UNIVERSITY OF SOUTHAMPTON

FACULTY OF MEDICINE

Human Development and Health

Role for acid-sensitive two-pore domain (K_{2P}) potassium channels in cancer

by

Sarah Williams

Thesis for the degree of Doctor of Philosophy

July 2014

UNIVERSITY OF SOUTHAMPTON

ABSTRACT

FACULTY OF MEDICINE, Human Development and Health

Doctor of Philosophy

ROLE FOR ACID-SENSITIVE TWO-PORE DOMAIN (K_{2P}) POTASSIUM CHANNELS IN CANCER

By Sarah Williams

K_{2P} channels are of broad interest to pathophysiology, including cancer biology, because they are active at all membrane potentials and, thereby, can influence cellular functions including the activity of other ion channels. To date, expression changes in four K_{2P} channels have been implicated in cancer and found to impact on cancer hallmark functions. However, no study has assessed the expression of all 15 K_{2P} channels in cancer or what functional roles K_{2P} multiple channels have in cancer cells. Therefore, the aim of this thesis was to investigate if acid-sensitive K_{2P} (TASK; K_{2P}3.1, K_{2P}9.1, and K_{2P}15.1) channel expression provides a functional advantage to human cancer cells. This research had two main lines of investigation: (i) to determine the K_{2P} channel mRNA and protein expression in a range of cancer tissues and cell lines, in order to establish clinically relevant model cancer cell lines that express K_{2P} channels, and (ii) to assess if TASK channel inhibition (using published inhibitors) has an impact on cell proliferation, apoptosis, or migration in cancer cell lines.

Bioinformatic analysis showed that K_{2P} channel mRNA was over- or underexpressed in a range of cancers, with several channels showing significant alterations. When the channel expression profile in cancer cell lines was studied, mRNA and protein expression data identified A549 (lung), HCT116 (colorectal), and 786-0 (renal) cells as model systems to study the role of TASK channels in cancer. Next, the role of TASK channels in cancer cell proliferation, apoptosis, and migration was examined. Colorectal cancer cell proliferation was significantly reduced following methanandamide or ruthenium red treatment, consistent with K_{2P}9.1 channel inhibition, suggesting that K_{2P}9.1 protein expression in colorectal cancer cell lines has a proliferative benefit. In contrast, TASK channel inhibition did not alter cellular functions in the other cell lines examined. Finally, the effect of conditions experienced within the cancer microenvironment was investigated. *N*-linked glycosylation was critical for K_{2P}3.1 channel surface expression, but not K_{2P}9.1. Incubation in either chronic hypoxia or low glucose failed to alter the cancer cell functions studied.

Overall this study had two main findings: (i) K_{2P} channel mRNA is both overexpressed and underexpressed in cancer, and (ii) that TASK channel inhibition had no impact on cellular functions in most of the cell lines studied. The combination of the functional data presented in this thesis, and published data which have linked K_{2P}9.1 channel activity to three cancer cell functions indicated that TASK channels may have a cell-specific role which could depend on the cancer type. This suggested that future studies are needed to determine what role the expression of multiple K_{2P} channels and other ion channels can have in cancer. In addition, to expanding on the findings from this thesis by determining if TASK channel activity can be detected in the cancer cell lines examined here, and using targeted TASK channel modulation to confirm the proliferative role of K_{2P}9.1 channels in colorectal cancer cells.

Table of contents

List of figures

List of tables

List of appendices

Declaration of authorship

I, Sarah Williams, declare that the thesis entitled

"Role for acid-sensitive two-pore domain (K_{2P}) potassium channels in cancer"

and the work presented in the thesis is both my own, and have been generated by me as the result of my own original research. I confirm that:

- this work was done wholly or mainly while in candidature for a research degree at this University;
- where any part of this thesis has previously been submitted for a degree or any other qualification at this University or any other institution, this has been clearly stated;
- where I have consulted the published work of others, this is always clearly attributed;
- where I have quoted from the work of others, the source is always given. With the exception of such quotations, this thesis is entirely my own work;
- I have acknowledged all main sources of help;
- where the thesis is based on work done by myself jointly with others, I have made clear exactly what was done by others and what I have contributed myself;
- parts of this work have been published as:
    1. Williams, S., Bateman, A. & O'Kelly, I. 2013. Altered expression of two-pore domain potassium (K_{2P}) channels in cancer. *PLoS One*, 8**,** e74589.
    2. Mant, A., Williams, S. & O'Kelly, I. 2013. Acid sensitive background potassium channels K_{2P}3.1 and K_{2P}9.1 undergo rapid dynamin-dependent endocytosis. *Channels,* 7**,** 0-14.
    3. Mant, A., Williams, S., Roncoroni, L., Lowry, E., Johnson, D. & O'Kelly, I. 2013. *N*-glycosylation-dependent control of functional expression of background potassium channels K_{2P}3.1 and K_{2P}9.1. *J Biol Chem,* 288**,** 3251-3264.

Signed: ……..

Date:……

Acknowledgements

I would like to thank my supervisors Dr. Ita O'Kelly and Dr. Andrew Bateman for their belief in my abilities, constant help, and support throughout the last three years. Thanks to everyone in the O'Kelly lab: Ita, Alex, Kelly, Laura and Jess, who have looked after me, kept me sane and provided fantastic science and life advice. Thanks to everyone in the surrounding research groups and the girls in PhD office for sharing the ups and downs of research with me, and for making it an enjoyable work environment. Also, I would like to thank Prof. David Wilson for providing expert advice with science and Corel Draw.

I would like to thank my friends and family, for listening to my potassium channel highs and lows, and for always being there. I would especially like to thank Katy Stubbs and Dave Madelin for the support, proof reading, cake, running motivation, and for keeping me balanced.

Finally I would like thank the Gerald Kerkut trust for funding this research and for giving me the opportunity to develop my learning, both within the lab and by attending scientific meetings.

Definitions and abbreviations

4-AP	4-aminopyridine
AA	Arachidonic acid
AE	Anion exchange protein
Akt	Protein kinase B
AMPK	AMP-activated protein kinase
ANOVA	Analysis of variance testing
AP-1	Activator protein 1
APS	Ammonium persulfate
AQP	Aquaporin
ASIC	Acid sensing ion channel
ATM	Ataxia telangiectasia mutated kinase
ATP	Adenosine triphosphate
ATR	Ataxia telangiectasia and Rad3 related kinase
AVD	Apoptotic volume decrease
Ba^{2+}	Barium
β-COP	β-coatomer protein
BK	Big-conductance K_{Ca} channel
BRCA1	Breast cancer susceptibility gene 1
BSA	Bovine serum albumin
Ca^{2+}	Calcium
CA	Carbonic anhydrase
CAMK	Calmodulin-dependent kinase
Ca_V	Voltage-gated Ca^{2+} channel
CDK	Cyclin-dependent kinases
cDNA	Complementary DNA
CGN	Cerebellar granule neuron
CHO	Chinese hamster ovary cells
Cl^-	Chloride
ClC	Voltage-gated Cl^- channel
CNS	Central nervous system
CO	Carbon monoxide
CO_2	Carbon dioxide

CRAC	Ca^{2+}-release-activated Ca^{2+} channels
CREB	cAMP response element binding protein
Cs^+	Caesium
DAB	Diaminobenzidine
DAG	Diacylglycerol
DEPC	Diethylphyrocarbonate
DMEM	Dulbecco's Modified Eagle Medium
DMEM Hams	DMEM with F-12 Ham nutrient supplement in 1:1 ratio
DTT	Dithiothreitol
E_X	Equilibrium potential
E_K	Equilibrium potential for K^+ ions
E2F	E2-binding transcription factor family
EATC	Ehrlich ascites tumour cells
ECL	Enhanced chemiluminescence
EDTA	Ethylenediaminetetraacetic acid
EEA1	Early endosome antigen 1
EGF	Epidermal growth factor
EGFR	Epidermal growth factor receptor
ELK-1	ETS domain-contain protein 1
EMT	Epithelial-mesenchymal transition
ENaC	Epithelial Na^+ channel
ER	Endoplasmic reticulum
ERα	Oestrogen receptor alpha
ERβ	Oestrogen receptor beta
FBS	Foetal bovine serum
G_1	Gap phase one
G_2	Gap phase two
G97E	TASK channel pore mutant
GABA	Gamma-aminobutyric acid
$GABA_A$	GABA ionotropic receptor
gDNA	genomic DNA
GF	Growth factor
GFP	Green fluorescent protein
GFP-K_{2P}3.1	GFP tagged human K_{2P}3.1

GFP-K_{2P}9.1	GFP tagged human K_{2P}9.1
GFP-K_{2P}15.1	N-terminal GFP tagged human K_{2P}15.1
GHK	Goldman-Hodkgin-Katz
GIRK	G-protein regulated K_{ir} channels
GLUT	Glucose transporter
GPCR	G-protein-coupled receptor
GR78	Glucose regulated protein 78 or Bip
GYG	glycine-tyrosine-glycine pore domain
GΩ	Gigaohm
h	Hours
H^+	Proton
H&E	Haematoxylin and eosin
HICC	Hypertonicity induced cation channel
HIF	Hypoxia-inducible factor
HRE	Hypoxia response element
HRP	Horse radish peroxidase
HV1	Voltage-gated proton channel
IC_{50}	Half maximal inhibition concentration
IGF-1	Insulin growth factor 1
IGFR	Insulin-like growth factor receptor
IK	Intermediate-conductance K_{Ca} channel
IL	Interleukin
IP_3	Inositol trisphosphate
IP_3R	Inositol trisphosphate receptor
IRK	classical K_{ir} channels
IUPHAR	International Union of Basic and Clinical Pharmacology
I-V	Current-voltage
K^+	Potassium
K_{ATP}	ATP-sensitive K_{ir} channels
K_{2P}	Two-pore domain potassium channels
K_{2P}15.1-GFP	C-terminal GFP tagged human K_{2P}15.1
K_{ca}	Calcium-gated potassium channels
KCh	Potassium channels
KCl	Potassium chloride

K_{ir}	Inward rectifier potassium channels
KO	Knockout
K_v	Voltage-gated potassium channels
M	Mitosis
MAPK	Mitogen-activated protein kinase
MCT	Monocarboxylate transporter
Meth	Methanandamide
MFI	Mean fluorescence intensity
Mg^{2+}	Magnesium
Min	minutes
MΩ	Megaohm
mRNA	Messenger RNA
MTS	3-(4,5-dimethylthiazol-2-yl)-5-(3-carboxymethoxyphenyl)-2-(4-sulfophenyl)-2H-tetrazolium inner salt
mV	Millivolts
N53Q	Glycosylation mutant
nA	Nanoamps
Na^+	Sodium
nACR	Nicotinic acetylcholine receptor
Na_V	Voltage-gated Na^+ channel
NCX	Na^+/Ca^{2+} co-transporter
NEB	Neuroepithelial body cells
NF-κB	Nuclear factor kappa-light chain enhancer of activated B cells
NFAT	Nuclear factor of activated T cells
NGF	Nerve growth factor
NHE1	Na^+/H^+ exchanger 1
NKCC1	Na^+-K^+-Cl^- co-transporter 1
NOX4	NADPH oxidase 4
o/n	Overnight
O_2	Oxygen
Orai	Store-operated Ca^{2+} channel
p	Membrane permeability
P	Pore domain
p53	Tumour antigen protein 53

pA	Picoamps
PASMC	Pulmonary artery smooth muscle cells
PBS	Phosphate buffered saline
pF	Picofarads
PFA	Paraformaldehyde
pK	Half maximal inhibition by pH
PKA	Protein kinase A
PKC	Protein kinase C
PI3K	phosphatidylinositol 4,5-bisphosphate 3 kinase
PIP_2	Phosphatidylinositol 4,5-bisphosphate
PLC	Phospholipase
PMCA	Plasma membrane Ca^{2+} ATPase
PDGF	Platelet derived growth factor
pTNM grading	pathology grading: tumour stage, lymph node invasion and metastasis
PUFA	Polyunsaturated fatty acids
qPCR	Quantitative real-time PCR
Rb	Retinoblastoma protein
rCGN	Rat cerebellar granule neurons
RMP	Resting membrane potential
RNAi	RNA interference
ROMK	renal outer medullary K_{ir} channels
ROI	Region of interest
ROS	Reactive oxygen species
Rpm	Rotations per minute
RR	Ruthenium red
RT	Room temperature
RT-PCR	Reverse-transcriptase PCR
RT-qPCR	Reverse-transcriptase quantitative PCR
RVD	Regulatory decrease in cell volume
RyR	Ryanodine receptor
s	Seconds
S	Synthesis
SDS	Sodium dodecyl sulfate
SDS-PAGE	SDS polyacrylamide gel electrophoresis

SDW	Sterile distilled water
SEM	Standard error of the mean
SERCA	Sarcoendoplasmic reticulum Ca^{2+} ATPase
siRNA	Small interfering RNA
SK	Small-conductance K_{Ca} channel
SOCE	Store operated Ca^{2+} entry
STAT-1	Signal transducer and activator of transcription 1
SUR	Sulfonylurea receptor
Ta	Annealing temperature
TAE buffer	Tris-acetate-EDTA buffer
TALK	TWIK-related alkaline-activated K_{2P} channel
TASK	TWIK-related acid-sensitive K_{2P} channel
TEA	Tetraethylammonium chloride
TEMED	Tetramethylethylenediamine
TFRC	Transferrin receptor
TGF	Transforming growth factor
THIK	TWIK-related halothane-inhibited K_{2P} channel
TK	Tyrosine kinase
T_m	Melting temperature
TM	Transmembrane domain
TNF	Tumour necrosis factor
TP53	Tumour protein 53
TREK	TWIK-related two-pore domain K_{2P} channel
TRESK	TWIK-related spinal cord localised K_{2P} channel
TRP	Transient receptor potential cation channels
TUNAL	TNF-related apoptosis-inducing ligand
TWIK	Two-pore domain weakly inward rectifying K_{2P} channel
UT	Untransfected
UV	Ultraviolent
VDAC	Voltage dependent anion channel
VEGF-A	Vascular endothelial growth factor-A
VEGFR	Vascular endothelial growth factor receptor
V_m	Membrane potential
VRAC	Volume regulated anion channel

W	Water
WT	Wild type
λ	Wavelength

Chapter 1

Introduction

1.1 Ion channels

Cellular homeostasis is maintained and regulated by the differential distribution of key physiological ions across the plasma membrane (Aidley and Stanfield, 1996; Alberts, 2008). The ionic gradients maintained across the plasma membrane vary depending on the specific ion (Figure 1.1 A); sodium (Na^+), chloride (Cl^-), and calcium (Ca^{2+}) ions are generally more concentrated in the extracellular environment, whereas potassium (K^+) concentrations are higher in the cell cytoplasm (Figure 1.1 C; Aidley and Stanfield, 1996; Alberts, 2008). In addition, ionic gradients are maintained between intracellular compartments, such as the endoplasmic reticulum (ER) and the cytoplasm (Alberts, 2008).

The generation of differential ion concentrations across a cell membrane creates electrochemical gradients for ion movement (Figure 1.1 A). The voltage at which the concentration and electrical gradients for a single ion will reach equilibrium and result in no net ion movement is known as the equilibrium potential (E_x). This voltage is calculated using the Nernst equation (Figure 1.1 B i; Aidley and Stanfield, 1996). This value varies depending on the specific ion concentrations, for K^+ ions E_K is approximately -86 mV, for Na^+ ions E_{Na} is +58 mV, and for Cl^- ions E_{Cl} is -51 mV (Figure 1.1 C).

The movement of ions across cell membranes is facilitated by specialised channels and transporters which form selective pores. These proteins are essential to both passive and active transport of ions across the membrane because lipid bilayers are impermeable to charged ions (Behrends, 2012). The selective transport of ions across the plasma membrane and tight regulation of ion channel and transporter activity is instrumental in the creation of the cell membrane potential (V_m): the electrical difference between the intracellular and extracellular environments (Aidley and Stanfield, 1996). The membrane potential of the cell is not controlled by a single ion, and in most cells K^+, Na^+, and Cl^- ions are the main contributors to the resting membrane potential (RMP; Aidley and Stanfield, 1996). As the Nernst equation will only take a single ion into consideration, to calculate the membrane potential the Goldman-Hodgkin-Katz (GHK) voltage equation is required (Figure 1.1 B ii). For a neuron, the RMP is usually -70 mV (Aidley and Stanfield, 1996; Alberts, 2008). This value is calculated using the GHK voltage equation, by taking into consideration the equilibrium potential for K^+, Na^+, and Cl^- ions, in addition to the relative permeability of the plasma membrane for each of these ions (membrane permeability is

proportional to the number of open channels; Aidley and Stanfield, 1996; Hodgkin and Huxley, 1945). For a neuron at rest, the relative membrane permeability (*p*) for each ion is typically 1: 0.05: 0.45 for p_K: p_{Na}: p_{Cl} (Aidley and Stanfield, 1996; Rosenberg, 1969). The RMP is often close to E_K, this is due to the high membrane permeability to K^+ ions at these potentials (which results from leak K^+ channel activity), although the contributions of other physiological ions prevent the RMP from reaching E_K (Aidley and Stanfield, 1996; Goldstein et al., 2001; Hodgkin and Huxley, 1945; Hodgkin and Huxley, 1947; Hodgkin and Katz, 1949). Once the RMP of a cell is established, a key transporter in maintaining this potential is the Na^+/K^+ ATPase, which is essential in regulating the intracellular concentrations of K^+ and Na^+ ions (Aidley and Stanfield, 1996; Alberts, 2008). For every adenosine triphosphate (ATP) molecule expended, the Na^+/K^+ ATPase will transport three Na^+ ions out of the cell and two K^+ ions into the cytoplasm, with the net efflux of positively charged ions maintaining the negative RMP (Aidley and Stanfield, 1996; Toyoshima et al., 2011).

Ion channels are highly selective pore forming transmembrane proteins, which allow ions to flow down their concentration gradients, across the plasma membrane at close to the rate of diffusion (Aidley and Stanfield, 1996; Catterall, 1995; Terlau and Stühmer, 1998). There are numerous types of ion channels, including Na^+, K^+, Ca^{2+}, and Cl^- channels, in addition to cation channels and ion transporters. For an overview of the different types of ion channels and their functional properties see the International Union of Basic and Clinical Pharmacology (IUPHAR) Database (www.iuphar-db.org). Due to the importance of regulating ionic gradients across the plasma membrane, ion channel activity is controlled and can be gated by a range of stimuli, including voltage, external and internal ligands, pH change, and mechanical force (Aidley and Stanfield, 1996; Catterall, 1995; Terlau and Stühmer, 1998). The importance of maintaining ionic gradients and the membrane potential across cellular membranes means that ion channels are fundamental in the regulation of many physiological processes, including cell excitability and Ca^{2+}-dependent intracellular signalling (Yellen, 2002).

A)

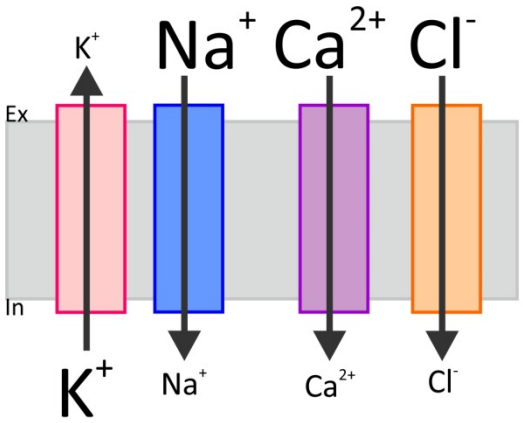

B)

i) Nernst equation $$Ex = \frac{RT}{zF} \ln\left(\frac{[X]_{ex}}{[X]_{in}}\right)$$

ii) GHK voltage equation $$V_m = \frac{RT}{F} \ln\left(\frac{p_K[K^+]_{ex} + p_{Na}[Na+]_{ex} + p_{Cl}[Cl^-]_{in}}{p_K[K^+]_{in} + p_{Na}[Na+]_{in} + p_{Cl}[Cl^-]_{ex}}\right)$$

Where:
E_x = equilibrium potential (mV)
R = gas constant (8.314 $J.K^{-1}.mol^{-1}$)
T = temperature, kelvin (37 °C = 310.15 K)
z = charge
F = Faraday's constant (96485 $c.mol^{-1}$)

$[X]_{ex}$ = extracellular concentration
$[X]_{in}$ = intracellular concentration
V_m = membrane potential
p_x = membrane permeability

C)

Ion	Intracellular concentration, $[X]_{in}$	Extracellular concentration, $[X]_{Ex}$	Equilibrium potential (mV), E_X	Direction of ion flux at a V_m of -70 mV
K^+	140 mM	5 mM	- 89	Efflux
Na^+	5-15 mM	145 mM	+ 60-90	Influx
Ca^{2+}	0.1 µM	1-2 mM	+ 123-132	Influx
Cl^-	5-15 mM	110 mM	- 53-83	Efflux/Influx

Figure 1.1: Overview of key cellular ionic gradients

A) The typical concentration gradients for key physiological ions, K^+, Na^+, Ca^{2+}, and Cl^-, maintained across the plasma membrane are shown by differences in text size. The direction of ion movement based on the concentration gradient for each ion is indicated.

B) Key equations used to calculate the electrical properties of the cell membrane: i) The Nernst equation calculates the voltage at which the concentration and electrical gradients for a single ion will reach equilibrium (equilibrium potential: E_X). ii) The Goldman-Hodgkin-Katz (GHK) voltage equation calculates the membrane potential (V_m) by considering the permeability of the cell membrane to each ion, in addition to the equilibrium potential.

C) Table indicating the typical ion concentrations for a mammalian cell and the equilibrium potential for each ion, which is calculated by the Nernst equation. The direction of ion flux at a V_m of -70 mV is also shown, this was calculated using the electrochemical driving force equation (where the driving force voltage (V_{DF}) = V_m - V_{eq}). Both ion efflux and influx is indicated for Cl^- ions, as efflux is predicted for $[Cl^-]_{in}$ = 5 mM, and influx for $[Cl^-]_{in}$ = 15 mM.

Figure based on Aidley and Stanfield (1996) and Alberts (2008).

1.2 Potassium channels

Potassium channels (KCh) are ubiquitously expressed membrane proteins and form the largest family of ion channels. In humans, there are 75 genes which encode KCh, these are divided into four superfamilies based on the membrane topology and functionality of the channels (Figure 1.2; IUPHAR Compendium; Adelman et al., 2013; Gutman et al., 2013a; Gutman et al., 2013b; Plant et al., 2014; Shieh et al., 2000). The four KCh superfamiles are: (i) voltage-gated (K_v) channels, (ii) calcium-gated (K_{Ca}) channels, (iii) inward rectifier (K_{ir}) channels, and (iv) two-pore domain (K_{2P}) channels.

KCh preferentially transport K^+ ions, due to a selectivity filter located within the pore domain (P) of the channel subunits (Doyle, 1998). This domain is formed of a tripeptide sequence motif, consisting of glycine-(tyrosine/leucine/phenylalanine)-glycine (G(Y/L/F)G) in the majority of KCh. Four P domains are required to form a functional channel with a complete selectivity filter (Doyle, 1998). The membrane topology of K_V and K_{Ca} channels have six transmembrane (TM) domains and one P domain (6TM/1P), therefore these channels will form functional tetramers (Figure 1.2 A). K_{ir} channel subunits have two TM domains and one P domain (2TM/1P) and will also form tetramers (Figure 1.2 B). The final KCh superfamily, the K_{2P} channel family are structurally distinct from other classes of KCh since they have two P domains and four TM domains (4TM/2P) in each channel subunit, meaning that they form functional dimers and not tetramers (Figure 1.2 C).

KCh activity is essential in controlling the membrane potential, therefore KCh activity is critical to the physiological properties of both excitable and non-excitable cells (Bayliss and Barrett, 2008; Sundelacruz et al., 2009). As a result, KCh activity is involved in many cellular functions including neuronal excitability, neurotransmitter release, volume control, smooth muscle contraction, heart rate regulation, and insulin secretion (Lesage and Lazdunski, 2000; Shieh et al., 2000; Wickenden, 2002).

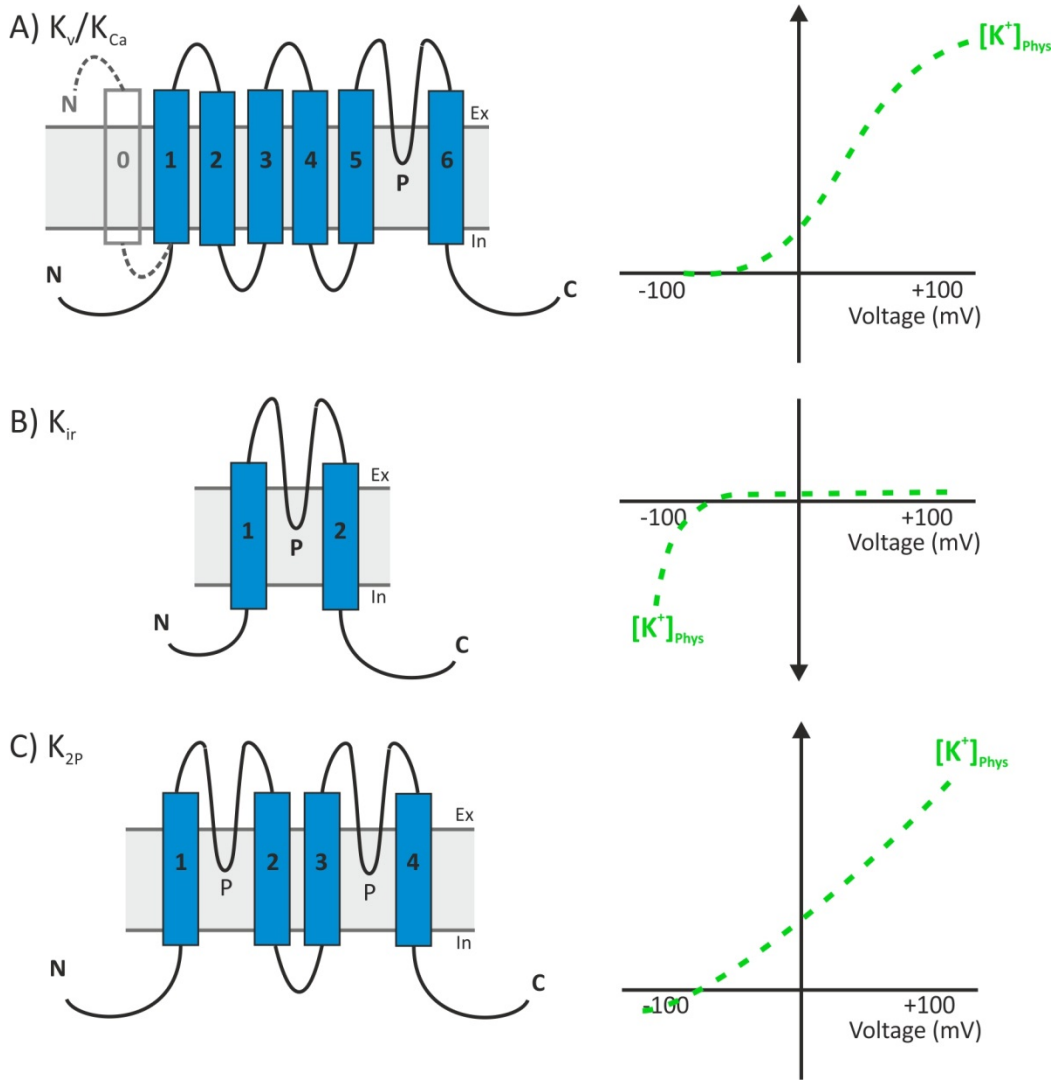

Figure 1.2: Membrane topology and functional properties of potassium channel subfamilies

The membrane topologies of the three types of potassium channel pore-forming subunits are shown, transmembrane (TM) helices are in blue and P indicates a pore domain. Graphs represent example current-voltage (*I-V*) relationships under physiological K^+ gradients ($[K^+]_{phys}$).

A) K_v and K_{Ca} channel subunits have six TM helices and one P domain (6TM/1P). $K_{Ca}1.1$ α subunits, which form BK channels in association with β subunits, have a 7TM/1P topology with an additional TM0 helix, and this is indicated in grey. K_V channels are activated by changes in voltage and conduct an outward current. K_{Ca} channels are activated by changes in voltage and/or Ca^{2+} concentrations and conduct an outward current. The *I-V* relationship shown is based on $K_V1.3$ channels, which activate at depolarised voltages.

B) K_{ir} channel subunits have two TM helices and one P domain (2TM/1P). At voltages positive to E_K, K_{ir} channels pass small outward currents due to pore blockage by intracellular cations. At voltage negative to E_K, the pore is unblocked and an inward K^+ current is conducted. The *I-V* relationship presented is based on $K_{ir}4.2$ channels.

C) K_{2P} channels have four TM helices and two P domains ($4TM/_{2P}$). K_{2P} channels are open rectifiers and will conduct outward currents under $[K^+]_{phys}$. The *I-V* relationship shown is based on $K_{2P}3.1$ channels.

Figure adapted from Goldstein et al. (2001) and Rodrigues et al. (2003).

1.2.1 K_V channels

The activity of K_V channels is gated by voltage. Thus, these channels are usually closed at the hyperpolarised RMP and open in response to membrane depolarisation at a specific activation voltage (Figure 1.2 A). The voltage sensitivity of K_V channels is conferred by the fourth TM domain (termed S4-helix; Figure 1.2 A) which acts as a voltage sensor. The composition of the S4-helix is unique with every third or fourth amino acid having a positive charge (either lysine or arginine), meaning that the S4-helix has a net positive charge (Jensen et al., 2012; Papazian et al., 1991; Terlau and Stühmer, 1998). Following membrane depolarisation the intracellular voltage becomes more positive with respect to the extracellular environment, causing outward movement of the S4-helix which results in a conformational change in the channel protein and opening of the channel pore (Jensen et al., 2012).

K_V channels are formed of tetramers of pore-forming α subunits (6TM/1P), which include K_V1.1-8, K_V2.1-2, K_V2.1-4, K_V4.1-3, K_V7.1-5, K_V10.1-2, K_V11.1-3, and K_V12.1-3 channels (Gutman et al., 2003). The activation voltage for most K_V channels lies between -30 and +50 mV, with the half-maximal activation voltage of K_V1.1, K_V2.1, and K_V3.1 channels (formed of α subunit tetramers) being -32.0 mV, +11.4 mV, and +16.0 mV, respectively (Gutman et al., 2013b). The kinetics and activity of K_V channels can be regulated by modulatory β subunits, which form heterotetramers with K^+-conducting α subunits, but cannot conduct K^+ alone (K_V5.1, K_V6.1-4, K_V8.1-2, and K_V9.1-3; Gutman et al., 2003; Gutman et al., 2013b; Shieh et al., 2000). In addition, accessory β subunits (K_Vβ1-3, Mink, MiRP1-3, KCNE1-like, and KCNIP1-4) can associate with tetrameric channels in a $\alpha_4\beta_4$ configuration (Gutman et al., 2003; Gutman et al., 2013b; Shieh et al., 2000). The association of K_V channels and accessory β subunits is critical for the physiological roles of certain channels (Abbott et al., 1999). In the heart, a prolonged ventricular action potential (elongated QT interval) is due to the slow onset of cell repolarisation in the myocardium, caused by delayed rectifier K^+ channels, K_V7.1-Mink (IK_S) and K_V11.1-MiRP1 (IK_r; Abbott et al., 1999; Curran et al., 1995; Ruscic et al., 2013; Shieh et al., 2000). The association of β subunits with K_V channels provides some of the characteristics which allow their function as delayed rectifiers. For example, the interaction of K_V7.1 with Mink (*KCNE1*) slows the movement of the S4-helix upon membrane depolarisation (Ruscic et al., 2013). In addition, MiRP1

subunits alter K_V11.1 channel gating, reduce channel conductance, and are required for the regulation of K_V11.1 by some anti-arrhythmic drugs (Abbott et al., 1999)

Multiple K_V channels are modulated by broad spectrum KCh blockers, including tetraethylammonium (TEA), 4-aminopyridine (4-AP), and α-dendrotoxin, although the selectivity of K_V channel subtypes to these inhibitors varies (see Table 1.1; Aidley and Stanfield, 1996; Gutman et al., 2003; Gutman et al., 2013b). The inhibitors described here are open channel blockers and will block the K_V channel pore from the extracellular side of the plasma membrane (Aidley and Stanfield, 1996; Catterall, 1995; Terlau and Stühmer, 1998).

1.2.2 K_{Ca} channels

K_{Ca} channels are grouped into big- (BK: K_{Ca}1.1 α subunits in association with β1-4 subunits, $\alpha_4\beta$), intermediate- (IK: K_{Ca}3.1), and small-conductance (SK: K_{Ca}2.1-3) channels based on their K^+ conductance properties (Wei et al., 2005). Generally, K_{Ca} channel activity causes membrane repolarisation following a rise in intracellular Ca^{2+}, which will modulate Ca^{2+} entry into the cell (Vergara et al., 1998; Wickenden, 2002). BK channels are activated by voltage and micromolar rises in intracellular Ca^{2+} and, like K_V channels, the voltage-sensitivity of BK channels is conferred by the fourth TM domain (Vergara et al., 1998; Xia et al., 2002). The Ca^{2+} sensitivity of BK channels is due to three divalent cation binding sites, located in the C-terminus of each subunit, and these are termed the Ca^{2+} binding bowl (Schreiber and Salkoff, 1997; Vergara et al., 1998; Xia et al., 2002). The physiological roles of BK channels are regulated by their association with accessory β subunits (β1-4), which can influence channel kinetics (Berkefeld et al., 2010). In adrenal chromaffin cells, different firing patterns are caused by the association of K_{Ca}1.1 with β subunits; either phasic relating to K_{Ca}1.1 subunits alone which are rapidly deactivating, or tonic corresponding to complexes of K_{Ca}1.1 tetramers with β2 or β3 subunits which are slowly deactivating (Berkefeld et al., 2010; Orio et al., 2002). β1 subunits are critical for the sensitivity of BK channels to Ca^{2+} in vascular smooth muscle cells and when β1 subunits are knocked out in mouse models increased vasoconstriction is observed (Berkefeld et al., 2010; Firth et al., 2011).

Table 1.1: Modulation of K_V channels by broad spectrum K^+ channel blockers

Inhibition of K_V channel α subunits by the broad spectrum K^+ blockers: tetraethylammonium (TEA), 4-aminopyridine (4-AP), and α-dendrotoxins. The characterised IC_{50} values are given for each compound.
Where a cell is left blank the channel is not inhibited by that compound.

Aidley and Stanfield (1996), Choi et al., (2011a), Gutman et al., (2003), Gutman et al., (2013b), Harvey, (2001), and Renganathan et al., (2009).

K_V subtype		**TEA**	**4-AP**	**α-dendrotoxin**
K_V1	$K_V1.1$	0.3 mM	290 μM	≈ 20 nM
	$K_V1.2$	560 mM	590 μM	≈ 17 nM
	$K_V1.3$	10 mM	195 μM	250 nM
	$K_V1.4$	> 100 mM	13 μM	> 100 nM
	$K_V1.5$	330 mM	270 μM	> 1000 nM
	$K_V1.6$	7 mM	1.5 mM	≈ 20 nM
	$K_V1.7$	150 mM	150 μM	
	$K_V1.8$	50 mM	1.5 mM	
K_V2	$K_V2.1$	13 μM	18 mM	
	$K_V2.2$	2.6 mM	1.5 mM	
K_V3	$K_V3.1$	0.2 mM	29 μM	> 1000 nM
	$K_V3.2$	0.1 mM	0.1 mM	> 100 nM
	$K_V3.3$	0.14 nM	1.2 mM	
	$K_V3.4$	0.3 mM		> 100 nM
K_V4	$K_V4.1$	> 10 mM	9 mM	> 300 nM
	$K_V4.2$		5 mM	
	$K_V4.3$		31 μM	
	$K_V4.4$			
K_V7	$K_V7.2$	0.16 mM		
	$K_V7.3$	> 30 mM		
	$K_V7.4$	3 mM		
	$K_V7.5$	> 30 mM		
K_V11	$K_V11.1$	600 mM	3.8 mM	

IK and SK channels are insensitive to changes in voltage, and are activated by increases in intracellular Ca^{2+} levels (Vergara et al., 1998; Wei et al., 2005). The regulation of IK and SK activity by Ca^{2+} is caused by indirect binding of Ca^{2+} ions to calmodulin, which is constitutively attached to the C-termini of these channels (Fanger et al., 1999; Xia et al., 1998). Calmodulin is considered an accessory β subunit of the channels (Berkefeld et al., 2010) and Ca^{2+} binding to calmodulin results in a conformational change that opens the channel pore (Schumacher et al., 2001; Xia et al., 1998). In the central nervous system (CNS), SK channels are expressed on the post-synaptic membranes of multiple neurons, for example in CA1 pyramidal neurons (Adelman et al., 2012). In these neurons, SK channel activity can limit synaptic excitability, by hyperpolarising the cell membrane which inhibits active NMDA receptors, reduces Ca^{2+} influx, and restricts the size of Ca^{2+} transients produced (Adelman et al., 2012).

There are a number of K_{Ca} channel inhibitors, these include the broad spectrum channel blocker TEA ($K_{Ca}1.1$ (BK) IC_{50} = 0.14 mM, and $K_{Ca}3.1$ (IK1) IC_{50} = 24 mM), in addition to toxins such as apamin ($K_{Ca}2.1$ (SK1) IC_{50} = 8 nM, $K_{Ca}2.2$ (SK2) IC_{50} = 200 pM, and $K_{Ca}2.3$ (SK3) IC_{50} = 10 nM), charybdotoxin ($K_{Ca}1.1$ (BK) IC_{50} = 2.9 nM), and iberiotoxin ($K_{Ca}1.1$ (BK) IC_{50} = 1.7 nM; Aidley and Stanfield, 1996; Catterall, 1995; Gutman et al., 2013a; Wei et al., 2005).

1.2.3 K_{ir} channels

At physiological membrane potentials, which are usually positive to E_K (-89 mV; Figure 1.1 C), K_{ir} channels will conduct small outward K^+ currents that cause a hyperpolarisation of the membrane potential (Figure 1.2 B; Adelman et al., 2013; Hibino et al., 2010). However, at membrane potentials negative to E_K K_{ir} channels allow inward rectification of K^+ ions (against their concentration gradient) causing membrane depolarisation (Adelman et al., 2013; Hibino et al., 2010). As result of this, K_{ir} channels can influence the membrane potential by either the influx or efflux of K^+ ions (Doupnik et al., 1995; Hibino et al., 2010; Nichols and Lopatin, 1997). K_{ir} channel subunits lack a voltage sensor domain and the voltage-dependent rectification of these channels is achieved by the binding of Mg^{2+} ions and polyamines to the cytoplasmic face of the channel (Lopatin et al., 1994; Mark and Herlitze, 2000; Yang et al., 1995). At depolarised membrane potentials,

the outward flow of K^+ ions is limited by the association of Mg^{2+} and polyamines to K_{ir} channels; these are removed at negative membrane potentials to allow the inward movement of K^+ ions (Lopatin et al., 1994; Mark and Herlitze, 2000; Yang et al., 1995). The regulation of K_{ir} channels is critical for their physiological roles and the channels are modulated by a range of stimuli including ATP, phosphorylation, G-proteins, and lipids (Adelman et al., 2013; Doupnik et al., 1995; Hibino et al., 2010; Nichols and Lopatin, 1997). There are four K_{ir} channel subfamilies, which are grouped by their regulation properties: (i) classical K_{ir} channels (IRK, K_{ir}2.1-4, K_{ir}7.1), (ii) renal outer medullary K_{ir} channels (ROMK, K_{ir}1.1), (iii) ATP-sensitive K_{ir} channels (K_{ATP}, K_{ir}6.1-2), and (iv) G-protein-coupled K_{ir} channels (GIRK, K_{ir}3.1-4; Adelman et al., 2013; Hibino et al., 2010).

For example, GIRK channels are activated by direct interaction of their N- and C-termini with G-proteins, as well as phosphatidylinositol 4,5-bisphosphate (PIP_2), intracellular Na^+, ethanol, and membrane stretch (Mark and Herlitze, 2000). A physiological role of GIRK channel activity is to regulate neuronal excitability, where activation of GIRK channels (by G-protein signalling) results in membrane hyperpolarisation and reduced action potential firing. In midbrain dopaminergic neurons, dopamine acts on synaptic D2 receptors (which are G-protein-coupled receptors (GPCR)); this causes GIRK activation and is thought to modulate the slow inhibitory post-synaptic currents (Luscher and Slesinger, 2010). The inhibition of K_{ATP} channels by ATP is caused by the interaction of K_{ir}6.1/K_{ir}6.2 subunits with the associated β accessory subunit sulfonylurea receptor (Nichols and Lopatin, 1997). K_{ATP} channels are essential for glucose-stimulated insulin secretion from pancreatic β-cells. Thus, in response to raised blood-sugar levels, increased glycolysis results in a rise in intracellular ATP that closes K_{ATP} channels, causing membrane depolarisation, voltage-gated Ca^{2+} (Ca_V) channel activation, rises in intracellular Ca^{2+} concentrations, and insulin secretion (Ashcroft, 2010; Koster et al., 2005; McTaggart et al., 2010).

1.2.4 K_{2P} channels

K_{2P} channels are functionally distinct compared to the other classes of KCh, in addition to being structurally different (Figure 1.2 C), with all functional K_{2P} channels possessing electrophysiological characteristics that closely resemble the theoretical leak K^+

current properties predicted by the GHK flux equation (Enyedi and Czirják, 2010; Goldstein et al., 2005; Goldstein et al., 2001; Hodgkin and Katz, 1949; Ketchum et al., 1995; Lesage et al., 1996): Thus: (i) The activity of K_{2P} channels should be independent of voltage, so that the probability of the channel being open is the same at all membrane potentials. (ii) The current is time independent, with no activation, deactivation, or inactivation kinetics, and follows changes in membrane potential. (iii) The current is non-rectifying; open rectification means that the direction of K^+ movement is determined by the K^+ gradient across the membrane. By satisfying these predicted criteria for a leak K^+ channel, K_{2P} channels compose the leak KCh family (Aidley and Stanfield, 1996; Enyedi and Czirják, 2010).

K_{2P} channels are open at all physiological membrane potentials and possess little activation or inactivation kinetics (Duprat et al., 1997; Lesage et al., 1996), although $K_{2P}6.1$ channels are reported to undergo partial inactivation at depolarised membrane potentials (Chavez et al., 1999; Patel et al., 2000). This means that when K_{2P} channels are expressed on the plasma membrane they are always active (unless they are modulated by internal and external stimuli) and will mediate the selective outward leak of K^+ ions from the cell. Open rectification means that K_{2P} channel currents are outward under physiological K^+ gradients and in symmetrical K^+ gradients there is no net movement of ions (linear current-voltage (*I-V*) relationship; Figure 1.5). However, not all K_{2P} channels completely satisfy this property and at certain voltages some K_{2P} channels (For example, $K_{2P}1.1$ and $K_{2P}6.1$) can show weak inward rectification (Figure 1.5 A; Chavez et al., 1999; Enyedi and Czirják, 2010; Kim et al., 2000).

A key physiological role of leak K^+ currents is to regulate the differential concentration of K^+ ions across the plasma membrane. Therefore, K_{2P} channels are critical in setting the membrane potential and regulating cellular input resistance. Secondarily, K_{2P} channel activity will regulate excitability, the shape of action potentials, and the activity of other ion channels (Lesage and Lazdunski, 2000).

1.3 K_{2P} channel family

The first K_{2P} channels were identified and cloned in the mid-nineties from yeast (TOK1; Ketchum et al., 1995) and Drosophila (ORK1; Goldstein et al., 1996). The first

mammalian K_{2P} channel was cloned in 1996 and was named two-pore domain weakly-inward rectifying K^+ channel (TWIK) for its unusual membrane topology and the weakly inward rectifying currents observed when the channel was expressed in *Xenopus* oocytes (Figure 1.2 C; Lesage et al., 1996). Following the discovery of subsequent K_{2P} channels, TWIK has been renamed as K_{2P}1.1 (Goldstein et al., 2005). The official nomenclature of K_{2P} channels is *KCNKX* for the gene and K_{2P}X.1 for the protein (Goldstein et al., 2005). Between 1996 and 2003, fourteen additional members of the K_{2P} channel family were identified. The fifteen K_{2P} channels are grouped into six subfamilies based on sequence homology and functional characteristics of the currents (Figure 1.3; Enyedi and Czirják, 2010; Goldstein et al., 2005). These K_{2P} channel subfamilies are: weak-inwardly rectifying TWIK, mechano-gated TREK, acid-sensitive TASK, alkaline-activated TALK, halothane-inhibited THIK, and spinal cord localised TRESK (Figure 1.3).

The K_{2P} channel family has low sequence homology between its members, for example K_{2P}1.1 and K_{2P}2.1 channels share only 28 % amino acid sequence homology (Figure 1.3; Fink et al., 1996). This contrasts with other KCh families, where the overall sequence similarity between members can reach 60 % (Enyedi and Czirják, 2010; Gutman et al., 2003). Despite sharing low amino acid sequence homology, all K_{2P} channel subunits, have the same membrane topology: a short N-terminus, long C-terminus, four TM domains, and two P domains (Figure 1.2 C; Goldstein et al., 2001). K_{2P}18.1 channels have the expected membrane topology (4TM/2P), but have a shorter C-terminus and a longer intracellular domain between TM2 and TM3 (Kang et al., 2004b; Sano et al., 2003). To date, no modulatory β subunits have been identified that interact with K_{2P} channels (Enyedi and Czirják, 2010).

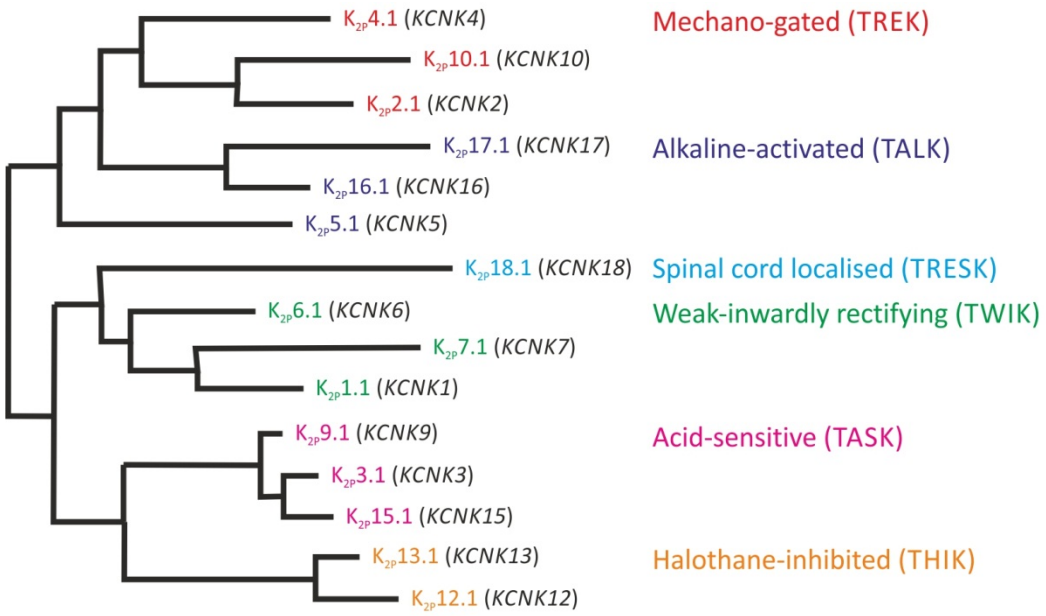

Figure 1.3: Human K_{2P} channel phylogenetic tree
K_{2P} channel family aligned by amino acid sequence and phylogenetic analysis. The channel subfamilies are grouped according to similarities in sequence and named using the IUPHAR derived K_{2P}X.1 nomenclature system; the gene names (*KCNKX*) are also given.
The six channel subfamilies are labelled in different colours.
Figure adapted from Goldstein et al. (2005).

The crystal structures of two K_{2P} channels ($K_{2P}1.1$ and $K_{2P}4.1$) have recently been resolved (Brohawn et al., 2012; Miller and Long, 2012). These structures showed that, although K_{2P} channels form dimers, the channels resemble the structure of a classical tetrameric KCh, such as $K_V1.2$ (Figure 1.4; Long et al., 2005; Miller and Long, 2012). As expected for a functional KCh, the K^+ conducting pore of K_{2P} channels is formed of four P domains (Brohawn et al., 2012; Miller and Long, 2012). TM2 and TM4 form the inner helices that line the channel pore, and TM1 and TM3 correspond to the outer helices of the channel (Figure 1.4 A; Brohawn et al., 2012; Miller and Long, 2012). The first extracellular loop, between TM1 and TM2, is longer than observed in other types of KCh, where this region is typically less than 20 amino acids compared to 56 amino acids in $K_{2P}1.1$. The crystal structure of $K_{2P}1.1$ revealed that this region forms an extracellular cap above the channel that is proposed to contain regulatory domains for the channels (Figure 1.4 A). In pH sensitive K_{2P} channels (TASK and TALK) this same region contains the amino acids responsible for channel modulation by changes in extracellular pH (Clarke et al., 2008; Miller and Long, 2012; Niemeyer et al., 2007).

K_{2P} channels are relatively insensitive to classical KCh blockers (TEA, 4-AP, caesium (Cs^+), and low concentrations of barium (Ba^{2+}); Lesage, 2003; Meadows and Randall, 2001). The insensitivity of K_{2P} channels to broad spectrum KCh blockers is caused by the extracellular cap, as this prevents access to the channel pore by these inhibitors (Figure 1.4 A; Brohawn et al., 2012; Miller and Long, 2012). Similarly, the cap domain is thought to preclude the accessibility of the K_{2P} channel pore to peptide toxins, such as α-dendrotoxin which blocks other K_V and K_{Ca} channels (Table 1.1).

Due to the recent and rapid identification of K_{2P} channel family, the physiological roles and selective pharmacological modulators of K_{2P} channels are still being determined. An overview of the activity and physiological roles of each K_{2P} channel subfamily has been given in the following sections, and the known characteristics of each K_{2P} channel is summarised in Appendix 1.

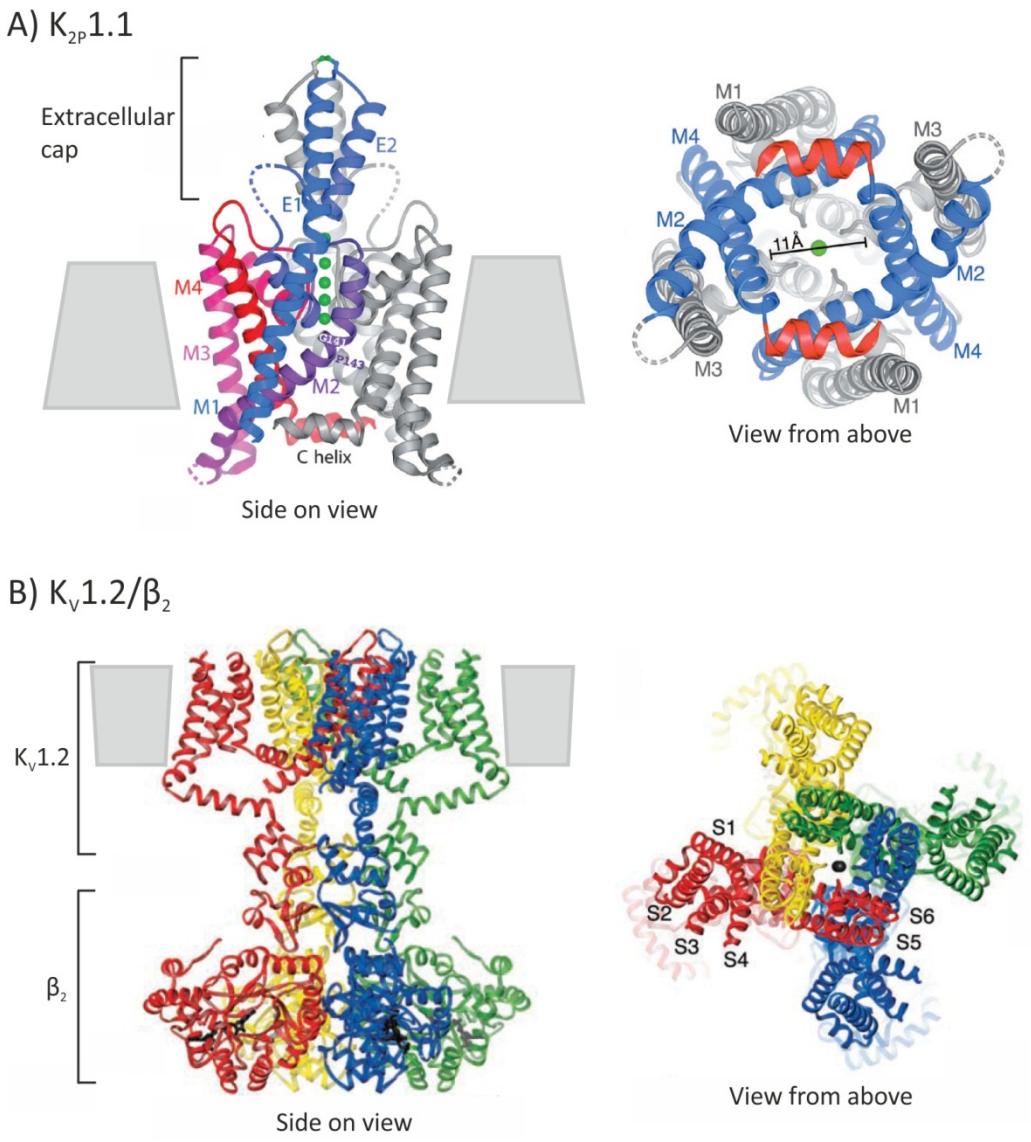

Figure 1.4: Crystal structures of $K_{2P}1.1$ and $K_V1.2/\beta_2$ channels
Crystal structures of (A) $K_{2P}1.1$ dimer and (B) $K_V1.2/\beta_2$ tetrameric complex.
For each channel a side view and the extracellular view from above are shown.
Figure adapted from Long et al. (2005) and Miller and Long (2012).

1.3.1 Overview of the TWIK channel family

The TWIK channel family has three members ($K_{2P}1.1$, $K_{2P}6.1$, and $K_{2P}7.1$). $K_{2P}1.1$ and $K_{2P}6.1$ channels show mild inward rectification in symmetrical K^+ gradients, although in physiological K^+ concentrations TWIK channels are outward rectifiers (Figure 1.5 A; Chavez et al., 1999; Lesage et al., 1996; Patel et al., 2000). The final TWIK family member, $K_{2P}7.1$ channel, is suspected to be non-functional due to trafficking defects, since when expressed in COS-7 cells $K_{2P}7.1$ is only localised to the ER (Salinas et al., 1999). $K_{2P}1.1$ and $K_{2P}6.1$ channels are inhibited by reductions in intracellular pH, and activated by protein kinase C (PKC) dependent pathways (Chavez et al., 1999; Lesage et al., 1996; Lesage and Lazdunski, 2000; Patel et al., 2000). The cell surface activity of $K_{2P}1.1$ channels is also modulated by a combination of inhibition caused by SUMOylation (Plant et al., 2012b; Rajan et al., 2005) and channel endocytosis (Feliciangeli et al., 2010).

$K_{2P}1.1$ channels are unique within the K_{2P} channel family, in that they can alter their ion permeability to conduct an inward Na^+ leak current when external K^+ or proton concentrations fall into the pathophysiological range (a serum K^+ concentration of ≈2 mM, and pH of less than 7; Chatelain et al., 2012; Ma et al., 2011). This switch in ion permeability is due to a threonine located adjacent to the selectivity filter in the first pore domain of the channel (TTGYG in $K_{2P}1.1$ compared to TIGYG in other K_{2P} channels; Chatelain et al., 2012; Ma et al., 2011). The electrophysiological consequence of $K_{2P}1.1$ channels conducting an inward Na^+ current is membrane depolarisation, although the physiological relevance of $K_{2P}1.1$ induced depolarisation has not been fully characterised (Chatelain et al., 2012; Ma et al., 2011). In human cardiac myocytes (which express endogenous $K_{2P}1.1$ channels) cultured in low external K^+ ion concentrations a depolarised membrane potential was observed in 45 % of cells (Ma et al., 2011). This effect was reduced in $K_{2P}1.1$ shRNA treated cells, suggesting that $K_{2P}1.1$ channels are involved in this depolarising response (Ma et al., 2011). In addition, the RMP of renal and pancreatic cells from $K_{2P}1.1^{-/-}$ knockout (KO) mouse models is more hyperpolarised than that observed in cells from wild type (WT) animals, and in these cells it is thought that $K_{2P}1.1$ channels are contributing a depolarising background conductance (Chatelain et al., 2012).

Representative *I-V* relationships for the K_{2P} channel subfamilies

A) TWIK (K_{2P}6.1)

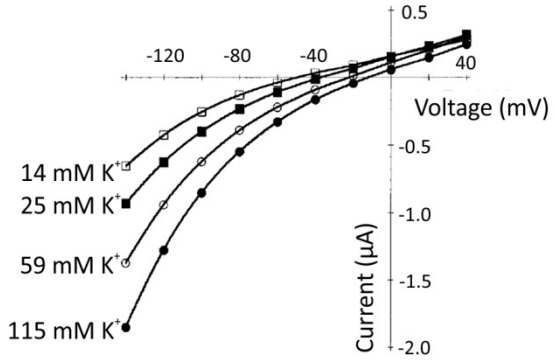

B) TREK (K_{2P}10.1)

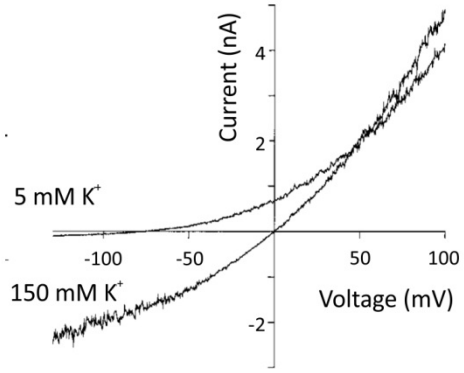

C) TASK (K_{2P}3.1)

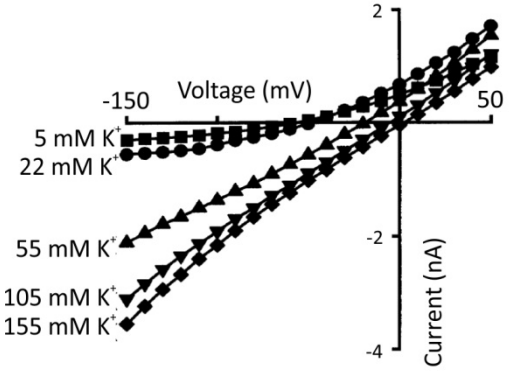

D) TALK (K_{2P}16.1)

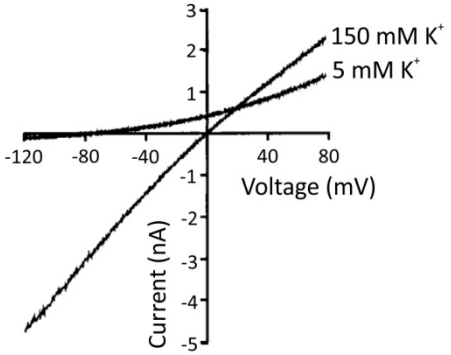

E) THIK (K_{2P}13.1)

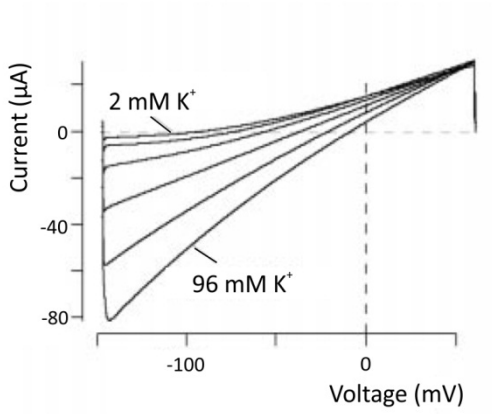

F) TRESK (K_{2P}18.1)

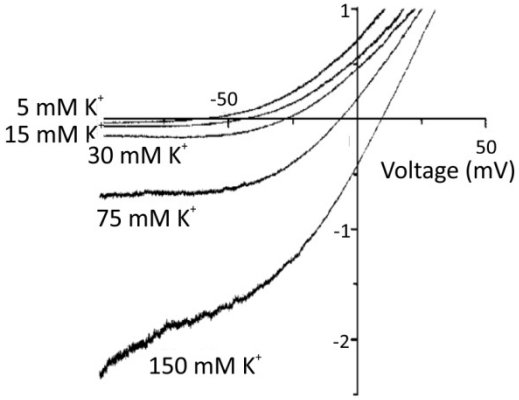

Figure 1.5: Representative *I-V* relationships for the K_{2P} channel subfamilies

Graphs represent example *I-V* relationships for K_{2P} channel members from the six subfamilies. The *I-V* relationships shown represent a variety of K^+ gradients from physiological (approximately 5 mM external) to symmetrical (approximately 150 mM external).
Figure adapted from Chavez et al. (1999), Duprat et al. (1997), Girard et al. (2001), Lesage et al. (2000), Rajan et al. (2001), and Sano et al. (2003).

A) TWIK channel subfamily: in near physiological K^+ gradients (14 mM external), $K_{2P}6.1$ expressing *Xenopus* oocytes show weak inward rectification (Chavez et al., 1999), and this is also observed in near symmetrical K^+ gradients (115 mM external). Oocytes were held at -80 mV and stepped between -120 to +40 mV, 1 s duration. For the functional properties of $K_{2P}1.1$ and $K_{2P}7.1$ channels see data presented in Lesage et al. (1996), Chatelain et al. (2012), and Salinas et al. (1999)

B) TREK channel subfamily: in physiological K^+ concentration (5 mM external) $K_{2P}10.1$ expressing COS-7 cells show outward rectification (Lesage et al., 2000), and continue to show slight outward rectification in symmetrical K^+ concentrations (150 mM external). Cells were held at -80 mV and stepped between -140 to +100 mV, 800 ms duration. For the functional properties of $K_{2P}2.1$ and $K_{2P}4.1$ channels see data presented in Patel et al. (1998), and Maingret et al. (1999a).

C) TASK channel subfamily: in physiological K^+ gradients (5mM external) $K_{2P}3.1$ expressing COS-7 cells show outward rectification (Duprat et al., 1997). In symmetrical K^+ gradients (155 mM external) the *I-V* relationship is linear, indicating open rectification. Cells were held at -80 mV and stepped between -150 to +50 mV, 500 ms duration. For the functional properties of $K_{2P}9.1$ and $K_{2P}15.1$ see data presented in Meadows and Randall (2001), and Ashmole et al. (2001).

D) TALK channel subfamily: in physiological K^+ gradients (5mM external) $K_{2P}16.1$ expressing COS-7 cells show outward rectification (Girard et al., 2001). In symmetrical K^+ gradients (155 mM external) the *I-V* relationship is linear, indicating open rectification. Cells were held at -80 mV and stepped between -130 to +80 mV, 800 ms duration. For the functional properties of $K_{2P}5.1$ and $K_{2P}17.1$ channels see data presented in Reyes et al. (1998), and Girard et al. (2001).

E) THIK channel subfamily: in near physiological K^+ gradients (2mM external) $K_{2P}13.1$ expressing *Xenopus* oocytes show outward rectification (Rajan et al., 2001). In high external K^+ gradients (96 mM external) the *I-V* relationship is near linear, with weak inward rectification at negative voltages (< -90 mV), indicating open rectification. Oocytes were held at -60 mV and voltage ramp applied between -160 to +40 mV, 105 mVs^{-1} duration. For the functional properties of $K_{2P}12.1$ see data presented in Rajan et al. (2001).

F) TRESK channel subfamily: in physiological K^+ gradients (5mM external) $K_{2P}18.1$ expressing L292 cells show outward rectification. In symmetrical K^+ concentrations (150 mM external) the *I-V* relationship continues to show slight outward rectification (Sano et al., 2003). Cells were held at -80 mV and stepped between -120 to +100 mV, 500 ms duration.

1.3.2 Overview of the TREK channel family

TREK channels (K_{2P}2.1, K_{2P}4.1, and K_{2P}10.1) are outward rectifiers in physiological K^+ gradients, and continue to show weak outward rectification in symmetrical K^+ gradients (Figure 1.5 B). TREK channels are activated by polyunsaturated fatty acids (PUFA: including arachidonic acid and lysophospholipids), intracellular pH, heat, and mechanical force via membrane stretch (Franks and Honoré, 2004; Heurteaux et al., 2004; Honore, 2007; Lesage et al., 2000; Maingret et al., 1999a; Maingret et al., 1999b; Maingret et al., 2000; Noël et al., 2011). In addition, K_{2P}2.1 and K_{2P}10.1 channel activity is increased by volatile anaesthetics (Heurteaux et al., 2004; Honore, 2007; Lesage et al., 2000). Physiologically TREK channels have been implicated in sensing the metabolic state of the cell, pain modulation, mediating the action of general anaesthetics, and neuroprotection (Alloui et al., 2006; Duprat et al., 2000; Franks and Honoré, 2004; Heurteaux et al., 2004; Honore, 2007; Lesage et al., 2000).

1.3.3 Overview of the TALK channel family

The *I-V* relationships of TALK channels (K_{2P}5.1, K_{2P}16.1, and K_{2P}17.1) show outward rectification in physiological K^+ gradients, whereas in symmetrical K^+ gradients the *I-V* relationship is linear showing open rectification (Figure 1.5 D). TALK channel activity is enhanced by changes in extracellular pH, for example the pK for K_{2P}5.1 is 8.0 (Girard et al., 2001; Niemeyer et al., 2007; Reyes et al., 1998). The pH sensitivity of K_{2P}5.1 channels is due to arginine 224, which is deprotonated under alkaline conditions and promotes channel opening (Niemeyer et al., 2007). In addition, TALK channel activity is potentiated by increased concentrations of intracellular nitric oxide and the application of volatile anaesthetics. In contrast, the channels are inhibited by local anaesthetics (Duprat et al., 2005; Girard et al., 2001; Niemeyer et al., 2007; Reyes et al., 1998). Based on their expression prolife and KO studies, TALK channel activity has been implicated in pancreatic function, cell volume regulation, and T lymphocyte proliferation (Barriere et al., 2003; Bittner et al., 2010; Bobak et al., 2011; Kirkegaard et al., 2010; L'Hoste et al., 2007a; Niemeyer et al., 2001).

1.3.4 Overview of the THIK channel family

Of the THIK channel subfamily (K_{2P}12.1 and K_{2P}3.1), only K_{2P}13.1 channels have been shown to be functional, with expression of rat or human K_{2P}12.1 channels in heterologous systems failing to pass recordable currents (Campanucci et al., 2005; Girard et al., 2001; Rajan et al., 2001). K_{2P}13.1 channels are outward rectifiers in physiological K^+ gradients, whereas in symmetrical K^+ gradients they show weak inward rectification, similar to members of the TWIK subfamily (Figure 1.5 E). K_{2P}13.1 channels are activated by PUFA, but inhibited by volatile anaesthetics and hypoxia (Campanucci et al., 2005; Rajan et al., 2001). As a result of their sensitivity to reduced oxygen (O_2) tensions, K_{2P}13.1 has been implicated in the cellular responses to hypoxia and brain ischemia (Campanucci et al., 2005), in addition to mediating the effects of volatile anaesthetics (Lazarenko et al., 2010).

1.3.5 Overview of the TRESK channel family

The TRESK channel subfamily has one member K_{2P}18.1, which in humans is localised to the spinal cord (Figure 1.5 F; Sano et al., 2003). TRESK channels are outward rectifiers, which are activated by Ca^{2+}-dependent phosphorylation and volatile anaesthetics, but inhibited by PUFA and intracellular acidification (Huang et al., 2008; Liu et al., 2004; Sano et al., 2003). TRESK channels are also thought to mediate the effects of volatile anaesthetics, as well as being linked to nociception and migraines (Lafreniere et al., 2010; Liu et al., 2004; Marsh et al., 2012).

1.4 Acid-sensitive K_{2P} channel family

This thesis is focused on the acid-sensitive K_{2P} (TASK: TWIK-related acid-sensitive K^+ channel) channel family. The TASK channel family has three members: K_{2P}3.1 (TASK-1), K_{2P}9.1 (TASK-3), and K_{2P}15.1 (TASK-5; Goldstein et al., 2005). K_{2P}3.1 was the first TASK channel cloned, based on sequence similarity to the previously isolated K_{2P}1.1 and K_{2P}2.1 channels (Duprat et al., 1997). K_{2P}3.1 channels have the predicted characteristics of an ideal background K^+ current, when expressed in *Xenopus* oocytes (Duprat et al., 1997). The currents are almost instantaneous with activation kinetics of < 10 ms and no current inactivation throughout the voltage pulse duration (Figure 1.6 A; Duprat et al., 1997). K_{2P}3.1

channels are open rectifiers, with the direction of the current carried by the channel depending on external K^+ concentration (Figure 1.5 C). Additionally, the experimental *I-V* relationship for $K_{2P}3.1$ has a close correlation to the ideal *I-V* relationship for a leak K^+ channel, as predicted by the GHK flux equation (Figure 1.6 B; Duprat et al., 1997). Injection of $K_{2P}3.1$ cRNA into oocytes, and expression of $K_{2P}3.1$ channels, shifts the RMP towards E_K, from -44 mV in uninjected oocytes to -85 mV in $K_{2P}3.1$ expressing oocytes (Duprat et al., 1997). $K_{2P}3.1$ currents are sensitive to changes in extracellular pH, with over 90 % inhibition observed at pH 6.5 with a pK of 7.3 (Figure 1.6 B; Bayliss et al., 2003; Duprat et al., 1997).

The second member of the TASK family, $K_{2P}9.1$, was isolated from rat (Kim et al., 2000), guinea pig (Rajan et al., 2000), and human tissues (Chapman et al., 2000; Rajan et al., 2000). Human $K_{2P}9.1$ has 62 % amino acid identity to $K_{2P}3.1$ channels (Chapman et al., 2000). Like $K_{2P}3.1$ channels, $K_{2P}9.1$ shows open rectification. Under low external K^+ concentrations, which resemble physiological K^+ gradients, $K_{2P}9.1$ channels conduct outward currents with the characteristics of an ideal background K^+ current with activation kinetics of less than 4 ms and non-inactivating currents (Figure 1.6 A; Chapman et al., 2000; Kim et al., 2000; Rajan et al., 2000). In addition, expression of $K_{2P}9.1$ cRNA in *Xenopus* oocytes shifts the RMP towards E_K (-79 mV in $K_{2P}9.1$ injected versus -34 mV in non-injected, Figure 1.6 C; Chapman et al., 2000). The activity of $K_{2P}9.1$ is also modulated by extracellular pH, although the channel is less sensitive than $K_{2P}3.1$, with a pK of 6.4 for human $K_{2P}9.1$ and 90 % channel inhibition observed at pH 5.0 (Figure 1.6 C; Chapman et al., 2000; Meadows and Randall, 2001).

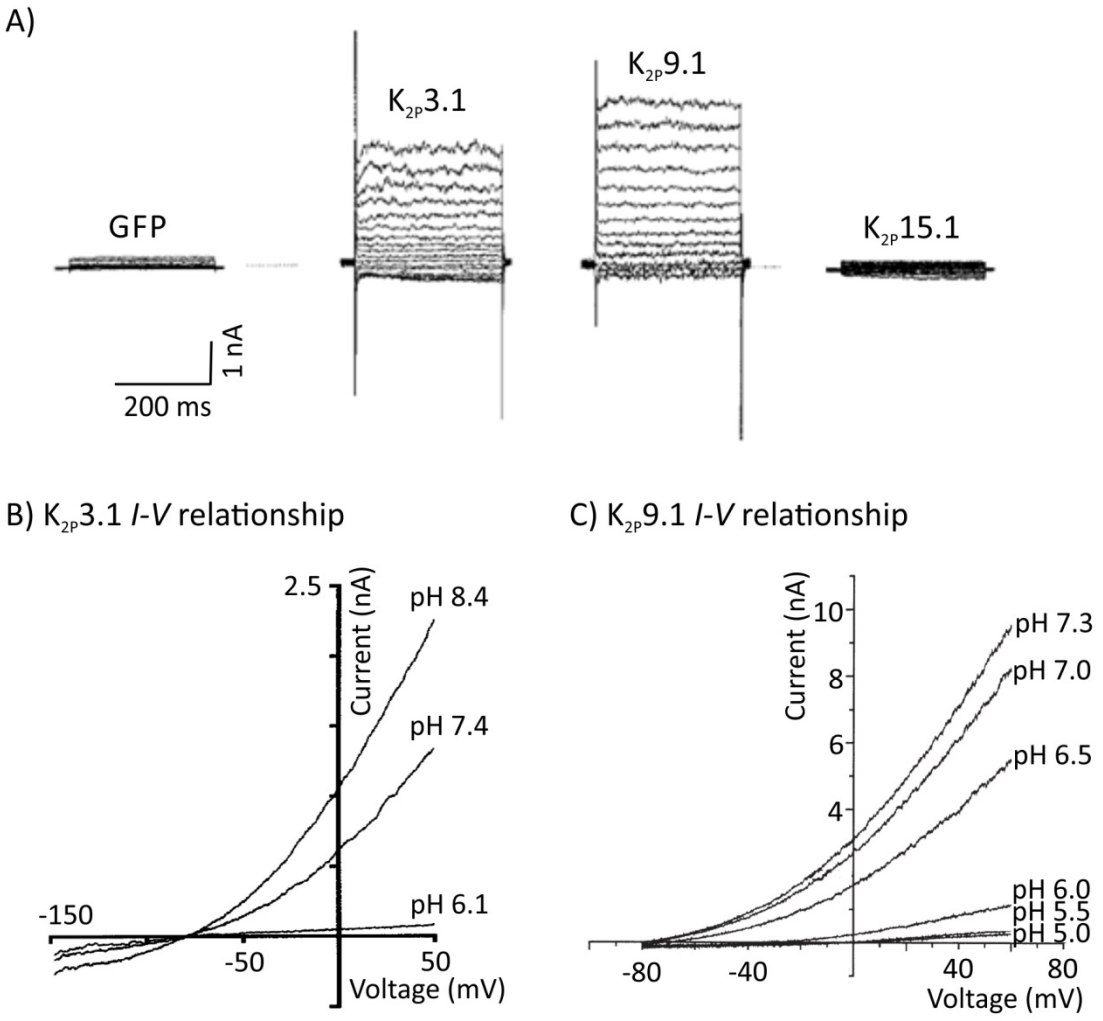

Figure 1.6: Whole-cell acid-sensitive K_{2P} channel recordings

A) Representative whole-cell current families from COS-7 cells expressing GFP alone or co-transfected with GFP and K_{2P}3.1, K_{2P}9.1, or K_{2P}15.1 channels. Both K_{2P}3.1 and K_{2P}9.1 channels produce instantaneous currents, while K_{2P}15.1 transfected cells showed currents comparable to GFP expression.
Cells were held at -80 mV and stepped between -120 to +60 mV, 400 ms duration.

B) *I-V* relationship of K_{2P}3.1 expressing COS-7 cells at physiological pH, pH 7.4. When the extracellular pH is increased to pH 8.4, K_{2P}3.1 currents are amplified. K_{2P}3.1 channels are inhibited when the extracellular pH is lowered to pH 6.1, shown by a current reduction and positive shift in reversal potential.
Cells were held at -80 mV and stepped between -150 to +50 mV, 500 ms duration.

C) *I-V* relationship of K_{2P}9.1 expressing HEK293 cells at physiological pH, pH 7.3. When the external pH is reduced (pH 5.5-7.0) K_{2P}9.1 currents are inhibited, shown by a reduction in outward currents and positive shift in reversal potential.
Cells were held at -80 mV and stepped between -80 to +80 mV, 200 ms duration.

Figure adapted from Kim and Gnatenco (2001), Duprat et al. (1997), and Meadows and Randall (2001).

K_{2P}15.1 is the third and final member of the TASK channel family. Human K_{2P}15.1 was cloned in 2001 from brain tissue and grouped into the TASK family based on sequence homology to K_{2P}3.1 and K_{2P}9.1 (55 % amino acid identity to K_{2P}3.1 and 58 % to K_{2P}9.1; Ashmole et al., 2001; Kim and Gnatenco, 2001). K_{2P}15.1 mRNA expression has been identified in many human tissues (Appendix 1), however when K_{2P}15.1 is expressed in heterologous expression systems (*Xenopus* oocytes or COS-7 cells) no background K^+ currents are elicited (Figure 1.6 A; Ashmole et al., 2001; Karschin et al., 2001; Kim and Gnatenco, 2001). K_{2P}15.1 channels possess a classical pore domain sequence (GYG) and it is assumed that the channel can pass K^+ ions, however a single nucleotide polymorphism in the first pore domain (EYG) has been identified in channels cloned from some human tissues (Kim and Gnatenco, 2001). Furthermore, altering the N- or C-termini of K_{2P}15.1, by replacing the protein sequences with sections of K_{2P}3.1 or K_{2P}9.1, fails to alter the functionality of the channel (Ashmole et al., 2001; Kim and Gnatenco, 2001). From these data it has been concluded that K_{2P}15.1 is non-functional, due to problems with the subcellular localisation and trafficking of the channel (Ashmole et al., 2001; Kim and Gnatenco, 2001).

TASK channels can form heterodimers, in addition to homodimers, with rat K_{2P}3.1 and K_{2P}9.1 subunits being shown to dimerise and create functional channels in heterologous and native expression systems (Czirjak and Enyedi, 2002a; Kim et al., 2009). The functional impacts of channel heterodimers have not been fully characterised, however K_{2P} channel heterodimers are known to result in channels with different conductance and modulatory properties, which may contribute to the physiological roles of these channels (Czirjak and Enyedi, 2002a; Kim et al., 2009; Plant et al., 2012b). For example, TASK channel heterodimers have an intermediate pH sensitivity compared to homodimeric channels, with a pK of 6.4, compared to pH 6.0 for rat K_{2P}9.1 homodimers and pH 6.8 for rat K_{2P}3.1 homodimers (Czirjak and Enyedi, 2002a). In rat carotid body glomus cells, K_{2P}3.1/K_{2P}9.1 heterodimers form the major O_2-sensitive background K^+ channel conductance, compared to channel homodimers (Kim et al., 2009). Additionally, formation of heterodimers between K_{2P}1.1 (TWIK channel) and TASK channels (K_{2P}3.1 and K_{2P}9.1) have been described in rat cerebellar granule neurons (rCGN; Plant et al., 2012b). Heterodimeric TASK and K_{2P}1.1 channels are silenced by SUMOylation, this is an additional modulation which is not present in TASK channel homo- or heterodimers, although the physiological implications of TASK/K_{2P}1.1 heterodimer SUMOylation in rCGN have not been characterised

(Plant et al., 2012b). Heterodimers are not formed between all K_{2P} channel members. Co-injection of human $K_{2P}3.1$ and $K_{2P}15.1$ cDNA into oocytes results in currents that are comparable to $K_{2P}3.1$ expression alone, suggesting that these channels do not form heterodimers and that $K_{2P}3.1$ channels do not rescue $K_{2P}15.1$ functionality (Ashmole et al., 2001).

1.4.1 Physiological roles of TASK channels

TASK channels are expressed in a wide range of cell types (Appendix 1). Both $K_{2P}3.1$ and $K_{2P}9.1$ are widely expressed across the CNS (Bayliss et al., 2003; Callahan et al., 2004; Karschin et al., 2001; Maingret et al., 2001; Talley et al., 2001). $K_{2P}3.1$ is highly expressed in cerebellar granule neurons (CGN), somatic motorneurons, ventrolateral medulla, and locus coeruleus (Bayliss et al., 2003; Karschin et al., 2001; Talley et al., 2001; Washburn et al., 2003). $K_{2P}9.1$ has a broader expression pattern, with high levels detected in raphe, hypothalamic, and tuberomammillary nuclei, in addition to CGN, somatic motorneurons, ventrolateral medulla, and locus coeruleus neurons (Bayliss et al., 2003; Callahan et al., 2004; Karschin et al., 2001; Marinc et al., 2011; Marinc et al., 2012; Talley et al., 2001; Washburn et al., 2003; Washburn et al., 2002). TASK channel activity is essential in regulating the RMP and cellular excitability of these neurons (Bayliss et al., 2003; Maingret et al., 2001). Furthermore, inhibition of TASK channels (by neurotransmitters, pH, or O_2) may trigger neuronal depolarisation and this can result in action potential generation via the activity of other classes of ion channels, such as voltage-gated Na^+ (Na_v) channels (Bayliss et al., 2003; Marinc et al., 2011; Williams et al., 2007b). The specific ion channels which may be activated following TASK channel inhibition will depend on the cell type in question, and, to date, these channels have not been characterised.

$K_{2P}3.1$ and $K_{2P}9.1$ are not exclusively expressed within the CNS and these channels are expressed in a wide range of peripheral tissues. The modulation of TASK channels by physiological stimuli (such as pH and O_2; see Section 1.4.2) means that these channels are expressed in a range of chemo- and nutrient-sensing cells, with roles for $K_{2P}3.1$ and $K_{2P}9.1$ channel activity being identified in the carotid body, adrenal glomerulus, and lung neuroepithelial body (NEB) cells (Czirjak et al., 2000; Duprat et al., 2007; Enyedi and Czirják, 2010; Kim et al., 2009; O'Kelly et al., 1998; Washburn et al., 2003).

Carotid body glomus cells are responsible for sensing reductions in O_2 tension and pH (Duprat et al., 2007). These conditions will induce cell depolarisation, Ca^{2+} entry, and neurotransmitter release (Duprat et al., 2007). TASK channels are thought to be involved in the depolarising response of these cells to environmental changes, since $K_{2P}3.1/K_{2P}9.1$ heterodimers are expressed in murine glomus cells, where they form the major outward background K^+ conductance and are inhibited by hypoxia and acidification (Buckler et al., 2000; Kim et al., 2009; Turner and Buckler, 2013).

NEB cells are responsible for O_2 sensing within the lung (Cutz and Jackson, 1999; O'Kelly et al., 1998). Neurotransmitter release from NEB cells is triggered by membrane depolarisation and intracellular Ca^{2+} signalling, which results from closure of O_2-sensitive KCh (Brazier et al., 2005; Cutz and Jackson, 1999). mRNA expression for both $K_{2P}3.1$ and $K_{2P}9.1$ channels has been detected in a model for NEB cells (H146 lung carcinoma cell line), with $K_{2P}9.1$ channels forming the major O_2-sensitive background K^+ current (Hartness et al., 2001; O'Kelly et al., 1998; O'Kelly et al., 1999).

Both $K_{2P}3.1$ and $K_{2P}9.1$ show high expression in adrenal glomerulosa cells, with $K_{2P}9.1$ channels contributing the dominant background outward K^+ current (Brenner and O'Shaughnessy, 2008; Czirjak and Enyedi, 2002b; Czirjak et al., 2000). Inhibition of TASK channels, by acidification and angiotensin II, results in aldosterone secretion by causing cell depolarisation and increased Ca^{2+} signalling (Brenner and O'Shaughnessy, 2008; Czirjak and Enyedi, 2002b; Czirjak et al., 2000).

1.4.2 TASK channel modulation

The expression and activity of TASK channels is modulated by a wide range of physiological and pharmacological stimuli, including trafficking signals, changes in the extracellular concentration of protons (pH), O_2, and neurotransmitters, as well as exposure to volatile anaesthetics and certain classic ion channel inhibitors (Figure 1.7). The impacts of these signalling molecules and pharmacological tools on TASK channel function are discussed in detail below.

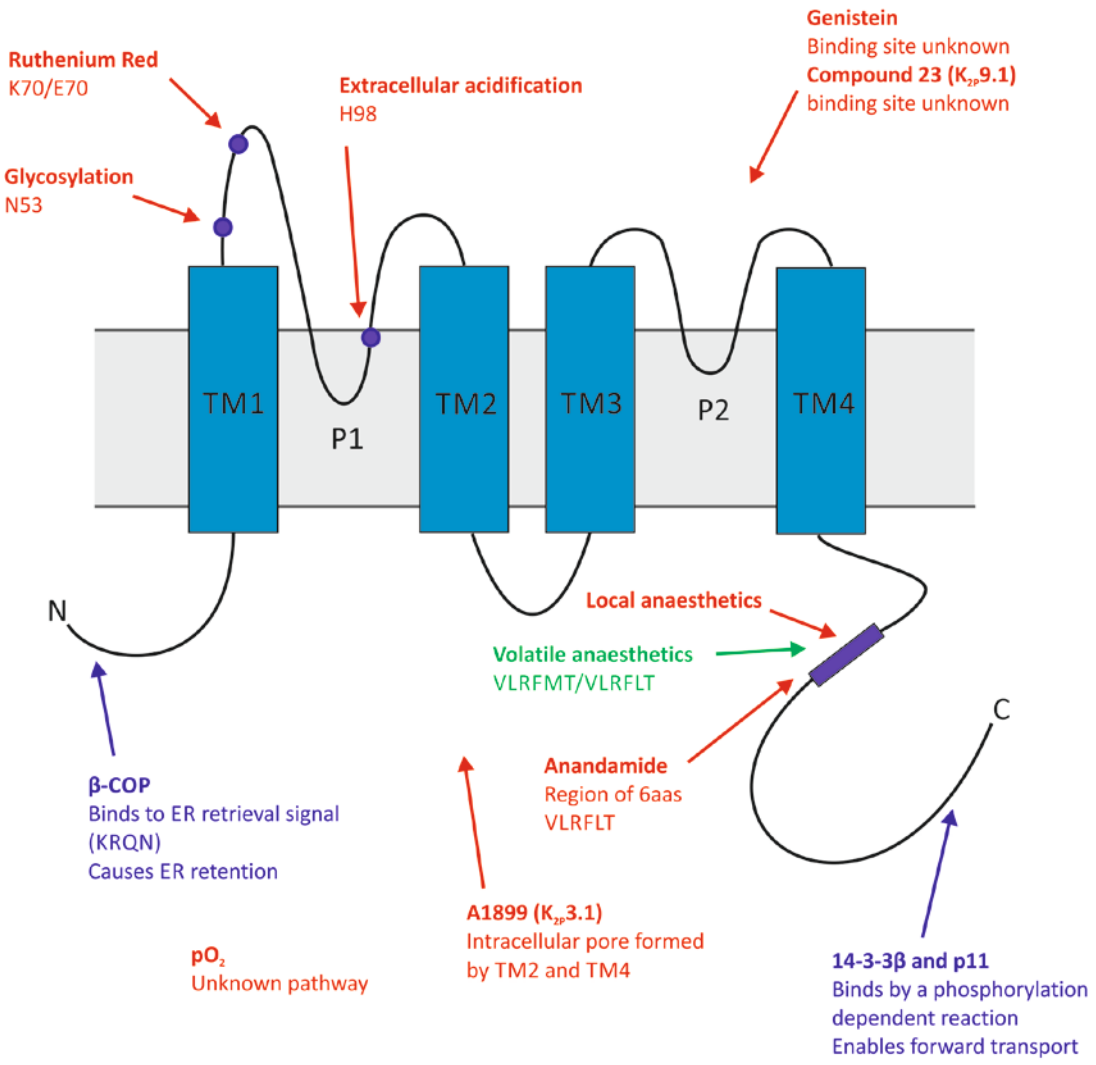

Figure 1.7: Physiological and pharmacological regulators of TASK channels

Summarising the modulatory sites of TASK channels, key residues are highlighted in blue and red indicates an inhibitory stimuli, whereas green indicates an excitatory stimuli.

Coburn et al., (2012), Czirják and Enyedi, (2003), Enyedi and Czirják, (2010), Gierten et al., (2008), Hartness et al., (2001), Kim et al., (2000), Lesage and Lazdunski, (2000), Meadows and Randall, (2001), O'Kelly et al., (2002), Streit et al., (2011), Talley and Bayliss, (2002), Veale et al., (2007a), and Yuill et al., (2007).

1.4.2.1 Trafficking

The expression of K_{2P} channels on the plasma membrane is tightly regulated by protein trafficking. The export of newly synthesised $K_{2P}3.1$ and $K_{2P}9.1$ channels from the ER through the forward transport pathway to the plasma membrane is closely regulated. TASK channels can only move forward in the secretary pathway to the cell surface, when the regulatory proteins, 14-3-3β and p11, bind to the C-terminal residues (MKRRSSV in $K_{2P}3.1$ and MKRRSV in $K_{2P}9.1$) in a protein kinase A (PKA)-dependent interaction (Figure 1.7; Mant et al., 2011; O'Kelly et al., 2002; O'Kelly and Goldstein, 2008; Rajan et al., 2002). Otherwise the channels are retained in the ER by binding of β-coatomer protein (β-COP) to a dibasic ER retrieval signal (KRQN) located on the N-terminus (Figure 1.7; O'Kelly et al., 2002; O'Kelly and Goldstein, 2008).

In addition to regulating the forward transport of TASK channels, the number of channels on the cell surface is controlled by protein retrieval. TASK channels have been shown to undergo dynamin-dependent endocytosis, which includes both clathrin-mediated endocytosis and caveolin-dependent endocytosis (Mant et al., 2013a). Clathrin-dependent endocytosis of $K_{2P}3.1$ is induced by nerve growth factor (NGF) in a rat adrenal medulla cell line (PC12; Matsuoka et al., 2013). Mutation of a dileucine motif (L263/L264) in the C-terminus of $K_{2P}3.1$ prevents channel endocytosis, induced by NGF, and may regulate clathrin-mediated retrieval (Matsuoka et al., 2013)

1.4.2.2 pH

Both $K_{2P}3.1$ and $K_{2P}9.1$ channels are inhibited by a decrease in extracellular pH, the pK for the modulation of human isoforms by extracellular acidification is pH 7.4 for $K_{2P}3.1$ and pH 6.4 for $K_{2P}9.1$ (Chapman et al., 2000; Duprat et al., 1997). The pH sensitivity of TASK channels is conferred by a conserved histidine residue at position 98 (H98), which is located in the first extracellular loop directly after the first pore domain (GYGH; Figure 1.7). If H98 is mutated to an asparate or glutamate, the pH sensitivity of TASK channels is lost (Lopes et al., 2000; Rajan et al., 2000). Protonation of H98 is proposed to inhibit TASK channels by causing closure of the channel pore by C-type gating (Mathie et al., 2010; Yuill et al., 2007). Protein modelling suggests that a water molecule stabilises the intramolecular interations

between H98 and theronine 89, keeping the pore open at neutral or alkaline pH (Stansfeld et al., 2008). When H98 is protonated, this water molecule is displaced and results in a closure of the channel pore (Stansfeld et al., 2008).

1.4.2.3 Oxygen

TASK channels are inhibited by acute hypoxia, with inhibition of human $K_{2P}3.1$ currents in stable transfected HEK293 cells, H146 cells, and rCGN being observed (Hartness et al., 2001; Lewis et al., 2001; O'Kelly et al., 1998; O'Kelly et al., 1999; Plant et al., 2002). However, in adrenal medulla cells TASK channel currents are not inhibited by acute hypoxia and this suggests that there is a system-specific response (Johnson et al., 2004). This is rationalised by the proposal that the modulation is likely to be independent of the channel and involve accessory proteins (Kemp et al., 2002; Lee et al., 2006; Wyatt et al., 2007). Several candidate proteins have been suggested to play this role, with the plasma membrane O_2-sensitive enzyme NOX4 (NADPH oxidase 4) being the most likely candidate identified to date (Buttigieg et al., 2012; Lee et al., 2006). When NOX4 is co-expressed with $K_{2P}3.1$ in HEK293 cells the inhibition of the channel in response to hypoxia is increased (Lee et al., 2006). In addition, knockdown of native NOX4 expression in HEK293 cells decreases the inhibition of heterologously expressed $K_{2P}3.1$ channels by acute hypoxia (Lee et al., 2006), and in H146 cells native NOX4 and $K_{2P}3.1$ protein is colocalised (Buttigieg et al., 2012). However, NOX enzymes do not fully account for the inhibition of O_2-sensitive K^+ currents in H146 cells; it has been suggested that multiple systems are present in native cells to mediate the effects of acute hypoxia (Johnson et al., 2004; O'Kelly et al., 2001).

AMPK (AMP-activated protein kinase) was described as an alternative candidate, with increased AMPK activity causing reduced whole-cell K^+ currents in rat carotid body glomus cells (Wyatt et al., 2007). However, when $K_{2P}3.1$, $K_{2P}9.1$, or $K_{2P}3.1/K_{2P}9.1$ channels were expressed in HEK293 cells, AMPK activity did not inhibit channel activity, although AMPK does modulate $K_{2P}2.1$ channels (Kréneisz et al., 2009). This suggests that AMPK does not directly modulate TASK channel activity, but may be involved in the hypoxia response of carotid body glomus cells, via the modulation of $K_{2P}2.1$ channels (Kréneisz et al., 2009; Wyatt et al., 2007).

The activity of $K_{2P}3.1$, $K_{2P}9.1$, and $K_{2P}3.1/K_{2P}9.1$ channels are increased by intracellular reactive oxygen species (ROS: application of H_2O_2 > 16 mM) in both heterologously (HeLa cells) and native expressing cells (rat carotid body glomus, rat adrenal cortical, and rCGN; Papreck et al., 2012). ROS are hypothesised to act on the C-termini of TASK channels, since when the C-terminus of $K_{2P}9.1$ is replaced with the same region from the ROS-insensitive channel, $K_{2P}10.1$, the modulation is lost (Papreck et al., 2012).

1.4.2.4 Neurotransmitters

TASK activity can be inhibited by neurotransmitters which activate $G\alpha_{q/11}$ protein coupled receptors, in both heterologous and native expressing cells (Czirjak and Enyedi, 2002b; Czirjak et al., 2000; Millar et al., 2000; Talley and Bayliss, 2002; Talley et al., 2000)., Activation of muscarinic M_3 receptors inhibits background outward K^+ currents in rCGN (Millar et al., 2000). In the same study, in *Xenpous* oocytes, application of muscarine was shown to inhibit $K_{2P}3.1$ channels. In motorneurons, the TASK-like background currents are inhibited by a range of neurotransmitters: serotonin, noradrenaline, substrate P, tryrotopin releasing horomone, and glutmate receptor agonists (Talley et al., 2000). Angiotensin II activates $G\alpha_{q/11}$ coupled receptors (AT_I receptor) in adrenal glomerulosa cells, which inhibits $K_{2P}3.1$ and $K_{2P}9.1$ channel activity, triggering a rise in intracellular Ca^{2+} (Czirjak and Enyedi, 2002b; Czirjak et al., 2000; Nogueira et al., 2010).

A region of six amino acids located at the interface of the fourth transmembrane domain and C-terminal tail (VLMFT in $K_{2P}3.1$ and VLRFLT in $K_{2P}9.1$) is essential for the channel modulation by neurotransmitters (Figure 1.7; Conway and Cotten, 2012; Talley and Bayliss, 2002). Replacement of these amino acids with the same region from $K_{2P}2.1$ channels causes loss of channel regulation by these modulators (Talley and Bayliss, 2002). The inhibition of TASK channels is caused by direct interaction of $G\alpha_{q/11}$ proteins to this motif and not by activation of kinase dependent pathways, although PKC activation can also inhibit TASK channels (Veale et al., 2007b).

1.4.2.5 Anaesthetics

K_{2P}3.1 and K_{2P}9.1 activity is increased by halogenated volatile anaesthetics, such as halothane and isoflurane, which act on the same motif as neurotransmitters (Figure 1.7 and Table 1.2; Conway and Cotten, 2012; Meadows and Randall, 2001; Patel et al., 1999; Talley and Bayliss, 2002). In contrast, local anaesthetics such as bupivacaine and lidocaine inhibit TASK channels (Table 1.2), although the mechanism of this inhibition is unknown (Du et al., 2011; Lesage and Lazdunski, 2000; Meadows and Randall, 2001). In K_{2P}2.1, lidocaine has been shown to reduce the open probability of the channel by a mechanism that is proposed to involve an interaction between the drug and phosphorylated serine resiudes in the C-terminal tail (Nayak et al., 2009).

1.4.2.6 Inhibitors

K_{2P}3.1 and K_{2P}9.1 channels are not inhibited by classical KCh blockers (Table 1.2) and, at this time, there is a lack of selective pharmacological agents that inhibit or augment the activity of specific K_{2P} channels. However, a number of semi-selective inhibitors of TASK channels have been identified: anandamide, ruthenium red, zinc, and genistein (Czirják and Enyedi, 2003; Gierten et al., 2008; Maingret et al., 2001; Veale et al., 2007a). Additionally, two targeted inhibitors have been designed for K_{2P}3.1 (A1899; Streit *et al.*, 2011) and K_{2P}9.1 (Compound 23; Coburn et al., 2012), although these were not commercially available for use in this thesis. The pharmacological profile of K_{2P}3.1 and K_{2P}9.1 channels is summarised in Table 1.2.

K_{2P}3.1 and K_{2P}9.1 are both sensitive to inhibition by the competitive tyrosine kinase (TK) inhibitor genistein (Gierten et al., 2008). K_{2P}3.1 is more sensitive to genistein than K_{2P}9.1, with an IC_{50} of 10 µM in *Xenopus* oocytes, although application of 100 µM genistein to K_{2P}9.1 expressing oocytes also causes a 60 % reduction in the magnitude of the current (Gierten et al., 2008). The precise mechanism for K_{2P}3.1 channel inhibition is unknown, with evidence suggesting that the effect of genistein is caused by blocking the channel pore and by modulating TK activity (Gierten et al., 2008). In support of genistein directly blocking K_{2P}3.1 channels, mutation of a putative TK phosphorylation site (Y323) or inhibition of tyrosine phosphatases failed to reduce channel inhibition (Gierten et al., 2008). In addition,

the rapid onset of inhibition following genistein application (< 1 min) suggests that a direct block is occurring from the extracellular side (Gierten et al., 2008). However, in support of TK modulation resulting in the inhibitory effects observed, a structural analogue of genistein which does not exert TK inhibitory effects (genistin) fails to reduce $K_{2P}3.1$ activity (Gierten et al., 2008). Of note, genistein is not selective for TASK channels and has numerous other cellular targets, including multiple protein kinases and DNA topoisomerase II (Akiyama et al., 1987; Akiyama and Ogawara, 1991; Peterson, 1995; Yan et al., 2010). Protein kinases which are inhibited by genistein include epidermal growth factor receptors (EGFR and HER2), mitogen-activated protein kinases (MAPK) 1/3, phosphatidylinositol 4,5-bisphosphate 3-kinase (PI3K), and Akt (protein kinase B). See Yan et al. (2010) for a comprehensive list of proteins targeted by genistein.

Anandamide is an endogenous cannabinoid neurotransmitter, that binds and activates cannabinoid receptors 1 and 2 (CB1 and CB2; Blankman and Cravatt, 2013). Anandamide has been found to inhibit both $K_{2P}3.1$ and $K_{2P}9.1$ channel activity (Veale et al., 2007a); whole-cell currents recorded from transformed tsA-201 variant of HEK293 cells expressing either channel are reduced by over 60 % following application of 3 μM methanandamide (a non-hydrolysable analogue of anandamide; Enyedi and Czirják, 2010; Maingret et al., 2001; Veale et al., 2007a). Anandamide acts on the same region of TASK channels as neurotransmitters and volatile anaesthetics, with deletion of this motif abolishing channel inhibition (Figure 1.7; Veale et al., 2007a). Anandamide also inhibits $K_V1.2$ channels with an IC_{50} of 2.7 μM (Poling et al., 1996).

Table 1.2: Pharmacological profile of $K_{2P}3.1$ and $K_{2P}9.1$ channels

The pharmacological modulation of $K_{2P}3.1$ and $K_{2P}9.1$ channels by classical K^+ channel inhibitors (4-AP, TEA, Cs^+, and Ba^{2+}), TASK channel inhibitors (A1899, anandamide, compound 23, genistein, ruthenium red, and zinc), and anaesthetics (volatile and local). Where characterised the IC_{50} values are given for each compound.
↓ indicates an inhibition and ↑ activation.

Buckler *et al.*, (2000), Clarke *et al.*, (2004), Coburn *et al.*, (2012), Conway and Cotten, (2012), Czirják and Enyedi, (2003), Du *et al.*, (2011), Duprat *et al.*, (1997), Gierten *et al.*, (2008), Kim *et al.*, (2000), Lesage, (2003), Maingret *et al.*, (2001), Meadows and Randall, (2001), Patel *et al.*, (1999), Rajan *et al.*, (2000), Streit *et al.*, (2011), and Veale *et al.*, (2007a).

Modulation	**Compound**	**Channel**	
		$K_{2P}3.1$	**$K_{2P}9.1$**
Classical K^+ channel inhibitors	4-AP	Not inhibited	Not inhibited
	TEA	Not inhibited	Not inhibited
	Cs^+	Not inhibited	Not inhibited
	Ba^{2+}	↓ insensitive to low concentrations (100 µM) but inhibited by > 10 mM	↓5 mM
TASK channel inhibitors	A1899	↓ 35 nM	↓ 320 nM
	Anandamide	↓ 700 nM	↓ IC_{50} not defined 80 % inhibition at 3 µM
	Compound 23	↓ 302 nM	↓ 35 nM
	Genistein	↓ 12.3 µM	↓ IC_{50} not defined 60 % inhibition at 100 µM
	Ruthenium red	Not inhibited	↓ 0.7 µM
	Zinc	Not inhibited	↓ 20 µM
Volatile anaesthetics	Halothane	↑ 0.3 mM	↑ IC_{50} not defined 134 % activation at 0.3 mM
	Isoflurane	↑ IC_{50} not defined 20 % activation at 2 mM	↑ IC_{50} not defined 25 % activation at 2.3 mM
Local anaesthetics	Bupivacaine	↓ 12.1 µM	↓ 27.6 µM
	Lidocaine	↓ 53.8 µM	↓ 86.5 µM

Out of the three functional TASK channels which have been currently been identified, ruthenium red is a selective inhibitor of homodimeric $K_{2P}9.1$ channels (IC_{50} = 0.7 μM) and does not alter the activity of $K_{2P}3.1$ homodimers or $K_{2P}3.1/K_{2P}9.1$ heterodimers (Czirjak and Enyedi, 2002a). The sensitivity of $K_{2P}9.1$ to ruthenium red is due to glutamate 70 (E70), which is located in the first extracellular loop, the corresponding residue in $K_{2P}3.1$ is a lysine (K70, Figure 1.7; Czirják and Enyedi, 2003). The ruthenium red sensitivity of $K_{2P}9.1$ requires two glutamate residues, since mutation of E70 in one subunit of $K_{2P}9.1$ homodimers (or in heterodimers) will cause a loss of channel inhibition (Czirják and Enyedi, 2003). Although ruthenium red is useful to discriminant the activity of $K_{2P}9.1$ homodimers from other TASK channels, this agent has a wide range of cellular targets that limit its utility as a specific blocker of $K_{2P}9.1$ homodimers in complex physiological systems such as native cells. Other targets for ruthenium red are reported to include Ca^{2+} binding proteins (Charuk et al., 1990) and Ca_V channels (mainly N- and P/Q-type; Tapia and Velasco, 1997). For N-type and P/Q-type Ca_V channels, ruthenium red inhibition has an IC_{50} of 0.7 μM (Cibulsky and Sather, 1999). As well as modulating Ca^{2+} channels, ruthenium red slows the inactivation of voltage-gated sodium channels (Stimers and Byerly, 1982), inhibits capsaicin sensitive non-selective cation channels (Dray et al., 1990), and inhibits $K_{Ca}1.1$ channel currents (Wu et al., 1999).

Zinc is also a more selective inhibitor of $K_{2P}9.1$ channels compared to $K_{2P}3.1$, with an IC_{50} of 20 μM for $K_{2P}9.1$ (Clarke et al., 2004). Both the H98 and E70 residues appear to be critical for this inhibition of $K_{2P}9.1$ channels, since mutation of both residues will reduce the zinc sensitivity of the channel (Clarke et al., 2004; Clarke et al., 2008). In addition, mutation of K70 in $K_{2P}3.1$ channels to a glutamate (K70E) increases the sensitivity of $K_{2P}3.1$ to zinc (Clarke et al., 2004).

A more selective blocker of $K_{2P}3.1$ channels, A1899, has recently been described by Streit et al. (2011). A1899 has an IC_{50} of 35 nM for $K_{2P}3.1$ channels expressed in *Xenopus* oocytes, compared to an IC_{50} of 320 nM for $K_{2P}9.1$ and 2.7 μM for $K_V1.1$ (Streit et al., 2011). Mutagenesis studies and patch clamp recordings show that A1899 is an open channel blocker, which binds between the second and fourth transmembrane helices of $K_{2P}3.1$ channels, in addition to interacting with the same motif as neurotransmitters, anaesthetics, and anandamide (Figure 1.7; Streit et al., 2011). High throughput screening and modification of a scaffold structure identified a selective $K_{2P}9.1$ inhibitor, named compound

23 (Coburn et al., 2012). Compound 23 has an IC_{50} of 35 nM for $K_{2P}9.1$ in transfected HEK293 cells, compared to 303 nM for $K_{2P}3.1$ (Coburn et al., 2012). To date, the binding location of Compound 23 to $K_{2P}9.1$ channels, and any additional cellular targets of the inhibitor have not been investigated (Coburn et al., 2012). Neither A1899, nor compound 23 were available for use in this thesis; therefore three other published TASK channel inhibitors were selected: methanandamide (the non-hydrolysable analogue of anandamide), genistein, and ruthenium red. These three compounds were chosen for use in this thesis despite their selectivity limitations. This meant that these inhibitors may target other proteins that could have roles in cancer cell biology, most notably cannabinoid receptors, tyrosine kinases, and calcium binding proteins, for methanandamide, genistein, and ruthenium red, respectively.

1.5 Cancer

Cancer is a major cause of death worldwide. In 2008 the World Health Organisation published a report stating that death from cancer is the third leading cause of mortality (Jemal et al., 2011). In the UK it is predicted that one in three people will develop cancer in their lifetime, with one in four men and one in five women estimated to die from the disease (Knowles and Selby, 2005).

The development of cancer, carcinogenesis, has shared characteristics with evolution, whereby there is a continuous selection pressure for cells that have a survival or proliferative advantage (Hanahan and Weinberg, 2000; Polyak et al., 2009). During carcinogenesis, a number of mutations can be accumulated to allow the progression from a normal cell into a neoplastic one; as a result of this many cancers (such as breast, colon, and prostate) have an age-dependent occurrence (King and Robins, 2006; Knowles and Selby, 2005; Weinberg, 2006). This is supported by the evidence that transforming cells, *in vitro*, from a normal phenotype into a carcinogenic one requires several transformation steps (Hahn et al., 1999; Hanahan and Weinberg, 2000; Land et al., 1983). For example, human embryonic HEK293 cells require two introduced genetic changes (cooperating oncogenes: human H-*Ras* and *c-Myc*), alongside the expression of telomerase to achieve tumorigenic competence (Hahn et al., 1999; Land et al., 1983).

It is widely accepted that the changes which occur during carcinogenesis can be linked to eight changes in normal cell physiology, known as the hallmarks of cancer (Figure 1.8): uncontrolled proliferation (due to self-sufficiency in growth factor (GF) signalling or insensitivity to anti-proliferative signalling), evasion of apoptosis, limitless replication, sustained angiogenesis, promotion of tissue invasion and metastasis, altered energy metabolism, and evasion of destruction by the immune system (Hanahan and Weinberg, 2011). It has been suggested that these cancer hallmarks can be acquired by tumour cells due to two enabling characteristics, genomic instability and promotion of tumour progression by the immune system (Hanahan and Weinberg, 2011). In general, cancer hallmarks are acquired by the accumulation of alterations in cell signalling pathways and some of the key signalling pathways are highlighted in Figure 1.9 (Bianco et al., 2006; Hanahan and Weinberg, 2011; King and Robins, 2006). Interplay exists between the components of cell signalling pathways, under both normal and cancerous conditions; a consequence of this is that a single abnormality can influence multiple effector proteins and cancer hallmarks (Bianco et al., 2006; Hanahan and Weinberg, 2011; Shaw and Cantley, 2006). Additionally, the accumulation of cancer hallmark functions (such as tumour growth, altered metabolism, and metastasis) can be promoted by the interactions between cancer cells and their surrounding environment (Chiche et al., 2010; Li and Li, 2012; Mucaj et al., 2012). Each of these areas of cancer research is explored in further detail in the following paragraphs:

1.5.1 The hallmarks of cancer

1.5.1.1 Enabling characteristic 1: Genomic instability

Genomic instability within cancer cells promotes the accumulation of genetic alterations, and this can be enhanced by the loss of DNA maintenance pathways (Hanahan and Weinberg, 2011). A key protein involved in maintaining genomic integrity is cellular tumour antigen protein 53 (p53), encoded by the *TP53* gene (Brown et al., 2009; Lane, 1992; Larkin and Jackson, 1999). p53 is activated following the detection of damaged DNA by ATR (Ataxia telangiectasia and Rad3 related) and ATM (Ataxia telangiectasia mutated) serine/threonine kinase signalling pathways (Brown et al., 2009; Shiotani and Zou, 2009). Once active, p53 can prevent cell division by stimulating the RNA transcription of multiple

proteins (for example p21 and GADD45) which bind to cell cycle proteins (including cyclins A and E) to cause cell cycle arrest (Haupt et al., 2003; Larkin and Jackson, 1999). Additionally, p53 can trigger apoptosis by inducing RNA transcription of pro-apoptotic proteins, such as Bax and FAS (Brown et al., 2009; Haupt et al., 2003). *TP53* is mutated in approximately 50 % of cancers which results in a loss of a critical DNA damage checkpoint and increases the frequency of cellular mutations (Brown et al., 2009; Haupt et al., 2003; Lane, 1992; Larkin and Jackson, 1999).

Telomerase is a specialised DNA polymerase that maintains and extends the chromosomal ends, the telomeric DNA. Telomerase has a role in maintaining genomic integrity, with a loss of telomerase activity leading to progressive shortening of the telomeric DNA and destabilisation of chromosomal DNA (Artandi and DePinho, 2010). Loss of telomeric DNA can induce a DNA damage response which involves p53. The importance of the combination of these pathways is shown by a p53 and telomerase mouse KO model, which has rapid tumour development compared to a p53 mouse KO model (Artandi and DePinho, 2010).

In cancer cells, gene expression can also be regulated by epigenetic changes in DNA methylation or histone modifications (Berdasco and Esteller, 2010). Hypomethylation in cancer is associated with genomic instability, with changes in the methylation pattern of the promoters of tumour suppressor proteins leading to gene silencing, such as in retinoblastoma protein (Rb) and breast cancer susceptibility gene 1 (BRCA1; Berdasco and Esteller, 2010).

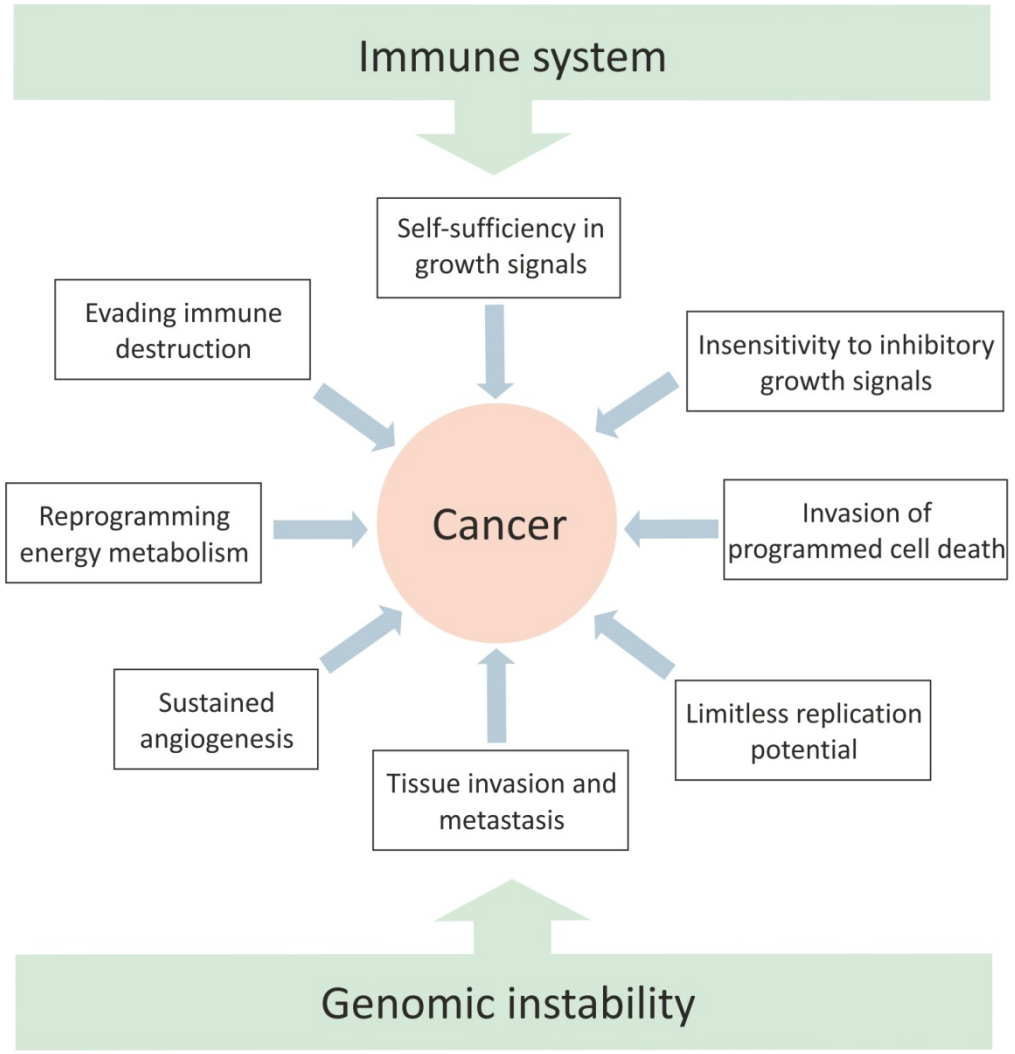

Figure 1.8: The hallmarks of cancer
During cancer development, cells can acquire functional abilities known as the hallmarks of cancer which allow for tumour growth and development.
Shown in green are two enabling characteristics which may encourage the development of these cancer hallmarks.
Figure adapted from Hanahan and Weinberg (2011).

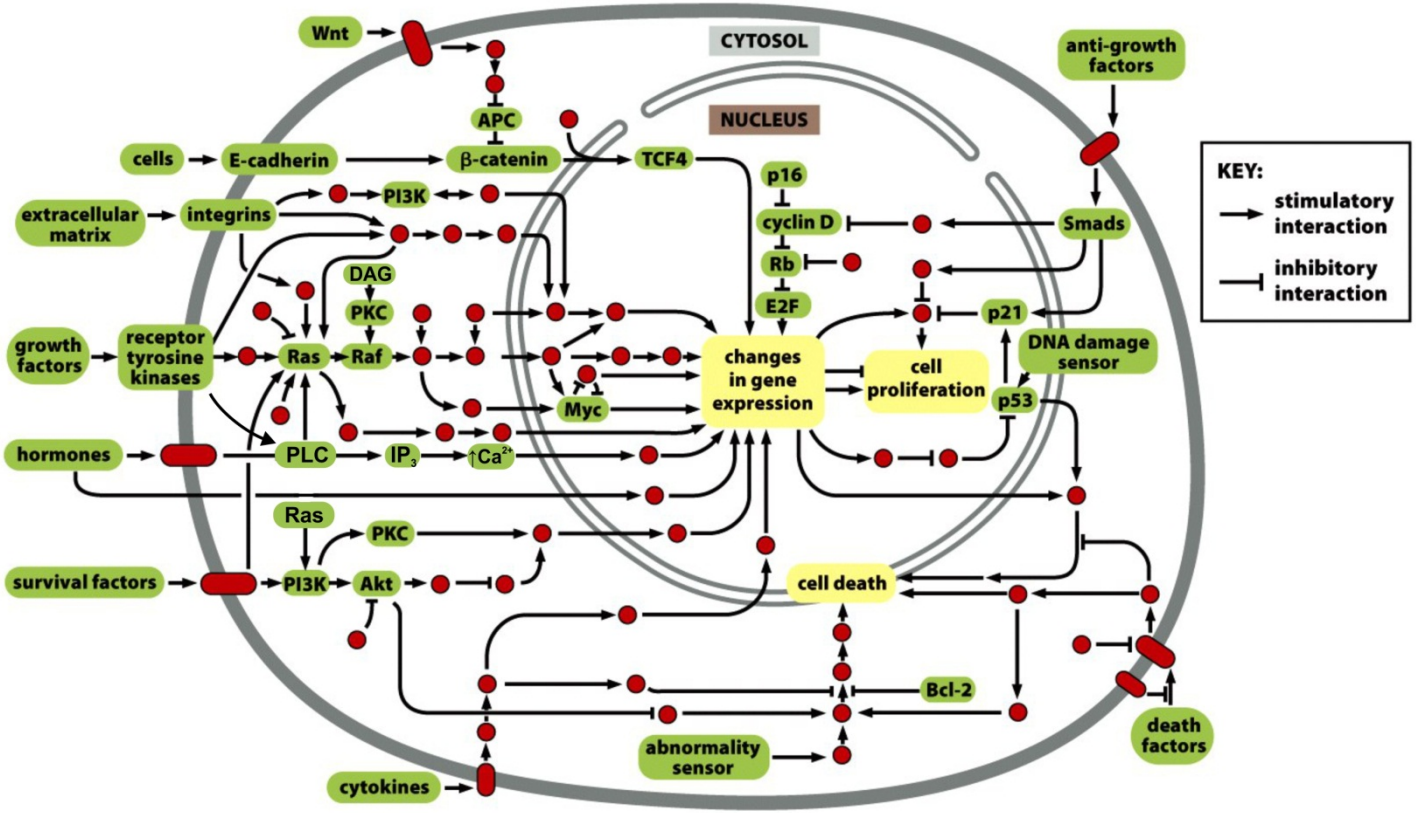

Figure 1.9: Key signalling pathways in cancer

Within a cancer cell, a number of signalling pathways can be altered, with both oncogenic proteins (e.g. PI3K, c-Myc, and Ras) and tumour suppressor proteins (e.g. Rb and p53) interacting within the same pathways. Key cancer proteins and stimuli are shown in green, with signalling proteins indicated by red circles. The stimulatory and inhibitory interactions between the different pathways are also shown.
Figure adapted from Alberts (2008).

1.5.1.2 Enabling characteristic 2: The immune system

Nearly all tumours are infiltrated by cells of the immune system (Grivennikov et al., 2010; Hanahan and Weinberg, 2011; Pages et al., 2009). It was originally thought that the immune system was involved in attempts to remove the cancer cells, but recent evidence showed that tumour associated inflammation can promote tumour growth and progression (Grivennikov et al., 2010). The precise pathways involved are still being characterised, however it has been suggested that inflammation can contribute to carcinogenesis by the release of bioactive molecules from immune cells, for example epidermal growth factor (EGF), transforming growth factor α (TGF-α), interleukin-6 (IL-6), and IL-11 (Grivennikov et al., 2010). These factors can stimulate downstream signalling pathways which activate transcription factors, including nuclear factor kappa-light chain enhancer of activated B cells (NF-κB), signal transducer and activator of transcription 1 (STAT-1), and activator protein 1 (AP-1). In addition to inducing signalling pathways involved in pro-survival or proliferative responses, such as Wnt/β-catenin pathways, inactivation of p53 signalling, cyclins D1 and D2 expression, and c-Myc pathways (Figure 1.9; Grivennikov et al., 2010; Hanahan and Weinberg, 2011). Furthermore, it has been suggested that the release of ROS from immune cells can cause DNA damage and enhance the genetic evolution of cancer cells (Grivennikov et al., 2010; Hanahan and Weinberg, 2011).

1.5.1.3 Cancer hallmark: self-sufficiency in growth signals

In general, non-cancerous cells spend a considerable portion of their lifetime within a quiescent growth state, known as G_0 (Witsch et al., 2010). During G_0, cells are neither dividing nor preparing to enter the cell cycle (Collins et al., 1997; Hanahan and Weinberg, 2000; Witsch et al., 2010). The cell cycle consists of four discrete stages, G_1 (Gap phase one), S (Synthesis: DNA duplication), G_2 (Gap phase two), and M (Mitosis: nuclear division and cytokinesis), and is monitored at three checkpoints, G_1/S, G_2, and M. To enable replication, non-cancerous cells require stimulation to progress from G_0 into a proliferative state (King and Robins, 2006). This stimulation usually involves extracellular GF (such as EGF and platelet derived growth factor (PDGF)), which activate cell signalling pathways to overcome inhibitory anti-growth signals and initiate the translation of proteins critical for G_1

progression (e.g. cyclins and cyclin-dependent kinases (CDKs), Figure 1.9; King and Robins, 2006; Witsch et al., 2010).

In cancer, uncontrolled cell proliferation can occur when cells become independent from normal GF signalling (Hanahan and Weinberg, 2000; Knowles and Selby, 2005; Witsch et al., 2010). There are several ways for cancer cells to become self-regulating, firstly, cancer cells may produce GF to act on their own receptors, or stimulate surrounding cells within the tumour microenvironment (such as cancer-associated fibroblasts) to secrete GF (Bhowmick et al., 2004; Hanahan and Weinberg, 2011). In breast cancer, secretion of hepatocyte GF by cancer-associated fibroblasts correlates with increased tumourigenesis (Tyan et al., 2011). Secondly, overexpression or constitutive activation of cell surface GF receptors allows cancer cells to become hyper-responsive to GF stimulation or independent from GF signalling (Knowles and Selby, 2005; Witsch et al., 2010). EGFR overexpression is detected in approximately 60 % of non-small cell lung cancers, and mutations are often detected within the kinase domain of the receptor (usually involving deletion of exon 19, or point mutations in exons 19 and 20; da Cunha Santos et al., 2011). These mutations commonly cause constitutive kinase activity and downstream signalling pathway activation (da Cunha Santos et al., 2011). Finally, overexpression or mutations in downstream signalling pathways can enhance the cellular response to normal GF receptor activation, for example in Ras, PI3K/Akt/mTOR, or MAPK signalling pathways (Figure 1.9; Bianco et al., 2006; Hanahan and Weinberg, 2011; Shaw and Cantley, 2006).

1.5.1.4 Cancer hallmark: insensitivity to inhibitory growth signals

Anti-proliferative signals will keep cells in a quiescent G_0 state and prevent entry into the G_1 phase of the cell cycle, with multiple anti-growth signals being transduced by Rb and related proteins, including p107 and p13 (Figure 1.9; Dick and Rubin, 2013; Hanahan and Weinberg, 2000; Hanahan and Weinberg, 2011). In its active, hypophosphorylated, state Rb will prevent cell proliferation, by binding and inhibiting the E2-binding transcription factor family (E2F), this prevents the activation of genes critical for G_1 progression (e.g. cyclins A and E; Dick and Rubin, 2013; Weinberg, 1995). Transforming growth factor β (TGF-β) has anti-proliferative effects, by preventing the phosphorylation of Rb and keeping it in an active state (Dick and Rubin, 2013; Hanahan and Weinberg, 2000; Hanahan and Weinberg, 2011; Weinberg, 1995).

PTEN phosphatase activity is also involved in anti-proliferative signalling. PTEN acts as a negative regulator of PI3K activity, by degrading PIP_3 and preventing downstream pro-growth signalling involving Akt and mTOR (Figure 1.9; Chalhoub and Baker, 2009). Loss of PTEN activity either by mutations (which are found in up to 20 % of skin, prostate, and CNS tumours) or promoter methylation (causing reduced expression), results in increased PI3K/Akt/mTOR signalling which can promote carcinogenesis (Chalhoub and Baker, 2009; Hanahan and Weinberg, 2011).

1.5.1.5 Cancer hallmark: evasion of programmed cell death

The size of a tumour cell population is determined by the rate of cell death, as well as proliferation, therefore cancer cells must acquire resistance to apoptosis (Hanahan and Weinberg, 2000). Apoptotic signalling pathways can be triggered by extrinsic signals (including TRAIL and Fas-L) mediated by tumour necrosis factor receptors (TNFR, Fas, and TRAIL), and intrinsic factors such as DNA damage involving p53 (Harris, 1996; Knowles and Selby, 2005; Ouyang et al., 2012; Portt et al., 2011). Activation of pro-apoptotic pathways changes the balance from anti-apoptotic BCl-2 family proteins (including Bcl-2, Bcl-w, and Mcl-1) to pro-apoptotic proteins (such as Bax and Bak) causing activation of caspases which leads to cell death (Adams and Cory, 2007). There are several ways by which cancer cells can limit apoptosis, a common alteration is the loss of p53 which is critical for sensing intrinsic cell damage and activating pro-apoptotic proteins (including Bid, DR5, and caspase-8; Haupt et al., 2003; Ouyang et al., 2012; Portt et al., 2011). Additionally, within cancer cells there is evidence for the upregulation of anti-apoptotic proteins and downregulation of pro-apoptotic proteins (Adams and Cory, 2007; Hanahan and Weinberg, 2011). Increased expression of anti-apoptotic proteins (such as Bcl-2, BAG-1, Bfl-1, and MCl-1) has been detected in multiple cancers including breast, leukaemia, melanoma, ovarian, and glioma (Placzek et al., 2010; Yang et al., 1999).

1.5.1.6 Cancer hallmark: limitless replicative potential

Most cells have an intrinsic program which will prevent unlimited proliferation. *In vitro* studies have shown that cultured cells undergo a limited number of divisions before

entering cell senescence; this growth limitation is related to the telomeres, the ends of the chromosomal DNA (Hayflick, 2000; Knowles and Selby, 2005). During each cell division the telomeric DNA becomes shorter, due to the inability of DNA polymerase to replicate the 3' end of a chromosome (King and Robins, 2006). This progressive shortening means that after a certain number of divisions (approximately 40) the chromosomal DNA will be exposed and this triggers cellular senescence (Shay and Wright, 2011). Increased telomerase activity is detected in approximately 90 % of malignant tumours and this reduces the loss of telomeric DNA during cell divisions preventing cellular senescence (Hanahan and Weinberg, 2011; Shay and Wright, 2011).

1.5.1.7 Cancer hallmark: sustained angiogenesis

Vasculature is required to deliver nutrients and O_2 to cells, in addition to removing waste products such as CO_2. For optimum nutrient delivery, cells need to be within the substrate diffusion limits, which is approximately 100-200 µm from a blood vessel (Hanahan and Weinberg, 2000; Hanahan and Weinberg, 2011; Trédan et al., 2007; Ward et al., 2013). Therefore, to develop and maintain cancer growth, the creation of blood vasculature is critical; without this tumours would not reach more than 1-2 mm in size (Knowles and Selby, 2005). During cancer progression, angiogenesis is initiated and sustained by an "angiogenic switch", which alters the balance between pro- and anti-angiogenic factors to trigger the development of new blood vessels (Baeriswyl and Christofori, 2009; Hanahan and Weinberg, 2011; Trédan et al., 2007). Vascular endothelial growth factor-A (VEGF-A) is considered to be the major pro-angiogenic factor in cancer (Baeriswyl and Christofori, 2009; Bianco et al., 2006; Hanahan and Weinberg, 2011). VEGF-A signalling can be upregulated by hypoxia and oncogenic signalling pathways, such as Ras and c-Myc (Figure 1.9; Baeriswyl and Christofori, 2009).

1.5.1.8 Cancer hallmark: tissue invasion and metastasis

Tumour metastases are one of the main causes of death from cancer (Hanahan and Weinberg, 2000). Metastasis is a multi-step process, where cancer cells must first migrate into the surrounding stroma, before invading nearby blood or lymphatic vessels which enable transportation around the body (Engbring and Kleinman, 2003; Talmadge and Fidler,

2010). Following this cancer cells must then arrest in a capillary bed before extravasation into the surrounding tissue, where the cells will re-establish a tumour producing a cancer metastasis (Engbring and Kleinman, 2003; Talmadge and Fidler, 2010).

The epithelial-mesenchymal transition (EMT) is a developmental program that has been implicated in the acquired ability of cancer cells to invade and metastasise (Hanahan and Weinberg, 2011; Kalluri and Weinberg, 2009; Yang and Weinberg, 2008). EMT is caused by a set of transcription factors (Snail, Slug, Twist, and Zeb1/2) which result in a number of cellular changes: loss of adherens junctions (reduced expression of E-cadherin), morphological changes toward a fibroblastic phenotype, expression of extracellular matrix degrading enzymes, and increased cell mobility (Kalluri and Weinberg, 2009; Peinado et al., 2004; Yang and Weinberg, 2008). Activation of EMT critical transcription factors can be triggered by a number of signalling pathways present within cancer cells, including TGF-β, Wnt/β-catenin, and Ras/MAPK (Figure 1.9; Kalluri and Weinberg, 2009; Yang and Weinberg, 2008).

1.5.1.9 Cancer hallmark: reprogramming energy metabolism

In order to support cell proliferation, tumour cells must adjust their energy metabolism. Cancer cells are commonly in a state of "aerobic glycolysis", where glucose is broken down into pyruvate to produce ATP even though O_2 is present; this phenomenon is known as the Warburg effect (Chiche et al., 2010; Gillies et al., 2008; Hanahan and Weinberg, 2011). Compared to energy production by oxidative phosphorylation, which results in 36 ATP molecules for the complete oxidation of one glucose molecule, aerobic glycolysis is more inefficient, creating only two ATP for the metabolism of one glucose molecule to pyruvate (Vander Heiden et al., 2009). However, the utilisation of aerobic glycolysis in cancer cells is thought to be beneficial due to the increased production of intermediate molecules, which are needed for other biosynthetic pathways, such as nucleotide and amino acid production (Vander Heiden et al., 2009). Components of the glycolytic pathway can be upregulated by hypoxic conditions, which are commonly found in the cancer microenvironment via hypoxia-inducible factor (HIF) 1α signalling, or by oncogenic signalling pathways, such as Ras and Akt (Figure 1.9; Bianco et al., 2006; Hanahan and Weinberg, 2011; Jones and Thompson, 2009).

1.5.1.10 Cancer hallmark: evading immune destruction

The current evidence suggests that the immune system has a role in both promoting and preventing carcinogenesis (Hanahan and Weinberg, 2011). The role of the immune system in preventing cancer development is supported by data from immunodeficient mouse models, since these mice develop carcinogen-induced tumours more quickly than the immunocompetent controls (Teng et al., 2008). The role of the immune system in tumour prevention appears to involve natural killer cells, $CD4^+$ and $CD8^+$ T lymphocytes (Hanahan and Weinberg, 2011; Teng et al., 2008). One way for cancer cells to evade immune destruction may be to secrete immunosuppressive factors, such as TGF-β, although the precise mechanisms and pathways involved are still being characterised (Hanahan and Weinberg, 2011).

1.5.2 Cancer microenvironment

Tumours are not just comprised of cancerous cells but form structures similar to functioning organs, with their growth and activity being supported by the surrounding microenvironment, this includes the tumour stroma and the environmental conditions experienced (Hanahan and Weinberg, 2011; Hu and Polyak, 2008). The tumour stroma is comprised of many cell types including cancer associated fibroblasts, immune cells, blood vessels, and smooth muscle cells (Hale et al., 2013; Hu and Polyak, 2008). These cells provide a supportive framework for the developing cancer, by secreting factors (extracellular matrix components, growth factors, and cytokines) which can encourage cancer growth, survival, and progression (Hale et al., 2013; Hu and Polyak, 2008).

Cancer cells are frequently under environmental stress conditions, which can occur as the cancer outgrows the gradient for nutrient delivery (Gillies et al., 2008). The development of new blood vessels will compensate for this nutrient deficiency to a certain extent, however due to the poor and abnormal structure of tumour vasculature this gradient is not always matched (Luo et al., 2009; Trédan et al., 2007). Therefore, it is common for regions within tumours to have inadequate nutrient supply, which can result in hypoxia, starvation, and acidosis (Chiche et al., 2010; Gillies et al., 2008; Luo et al., 2009; Ward et al., 2013).

The physiological O_2 tension for the majority of tissues within the body is between 2-9 % O_2, but in tumours this can often fall below 2 % O_2 (Bertout et al., 2008; Mucaj et al., 2012). One mechanism used by tumour cells to compensate for poor O_2 supply is the upregulation of HIFs and utilisation of anaerobic glycolysis (Mucaj et al., 2012). In hypoxia, HIF activity can alter tumour metabolism by modulating the expression of genes which can promote cell proliferation and survival (Chiche et al., 2010; Mucaj et al., 2012; Trédan et al., 2007). A target of HIF is the oncogene c-Myc, and increased expression of c-Myc in cancer cells under energetic stress (glucose deprivation and hypoxia) can drive proliferation (Le et al., 2012). Hypoxia has also been found to induce a selection pressure for cancer cells with a more aggressive phenotype, for example by selecting for cancer cells that are insensitive to p53-mediated apoptosis (Trédan et al., 2007). It has been hypothesised that a loss of p53 expression in cancer cells will be beneficial under hypoxic conditions as it will prevent activation of p53-dependent apoptotic pathways (Graeber et al., 1996; Trédan et al., 2007).

As a result of the Warburg effect, the majority of tumours utilise aerobic glycolysis for energy production, therefore cancer cells have a higher glucose uptake and metabolism, compared to normal cells (DeBerardinis et al., 2008; Gillies et al., 2008; Hanahan and Weinberg, 2011). To support this, many tumour cells upregulate the glucose transporter GLUT-1 (Jones and Thompson, 2009). Glucose starvation can also trigger upregulation of glucose regulated protein 78 (GRP78 or Bip); physiologically GRP78 is involved in the ER response to cell stress and its expression has been implicated in the adaptation of cancer cells to the microenvironment (Li and Li, 2012).

These environmental alterations, hypoxia and low glucose, will cause extracellular acidification of the tumour microenvironment (Chiche et al., 2010; Gatenby et al., 2007; Ward et al., 2013). The decrease in extracellular pH is directly correlated to reduced O_2 and in regions greater than 300 µm from a blood vessel the pH can drop from pH 7.4 to 6.0 (Chiche et al., 2010; Gatenby et al., 2007; Ward et al., 2013). In addition, upregulation of systems to modulate intracellular pH (such as the Na^+/H^+ exchanger) can lead to further extracellular acidification (Chiche et al., 2010). In summary, these environmental stress conditions induce a selection pressure for cells which can proliferate and survive under these conditions (Gatenby et al., 2007; Gillies et al., 2008; Graeber et al., 1996; Williams et al., 1999); thus providing a driving force for cancer progression into metastasis (Anderson et al., 2006).

1.5.3 Cancer cell signalling pathways

A number of cell signalling pathways that are altered in cancer and involved in cancer hallmark functions have been highlighted, for example EGF signalling, Rb signalling, p53 DNA repair pathways, and PI3K/Akt/mTOR signalling (Figure 1.9; Bianco et al., 2006; Brown et al., 2009; Hanahan and Weinberg, 2011; Normanno et al., 2006; Park et al., 2012; Vara et al., 2004). In addition to these signalling pathways, Ca^{2+} is a key intracellular messenger in both normal and cancer cells (Prevarskaya et al., 2013).

Intracellular Ca^{2+} signalling involves Ca^{2+} release from internal stores, such as the ER, and occurs by two general methods, Ca^{2+} induced release and receptor stimulated release (Prevarskaya et al., 2013). Activation of multiple GPCR (e.g. acetylcholine, glutamate, angiotensin II, endothelin, and lipid) and receptor TK (EGFR, insulin-like growth factor receptor (IGFR), PDGFR, and VEGFR) can stimulate Ca^{2+} signalling, and these events are mediated by phospholipase C (PLC, in particular PLCβ for GPCR events and PLCγ for receptor TK events, Figure 1.10; Berridge, 1993; Clapham, 2007; Park et al., 2012; Prevarskaya et al., 2013; Raimondi and Falasca, 2012). For example, PLCγ is activated by interacting with phosphorylated EGFR, via the SH2 protein domain within the PLCγ protein (Park et al., 2012). In its active form, PLC will cleave the plasma membrane lipid phosphatidylinositol 4,5-bisphosphate (PIP_2) into the second messengers diacylglycerol (DAG) and inositol trisphosphate (IP_3, Figure 1.10; Clapham, 2007; Park et al., 2012; Raimondi and Falasca, 2012). Both DAG and IP_3 have multiple downstream consequences (Figure 1.10), with IP_3 being critical for Ca^{2+}-dependent signalling by opening IP_3 receptors (non-selective cation channels) located on the ER membrane, which causes Ca^{2+} release from the ER and a rise in cytoplasmic Ca^{2+} (Park et al., 2012; Prevarskaya et al., 2013; Raimondi and Falasca, 2012). Ca^{2+} release from the ER can induce further Ca^{2+} influx into the cytoplasm, via plasma membrane channels (such as store-operated Ca^{2+} entry channels, formed of Orai and STIM complexes, and TRP channels) and ER localised ryanodine receptors (Ca^{2+}-activated Ca^{2+} channels, Figure 1.10; Chen et al., 2013; Davis et al., 2013; Fioro Pla and Gkika, 2013; Prevarskaya et al., 2013; Yang et al., 2009).

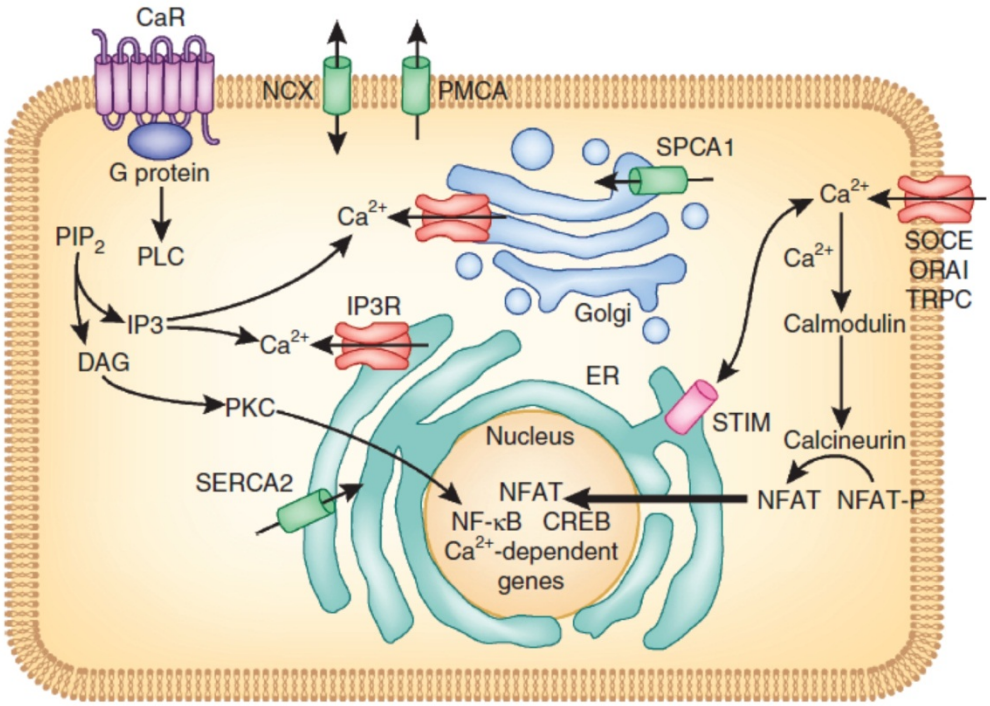

Figure 1.10: Ca^{2+}-dependent cell signalling pathways

The major components which regulate intracellular Ca^{2+} signalling are shown.

Activation of PLC by cell surface receptors results in DAG and IP_3 generation, from PIP_2. IP_3 stimulates Ca^{2+} release from internal Ca^{2+} stores, via IP_3 receptors; the ER and Golgi apparatus are shown. Increased cytoplasmic Ca^{2+} stimulates further Ca^{2+} influx through plasma membrane channels, store-operated Ca^{2+} entry (SOCE; formed by interactions between STIM1 and Orai channels) and TRP channels. The rise in intracellular Ca^{2+} will activate Ca^{2+}-dependent signalling proteins (calmodulin and calcineurin), which leads to activation of Ca^{2+}-dependent transcription factors (NFAT, NF-κB, and CREB) and gene transcription.

To prevent cell death events from prolonged Ca^{2+} signalling, Ca^{2+} ATPases regulate cytoplasmic Ca^{2+} levels by replenishing internal stores (SERCA and SPCA1) and pumping Ca^{2+} out of the cell (PMCA).

Figure from Mascia et al. (2012).

The rise in intracellular Ca^{2+} has a range of direct and indirect consequences on cellular functions. Ca^{2+} will bind and activate a range of signalling proteins, including calmodulin, calmodulin-dependent kinases (CAMK), and calcineurin (Figure 1.10; Mascia et al., 2012; Prevarskaya et al., 2013). These proteins regulate the activation of a range of transcription factors, such as AP-1, CREB (cAMP response element binding protein), NFAT (nuclear factor of activated T cells), and NF-κB (Carafoli, 2002; Mascia et al., 2012; Prevarskaya et al., 2013). For example, calcineurin will dephosphorylate NFAT which causes translocation of NFAT to the nucleus, where it stimulates gene expression of pro-growth factors, e.g. c-Myc, cyclin E, and E2F transcription factors (Carafoli, 2002; Mascia et al., 2012). Ca^{2+} can also stimulate Ras and MAPK signalling cascades, by Ca^{2+}-induced binding of calmodulin to the N-termini of Ras guanine nucleotide exchange proteins (Clapham, 2007; Freshney et al., 1997).

Cancer cells can alter the intracellular Ca^{2+} levels, by manipulation of components of Ca^{2+} signalling pathways, which can promote beneficial cancer hallmarks such as cell growth, apoptosis resistance, and metastases (Figure 1.10; Akl and Bultynck, 2013; Clapham, 2007; Prevarskaya et al., 2013). As a result of this, abnormalities are detected in a number of proteins within Ca^{2+}-dependent signalling pathways in cancer (Prevarskaya et al., 2013). Alterations can occur at the receptor level, for example EGFR signalling is commonly dysregulated, and overexpression of EGFR and HER3 has been detected in 50-70 % of lung, breast, and colon cancers (Bianco et al., 2006; Normanno et al., 2006). Altered expression of PLC has also been detected in cancer; PLCγ is considered to be a tumour promoter and is generally activated following GF signalling (Clapham, 2007; Park et al., 2012). Overexpression of PLCγ protein is detected in breast cancer tissue compared to normal tissue (Raimondi 2012). Furthermore, when PLCγ expressing breast cancer cells (MDA-MB-231 cells) were injected into mice increased tumour formation was detected compared to untransfected cells (Raimondi 2012).

Alterations can also occur at the Ca^{2+} release level. In colorectal, glioblastoma, liver, and prostate cancers, increased IP_3 receptor expression has been found to correlate with more aggressive tumours and poor survival (Akl and Bultynck, 2013). Increased expression of plasma membrane Ca^{2+} channels, such as Orai channels, are also detected in cancer (Table 1.3; McAndrew et al., 2011; Prevarskaya et al., 2013; Yang et al., 2009). ER Ca^{2+} pumps (SERCA) that are responsible for the active transport of Ca^{2+} from the cytoplasm into

the ER, are downregulated in aggressive prostate and colorectal cancers (Prevarskaya et al., 2013). This is thought to prevent apoptosis, by limiting the ER stress that can result from rapid Ca^{2+} reloading (Prevarskaya et al., 2013).

1.5.4 Roles of ion channels and transporters in cancer

In addition to changes in Ca^{2+} signalling, over the last 15 years, alterations to numerous types of ion channels and transporters have been identified in cancer (Table 1.3; Pedersen and Stock, 2013). By regulating cellular processes, ion channels and transporters have been shown to impact on nearly all cancer hallmark functions (Table 1.3). Furthermore, the interactions formed between different ion channels and transporters are essential to create a functional response from the coordinated movement of ions across the cell membrane (Figure 1.11).

The functional impacts of ion channels and transporter alterations are still being characterised, however it has been suggested that there are four general methods by which ion channels and transporters can influence cancer cell functions (Figure 1.11; Arcangeli and Becchetti, 2010; Becchetti et al., 2013; Kunzelmann, 2005; Schwab et al., 2012):

(i) By regulation of the membrane potential.

(ii) By modulating intracellular Ca^{2+} signalling.

(iii) By controlling the cell volume.

(iv) By regulating the intracellular pH.

Examples of ion channels and transporters which contribute to these ionic processes and how they can influence cancer cell functions are outlined in the following sections in further detail.

1.5.4.1 Regulation of the membrane potential

Changes in the membrane potential which result from altered ion channel activity have been found to be critical for cell cycle progression in both normal and cancer cells (Figure 1.11 A; Arcangeli and Becchetti, 2010; Wonderlin and Strobl, 1996). During the G_1/S transition, a transient hyperpolarisation caused by K^+ efflux is required, whereas

depolarisation caused by Cl^- efflux is essential at the G_2/M transition (Figure 1.11 A; Blackiston et al., 2009; Molenaar, 2011). A number of KCh have been linked to membrane potential hyperpolarisation and cell cycle progression in cancer cells (discussed further in Section 1.6.3), these include K_V10.1 (breast and ovarian cancers), K_V11.1 (breast, lung, neuroblastoma, and ovarian cancers), and K_{Ca}3.1 (breast and prostate cancers; Asher et al., 2011; Crociani et al., 2003; Glassmeier et al., 2012; Lallet-Daher et al., 2009; Ouadid-Ahidouch et al., 2000; Ouadid-Ahidouch et al., 2004). G_2/M depolarisation is caused by Cl^- efflux, via ClC-3 channels, in glioblastoma cells (Molenaar, 2011). ClC-3 channel activity is dependent on Ca^{2+} influx (due to channel phosphorylation by CAMKII) and inhibition of TRPC6 (Ca^{2+}-permeable transient receptor potential canonical channel protein 6) results in cell cycle arrest at G_2/M, due to reduced Ca^{2+} influx and ClC-3 activity (Cuddapah and Sontheimer, 2010; Ding et al., 2010; Molenaar, 2011).

The membrane potential of cancer cells if often depolarised compared to normal cell counterparts (Arcangeli et al., 1995; Olsen and Sontheimer, 2004; Sundelacruz et al., 2009). At depolarised membrane voltages (between -20 and -60 mV) continuous Na^+ influx (caused by partial Na_V channel activation and incomplete inactivation) is observed (Figure 1.11; Blackenbury, 2012; Campbell et al., 2013; Gillet et al., 2009; Roger et al., 2007; Yang and Blackenbury, 2013). Increased Na^+ influx resulting from persistent Na_V channel activity has been found to promote cancer cell migration and invasion (Campbell et al., 2013; Gillet et al., 2009). The specific Na_V channels which have been linked cancer cell invasion are highlighted in Table 1.3. Increased Na^+ influx is proposed to alter cancer cell volume control (Section 1.5.4.3) and intracellular pH regulation (Section 1.5.4.4), and this is thought to lead to invasive phenotypes (Figure 1.11).

Table 1.3: Ion channels and transporters linked to cancer hallmark functions
Examples of ion channels and transporters that have been linked to cancer cell hallmark functions.

Abbreviations:
Calcium (Ca^{2+}) channels: voltage-gated (Ca_V), plasma membrane Ca^{2+} ATPase (PMCA), sarcoendoplasmic reticulum Ca^{2+} ATPase (SERCA), store-operated (Orai), transient receptor potential (TRP), IP_3 receptor (IP_3R), and ryanodine receptor (RyR).
Chloride (Cl^-) channels: voltage-gated (ClC), voltage-dependent anion channel (VDAC), and volume regulated anion channel (VRAC).
Potassium (K^+) channels: voltage-gated (K_V), calcium-gated (K_{Ca}), inward rectifying (K_{ir}), and two-pore domain (K_{2P}).
Sodium (Na^+) channels: epithelial Na^+ channel (ENaC), and voltage-gated (Na_V).
Other channels: acid sensing ion channels (ASIC), aquaporins (AQP), GABA ionotropic receptor ($GABA_A$), hypertonicity induced cation channel (HICC), nicotinic acetylcholine receptors (nACRs), and voltage-gated proton channel (HV1).
Transporters: anion exchange protein (AE), carbonic anhydrase (CA), glucose transporter (GLUT), Na^+/Ca^{2+} co-transporter (NCX), Na^+/H^+ exchanger (NHE1), Na^+-K^+-Cl^- co-transporter (NKCC1), and monocarboxylate transporter (MCT).

(1) Kunzelmann (2005), (2) Pei et al. (2003), (3) Voloshyna et al. (2008), (4) Monteith et al. (2012), (5) Ding et al. (2010), (6) Molenaar (2011), (7) Becchetti (2011), (8) Fraser and Pardo (2008), (9) Lehen'kyi et al. (2011), (10) Arcangeli and Becchetti (2010), (11) Mijatovic et al. (2008), (12) McAndrew et al. (2011), (13) Frede et al. (2013), (14) DeCoursey (2013), (15) Capiod (2012), (16) Lehen'kyi et al. (2007), (17) Numata et al. (2008), (18) Pedersen et al. (2013), (19) Benga and Huber (2012), (20) Leanza et al. (2013), (21) Yu (2003), (22) VanHouten et al. (2010), (23) Fioro Pla and Gkika (2013), (24) Arcangeli (2011), (25) Cuddapah and Sontheimer (2011), (26) Black and Waxman (2013), (27) Schwab et al. (2012), (28) Prevarskaya et al. (2007), (29) Cuddapah and Sontheimer (2010), (30) Amith and Fliegel (2013), (31) Yang et al. (2009), (32) Brackenbury (2012), (33) Campbell et al. (2013), (34) Lee et al. (2012), (35) Becchetti et al. (2013), (36) Fiorio Pla et al. (2011), (37) Crociani et al. (2013), (38) Downie et al. (2008), (39) Grgic et al. (2005), (40) Maldonado and Lemasters (2012).

Cancer hallmark function	**Ion channels and transporters**	**Ref.**
Uncontrolled cell proliferation	Ca^{2+} channels: Ca_V3, T-type Ca_V, Orai1, TRPC3, TRPC6, TRPV6, IP_3R Cl^- channels: ClC-3 K^+ channels: $K_V1.3$, $K_V1.5$, $K_V10.1$, $K_V11.1$, $K_{Ca}1.1$, $K_{Ca}3.1$, $K_{ir}4.1$, $K_{2P}2.1$, $K_{2P}9.1$ Other channels: H_V1, $GABA_A$, nAChRs Transporters: Na^+/K^+ ATPase, Ca-IX, Ca-XII	1-16
Evasion of apoptosis	Ca^{2+} channels: L-type Ca_V, Orai1, TRPM8 Cl^- channels: ClC-4, VDAC K^+ channels: $K_V1.3$, $K_V11.1$, $K_{Ca}1.1$, $K_{Ca}3.1$, $K_{2P}9.1$ Na^+ channels: ENaC, $Na_V1.2$, $Na_V1.5$, $Na_V1.6$, $Na_V1.7$, β subunits 1/4 Other channels: HICC, AQP4 Transporters: Na^+/K^+ ATPase, NHE1, NKCC1, NCX, Ca-IX, Ca-XII, PMCA2, SERCA	2, 4, 8-11, 17-22
Tissue invasion and metastasis	Ca^{2+} channels: T-type Ca_V, Orai1+STIM1, TRPC1, TRPC3, TRPC6, TRPM7, TRPM8, TRPV1, TRPV2, TRPV4, TRPV6, RyR, IP_3R Cl^- channels: ClC-3, VRAC K^+ channels: $K_V10.1$, $K_V11.1$, $K_{Ca}1.1$, $K_{Ca}2.3$, $K_{ir}4.2$, $K_{2P}9.1$ Na^+ channels: $Na_V1.2$, $Na_V1.5$, $Na_V1.6$, $Na_V1.7$, ENaC Other channels: HICC, AQP1, AQP4, ASIC1, ASIC2, ASIC3 Transporters: Na^+/K^+ ATPase, NHE1, NKCC1, SERCA	4, 6, 8, 10-13, 19, 23-35
Increased angiogenesis	Ca^{2+} channels: Orai1+STIM1, TRPC1, TRPC6, TRPV4 K^+ channels: $K_V10.1$, $K_V11.1$, $K_{Ca}1.1$, $K_{Ca}3.1$	4, 36-39
Reprogramming energy metabolism	Cl^- channels: VDAC Transporters: GLUT-1, Na^+/K^+ ATPase, NHE1, MCT14, AE1, Ca-IX	1, 30, 40

A) Membrane potential

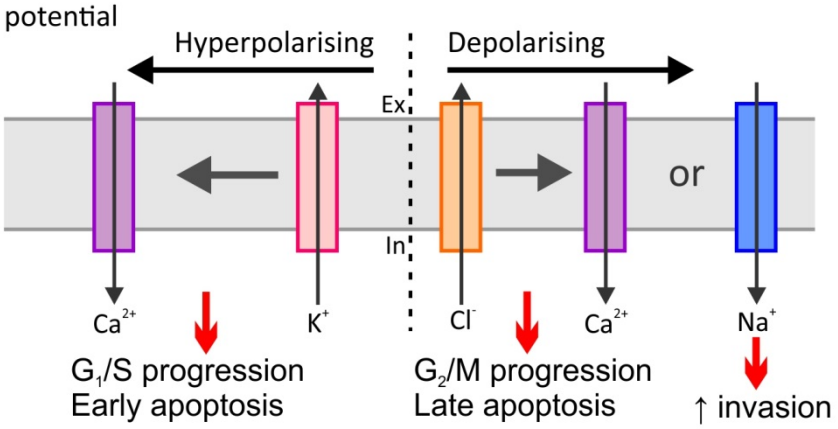

B) Ca^{2+} signalling

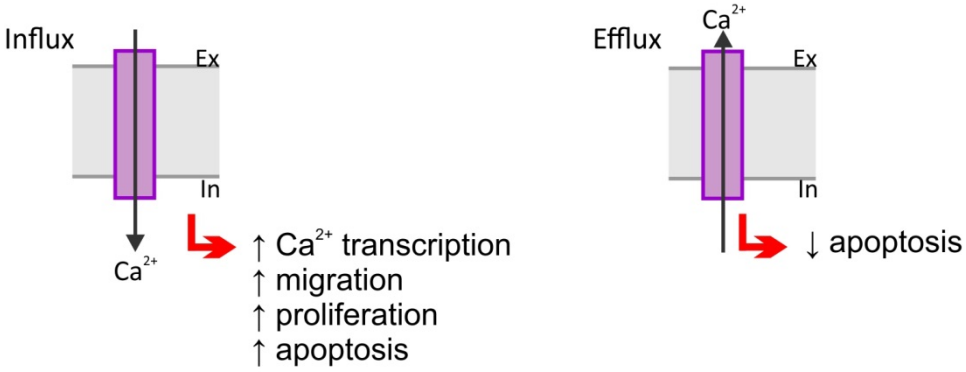

C) Cell volume

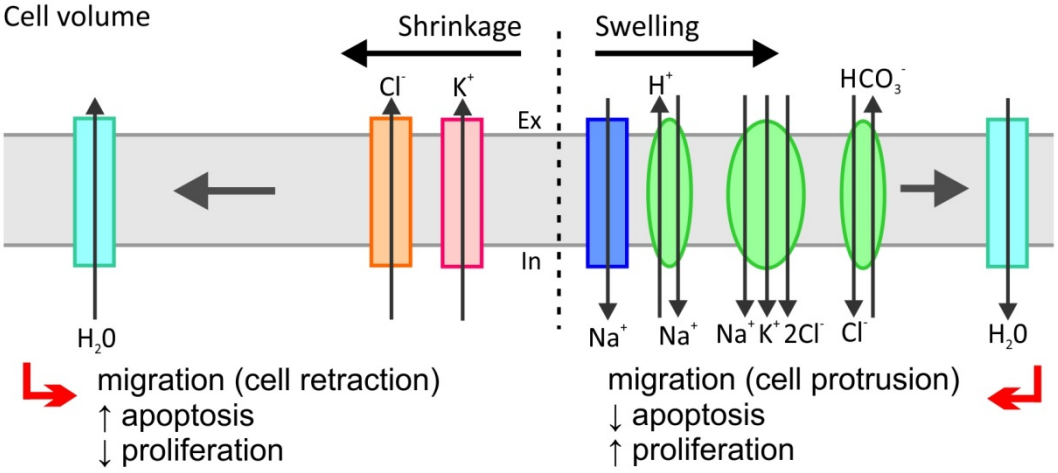

D) Intracellular pH

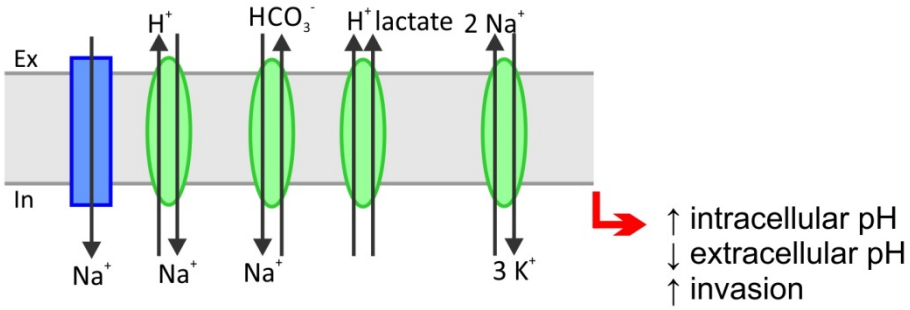

Figure 1.11: Functional consequences of ion channel and transporter expression

Figure demonstrating four methods by which ion channel and transporter activity can impact on cellular functions:

A) Membrane potential (V_m). By altering the membrane potential of the cell, ion channels can impact on the activity of other channels and Ca^{2+}-dependent signalling events. In the cell cycle, transient changes in the membrane potential are essential for progression. During the G_1/S transition, a transient hyperpolarisation caused by K^+ efflux is required, whereas depolarisation caused by Cl^- efflux is essential at the G_2/M transition. The membrane potential of cancer cells if often depolarised and this promotes continuous Na^+ influx and invasive phenotypes.

B) Ca^{2+} signalling. Ca^{2+} influx results in activation of downstream Ca^{2+} signalling events, which can lead to Ca^{2+}-dependent transcription and has functional consequences (proliferation and migration). Ca^{2+} efflux systems are required to regulate intracellular Ca^{2+} concentrations, which will prevent Ca^{2+} overload and apoptosis.

C) Cell volume. Changes in cell volume require the coordinated activity of multiple channels and transporters, for cell shrinkage net K^+ and Cl^- efflux results in H_2O efflux, whereas for cell swelling net Na^+ and Cl^- influx causes H_2O influx.

D) Intracellular pH. To increase the intracellular pH, coordinated ion channel and transporter activity is needed, which results in net H^+ efflux.

Figure adapted from Becchetti (2011), Blackiston et al. (2009), Cuddapah and Sontheimer (2011), Fiske et al. (2006), Kunzelmann (2005), Pedersen et al. (2013), Schwab et al. (2012), and Yu (2003).

Membrane potential changes are also involved in cell apoptosis and migration. Early apoptotic pathways involve enhanced K^+ efflux, which results in an initial hyperpolarisation of the membrane potential, followed by Ca^{2+} overload, and depolarising events of the plasma and mitochondrial membranes (Lehen'kyi et al., 2011; Yu, 2003). In order to resist apoptosis, some cancers downregulate specific KCh (decreased mitochondrial $K_V1.5$ expression is detected in lung and glioblastoma cancer cell lines), or upregulate certain transporters to restore intracellular K^+ ion concentrations (such as Na^+/K^+ ATPase; Bonnet et al., 2007; Lehen'kyi et al., 2011; Yu, 2003). Activation of TRPM8 channels in bladder cancer cells results in Na^+/Ca^{2+} entry and causes mitochondrial membrane depolarisation leading to cell death (Lehen'kyi et al., 2011).

1.5.4.2 Ca^{2+} signalling

Membrane potential changes can alter the driving force for Ca^{2+} entry into the cell, the response caused depends on the voltage change and the subset of Ca^{2+} channels expressed (Becchetti, 2011; Schwab et al., 2012). K^+ efflux results in membrane potential hyperpolarisation and increases the electrical driving force for Ca^{2+} entry through voltage-independent Ca^{2+} channels, such as TRP channels (Schwab et al., 2012). Increased expression of TRPV6 channel protein (Ca^{2+} selective and constitutively activate channels) correlates with prostate cancer invasion and progression (Lehen'kyi et al., 2007). TRPV6 overexpression has also been detected in thyroid, colon, ovarian, and breast cancers (Monteith et al., 2012). Ca^{2+} influx, through TRPC3 and TRPC6 channels, is also linked to membrane depolarisation that occurs during G_2/M progression (Monteith et al., 2012). Ca_V channels are activated by membrane depolarisation and cause Ca^{2+} influx, increased Ca_V channel expression has been detected in a number of cancers, including $Ca_V3.2$ in prostate cancer and $Ca_V1.2$ in colon cancer (Fiske et al., 2006; Li and Xiong, 2011). In addition, localised Ca^{2+} entry through store-operated Ca^{2+} entry channels has been linked to cancer cell functions (Feng et al., 2010; Monteith et al., 2012; Yang et al., 2009). Store-operated Ca^{2+} entry is required for breast cancer migration, with Orai1 and STIM1 protein overexpression correlating with poor prognosis in breast cancer (McAndrew et al., 2011; Yang et al., 2009). Inhibition of Orai1 also results in decreased breast cancer cell line proliferation due to reduced Ca^{2+} influx, this decreases ERK1/2 phosphorylation and cyclin D1 activity (Feng et al., 2010; Monteith et al., 2012).

Ca^{2+} influx will trigger downstream signalling events which can have long-term functional consequences (Figure 1.10). For example, by modulating the activity of Ca^{2+}-dependent transcription factors (such as NFAT, NF-κB, and CREB) which regulate cell cycle proteins (cyclins D and E, CDKs, c-Myc, and E2F), in addition to influencing calmodulin-dependent signalling pathways (Figure 1.10; Monteith et al., 2012; Prevarskaya et al., 2013).

Ca^{2+} transporters have also been proposed to be involved in the regulation of cancer cell functions, for example it has been hypothesised that Na^+/Ca^{2+} exchanger (NCX1) will promote Ca^{2+} influx/Na^+ efflux and altered Ca^{2+} signalling in response to the high intracellular Na^+ levels which have been observed in cancer cells (Blaustein and Lederer, 1999; Dong et al., 2010, Monteith et al., 2007). Depending on the concentrations gradients, NCX1 can transport Ca^{2+} and Na^+ ions in either direction (Monteith et al., 2007). It has been found that in pancreatic cancer cells, decreased Ca^{2+} entry caused by knocking down NCX1 expression reduces cancer cell motility (Dong et al., 2010). Although, altered NCX1 expression has not been identified in cancer tissue, compared to matched normal tissue controls, within the published literature.

Generally, the upregulation of channels and transporters to allow Ca^{2+} influx is beneficial to cancer cells, however a balance is required with Ca^{2+} efflux to prevent Ca^{2+} overload and apoptosis (Monteith et al., 2012). As a result of this, the upregulation of Ca^{2+} ATPases to transport Ca^{2+} from the cytoplasm, against its concentration gradient, either into the ER (sarcoendoplasmic reticulum Ca^{2+} ATPase; SERCA) or extracellular environment (plasma membrane Ca^{2+} ATPase; PMCA) has been observed in cancer cells (Table 1.3; Monteith et al., 2012; VanHouten et al., 2010). For example, in breast cancer cell lines, PMCA2 expression will reduce apoptosis and this may be involved in the cancer cells acquiring an anti-apoptotic phenotype (Monteith et al., 2012; VanHouten et al., 2010). In support of this, the overexpression of PMCA2 protein in breast cancer tissue correlates with poor prognosis (VanHouten et al., 2010).

1.5.4.3 Cell volume

In addition to regulating the membrane potential and Ca^{2+} signalling, ionic gradients are essential in determining cell volume, by influencing the movement of water across the plasma membrane (Becchetti, 2011; Lang et al., 1998; Lang et al., 2007; Lang et

al., 2005). Cell volume regulation is linked to a number of cancer hallmark functions, including proliferation, apoptosis, and migration. For cell migration, cooperative activity of ion channels and transporters is required, which enables cell swelling at the leading edge and cell shrinkage at the trailing edge (Schwab et al., 2012). At the leading edge, cell swelling occurs due to net Na^+, Cl^-, and water uptake; to facilitate this many cancer cells upregulate multiple channels and transporters: epithelium Na^+ channel (ENaC: Na^+ influx), Na^+/H^+ exchanger (NHE1: H^+ efflux and Na^+ influx), Na^+-K^+-Cl^- co-transporter (NKCC1: influx of Na^+, K^+ and 2 Cl^- ions), anion exchange protein 2 (AE2: Cl- influx and $HCO3^-$ efflux), and aquaporin 1/4 (AQ1/4: water influx, Figure 1.11 C; Benga and Huber, 2012; Black and Waxman, 2013; Li and Xiong, 2011; Ousingsawat et al., 2008; Schwab et al., 2012). Cell shrinkage occurs at the trailing edge due to net KCl efflux which results in a loss of water and several ion channels have been linked to this: ClC-3 (Cl^- efflux), volume regulated anion channel (VRAC: Cl^- efflux), KCh ($K_{Ca}3.1$ and $K_V1.3$: K^+ efflux) and AQP (Figure 1.11 C; Benesova et al., 2012; Bobak et al., 2011; Huang et al., 2012; Lang et al., 2005; Pedersen et al., 2013; Schwab et al., 2012).

Cell volume control is also critical in regulating proliferation and apoptosis. In cancer, some channels involved in increasing cell volume are upregulated to resist the cell shrinkage which is associated with apoptosis (Benga and Huber, 2012; Pedersen et al., 2013). For example, cell shrinkage can be counteracted by upregulation of NHE1, NKCC1 and hypertonicity induced cation channel (HICC: molecular identity is currently unknown; Amith and Fliegel, 2013; Garzon-Muvdi et al., 2012; Numata et al., 2008; Pedersen et al., 2013; Pedersen and Stock, 2013).

1.5.4.4 Intracellular pH

Upregulation of channels and transporters that regulate intracellular pH is critical in the metabolic programming of highly glycolytic cancer cells (Figure 1.11 D), since increased glucose metabolism produces acidic by-products (such as lactate and carbonic acids) resulting in intracellular acidification (Pouyssegur et al., 2006). To compensate for this, cancer cells often have alkaline intracellular pH due to the upregulation of proton pumps, such as NHE1, H^+/lactate transporter, and Na^+-HCO_3 co-transporter (Amith and Fliegel, 2013; Arcangeli, 2011; Izumi et al., 2003; Pedersen and Stock, 2013). This upregulation contributes to the acidic pH of the surrounding cancer microenvironment and promotes

cell invasion (Arcangeli, 2011; Izumi et al., 2003). Co-expression of $Na_V1.5$ and NHE1 in breast cancer cells enhances H^+ efflux and pH-dependent extracellular matrix degradation, by favouring the proteolytic activity of cysteine cathepsins B and S which promote cell invasion (Brackenbury, 2012; Gillet et al., 2009). Increased Na^+/K^+ ATPase activity may act in combination with NHE1 to restore low intracellular Na^+ concentrations, and Na^+/K^+ ATPase α subunit overexpression has been detected in colon and lung cancers (Kunzelmann, 2005; Mijatovic et al., 2008).

1.5.4.5 Regulation of ion channel and transporter expression (mRNA and protein) and activity by cancer cell signalling pathways

Altering the mRNA and protein expression levels of subsets of ion channels and transporters in cancer may allow beneficial cellular functions to be acquired, for example cell proliferation, without detrimental effects, such as increased apoptosis. One way by which the expression and activity of ion channels and transporters may be controlled is via cell signalling pathways, with many channels regulated by key pathways involved in cancer cell functions (Arcangeli, 2011; Becchetti, 2011; Fraser et al., 2014; Frede et al., 2013; Pedersen et al., 2013). In non-small lung cancer cells (H460 cell line) $Na_V1.7$ mRNA is upregulated via EGFR/ERK1/ERK2 signalling, which results in increased $Na_V1.7$ channel activity at the cell surface and cell invasion (Campbell et al., 2013; Fraser et al., 2014). In addition, cell migration in rat prostate cancer cells (PCa cell line) is enhanced by a functional upregulation of the $Na_V1.7$ α subunit, which is stimulated by EGF and NGF signalling pathways (Brackenbury and Djamgoz, 2007; Frazer et al., 2014; Uysal-Onganer and Djamgoz, 2007). In ovarian cancer cells, EGF signalling upregulates TRPC3 activity which may provide proliferative benefits, in addition AQP3 protein expression is increased by EGF/Akt/ERK signalling (Frede et al., 2013). A number of KCh are also regulated by GF. For example, in rat arterial smooth muscle cells IGF-1 inhibits K_{ATP} channel currents, via PI3K signalling (Hayabuchi et al., 2008), whereas induction of TGF-β/Ras/MEK/ERK signalling in fibroblasts upregulates Ca^{2+}-activated K^+ currents (Peña et al., 2000).

In summary, the variety of cellular functions which can be altered by ionic signalling pathways means that changes to ion channel and transporter expression and activity can have a multiple consequences in cancer. Thus, understanding the interactions formed

between different classes of ion channels and transporters will be critical in designing cancer therapies targeted against these proteins.

1.6 Functional roles of potassium channels in cancer

Growing *in vitro* and *in vivo* evidence has implicated altered ion channel expression in cancer, with the activity of KCh being implicated in cancer hallmarks and tumour progression (Fiske et al., 2006; Hanahan and Weinberg, 2000; Hanahan and Weinberg, 2011; Kunzelmann, 2005; Pedersen and Stock, 2013; Schönherr, 2005). To date, members of all four KCh superfamilies (K_V, K_{Ca}, K_{ir}, and K_{2P}) have been identified in a range of cancer types where they are associated with cancer cell functions (summarised in Table 1.4). This project is focused on the TASK channel family, based on the evidence for altered $K_{2P}9.1$ channel activity in cancer (Section 1.7.1). To understand the potential implications of altered K^+ efflux through K_{2P} channels in cancer, the published roles of KCh in both normal and cancer cell biology need to first be considered. The published evidence linking altered KCh expression and activity to cancer hallmark functions is presented in the following sections.

Table 1.4: Summary of potassium channel expression in cancer

Cancers where potassium channel expression has been detected; data are from either patient tissues or cell lines. At a cellular level, the functional impacts caused by aberrant expression of a particular channel are described.

Potassium channels are divided into superfamily groupings: voltage-gated (K_V), calcium-gated (K_{Ca}), inward rectifying (K_{ir}), and two-pore domain (K_{2P}).

(1) Wang et al. (2012), (2) Jang et al. (2009a), (3) Abdul and Hoosein (2006), (4) (Brevet et al., 2009a), (5) Brevet et al. (2009b), (6) Zheng et al. (2011), (7) Arvind et al. (2012), (8) Menéndez et al. (2010), (9) (Jang et al., 2009b), (10) Kim et al. (2010), (11) Rodriguez-Rasgado et al. (2012), (12) Menendez et al. (2012), (13) Wu et al. (2012), (14) Asher et al. (2011), (15) Agarwal et al. (2010), (16) Spitzner et al. (2008), (17) Ding et al. (2008b), (18) Ding et al. (2007), (19) Hammadi et al. (2012), (20) Wadhwa et al. (2009), (21) Huang et al. (2012), (22) Lastraioli (2004), (23) Afrasiabi et al. (2010), (24) Glassmeier et al. (2012), (25) Ding et al. (2008a), (26) Fortunato et al. (2010), (27) Banderali et al. (2011), (28) Shao et al. (2008), (29) Ma et al. (2012), (30) Ousingsawat et al. (2007), (31) Han et al. (2008), (32) Steinle et al. (2011), (33) Khaitan et al. (2009), (34) Coiret et al. (2007), (35) Cambien et al. (2008), (36) Chantôme et al. (2009), (37) Potier et al. (2006), (38) Potier et al. (2010), (39) Catacuzzeno et al. (2011), (40) Schmidt et al. (2010), (41) Lai et al. (2011), (42) Lallet-Daher et al. (2009), (43) Faouzi et al. (2010), (44) Lee et al. (2010), (45) Stringer et al. (2001), (46) Plummer et al. (2005), (47) Choi et al. (2011b), (48) Tan et al. (2008), (49) Veeravalli et al. (2012), (50) Park et al. (2008), (51) Huang et al. (2009), (52) Nunez et al. (2013), (53) Suzuki et al. (2012), (54) Voloshyna et al. (2008), (55) Innamaa et al. (2013a), (56) Nogueira et al. (2010), (57) Alvarez-Baron et al. (2011), (58) Mu et al. (2003), (59) Kim et al. (2004), (60) Kosztka et al. (2011), (61) Lee et al. (2012), (62) Innamaa et al. (2013b).

Channel	Expression detected	Functional impact	Ref
$K_V1.3$	Breast, lung, lymphoma, pancreatic, prostate	Apoptosis, poor prognosis, proliferation	1-5
$K_V1.4$	Gastrointestinal	Gene silencing	6
$K_V1.5$	Brain	Increased survival	7
$K_V3.4$	Head and neck	Proliferation	8
$K_V4.1$	Breast, gastrointestinal	Proliferation	9,10
$K_V10.1$	Bone, breast, cervical, colorectal, head and neck, kidney, leukaemia (acute myeloid), oesophageal, ovarian	Biomarker, migration, proliferation, poor prognosis	11-20
$K_V10.2$	Brain, kidney	Proliferation	20,21
$K_V11.1$	Breast, colorectal, gastrointestinal, head and neck, kidney, leukaemia (acute myeloid), lung, melanoma, oesophageal, ovarian, retinoblastoma, thyroid	Migration, proliferation, poor prognosis,	12,14,20,22-28
$K_{Ca}1.1$	Bone, brain, breast, ovarian, prostate	Apoptosis, metastases, microenvironment regulation, migration, proliferation	29-35
$K_{Ca}2.3$	Breast, colon, melanoma	Migration	36-38
$K_{Ca}3.1$	Brain, breast, colorectal, melanoma, prostate	Migration, proliferation	39-43
$K_{ir}2.2$	Breast, gastrointestinal, prostate	Cell cycle progression	44
$K_{ir}3.1$	Breast, lung, pancreatic	Metastases, proliferation	4,45,46
$K_{ir}3.4$	Aldosterone-producing adenomas	Mutations detected	47
$K_{ir}4.1$	Brain	Migration, poor prognosis	48,49
$K_{ir}6.1$/ $K_{ir}6.2$	Brain, breast, melanoma, uterine	Apoptosis, cell cycle progression, proliferation	50-53
$K_{2P}2.1$	Prostate, ovarian	Proliferation	54,55
$K_{2P}3.1$	Aldosterone-producing adenomas	Aldosterone production	56
$K_{2P}5.1$	Breast	Proliferation	57
$K_{2P}9.1$	Breast, colorectal, lung, melanoma, Ovarian	Apoptosis, migration, mitochondrial function, proliferation	58-62

1.6.1 Potassium channels as cancer biomarkers

In addition to having functional roles in cancer cells, the distinct expression patterns of specific KCh in cancer has led to the proposal that these proteins might be useful biomarkers for certain cancer types (D'Amico M et al., 2013; Rodriguez-Rasgado et al., 2012). For example, the expression of $K_V10.1$ is altered in a number of cancers (Table 1.4) and may serve as a biomarker for cervical, colorectal, and breast cancers, with channel expression detected in pre-cancerous and malignant cells but not normal tissue (Rodriguez-Rasgado et al., 2012). Overexpression of $K_V10.1$ channels correlates with poor prognosis in breast, cervical, colorectal, and ovarian cancers (Asher et al., 2010; Ousingsawat et al., 2007; Rodriguez-Rasgado et al., 2012). Similarly, in a study of twelve cancer types compared to matched normal tissue controls, Bielanska et al. (2009) found that $K_V1.3$ protein expression was upregulated in 75 % of colorectal cancers, but not in the other eleven types. In contrast, $K_V1.5$ exhibited altered protein expression in all cancer types examined, with the exception of ovarian cancers (Bielanska et al., 2009). $K_V1.5$ showed high differential protein expression in bladder, renal, and skin cancers which may suggest that it could be used as a biomarker for cancer cells in these tissue types (Bielanska et al., 2009). To date, no evidence has suggested that K_{2P} channels expression has a role as biomarkers for specific cancers. Therefore, expanding upon the published data showing K_{2P} channel expression in cancer will be critical to determine if any K_{2P} channels are suitable cancer biomarkers.

1.6.2 Role of potassium channels in membrane potential control

A key role of KCh activity is to maintain the difference in K^+ concentrations across the plasma membrane, which is essential for setting the membrane potential of the cell. The membrane potential has been found to correlate with the proliferative potential of the cell and fast growing cells, such as cancer cells, commonly have a more depolarised RMP than their normal counterparts (Arcangeli et al., 1995; Enyedi and Czirják, 2010; Felipe et al., 2006; Olsen and Sontheimer, 2004; Sundelacruz et al., 2009). For example, glioma cells have a RMP of -40 mV compared to -80 mV for non-cancerous astrocytes (Olsen and Sontheimer, 2004). KCh activity causes hyperpolarisation of the membrane potential and based on this evidence this could be assumed to be anti-proliferative (Arcangeli et al., 1995; Olsen and Sontheimer, 2004; Sundelacruz et al., 2009). However, early evidence showed

that the proliferation of human breast carcinoma MCF-7 cells could be inhibited by broad spectrum KCh inhibition (using TEA, 4-AP, quinidine, glibenclamide, or linogliride; Wonderlin and Strobl, 1996). Since this discovery, it has been found that as cells proceed through the cell cycle ion channel activity changes and this is believed to be instrumental in driving the oscillatory rhythm of the cell cycle (Kunzelmann, 2005; Sundelacruz et al., 2009). A transient hyperpolarisation caused by K^+ efflux is required for cell cycle progression through the G_1/S transition (Arcangeli et al., 1995; Pardo, 2004; Sundelacruz et al., 2009; Wang, 2004; Wonderlin and Strobl, 1996). Regulation of the membrane potential also alters the electrochemical driving force for Ca^{2+} and Na^+ entry into the cell (Figure 1.11). Membrane hyperpolarisation, which may occur as a result of KCh overexpression, will increase Ca^{2+} influx through voltage-independent Ca^{2+} channels (such as TRP channels). In contrast, membrane depolarisation, which may occur in response to decreased KCh activity, will result in Ca^{2+} entry through Ca_V channels (Schwab et al., 2012). A depolarised membrane potential will also result in a persistent Na^+ influx (through Na_V channels; Section 1.5.4.1) and this promotes invasive phenotypes (Blackenbury, 2012; Campbell et al., 2013; Gillet et al., 2009; Roger et al., 2007; Yang and Blackenbury, 2013).

1.6.3 Role of potassium channels in cell proliferation

In glial progenitor cells, inhibiton of KCh using TEA prevents G_1 progression and causes an accumulation of CDK inhibitors, suggesting that KCh activity can regulate cell cycle proteins (Ghiani et al., 1999). KCh activity can also be regulated by GF. Thus, Gamper et al. (2002) showed that the mRNA expression of several K_V channels (K_V1.1-4, K_V3.1, and K_V3.4) expressed in HEK293 cells were upregulated in response to IGF-1 treatment. In addition, a study of three cancer cell lines showed that EGF exposure causes K^+-dependent membrane hyperpolarisation, intracellular Ca^{2+} oscillations, and fluctuations in the membrane potential, although the resulting effects on proliferation were not studied (Pandiella et al., 1989). In SH-SY5Y neuroblastoma cells, K_V11.1 mRNA expression has been shown to vary throughout the cell cycle, with increased K_V11.1 mRNA correlating with membrane hyperpolarisation and an inhibition of K_V11.1 activity preventing cell proliferation (Crociani et al., 2003). The precise functional impacts of membrane potential alterations caused by KCh are unclear; however experimental data indicated that KCh activity can influence cell growth by regulating Ca^{2+} signalling and cell volume (Bortner and Cidlowski, 2007; Felipe et al., 2006; Lang et al., 1998; Pardo, 2004; Wang, 2004). At this

time, there has been little investigation into how KCh activity can impact on other ion channels expressed in cancer cells (see Table 1.3 and Figure 1.11). However, one characterised example is in LNCaP prostate cancer cells where $K_{Ca}3.1$ activation has been shown to result in membrane hyperpolarisation (from -47 mV at rest to -71 mV) and promote Ca^{2+} entry through TRPV6 cation channels (Lallet-Daher et al., 2009).

A well characterised role of KCh activity in cell proliferation is during T lymphocyte activation and subsequent divisions. DeCoursey et al. (1984) discovered that the application of broad spectrum KCh inhibitors (TEA and 4-AP) reduces the whole-cell outward currents and mitogen-stimulated activation of T lymphocytes. At rest, two classes of KCh ($K_V1.3$ and TASK channels) contribute to the RMP (-50 mV) in lymphocytes (Cahalan et al., 2001; Meuth et al., 2008a; Panyi et al., 2004; Pardo, 2004). Activation of T lymphocytes stimulates Ca^{2+} influx, which causes a depolarisation of the membrane potential and increases $K_V1.3$ channel activity, in addition to activating $K_{Ca}3.1$ channels (Panyi et al., 2004). KCh activity will result in a membrane hyperpolarisation which increases the driving force for Ca^{2+} entry via Ca^{2+}-release-activated channels (CRAC) which have increased activity at negative membrane potentials (Cahalan et al., 2001; Panyi et al., 2004). The prolonged stimulation of Ca^{2+} influx, triggered by KCh activity, is proposed to cause a sustained response which can influence gene expression (Panyi et al., 2004). Although TASK channel activity is independent of membrane potential changes, the channels have been shown to be involved in T lymphocyte activation, as reduced cytokine (IFNγ and IL-2) secretion and proliferation was measured in the presence of the TASK channel inhibitors anandamide and ruthenium red (Meuth et al., 2008a). The role played by TASK channel activity in T lymphocyte activation has not been defined. However, TASK channel activity has been hypothesised to regulate K^+ efflux and hyperpolarise the membrane potential (alongside $K_V1.3$ and $K_{Ca}3.1$ channel activity), a process which is critical for regulating Ca^{2+} entry via CRAC channels (Meuth et al., 2008a).

Controlling the cell volume is also essential for proliferation, with an increased cell volume required as cells undergo mitosis and split into two daughter cells (Bortner and Cidlowski, 2007; Lang et al., 1998; Wang, 2004). In glioma cells, there is a narrow volume range where the cell growth rates will be the highest (Pardo, 2004). KCh inhibiton in SH-SY5Y neuroblastoma cells prevents proliferation, by causing a 25 % increase in cell volume (Rouzaire-Dubois and Dubois, 1998).

In cancer, there are numerous examples where KCh channel activity provides a proliferative advantage, by the regulation of Ca^{2+} signalling and/or cell volume (Table 1.4). In MCF-7 breast cancer cells, $K_V10.1$ channel inhibition prevents IGF-1-induced CDK upregulation and causes G_1 cell cycle arrest (Borowiec et al., 2011; Borowiec et al., 2007). The activity of $K_V11.1$ and $K_{Ca}3.1$ channels is essential for MCF-7 cell cycle progression, by causing membrane hyperpolarisation which is required at the G_1/S checkpoint, inhibition of both channels results in cell cycle arrest and CDK p21 accumulation (Faouzi et al., 2010; Ouadid-Ahidouch and Ahidouch, 2008; Ouadid-Ahidouch et al., 2004). In addition, when $K_V11.1$ and $K_{Ca}3.1$ channels are inhibited the intracellular Ca^{2+} concentration during the G_1 phase is reduced, suggesting that the activity of these channels regulates Ca^{2+} signalling (Ouadid-Ahidouch and Ahidouch, 2008). $K_{Ca}1.1$ channel activity may also be involved, as $K_{Ca}1.1$ activation in MCF-7 cells by 17-β-estradiol results in a modest increase in cell proliferation (Coiret et al., 2005; Oeggerli et al., 2012). KCh activity also influences MCF-7 cell volume, with $K_V7.1$ and $K_V11.1$ channel activity being involved in the regulatory decrease in volume response (RVD response) that occurs following hyposmotic shock induced cell swelling (Linsdell et al., 2008; vanTol et al., 2007). Inhibition of these channels prevents this RVD response. While the functional consequences of this in MCF-7 cells have yet to be identified, it is likely that this would prevent cell growth or induce apoptosis (Linsdell et al., 2008; vanTol et al., 2007).

In addition, $K_V11.1$ channels have a proliferative role in other cancer cell lines. Inhibition of $K_V11.1$ channel activity in SW2 small cell lung carcinoma cells results in membrane potential depolarisation, by 10 mV, and $K_V11.1$ siRNA knockdown results in a 50 % reduction in cell growth (Glassmeier et al., 2012). Knockdown of $K_V11.1$ mRNA expression in SH-SY5Y neuroblastoma cells also reduces cell growth by causing G_1 cell cycle arrest (Zhao et al., 2008). Inhibition of $K_V10.1$ or $K_V11.1$ channels in ovarian carcinoma SK-OV-3 cells decreases proliferation and causes accumulation of cells in the S phase (Asher et al., 2011). The downstream proliferative consequences of KCh activity have not been extensively characterised. However, as highlighted above, one example is LNCaP prostate cancer cells, where $K_{Ca}3.1$ activation promotes Ca^{2+} entry through TRPV6 cation channels and proliferation (Lallet-Daher et al., 2009).

1.6.4 Role of potassium channels in apoptosis

KCh activity is also involved in regulating apoptosis, with the activity of some channels promoting apoptosis while others reduce cell death (Lang et al., 2005; Wang, 2004). An early indicator of apoptosis is cell shrinkage, which is caused by the efflux of K^+ ions (Bortner and Cidlowski, 2007; Bortner et al., 1997; Dezaki et al., 2012). Lymphocyte cell death can be triggered by K^+ ion efflux; this can be inhibited by culturing cells in high external K^+ concentrations which reduces the driving force for K^+ efflux (Bortner et al., 1997). At physiological K^+ concentrations, cultured rCGN will undergo apoptosis due to outward flow of K^+ ions through TASK channels, and disruption of TASK channel activity using inhibitors (anandamide and ruthenium red) or targeted channel knockdowns protects these cells from K^+ mediated apoptosis (Lauritzen et al., 2003). In cortical neurons, application of broad spectrum KCh inhibitors (TEA and 4-AP) reduces the outward whole-cell K^+ currents and causes apoptosis (Yu et al., 1997). In erythrocytes, osmotic shock causes enhanced Ca^{2+} entry leading to increased efflux of K^+ (via $K_{Ca}3.1$ channels), Cl^-, and water which causes cell shrinkage and apoptosis (Lang et al., 2003).

In addition to having a proliferative role, $K_V11.1$ activity has also been linked to apoptosis in a number of cancer cell lines (Jehle et al., 2011). Reduction of $K_V11.1$ activity (by inhibitors or RNA interference) increases apoptosis in heterologously expressing HEK293 cells, as well as colorectal (HCT116) and gastrointestinal cancer cell lines (SGC7901, AGS, MGC803, and MKN45; Gong et al., 2010; Shao et al., 2005; Thomas et al., 2008; Zhang et al., 2012).

In CaCo-2 colorectal cancer cells, deoxycholate induces cell death by causing membrane hyperpolarisation and Ca^{2+} entry (Gerbino et al., 2009). Membrane hyperpolarisation in CaCo-2 cells is triggered by increased K_{Ca} currents, with exposure to K_{Ca} inhibitors (charybdotoxin and apamin) reducing the membrane hyperpolarisation and cell death triggered by deoxycholate (Gerbino et al., 2009). TNF-related apoptosis-inducing ligand (TUNAL) causes cell death in D54-MG glioblastoma cell line, by triggering an apoptotic volume decrease response, involving K^+ efflux through $K_{Ca}1.1$ channels (McFerrin et al., 2012). In HeLa cervical cancer cells, inhibition of $K_{Ca}1.1$ channels (using iberiotoxin) increases cell death and correlates with TP53 upregulation (Han et al., 2007). In contrast,

activation of $K_{Ca}1.1$ channels increases cell death in MDA-MB-231 breast carcinoma cells (Ma et al., 2012).

A number of ion channels are localised with the mitochondria membrane and have been implicated in the regulation of cell death (Gulbins et al., 2010; Leanza et al., 2013; Leanza et al., 2012). Lymphocytes express functional $K_V1.3$ channels within the inner mitochondrial membrane (mito$K_V1.3$; Gulbins et al., 2010). Inhibition of mito$K_V1.3$ activity, by membrane permeable inhibitors (Psora-4, PAP-1 and clofazimine) or binding of the apoptotic signalling protein Bax, causes mitochondrial hyperpolarisation and downstream cell death signalling events (such as ROS production and cytochrome C uncoupling; Gulbins et al., 2010; Leanza et al., 2012). Expression of mito$K_V1.3$ channels has been identified in breast (MCF-7) and prostate (PC3) cancer cells lines, although the functional impact on cell death has not been characterised (Gulbins et al., 2010).

1.6.5 Role of potassium channels in cancer metastasis

In a similar manner to regulating proliferation and apoptosis, KCh activity has also been shown to modulate cell migration, by altering the membrane potential, cell volume control, and intracellular Ca^{2+} signalling (Fiske et al., 2006; Schwab et al., 2012). Cell volume control is essential in migration, with cell retraction requiring volume shrinkage, due to water efflux which is driven by K^+ and Cl^- channel activity (Figure 1.11 C; Schwab et al., 2012; Sontheimer, 2008). Additionally, KCh may be involved in cytoskeletal rearrangements; for example in lymphocytes $K_V1.3$ interacts with integrin and other cell adhesion molecules (Levite et al., 2000). $K_V1.3$ activity is involved in the migration of lymphocytes, with $K_V1.3$ channel inhibition preventing cell migration by reducing Ca^{2+} signalling and integrin activation (Levite et al., 2000; Matheu et al., 2008). Furthermore, $K_V1.3$ and β_1-integrin are associated in melanoma cell lines (Artym and Petty, 2002). $K_V1.1$ activity has been linked to gastrointestinal epithelial cell migration by modulating Ca^{2+} signalling (Rao et al., 2002; Wang et al., 2000).

In cancer, altered KCh expression has been found to correlate with tumour metastases (Fiske et al., 2006). $K_{ir}3.1$ mRNA is overexpressed in 30 % of breast cancers compared to matched normal tissue controls and correlates with breast cancers which have invaded into surrounding lymph nodes (Stringer et al., 2001). Additionally, in breast

cancer higher $K_{Ca}1.1$ mRNA expression is detected in brain metastases compared to metastases present in other organs (Khaitan et al., 2009). Higher $K_{Ca}3.1$ protein expression has been detected in breast and prostate cancers which have metastasised to the bone (Chantôme et al., 2013). In metastatic gliomas reduced $K_V1.5$ mRNA expression is detected compared to low-grade glioblastoma (Preußat et al., 2003). In prostate cancer cell lines, differences in the whole-cell K^+ currents are detected depending on the invasive phenotypes; higher Ca^{2+}-activated currents are observed in invasive PC3 prostate carcinoma cells and larger voltage-sensitive K^+ currents are identified in the weakly metastatic LNCaP cells (Laniado et al., 2001).

The functional consequences of a number of KCh linked to breast cancer metastasis have been investigated. In the metastatic MDA-MB-231 breast cancer cell line, inhibition or knockdown of $K_V10.1$ results in membrane depolarisation, reduced Ca^{2+} entry, and cell migration (Hammadi et al., 2012). Ca^{2+} entry, stimulated by $K_V10.1$ activity, occurs through Orai1 containing CRAC channels, with increased expression of both channels ($K_V10.1$ and Orai1) correlating with invasive breast cancers and lymph node metastasis (Hammadi et al., 2012). Breast cancer cell metastasis is also likely to involve $K_{Ca}3.1$ channels, since $K_{Ca}3.1$ activity can also regulate Ca^{2+} entry through Orai1 channels, with both proteins associating in lipid rafts present on the plasma membrane during cell migration (Chantôme et al., 2013). The migration of melanoma cell lines is stimulated by $K_V11.1$ activity and this response is hypothesised to involve MAPK signalling, since $K_V11.1$ inhibition reduces MAPK phosphorylation (Afrasiabi et al., 2010). $K_{Ca}2.3$ is also expressed in melanomas, but not normal melanocytes, with knockdown of $K_{Ca}2.3$ in melanoma cell lines resulting in membrane depolarisation and reduced migration (Chantôme et al., 2009).

1.6.6 Role of potassium channels in angiogenesis

VEGF stimulates angiogenesis by increasing vascular endothelial cell proliferation (Hoeben et al., 2004). KCh activity is involved in angiogenesis and the proliferation of vascular endothelial cells is triggered by K^+-dependent membrane hyperpolarisation and Ca^{2+} influx (Erdogan et al., 2005; Grgic et al., 2005; Michaelis and Fleming, 2006). K_{Ca} channel activity ($K_{Ca}1.1$ and $K_{Ca}3.1$) is critical for the VEGF induced membrane hyperpolarisation and this response is prevented by exposure to K_{Ca} channel inhibitors (margatoxin, charaboxytoxin, clotrimazole, and TRAM-34; Erdogan et al., 2005; Grgic et al.,

2005; Michaelis and Fleming, 2006). Angiogenesis is reduced by 85 % *in vivo* when mice are treated with $K_{Ca}3.1$ inhibitors (Grgic et al., 2005). In addition, $K_{Ca}3.1$ activity is essential for vascular remodelling during pregnancy, vascular smooth muscle proliferation, and EGF-induced angiogenesis in the cornea (Bi et al., 2013; Grgic et al., 2005; Rada et al., 2012; Yang et al., 2013). Knocking down $K_{Ca}3.1$ expression in coronary artery smooth muscle cells reduces the increase in intracellular Ca^{2+} which is required to stimulate cell proliferation (Bi et al., 2013).

Compared to normal tissue, increased $K_{Ca}1.1$ and $K_{Ca}3.1$ mRNA expression is detected in endothelial cells from colorectal adenocarcinomas (Köhler et al., 2000). Although, the amplitude of Ca^{2+}-activated K^+ currents were comparable in cancerous and non-cancerous endothelial cells, the increased K_{Ca} channel expression in cancer endothelial cells correlates with a larger hyperpolarisation response to bradykinin (Köhler et al., 2000). K_V channel activity has also been linked to cancer angiogenesis. In heterologous expression systems, $K_V10.1$ expression promotes VEGF secretion, with this response correlating to the upregulation of HIF1 (Downie et al., 2008). $K_V10.1$ activity is hypothesised to be involved in the hypoxic response of cells which can induce angiogenesis (Downie et al., 2008). In glioblastoma tissue and cell lines (U138 and A172), $K_V11.1$ expression is upregulated and increased $K_V11.1$ activity stimulates VEGF secretion (Masi et al., 2005). Overexpression of $K_V11.1$ (mRNA and protein) and components of the VEGF-A pathway (increased mRNA expression of *vegf-a*, *flt-1*, *kdr*, and *hif-1α*) were detected in two sporadic retinoblastomas compared to normal tissue, suggesting a correlation between $K_V11.1$ and VEGF-A pathway expression (Fortunato et al., 2010).

1.7 Evidence linking K_{2P} channel expression to cancer

Of the fifteen K_{2P} channels only two members, $K_{2P}2.1$ (*KCNK2*) and $K_{2P}9.1$ (*KCNK9*), have been described to be overexpressed in cancer (Mu et al., 2003; Voloshyna et al., 2008). However, two other K_{2P} channels ($K_{2P}3.1$ (*KCNK3*) and $K_{2P}5.1$ (*KCNK5*)) have been identified in cancer cell lines (Alvarez-Baron et al., 2011; Nogueira et al., 2010). The published evidence linking these K_{2P} channels to cancer is outlined in the following sections:

1.7.1 $K_{2P}9.1$

$K_{2P}9.1$ was the first K_{2P} channel identified to play a role in cancer. Mu et al. (2003) described $K_{2P}9.1$ as a proto-oncogene, following the detection of genomic overexpression of *KCNK9* gene locus (8q24.3) in 10 % of breast carcinomas. The authors described the location of *KCNK9* on chromosome 8 as an amplification epicentre since *KCNK9* is encoded close to the published oncogene *c-Myc* (Mu et al., 2003). However, *KCNK9* amplification did not always correlate with an increase in *c-Myc* gene expression and the upregulation of *KCNK9* is hypothesised to be independent of *c-Myc* (Mu et al., 2003). *KCNK9* gene amplification correlated with at least a 5-fold mRNA upregulation in 44 % of breast cancer samples (Mu et al., 2003). Mu et al. (2003) also assessed $K_{2P}9.1$ protein expression in breast cancer and also found that 44 % of breast cancer tissue showed increased $K_{2P}9.1$ staining compared to normal tissue samples (Mu et al., 2003). These expression data suggested that an upregulation of $K_{2P}9.1$ at a genomic and mRNA level leads to increased protein expression.

Since this initial report, a number of studies have also shown $K_{2P}9.1$ channels to have a carcinogenic role (Liu et al., 2005; Mu et al., 2003; Pei et al., 2003). Overexpression of $K_{2P}9.1$ channels in mammary epithelial derived NmuMG or fibroblast NIH-3T3 cell lines did not result in a cancerous transformation of the cells (Mu et al., 2003). However, tumours developed within 3 months when these cells were injected into mouse models (Mu et al., 2003). In addition, mice injected with C8 fibroblasts (partially transformed mouse embryonic fibroblasts) stably expressing WT $K_{2P}9.1$ had increased tumour formation compared to those expressing a non-functional channel, suggesting that the oncogenic ability of $K_{2P}9.1$ relies on the functionality of the channel (Pei et al., 2003). Expression of a dominant-negative mutant channel ($K_{2P}9.1_{G95E}$) in Ben lung carcinoma cells, which have native $K_{2P}9.1$ expression, reduced proliferation by 50 % compared to untransfected cells, indicating that WT $K_{2P}9.1$ activity provides a growth advantage (Pei et al., 2003).

$K_{2P}9.1$ protein expression has now been identified in several carcinomas. $K_{2P}9.1$ protein was detected in 46 % of colorectal carcinomas compared to colorectal adenomas which did not express $K_{2P}9.1$ protein, suggesting that $K_{2P}9.1$ expression may be linked to colorectal cancer development (Kim et al., 2004). $K_{2P}9.1$ immunopositivity has also been observed in melanoma and ovarian carcinoma tissue sections, although in both cases the

expression levels were not different compared to benign melanocytes or normal ovarian epithelium, respectively (Innamaa et al., 2013b; Pocsai et al., 2006).

In addition, studies have shown that TASK channel activity is involved in the regulation of apoptosis. $K_{2P}3.1$ and $K_{2P}9.1$ channel activation in glioma cells by isoflurane results in an increase in the number of cells undergoing cell death (via necrosis or apoptosis; Meuth et al., 2008b). $K_{2P}9.1$ inhibition (by methanandamide or zinc) in ovarian cancer cell lines (SKOV-3 and OVCAR-3) will also increase apoptosis by 60 % compared to untreated cells (Innamaa et al., 2013b). In contrast, expression of $K_{2P}9.1$ in C8 fibroblasts results in reduced cell death following TNF-stimulation and this effect is not observed when a non-functional $K_{2P}9.1_{G95E}$ channel is expressed (Pei et al., 2003). Furthermore, stable expression of $K_{2P}9.1$ (or $K_{2P}3.1$) in C8 fibroblasts enhances survival under cell stress conditions (serum starvation and hypoxia), compared to control conditions or untransfected cells (shown by decreased expression of apoptotic markers; Liu et al., 2005). $K_{2P}9.1$ activity has also been linked to the migration of MDA-MB-231 breast cancer cells, where a siRNA knockdown of $K_{2P}9.1$ expression will increase migration, but overexpression of the WT channel will reduce migration (Lee et al., 2012).

In WM35 melanoma cells, $K_{2P}9.1$ channel protein colocalises with the mitochondria, in addition to being detected on the cell surface (Rusznak et al., 2008). Knockdown of $K_{2P}9.1$ in WM35 cells cause reduced cell numbers and mitochondrial function (Kosztka et al., 2011). The authors hypothesise that $K_{2P}9.1$ channels expressed within the mitochondrial membranes will support mitochondrial activity, ATP production, and this enhances cell survival (Kosztka et al., 2011).

These studies suggest that $K_{2P}9.1$ activity is involved in regulating three key cancer cell hallmark functions (proliferation, apoptosis, and migration) and it has been hypothesised that the functional effect of $K_{2P}9.1$ expression may depend on the cancer cell type (Patel and Lazdunski, 2004). In addition, the regulation of TASK channels by environmental parameters may mean that expression of $K_{2P}9.1$ may provide an oncogenic advantage to tumour cells in cell stress conditions (hypoxia or starvation; Liu et al., 2005; Mu et al., 2003).

1.7.2 K_{2P}2.1

Increased K_{2P}2.1 protein expression has been detected in prostate adenocarcinoma tissue compared to normal prostate epithelium (Voloshyna et al., 2008). When K_{2P}2.1 expression is knocked down in PC3 prostate carcinoma cells there is 45 % reduction in proliferation, however K_{2P}2.1 overexpression in Chinese hamster ovary (CHO) cells increased cell cycle progression (20 % rise in the number of cells in S phase; Voloshyna et al., 2008).

K_{2P}2.1 and K_{2P}10.1 protein expression have also been identified in both ovarian carcinomas and normal ovarian epithelium tissue (Innamaa et al., 2013a), suggesting that there is no differential expression of these channels in ovarian cancer. Innamaa et al. (2013a) proposed that K_{2P}2.1 channels may have a functional role in ovarian cancer cell lines (SKOV-3 and OVCAR-3), since decreased proliferation and increased apoptosis were observed following K_{2P}2.1 inhibition (using curcumin and L-methionine treatment). While these data indicated that K_{2P}2.1 channels may play a role in ovarian cancer cell death, curcumin and L-methionine have other cellular targets which were not investigated in this study (Innamaa et al., 2013a).

1.7.3 K_{2P}3.1

There is some evidence which suggests that the expression of K_{2P}3.1 channels may be altered in cancer. Downregulation of the *KCNK3* gene was observed in colorectal cancers from patients with an unfavourable prognosis, compared to those with a more favourable outcome (Cavalieri et al., 2007). K_{2P}3.1 mRNA has been detected in aldosterone-producing adrenal adenomas (benign tumours), however this expression was not differential compared to normal tissue controls (Nogueira et al., 2010). Expression of either K_{2P}3.1 or K_{2P}9.1 channel protein, but not both, are increased in medulloblastoma tissue and cell lines compared to normal tissue controls (Ernest et al., 2010). In addition, a TASK-like background K^+ current has been identified in the DAOY medulloblastoma cell line (Ernest et al., 2010). However, no functional consequences linked to K_{2P}3.1 activity in these cancers have been identified.

1.7.4 $K_{2P}5.1$

Transcriptome analysis of the human T47D ductal breast cancer cell line, measured in response to oestrogen receptor (ERα and ERβ) signalling, showed that $K_{2P}5.1$ mRNA was upregulated by proliferative ERα signalling but downregulated by anti-proliferative ERβ signalling (Williams et al., 2007a). In T47D and MCF-7 breast cancer cell lines, $K_{2P}5.1$ mRNA, protein, and functional (outward acid-sensitive K^+ currents) expression has been shown to increase in response to ERα signalling (caused by 17β-estradiol stimulation; Alvarez-Baron et al., 2011). This regulation is due to an oestrogen response element in the promoter of the *KCNK5* gene (Alvarez-Baron et al., 2011). siRNA knockdown of $K_{2P}5.1$ channel expression causes a modest reduction in the basal proliferation of T47D cells, but significant decreases in the oestrogen-induced proliferation, this suggests that $K_{2P}5.1$ has a role in oestrogen-induced cell growth (Alvarez-Baron et al., 2011). The expression of $K_{2P}5.1$ protein in breast cancer tissue samples has yet to be examined, so it is unknown if $K_{2P}5.1$ is differentially expressed in cancer compared to normal breast tissue.

1.7.5 Expression of other K_{2P} channels in cancer

Hypermethylation of gene promoters is responsible for gene silencing (Berdasco and Esteller, 2010). In cancer, the hypermethylation of ion channel genes (Ca^{2+} channel; *CACNAIG* and Na^+ channel; *SLC5A8*) is thought to have a role in tumour suppression (Shu et al., 2006). The promoter of *KCNK15,* which encodes $K_{2P}15.1$, has been found to be hypermethylated in colorectal and leukaemia cancer cell lines (Shu et al., 2006). The functional implications of altered *KCNK15* gene expression are unknown, as this channel is thought to be non-functional (Kim and Gnatenco, 2001). Additionally, *KCNK2* (encoding $K_{2P}2.1$) is differentially methylated in acute lymphoblastic leukaemia compared to normal lymphocytes (Taylor et al., 2007). Three separate microarray analyses have found altered gene copy numbers for *KCNK12* in cancer compared to normal tissue. Increased *KCNK12* copy numbers were detected in synovial sarcoma (Nakagawa et al., 2006a) and peripheral nerve sheath tumours (Nakagawa et al., 2006b), in addition to reduced copy numbers in 52 % of tubular breast cancers (Riener et al., 2008). This evidence suggested that wider range of K_{2P} channels may be expressed in cancer than has been identified in published studies at this time.

1.8 Summary of the current evidence which has linked TASK channel expression and activity to cancer

A number of studies have identified altered expression and functional roles for TASK channels in cancer, following the discovery of genomic amplification of *KCNK9* in breast cancer (Mu et al., 2003). K_{2P}9.1 protein has now been detected in several cancers, with differential expression (compared to control tissue) observed in breast and colon cancers. In addition, K_{2P}9.1 protein has been identified in ovarian cancers and melanomas, although in these cancers the expression detected was not altered compared to matched normal tissue controls (Innamaa et al., 2013b; Kim et al., 2004; Mu et al., 2003; Pocsai et al., 2006). K_{2P}3.1 channels have been linked to poor prognosis in colon cancer (gene downregulation; Cavalieri et al., 2007) and detected in adrenal adenoma tissue (mRNA; Nogueira et al., 2010).

Pei et al. (2003) showed that expression of a functional K_{2P}9.1 channel, which can conduct K^+ ions, promoted proliferation in C8 fibroblasts and lung cancer cells. Following this study, K_{2P}9.1 channel activity has been linked to three cancer cell functions: proliferation (Kosztka et al., 2011; Pei et al., 2003), apoptosis (Innamaa et al., 2013b; Meuth et al., 2008b; Pei et al., 2003), and migration (Lee et al., 2012). However, the specific functional implications of K_{2P}9.1 channel activity in cancer are not clear. K_{2P}9.1 expression is beneficial in certain cell types by promoting cell growth (lung cancer and melanoma cells) and resistance to apoptosis (C8 fibroblasts and ovarian cancer cells), but K_{2P}9.1 channel activity is detrimental in glioma cells as it encourages cell death. In addition, K_{2P}3.1 and K_{2P}9.1 channels are hypothesised to promote cell survival under environmental stress conditions which are experienced within the cancer microenvironment (such as hypoxia or nutrient restriction; Liu et al., 2005; Rusznak et al., 2008).

Physiologically, in non-cancer cells, a fundamental role of TASK channel activity is to influence the membrane potential, which can impact on the activity of other ion channels (Introduction 1.2.4 and 1.5.4; Enyedi and Czirják, 2010; Goldstein et al., 2001). Consequently, this could be the basis of the functional role of TASK channels in cancer. However, this is an emerging area of research with a limited number of reports, several of which suggest that the functional impact of TASK channel expression on cancer cells is not universal, and this is comparable to the functional roles of other ion channels in cancer

(Figure 1.11). Therefore, the consequence of TASK channel activity in cancer may depend on the other channels and transporters which are expressed in a given cancer cell type. The current hypotheses (which have been based on the functional roles resulting from the overexpression of other classes of KCh in cancer cells) are that, in addition to regulating the membrane potential, increased TASK channel activity may also influence Ca^{2+}-dependent signalling and cell volume control (Figure 1.12). In summary, the published evidence and hypotheses have suggested that modulation of TASK channel activity in cancer cells could have functional impacts, either or by altering the activity of other ion channels or by directly regulating cancer hallmark functions (Figure 1.11).

1.8.1 Key research questions arising from the literature

Despite the identification of *KCNK9* as a proto-oncogene eleven years ago, the role of K_{2P} channels in cancer cells is an emerging area of research. Thus, understanding how K_{2P} channel activity influences the membrane potential and other ion channels expressed in cancer cells is a critical question which requires investigation. However, prior to addressing these critical research questions there are several lines of investigation which need addressing. These lines of investigation include, establishing the extent of K_{2P} channel expression in cancer, and determining the functional effects of TASK channel activity in cancer cells. Therefore, the key research questions surrounding this project are outlined below:

(i) Four K_{2P} channels have been linked to cancer to date. However, no comprehensive study has been conducted to determine if the expression profile of the entire K_{2P} channel family undergoes alterations in cancer. The expression of different K_{2P} channels may promote different functional advatanges to cancer cells, due to the different regulation properties of the K_{2P} channel family.

(ii) The published studies which have identified functional roles for $K_{2P}9.1$ channel expression in cancer cells have linked channel activity to three cancer hallmark functions. However, no study has been conducted to investigate what accounts for the apparent cell-specific roles of $K_{2P}9.1$ channel expression in cancer cells. This effect is hypothesised to depend on the other channels expressed within the cancer cells. Therefore, will the functional impact of TASK channel activity on cancer cells vary depending on cancer type or K_{2P} channel expression patterns?

(iii) It has been hypothesised that the regulation of TASK channel activity by acute alterations in the environment (e.g. hypoxia and pH) is involved in the advantages of channel expression in cancer. However, no study has investigated the regulation of channel activity by chronic environmental alterations which are experience in the cancer microenvironment.

The data presented in this thesis aimed to explore these questions by examining the overall hypothesis and chapter aims outlined in Section 1.9.

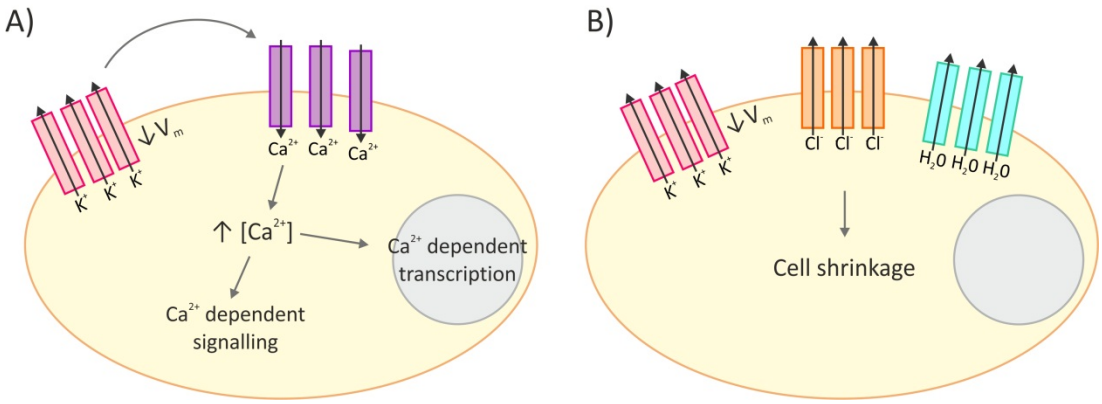

Figure 1.12: Potential impacts of increased TASK channel activity on cancer cell functions

Illustrating two potential mechanisms for how increased TASK channel activity in a cancer cell can impact on cellular functions. These mechanisms are based on the published hypotheses for how increased KCh activity can influence cancer cell functions. See Figure 1.11, for an overview of other ionic signalling pathways which have been identified in cancer.

A) TASK channel activity (red) causes membrane potential hyperpolarisation (↓ V_m). This increases the driving force for Ca^{2+} entry, via voltage independent Ca^{2+} channels (purple) e.g. TRP channels. The subsequent increase in intracellular Ca^{2+} concentrations may have downstream effects, such as Ca^{2+}-dependent cell signalling and transcription.

B) Cooperative TASK channel activity (red) and Cl^- channel activity (orange) will result in the efflux of K^+ and Cl^- ions from the cell, this leads to water efflux via aquaporins (blue) which causes cell shrinkage.

Figure is based on the data and hypotheses from Bortner and Cidlowski (2007), Felipe et al. (2006), Kunzelmann (2005), Lang et al. (1998), Lallet-Daher et al. (2009), Pardo, (2004), Pardo and Stuhmer (2014), Wang (2004), and Wonderlin and Strobl, 1996.

1.9 Hypothesis and aims

The expression of TASK channels in cancer will provide a functional advantage to cancer cells. To investigate this hypothesis, and some of the key research questions which have emerged from the field, this study has four specific aims:

i) To utilise bioinformatics to examine the mRNA expression profile of K_{2P} channels in cancer tissues compared to matched normal tissue controls. This approach was selected as it allowed the expression profile in cancer tissue of all members of the K_{2P} channel family to be determined.

ii) To identify clinically relevant model cancer cell lines, through the characterisation of TASK channel expression in human cancer cell lines and tissues. This allowed any impacts of TASK channel inhibition on cancer cell functions to be related to the channel expression profile in Aims (iii) and (iv).

iii) To determine the impact of TASK channel inhibition on cancer cell functions under normal cell culture conditions.

iv) To determine the regulation of TASK channels by environmental conditions and the impact of this on cancer cell functions.

Chapter 2

Materials and Methods

2.1 Chemicals and reagents

Unless otherwise stated, all chemicals and reagents were obtained from Sigma-Aldrich.

2.2 Bioinformatics

Analysis of K_{2P} channel mRNA expression in cancer (meta-analysis of *KCNK* genes and related statistical analyses) was performed using the online cancer microarray database, Oncomine (www.oncomine.org, Compendia biosciences, Ann Arbor, MI, USA). Oncomine collects publicly available cancer microarray studies and reprocesses all data imposing the same analysis criteria (Rhodes et al., 2004). The mRNA expression data are organised into cancer types defined within the original publications and all data were extracted from Oncomine between August 2012 and January 2013. All the datasets used from Oncomine in this thesis, including histological classification of the cancer tissues examined in each dataset, are referenced in Appendix 2.

Only datasets examining the mRNA expression of K_{2P} channels in cancer tissues matched with normal tissue controls (cancer vs. normal) were included in this study and threshold criteria had to be achieved by each study for inclusion in the analysis. The threshold search criteria used for this study were a p-value < 0.05, a fold change > 2, and a gene rank percentile < 10 %. The p-values presented in this study were calculated by Oncomine using a two-sided Student's *t*-test with multiple testing correction and a p-value less than 0.05 was considered significant (Rhodes et al., 2007; Rhodes et al., 2004). Multiple testing correction was performed using the false discovery rate method, corrected p-values (Q-values) were calculated as Q = NP / R, where P = p-value, N = total number of genes, and R = sorted rank of p-value (Rhodes et al., 2007; Rhodes et al., 2004). Fold change is defined as the linear change in mRNA for the gene of interest in cancer tissue when compared to the normal expression level for that tissue. In this thesis a fold change of < 2 was included for analysis. For each dataset, the genes studied are ranked by their p-value and the gene rank percentile is the percentage ranking of the gene of interest compared to all other genes analysed in that dataset based on their p-values. The average number of genes examined in the microarray data presented in this study was approximately 14,000 genes.

Only datasets in which the K_{2P} channel of interest was in the top 10 % of genes changed were included. Additionally, these threshold values are connected by the Boolean AND, therefore an analysis was only classed as above threshold when it met all three criteria.

Initially K_{2P} channels (*KCNK1-18*) were examined across a range of 20 cancer types which have been grouped by their tissue of origin (Table 2.1), comparing the mRNA expression in that cancer type to normal tissue controls. The gene summary view in Oncomine was utilised during this analysis and presented in this thesis, with the gene expression ranking indicated by colour shading. Expression colouring for a gene in a particular cancer related to the gene rank percentile for the highest ranked above threshold analysis.

Further analysis was performed on each K_{2P} channel in the most prevalent cancer types based on the GLOBACON 2008 World Health Organisation rankings (http://globocan.iarc.fr/; Ferlay et al., 2008). Lymphoma, myeloma, sarcoma, liver, and ovarian cancers were removed from further analysis due to low K_{2P} channel mRNA expression (Table 2.1). The subtype 'other cancers' which is defined as cancers that do not fall into the prescribed subtypes (e.g. uterine and adrenal cancers) was also removed from further analysis, as the large diversity of cancer subtypes within this group would make detailed analysis uninformative (Table 2.1). All above threshold analyses for each K_{2P} channel were extracted from Oncomine and compiled using the threshold criteria described above. Once all above threshold data for each K_{2P} channel had been compiled, comparative meta-analysis was performed on each cancer subtypes with more than three datasets available ($n \geq 3$), these analyses provide a median gene rank and median p-value for that cancer subtype.

Table 2.1: Cancer inclusion

Shown are the 20 cancer types examined in the gene summary view and those included for comparative meta-analysis (indicated by X). The number of above threshold datasets for K_{2P} channel mRNA expression are also indicated.

Cancer	Number of above threshold datasets	Used for detailed analysis
Bladder	3	X
Brain and CNS	8	X
Breast	9	
Cervical	3	X
Colorectal	4	X
Gastrointestinal	3	X
Head and Neck	6	X
Kidney	6	X
Leukaemia	3	X
Liver	1	
Lung	8	X
Lymphoma	2	
Melanoma	3	X
Myeloma	1	
Oesophageal	4	X
Other	7	
Ovarian	0	
Pancreatic	5	X
Prostate	4	X
Sarcoma	1	

2.3 Molecular Biology

2.3.1 Bacterial transformation

Transformation of competent cells was performed in different types of *E. coli* cells depending on the experiment requirements. DH5α *E. coli* cells (Invitrogen) were transformed to prepare DNA for most manipulations, except for site-directed mutagenesis products (Method 2.3.5) where XL10-Gold Ultracompetent *E. coli* cells (Agilent Technologies) were used.

To transform DH5α *E. coli* cells, 50 µl of competent bacteria were thawed on ice, mixed with 1-100 ng of DNA, and incubated on ice for 30 minutes (min). Cells were subjected to heat shock at 42 °C for 20 seconds (s), incubated on ice for 2 min, mixed with 950 µl of LB medium, and incubated at 37 °C, 225 rpm for 1 hour (h). The culture was centrifuged at 3,000 g for 5 min and the bacteria pellet was resuspended in 100 µl of LB medium. Bacteria were then plated on LB agar plates containing the appropriate selective antibiotic and incubated at 37 °C overnight (o/n).

For XL10-Gold Ultracompetent *E. coli* cell transformation, 70 µl of competent bacteria were thawed on ice, mixed with 25 mM β-mercaptoethanol, and incubated on ice for 10 min. 1-100 ng purified DNA from a single mutagenesis reaction was added and cell incubated for a further 30 min on ice. Cells were subjected to heat shock at 42 °C for 30 s and incubated on ice for 2 min. After addition of 900 µl of NZY^+ medium (5 g/l yeast extract, 5 g/l NaCl, 10 g/l NZ amine-A casein hydrolysate, 12.5 mM $MgCl_2$, 12.5 mM $MgSO_4$, 20 mM glucose, pH 7.5; preheated at 42 °C) cells were incubated at 37 °C, 225 rpm for 1 h. The culture was centrifuged at 3,000 g for 5 min and the bacteria pellet was resuspended in 100 µl of NZY^+ medium. Cells were then plated on solid LB agar containing the appropriate selective antibiotic and incubated at 37 °C o/n.

2.3.2 Bacterial cultures

Bacterial cultures were used for DNA transformations (Method 2.3.2) and extractions (Method 2.3.6). All cultures were handled under sterile conditions. Cultures

were initiated from either bacterial stocks, stored at -80 °C in Luria Broth (LB) medium (10 g/l enzymatic digest of casein, 5 g/l NaCl, 5 g/l yeast extract) containing 20 % glycerol, or single colonies selected from LB agar plates (10 g/l enzymatic digest of casein, 5 g/l NaCl, 5 g/l yeast extract, 15 g/l agar). LB agar plates contained a selective antibiotic either 50 µg/ml ampicillin or 50 µg/ml kanamycin. All bacterial cultures were grown in LB medium in presence of a selective antibiotic at 37 °C, 225 rpm. Specific volume and culture time periods are detailed in individual experiments. Glycerol stocks of bacterial cultures were made by freezing at -80 °C in LB medium containing 20 % glycerol.

2.3.3 cDNA constructs

In this study, a variety of cDNA constructs encoding TASK channels were utilised (Table 2.2) for site-directed mutagenesis (Method 2.3.5) and cell line transfections (Method 2.4.4). The known expression and functional properties (production of TASK channel currents) of the cDNA constructs used in this thesis are shown in Table 2.2 (Ashmole et al., 2001; Mant et al., 2011; O'Kelly et al., 2002; Roncoroni Thesis., 2012).

2.3.4 siRNA constructs

To examine the effects of K_{2P} channel knockdown by RNA interference (RNAi), commercially available small interfering RNA (siRNA, Qiagen; Table 2.4) and DNA plasmids encoding siRNA were utilised (abm® Canada; Table 2.5).

Qiagen siRNA are designed using the HP OnGuard siRNA design software against NCBI reference sequences and are predicted to give up to 70 % gene silencing when four siRNA are used in combination. The siRNA plasmids used encode the double stranded siRNA sequences and green fluorescence protein (GFP) independently within the vector (Figure 2.1). The siRNA sequences encoded by these plasmids are predicted to bind to the target gene based on the abm® design software and to result in up to 70 % gene silencing when a combination of four plasmids are used.

Table 2.2: cDNA plasmids utilised in this study

cDNA constructs used in this study. Shown for each construct are the name, plasmid backbone, protein tags, and antibiotic resistance.

Construct	Plasmid backbone	GFP tag	Other tags	Antibiotic resistance	
				Bacterial	Mammalian
eGFP	pEGFP-C1	n/a	n/a	Kanamycin	G418
GFP-hK_{2P}3.1	pEGFP-C1	N-terminal	n/a	Kanamycin	G418
hK_{2P}3.1	pRAT	n/a	n/a	Ampicillin	G418
GFP-hK_{2P}9.1	pEGFP-C1	N-terminal	n/a	Kanamycin	G418
GFP-hK_{2P}15.1	pEGFP-C1	N-terminal	n/a	Kanamycin	G418
hK_{2P}15.1-GFP	pEGFP-N1	C-terminal	n/a	Kanamycin	G418
rK_{2P}3.1	pcDNA3.1+	n/a	n/a	Ampicillin	G418
GFP-rK_{2P}3.1-HA	pcDNA3.1+	N-terminal	HA tag	Ampicillin	G418
rK_{2P}9.1	pcDNA3.1+	n/a	n/a	Ampicillin	G418
GFP-rK_{2P}9.1-HA	pcDNA3.1+	N-terminal	HA tag	Ampicillin	G418

Table 2.3: Characteristics of the cDNA plasmids utilised in this study
Known characteristics of cDNA constructs used in this study. Shown are the expression and functional properties for each cDNA construct.

Construct	Protein expression	Functionality
eGFP	Correct protein targeting: cytoplasmic localisation (confocal microscopy)	n/a
GFP-hK_{2P}3.1	Not characterised	Not characterised
hK_{2P}3.1	Not characterised	Functional and produces characteristic TASK channel currents (whole-cell patch clamp in HEK293 cells)
GFP-hK_{2P}9.1	Correct protein targeting: plasma membrane localisation (flow cytometry)	Not characterised
GFP-hK_{2P}15.1	Correct protein targeting: ER localisation (confocal microscopy)	Non-functional channel (as expected)
hK_{2P}15.1-GFP	Correct protein targeting: ER localisation (confocal microscopy)	Non-functional channel (as expected)
rK_{2P}3.1	Not characterised	Functional: and produces characteristic TASK channel currents (whole-cell patch clamp in HEK293 cells)
GFP-rK_{2P}3.1-HA	Correct protein targeting: plasma membrane localisation (confocal microscopy and flow cytometry)	Not characterised
rK_{2P}9.1	Not characterised	Functional: and produces characteristic TASK channel currents (whole-cell patch clamp in HEK293 cells)
GFP-rK_{2P}9.1-HA	Correct protein targeting: plasma membrane localisation (confocal microscopy and flow cytometry)	Not characterised

Table 2.4: siRNA utilised in this study

Commercially available siRNA (Qiagen) used for RNAi in this study, the target gene and sequence are shown.

siRNA	Target gene	Target sequence
Hs_*KCNK3*_6	*KCNK3*	CGCACTGGAGGTTCAAGCTAA
Hs_*KCNK3*_7	*KCNK3*	CGCCGACGTGTCCATGGCCAA
Hs_*KCNK3*_2	*KCNK3*	CTGATAATTACCCACTCTTAA
Hs_*KCNK3*_5	*KCNK3*	CAGACTCACCATAATTGCTGA
Hs_*KCNK9*_3	*KCNK9*	CCGCAACAGCATGGTCATTCA
Hs_*KCNK9*_4	*KCNK9*	CCTCAGGTTCTTGACCATGAA
Hs_*KCNK9*_1	*KCNK9*	TGGCCTTTAGCTTTATGTATA
Hs_*KCNK9*_2	*KCNK9*	CGCGAGGAGGAGAAACTCAAA
Control	n/a	Annealed double stranded siRNA

Table 2.5: siRNA plasmids utilised in this study

Plasmids encoding double stranded siRNA (abm® Canada) were used in this study for RNAi. For each construct the name, siRNA sequence and plasmid backbone are shown.

Construct	siRNA (5'-3')	Plasmid
KCNK3-263	TCACCGTCATCACCACCAT	piLenti-siRNA-GFP
KCNK3-313	GGCGGCAAGGTGTTCTGCATGTTCTACGC	piLenti-siRNA-GFP
KCNK3-663	GGCCTTCAGCTTCGTCTACATCCTTACGG	piLenti-siRNA-GFP
KCNK3-723	CGTGGTGCTGCGCTTCATGACCATGAACG	piLenti-siRNA-GFP
KCNK9-414	CCTGCTGAAGCGCATTAAGAAGTGCTGTG	piLenti-siRNA-GFP
KCNK9-663	GGCCTTTAGCTTTATGTATATCCTGGTGG	piLenti-siRNA-GFP
KCNK9-802	CGCAACAGCATGGTCATTCACATCCCTGA	piLenti-siRNA-GFP
KCNK9-1055	GCTCCATCTCTCCTGGGTTACACAGCTTT	piLenti-siRNA-GFP
Scrambled	GGGTGAACTCACGTCAGAA	piLenti-siRNA-GFP

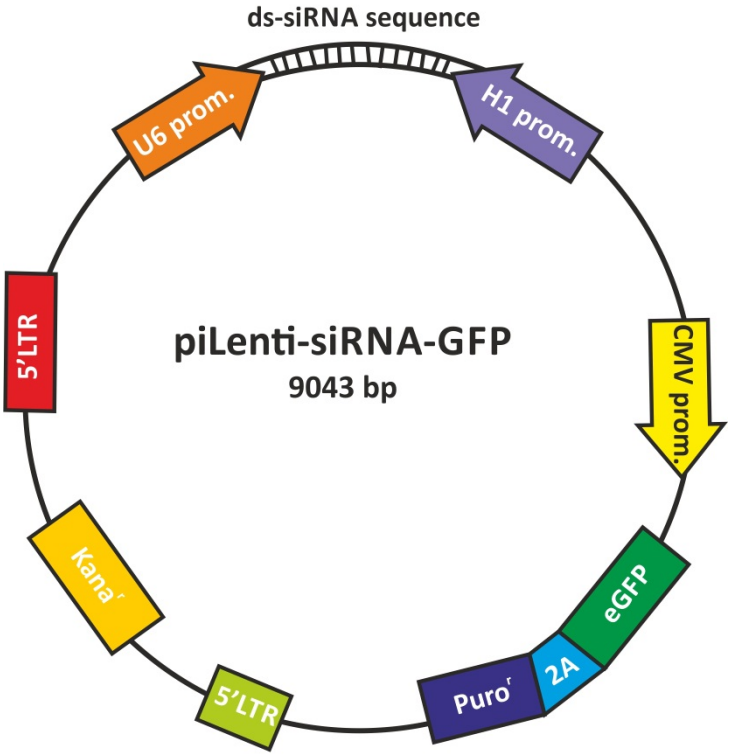

Figure 2.1: siRNA plasmid construct map

piLenti-siRNA-GFP plasmid encoding double stranded siRNA sequences under U6 and H1 promoters were used in this study for RNAi. GFP is also encoded in the plasmid under the control of a CMV promoter.

The plasmid contains both kanamycin (bacterial) and puromycin (mammalian) resistance genes for antibiotic selection.

Based on plasmid map provided by abm® Canada.

2.3.5 Site-directed mutagenesis

Site-directed mutagenesis was utilised to create $K_{2P}3.1$ and $K_{2P}9.1$ channels with a disrupted pore domain at glycine 97 (G97), for this the Agilent Technologies QuikChange® mutagenesis protocol was used. Mutagenesis primers were designed according to the recommended guidelines (between 25-45 base pairs (bp) in length and a melting temperature (T_m) ≥ 78 °C) to insert a glutamate residue (E) at G97 in both GFP-h$K_{2P}3.1$ and GFP-h$K_{2P}9.1$ cDNA constructs (Table 2.6).

To perform site-directed mutagenesis polymerase chain reactions (PCR), *PfuUltra* high-fidelity DNA polymerase (Agilent Technologies) was used, with an annealing temperature (Ta) of 55 °C. For this, a 50 µl reaction was set up containing: 1x *PfuUltra* buffer, 50 ng plasmid DNA template, 125 ng sense primer, 125 ng anti-sense primer, 1 µl 10 mM dNTP mix, sterile water (to 49 µl), and 1 µl *PfuUltra* DNA polymerase (2.5 U/µl). The PCR conditions used are outlined in Table 2.7.

PCR products were then DpnI-digested to cleave the methylated template DNA; 10 U of DpnI (New England Biolabs) was added to the PCR reaction and incubated at 37 °C for 1 h. After DpnI digestion, the DNA was transformed into XL10-Gold Ultracompetent *E. coli* cells (Agilent Technologies; Method 2.3.2). Minipreps (Method 2.3.6) were utilised to isolate plasmid DNA from single bacterial colonies. The extracted DNA was then sequenced (Method 2.3.8) to ensure it encoded the mutated region.

Table 2.6: Mutagenic primers

Primers used to mutate the pore domains of $K_{2P}3.1$ and $K_{2P}9.1$. The target gene and the sequence of each primer are shown, highlighted in bold are the mismatched bases which will introduce the target mutation.

Target	Primer	Sequence (5'-3')
KCNK3	*KCNK3* G97E sense	CCATCGGCTACG**A**GCACGCGGCACC
	KCNK3 G97E anti-sense	GGTGCCGCGTGC**T**CGTAGCCGATGG
KCNK9	*KCNK9* G97E sense	TCACCACCATAGGTTATG**A**GCACGCTGCACC
	KCNK9 G97E anti-sense	GGTGCAGCGTGC**T**CATAACCTATGGTGGTGA

Table 2.7: Mutagenesis PCR conditions

Conditions used for site-directed mutagenesis PCR reactions.

Step	Conditions
Initial Denaturation	95 °C, 30 s
Cycles	12-18 cycles
Denaturation	95 °C, 30 s
Annealing	55 °C, 1 min
Elongation	68 °C, 8 min (1 min/kb of plasmid)
Final Extension	68 °C, 20 min

2.3.6 DNA preparation

A range of DNA preparations were utilised depending on the DNA concentration, level of purity, and quantity of DNA required. Generally DNA required for sequencing (Method 2.3.8) and bacterial transformations (Method 2.3.2) were prepared through miniprep purifications, while DNA required for cell line transfections (Methods 2.4.4) and further plasmid manipulations were prepared through maxiprep purifications.

The main steps followed for DNA purification protocols are summarised in Table 2.8 and the compositions of the different buffers used for Promega Wizard® Plus Minipreps in Table 2.9. The composition of reagents used in the Sigma GenElute™ HP plasmid Maxiprep are not disclosed by the company, but they are likely to be comparable to those used for minipreps.

To perform miniprep DNA purifications the Promega Wizard® *Plus* Minipreps DNA purification system was used. After DNA transformation, a single colony from the LB agar plate was grown o/n in 3-10 ml of LB medium containing the appropriate selective antibiotic (Method 2.3.1). The culture was centrifuged at 10,000 g, 4 °C for 10 min, the medium removed and the pellet was resuspended in 300 µl of cell resuspension buffer (50 mM TrisHCl pH 7.5, 10 mM ethylenediaminetetraacetic acid (EDTA), 100 µg/ml RNase A). Bacteria were lysed in 300 µl cell lysis buffer (200 mM NaOH, 1 % sodium dodecyl sulfate (SDS)) and inverted 4 times to produce a clear suspension. To neutralise the lysis buffer and to precipitate bacterial proteins and genomic DNA, 300 µl cold neutralisation solution (1.32 M potassium acetate, pH 4.8) was added and tubes inverted 4 times, after which this was centrifuged at 10,000 g for 5 min. The supernatant containing plasmid DNA was added to Wizard® Minicolumn and centrifuged at 10,000 g for 1 min, the flow-though was discarded. The DNA bound to the column was washed twice, each time 750 µl of wash solution (80 mM potassium acetate, 8.5 mM TrisHCl (pH 7.5), 40 µM EDTA, 55 % ethanol) was added to the column and the column was centrifuged at 10,000 g for 1 min, discarding the flow-through. The column was then centrifuged at 10,000g for 2 min to remove any residual ethanol. 50 µl of 10 mM TrisHCl (pH 8.5) was added to elute the DNA form the column and the column was centrifuged at 10,000 g for 1 min. The DNA was quantified through UV spectrophotometry (Method 2.3.7).

Table 2.8: DNA preparation steps

Summary of the main steps used to obtain DNA by either miniprep or maxiprep protocols.

Step	Miniprep	Maxiprep
Starting culture	3-10 ml	200-300 ml
Pelleting	10,000 g, 4 °C, 10 min	10,000 g, 4 °C, 10 min
Cell resuspension	300 µl resuspension buffer	12 ml resuspension buffer
Cell lysis	300 µl cell lysis buffer	12 ml cell lysis buffer
Neutralisation	300 µl neutralisation buffer	12 ml neutralisation buffer
Centrifugation	10,000g, 5 min	10,000g, 5 min
Column equilibration	-	12 ml column preparation solution 3,000 g, 2min
DNA binding	10,000 g, 1 min	3,000 g, 2 min
Washing	750 µl wash solution 10,000 g, 1 min Twice	12 ml wash solution 3,000 g, 2-5 min Twice
DNA elution	50 µl elution buffer 10,000 g, 1 min	3 ml elution buffer 3,000 g, 5 min
DNA precipitation	-	2.1 ml isopropanol 300 µl 3 M sodium acetate (pH 5.2)
Centrifugation	-	12,000 g, 4 °C, 30 min
DNA wash	-	1.5 ml 70 % ethanol
Centrifugation	-	12,000 g, 10 min
Pellet resuspension	-	100-200 µl 10 mM TrisHCl (pH 8.4)
DNA quantification	UV spectrophotometry, 260 nm	UV spectrophotometry, 260 nm

Table 2.9: Buffers used for miniprep DNA preparation

Promega Wizard® *Plus* minipreps buffer composition used for DNA preparations.

Buffer	Miniprep buffer composition
Cell resuspension buffer	50 mM TrisHCl pH 7.5 10 mM EDTA 100 µg/ml RNase A
Cell lysis buffer	200 mM NaOH 1 % SDS
Neutralisation buffer	1.32 M potassium acetate pH 4.8
Wash buffer	80 mM potassium acetate 8.5 mM TrisHCl pH 7.5 40 µM EDTA 55 % ethanol
Elution	10 mM TrisHCl pH 8.4

To perform maxiprep purifications, Sigma GenElute™ HP plasmid Maxiprep purification kits were used. After DNA transformation, a single colony from the LB agar plate was grown o/n in 200-300 ml of LB containing the appropriate selective antibiotic (Method 2.3.1). The culture was centrifuged at 10,000 g, 4 °C for 10 min, LB medium removed and the pellet was resuspended in 12 ml of resuspension buffer. Bacteria were lysed by adding 12 ml of cell lysis buffer, inverted 6 times and the lysate was incubated for 5 min at room temperature (RT). To neutralise the lysis buffer and to precipitate bacterial proteins and genomic DNA, 12 ml of cold neutralisation solution was added and inverted 6 times. 9 ml of binding solution was added, the mixture was inverted twice and transferred into the filter syringe barrel and incubated for 5 min. During this time the spin column was assembled and washed with 12 ml of column preparation solution, then centrifuged at 3,000 g for 2 min. After incubation the bacterial lysate was added to the spin column through the filter syringe to remove insoluble debris. The columns were centrifuged at 3,000g for 2 min and elution was discarded. Once all lysate was passed through the column, the column was washed with 12 ml of wash solution 1, centrifuged at 3,000 g for 2 min and the elution was discarded. The column was then washed with 12 ml of wash solution, centrifuged 3,000 g for 5 min and the elution was discarded. The DNA was eluted by adding 3 ml elution buffer (10 mM TrisHCl pH 8.5) to the column and centrifuging at 3,000 g for 5 min. The eluted DNA was concentrated by precipitation, by adding 2.1 ml (0.7 volumes) isopropanol and 300 µl (0.1 volumes) 3 M sodium acetate (pH 5.2) and immediately centrifuged at 3,000 g, 4 °C for 1 h. The resultant pellet was washed in 1.5 ml 70 % ethanol and centrifuged at 3,000 g, 4 °C for 30 min. The DNA contained in the pellet was resuspended in 100-200 µl of 10 mM TrisHCl (pH 8.5) and quantified through UV spectrophotometry (Method 2.3.7).

2.3.7 Nucleic acid quantification

DNA obtained from minipreps and maxipreps (Method 2.3.6) and extracted RNA (Method 2.3.9) was quantified through UV spectrophotometry. Sample concentration was estimated by its light absorption at a wavelength (λ) of 260 nm (OD_{260}). DNA or RNA quality was assessed by comparing the light absorption values of the sample at 230 nm (OD_{230}) compared to OD_{260}, and at 280 nm (OD_{280}) compared to OD_{260}. An OD_{260}/OD_{230} ratio greater than 1.5 indicated negligible contamination by organic compounds or guanidium salt

(present in DNA purification columns). An OD_{260}/OD_{280} ratio of approximately 1.8 indicated a DNA pure sample, with no RNA or protein contaminants, or an OD_{260}/OD_{280} ratio 2 for an RNA pure sample, with no DNA or contaminants.

2.3.8 DNA sequencing

Mutagenesis products (Method 2.3.5) and purified PCR products (Method 2.3.16) were sequenced by SourceBioscience Life Sciences. Template DNA and primers were supplied to the company at the following concentrations: for plasmid DNA at 100 ng/µl, PCR products at 1 ng/µl for every 100 bp of product, and primers at 3.2 pmol/µl.

2.3.9 RNA extraction

To examine transcript expression, total mRNA was extracted from cell line pellets and human foetal tissue samples for PCR analysis. Human foetal tissues were used to create a cDNA pool containing multiple tissues likely to express K_{2P} channel mRNA. Pooled cDNA was used for the optimisation of primer conditions to detect K_{2P} channel expression by RT-PCR (Method 2.3.14). All materials used throughout the RNA extraction were RNase free, or treated with diethylpyrocarbonate (DEPC) to inactivate RNase activity.

Human foetal tissue samples were collected from women undergoing termination of pregnancy between 8-12 weeks post conception. Tissue was collected under guidelines issue by the Polkinghome Report and with ethical approval from the Southampton and South West Hampshire Local Research Ethics Committee. Tissues were stabilised in RNAlater (Qiagen) and stored at -20 °C prior to RNA extraction. Cell lines were harvested prior to RNA extraction, by trypsinisation and centrifugation (Method 2.4.3).

Foetal tissue was transferred to a fresh tube and homogenised with 1 ml TRIZOL (Invitrogen) before resuspension by pipetting. Cell pellets were resuspended in 1 ml TRIZOL and transferred to an RNase free tube. The lysates were incubated at RT for 5 min before centrifuging at 12,000 g, 4 °C for 10 min. The aqueous supernatant was then transferred into a fresh tube, where 200 µl chloroform was added, the tube was vortexed for 15 s and incubated at RT for 15 min, before centrifuging at 12,000 g, 4 °C for 15 min. This resulted in

separation of the contents into three phases: the lower organic phase containing proteins, the interphase containing DNA, and the upper aqueous phase containing RNA. The clear aqueous phase containing the RNA was removed and transferred to a fresh tube, 500 µl isopropanol and 1 µl (20 µg/µl) glycogen were added, and the tube was mixed well. At this stage the sample was either left at -20 °C o/n or -80 °C for 30 min. Following freezing the sample was centrifuged at 12,000 g, 4 °C for 10 min and the supernatant removed. The resulting pellet, which contained the RNA, was washed with 1 ml 75 % ethanol, vortexed and centrifuged at 7,500 g, 4 °C for 5 min. The supernatant was removed and the wash step was repeated twice. The pellet was air dried for 10 min before being resuspended in 30-50 µl RNase free water. The RNA obtained was quantified by UV spectrophotometry (Method 2.3.7) and the RNA was stored at -80 °C.

2.3.10 RNA purification

RNA was purified using the Qiagen RNeasy Plus Mini Kit to remove any remaining genomic DNA (gDNA). The compositions of buffers used for RNA purification have not been disclosed by the company. To a maximum of 50 µl RNA, 350 µl lysis (RLT Plus) buffer was added and the mixture transferred to the column matrix designed to bind gDNA (gDNA eliminator column). This was centrifuged at 8,000 g for 30 s and the column was discarded. 525 µl ethanol was added to the flow-through and mixed by pipetting. 700 µl of the sample was transferred to an RNeasy Mini spin column (silica membrane designed to trap RNA), centrifuged at 8,000 g for 15 s and the flow-through discarded. The spin column was transferred to a new 2 ml collection tube and 500 µl wash buffer (RPE + ethanol, to provide ideal binding conditions) was added, this was centrifuged at 8,000 g for 15 s and the flow through discarded, this step was then repeated. The spin column and collection tube was then centrifuged at full speed for 1 min. Following centrifugation the spin column was placed in a 1.5 ml collection tube. The RNA was eluted in RNAse free water (in the same volume as the initial sample usually 30-50 µl), water was added to the column and centrifuged at 8,000 g for 1 min. The column was discarded and the purified RNA was stored at -80 °C.

2.3.11 cDNA synthesis

Purified total mRNA extracted from cells or tissue (Method 2.3.9) was reverse transcribed into cDNA for analysis by reverse transcriptase PCR (RT-PCR). A 14 µl reaction containing 1 µg of extracted mRNA, 1 µl of 10 mM dNTP mix (dATP, dCTP, dGTP, and dTTP), 1 µl of random primers (a selection of randomly synthesised hexadeoxyneucleotides; Promega), and sterile distilled water (SDW) was set up. This reaction was incubated at 65 °C for 5 min and then cooled on ice for 1 min. The reaction was brought to a final volume of 20 µl by the addition of 4 µl of 5x First Strand Buffer (Invitrogen), 1 µl of 0.1 M dithiothreitol (DTT; Invitrogen) and 1 µl SuperScript Reverse Transcriptase III (Invitrogen). The reaction was incubated at 25 °C for 5 min, then 55 °C for 1 h before being inactivated at 70 °C for 15 min. The resulting cDNA was stored at -20 °C.

2.3.12 Reverse transcriptase PCR

RT-PCR reactions were used to detect housekeeping genes and K_{2P} channel mRNA from cDNA synthesised from total RNA (Method 2.3.11). All reactions were performed at a total volume of 20 µl in a mix of cDNA template, dNTPs, GoTaq DNA polymerase, and buffer (Promega; Table 2.10). Each PCR cycle had three phases, DNA denaturation, primer annealing, and DNA extension, with the number of cycles varying depending on the reaction. The PCR reaction was completed with a final DNA extension phase.

cDNA expression was examined using exon-spanning primers (Figure 2.2). Exon-spanning primers allowed mRNA product to be determined from any potential genomic contamination, since if gDNA was amplified it would run at a much larger size due to the presence of the intronic DNA. Primers designed against transferrin receptor (TFRC) were used as a housekeeping gene to check the quality of the cDNA (Figure 2.2 A). Expression of K_{2P} channel mRNA was analysed by using primers designed against the mRNA sequence for the genes (Figure 2.2 and Table 2.12). The Ta for each primer pair was determined by the primer characteristics and performing RT-PCR at a range of temperatures (Figure 2.4 and Table 2.11).

Table 2.10: PCR compositions

Compositions of standard PCR reactions and those with DMSO and Betaine added. All reactions were 20 µl in total.

Composition	**Standard reaction**	**Reactions with DMSO + Betaine**
Template cDNA	1 – 5 µl	1 – 5 µl
GoTaq buffer 5x	4 µl	4 µl
10 mM dNTP mix	0.5 µl	0.5 µl
Forward primer 5 µM	2.5 µl	2.5 µl
Reverse primer 5 µM	2.5 µl	2.5 µl
DMSO	-	0.4 µl
Betaine 5 M	-	2 µl
Taq DNA Polymerase (5 U/µl)	0.25µl	0.25 µl
SDW	to 20 µl	to 20 µl

Table 2.11: RT-PCR conditions

PCR cycle conditions used for RT-PCR reactions.

Step	**TA gradients**	**TFRC**	***KCNK* genes**
Initial Denaturation	93 °C, 3 min	93 °C, 3 min	93 °C, 3 min
Cycles	35 cycles	35 cycles	40 cycles
Denaturation	93 °C, 1 min	93 °C, 1 min	93 °C, 1 min
Annealing	Range, 1 min	58.5 °C, 1 min	69.0 °C, 1 min
Elongation	72 °C, 1 min	72 °C, 1 min	72 °C, 1 min
Final Extension	72 °C, 10 min	72 °C, 10 min	72 °C, 10 min

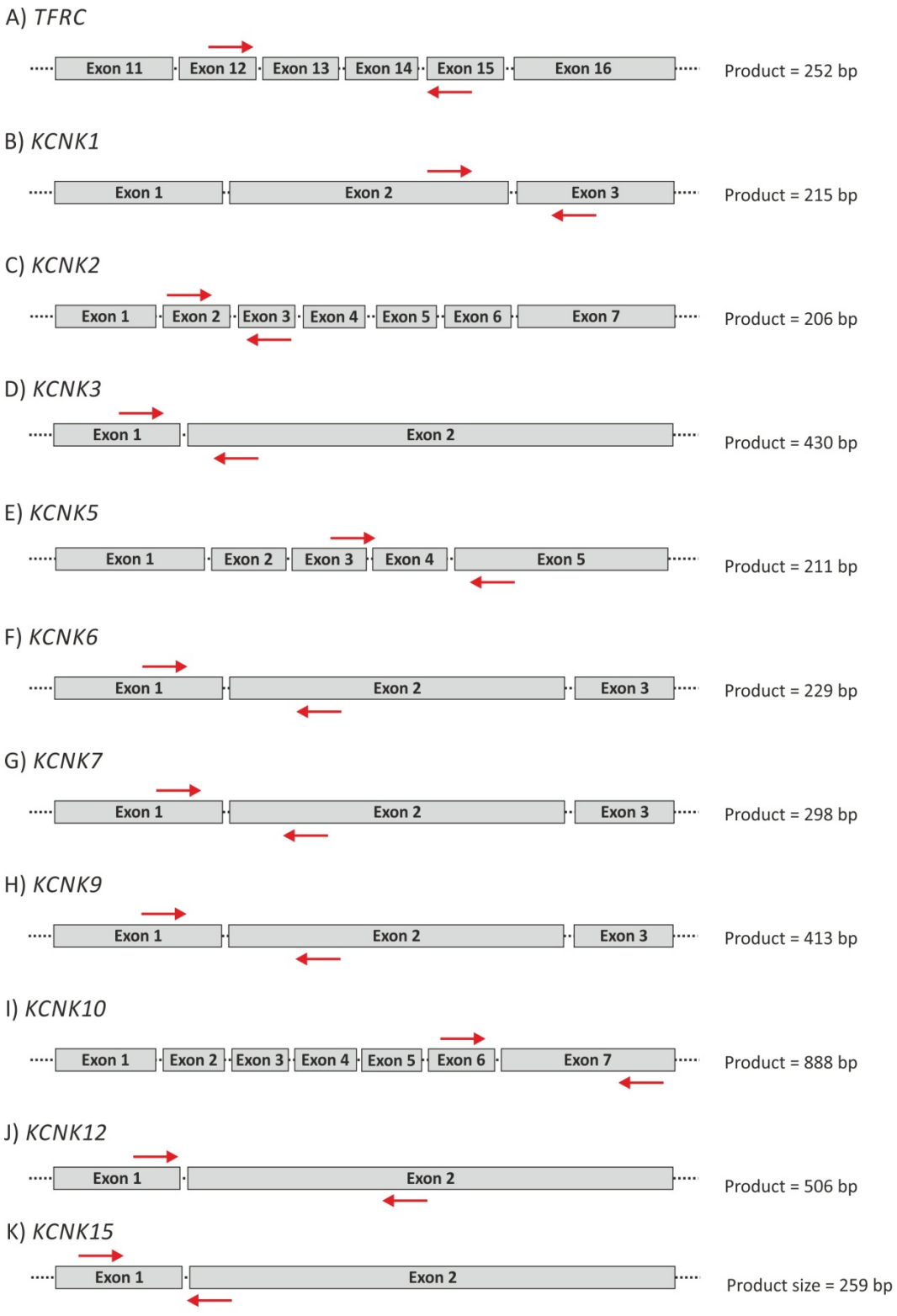

Figure 2.2: Annealing locations of primers used for RT-PCR reactions
Exon-spanning primers were designed for the amplification of RT-PCR products. Gene structures are shown for (A) Transferrin receptor (*TFRC*) and (B-K) *KCNK1-15*.
mRNA structure shown in grey with exons labelled and exon-exon junctions shown as a gap. Primer annealing locations are indicated by red arrows with the predicted product size indicated in base pairs (bp).

Table 2.12: Primers utilised for RT-PCR

Summary of the primers used to detect transferrin receptor and K_{2P} channel mRNA expression in cell lines and tissues. The target gene and the sequence of each primer are shown as well as the expected product size in base pairs (bp) and optimised annealing temperature (Ta).

Target	Primer	Sequence	Product size	Ta
TFRC	TFRC-F	5' – GCAGAAGCATTATCTTTGCCAG	252 bp	58.5 °C
	TFRC-R	5' – CCCAGTTGCTGTCCTGATATAG		
KCNK1	KCNK1F	5' – TTATTTCCCTGAGCACCATTG	215 bp	63 °C
	KCNK1R	5' – CACCTGATCCTCGTCCTTGT		
KCNK2	KCNK2F	5' – TGTTCAAAGCATTGGAGCAG	206 bp	56 °C
	KCNK2R	5' – GGAACTTCCCAAATCCCAGT		
KCNK3	KCNK3F	5' – CAACCTCAGCCAGGGCGGCTAC	430 bp	69.0 °C
	KCNK3R	5' – GATGAAGCAGTAGTAGTAGGCCTGG		
KCNK5	KCNK5F	5' – CACGTGCACAGTCATCTTCA	211 bp	62 °C
	KCNK5R	5' – CCAGAGCTCCACGAAGTAGC		
KCNK6	KCNK6F	5' – GTCGTGCTTGCTAACGCTTC	229 bp	62 °C
	KCNK6R	5' – GAGTCAGCAGCAGTGACAGG		
KCNK7	KCNK7F	5' – GAAGAGCTGCTGGGCACT	298 bp	64 °C
	KCNK7R	5' – GTGACAGCTGCCAGTGGAC		
KCNK9	KCNK9F	5' – GAAGTACAACATCAGCAGCGAGGAC	413 bp	65.0 °C
	KCNK9R	5' - GGAAGAAGCTCCACTCCTCACACTG		
KCNK10	KCNK10F	5' – GATCGGAGATTGGCTACGGG	888 bp	60 °C
	KCNK10R	5' – CTTGGTGTGTCCTGCGTTTG		
KCNK12	KCNK12F	5' – CCGTGGTGTCAACCATAGGTTTC	506 bp	62 °C
	KCNK12R	5' – CGAGTAAATGCAGCACACGC		
KCNK15	KCNK15F	5' – GTCCTGTGCACCCTGTGTTA	259 bp	58 °C
	KCNK15R	5' – GGCCGTACTCGATGGTAGTG		

2.3.13 Housekeeping gene detection

After synthesis, cDNA quality was verified by performing a control PCR reaction for a housekeeping gene mRNA, using TFRC. To detect TFRC primers TFRC-F and TFRC-R were used (Table 2.12), TFRC-F primes in exon 12 before the exon junction at 1476 bp and TFRC-R primes in exon 15 after the exon junction at 1706 bp (Figure 2.2). This resulted in amplification of a 252 bp product. TFRC mRNA expression was detected in all cDNA samples used for RT-PCR at the expected product size (252 bp), but not in the matched no reverse transcriptase control for each sample (example gel; Figure 2.3). By checking no products were amplified in the no reverse transcriptase control it ensured there was no contamination of the cDNA samples

2.3.14 Optimisation of *KCNK* gene PCR conditions

The presence of K_{2P} channel mRNA in human cancer cell lines was examined using exon spanning primers for each channel (Table 2.12). The priming locations and resulting products of all primers used in this study are shown in Figure 2.2. These primers were optimised on pooled human foetal cDNA (containing a combination of brain, kidney, limb, lung, placenta, and spinal cord) by performing Ta gradients (Figure 2.4). An optimal Ta was selected for each primer pair based on both the detection of the strongest product band and minimal non-specific products (Table 2.12 and Figure 2.4).

2.3.15 DNA electrophoresis

The products from PCR reactions were visualised using DNA electrophoresis. The reaction buffer used for PCR reactions included a loading buffer for electrophoresis. Therefore 5-10 µl of the total PCR reaction was separated on agarose gels (1 % agarose, Tris-acetate-EDTA buffer with either 5 µl ethidium bromide or 5 µl Nancy-520 dye (ethidium bromide substitute)) in Tris-acetate-EDTA buffer (TAE; 40 mM TrisBase, 1 mM EDTA pH 8.0, 20 mM acetic acid) at RT using a voltage of between 70-100 V. Once good separation was achieved, DNA gels were visualised using the UVP Gel Doc-IT system by exposing the gel to UV light.

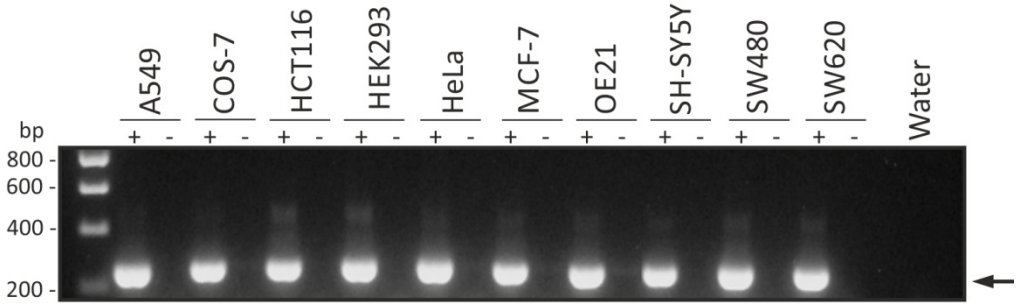

Figure 2.3: Example detection of transferrin receptor mRNA expression in cancer cell lines

PCR products were amplified with TFRC-F and TFRC-R primers from cancer cell line cDNA.
(+) Reverse transcriptase included in cDNA synthesis.
(-) No reverse transcriptase control.
Water was used as a no cDNA template control.
Predicted product size of 252 bp, indicated by arrow.

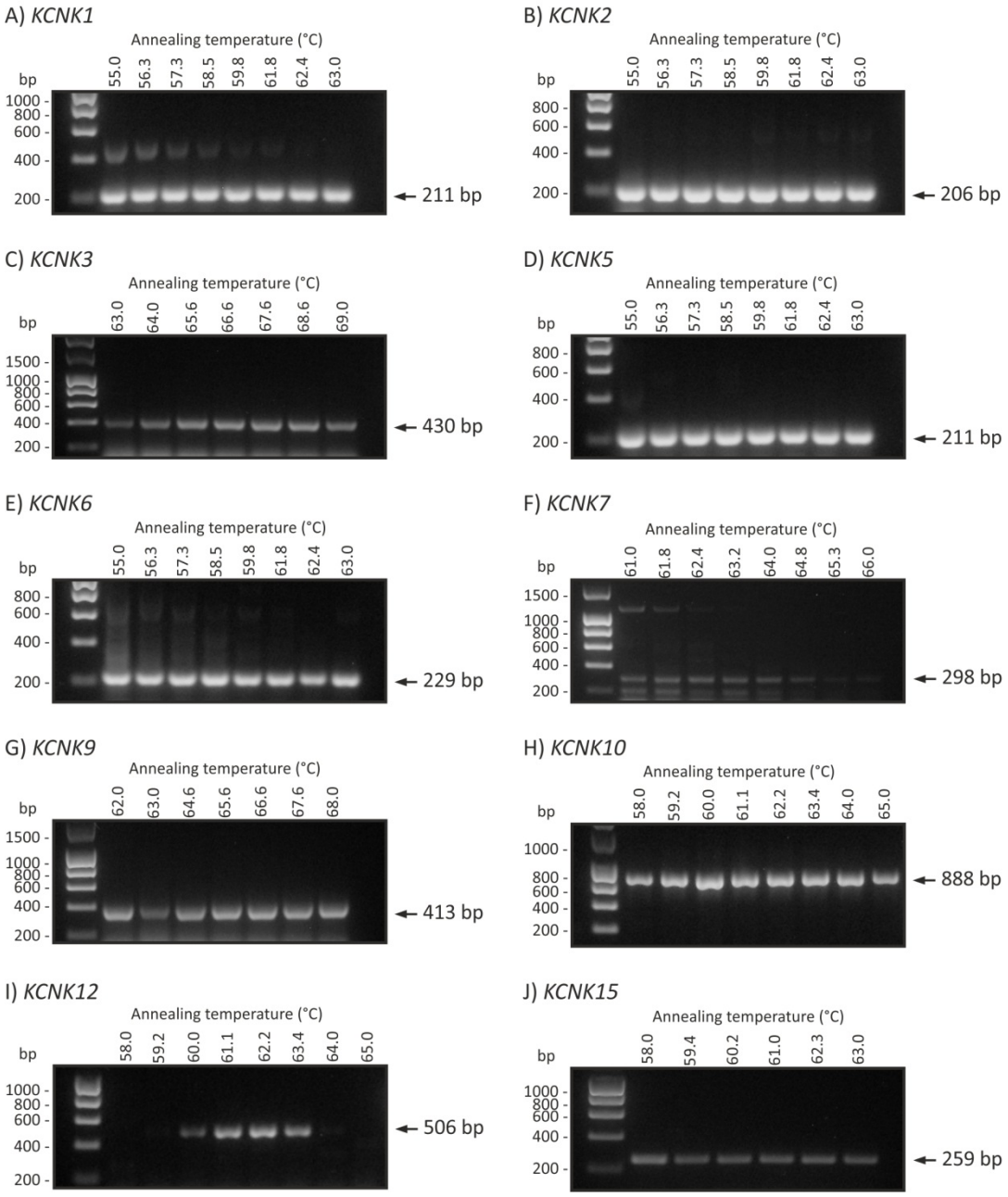

Figure 2.4: Optimisation of K_{2P} channel primer annealing temperatures

1 % agarose gel showing the PCR products obtained across a range of annealing temperatures (Ta) from pooled foetal cDNA with primers designed again K_{2P} channel family members.

(A) *KCNK1*, (B) *KCNK2*, (C) *KCNK3*, (D) *KCNK5*, (E) *KCNK6*, (F) *KCNK7*, (G) *KCNK9*, (H) *KCNK10*, (I) *KCNK12*, and (J) *KCNK15*.

Expected product size for each channel is indicated by an arrow and shown in base pairs (bp).

2.3.16 mRNA expression quantification

To quantify the mRNA product expression following RT-PCR (Method 2.3.12), the mean intensity of PCR product bands was calculated using ImageJ analysis software using the image obtained by gel electrophoresis (Method 2.3.15). For each sample, K_{2P} channel mRNA expression was normalised to TFRC housekeeping gene expression.

2.3.17 DNA gel extraction

To obtain DNA products from RT-PCR reactions (Method 2.3.12), DNA separated by electrophoresis (Method 2.3.15) was extracted from agarose gels and purified using the Sigma GenElute gel extraction kit. The compositions of reagents used in this kit were not disclosed by the company. All centrifugation steps were performed at 12,000 g. The band of interest was isolated from the agarose gels using a clean scalpel and transferred to an eppendorf tube. The excised agarose band was weighed and 300 µl of gel solubilisation solution was added for every 100 mg of agarose gel, usually 600 µl. The gel mixture was vortexed and incubated at 60 °C until the gel was completely dissolved. Whilst performing the gel incubation the binding column was prepared by adding 500 µl column preparation solutions and spinning for 1 min, discarding the flow-through. Once dissolved 200 µl isopropanol was added to the gel mixture and mixed, this was then transferred to the binding column, centrifuged for 1 min, and the resulting flow-through discarded. The binding column was then washed with 700 µl wash solutions, centrifuging for 1 min, and discarding the flow-through. The column was centrifuged for an additional 1 min to remove any residual ethanol. The binding column was transferred to a clean tube and 40 µl elution solution added to the column membrane. The column was incubated for 1 min and the DNA eluted by centrifuging for 1 min. The DNA obtained was quantified by UV spectrophotometry (Method 2.3.7) and stored at -20 °C.

2.4 Cell line studies

The cancer cell lines used in this thesis were selected to cover a wide range of cancer types, reflecting the published studies which have examined K_{2P} channels in cancer and the mRNA expression data obtained from Oncomine (Method 2.2). Additionally, COS-7,

HEK293, and HeLa cell lines were used for heterologous expression of cDNA constructs (Method 2.4.4), due to their high transfection efficiency (usually between 60-90 %) which allowed optimal channel expression.

2.4.1 Cell culture

All cell culture reagents were purchased from Invitrogen unless otherwise stated. Cell lines (Table 2.13) were grown in either Dulbecco's Modified Eagle Medium (DMEM), DMEM Hams (DMEM with F-12 Ham nutrients in 1:1 ratio), or RPMI 1640, as indicated. Cell culture medium was supplemented with 10 % foetal bovine serum (FBS) and antibiotics (100 U/ml Penicillin and 100 µg/ml Streptomycin). Cells were incubated at 37 °C in a humidified atmosphere with 5 % CO_2 and passaged using 0.05 % Trypsin-EDTA at 80-90 % confluence or every two days.

Cell lines were tested for mycoplasma on a yearly basis, or when new cell stocks were received from the ATCC® and other research groups. All cell lines used in this thesis tested negative for mycoplasma. Mycoplasma testing was carried out using *e*-Myco Mycoplasma PCR detection kit (Abbott Molecular Inc.) and this kit detects the presence of the mycoplasma 16S ribosomal RNA subunit gene in cultured cells. Briefly cells were grown to 80 % confluence in culture and harvested by trypsinisation (Method 2.4.3), after which cell pellets were resuspended in media. 1 ml of cell suspension was transferred to an eppendorf tube and the cells were pelleted by centrifuging at 1,500 g for 2 min. The cell pellet was resuspended in 1 ml sterile PBS and pelleted by centrifuging at 1,500 g for 2 min. This wash was repeated once more before resuspending the cell pellet in 100 µl PBS. Samples were heated to 95 °C for 10 min, vortexed, and pelleted by centrifuging at 16,000 g for 2 min. The supernatant was transferred to a clean tube and used as template for PCR reactions, 10 µl of template and 10 µl of sterile water were added to an *e*-Myco Mycoplasma PCR detection tube. PCR was then performed on this mixture using the following program: initial denaturation at 94 °C for 1 min followed by 35 cycles of denaturation at 94 °C for 30 s, annealing at 60 °C for 20 s, extension at 72 °C for 1 min and a final extension at 72 °C for 5 min. PCR products were detected using DNA gel electrophoresis (Method 2.3.15).

Table 2.13: Cell lines

Cell lines cultured throughout the duration of this study. The name of each cell line together with a description of the cell type, culture media required, and the original reference are provided.

(1) Williams et al. (1978), (2) Giard et al. (1973), (3) Gluzman (1981), (4) Brattain et al. (1981), (5) Graham et al. (1977), (6) Scherer et al. (1953), (7) Soule et al. (1973), (8) Rockett et al. (1997), (9) Rockett et al. (1997), (10) Biedler et al. (1978), (11) Leibovitz et al. (1976), and (12) Leibovitz et al. (1976).

Cell line	Description	Culture Media	Ref
786-0	Human clear cell renal carcinoma	RPMI 1640	1
A549	Human lung carcinoma	DMEM Ham's F-12	2
COS-7	African green monkey fibroblast-like	DMEM	3
HCT116	Human colorectal carcinoma	DMEM	4
HEK293	Human embryonic kidney derived	DMEM	5
HeLa	Human cervical adenocarcinoma	RPMI 1640	6
MCF-7	Human breast adenocarcinoma	DMEM	7
OE19	Human oesophageal adenocarcinoma	RPMI 1640	8
OE21	Human oesophageal squamous cell carcinoma	RPMI 1640	9
SH-SY5Y	Human neuroblastoma	DMEM Ham's F-12	10
SW480	Human colorectal adenocarcinoma	DMEM	11
SW620	Human colorectal adenocarcinoma (derived from lymph node metastases)	DMEM	12

2.4.2 Cell treatments

Cells were grown under control culture conditions at 20 % O_2 and 2-4.5 g/l glucose (4.5 g/l for DMEM, 3.2 g/l for DMEM Ham's F-12 and 2.0 g/l for RMPI 1640). In experiments to examine the role of environmental parameters on cell line functions, cells were cultured in altered glucose concentrations or O_2 tensions. For studies examining the role of O_2 on cellular functions, cells were cultured in either 20 % O_2 (normoxia) or 5 % O_2 (hypoxia) for 24-48 h prior to experiments. To examine the role of glucose concentration on cellular functions, cells were cultured in control media or media containing 0.5 g/l glucose (low glucose) for 24 h prior to experiments. To examine channel glycosylation, transfected cells (Method 2.4.4) were treated o/n (for 16 h) with 1.0 g/ml tunicamycin prior to harvesting for western blot analysis (Method 2.4.3).

2.4.3 Cell line harvesting

For RNA extraction cell lines were grown in a 75 cm^2 tissue culture flask for 48 h prior to harvesting. For protein analysis cells lines were grown on 10 cm^2 petri dishes for 24 h prior to transfection or harvesting.

The media was aspirated from the flask and the cells washed with 1 ml 0.05 % Trypsin-EDTA. The flask was then incubated with 3 ml 0.05 % Trypsin-EDTA at 37 °C for 3 min. After incubation the cells were dislodged by tapping the flask. 5 ml media was added to the flask to inactivate the trypsin and dislodge the remaining cells. The cells were centrifuged at 1,200 g for 3 min. The media was aspirated and the cell pellet was stored at -20 °C o/n or -80 °C for prolonged storage. For protein analysis, the resulting pellets were incubated on ice and the protein harvested immediately (Method 2.5.4.1).

2.4.4 Cell transfection

Cells were transfected with DNA plasmids (Table 2.2) for stable cell line generation (Method 2.4.5.2), protein studies (Methods 2.5.3 and 2.5.4), and electrophysiology (Method 2.8). For RNA knockdowns, cells were transfected with siRNA alone (Table 2.4) or siRNA plasmids (Table 2.5).

2.4.4.1 cDNA plasmid transfection

cDNA plasmids were transfected into cell lines using jetPEI (Polyplus). Cells were grown in media without antibiotics 24 h prior to transfection. Cells were seeded into 6 well plates on 22 mm sterile glass coverslips for immunocytochemistry (50,000-200,000 cells per well; Method 2.5.3) and electrophysiology (20,000 cells per well; Method 2.8). Cells were seeded into 10 cm^2 petri dishes for protein extraction (350,000-500,000 cells per dish; Method 2.5.4.1) and stable cell line generation (50,000-100,000 cells per dish; Method 2.4.5.2).

For transfection with jetPEI, two solutions A and B were freshly prepared as indicated in Table 2.14, vortexed and centrifuged. Solution B was added dropwise to solution A and then vortexed immediately and briefly centrifuged. The DNA-jetPEI mix was incubated at RT for 20-30 min. Following incubation, cells were covered by the DNA-jetPEI mix and incubated for 4 h at 37 °C after which the media was changed and the cells were harvested 24 h later.

2.4.4.2 siRNA transfection

siRNA (Table 2.4) were transfected into cell lines using Interferin (Polyplus). Cells were seeded 24 h prior to transfection in complete media and 50,000-100,000 cells were seeded into 6 well culture plates.

For transfection with Interferin, reagents were prepared as indicated in Table 2.15. 50 nM siRNA was added to the 200 µl of media without serum, vortexed, and centrifuged. The required volume of Interferin was then added to the tube and vortexed immediately and briefly centrifuged. The siRNA-Interferin mix was incubated at RT for 10 min. Following incubation, cells were covered by the siRNA-Interferin mix and incubated o/n at 37 °C, after which the media was changed. Channel knockdowns were assessed either 48-72 h post-transfection (Method 2.4.5.2).

Table 2.14: Solution composition for jetPEI transfections

Solution composition for DNA transfections using jetPEI.

	Culture dish	NaCl (150 mM)	DNA	jetPEI
Solution A	6 well plate	50 µl	0.5-2 µg	-
	10 cm^2 dish	250 µl	7.5 µg	-
Solution B	6 well plate	350 µl	-	3-6 µl
	10 cm^2 dish	450 µl	-	20-30 µl

Table 2.15: Solution composition for Interferin transfections

Solution composition for siRNA plasmid transfection using Interferin.

Reagent	6 well plate
siRNA	50 nM
Media (no serum)	200 µl
Interferin	6-10 µl

2.4.4.3 Polyclonal stable cell line generation

To assess channel knockdowns, a polyclonal transfected cell population were selected using antibiotic treatment where cells expressing the cDNA constructs were resistant to the antibiotic used. Once all cells in a control untransfected cell population had died as a result of the antibiotic treatment, the transfected cells were considered to be polyclonal transfected population. The selection of transfected cells usually took between 1-3 weeks. Cells were treated with 0.5-1 mg/ml G418 for cDNA plasmids (Table 2.2) encoding a G418 resistance gene, and 2 μg/ml puromycin for cells expressing siRNA plasmids (Table 2.5) which encoded a puromycin resistance gene.

2.5 Protein expression studies

2.5.1 TASK channel antibodies

A number of commercially available antibodies targeted against TASK channel protein were characterised in this thesis (Table 2.16). The binding location of each antibody and the corresponding epitope, when revealed by the company, are shown in Table 2.16.

2.5.2 Immunohistochemistry

2.5.2.1 Fixation of cell lines into agarose cylinders

Cell lines were fixed into paraffin blocks to allow optimisation of immunohistological conditions. Cells were either grown in 75 cm^2 culture flasks or transfected in 10 cm^2 petri dishes for 24 h prior to fixation (Method 2.4.4).

Table 2.16: Commercial antibodies used for detection of TASK channel protein

Description of the primary antibodies used for TASK channel protein detection in this thesis, and their binding locations.

Target channel	Antibody	Clonality	Host	Reactivity	Binding location
K_{2P}3.1	Sigma anti-K_{2P}3.1 (P0981)	Polyclonal	Rabbit	Human, rat	C-terminus, amino acid residues 252-269 (EDEKRDAEHRALLTRNGQ)
K_{2P}9.1	Alomone anti-K_{2P}9.1 (APC-044)	Polyclonal	Rabbit	Human, rat	First extracellular loop, amino acid residues 57-73 in rat K_{2P}9.1 (DDYQQLELVILQSEPHR)
	Proteintech anti-K_{2P}9.1 (180331-1-AP)	Polyclonal	Rabbit	Human	C-terminus
	Santa Cruz anti-K_{2P}9.1 (sc-11320)	Polyclonal	Goat	Human	Near C-terminus
	Sigma anti-K_{2P}9.1 (K0514)	Monoclonal	Human	Mouse	C-terminus, amino acid residues 360-374 (SFTDHQRLMKRRKSV)
K_{2P}15.1	Lifespan Biosciences anti-K_{2P}15.1 (LS-C120230)	Polyclonal	Rabbit	Human	C-terminus
	Proteintech anti-K_{2P}15.1 (18059-1-AP)	Polyclonal	Rabbit	Human	From TM2 to C-terminus

Cells were harvested by trypsinisation and pelleted by centrifugation (1,200 g for 3 min). The cell pellet was fixed in 1 ml 36.5-80 % formaldehyde solution o/n on a shaker. After fixation, the cells were re-pelleted by centrifugation (5,000 g for 5 min) the formalin removed and the pellet washed with PBS. The cells were then re-pelleted and the PBS removed. The resulting cell pellet was resuspended in 500 µl 1 % agarose in PBS and this was then transferred to an eppendorf mould and allowed to solidify. Once set, the cylinder was transferred to DEPC 70 % ethanol for embedding (Method 2.5.2.2).

2.5.2.2 Embedding into paraffin blocks

Agarose cylinders containing fixed cells (Method 2.5.2.2) were embedded into paraffin blocks. The cylinders were washed in increasing concentrations of DEPC ethanol (70 %, 80 %, 90 %, and 100 %) where the agarose was incubated for 2 h on a rocker with each concentration. The agarose was transferred into chloroform o/n. The cylinder was then placed into paraffin wax and left at 72 °C for 2 h and this was repeated 3 times with the final treatment performed under vacuum. Finally, the agarose cylinders were placed into a wax filled cassette and left on a cold plate to set. Once set the paraffin blocks were stored at 4 °C, before cutting and mounting onto glass slides (Method 2.5.2.5).

2.5.2.3 Cancer tissue

Ethical approval for the study of human cancer tissue was submitted via IRAS to the Southampton and South West Hampshire REC (B) and was approved on the 21st May 2009 (REC 09/H0504/66). Patient cancer tissue samples used for immunohistochemical staining in this study were fixed in formalin and embedded in paraffin blocks by Southampton General Hospital Pathology (Table 2.17). Most of the human carcinoma samples examined in this thesis were classified using the pathological TNM (pTNM) grading system (Table 2.17). Where T indicates the tumour stage relating the size and extent of the original tumour, N corresponds to the degree of local lymph node invasion, and M shows whether the tumour has metastasised (National Cancer Institute, NIH 2013).

Table 2.17: Human cancer tissue

Summary of human cancer tissues utilised in this study. Each tissue block was given a reference letter (A-S). The pathology reference, cancer diagnosis, and tumour stage for each sample are indicated.

Tissue		Cancer	Stage
Sample	**Pathology reference**		
A	04120520J (7E)	Oesophageal adenocarcinoma	3
B	0408274B (C)	Oesophageal adenocarcinoma	3
C	0324432X (4A)	Oesophageal adenocarcinoma	3
D	0319259X (1D)	Oesophageal adenocarcinoma with Barrett's oesophagus	1
E	03HS19173V (1E)	Oesophageal adenocarcinoma	3
F	02HS21930W (2E)	Oesophageal adenocarcinoma	3
G	02HS20632V (2B)	Oesophageal adenocarcinoma	3
H	02HS21930W (2F)	Oesophageal adenocarcinoma	3
I	04HS06197T (2C)	Oesophageal adenocarcinoma	2
J	04HS18459C (1B)	Oesophageal adenocarcinoma	3
K	06HS26249N (1)	Lung squamous cell carcinoma	2
L	04HS20896A (3D)	Lung squamous cell carcinoma	1
M	06HS06409A (7C)	Lung squamous cell carcinoma	3
N	06HS18973U (2G)	Pancreatic ductal adenocarcinoma	1
O	06HS22055F (2D)	Pancreatic adenocarcinoma	4
P	06HS28521A (2B)	Pancreatic adenocarcinoma	2
Q	06HS02665C (D)	Renal oncocytoma	Benign
R	04HS26340S (D)	Renal carcinoma	3
S	06HS01257T (D)	Renal carcinoma	Low grade

2.5.2.4 Coating of glass slides

Glass slides were cleaned and coated with aminoalkylsilane to encourage the adhesion of tissue sections (Table 2.18).

2.5.2.5 Microtome sectioning and mounting of tissue

All surfaces and tools were cleaned with 0.1 % DEPC ethanol before use. Using a Leica RM2135 microtome 5-10 µm sections were cut from the paraffin embedded tissue blocks. Sections were mounted onto coated slides (Method 2.5.2.4) with every 9th section being mounted onto a separate slide for haematoxylin and eosin (H&E) staining (Method 2.5.2.6). 0.1 % DEPC water was applied under each section and the slides placed on a slide warmer at 42 °C. The water was then aspirated from the slides and the slides dried o/n at 37 °C before being stored at 4 °C.

2.5.2.6 Haematoxylin and eosin staining

H&E staining was used for tissue identification, for this the cell nuclei and cytoplasm were stained with haematoxylin and eosin respectively. Sections which were mounted for H&E staining were put through the steps outlined in Table 2.19.

2.5.2.7 Immunohistochemical staining of tissue sections

The steps involved in immunohistochemical staining of tissue sections are outlined in Table 2.20. Briefly, tissue sections were rehydrated (Table 2.21) before antigen retrieval pre-treatment was employed. Slides were either boiled in 0.01-0.1 M sodium citrate pH 6.0 for 0-20 min or heated in 8 mM TrisHCl buffer pH 8.4 for 0-20 min, and then cooled for 20 min. Cooled slides were washed in PBS for 5 min. For experiments using non-fluorescent secondary antibodies, the endogenous peroxidase activity was blocked by incubating tissue sections with 3 % H_2O_2 in PBS for 20 min at RT. The slides were then washed in PBS for 5 min.

Table 2.18: Pre-treatment of glass slides for tissue sections

Pre-treatment steps for the cleaning and coating of glass slides used for mounting tissue sections

Treatment	Time
RNAse free wash	
0.1 % DEPC water + 0.01 % DEPC	5 min
Ethanol + 0.01 % DEPC	5 min
Ethanol + 0.01 % DEPC	5 min
Filtered air to dry	20 min
Acid wash	
70 % ethanol + 10 % hydrochloric acid	1 min
0.1 % DEPC water	1 min
Ethanol	1 min
Filtered air to dry	20 min
Silane treatment	
2 % aminoalkylsilane in acetone	15 s
0.01 % DEPC water (x5)	Move up/down 10 times
Filtered air to dry	20 min
Drying	
37 °C oven	o/n

Table 2.19: H&E staining of mounted tissue sections

Outlining the steps used for H&E staining of mounted tissue sections

Step	Time
Dehydration	
Xylene (x2)	3 min
100 % ethanol	2 min
90 % ethanol	2 min
Distilled water	2 min
Haematoxylin staining	
Filtered haematoxylin	5 min
Running water	5 min
Eosin staining	
Eosin	3 min
Distilled water	2 min
Distilled water	2 min
Rehydration	
90 % ethanol	2 min
100 % ethanol	2 min
Xylene (x2)	2 min, leave in for mounting
Mounting	
Entellan	Mount and dry o/n

Table 2.20: Overview of the immunohistochemical staining of tissue
Outlining the main steps in fluorescent or enzymatic labelling of mounted tissue sections

Step	**Staining**	
	Fluorescence	**Enzymatic**
Rehydration	Table 2.21	Table 2.21
Antigen retrieval	0-20 min in sodium citrate or Tris buffer	0-20 min in sodium citrate or Tris buffer
Endogenous peroxidise removal	-	3 % H_2O_2 in PBS, 20 min RT on shaker
Endogenous Biotin Blocking	15 min Avidin D solution 15 min Biotin solution	15 min Avidin D solution 15 min Biotin solution
Primary Antibody	o/n, 4 °C in moist container	o/n, 4 °C in moist container
Secondary Antibody	1 h, RT in moist container	1 h, RT in moist container
Streptavidin	Fluorescence conjugated streptavidin	HRP conjugated streptavidin
DAB staining	-	5 min solution A 3 min solution B
Counter stain	-	2 min toluidine blue 30 s haematoxylin
Dehydration	Table 2.21	Table 2.21
Mounting	Vectashield® with DAPI	Entellan

Table 2.21: Rehydration and dehydration steps
Outlining the rehydration and dehydration steps for slides during immunohistochemical experiments

Rehydration		
Solution	**All slides**	
Xylene	2 min	
Xylene	2 min	
100 % ethanol	2 min	
90 % ethanol	2 min	
70 % ethanol	2 min	
Water	2 min	
Dehydration		
Solution	**Fluorescence staining**	**H&E or enzymatic staining**
70 % ethanol	2 min	10 s
90 % ethanol	2 min	10 s
100 % ethanol	2 min	2 min
Xylene	2 min	2 min
Xylene	2 min	2 min, leave in for mounting
100 % ethanol	Before mounting	-

In lung, renal, and pancreatic tissue samples, the presence of endogenous biotin was blocked using a biotin blocking kit (SP-2001, Vector Laboratories). Each section was incubated with 20 µl avidin D solution for 15 min at RT, briefly washed in PBS, then incubated with 20 µl biotin solution for 15 min at RT and this was followed by a 5 min PBS wash.

Three 5 min PBS washes were performed between each of the antibody incubation steps. Following PBS washes, the tissue slides were incubated with primary antibodies (Table 2.22) diluted in 0.1 % Triton X-100 in PBS and 3 % serum (with serum species matching the species in which the secondary antibody is raised). Slides were incubated with primary antibodies o/n at 4 °C in a humidified container. Slides were then washed and incubated with the appropriate secondary antibodies (Table 2.22) diluted in 0.1 % Triton X-100 in PBS for 1 h at RT in a humidified container. After three 5 min PBS washes, Slides were incubated with a fluorochrome or horseradish peroxidase (HRP) conjugated streptavidin (Table 2.22) diluted in 0.1 % Triton X-100 in PBS for 30 min at RT in a humidified container.

Slides were washed three times in PBS (5 min each), and if slides were incubated with HRP conjugated streptavidin staining was visualised using diaminobenzidine (DAB, Merck). Sections were incubated with solution A (1 tablet per 10 ml water) for 5 min followed by solution B (1 tablet per 10 ml water, 0.01 % H_2O_2) for 3 min, after DAB incubation slides were washed in PBS for 5 min. The DAB stained tissue sections were counter-stained for the cell nuclei, with either filtered haematoxylin for 30 s or toluidine blue (10 ml stock solution, 1 % toluidine blue in ethanol, in 240 ml water) for 2 min. After counterstaining the slides were washed in water, 5 min for haematoxylin staining or briefly submerged (for less than 5 s) for toluidine blue staining. All slides were then dehydrated according to the steps in Table 2.21 and a coverslip was then mounted onto the slide using Vectashield® with DAPI (H-1200, Vector laboratories) for fluorescent staining or entellan (Fisher) for colour staining.

Table 2.22: Antibodies used for immunohistochemical reactions

Antibodies and concentrations used for protein detection by immunohistochemistry

Primary antibodies				
Antibody	**Company**	**Reactivity**	**Host**	**Conc. (µg/ml)**
Anti-K_{2P}3.1	P0981, Sigma	Human, rat	Rabbit	12
Anti-K_{2P}9.1	sc-11320 Santa Cruz	Human	Goat	20
Anti-cytokeratin	MNF116, DakoCytomation	Human, cow, rabbit, rat	Mouse	2.32
Secondary antibodies				
Antibody	**Company**	**Reactivity**	**Host**	**Conc. (µg/ml)**
Anti-goat biotinylated	BA-9500, Vector Laboratories	Goat	Horse	1.5
Anti-rabbit biotinylated	BA-1000, Vector Laboratories	Rabbit	Goat	1.5
Anti-mouse biotinylated	BA-2000, Vector Laboratories	Mouse	Horse	1.5
Streptavidin				
Antibody	**Company**	**Reactivity**	**Host**	**Conc. (µg/ml)**
Streptavidin-texas red	SA-5006, Vector Laboratories	-	-	2
Streptavidin-HRP	SA-5004, Vector Laboratories	-	-	2

2.5.3 Immunofluorescence

Immunofluorescence was used to assess the endogenous expression of K_{2P} channel protein, the specificity of the primary antibodies, and protein colocalisation. The steps involved in immunofluorescent staining of cells are outlined in Table 2.23, and all solutions were filter sterilised before use with a 0.22 μm filter (Millipore).

Cells were either transfected 24 h prior to immunofluorescence staining (Method 2.4.4) or plated out at 50-80 % confluence on sterilised coverslips in 6 well plates, and allowed to seed for 24 h. After 24 h, the media was removed and the cells were washed with PBS and fixed in 4 % paraformaldehyde (PFA). After fixing, the PFA was quenched using 100 mM glycine in PBS and cells were permeabilised with 0.1 % Triton X-100 in PBS. Before incubation with the primary antibodies the cells were blocked with 1 ml 3 % bovine serum albumin (BSA) for 1 h.

Three PBS washes were performed between each of the antibody incubation steps. The primary antibodies (Table 2.24) were diluted in 1 % BSA. Each coverslip was covered with parafilm, the samples placed in a humidity chamber and incubated at 4 °C o/n. After incubation the cells were washed and incubated with the secondary antibody (Table 2.24) diluted in 1 % BSA for 1 h at RT. After incubation the cells were washed and if a biotinylated secondary antibody was used the cells were incubated with streptavidin in 1 % BSA for 30 min at RT. After incubation the cells were washed and the coverslips were either mounted using Vectashield® with DAPI, or incubated with a separate DAPI nuclear stain (1:10,000 in PBS) for 5 min RT and mounted using aqueous mountant (Biomedical Imaging Unit, Southampton). In both cases, the coverslips were mounted onto glass slides and sealed with nail varnish.

Table 2.23: Overview of the steps involved in immunofluorescence
Outlining the main steps involved in the immunofluorescent staining of cultured cells.

Step		**Time**
Wash	PBS, 3x	-
Fixing	4 % PFA in PBS, 1 ml per well	7 min
Wash	PBS, 3x	-
Quenching	100 mM glycine in PBS (autoclaved), 1 ml per well	10 min
Wash	PBS, 3x	-
Permeablisation	0.1 % triton X-100 in PBS, 1 ml per well	7 min
Wash	PBS, 1x	-
Blocking	3 % BSA in PBS, 1 ml per well	1 h
Wash	PBS, 3x	-
Primary antibody	Diluted into 1 % BSA in PBS, 100 µl per well	o/n, 4 °C
Wash	PBS, 3x	-
Secondary antibody	Diluted into 1 % BSA in PBS, 500 µl per well	1 h, RT
Wash	PBS, 3x	-
Streptavidin (if applicable)	Diluted into 1 % BSA in PBS, 500 µl per well	30 min, RT
Wash	PBS, 3x	-
Nuclear stain	Incubation with DAPI in PBS (1:10,000), 500 µl per well	5 min, RT
Wash	PBS, 1x	-
Mounting	Aqueous mountant or Vectashield® with DAPI	-

Table 2.24: Antibodies used for immunofluorescence

Overview of the antibodies and concentrations used for immunofluorescent detection of transfected and endogenous K_{2P} channels.

Primary antibodies				
Antibody	**Company**	**Reactivity**	**Host**	**Conc. (µg/ml)**
Anti-Calnexin (ER staining)	Ab22595, Abcam	Mouse, Rat, Human, Marmoset (common)	Rabbit	1
Anti-58K Golgi (Golgi apparatus staining)	Ab27043, Abcam	Rat, Hamster, Cow, Dog, Human, Monkey, African Green Monkey	Mouse	1
Lectins-TRITC (plasma membrane staining)	L5266, Sigma	N-acetyl-β-D-glucosaminyl residues	Triticum vulgaris (wheat)	0.1
Anti- K_{2P}3.1	P0981, Sigma	Human, rat	Rabbit	12
Anti- K_{2P}9.1	APC-044, Alomone	Human, Rat	Rabbit	7.5
Anti- K_{2P}9.1	180331-1-AP, Proteintech	Human	Rabbit	0.13
Anti- K_{2P}9.1	sc-11320, Santa Cruz	Human	Goat	4-20
Anti-K_{2P}9.1	K0514, Sigma	Human	Mouse	48
Anti-K_{2P}15.1	LS-C120230, Lifespan Biosciences	Human	Rabbit	10-20
Anti-K_{2P}15.1	18059-1-AP, Proteintech	Human	Rabbit	0.13
Secondary antibodies				
Antibody	**Company**	**Reactivity**	**Host**	**Conc. (µg/ml)**
Anti-goat Alexa 647	A-21469, Invitrogen	Goat	Chicken	2
Anti-goat biotinylated	BA-9500, Vector Laboratories	Goat	Horse	1.5
Anti-mouse biotinylated	BA-2000, Vector Laboratories	Mouse	Horse	1.5
Anti-rabbit Alexa 594	A-11072, Invitrogen	Rabbit	Goat	2
Anti-rabbit biotinylated	BA-1000, Vector Laboratories	Rabbit	Goat	1.5
Streptavidin				
Antibody	**Company**	**Reactivity**	**Host**	**Conc. (µg/ml)**
Streptavidin-texas red	SA-5006, Vector Laboratories	-	-	2
Streptavidin-Dylight 488	SA-5488-1, Vector Laboratories	-	-	2

2.5.4 Western blotting

Western blotting was used to characterise the ability of the primary antibodies utilised in this thesis to detect TASK channel protein (Table 2.16). This approached would have allowed the assessment of endogenous TASK channel protein expression in cancer cell lines.

2.5.4.1 Cell lysis

To determine the specificity of the primary antibodies for TASK channel protein, cells were transfected in petri dishes 24 h prior to harvesting (Method 2.4.4), while non-transfected cells were seeded into petri dishes 24 h prior to harvesting (Method 2.4.3). Cell pellets were resuspended in 100 µl of lysis buffer (Table 2.25) on ice, with the lysis buffer chosen depended on the experimental conditions. The cell lysate was homogenised manually or by sonication. For manual homogenisation the cell lysate was drawn through a syringe and needle 10 times and incubated on ice for 15 min after which the homogenisation and incubation was repeated. For homogenisation by sonication the cell lysate was sonicated in a water bath for 1 min, and then incubated on ice for 5 min. This was repeated 3 times and the homogenate was then incubated on ice for a further 15 min. After homogenisation, the cell lysate was centrifuged at 2,500 g at 4 °C for 15 min to remove the nuclear fraction. The supernatant represents the whole cell lysate and was either used immediately for pull down assays (Method 2.5.4.3) and protein electrophoresis (Method 2.5.4.5), or underwent further centrifugation to obtain the membrane fraction.

2.5.4.2 Membrane fractionation

To enrich for the membrane protein fraction, whole cell lysates were centrifuged at 50,000 g for 30 min at 4 °C in the TL100 ultracentrifuge (Beckman Coulter). The resulting pellet contained the crude membrane fraction (organelle and plasma membranes), and the supernatant was discarded. This pellet was either resuspended into loading buffer for protein electrophoresis (Table 2.26 and Method 2.5.4.5) or lysis buffer for protein quantification (Method 2.5.4.4).

Table 2.25: Lysis buffers

Outlining the lysis buffers used for the solubilisation of cell pellets.

Buffer	Composition
Cell lysis buffer	10 mM Tris buffer pH 7.5, 150 mM NaCl, 0.5 % NP40, protease inhibitors 1x
IP buffer	10 mM Tris buffer pH7.5, 150 mM NaCl, 15mM $MgCl_2$, 1 % NP40, protease inhibitors 1x
RIPA buffer	PBS, 50 mM Tris, 150 mM NaCl, 0.01 % SDS, 1 % NP40, 0.5 % Na-deoxycholate, protease inhibitors

2.5.4.3 GFP pull down

GFP tagged transfected proteins were purified from whole cell lysates (Method 2.5.4.1) using a GFP pull down with GFP binder beads (GFP-trap®-A; Chromotek). 500 µl dilution buffer (10 mM TrisHCl buffer pH 7.5, 150 mM NaCl, 0.5 mM EDTA, protease inhibitors 1x) was added to whole cell protein lysate. A 10 µl sample of the whole cell lysate was then removed and stored at -80 °C to be used as the input sample for protein electrophoresis. The remaining sample (500 µl) was incubated with 10 µl equilibrated GFP binder beads and the sample was rotated o/n at 4 °C.

Following incubation the GFP trap beads were pelleted by centrifugation at 2,400 g, for 1 min. The supernatant was removed and 1 ml dilution buffer was added to the beads. The beads were washed by rotating the sample 2-15 min at RT before re-pelleting. This washing step was repeated with fresh dilution buffer 3-5 times. After the final wash the sample was either eluted in low pH buffer or loading buffer. For low pH elution, the pellet was incubated with 30 µl glycine elution buffer (150 mM NaCl, 200 mM glycine, pH 2) and centrifuged at 10,000 g for 2 min. This supernatant was transferred to a fresh tube and corresponded to low pH-eluted binding proteins. To neutralise low pH, 5 µl of TrisHCl buffer pH 9 was added to both the supernatant and the pellet. Strongly interacting proteins were eluted by incubating the pellet with 30 µl of loading buffer (12 % SDS, 2 M urea, 250 mM Tris buffer pH 6.8, 35 % Glycerol, Bromophenol blue, 50 mM DTT; Table 2.26), boiling the for 5 min at 95 °C and collecting the supernatant after centrifugation (Method 2.5.4.5).

2.5.4.4 Protein quantification

Protein samples were quantified using a colorimetric assay (DC Protein Assay kit; BioRad) which is based on the Lowry method (Lowry et al., 1951). For the calibration curve which is used as a reference, five BSA protein samples of known concentration (1 to 10 mg/ml) and final volume of 5 µl in lysis buffer were set up. Samples from the cell lysates were also prepared at 1:1 and 1:5 dilutions. To enable reduction-oxidation reactions and a colour change, 25 µl of alkaline copper tartrate solution (98 % buffer A, 2 % buffer S) was added to each sample, the samples were then mixed with 200 µl of buffer B (containing Folin) The reactions were incubated at RT for 15 min to allow reduction of the Folin and the

oxidation of the aromatic residues in the protein samples. The concentration of reduced Folin in the sample was quantified by UV spectrophotometry at 750 nm wavelength. Since protein concentration in the samples is proportional to the reduced Folin concentration, the sample concentration was calculated by referring to the calibration curve.

2.5.4.5 Protein electrophoresis

Protein electrophoresis was used to separate proteins for western blot analysis (Method 2.5.4.6), the composition of different buffers and reagents used are outlined in Table 2.26. Polyacrylamide gels were produced with a stacking gel (2-3 cm polymerised 4 % polyacrylamide layer; Table 2.26) on top of a resolving gel (7.5-12 % polyacrylamide layer with 8 M urea added; Table 2.26). Protein samples were mixed with loading buffer (Table 2.26), incubated at 37°C for 10 min and centrifuged at 12,000 g for 1 min. For experiments studying the effect of channel glycosylation, protein samples were incubated with 100-200 mM DTT for 30 min at RT prior to loading buffer addition. Samples from GFP pull down assays were either eluted in low pH and mixed with loading buffer for electrophoresis or eluted in 30 µl of loading buffer and loaded directly onto the gels. Samples were loaded onto polyacrylamide gels and separated by SDS gel electrophoresis (SDS-PAGE) in running buffer (Table 2.26) by applying a voltage of 60-100 V for 1-2 h. After separation, the proteins on the gel were transferred to a nitrocellulose membrane for western blot analysis (Method 2.5.4.6).

2.5.4.6 Western blotting

Western blot analysis was used to examine the protein of interest after sample separation by protein electrophoresis (Method 2.5.4.5). The main steps in western blot analysis are outlined in Table 2.27, and the buffers used are shown in Table 2.28. The antibodies and concentrations used for protein detection are specified in Table 2.29.

Table 2.26: Reagents and buffer used for protein electrophoresis

Summarising the composition of gels and buffers utilised in protein electrophoresis. Abbreviations used: sodium dodecyl sulphate (SDS), tetramethylethylenediamine (TEMED) and ammonium persulfate (APS).

Reagent	Composition
Loading buffer	12 % SDS 250 mM TrisHCl pH 6.8 2 M urea 35 % glycerol 50 mM DTT Bromophenol blue
Resolving gel: 7.5 % polyacrylamide	7.28 % acrylamide 0.32 % bis-acrylamide 375 mM TrisHCl pH 8.8 8 M urea 0.1 % SDS 0.05 % TEMED 0.05 % APS
Resolving gel: 12 % polyacrylamide	11.68 % acrylamide 0.22 % bis-acrylamide 375 mM TrisHCl pH 8.8 8 M urea 0.1 % SDS 0.05 % TEMED 0.05 % APS
Stacking gel: 4 % polyacrylamide	3.84 % acrylamide 0.104 % bis-acrylamide 1.25 mM TrisHCl pH 6.8 0.1 % SDS 0.1 % TEMED 0.05 % APS
Running buffer	25 mM Tris 192 mM glycine 0.1 % SDS

Table 2.27: Western blot analysis.

Outlining the main steps used to perform western blot analysis.

Step	Procedure
Protein transfer	Transfer onto nitrocellulose membrane, 250 mA for 2 h.
Ponceau S staining	Stain for 5 min Wash with water
Labelling	Blocking solution for 5 min then 1 h Incubate with primary antibody o/n 4°C Wash in blocking solution 3x, 15 min each Incubate with secondary antibody for 1 h Wash in TBST solution 3x, 15 min each
Detection	Incubation in ECL solution for 5 min Exposure to film in dark room

Table 2.28: Western blot solutions

Showing the composition of the solutions used to perform western blot analysis.

Solution	Composition
Transfer buffer	20 mM Tris 153 mM glycine 20 % methanol
Ponceau S	1 % acetic acid 0.1 % ponceau red
Blocking buffer	50 mM TrisHCl pH 7.4 150 mM NaCl 0.05 % Tween 20 100 g/l non-fat dry milk powder
TBST solution	50 mM TrisHCl pH 7.4 150 mM NaCl 0.05 % Tween 20

Table 2.29: Antibodies used for western blotting

Showing the antibodies and dilutions used for protein detection by western blot analysis.

Primary antibodies				
Antibody	**Company**	**Reactivity**	**Host**	**Conc. (µg/ml)**
Anti-GFP	ab290, Abcam	all variants of *Aequorea victoria* GFP	Rabbit	2.5-5
Anti-HA	16B12, Covance	HA epitopes	Mouse	1
Anti-K_{2P}3.1	P0981, Sigma	Human, rat	Rabbit	3
Anti-K_{2P}9.1	APC-044, Alomone	Human, rat	Rabbit	1.88
Anti-K_{2P}9.1	sc-11320, Santa Cruz	Human	Goat	1
Anti-K_{2P}9.1	K0514, Sigma	Human	Mouse	12
Secondary antibodies				
Antibody	**Company**	**Reactivity**	**Host**	**Conc. (µg/ml)**
Anti-goat IgG HRP conjugated	P0449, DAKOCytomation	Goat	Rabbit	0.5
Anti-rabbit IgG HRP conjugated	P0447, DAKOCytomation	Rabbit	Goat	0.25
Anti-mouse IgG HRP conjugated	P0448, DAKOCytomation	Mouse	Goat	1

Following protein electrophoresis, proteins from the polyacrylamide gels were transferred onto a nitrocellulose membrane (GE Healthcare). The transfer chamber was assembled inside a plastic perforated cassette by placing the polyacrylamide gel and the nitrocellulose membrane in between two layers, with the inner layer made of two pieces of filter paper and the external layer consisting of a sponge. The protein transfer was carried out at 250 mA, 4 °C for 2 h in transfer buffer (20 mM TrisHCl, 153 mM glycine, 20 % methanol). Proteins transferred to the nitrocellulose membrane were visualised by incubating the membrane with Ponceau S solution (1 % acetic acid, 0.1 % Ponceau S) for 5 min. After Ponceau S staining the membrane was rinsed with water and the ladder and lanes were marked with pencil. To minimise non-specific antibody binding, the membrane was then incubated in blocking buffer (10 % non-fat dry milk in TBST solution; Table 2.28) for 5 min and then for 1 h in fresh buffer. The membrane was incubated o/n at 4°C with the primary antibody (Table 2.29) diluted in blocking buffer. After primary antibody incubation, the membrane was washed 3 times for 15 min each with blocking buffer to remove excess antibody. The membrane was incubated with an HRP conjugated secondary antibody (Table 2.29) diluted in blocking buffer for 1 h at RT. After secondary antibody incubation the membrane was washed 3 times with Tris-Buffered-Saline-Tween (TBST) solution (50 mM TrisHCl pH 7.4, 1500 mM NaCl, 0.05 % Tween20; Table 2.28) for 15 min each to remove any excess antibody.

After washing, the membrane was incubated for 5 min with either pico or femto sensitivity enhanced chemiluminescence (ECL) solution (Pierce) depending on the strength of the signal to be detected. ECL was prepared by mixing both solutions in a 1:1 ratio. Protein signal was detected by exposing the membrane to film in a development cassette in a dark room for a variable period of time (3 s to 1 h) depending on signal strength. The film was then developed in development solution (Kodak) for up to 5 min, washed in water, incubated with fixer solution (Kodak) for 5 min, washed in water, and air dried.

2.6 Microscopy

Following immunohistochemical (Method 2.5.2.7) and immunofluorescent staining (Method 2.5.3), samples were analysed by light (Method 2.6.1) or confocal microscopy (Method 2.6.2).

2.6.1 Light microscopy

Light microscopy was used to examine immunohistochemical cancer tissue staining (Method 2.5.2.7), immunofluorescent TASK channel antibody staining (Method 2.5.3), and cell migration assays (Method 2.7.4).

Stained slides were imaged using the Axioplan 2 imaging microscope (Carl Zeiss) and images were captured and processed using AxioVision 4.8 software. Images were acquired with a variety of magnification objective lenses: 10x Zeiss PlanNEOFLUAR 10x/0,30, 20x Zeiss PlanNEOFLUAR 20x/0,50, 40x Ph2 PlanNEOFLUAR 40x/0,75, and 63x Ph3 Plan-APOCHROMAT 63x/1,40 oil. Images were acquired in xyz scan mode at 520 Hz scanning speed. Scanned fields of view were 23 x 23 mm. Each image was generated at 512 x 512 pixels, with 8-bit colour resolution. For detection of enzymatic immunohistochemical staining (Method 2.5.2.7) a white light source was used (HAL 100 halogen illuminator). For detection of epifluorescent staining (Method 2.5.3), a HBO103 mercury vapour short-arc lamp emitting at light at various wavelengths (from 289 to 579 nm) was used as the excitation light source; in combination with emission filters to observe DAPI (peak emission = 461 nm), FITC/GFP (peak emission = 519 nm), and Texas red fluorescence (peak emission = 613 nm). For fluorescence imaging, each channel was set to the maximum exposition time which gave no signal detection in the control sample (usually a no primary antibody incubation sample). For analysis of cell migration (Method 2.7.4), cells were imaged using the Zeiss Observer Z1 microscope and the images captured using AxioVision 4.8 software. Images were acquired with a 10x magnification lens (10x Zeiss A Pla 10x 0.25 Ph1) and a phase contrast filter.

2.6.2 Confocal microscopy

Confocal microscopy was used when increased detection sensitivity and staining resolution was required. For these reasons, confocal microscopy was used to assess endogenous TASK channel staining, analyse protein colocalisation, and quantify protein staining following siRNA transfection (Method 2.4.5.1).

Images were acquired with the inverted confocal microscope Leica TCS SP5 II (Leica). Confocal images were acquired in xyz scan mode with 90 ° rotation at 600 Hz scanning speed using an x63 HCX Plan Apo Lambda Blue NA 1.4 UV oil immersion objective and a pinhole of 1 Airy Unit. Scanned fields of view were 124 x 124 µm. Z-slices were taken every 1 µm for examination of native TASK channel expression or 0.5 µm for colocalisation experiments. Each Z-slice was generated as the average of 4 acquired frames at 1024 x 1024 pixels with 8-bit colour resolution.

To specifically excite each fluorophore used for immunofluorescent staining (Method 2.5.3), different lasers emitting at specific wavelengths were employed as the excitation light source. DAPI (nuclear counterstain) was excited with a soft UV diode laser at 405 nm, green stains (FITC and GFP) were excited with an Argon laser at 488 nm, mid red dyes (e.g. Alexa Fluor® 594) were excited with a yellow diode-pumped solid state (DPSS) laser at 561 nm, and far red dyes (e.g. Alexa Fluor 647®) were excited with a Helium-Neon (NeNe) laser at 594 and 633 nm. All lasers were used at 30 % power.

Confocal images (Method 2.6.2) were visualised and exported using LAS AS Lite software, images are presented as single slices or z-stacks. To determine channel knockdowns, the antibody signal for the channel of interest was compared between siRNA transfected cells and untransfected cells using the LAS AS Lite software. For A549 cells, a line defining the region of interest (ROI) was traced across 20 cells from two separate fields of view and the mean fluorescence intensity (MFI) of the channel staining signal was quantified along the ROI. For HCT116 cells, the MFI of the three separate fields of view were calculated. To verify protein colocalisation, a single Z-slice was analysed using LAS AS Lite software by drawing a transect line to define the region of ROI across a transfected cell. The fluorescence intensity of each staining signal was quantified along the ROI. Colocalisation was demonstrated by fluorescence intensity overlap between both staining signals which indicated that the proteins of interest were in the same location.

2.7 Functional assays

To investigate the role of KCh activity in cancer cell functions, proliferation (Method 2.7.2), apoptosis (Method 2.7.3), and migration (Method 2.7.4) assays were

performed. Assays were carried out in control conditions and in the presence of channel inhibitors (Method 2.7.1) or environmental regulation (Method 2.4.2).

2.7.1 Inhibitors

TASK channels were inhibited with 0.1-100 µM genistein (G6649, Sigma), 0.1-50 µM methanandamide (M186, Sigma), and 0.1-100 µM ruthenium red (R2751, Sigma). Broad spectrum KCh inhibition using 0.1-20 mM 4-aminopyridine (4-AP; 275875 Sigma) was utilised for functional assays and 30 mM tetraethylammonium (TEA; T2265, Sigma) for electrophysiological recordings. 10 µM etoposide (E1838, Sigma) was used as a positive control for apoptosis analysis (Method 2.7.3)

2.7.2 Proliferation

MTS assays (3-(4,5-dimethylthiazol-2-yl)-5-(3-carboxymethoxyphenyl)-2-(4-sulfophenyl)-2H-tetrazolium inner salt, CellTiter 96 aqueous non-radioactive cell proliferation assay kit; Promega) were used to measure the number of viable cells following channel modulation. In this assay, the tetrazolium dye is reduced to a formazan product by the mitochondria of living cells; this is quantified by measuring the absorbance at 490 nm. Therefore, the resulting absorbance is proportional to the number of cells. If the modulation tested was not causing cell death, which was assessed in separate assays by flow cytometry (Method 2.7.3), any change in cell numbers are likely to be caused by altered proliferation. Cell numbers were assessed, by MTS assays, following a 24 h treatment with KCh modulation. This time point was selected so that sufficient time was given for chronic channel modulation and cell cycle progression, without the need for the cell media to be changed during the assay.

Cells were seeded in triplicate in a 96 well plate with 5,000 cells/100 µl media per well, blank wells with media no cells were also set up in triplicate. The plate was incubated for 24 h, at 37 °C (5 % CO_2). After 24 h the media was aspirated, 100 µl fresh media added ± inhibitors (Method 2.7.1) and the cells were then incubated for a further 24 h. To assess environmental regulation on cell line proliferation, after cell seeding for 24 h, cells were cultured under altered environmental parameters (Method 2.4.2; low glucose or hypoxia)

alongside channel inhibitors for 24 h. Proliferation was assessed after 24 h by addition of 20 µl MTS reagent to each well and incubation for 2 h after which absorbance of each well in the plate was measured at 490 nm using the FLUOstar OPTIMA plate reader (BMG Labtech).

All data were analysed using GraphPad Prism 6 to calculate the IC_{50} for each inhibitor treatment. If inhibition reached a 50 % growth inhibition once the IC_{50} was calculated, the statistical significance of these results were calculated using a Student's t-test (Method 2.9). For data examining the effect of environmental regulation on cell proliferation, the average absorbance was assessed using GraphPad Prism 6 for each condition and the significance calculated using ANOVA testing (Method 2.9).

2.7.3 Apoptosis

The apoptotic response of cells to channel knockdown and inhibitors was measured using flow cytometry with staining for extracellular phosphatidylserines using annexin V and a dead cell stain. In viable cells, phosphatidylserines are located on the cytoplasmic side of the plasma membrane and when cells become apoptotic they are moved onto the extracellular surface of the plasma membrane.

Cells were seeded into 6 well plates 72 h prior to analysis by flow cytometry. For each experiment wells were plated for treatment conditions and controls. As a positive control an apoptosis inducer (etoposide) was used and on the day of seeding, the cells were treated o/n with 10 µM etoposide and the media changed the 16 h later. 24-48 h prior to flow cytometry analysis cells were treated with altered environmental stimuli (Method 2.4.2) and/or channel inhibitors (Method 2.7.1). To assess the effect of a functional channel knockdowns on cell death, cells were transfected with GFP tagged pore mutant (G97E) channels 24 h prior to apoptosis analysis (Method 2.4.5). Apoptosis was measured at either 24 h or 48 h time points as this allowed sufficient time for cell death to occur, in addition this allowed any cell death effects observed at 48 h to be related to the proliferative response observed at 24 h (Method 2.7.2).

All washing steps were performed by adding 500 µl of buffer to cell pellets, vortexing and centrifuging for 1,400 g at 4 °C for 3 min. Cells were harvested by trypsin and washed once with PBS, cell lysates were then transferred to flow cytometry analysis tubes (BD Biosciences). Cell pellets were washed, vortexed, and pelleted 3 times in flow cytometry buffer (1 % FBS in PBS). Cells pellets were then washed in 500 µl annexin V binding buffer (10 mM HEPES, 140 mM NaCl, 25 mM $CaCl_2$, pH 7.4), vortexed, and pelleted. For cell staining, cells were incubated for 15-30 min in the dark with 100 µl annexin V FITC (courtesy of Patrick Dunz; Cancer Sciences division, University of Southampton) diluted 1:100 in annexin V binding buffer for untransfected cells, or annexin V Alexa Fluor® 647 (1:50; Invitrogen) for GFP transfected cells. Immediately prior to analysis, cells were stained with 500 µl SYTOX AADvanced Dead Cell Stain (Invitrogen) diluted 1:1000 in binding buffer, to label dead cells.

Cells were analysed immediately after staining using the FACSCanto I flow cytometer (BD Biosciences). Compensation controls were set up for each individual experiment using cells population which were untransfected and unstained, GFP transfected and unstained, annexin V stained alone, and SYTOX stained alone. Gates were drawn to represent cell population and 5,000-20,000 events were measured from this population. Data were analysed by quadrant analysis to represent four staining populations (SYTOX stained (Q1; dead/damaged), annexin V and SYTOX stained (Q2; late apoptosis), unstained (Q3; live), annexin V stained (Q4; early apoptosis)) and extracted using the FACSDiva software. The percentages of annexin V positive cells (for the cell or GFP expressing cell populations) are presented and the statistical significance was calculated using ANOVA testing in GraphPad Prism 6 (Method 2.9).

2.7.4 Migration

The ability of A549 lung cancer cells to migrate following pharmacological inhibition was examined using wound healing assays. A549 cells were seeded at 350,000 cells per well into 0.01 % poly-L-lysine coated 6 well plates, since this density reached > 90 % confluent at start the assay. For experiments examining altered environmental conditions, cells were treated for 24 h with altered environmental stimuli, following cell seeding for 4 h (Method 2.4.2). For all experiments, channel inhibitors were added at time point 0 h

(Method 2.7.1). During optimisation experiments, A549 cells closed the wound between 9-12 h. Therefore, a time course from 0-9 h (assessing migration at 3 h intervals) was used to examine the migration of A549 cells. Due to this rapid migration of A549 cells (< 9 h), the cells were not serum starved during the assay.

At time point 0 h, the media was aspirated from the wells, and a guideline was drawn on the underside of the plate. Two wounds were made in each well perpendicular to the guideline using a p200 pipette tip. The cells were then washed 3 times in PBS before the media was replaced. To assess the migration of cells, the wounds were imaged (Method 2.6.1) at various time points from 0-9 h taking two images for each scratch (above and below the guideline). To quantify the migration of cells the wound was measured using TScratch image analysis software (Gebäck et al., 2009) by determining the area of the field covered by cells. The percentage of the field of view covered by cells was presented and statistical significance calculated using GraphPad Prism 6 (Method 2.9).

2.8 Electrophysiology

2.8.1 Cell culture for electrophysiological analysis

To assess the activity of endogenous or transiently expressed TASK channels in cultured cell lines whole-cell patch clamp experiments were performed. To ensure consistent and comparable recordings, the cells (A549 and HEK293) used for electrophysiological experiments in this study originated from a single culture source. In addition, the expression of endogenous TASK channels in A549 cells were regularly checked, at an mRNA level (using RT-PCR; Method 2.3.12). The electrophysiological properties (current amplitude and reversal potential) of uninhibited A549 and untransfected HEK293 cells were comparable throughout the duration of this study.

For transfected channel recordings, HEK293 cells were plated 24 h prior to recording onto 22 mm sterile glass coverslips in 6 well plates, in single cell suspension at a low density (20,000 cells per well). The cells were seeded for 4 h before transfection using jetPEI (Method 2.4.5); the cDNA plasmids and concentrations which were transfected into HEK293 cells for electrophysiological experiments are shown in Table 2.30. Cells were

typically analysed by whole-cell patch clamp experiments 16-24 h after transfection and generally between 50-70 % of the cells were transfected (identified by GFP fluorescence). For endogenous channel recordings, A549 cells were plated in single cell suspension, at a low density (20,000 cells per well), onto 22 mm sterile glass coverslips in 6 well plates, 24 h prior to whole-cell patch clamp experiments.

To characterise the regulation of endogenous TASK channel activity by environmental conditions (Method 2.8.2), A549 cells were cultured in 0.5 g/l glucose media or 5 % O_2 for 24 h prior to whole-cell patch clamp analysis (Method 2.4.2). To examine the impact of chronic hypoxia on transfected channels expressed in HEK293 cells (Method 2.4.5), the cells were cultured in 5 % O_2 for 24 h after the media was changed following incubation with the DNA complexes.

2.8.2 Whole-cell patch clamp experiments

Electrodes for whole-cell patch clamp experiments were pulled from Brososilicate glass capillaries (1B150-4, World Precision Instruments) using the two-stage Narishige PC-10 pipette puller (Narishige Scientific Instrument Laboratory). Tips were then heat polished, using a Narishige MF-830 microforge, to produce electrodes with a resistance of 2-5 megaohm (MΩ) when backfilled with filtered intracellular solution (Table 2.31). For recordings, cells were placed in a bath of extracellular solution (Table 2.31). A gigaohm (GΩ) seal was achieved between a single cell and the electrode by applying suction, with further suction pulses being applied to rupture the membrane under the pipette to enable a whole-cell configuration. Following the successful transition to the whole-cell configuration, the capacitance transients were compensated for and measured.

All recordings were performed using an Axopatch 200B amplifier (Axon instruments), in combination with Clampex 10.2 software and an Axon Digidata 1400A (Axon instruments). Cells were held at a holding potential of -60 mV and test potentials were applied between -100 mV to +90 mV (10 mV steps, for 50 (HEK293 cells) or 70 ms duration (A549 cells)), and the current evoked recorded. To measure the effect of channel inhibitors or altered pH, perfusion was applied to the cells for 2-3 min between recordings to ensure complete exchange of the bath solution.

Table 2.30: cDNA plasmids used for patch clamp analysis

The channel cDNA constructs, plasmid backbone, and quantity of DNA (µg) transfected into cells for electrophysiological analysis are shown.

Construct	Plasmid	DNA (µg)
Human $K_{2P}3.1$ (untagged)	pRAT	2.0
Human wild type GFP-$K_{2P}3.1$	pEGFP-C1	2.0
Human GFP-$K_{2P}3.1_{G97E}$	pEGFP-C1	2.0
Rat wild type $K_{2P}3.1$	pcDNA3.1+	1.5
Rat $K_{2P}3.1_{N53Q}$	pcDNA3.1+	1.5
Human wild type GFP-$K_{2P}9.1$	pEGFP-C1	1.0
Human GFP-$K_{2P}9.1_{G97E}$	pEGFP-C1	1.0
Rat wild type $K_{2P}9.1$	pcDNA3.1+	0.1-0.25
Rat $K_{2P}9.1_{N53Q}$	pcDNA3.1+	0.1-0.25
GFP (alongside untagged channels)	pEGFP-C1	0.25-0.75

Table 2.31: Solutions used for whole-cell patch clamp experiments

Showing the basic composition of solutions used for whole-cell patch clamp recordings

Solution	Composition
Intracellular solution	150 mM KCl 1 mM $MgCl_2$ 10 mM HEPES 2 mM EGTA pH 7.2
Extracellular solution	135 mM NaCl 5 mM KCl 1 mM $MgCl_2$ 10 mM HEPES 1 mM $CaCl_2$ (20 mM Glucose for control A549 recordings) pH 6.0-7.8
Extracellular solution With TEA	135 mM NaCl 5 mM KCl 1 mM $MgCl_2$ 10 mM HEPES 1 mM $CaCl_2$ 30 mM TEA pH 6.0-7.8

All experiments were carried out at RT and current data were analysed using the Clampfit 10.2 software. The inclusion criteria for analysis were: (i) the current evoked at -100 mV must not be more than half of the maximal current recorded, (ii) the current-voltage (*I-V*) relationship must have a negative reversal potential, and (iii) the *I-V* relationship must not be linear.

GraphPad Prism 6 was used to plot and calculate the statistical significance of the whole-cell patch clamp data (Method 2.9). The replicate values for whole-cell patch clamp experiments are the number of cells (n) recorded, corresponding to recordings made on multiple experimental days. The quantification of whole-cell current data are presented as the current amplitude, either in picoamps (pA) or nanoamps (nA), observed at a particular voltage (+40 mV for native channel recordings or +60 mV for transfected channel recordings). This measurement was appropriate for the data presented in this thesis due to both A549 and HEK293 cells being cultured cell lines. This meant that there was little variation in cell size, which may have impacted on the size of the currents observed. As a result of this, the membrane capacitances recorded were within the same range, from approximately 2.0-3.0 pF (picofarads) for A549 cells and 1.5-2.5 pF for HEK293 cells.

2.9 Statistics

All data are presented as the average ± standard error of the mean (SEM), which were calculated as the standard deviation divided by the square root of the number of samples (n). Statistically significant differences between different sets of data were calculated in GraphPad Prism 6 statistical software using a Student's *t*-test or analysis of variance testing (ANOVA) with post-hoc multiple comparisons testing. The post-hoc test used depended on the experimental design, and was typically Dunnett's, Turkey's, or Sidak's testing. The levels of significance used are: ns non-significant, * $p < 0.05$, ** $p < 0.01$, *** $p < 0.001$, and **** $p < 0.0001$.

Chapter 3

Results

Bioinformatic analysis of K_{2P} channel mRNA expression in human cancers

3.1 Introduction

K_{2P} channels have emerged as a potential target for cancer therapies over the last eleven years (Introduction 1.7). To date, four of the fifteen members of the K_{2P} channel family have been implicated in cancer: K_{2P}2.1, K_{2P}3.1, K_{2P}5.1, and K_{2P}9.1 (Introduction 1.7). However, no comprehensive study has been conducted to determine if the entire K_{2P} channel family undergo alterations in cancer. Therefore, the aim of this chapter was to use bioinformatic analysis to examine the mRNA expression of all fifteen K_{2P} channels in twenty cancer tissues from human patients compared to matched normal, healthy controls (see Section 3.1.1 for the overall and specific aims of this Chapter).

The lack of expression data on the K_{2P} channel family in cancer meant that it was unclear to what extent mRNA or protein levels were altered in disease tissue; for example, were K_{2P} channels only overexpressed in cancer or does channel underexpression also occur? Additionally, published work has focused on studying the expression of individual K_{2P} channels in single cancer types. Thus, no study has been conducted to determine if altered K_{2P} channel expression correlates to different cancer types. If specific K_{2P} channels/subfamilies were altered within one cancer type this may provide an indication of any functional advantages the channels are providing based on their published physiological functions. To address these questions, a bioinformatic approach was selected by utilising the online cancer microarray database Oncomine (www.oncomine.org; Method 2.2).

The use of Oncomine to conduct an expression study has a number of benefits: (i) all fifteen K_{2P} channels can be studied in the same twenty cancer types, (ii) the expression in cancer tissues can be compared to matched normal tissue controls, thereby providing a measure of the expression alterations, and (iii) all the data available on Oncomine has been processed using the same criteria, meaning that direct comparisons can be made between different channels and studies. Thus, Oncomine analysis allowed a wide scale expression study to be performed on K_{2P} channels in cancer and provided a substantial amount of new information on the expression of K_{2P} channels in cancer.

Oncomine is used here with a number of caveats that should be considered when interpreting the data. These limitations are discussed further in Section 3.3. However, the

most significant limitation is that this study only examined K_{2P} channel mRNA expression in cancer, therefore any implications for K_{2P} channel protein levels and activity would require further investigation. Nevertheless, use of Oncomine in this study revealed that nine K_{2P} channels are significantly altered in cancer, compared to the four channels which had been previously identified from published studies.

3.1.1 Aim

Determining the expression profile of K_{2P} channels in cancer cells is important because alterations to K_{2P} channel expression and activity could have profound implications for cancer cell function. The current hypothesis for how this might occur is that altered K_{2P} channel activity will change the membrane potential of cancer cells and, thereby, the activity of other ion channels (see Figure 1.12 and Introduction 1.8). The aim of this chapter is divided into three specific points based on the questions raised in published literature, these points are summarised below:

1. To determine which members of the K_{2P} channel family undergo expression alterations in cancer.
2. To examine if K_{2P} channels undergo both over- and underexpression in cancer.
3. To assess if any K_{2P} channels/subfamilies can be linked to specific cancer types.

3.2 Analysis of K_{2P} channel mRNA expression in human cancers

In this chapter, the mRNA expression of the entire K_{2P} channel family, encoded by *KCNK1-18* genes, was characterised across 20 cancer types compared to matched normal tissue controls. To achieve this experimental goal, bioinformatic analysis of K_{2P} channel mRNA in human cancers was performed using the publically available cancer microarray database, Oncomine (www.oncomine.org; Method 2.2). Searches were performed using the following threshold values: p-value < 0.05, fold change > 2, and gene rank percentile < 10 %. Initially, a gene summary approach was utilised to get a global view of the K_{2P} channel mRNA expression in cancer. Coloured shading was used to represent the gene rank

percentile score (either top 1 %, 5 %, or 10 % of genes with altered expression) for a given channel within a cancer type; this ranking was based on the presence of one or the highest ranked above threshold analysis.

Of the 20 cancer types present on Oncomine, six cancers exhibited mRNA overexpression compared to matched normal tissue controls for at least three K_{2P} channels: breast, kidney, leukaemia, lung, lymphoma, and "other" cancers (Figure 3.1). Six cancers showed no overexpression of K_{2P} channel mRNA: colorectal, liver, melanoma, myeloma, ovarian, and prostate (Figure 3.1). Examining the pattern of K_{2P} channel mRNA overexpression revealed that four channels were overexpressed in over five different cancer types (Figure 3.1): K_{2P}1.1 (12/20), K_{2P}3.1 (7/20), K_{2P}5.1 (5/20), and K_{2P}12.1 (5/20). In contrast, four channels did not show mRNA overexpression in these cancers (Figure 3.1): K_{2P}4.1, K_{2P}7.1, K_{2P}16.1, and K_{2P}18.1. Additionally, there was no obvious pattern for one K_{2P} channel subfamily being more upregulated than another.

The underexpression of K_{2P} channel mRNA was examined in the same 20 cancer types (Figure 3.2). There was an increase in the number of results for K_{2P} channel mRNA underexpression with 54 above threshold analyses, compared to 42 for overexpression (Figure 3.1). This suggested that there is more K_{2P} channel underexpression in cancer at an mRNA level. Over 50 % (11/20) of the cancer types examined had mRNA underexpression for at least three K_{2P} channels (Figure 3.2): brain and CNS, breast, colorectal, gastrointestinal, head and neck, kidney, lung, melanoma, "other" cancers, prostate, and sarcoma (Figure 3.2). In addition, six K_{2P} channels showed mRNA underexpression in over five cancer types (Figure 3.2): K_{2P}1.1 (7/20), K_{2P}2.1 (5/20), K_{2P}3.1 (10/20), K_{2P}5.1 (10/20), K_{2P}7.1 (8/20), and K_{2P}10.1 (5/20). There was also no indication for one K_{2P} channel subfamily being more downregulated than another.

The mRNA of three K_{2P} channels (K_{2P}4.1, K_{2P}16.1, and K_{2P}18.1) did not show any alterations in the cancers examined, despite the presence of datasets examining these genes (Figures 3.1 and 3.2).

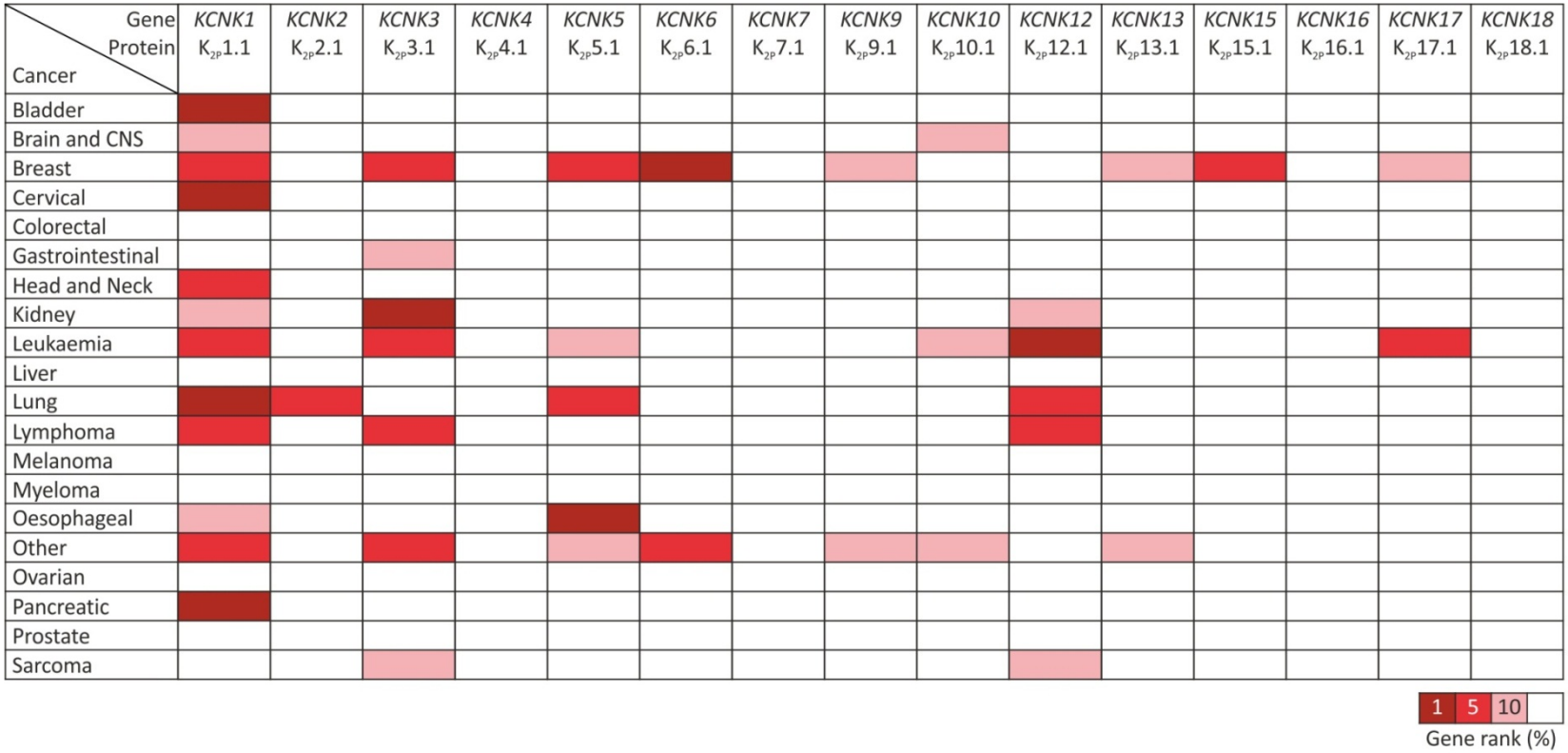

Figure 3.1: Overexpression summary of K_{2P} channel mRNA expression in cancer

Overexpression of K_{2P} channel mRNA (*KCNK1-18*) was assessed in 20 cancer types, compared to normal tissue controls. The protein nomenclature is indicated for each gene.

The search criteria applied were, for mRNA datasets looking at cancer vs. normal expression, with threshold values for inclusion: p-value < 0.05, fold change > 2, and gene rank percentile < 10 %.

Overexpression of K_{2P} channel mRNA in different cancer types is indicated by red shading, where the degree of colour correlates to the gene rank percentile (%) of the highest ranked analysis.

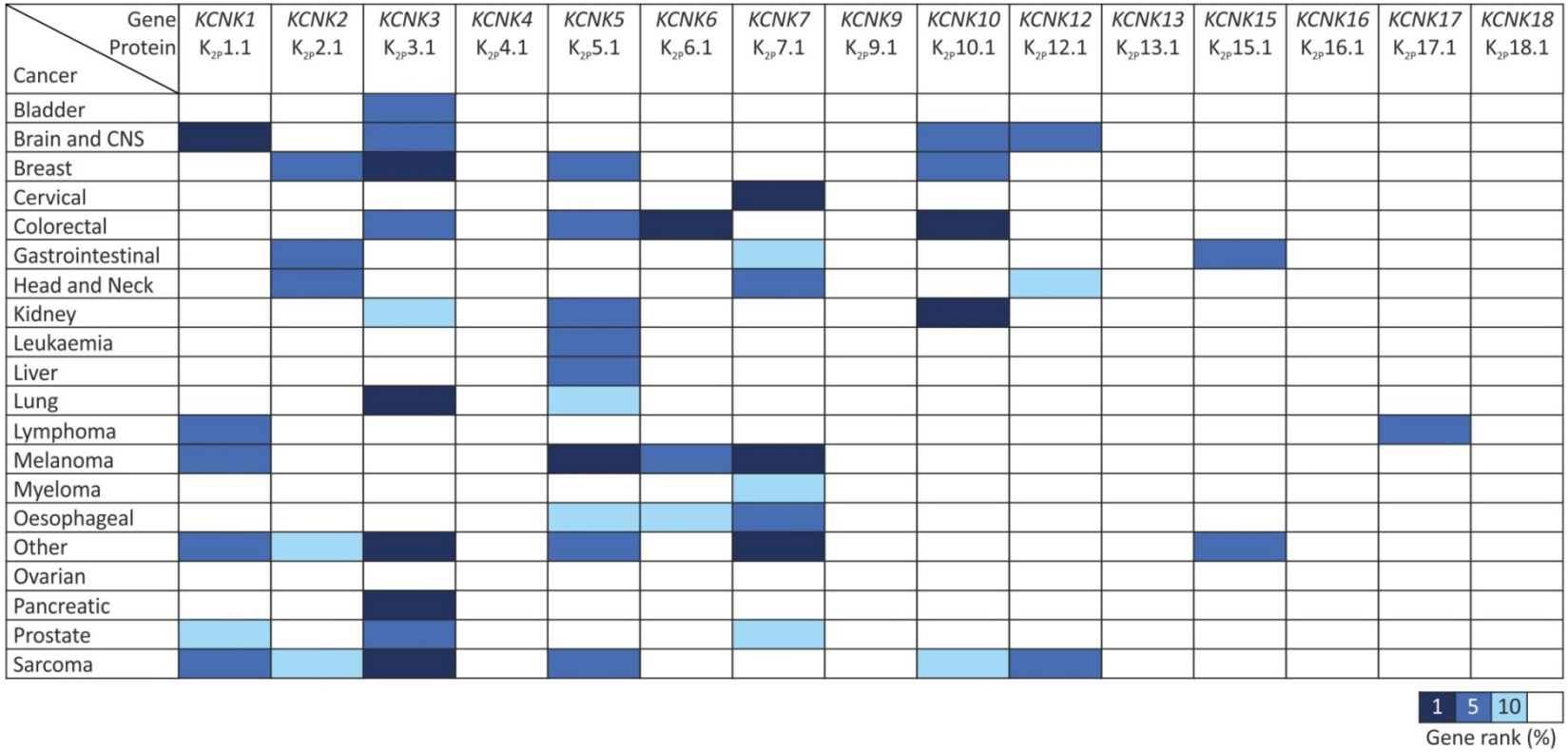

Figure 3.2: Underexpression summary of K_{2P} channel mRNA expression in cancer

Underexpression of K_{2P} channel mRNA (*KCNK1-18*) was assessed in 20 cancer types, compared to normal tissue controls. The protein nomenclature is indicated for each gene.

The search criteria applied were, for mRNA datasets looking at cancer vs. normal expression, with threshold values for inclusion: p-value < 0.05, fold change > 2, and gene rank percentile < 10 %.

Underexpression of K_{2P} channel mRNA in different cancer types is indicated by blue shading, where the degree of colour correlates to the gene rank percentile (%) of the highest ranked analysis.

In some cases, channels had rankings for both mRNA over- and underexpression in a particular cancer type. For example, in brain and CNS cancers, K_{2P}1.1 mRNA was ranked in the top 10 % for overexpression and top 1 % for underexpression. This can occur due to the broad cancer groupings, which include many cancer subtypes. The coloured shading in the data Figures 3.1 and 3.2 only represented the highest ranking analysis in that category. Therefore, if one cancer subtype showed mRNA overexpression whilst another showed underexpression, the channel will have a gene rank percentile for both mRNA over- and underexpression.

To get a more detailed picture of the K_{2P} channel mRNA expression in cancer, each channel (with the exception of K_{2P}4.1, K_{2P}16.1, and K_{2P}18.1) was further examined in 14 cancer types. The results of these analyses are grouped by the K_{2P} channel subfamilies. Six cancers were excluded from this analysis due to low dataset numbers or high cancer subtype diversity (Table 2.1). This analysis was performed using the same search criteria: comparing mRNA expression in cancer to normal tissue and the search threshold values (p-value < 0.05, fold change > 2, and gene rank percentile < 10 %). Comparative meta-analysis was performed for the channel of interest when at least three studies (n ≥ 3) in a particular cancer subtype were available. If the median ranked analysis had a significant p-value (p < 0.05), it indicated that the expression trend observed was likely to be significant.

3.2.1 Analysis of TWIK channel family expression in cancer

K_{2P}1.1 mRNA showed the widest expression of the entire K_{2P} channel family across the cancers examined (10/20 cancers), with a general trend for overexpression (Table 3.1). The most significant K_{2P}1.1 mRNA overexpression was detected in lung adenocarcinomas. K_{2P}1.1 mRNA was not exclusively overexpressed, significant underexpression was observed in glioblastomas and melanomas (Table 3.1). The mRNA of the other two TWIK subfamily members K_{2P}6.1 (2/20 cancers) and K_{2P}7.1 (4/20 cancers) were generally underexpressed in cancer (Table 3.2). The potential functional implications resulting from alterations in TWIK family mRNA expression in cancer are discussed in Section 3.3.2.1.

Table 3.1: TWIK channel family member, *KCNK1*, expression in cancer

The above threshold data for the TWIK family member, *KCNK1*, are shown. Data are divided into each cancer type and subtypes. The p-value, fold change, and gene rank percentile (%) for above threshold data are given. The threshold values used were: p-value < 0.05, fold change > 2, and gene rank percentile < 10 %.

Comparative meta-analysis was performed when n ≥ 3 analyses were available. This gave the median gene rank and median p-value.

Overexpression (↑) and underexpression (↓) are indicated in red and blue respectively.

mRNA	Cancer	Subtype	Above threshold analyses				Median values		
			p-value	Fold change	%	Ref	p-value	Gene rank	n
KCNK1	Bladder	Infiltrating	↑ 1.05E-10	2.283	1	2	1.60E-04	1306	4
			↑ 6.67E-08	2.701	7	1			
		Superficial	↑ 1.12E-16	5.285	3	2	0.005	2543	4
			↑ 2.79E-08	2.385	1	1			
	Brain	Astrocytoma	↓ 3.75E-08	-4.168	4	9	0.028	1042	4
			↓ 8.09E-08	-6.64	1	8			
		Glioblastoma	↓ 1.72E-24	-9.574	2	9	5.14E-06	560.5	8
			↓ 1.80E-14	-20.541	3	10			
			↓ 1.07E-08	-8.483	3	3			
			↓ 1.03E-05	-13.309	4	6			
			↑ 5.89E-04	3.178	6	5			
		Medulloblastoma	↓ 2.60E-08	-14.207	2	7	-	-	2
			↓ 5.48E-05	-10.211	2	7			
		Oligodendrioglioma	↓ 5.42E-16	-4.813	1	9	0.002	1633	3
			↓ 2.00E-03	-3.963	9	4			
	Breast	Ductal	↑ 5.23E-04	2.515	5	16	0.002	2547	12
			↑ 7.18E-04	3.965	5	12			
			↑ 1.00E-03	2.405	5	15			
			↑ 4.00E-03	2.661	9	12			
			↑ 1.10E-02	2.4	9	13			
		Lobular	↑ 2.20E-02	2.177	4	13	0.031	3848	5
	Cervical	Squamous cell	↑ 9.70E-13	2.949	1	20	0.043	3326	5
	Head and Neck	Tongue squamous cell	↑ 2.98E-10	2.277	3	34	4.67E-05	662.5	4
			↑ 9.00E-05	2.784	3	35			
			↑ 3.35E-06	2.88	10	31			
	Leukaemia	Acute lymphocytic	↑ 4.00E-03	2.173	5	42	9.04E-07	4799	7
	Lung	Adenocarcinoma	↑ 3.59E-07	3.984	2	52	8.51E-13	511	7
			↑ 5.38E-07	2.141	3	46			
			↑ 2.35E-05	4.641	1	47			
			↑ 6.21E-05	2.137	8	51			
		Squamous cell	↑ 5.98E-08	2.138	9	49	0.002	852	6
			↑ 2.61E-06	7.79	2	47			
	Melanoma	Melanoma	↓ 7.58E-04	-2.769	4	56	0.002	1487	4
			↓ 1.55E-04	-5.725	3	57			
	Oesophageal	Barrett's	↑ 1.60E-02	2.352	7	62	0.032	2211	4
	Pancreas	Adenocarcinoma	↑ 9.83E-10	3.526	5	71	0.008	787.5	8
			↑ 2.61E-04	6.584	3	72			
			↑ 1.41E-04	6.62	5	73			
			↑ 1.21E-08	4.613	1	74			
			↑ 2.00E-03	2.685	9	75			

Table 3.2: TWIK channel family members, *KCNK6* and *KCNK7*, expression in cancer

The above threshold data for TWIK family members, *KCNK6* and *KCNK7*, are shown. Data are divided into each cancer type and subtypes. The p-value, fold change, and gene rank percentile (%) for above threshold data are given. The threshold values used were: p-value < 0.05, fold change > 2, and gene rank percentile < 10 %.
Comparative meta-analysis was performed when n ≥ 3 analyses were available. This gave the median gene rank and median p-value.
Overexpression (↑) and underexpression (↓) are indicated in red and blue respectively.

mRNA	Cancer	Subtype	Above threshold analyses				Median values		
			p-value	Fold change	%	Ref	p-value	Gene rank	N
KCNK6	Breast	Ductal	↑ 2.77E-19	2.161	9	17	0.076	5236	10
			↑ 1.00E-03	2.765	1	14			
		Invasive	↑ 5.44E-04	3.237	1	14	0.059	4104	4
	Colorectal	Adenocarcinoma	↓ 1.77E-18	-2.071	4	26	0.028	4860	11
			↓ 2.38E-15	-2.11	7	26			
			↓ 9.37E-15	-2.136	1	26			
	Melanoma	Melanoma	↓ 2.01E-04	-2.209	3	57	-	-	2
	Oesophageal	Adenocarcinoma	↓ 2.20E-12	-2.223	8	61	2.20E-12	1409	3
KCNK7	Cervical	Squamous cell	↓ 5.62E-10	-6.76	1	21	7.99E-04	519	5
			↓ 1.86E-08	-3.055	1	22			
			↓ 7.99E-04	-3.315	5	22			
	Gastrointestinal	Adenocarcinoma	↓ 1.60E-02	-2.336	10	29	0.446	9583	5
	Melanoma	Melanoma	↓ 7.33E-09	-64.334	1	57	0.004	2573	3
	Oesophageal	Adenocarcinoma	↓ 2.40E-17	-2.681	4	61	2.40E-17	667	3
			↓ 3.74E-04	-9.38	2	62			
		Barrett's	↓ 1.12E-10	-2.608	5	61	1.12E-10	794.0	3
			↓ 3.00E-03	-2.586	3	60			

3.2.2 Analysis of TREK channel family expression in cancer

Overall, the TREK family was significantly underexpressed in cancer, with K_{2P}10.1 mRNA showing the widest range of expression (Table 3.3). These data differ from published work which has identified K_{2P}2.1 protein overexpression in invasive prostate adenocarcinomas (Voloshyna et al., 2008). No alterations of K_{2P}2.1 mRNA were detected in prostate cancers (Table 3.3), therefore, in prostate adenocarcinomas, K_{2P}2.1 expression may only be altered at a protein level. Currently no studies have described differential K_{2P}10.1 mRNA expression in cancer, although K_{2P}2.1 and K_{2P}10.1 protein has been detected in both cancerous and normal ovarian tissue (Innamaa et al., 2013a). The potential functional implications resulting from alterations to TREK family mRNA expression in cancer are discussed in Section 3.3.2.2.

3.2.3 Analysis of TASK channel family expression in cancer

Of the entire K_{2P} channel family, K_{2P}3.1 was the second most altered channel in the cancers examined, with a general trend for underexpression (Table 3.4). The most significant K_{2P}3.1 mRNA underexpression detected was in lung squamous cell carcinomas. K_{2P}3.1 mRNA was also significantly overexpressed in invasive breast and clear cell kidney cancers (Table 3.4). Prior to this study, differential expression of K_{2P}3.1 mRNA had not been described in cancer, although K_{2P}3.1 mRNA expression was detected in adrenal adenoma tissue (Nogueira et al., 2010) and medulloblastoma cell lines (protein and functional currents; Ernest et al., 2010).

K_{2P}9.1 showed no significant mRNA expression changes in the cancers analysed, following comparative meta-analysis (Table 3.4). These findings differed from data presented by Mu et al. (2003), which show amplification of K_{2P}9.1 mRNA in 44 % of breast and 35 % of lung cancers, compared to matched normal tissue controls. There is no simple explanation for these differences; one reason may be that different cancer subtypes were analysed by the two studies. In the majority of breast cancer samples examined by Mu et al. (2003), *KCNK9* genomic amplification was detected and this information was not available for the studies analysed on Oncomine. Additionally, alterations to K_{2P}9.1 channels at a protein level may be more common in cancer. For example, differential K_{2P}9.1 protein

overexpression has been identified in colorectal carcinomas (Kim et al., 2004), although the authors did not examine K_{2P}9.1 mRNA in this study.

The mRNA levels for K_{2P}15.1, the non-functional TASK channel family member, was significantly altered in two cancers and showed no trend for over- or underexpression (Table 3.4). The potential functional implications resulting from alterations in the mRNA levels of all three members of the TASK family in cancer are discussed in Section 3.3.2.3.

3.2.4 Analysis of TALK channel family expression in cancer

Only one TALK channel, K_{2P}5.1, was significantly altered in cancer (4/20 cancers), with a general trend for mRNA underexpression (Table 3.5). Although, the most significant alteration of K_{2P}5.1 mRNA identified was overexpression in lung adenocarcinomas (Table 3.5). K_{2P}5.1 channels have been previously described to have a role in breast cancer cells, where K_{2P}5.1 expression (mRNA and acid-sensitive currents) was upregulated by proliferative oestrogen receptor α signalling (Alvarez-Baron et al., 2011; Williams et al., 2007a). Alvarez-Baron et al. (2011) did not examine the expression of K_{2P}5.1 mRNA or protein in breast cancer tissue, and the data presented here did not identify any alterations to K_{2P}5.1 mRNA in breast cancers (Table 3.5). Therefore, the regulation of K_{2P}5.1 expression by oestrogen receptor signalling may be critical for the role of this channel in breast cancer. The potential functional implications resulting from alterations in K_{2P}5.1 channel expression in cancer are discussed in Section 3.3.2.4.

3.2.5 Analysis of THIK channel family expression in cancer

Of the THIK channel family, only K_{2P}12.1 showed significantly altered mRNA expression in cancer (3/20 cancers) with a general trend for overexpression (Table 3.6). K_{2P}12.1 mRNA was most significantly altered in acute lymphocytic leukaemia (Table 3.6). These analyses originate from the same dataset; therefore this comparison may not be a true representation of K_{2P}12.1 mRNA expression. The potential functional implications resulting from alterations in K_{2P}12.1 channel expression in cancer cells are discussed in Section 3.3.2.5.

Table 3.3: TREK channel family expression in cancer

The above threshold data for TREK family members, *KCNK2* and *KCNK10*, are shown. Data are divided into each cancer type and subtypes. The p-value, fold change, and gene rank percentile (%) for above threshold data are given. The threshold values used were: p-value < 0.05, fold change > 2, and gene rank percentile < 10 %.
Comparative meta-analysis was performed when n ≥ 3 analyses were available. This gave the median gene rank and median p-value.
Overexpression (↑) and underexpression (↓) are indicated in red and blue respectively.

mRNA	Cancer	Subtype	Above threshold analyses				Median value		
			p-value	Fold change	%	Ref	p-value	Gene rank	N
KCNK2	Breast	Invasive	↓ 5.70E-05	-2.23	4	19	0.349	8095	11
	Gastrointestinal	Adenocarcinoma	↓ 6.43E-05	-5.469	2	28	9.32E-04	1555	3
	Head and Neck	Squamous cell	↓ 2.24E-05	-3.693	2	30	-	-	2
	Lung	Squamous cell	↑ 2.98E-04	2.111	5	48	0.696	6505	5
KCNK10	Brain	Glioblastoma	↓ 1.81E-17	-4.843	5	9	5.03E-05	908	5
			↓ 1.56E-10	-2.974	6	10			
			↓ 8.63E-04	2.547	7	5			
	Breast	Ductal	↓ 1.00E-03	-2.294	2	18	0.15	6686.5	10
			↓ 3.85E-04	-3.523	2	14			
		Lobular	↓ 3.50E-02	-3.576	5	14	0.086	2913	3
	Colorectal	Adenoma	↓ 3.61E-11	-2.758	1	25			2
		Adenocarcinoma	↓ 1.74E-25	-7.227	1	26	8.12E-07	372.5	14
			↓ 3.19E-22	-7.914	2	26			
			↓ 2.85E-18	-6.275	1	26			
			↓ 2.07E-14	-4.83	2	26			
			↓ 1.11E-07	-6.275	2	26			
			↓ 3.42E-07	-2.503	3	26			
		Carcinoma	↓ 5.65E-10	-3.37	5	23	3.59E-07	759	4
			↓ 7.55E-08	-2.155	3	25			
			↓ 7.17E-07	-2.41	5	25			
	Kidney	Clear cell	↓ 2.17E-10	-4.752	1	38	6.35E-05	500	4
			↓ 1.11E-06	-2.748	7	36			
			↓ 1.19E-06	-2.783	5	36			
	Leukaemia	Acute myeloid	↑ 2.00E-02	2.615	10	44	0.024	6040	4

Table 3.4: TASK channel family expression in cancer

The above threshold data for TASK family members, *KCNK3*, *KCNK9*, and *KCNK15*, are shown. Data are divided into each cancer type and subtypes. The p-value, fold change, and gene rank percentile (%) for above threshold data are given. The threshold values used were: p-value < 0.05, fold change > 2, and gene rank percentile < 10 %.
Comparative meta-analysis was performed when n ≥ 3 analyses were available. This gave the median gene rank and median p-value.
Overexpression (↑) and underexpression (↓) are indicated in red and blue respectively.

mRNA	Cancer	Subtype	Above threshold analyses				Median value		
			p-value	Fold change	%	Ref	p-value	Gene rank	n
KCNK3	Bladder	Infiltrating	↓ 6.57E-13	-3.045	5	1	0.0850	1395	4
		Superficial	↓ 5.79E-11	-4.046	6	1	0.09	2901	4
	Brain	Astrocytoma	↓ 3.00E-03	-2.156	9	9	0.003	1629	3
		Glioblastoma	↓ 6.20E-08	-5.468	10	10	0.007	1486	7
			↓ 2.61E-05	-4.471	3	10			
	Breast	Invasive	↑ 4.41E-17	2.782	4	11	0.005	8863	13
			↑ 1.50E-02	2.958	6	14			
			↓ 1.00E-03	-2.375	7	17			
	Colorectal	Colon adenoma	↓ 2.37E-04	-2.493	10	24	5.01E-04	2203.5	4
	Gastrointestinal	Adenocarcinoma	↑ 2.85E-04	3.567	6	28	1.00	10604	6
	Kidney	Clear cell	↑ 1.53E-14	8.407	1	36	1.14E-04	990	6
			↑ 2.57E-07	6.014	5	36			
			↑ 4.01E-05	4.541	7	38			
			↑ 8.98E-04	6.344	6	41			
	Leukaemia	Acute lymphocytic	↑ 1.30E-02	2.177	9	42	0.994	8503	7
		Chronic lymphocytic	↑ 4.00E-03	2.681	5	42	0.482	4081.5	4
	Lung	Adenocarcinoma	↓ 6.55E-34	-4.136	1	50	4.33E-11	146.5	6
			↓ 8.44E-20	-6.89	1	49			
			↓ 8.67E-11	-7.375	2	52			
			↓ 4.11E-10	-2.367	1	51			
			↓ 2.54E-06	-7.399	3	47			
			↓ 1.08E-04	-3.803	4	48			
		Squamous cell	↓ 5.90E-20	-12.756	2	49	5.90E-20	343	5
			↓ 3.86E-06	-8.471	3	47			
			↓ 1.58E-05	-4.28	3	48			
			↓ 2.00E-03	-2.422	7	53			
	Pancreas	Adenocarcinoma	↓ 7.34E-06	-6.459	1	74	2.46E-07	2997	7
			↓ 4.72E-05	-5.03	1	72			
			↓ 1.19E-04	-2.191	3	75			
	Prostate	Carcinoma	↓ 2.72E-08	-2.034	3	77	0.029	1515	13
			↓ 1.02E-04	-2.638	2	79			
			↓ 8.94E-04	-3.106	4	76			
KCNK9	Breast	Invasive	↑ 1.16E-12	3.95	9	11	0.459	10188.5	14
KCNK15	Breast	Ductal	↑ 1.00E-03	5.046	6	12	0.008	1578	6
			↑ 8.00E-03	2.283	9	12			
			↑ 4.10E-02	8.774	8	14			
	Gastrointestinal	Adenocarcinoma	↓ 3.00E-03	-2.189	5	29	0.043	2990	5

Table 3.5: TALK channel family expression in cancer

The above threshold data for TALK family members, *KCNK5* and *KCNK17*, are shown. Data are divided into each cancer type and subtypes. The p-value, fold change, and gene rank percentile (%) for above threshold data are given. The threshold values used were: p-value < 0.05, fold change > 2, and gene rank percentile < 10 %.
Comparative meta-analysis was performed when n ≥ 3 analyses were available. This gave the median gene rank and median p-value.
Overexpression (↑) and underexpression (↓) are indicated in red and blue respectively.

mRNA	Cancer	Subtype	Above threshold analyses				Median value		
			p-value	Fold change	%	Ref	p-value	Gene rank	n
KCNK5	Breast	Ductal	↑ 2.14E-04	2.977	3	12	0.233	4729	9
			↓ 7.70E-04	-3.629	4	12			
			↓ 2.00E-03	-2.498	2	18			
			↓ 1.00E-03	-3.856	6	12			
	Colorectal	Adenocarcinoma	↓ 2.42E-12	-3.18	3	26	2.35E-07	1052	11
			↓ 1.95E-11	-2.498	5	26			
			↓ 7.86E-08	-3.199	2	26			
	Kidney	Clear cell	↓ 1.07E-04	-3.693	3	40	4.94E-04	1440.5	4
			↓ 1.67E-04	-2.409	9	38			
	Leukaemia	Acute Myeloid	↓ 1.30E-02	2.172	8	44	0.591	8006	4
		Chronic Lymphocytic	↓ 4.97E-39	-2.039	5	43	-	-	2
	Lung	Adenocarcinoma	↑ 4.27E-06	2.145	3	52	1.78E-08	1296	3
		Squamous cell	↓ 9.14E-14	-2.192	6	49			2
	Melanoma	Melanoma	↓ 5.02E-10	-6.576	2	58	0.004	1815	3
			↓ 4.00E-03	-2.869	10	57			
	Oesophageal	Adenocarcinoma	↑ 5.17E-12	2.077	4	61	0.500	2226	4
			↑ 2.31E-04	2.481	2	62			
			↓ 6.98E-04	-2.281	8	63			
		Barrett's	↑ 1.60E-11	5.57	1	61	0.507	2216.5	4
			↑ 1.50E-02	2.019	7	62			
KCNK17	Breast	Invasive	↑ 2.20E-02	3.265	8	14	0.752	14529	12

Table 3.6: THIK channel family expression in cancer

The above threshold data for THIK family members, *KCNK12* and *KCNK13*, are shown. Data are divided into each cancer type and subtypes. The p-value, fold change, and gene rank percentile (%) for above threshold data are given. The threshold values used were: p-value < 0.05, fold change > 2, and gene rank percentile < 10 %.
Comparative meta-analysis was performed when n ≥ 3 analyses were available. This gave the median gene rank and median p-value.
Overexpression (↑) and underexpression (↓) are indicated in red and blue respectively.

mRNA	Cancer	Subtype	Above threshold analyses				Median value		
			p-value	Fold change	%	Ref	p-value	Gene rank	N
KCNK12	Brain	Astrocytoma	↓ 8.77E-08	-4.126	5	9	-	-	2
			↓ 3.00E-03	-3.054	10	9			
		Glioblastoma	↓ 1.81E-23	-7.969	2	9	0.001	1557.5	4
			↓ 3.32E-09	-4.925	8	10			
	Leukaemia	Acute Lymphocytic	↑ 5.75E-75	3.532	1	43	5.99E-33	201	3
			↑ 4.96E-34	3.301	3	43			
			↑ 5.99E-33	8.691	2	43			
	Lung	Adenocarcinoma	↑ 9.84E-06	2.803	4	52	1.09E-05	2243	3
KCNK13	Breast	Invasive	↑ 3.35E-12	3.193	10	11	0.399	10349	11
			↑ 4.99E-08	2.05	10	17			

3.3 Discussion

The aim of the data presented in this chapter was to examine the mRNA expression pattern of all members of the K_{2P} channel family in cancer tissues compared to matched normal tissue controls. To address this aim the mRNA expression of each individual K_{2P} channel was analysed in 20 distinct cancer types, by performing bioinformatic analysis using the online cancer microarray database Oncomine. This technique was selected because; (i) it allowed the mRNA expression of the entire K_{2P} channel family to be studied, (ii) the mRNA expression could be compared to matched normal tissue controls, which provided information on whether the expression patterns were differential, and (iii) it allowed the analysis of each K_{2P} channel in cancer to be performed in a uniform manner so that comparisons could be made between different channels and cancer.

This approach led to four main conclusions:

(i) The mRNA levels of K_{2P} channels were significantly altered in 14 of the 20 cancer types examined.

(ii) The mRNA expression level of nine K_{2P} channel from five subfamilies are significantly altered in at least one cancer type

(iii) K_{2P} channel mRNA can be both over- and underexpressed in cancer

(iv) Within a single cancer type, multiple K_{2P} channels are expressed at an mRNA level.

Each of these findings is discussed in detail below.

3.3.1 K_{2P} channel mRNA was significantly altered in 14 cancer types

Examining the mRNA expression of all 15 K_{2P} channels in 20 cancer types revealed that in 14 cancers, significant over- and underexpression of channel mRNA occurred compared to normal tissue. These expression data showed wider expression of K_{2P} channels in cancer than would be predicted based on the published data, which had only linked K_{2P}2.1, K_{2P}3.1, K_{2P}5.1, and K_{2P}9.1 to cancer (Introduction 1.7). The widespread expression of K_{2P} channel mRNA in cancer suggested that the expression of K_{2P} channels may provide a critical functional advantage to cancer cells. K_{2P} channel activity is hypothesised to be beneficial to cancer cells by regulating the membrane potential and, thereby, impacting on the activity of other ion channels, which may result in functional

advantages (Enyedi and Czirják, 2010; Lee et al., 2012; Mu et al., 2003; Patel and Lazdunski, 2004; Pei et al., 2003; Voloshyna et al., 2008). However, at this time, the influence of altered K_{2P} channel expression on other ion channels and transporters present in cancer cells has not been described.

It is important to appreciate the limitations of using Oncomine for this type of analysis. Comparative meta-analysis was used in this chapter to assess the significance of the above threshold results. However, in some cases the number of analyses examining K_{2P} channels in certain cancer subtypes were limited ($n \leq 2$), this meant that comparative meta-analysis could not be performed. Appendix 3 shows the K_{2P} channel mRNA expression data where less than two analyses were available. Where insufficient studies are available, it may be premature to include/discount the K_{2P} channel expression until further investigations have been undertaken. Furthermore, in some cases, such as for $K_{2P}12.1$ mRNA overexpression altered in acute lymphocytic leukaemia (Table 3.6), the multiple analyses which were compared originated from the same dataset. This may impact on the significance of this comparison, as the data were generated by the same research group and may have utilised the same experimental set up, meaning that the results are not from independent research studies. However, these comparisons still provided an indication of the K_{2P} channel expression in that cancer type. Another limitation of this study was that it only enabled the characterisation of K_{2P} channel mRNA expression in cancer. This could mean that the expression changes observed in this chapter may only occur at the mRNA level. Therefore, the expression patterns identified in this chapter will require further examination to determine if these alterations correlate with protein expression and channel activity. Therefore, a key question that arises from this work is: will the significant changes in K_{2P} channel mRNA that were observed in these 14 cancers occur at a protein level and relate into alterations in channel activity?

3.3.2 Nine members of the K_{2P} channel family showed significant alterations in cancer

Nine K_{2P} channels showed significant mRNA alterations in cancer; most notably $K_{2P}1.1$, $K_{2P}3.1$, $K_{2P}5.1$, and $K_{2P}10.1$ were significantly altered in over four cancer types. Of the nine K_{2P} channels which showed significant alterations, seven channels ($K_{2P}1.1$, $K_{2P}3.1$,

K_{2P}6.1, K_{2P}7.1, K_{2P}10.1, K_{2P}12.1, and K_{2P}15.1) had not previously been identified in cancer tissue or linked to cancer cell functions. The specific implications which may result from alterations in expression of these K_{2P} channel subfamilies are discussed below. However, in the broader context this study has provided information on seven K_{2P} channels that were not known to have expression in cancer, as well as identifying novel cancers where mRNA expression alterations for K_{2P}2.1 (gastrointestinal adenocarcinomas; Table 3.3) and K_{2P}5.1 (colorectal adenocarcinoma, lung adenocarcinoma, melanoma, and renal clear cell carcinoma; Table 3.5) channels occur.

3.3.2.1 Potential functional implications of alterations to TWIK channel mRNA in cancer

The data presented in this chapter showed that K_{2P}1.1 mRNA was generally overexpressed in the cancers examined (Table 3.1). To date, no studies have implicated TWIK channels in cancer and the physiological roles (in normal cells) of this channel subfamily are relatively unknown. Published data has shown that K_{2P}1.1 channels can alter their ion permeability, depending on the external K^+ concentration and pH, to allow an inward Na^+ current which will result in membrane depolarisation (Chatelain et al., 2012; Ma et al., 2011). Thus, overexpression of K_{2P}1.1 channels in cancer cells may be beneficial by altering the ionic currents in response to environmental cues, or by maintaining a depolarised membrane potential. A depolarised membrane potential is generally associated with highly proliferating and/or strongly invasive cancer cells (Arcangeli and Becchetti, 2010; Brackenbury, 2012; Blackiston et al., 2009; Molenaar, 2011; Wonderlin and Strobl, 1996).

In contrast to K_{2P}1.1, mRNAs for the related channels, K_{2P}6.1 and K_{2P}7.1 were generally underexpressed in cancer (Table 3.2). With the exception of regulating background K^+ currents (Chavez et al., 1999; Patel et al., 2000), no published studies have linked K_{2P}6.1 channels to functional roles which may be relevant in cancer cells. Therefore, the functional consequences of K_{2P}6.1 channel underexpression may involve membrane depolarisation, which could influence the activity of other ion channels. K_{2P}7.1 is a non-functional channel due to ER retention (Salinas et al., 1999); hence the consequence of K_{2P}7.1 mRNA downregulation in cancer is also unknown. A potential hypothesis is that K_{2P}7.1 may cause ER retention of other K_{2P} channels if channel heterodimers are formed. ER

retention caused by channel dimerisation has been demonstrated by the expression of a $K_{2P}3.1$ trafficking mutant (which lacks the C-terminal valine 395) alongside WT $K_{2P}3.1$ channels (O'Kelly et al., 2002; O'Kelly and Goldstein, 2008). Therefore, downregulation of ER retained K_{2P} channels, such as $K_{2P}7.1$, could decrease the cell surface expression of other K_{2P} channels and this may have functional implications.

3.3.2.2 Potential functional implications of alterations to TREK channel mRNA in cancer

The mRNA expression data presented in this chapter showed that $K_{2P}10.1$ mRNA was the most significantly altered TREK channel (4/20 cancers) with a trend for mRNA underexpression (Table 3.3). The current research has focused on the role of $K_{2P}2.1$ channels in cancer (Bittner et al., 2013; Lauritzen et al., 2005; Voloshyna et al., 2008); with several studies linking $K_{2P}2.1$ channel expression to cancer cell functions. The roles of $K_{2P}2.1$ channels may correlate with the functional impact of $K_{2P}10.1$ expression on cancer cells, due to the similarities in TREK channel activity and modulation (Appendix 1). $K_{2P}2.1$ activity has been found to promote proliferation in PC3 prostate cancer cells (Voloshyna et al., 2008). TREK channels may also be involved in cancer cell migration, as TREK channel activity is enhanced by mechanical force transmitted through the lipid bilayer and this is an effect which can be triggered by cytoskeletal disruption (Lauritzen et al., 2005; Maingret et al., 1999b; Noël et al., 2011). Enhanced lymphocyte migration across brain microvascular endothelial cells was observed in $K_{2P}2.1^{-/-}$ KO mouse models (Bittner et al., 2013). This migratory effect was caused by an upregulation of cellular adhesion molecules (ICAM1, VCAM1, and PEDCAM1) in $K_{2P}2.1^{-/-}$ endothelial cells and facilitated lymphocyte migration into the brain (Bittner et al., 2013). In summary, these published studies suggested that $K_{2P}10.1$ channel mRNA underexpression in cancer may provide a migratory advantage to cancer cells.

3.3.2.3 Potential functional implications of alterations to TASK channel mRNA in cancer

The data presented in this chapter revealed that $K_{2P}3.1$ was the most significantly altered TASK channel at an mRNA level in cancer (8/20 cancers). No functional

consequences have been linked to altered K_{2P}3.1 expression in cancer cells within published literature. However, K_{2P}9.1 activity has been linked to multiple cancer cell functions (proliferation, apoptosis, and migration) and no clear role has emerged for TASK channel activity in cancers (Introduction 1.8; Innamaa et al., 2013b; Lee et al., 2012; Liu et al., 2005; Meuth et al., 2008b; Pei et al., 2003).

The data presented in this chapter provided the first description of TASK channel mRNA underexpression in cancer. Reduced expression of TASK channels may be advantageous in cancer as TASK channel activity has been published to promote cell death in certain cell types, e.g. rCGN and glioma cells (Lauritzen et al., 2003; Meuth et al., 2008b). Exploring the functional impact of TASK channel expression on cancer cells will be the focus of this thesis.

3.3.2.4 Potential functional implications of alterations to TALK channel mRNA in cancer

K_{2P}5.1 was the only member of the TALK channel family which showed significant expression alterations in the cancers examined in this chapter (4/20 cancers). To date, published data have linked K_{2P}5.1 activity to cell proliferation and cell volume control. K_{2P}5.1 mRNA expression is upregulated by oestrogen and this has been implicated in the promotion of oestrogen-induced cell proliferation in breast cancer cells (Alvarez-Baron et al., 2011). K_{2P}5.1 channel activity has also been linked to cell volume control in Ehrlich ascites tumour cells and mouse renal proximal tubules (Kirkegaard et al., 2010; L'Hoste et al., 2007b; Niemeyer et al., 2001). In mouse renal proximal tubules, cell death signalling induced an outward K^+ conductance with the characteristics of K_{2P}5.1 channels. This finding suggested that K_{2P}5.1 is involved in the apoptotic volume decrease of these cells (L'Hoste et al., 2007b). In summary, the published data on K_{2P}5.1 channels in cancer indicated that a major effect of K_{2P}5.1 overexpression could be providing a proliferative advantage to cancer cells, whereas K_{2P}5.1 downregulation may prevent cell death which results from a cell volume decrease. Additionally, the regulation of K_{2P}5.1 expression by oestrogen signalling pathways in breast cancer (Alvarez-Baron et al., 2011) indicates that the regulation of K_{2P}5.1 channel expression by cell signalling pathways could result in cell-specific roles.

3.3.2.5 Potential functional implications of alterations to TALK channel mRNA in cancer

In the THIK channel family, K_{2P}12.1 showed significantly altered mRNA expression in cancer (3/20 cancers) and a general trend for overexpression. K_{2P}12.1 is a non-functional K_{2P} channel; however unlike K_{2P}7.1 and K_{2P}15.1 channels which are ER retained (Ashmole et al., 2001; Salinas et al., 1999), K_{2P}12.1 channels are detected on the cell surface so it is thought that the lack of functionality is not due to improper trafficking (Rajan et al., 2001). The implications of altered K_{2P}12.1 expression in cancer are unknown, but a potential consequence could be to silence other K_{2P} channels. If channel silencing occurred it may result in membrane depolarisation (Enyedi and Czirják, 2010; Plant et al., 2012). For example, dimerisation of SUMOylated K_{2P}1.1 channels (which are silent and do not pass K^+ ions) with unmodified K_{2P}1.1 or TASK channels causes an inhibition of outward K^+ leak currents, despite the presence of these channels on the cell surface (Plant et al., 2012; Rajan et al., 2005).

3.3.2.6 Six K_{2P} channels were not altered within the cancers examined

Six channels failed to show any significant expression alterations following the mRNA analyses conducted in this chapter. These were K_{2P}4.1, K_{2P}9.1, K_{2P}13.1, K_{2P}16.1, K_{2P}17.1, and K_{2P}18.1. For three of these six channels (K_{2P}4.1, K_{2P}16.1, and K_{2P}18.1), no expression alterations were observed which ranked above the search threshold values used. In other cases the expression alterations observed did not remain significant following comparative meta-analysis, for example K_{2P}9.1 mRNA overexpression in invasive breast cancers (Table 3.4). This finding was surprising as K_{2P}9.1 has been published to show mRNA amplification in 44 % of breast cancer samples (Mu et al., 2003). The numbers analysed by Mu et al. (2003) were lower than in the datasets present on Oncomine and this may account for the mRNA expression differences observed. Overexpression of K_{2P}9.1 channel protein has also been observed for breast and colon cancer tissue (Kim et al., 2004), thus for K_{2P}9.1 channels alterations at a protein level may be more common.

A further limitation of assessing K_{2P} channel expression in cancer using Oncomine, in addition to those described above (Section 3.3.1), was that the number of datasets examining a specific K_{2P} channel was low in some cases. There are a total of 156 datasets

on Oncomine which examine K_{2P} channel mRNA in cancers compared to normal controls (Oncomine, 2013). For K_{2P}1.1 (the first K_{2P} channel cloned) there are 146 datasets, whereas for K_{2P}18.1 (the final family member identified) there are only 12 datasets. This may have limited the detection of K_{2P}18.1 mRNA alterations in cancer, although it should be noted that no alterations were observed within the datasets available.

In conclusion, this study identified nine K_{2P} channels which showed significant expression alterations in cancer and warrant further investigation within the specific cancer types (shown in Tables 3.1 to 3.6). For this, it will be important to determine the protein expression and levels of channel activity, as well as determining if expression changes only occur at a protein level for the channels which were not significantly altered at an mRNA level, such as for K_{2P}9.1 channel expression in breast cancer.

3.3.3 K_{2P} channel mRNA can be over- and underexpressed in cancer tissue

The mRNA expression data presented in this chapter revealed that in addition to significant K_{2P} channel mRNA overexpression (Figure 3.1), that channel underexpression (Figure 3.2) also occurs in cancer. Underexpression of K_{2P} mRNA was not expected based on the current literature which described overexpression of K_{2P}9.1 (Kim et al., 2004; Mu et al., 2003) and K_{2P}2.1 (Voloshyna et al., 2008) protein in cancer tissues (Introduction 1.7). However, if over/underexpression alterations to channel mRNA results in an increase/decrease of K_{2P} channel activity, both could have significant implications for the physiological roles played by other ion channels expressed within cancer cells.

The precise functional impacts of K_{2P} channel overexpression are unknown; however increased K^+ efflux resulting from KCh activity in cancer has been shown to provide a number of functional advantages (Figure 1.11 and Introduction 1.6). For example, K^+ efflux and membrane hyperpolarisation can increase the electrical driving force for Ca^{2+} entry into cells, stimulate Ca^{2+}-dependent signalling, and promote cell proliferation. This effect has been observed in LNCaP prostate cancer cells, where K^+ efflux through K_{Ca}3.1 channels causes Ca^{2+} entry through TRPV6 channels (Lallet-Daher et al., 2009). In addition, cooperative activity of K^+ and Cl^- channels results in water efflux and cell shrinkage, this is

critical for the regulation of cancer cell migration and proliferation (Lang et al., 1998; Lang et al., 2007; Pedersen et al., 2013; Rouzaire-Dubois and Dubois, 1998).

In this chapter, widespread K_{2P} channel mRNA underexpression was also observed in the cancers examined (Figure 3.2). If this underexpression caused a decrease in K_{2P} channel protein and less channel activity on the cell surface, this may result in membrane depolarisation which could alter the activity of other ion channels and increase cellular excitability (Campanucci et al., 2005; Duprat et al., 1997; Enyedi and Czirják, 2010; Kim et al., 2000; Lesage and Lazdunski, 2000; Rajan et al., 2000). Reduced K_{2P} channel expression had not been previously identified, however underexpression of other classes of KCh have been described in cancer cells. For example, in metastatic gliomas $K_V1.5$ protein expression is reduced compared to low grade glioblastomas (Preußat et al., 2003). Additionally, the surface expression of K_{ir} channels ($K_{ir}2.3$ and $K_{ir}4.1$) is reduced in gliomas, due to channel localisation on the nuclear membranes, and this is thought to contribute to the depolarised RMP (approximately -20 mV; Molenaar, 2011).

Reduced K^+ efflux caused by decreased KCh expression or activity could have a number of functional advantages which are likely to depend on the other channels expressed within the cancer cell. Membrane depolarisation may encourage cell cycle progression through the G_2/M checkpoint, in addition to Ca^{2+} entry through Ca_V and TRP channels (Blackiston et al., 2009; Molenaar, 2011; Monteith et al., 2012). Membrane depolarisation could also result in the activation of other voltage-gated ion channels which may provide additional functional advantages (Figure 1.11). These include: K_V channels which may influence a wide range of cancer cell functions (Table 1.4), Ca_V channels which may stimulate Ca^{2+} signalling events and Ca^{2+}-dependent transcription (Fiske et al., 2006; Li and Xiong, 2011), and Na_V channels which may promote cancer cell invasion and metastases (Brackenbury, 2012; Campbell et al., 2013).

The limitations of these findings are the same as described in Section 3.1.1. Therefore, without further investigations to confirm if K_{2P} channel activity is increased in cancer, the effects of altered mRNA expression on other ion channels and cellular functions are speculative. In summary, the data presented in this chapter showed that K_{2P} channel mRNA can be both increased and decreased in cancer, and future studies will be required to determine the consequences of these alterations.

3.3.4 Multiple K_{2P} channels are expressed within a single cancer type

The data presented in this chapter revealed that the mRNA levels of multiple K_{2P} channels can be both detected and altered, compared to controls, within a single cancer subtype. Whether or not multiple K_{2P} channels are expressed in cancer had not been investigated prior to this study, as published studies have only focused on a single channel. The functional consequences of this finding are unknown, although evidence from heterologous and endogenous expression systems showed that heterodimers can form between $K_{2P}1.1$, $K_{2P}3.1$, and $K_{2P}9.1$ channels, with consequence for how excitable cells respond to drugs and changes in pH (Czirjak and Enyedi, 2002a; Kim et al., 2009; Plant et al., 2005; Plant et al., 2012b). Currently, it is not known which other members of the K_{2P} channel family can form heterodimers with each other. However, the different regulation properties of the K_{2P} channel family (such as pH and O_2 sensitivity; Appendix 1) means that understanding the interactions formed between different channels in cancer will be essential to establish the functional implications resulting from the expression of different K_{2P} channel subsets. For example, upregulation of a functional K_{2P} channel or downregulation of a K_{2P} channel which can silence other K_{2P} channels (such as $K_{2P}1.1$) may cause membrane hyperpolarisation. On the contrary, downregulation of a functional K_{2P} channel or upregulation of an inhibitory K_{2P} channel could result in membrane depolarisation. These alterations may result in different advantageous cellular functions, with the precise impact likely to depend on which other channels are expressed within the cancer cell (Figure 1.10).

In conclusion, the data presented in this chapter provided evidence that K_{2P} channel mRNA is altered in a wide range of cancers. Additionally, this study has identified candidate K_{2P} channels which show significant alterations in the cancers examined and warrant further investigation, notably $K_{2P}1.1$, $K_{2P}3.1$, $K_{2P}5.1$, and $K_{2P}10.1$. This thesis focused on the TASK channel subfamily and the data presented here provide the first evidence for differential expression of $K_{2P}3.1$ and $K_{2P}15.1$ mRNA in cancer compared to normal tissues. To enable the functional implications of TASK channel expression on cancer cell biology to be investigated, clinically relevant model cancer cell lines with TASK channel expression were required. Consequently, characterising the expression of TASK channels in cancer cell lines was the next aim of this thesis.

3.4 Publications arising

Tables 3.1 to 3.6 are published in: Williams, S., Bateman, A. & O'Kelly, I. 2013. Altered expression of two-pore domain potassium (K_{2P}) channels in cancer. *PLoS One*, 8**,** e74589.

Chapter 4

Results

TASK channel expression profile in human cancer cell lines and tissue

4.1 Introduction

The aim of this chapter was to define the TASK channel expression profile of clinically relevant human cancer cell lines. The bioinformatic data presented in Chapter 3 indicated that the mRNA expression of the entire K_{2P} channel family, including members of the TASK channel subfamily, undergo significant alterations in cancer. Additionally, the data described in Chapter 3 revealed that the mRNA of multiple K_{2P} channels can be detected within a single cancer type. These findings were distinct from published literature which, despite multiple studies, has focused on the role of single K_{2P} channel subtypes within a cancer type (see Introduction 1.7). Therefore, understanding the impact of multiple K_{2P} channels and subfamilies on the physiology of cancer cells is not yet understood. Despite the critical importance of understanding the role of multiple K_{2P} channels in cancer, such an analysis was beyond the scope of a single PhD project. Therefore, this project focused on the TASK channel subfamily ($K_{2P}3.1$, $K_{2P}9.1$, and $K_{2P}15.1$ channels; Figure 1.3) because: (i) the bioinformatics data presented in Chapter 3 suggested that there were marked changes in the expression of this group of background potassium channels at the mRNA level; (ii) the TASK channels are an important research focus for this lab and (iii), the TASK channels have been demonstrated to play key roles in the cell biology, pathophysiology, and pharmacological responses of numerous tissues (see Introduction 1.4 and 1.8 for more details).

Several lines of evidence support the idea that altered TASK channel expression might play a functional role in the biology of clinically relevant cancer cell lines. The same data also support the overarching hypothesis of this thesis: does the expression of TASK channels in cancer provide a functional advantage to cancer cells? The data presented in Chapter 3 identified, for the first time, alterations to TASK channel mRNA in several cancers. Changes in mRNA levels may result in changes to TASK protein level and activity which could have functional impacts on cancer cells. For example, $K_{2P}3.1$ mRNA expression was significantly altered in 6 of the 20 cancers examined in Chapter 3 (Table 3.4). Differential expression of $K_{2P}3.1$ channels has not been identified in the literature, although $K_{2P}3.1$ expression has been described in three cancers: adrenal adenoma tissue (mRNA; Nogueira et al., 2010), medulloblastoma cell lines (protein and acid-sensitive currents; Ernest et al., 2010), and lung cancer cell lines (mRNA and acid-sensitive currents; Hartness et al., 2001). $K_{2P}9.1$, the second member of the TASK family, has been identified as a potential proto-

oncogene (Mu et al., 2003). K_{2P}9.1 channel overexpression has been identified in breast (mRNA and protein; Mu et al., 2003) and colorectal cancers (protein; Kim et al., 2004) compared to normal tissues. K_{2P}9.1 channel activity has been linked to tumour formation (in mouse models; Mu et al., 2003) as well as increased cell proliferation (Mu et al., 2003; Pei et al., 2003), reduced apoptosis (Innamaa et al., 2013b; Meuth et al., 2008b; Pei et al., 2003), and decreased migration (Lee et al., 2012). Despite this published evidence, it should be noted that K_{2P}9.1 mRNA expression was not significantly altered within the cancers examined in Chapter 3 (Table 3.4). Finally, bioinformatic data presented in Chapter 3 showed that K_{2P}15.1 mRNA was significantly altered in two cancers (Table 3.4). K_{2P}15.1 is the non-functional TASK channel family member and K_{2P}15.1 protein expression had not been described in either normal or cancer tissue prior to this investigation.

To date, no comprehensive study has been conducted to establish cancer cell lines with robust TASK channel expression and a clinical relevance to be used as model cell lines. Therefore, the aim of the experiments presented in this chapter was to characterise the expression profile of TASK channels in clinically relevant model cancer cells. Cancer cell lines are commonly used as *in vitro* models of the diseased state for multiple reasons. These include ease of cell culture, the fact that they provide a relatively homogenous cell source, and that cancer cells offer a standardised model for use in different research studies (Burdall et al., 2003). The human cancer cells lines (Table 2.13) utilised in this thesis were selected to represent the cancer types shown to exhibit altered K_{2P} channel mRNA expression in Chapter 3. In these cell lines it was important to examine both TASK channel mRNA and protein expression. This established if the detection of TASK channel mRNA resulted in protein production and provided a qualitative assessment of the protein expression levels (which can be further related into channel activity). RT-PCR was utilised to examine the expression of TASK channel mRNA in cancer cell lines. This technique was selected as it enabled the use of exon-spanning primers (see Method 2.3.12) which prevented the amplification of genomic products, thereby ensuring that any results were from the expression of TASK channel mRNA. In addition, RT-PCR is a well-established method of mRNA expression analysis and has been widely used when studying TASK channels (Duprat et al., 1997, Hartness et al., 2001, Lee et al., 2012, Rajan et al., 2000). To study the expression of TASK channel protein in cancer cell lines, the specificity of commercially available antibodies to TASK channel protein needed to be determined. Determining the specificity of TASK channel antibodies was an essential part of this project

as a lack of reliable antibodies had been a limitation of studying K_{2P} channel protein within the literature (Kovacs et al., 2005, Mant et al., 2013, Plant et al., 2012b). Once the specificity of TASK channel antibodies was confirmed, endogenous TASK channel protein expression was assessed in cancer cell lines using immunofluorescence and confocal microscopy. This approach was selected to provide the highest detection sensitivity in permeabilised cells. After confirming that TASK channel protein was detected in cell lines where channel mRNA was present, whole-cell patch clamp experiments were conducted to determine if endogenous TASK-like currents could be isolated within cancer cell lines. Time restrictions limited the depth of this investigation and only the lung cancer cell line A549 was assessed. For the final experiments presented in this chapter, immunohistochemistry and the antibodies characterised in this study were used to determine if TASK channel protein could be observed within cancerous cells in human patient tissues. Immunohistochemistry is a well published technique used to examine protein expression in patient tissue samples and has been previously utilised when studying K_{2P}9.1 protein expression (Kim et al., 2004, Kovacs et al., 2005, Mu et al., 2003, Pocsai et al. 2006). Therefore, in summary the overall and specific aims of this chapter are as follows:

4.1.1 Aims

To define the TASK channel expression profile in clinically relevant human cancer cell lines in order to determine which cell lines to use as models for functional studies in subsequent chapters. To address this, this work has five specific aims:

1. To examine the mRNA expression of K_{2P} channels in a range of human cancer cell lines using RT-PCR.
2. To characterise the ability of commercially available antibodies to detect specific TASK channel proteins.
3. To assess the expression of TASK channel protein in human cancer cell lines.
4. To use whole-cell patch clamp experiments to determine if functional TASK channels can be detected in A549 lung cancer cells. This cell line was selected based on the identification of K_{2P}3.1 and K_{2P}9.1 expression at an mRNA and protein level.
5. To provide a clinical relevance to the TASK channel expression detected within cancer cell lines by examining if TASK channel protein is detectable in patient

cancer tissue samples (tissue samples of oesophageal, lung, pancreatic, and renal cancers were examined, this selection was based on mRNA expression findings from Chapter 3 and tissue availability).

4.2 Analysis of K_{2P} channel mRNA expression in human cancer cell lines

Initially, eleven cancer cell lines that reflected a wide range of cancer types (Table 2.13) were screened for the presence of K_{2P}3.1, K_{2P}9.1, and K_{2P}15.1 mRNA. In addition, bioinformatic data revealed that multiple K_{2P} channels were altered (at an mRNA level) in a wide range of cancers (with the exception of K_{2P}4.1, K_{2P}13.1, K_{2P}16.1, K_{2P}17.1, and K_{2P}18.1). At this time there is little published information on the mRNA expression of the entire K_{2P} channel family in cancer cell lines. Therefore, to further characterise the cancer cell lines utilised in this study, the mRNA expression of six additional K_{2P} channels from other subfamilies (K_{2P}1.1, K_{2P}2.1, K_{2P}5.1, K_{2P}7.1, K_{2P}10.1, and K_{2P}12.1) was assessed in selected cancer cell lines to reflect the expression profile observed in Chapter 3.

The expression profile of K_{2P} channel mRNA in cancer cell lines was established using reverse transcriptase PCR (RT-PCR) with exon-spanning primers, this ensured mRNA amplification over any genomic products (Method 2.3.12). The primers and optimised PCR conditions used for RT-PCR analysis are described in Table 2.12 and Figure 2.4. Prior to studying K_{2P} channel expression, all synthesised cDNA was examined for transferrin receptor expression; this checked the quality of the cDNA and ensured no contaminants were present (see Figure 2.3 for an example gel).

4.2.1 K_{2P}3.1 (*KCNK3*) mRNA expression

Eleven human cancer cell lines and two control cell lines, used for heterologous expression in this study (COS-7 monkey fibroblast-like and HEK293 human embryonic kidney), were examined for *KCNK3* mRNA expression (using KCNK3F and KCNK3R primers, Ta = 69 °C; Figure 2.4). *KCNK3* PCR product was detected at the expected size (430 bp) in five of the human cancer cell lines examined (Figure 4.1): A549 lung, HeLa cervical, MCF-7

breast, SH-SY5Y neuroblastoma, and 786-0 renal. Amplification of the correct PCR product, at 430 bp, was confirmed by DNA sequencing in two cell lines: A549 and 786-0 (indicated by *; Figure 4.1). Sequenced PCR products had over 88 % identity to the *KCNK3* mRNA reference sequence (*Homo sapiens*; NM_002246.2), with mismatch due to ambiguous bases (N) present throughout the sequencing read: 100 % for A549 cells (261 matched bp) and 88 % for 786-0 cells (230/260 matched bp). No PCR products were detected in colorectal (HCT116, SW480, and SW620) or oesophageal (OE19 and OE21) cancer cell lines, in addition to control cell lines (COS-7 and HEK293; Figure 4.1).

4.2.2 $K_{2P}9.1$ (*KCNK9*) mRNA expression

In comparable PCR reactions, *KCNK9* mRNA expression was examined in all eleven human cancer cell lines and the two control cell lines (using KCNK9F and KCNK9R primers, Ta = 65 °C; Figure 2.4). *KCNK9* PCR product was detected at the expected size (413 bp) in six of the human cancer cell lines examined (Figure 4.2): A549 lung, MCF-7 breast, HCT116 colorectal, SW480 colorectal, SW620 colorectal, and SH-SY5Y neuroblastoma. *KCNK9* product was also detected in HEK293 cells, which are used in this study for heterologous expression of TASK channels. Amplification of the correct PCR product, at 413 bp, was confirmed by DNA sequencing in two cells lines: A549 and SH-SY5Y cells (indicated by *, Figure 4.2). The sequenced PCR products had over 200 bp with 100 % identity to the *KCNK9* mRNA reference sequence (*Homo sapiens*; NM_016601.2): A549 cells (261 matched bp) and SH-SY5Y cells (204 matched bp).

A higher product band at 600 bp was detected for 786-0 renal cancer cells and a lower product band (300 bp) was observed for PC3 prostate cancer cells, these are not predicted to correspond to *KCNK9* PCR products (Figure 4.2). The identity of these non-specific products was not investigated by DNA sequencing. No products were detected for HeLa cervical and oesophageal (OE19 and OE21) cancer cell lines, in addition to COS-7 cells (Figure 4.2).

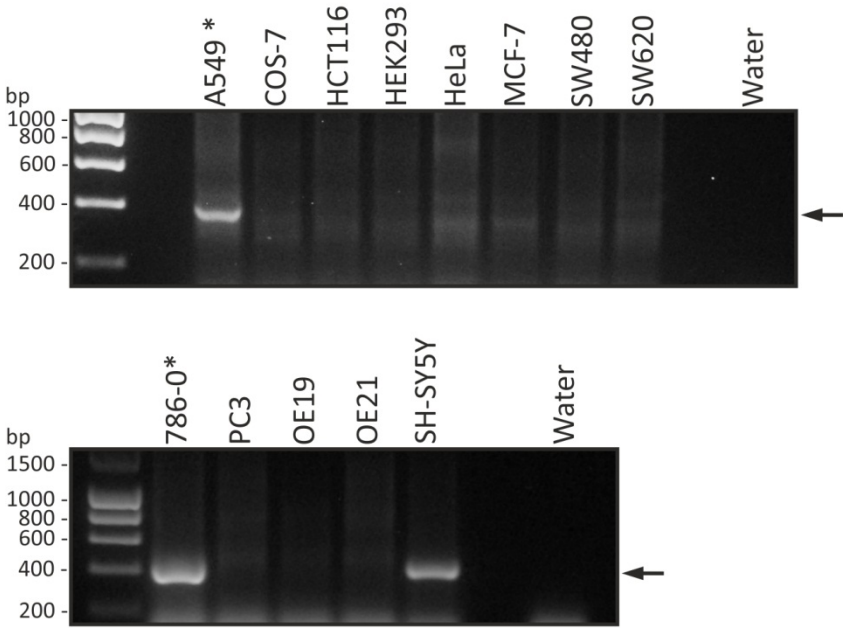

Figure 4.1: *KCNK3* mRNA expression in human cancer cell lines
KCNK3 PCR product was amplified at the predicted size of 430 bp (indicated by an arrow) from breast (MCF-7), cervical (HeLa), lung (A549), neuroblastoma (SH-SY5Y), and renal (786-0) cancer cell line cDNA.
No PCR products were detected at 430 bp in colorectal (HCT116, SW480, and SW620), prostate (PC3) and oesophageal (OE19 and OE21) cancer cell line cDNA, in addition to HEK293 (human embryonic kidney) and COS-7 (monkey fibroblast-like) cell line cDNA.

PCR products were amplified using KCNK3F and KCNK3R primers, with a Ta of 69 °C.
Water was run as a no cDNA template control to ensure no PCR contamination.

* indicates where the PCR product has been confirmed to be *KCNK3* by DNA sequencing.

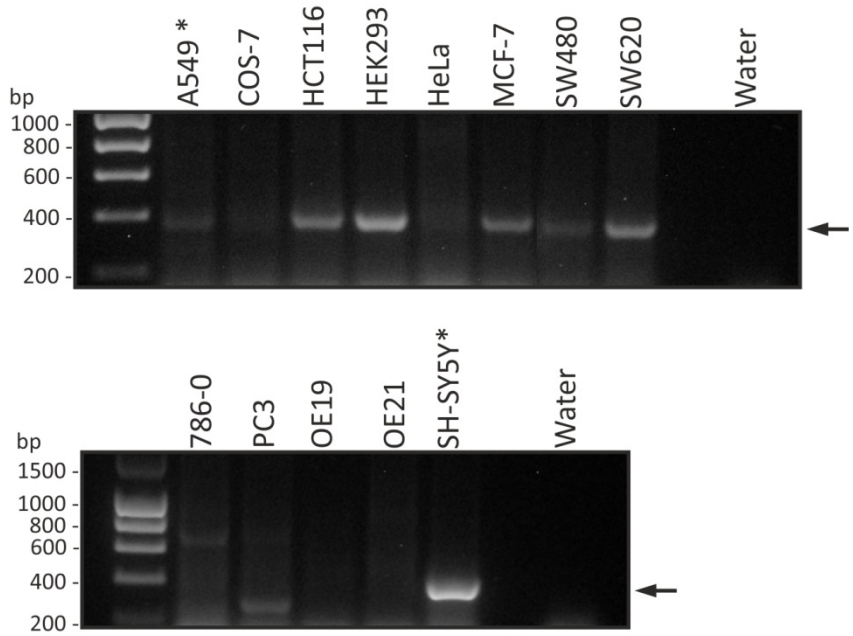

Figure 4.2: *KCNK9* mRNA expression in human cancer cell lines

KCNK9 PCR product was amplified at the predicted size of 413 bp (indicated by an arrow) from breast (MCF-7), cervical (HeLa), colon (HCT116, SW480, and SW620), and neuroblastoma (SH-SY5Y) cancer cell line cDNA. In addition, *KCNK9* PCR product was detected in HEK293 (embryonic kidney) cell line cDNA.
No PCR products were detected, at 413 bp, in cervical (HeLa), renal (786-0), prostate (PC3), and oesophageal (OE19 and OE21) cancer cell lines, in addition to COS-7 (monkey fibroblast-like) cell line cDNA.

PCR products were amplified using KCNK9F and KCNK9R, with a Ta of 65 °C.
Water was run as a no cDNA template control to ensure no PCR contamination.

* indicates where the PCR product has been confirmed to be *KCNK9* by DNA sequencing.

4.2.3 K_{2P}15.1 (*KCNK15*) mRNA expression

KCNK15 mRNA expression was also examined in the same eleven human cancer cell lines (using KCNK15F and KCNK15R primers, Ta = 58 °C; Figure 2.4). *KCNK15* PCR product, at the expected size (259 bp), was detected in all nine of the human cancer cell lines examined (Figure 4.3). Although PCR product was detected for 786-0 renal and OE21 oesophageal cancer cells, these bands appear slightly higher and are fainter than those in the other cell lines so may not correspond to a specific *KCNK15* product (Figure 4.3). An additional product band at 500 bp was detected in 786-0 which was not predicted to correspond to a *KCNK15* PCR product (Figure 4.3). The two PCR product bands for 786-0 were extracted and sent for DNA sequencing, although the DNA failed to result in any readable sequence so the identity of these bands are unknown. Amplification of the correct *KCNK15* PCR product at 259 bp was confirmed by DNA sequencing in three cells lines: A549 lung, OE19 oesophageal, and SW480 colorectal (indicated by *, Figure 4.3). Sequenced PCR products showed over 92 % identity to the *KCNK15* mRNA reference sequence (*Homo sapiens*; NM_022358.3), with any mismatch due to ambiguous bases (N) detected in the sequencing read: 99 % for A549 (209/211 matched bp), 92 % for OE19 (128/139), and 99 % for SW480 cells (216/218 matched bp).

4.2.4 K_{2P}1.1 (*KCNK1*) mRNA expression

KCNK1 (K_{2P}1.1) mRNA expression was examined in all eleven human cancer cell lines utilised in this study. These cancer cell lines were selected to reflect the expression data observed in Chapter 3, where *KCNK1* mRNA was altered in 10 of the 20 cancers examined (Table 3.1). *KCNK1* PCR product (211 bp) was detected in ten of these cancer cell lines (Figure 4.4 A) and sequencing confirmed the correct amplification of *KCNK1* product (Table 4.1), with over 140 matched bases to the *KCNK1* mRNA reference sequence (*Homo sapiens*; NM_002245.3). *KCNK1* expression was observed in two colorectal cells lines (SW480 and HCT116); no product was observed for SW620 colorectal cells although a higher band (400 bp) was detected. This band is not predicted to be a *KCNK1* specific product and DNA sequencing showed it corresponded to mitochondrial genome DNA (*Homo sapiens*; NC_012920.1).

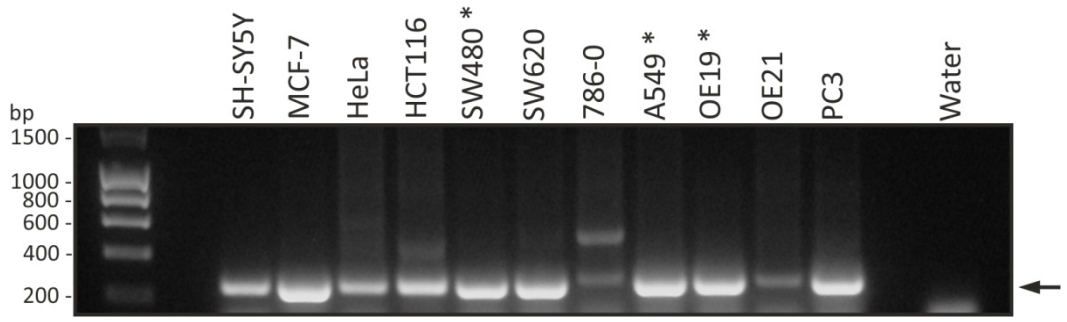

Figure 4.3: *KCNK15* mRNA expression in human cancer cell lines
KCNK15 PCR product was amplified, at the predicted size of 259 bp (indicated by an arrow), from breast (MCF-7), cervical (HeLa), colon (HCT116, SW480, and SW620), lung (A549), oesophageal (OE19), prostate (PC3), and neuroblastoma (SH-SY5Y) cancer cell line cDNA. No PCR products were detected at 259 bp in renal (786-0) and oesophageal (OE21) cancer cell lines.

PCR products were amplified using KCNK15F and KCNK15R, with a Ta of 65 °C.
Water was run as a no cDNA template control to ensure no PCR contamination.

* indicates where the PCR product has been confirmed to be *KCNK15* by DNA sequencing.

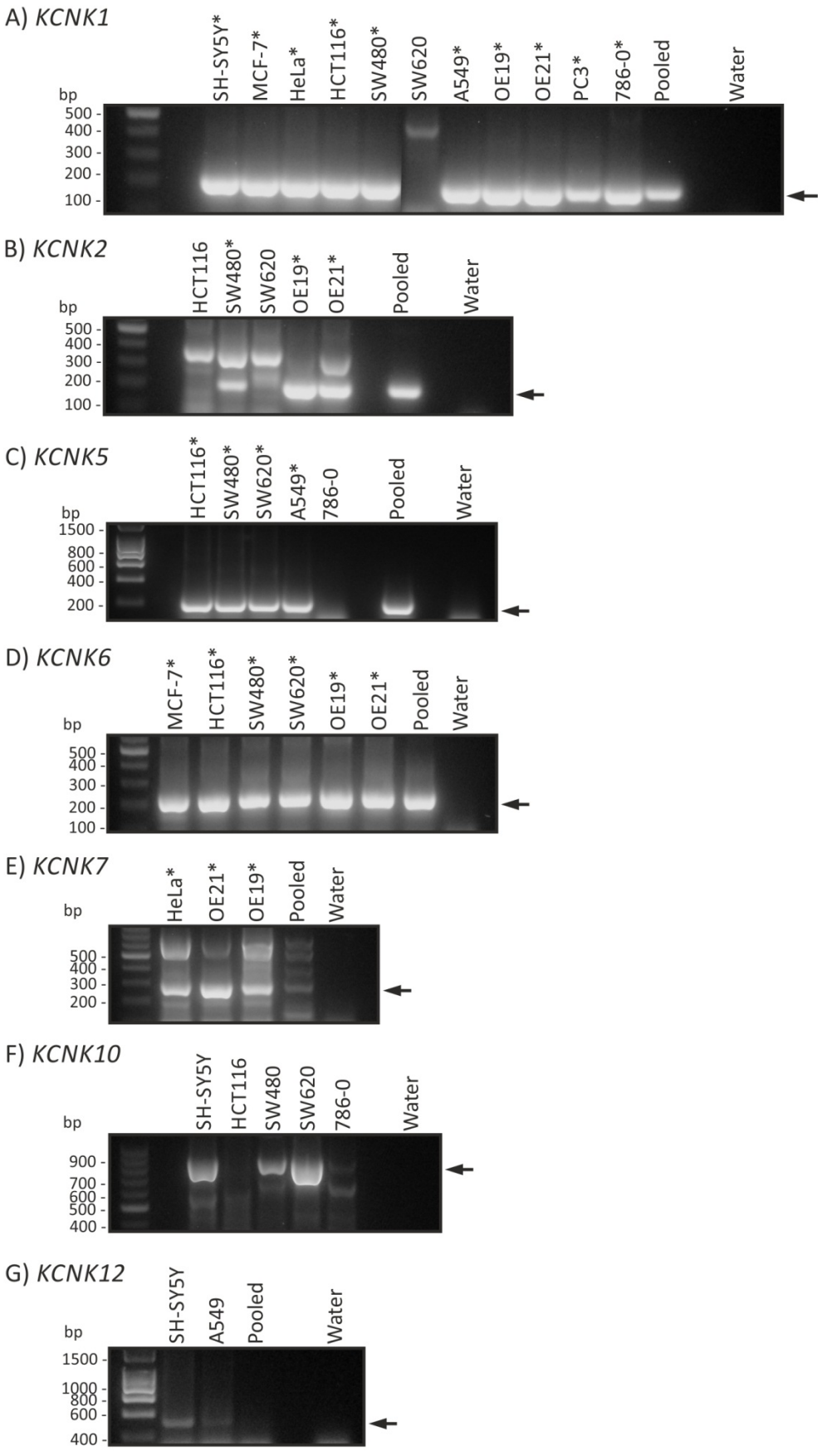
A) KCNK1
SH-SY5Y*
MCF-7*
HeLa*
HCT116*
SW480*
SW620
A549*
OE19*
OE21*
PC3*
786-0*
Pooled
Water
bp
500
400
300
200
100
B) KCNK2
HCT116
SW480*
SW620
OE19*
OE21*
Pooled
Water
bp
500
400
300
200
100
C) KCNK5
HCT116*
SW480*
SW620*
A549*
786-0
Pooled
Water
bp
1500
800
600
400
200
D) KCNK6
MCF-7*
HCT116*
SW480*
SW620*
OE19*
OE21*
Pooled
Water
bp
500
400
300
200
100
E) KCNK7
HeLa*
OE21*
OE19*
Pooled
Water
bp
500
400
300
200
F) KCNK10
SH-SY5Y
HCT116
SW480
SW620
786-0
Water
bp
900
700
600
500
400
G) KCNK12
SH-SY5Y
A549
Pooled
Water
bp
1500
1000
800
600
400

Figure 4.4: K_{2P} channel mRNA expression in human cancer cell lines

K_{2P} channel mRNA product was amplified, using exon-spanning primers, from cancer cell line cDNA. Cancer cell lines were selected to reflect the K_{2P} channel mRNA expression data observed in Chapter 3.
Pooled cDNA was run as a positive control for K_{2P} channel mRNA expression and water as a no cDNA template control to ensure no PCR contamination.
Predicted PCR product size is indicated by an arrow. * indicates where the PCR product has been confirmed by DNA sequencing.

A) *KCNK1* PCR product amplified from breast (MCF-7), cervical (HeLa), colon (HCT116, and SW620), lung (A549), neuroblastoma (SH-SY5Y), oesophageal (OE19 and OE21), prostate (PC3), and renal (786-0) cancer cell line cDNA.
PCR products were amplified using KCNK1F and KCNK1R primers, Ta = 63 °C. Predicted product size is 211 bp.

B) *KCNK2* PCR product amplified from colon (SW480) and oesophageal (OE19 and OE21) cancer cell line cDNA.
PCR products were amplified using KCNK2F and KCNK2R primers, Ta = 56 °C. Predicted product size is 206 bp.

C) *KCNK5* PCR product amplified from colon (HCT116, SW480, and SW620) and lung (A549) cancer cell line cDNA.
PCR products were amplified using KCNK5F and KCNK5R primers, Ta = 62 °C. Predicted product size is 211 bp.

D) *KCNK6* PCR product amplified from breast (MCF-7), colon (HCT116, SW480, and SW620), and oesophageal (OE19 and OE21) cancer cell line cDNA.
PCR products were amplified using KCNK6F and KCNK6R primers, Ta = 62 °C. Predicted product size is 229 bp.

E) *KCNK7* PCR product amplified from cervical (HeLa) and oesophageal (OE19 and OE21) cancer cell line cDNA.
PCR products were amplified using KCNK7F and KCNK7R primers, Ta = 64 °C. Predicted PCR product size is 298 bp.

F) *KCNK10* PCR product amplified from colon (SW480) and renal (786-0) cancer cell line cDNA.
PCR products were amplified using KCNK10F and KCNK10R primers, Ta = 60 °C. Predicted product size is 888 bp.

G) *KCNK12* PCR product amplified from lung (A549) and neuroblastoma (SH-SY5Y) cancer cell line cDNA.
PCR products were amplified using KCNK12F and KCNK12R primers, Ta = 63 °C. Predicted product size is 506 bp.

4.2.5 K_{2P}2.1 (*KCNK2*) mRNA expression

KCNK2 (K_{2P}2.1) mRNA expression was significantly altered in gastrointestinal adenocarcinomas (Table 3.3). No gastrointestinal cancer cell lines were available for RT-PCR analysis, so *KCNK2* mRNA expression was examined in colorectal (HCT116, SW480, and SW620) and oesophageal (OE19 and OE21) cancer cell lines. *KCNK2* PCR product (206 bp) was detected in SW480, OE19, and OE21 cell lines (Figure 4.4 B), DNA sequencing confirmed correct amplification of *KCNK2* in these cell lines (Table 4.1). Sequenced DNA had over 139 matched bases to the *KCNK2* mRNA reference sequence (*Homo sapiens*; NM_014217.3). A higher band (350 bp) was also detected in all cell lines which was not predicated to be a *KCNK2* specific PCR product and when sequenced corresponded to enolase 1α transcript variant 2 mRNA (*Homo sapiens*; NM_001201483.1).

4.2.6 K_{2P}5.1 (*KCNK5*) mRNA expression

KCNK5 (K_{2P}5.1) mRNA expression was significantly altered in colorectal, lung, and renal cancers (Figure 3.5). Therefore, *KCNK5* mRNA expression was examined in colorectal (HCT116, SW480, and SW620), lung (A549), and renal (786-0) cancer cell lines. *KCNK5* PCR product (211 bp) was detected in both colorectal and lung cell lines, but not 786-0 renal cells (Figure 4.4 C). Sequencing confirmed correct amplification of *KCNK5* mRNA product (211 bp) in positive cell lines (Table 4.1), with 157 matched bases to the *KCNK5* mRNA reference sequence (*Homo sapiens*; NM_003740.3).

4.2.7 K_{2P}6.1 (*KCNK6*) mRNA expression

KCNK6 (K_{2P}6.1) mRNA expression was significantly altered in breast, colorectal, and oesophageal cancers (Figure 3.2). Thus, *KCNK6* mRNA expression was examined in breast (MCF-7), colorectal (HCT116, SW480, and SW620), and oesophageal (OE19 and OE21) cancer cell lines. Positive *KCNK6* expression (PCR product; 229 bp) was detected in all of these cell lines (Figure 4.4 D) and sequencing confirmed detection of *KCNK6* mRNA (Table 4.1), with over 170 matched bases to the *KCNK6* mRNA reference sequence (*Homo sapiens*; NM_004823.1).

4.2.8 K_{2P}7.1 (*KCNK7*) mRNA expression

KCNK7 (K_{2P}7.1) mRNA expression was significantly altered in cervical and oesophageal carcinomas (Figure 3.2). Therefore, *KCNK7* mRNA expression was examined in cervical (HeLa) and oesophageal (OE19 and OE21) cancer cell lines. *KCNK7* PCR product (298 bp) was detected in all three of these cells lines (Figure 4.4 E) and sequencing confirmed detection of *KCNK7* mRNA (Table 4.1), with over 190 matched bases to the mRNA reference sequences of all four *KCNK7* transcript variants (*Homo sapiens*; A: NM_033347.1, B: NM_033348.1, C: NM_005714.1, and D: NM_033455.1). In addition to the correct product band, a series of higher running bands were detected which are not predicted to be *KCNK7* specific, although the identity of these bands was not examined.

4.2.9 K_{2P}10.1 (*KCNK10*) mRNA expression

KCNK10 (K_{2P}10.1) mRNA expression was significantly altered in brain, colorectal, and renal cancers (Figure 3.3), therefore expression was examined in neuroblastoma (SH-SY5Y), colorectal (HCT116, SW480, and SW620), and renal (786-0) cancer cell lines. Of these cell lines, *KCNK10* PCR product was detected in one colorectal (SW480) cell line and a faint band in 786-0 renal cells (Figure 4.4 F). In SH-SY5Y and SW620 bands are detected, but they appear to be running at lower size (750 bp) compared to the other cell lines and are not at the expected size (888 bp). PCR product sequencing failed to produce any readable sequence, so confirmation of the correct *KCNK10* mRNA product was not possible.

4.2.10 K_{2P}12.1 (*KCNK12*) mRNA expression

The final K_{2P} channel examined was *KCNK12* (K_{2P}12.1), data from Oncomine show *KCNK12* mRNA was significantly altered in brain and lung cancers (Figure 3.6). Therefore, *KCNK12* mRNA expression was examined in neuroblastoma (SH-SY5Y) and lung (A549) cancer cell lines. *KCNK12* PCR product (506 bp) was successfully detected in both of these cell lines (Figure 4.4 G; Table 4.1). However, PCR product sequencing also failed to produce any readable sequence, so confirmation of the correct *KCNK12* mRNA product was not possible.

4.2.11 Expression of K_{2P} channel mRNA in human cancer cell lines

The aim of these experiments was to characterise the mRNA expression of the TASK channel family in the cancer cell lines examined. RT-PCR analysis revealed that K_{2P} channel mRNA was expressed in a wide range of cancer cell lines (Table 4.1) and in many cases the PCR products reflected the mRNA expression profile observed in Chapter 3. The RT-PCR data presented here showed that within a single cancer cell line the mRNA for several K_{2P} channels were expressed (summarised in Table 4.1). This strengthened the findings from Chapter 3 which suggested that multiple channels are expressed within a given cancer type. This further indicated that the expression of multiple K_{2P} channels may occur in cancer tissues and that this could have clinical relevance. As discussed in Chapter 3 (Section 3.3), there is no evidence to indicate how the activity of multiple K_{2P} channels will impact on cancer cell functions.

K_{2P}3.1, which was the most significantly altered TASK channel in Chapter 3, was expressed in the fewest number of cancer cell lines, with the highest levels of mRNA product detected in A549 lung, 786-0 renal, and SH-SY5Y neuroblastoma cells (Figure 4.1). Expression of K_{2P}9.1 mRNA was detected in a wider range of cancer cell lines, with high levels of PCR product identified in breast (MCF-7), colorectal (HCT116, SW480, and SW620), and neuroblastoma (SH-SY5Y) cells (Figure 4.2). In addition, K_{2P}9.1 mRNA was detected in HEK293 cells, which are used for heterologous expression in this study. K_{2P}15.1, the non-functional member of TASK channel family, was also detected in nine of the eleven human cancer cell lines examined (Figure 4.3). The oesophageal cancer cell line, OE21, was the only cell line examined that was negative for all members of the TASK channel family, at an mRNA level (Table 4.1).

Table 4.1: K_{2P} channel mRNA expression in human cancer cell lines

Summary of the K_{2P} channel mRNA expression observed in human cancer cell lines by RT-PCR.
Positive (+) and negative (-) expression is shown. Blank cells indicate where expression was not examined.
* indicates confirmation of mRNA product by DNA sequencing, with the number of matched bases (bp) shown.

Cancer	Cell line	mRNA									
		KCNK1	***KCNK2***	***KCNK3***	***KCNK5***	***KCNK6***	***KCNK7***	***KCNK9***	***KCNK10***	***KCNK12***	***KCNK15***
Brain	SH-SY5Y	+* 144 bp		+				+* 204 bp	+	+	+
Breast	MCF-7	+* 155 bp		+		+* 183 bp		+			+
Cervical	HeLa	+* 161 bp		+			+* 232 bp	-			+
Colorectal	HCT116	+* 157 bp	-	-	+* 157 bp	+* 181 bp		+	-		+
	SW480	+* 160 bp	+* 143 bp	-	+* 157 bp	+* 180 bp		+	-		+* 216 bp
	SW620	-	-	-	+* 157 bp	+* 181 bp		+	+		+
Lung	A549	+* 161 bp		+* 261 bp	+* 157 bp			+* 261 bp		+	+* 209 bp
Oesophageal	OE19	+* 160 bp	+* 140 bp	-		+* 172 bp	+* 199 bp	-			+* 128 bp
	OE21	+* 160 bp	+* 139 bp	-		+* 174 bp	+* 228 bp	-			-
Prostate	PC3	+* 161 bp		-				-			+
Renal	786-0	+* 161 bp		+* 230 bp	-			-			-

The levels of K_{2P} channel PCR products detected within the cancer cell lines examined varied. RT-PCR is not a quantitative measure of mRNA expression, therefore from these experiments reliable conclusions about the different levels of channel expression cannot be made. As a means to quantify TASK channel mRNA, reverse transcriptase quantitative PCR (RT-qPCR) was tested during this study, however the probes used (*KCNK3*, *KCNK9*, β-actin, GAPDH, HPRT1; Applied Biosystems) were unsuitable for validation by the ΔΔCt method (data not shown). This meant that the standard curve method, together with a suitable positive expression control that could not be identified, would have been required. These technical problems meant that, at this time, RT-qPCR cannot be used to quantitatively determine K_{2P} channel mRNA expression in cancer cell lines.

In summary, examining the mRNA expression of K_{2P} channels in these cell lines using RT-PCR provided an indication of which K_{2P} channels are expressed (Table 4.1). However, mRNA expression may not correlate with protein expression and functional channel activity. Therefore, the rationale for the following experiments in this chapter was to identify which of the cancer cell lines positive for channel mRNA also had robust protein expression.

4.3 Optimisation of antibodies to detect TASK channel protein expression

Before TASK channel expression could be studied at a protein level in cancer cells, the reliability of commercially available antibodies targeted against the channels needed to be determined (Table 2.16). Therefore, the aim of this series of experiments was to identify commercially available antibodies which could specifically detect TASK channel protein. To achieve this, immunofluorescence was used to compare the fluorescent staining produced by the primary antibodies against GFP tagged channels heterologously expressed in COS-7, HEK293, or HeLa cells (Table 2.2; Method 2.5.3). Transfected cells were used so that channel protein detection could be confirmed in an expression system with high levels of TASK channel protein. Epifluorescence microscopy was utilised for staining detection (Method 2.6.1), selecting exposure times which gave the maximal staining detection without background staining. The same exposure times were used to detect GFP, TASK channel antibody, and no primary control staining.

Additionally, western blot conditions were examined to determine if the antibodies are suitable for channel protein detection by this method (Method 2.5.4). This would allow the protein expression to be quantified, as this was a limitation of the mRNA expression data presented in Result 4.2. Initially, experiments were conducted to determine if the channel antibody could replicate the binding pattern observed using a GFP specific antibody (Ab290, Abcam), when blotting against protein from cells expressing GFP tagged channels. Secondly, conditions were optimised for endogenous protein detection by assessing different cell lysis conditions in combination with membrane fractionation. Finally, using optimised conditions, experiments were conducted to determine if endogenous TASK channel protein can be detected in cancer cell lines (data presented in Section 4.4).

4.3.1 Detection of human $K_{2P}3.1$ protein expression

One commercially available antibody, Sigma anti-$K_{2P}3.1$ (P0981; Table 2.16), was examined and optimised for the detection of human $K_{2P}3.1$ protein.

4.3.1.1 $K_{2P}3.1$ protein detection by immunofluorescence

The specificity of Sigma anti-$K_{2P}3.1$ for $K_{2P}3.1$ detection by immunofluorescence was determined in HEK293 cells transfected with N-terminally GFP tagged human $K_{2P}3.1$ (GFP-$K_{2P}3.1$), fixed 24 h post-transfection. Antibody specificity was assessed by examining the overlap between the GFP signal (shown in green; Figure 4.5 A, D) and the signal due to the TASK channel specific antibody (shown in red; Figure 4.5 B). Areas of overlapping fluorescence appear yellow (overlapped signals with addition of DAPI (shown in blue); Figure 4.5 C). The fluorescence caused by primary antibody incubation was compared to untransfected cells in the same field of view and a no primary antibody incubation control.

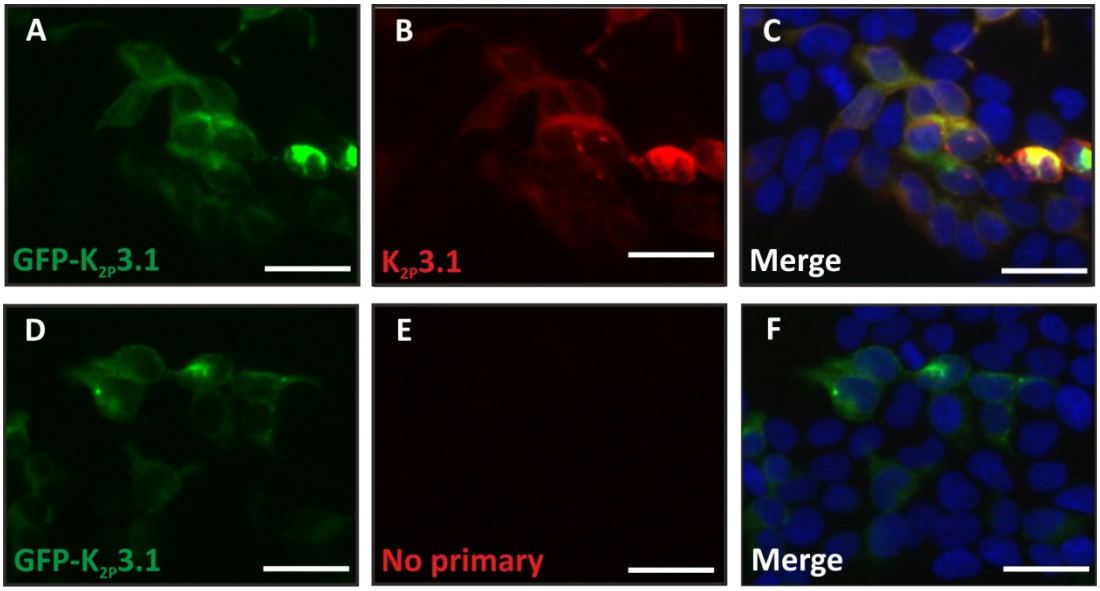

Figure 4.5: Detection of GFP-K_{2P}3.1 by Sigma anti-K_{2P}3.1 antibody
HEK293 cells transiently expressing GFP tagged human K_{2P}3.1.

A, D) Transfected channel was detected by GFP fluorescence signal.
B) Immunolabelling for K_{2P}3.1 using Sigma polyclonal anti-K_{2P}3.1 antibody.
E) No primary antibody incubation control.
C, F) Overlapped fluorescence signals including nuclear stain (DAPI).

All scale bars are 30 µm.

Incubation with Sigma anti-K_{2P}3.1 antibody (Figure 4.5 B) resulted in a similar fluorescence pattern to GFP-K_{2P}3.1 (Figure 4.5 A) and the overlapping signals (Figure 4.5 C) provide evidence that Sigma anti-K_{2P}3.1 is specifically binding to the channel. The signal resulting from primary antibody incubation was only seen in transfected cells compared to untransfected HEK293 cells (non-green cells; Figure 4.5 C). The antibody appeared to bind to transfected cells expressing lower amounts of the channel and not just those showing high expression, suggesting that the signal is specific and not just caused by binding to protein aggregates. The optimal antibody concentration for K_{2P}3.1 detection by this method was 12 µg/ml.

4.3.1.2 Detection of K_{2P}3.1 protein by western blot

The specificity of the Sigma anti-K_{2P}3.1 antibody to detect GFP-K_{2P}3.1 protein by western blotting was determined (Method 2.5.4), comparing antibody binding to a GFP specific antibody (5 µg/ml). For western blot detection, HEK293 cells expressing GFP-K_{2P}3.1 channels were lysed 24 h post-transfection and enriched for the crude membrane protein fraction using an ultracentrifugation step (50,000 g, 30 min; Method 2.5.4.2). GFP-K_{2P}3.1 has a predicted molecular weight of 72 kDa.

Incubation with the anti-GFP antibody (Figure 4.6 A) produced two bands in the transfected protein lane, one at approximately 66 kDa which is most likely to be GFP-K_{2P}3.1 and a higher band above the 116 kDa marker. Immunoblotting for GFP-K_{2P}3.1 protein using Sigma anti-K_{2P}3.1 antibody (3 µg/ml; Figure 4.6 B) resulted in a comparable band pattern to the GFP antibody (a lower band at 66 kDa and a higher band above the 116 kDa ladder). Both antibodies showed binding that was specific to the transfected protein and no binding was detected in the untransfected lane (Figure 4.6). The higher band detected by both GFP and K_{2P}3.1 antibody staining was likely to be caused by improperly solubilised or aggregated proteins, and this has been regularly observed by our lab when blotting transfected proteins.

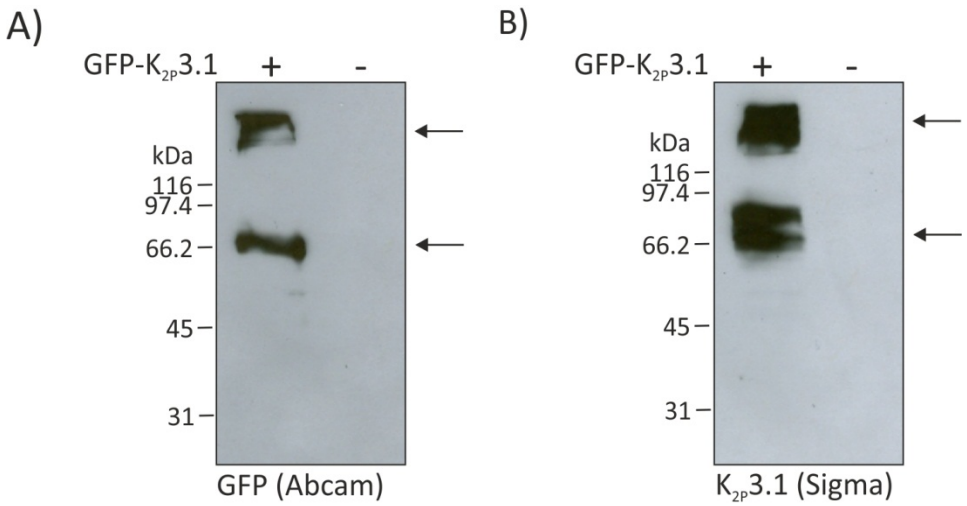

Figure 4.6: Detection of GFP-K_{2P}3.1 protein following membrane fractionation

HEK293 cells transiently expressing GFP-K_{2P}3.1 (+) were lysed 24 h post transfection and untransfected HEK293 cells (-) were run as a negative expression control.
Samples were enriched for the membrane faction by ultracentrifugation.
Proteins were visualised using antibodies for (A) GFP (Abcam) and (B) K_{2P}3.1 (Sigma).

The expected size for GFP-K_{2P}3.1 is 72 kDa.

A range of cell lysis conditions (alongside membrane fractionation and the validated $K_{2P}3.1$ antibody (which successfully identifies GFP-$K_{2P}3.1$; Figure 4.6) were examined to see if the solubilisation of $K_{2P}3.1$ protein could be improved and if endogenous $K_{2P}3.1$ protein could be detected (Figure 4.7). For this, A549 lung cancer cells were used; these cells endogenously express $K_{2P}3.1$ mRNA (Table 4.1). A549 cell pellets (harvested from T175 culture flasks) were lysed using one of three lysis buffers (cell lysis (CL), IP, or RIPA buffer; Table 2.25) in combination with manual homogenisation or sonication. After cell lysis, the lysate was enriched for the membrane protein fraction (Method 2.5.4.2) and prior to gel loading the samples were incubated at either 37 or 90 °C in loading buffer (Table 2.26). Samples were separated by SDS-PAGE electrophoresis on 12 % acrylamide gels with 8 M urea added, to further disrupt any hydrophobic protein interactions.

Native $K_{2P}3.1$ has a predicted molecular weight of 45 kDa. When blotting for endogenous $K_{2P}3.1$ protein in A549 cells (Figure 4.7 A), bands were detected in all lanes with the strongest band corresponding to a molecular weight of approximately 80 kDa making it unlikely to be endogenous $K_{2P}3.1$ protein. When comparing solubilisation conditions, no visual difference in the amount of protein was identified, except when the sample was heated to 90 °C which reduced the intensity of the 80 kDa band (lane 8; Figure 4.7 A). Since no differences in $K_{2P}3.1$ detection were observed, RIPA buffer (the most denaturing cell lysis buffer) in combination with sonication and a pre-loading incubation of 37 °C (lane 6; Figure 4.7 A) was selected to assess if native protein expression could be detected in other cancer cell lines (Figure 4.7 B). Five human cancer cell lines were assessed for $K_{2P}3.1$ protein expression by western blot detection (Table 4.1). In addition, further optimisation of $K_{2P}3.1$ solubility was tested, by resuspending the membrane fraction pellets in either RIPA lysis buffer then loading buffer (A549 (1)) or directly into loading buffer (A549 (2); Figure 4.7 B). No differences in $K_{2P}3.1$ protein detection were observed between the two conditions (Figure 4.7 B). Immunoblotting for $K_{2P}3.1$ protein (with Sigma anti-$K_{2P}3.1$) failed to result in any bands at the predicted molecular weight (45 kDa) in these cell lines (Figure 4.7 B), although a band was detected at 55 kDa which could be $K_{2P}3.1$ protein. However, this band was present in all cell lines, regardless to whether $K_{2P}3.1$ mRNA expression was observed (Figure 4.1), and was strongest in OE21 cells which are negative for $K_{2P}3.1$ mRNA.

A)

Cell lysis	CL	CL	IP	IP	RIPA	RIPA	RIPA	RIPA
Homogenisation	M	S	M	S	M	S	M	S
Preheated (° C)	37	37	37	37	37	37	90	90

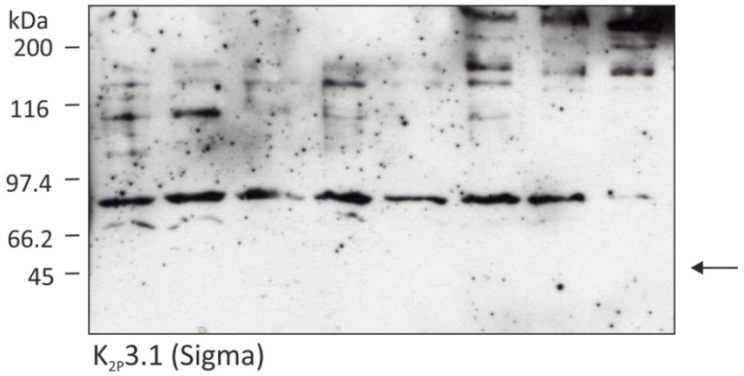

$K_{2P}3.1$ (Sigma)

B)

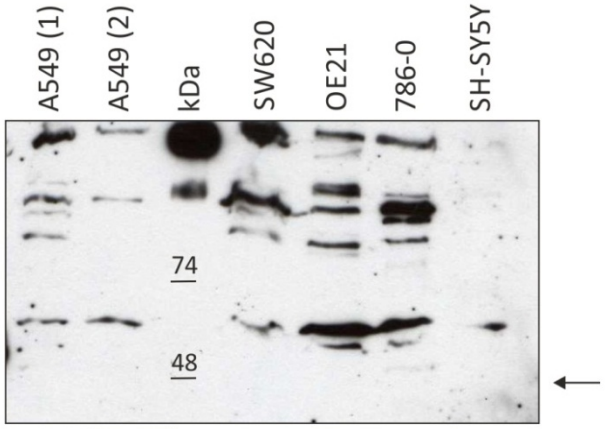

$K_{2P}3.1$ (Sigma)

Figure 4.7: Endogenous $K_{2P}3.1$ protein detection in human cancer cell lines

A) Optimisation of western blot conditions to detect $K_{2P}3.1$ protein in A549 lung cancer cell line.

Cells were lysed in either cell lysis buffer (CL), IP lysis buffer (IP) or RIPA buffer (RIPA), and homogenised manually (M) or by sonication (S). Cell lysates were enriched for the channel by membrane fractionation and preheated to 37 or 90 °C for 10 min before separation by SDS-PAGE electrophoresis on 12 % acrylamide gels (+ 8 M urea).

B) Failed detection of $K_{2P}3.1$ protein in human cancer cell lines.

Cells were lysed in RIPA buffer and the membrane fraction was resuspended directly into loading buffer (LB) for all samples except A549 (2) which was resuspended in RIPA buffer before LB addition. Cell lines: A549 lung (positive for $K_{2P}3.1$ mRNA), SW620 colorectal (negative for $K_{2P}3.1$ mRNA), OE21 oesophageal (negative for $K_{2P}3.1$ mRNA), 786-0 renal (positive for $K_{2P}3.1$ mRNA), and SH-SY5Y neuroblastoma (positive for $K_{2P}3.1$ mRNA) cancer cell lines.

Sigma anti-$K_{2P}3.1$ was used for immunolabelling. The expected size for $K_{2P}3.1$ protein is 45 kDa (indicated by arrow).

In conclusion, these experiments show that Sigma anti-K_{2P}3.1 is suitable for the detection of overexpressed K_{2P}3.1 channel protein by immunofluorescence and western blotting. However, this antibody is not suitable for the detection of endogenous K_{2P}3.1 channels by western blotting and this may be due to sub-optimal protein solubilisation conditions. Therefore, to enable assessment of endogenous K_{2P}3.1 protein expression in cancer cell lines, immunofluorescent staining in combination with confocal microscopy was used, since this gave higher detection sensitivity (Result 4.4.1).

4.3.2 Detection of human K_{2P}9.1 protein expression

Four commercially available antibodies targeted against human K_{2P}9.1 protein were tested (Table 2.16): Alomone polyclonal (APC-044), Proteintech polyclonal (180331-1-AP), Santa Cruz polyclonal (sc-11320), and Sigma monoclonal (K0514).

4.3.2.1 Detection of K_{2P}9.1 protein by immunofluorescence

The specificity of K_{2P}9.1 antibodies were tested in the same manner as for the K_{2P}3.1 antibody tested, by comparing the fluorescence patterns between GFP tagged human K_{2P}9.1 expressing cells to the staining produced by the primary antibody. Of the four commercially available antibodies targeted against K_{2P}9.1, only Santa Cruz polyclonal anti-K_{2P}9.1 showed a binding pattern comparable to GFP-K_{2P}9.1 that was not observed in untransfected cells.

Alomone anti-K_{2P}9.1 polyclonal antibody (7.5 µg/ml) did not recognise transfected GFP-K_{2P}9.1 in HEK293 cells (Figure 4.8 i); the primary antibody produced high background staining (Figure 4.8 i; B) compared to a no primary antibody incubation control (Figure 4.8 i; E). No specific binding of the antibody to the transfected channel protein was detected when comparing the GFP fluorescence to the signal from Alomone anti-K_{2P}9.1 binding (Figure 4.8 i; C). The antibody signal showed a nuclear staining pattern, which was also detected in untransfected HEK293 cells (positive for K_{2P}9.1 mRNA expression; Figure 4.2), however this staining was not increased by expression of GFP-K_{2P}9.1 channels making it unlikely to be K_{2P}9.1 specific binding (Figure 4.8 i; B).

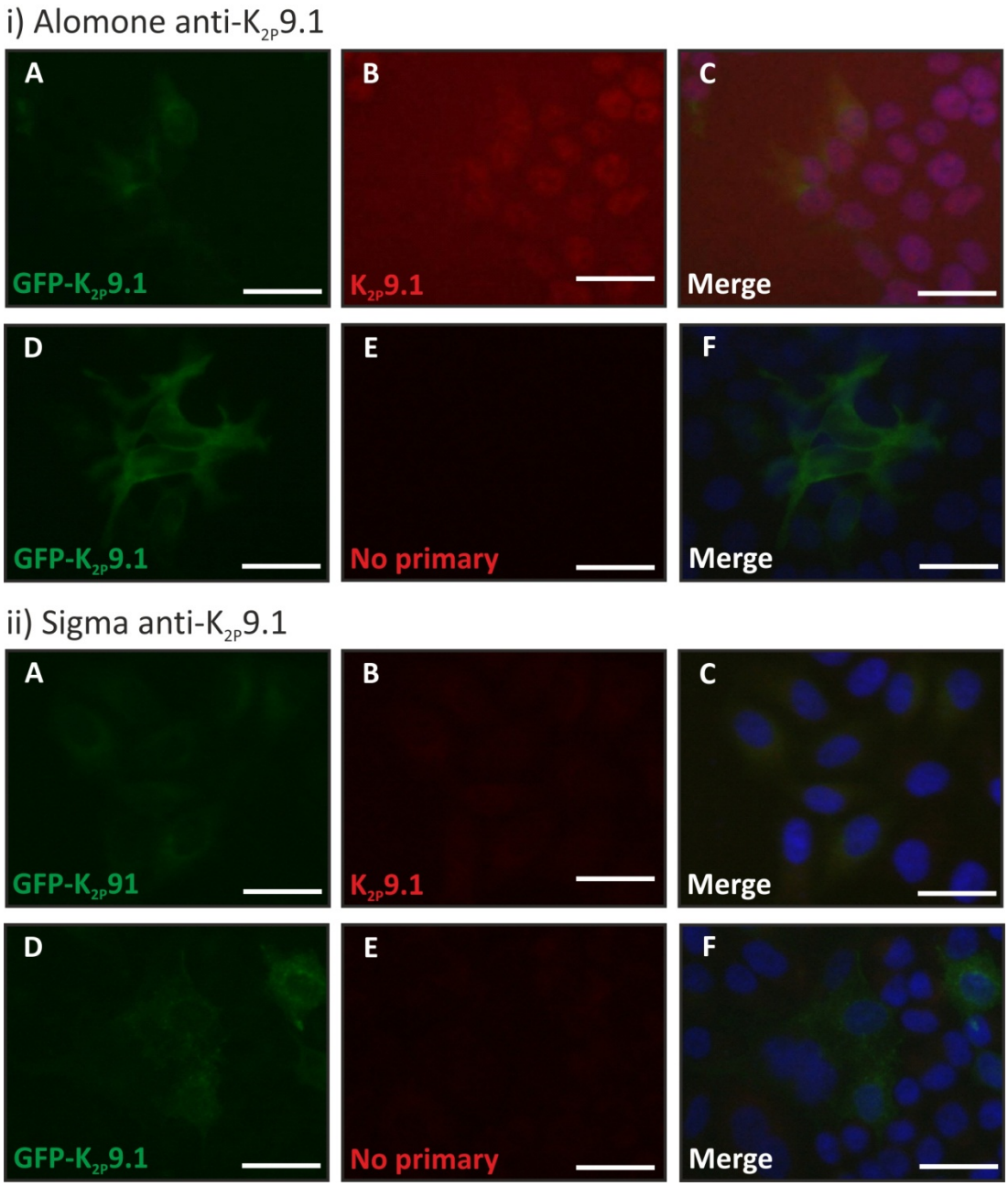

Figure 4.8: Failed detection of GFP-K_{2P}9.1 protein by K_{2P}9.1 antibodies

i) HEK293 cells transiently expressing GFP tagged human K_{2P}9.1.
A, D) Transfected channel was detected by GFP fluorescence signal.
B) Immunolabelling for K_{2P}9.1 using Alomone polyclonal anti-K_{2P}9.1 antibody.
E) No primary antibody incubation control.
C, F) Overlapped fluorescence signals including nuclear stain (DAPI).

ii) HeLa cells transiently expressing GFP tagged human K_{2P}9.1.
A, D) Transfected channel was detected by GFP fluorescence signal.
B) Immunolabelling for K_{2P}9.1 using Sigma monoclonal anti-K_{2P}9.1 antibody.
E) No primary antibody incubation control.
C, F) Overlapped fluorescence signals including nuclear stain (DAPI).

All scale bars are 30 µm.

Sigma anti-K_{2P}9.1 monoclonal antibody (48 µg/ml) failed to specifically recognise transfected GFP-K_{2P}9.1 protein in HeLa cells (Figure 4.8 ii). Incubation with the primary antibody produced a cytoplasmic binding pattern (Figure 4.8 ii; B) which when compared with the GFP-K_{2P}9.1 fluorescence (Figure 4.8 ii; A) caused signal overlap (Figure 4.8 ii; C). However, this was considered to be non-specific as the staining was observed in both transfected and untransfected HeLa cells, which do not express endogenous K_{2P}9.1 mRNA (Figure 4.2).

Proteintech anti-K_{2P}9.1 monoclonal antibody (0.13 µg/ml) recognised transfected GFP-K_{2P}9.1 protein in COS-7 cells (Figure 4.9 i). Incubation with the primary antibody produced a cytoplasmic binding pattern (Figure 4.9 i; B), that resulted in signal overlap (Figure 4.9 i; C) when compared with the GFP-K_{2P}9.1 fluorescence (Figure 4.9 i; A). However, low level non-specific binding of the primary antibody to untransfected COS-7 cells was observed (Figure 4.9 i; B); since COS-7 cells do not express native K_{2P}9.1 mRNA (Figure 4.2) this antibody was considered unsuitable for subsequent experiments.

Incubation with Santa Cruz anti-K_{2P}9.1 polyclonal antibody recognised transfected GFP-K_{2P}9.1 protein in HEK293 cells, when used at a range of concentrations from 2-20 µg/ml (Figure 4.9 ii). Staining caused by primary antibody binding (Figure 4.9 ii; B) showed a similar pattern to the GFP-K_{2P}9.1 (Figure 4.9 ii; A) and the overlap of the fluorescent signals suggested that Santa Cruz anti-K_{2P}9.1 is specifically binding to the channel protein (Figure 4.9 ii; C). The signal resulting from primary antibody incubation was only seen in transfected cells compared to untransfected HEK293 cells (non-green cells; Figure 4.9 ii; C). In addition, the antibody appears to bind to transfected cells expressing lower levels of the protein and not just those expressing higher amounts, this further suggests that the signal is specific and not just caused by binding to protein aggregates. HEK293 cells express endogenous K_{2P}9.1 mRNA (Figure 4.2); however the conditions used in this experiment (2 µg/ml antibody and epifluorescent microscopy) were not sensitive enough to detect endogenous K_{2P}9.1 protein levels which are lower than the overexpressed GFP-K_{2P}9.1 protein. Consequently, for experiments examining endogenous K_{2P}9.1 protein expression in cancer cell lines, the highest antibody concentration tested was used (20 µg/ml) in combination with confocal microscopy to give the highest sensitivity for staining detection (Result 4.4).

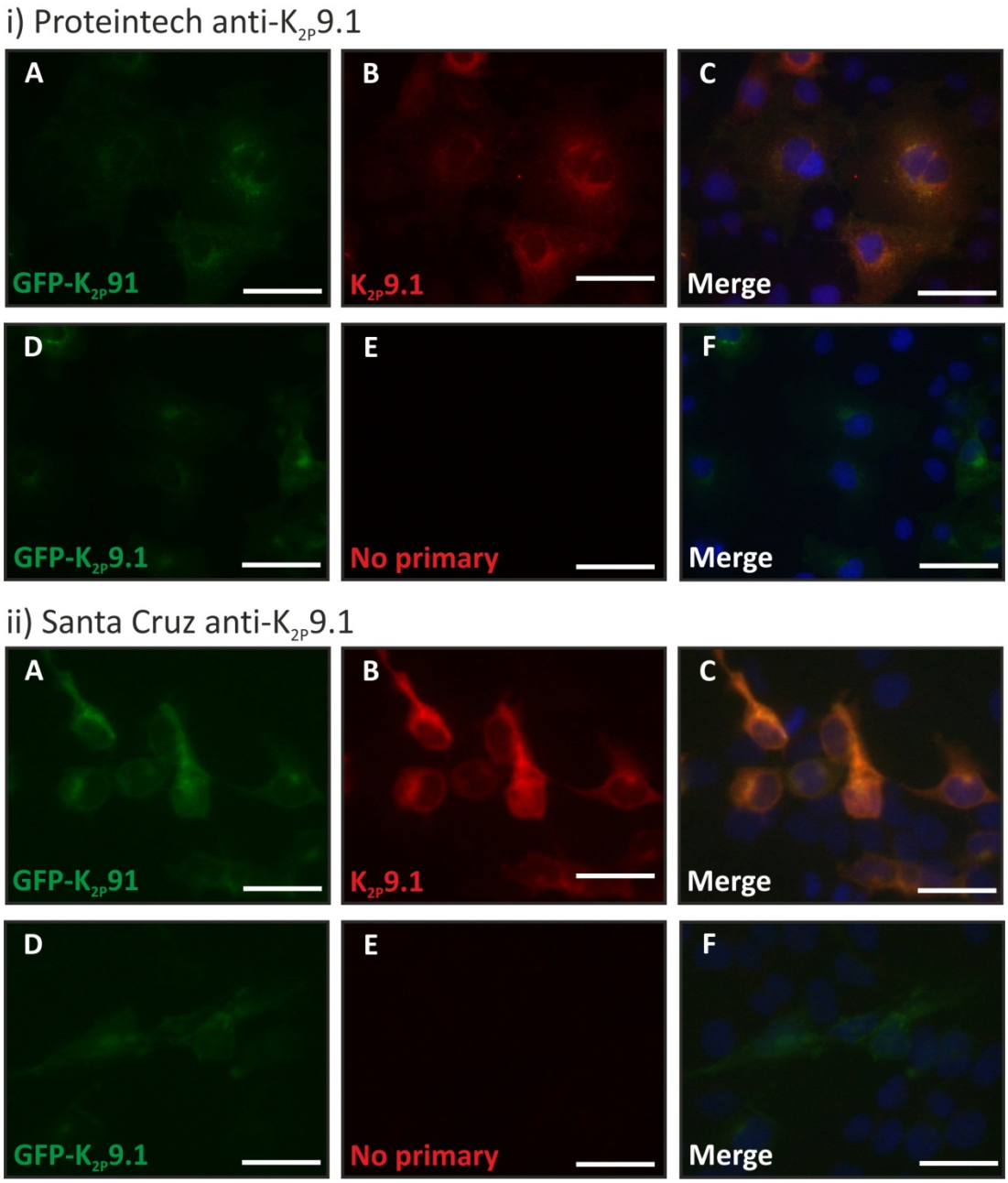

Figure 4.9: Detection of GFP-K_{2P}9.1 protein by K_{2P}9.1 antibodies

i) COS-7 cells transiently expressing N-terminally GFP tagged human K_{2P}9.1.
A, D) Transfected channel was detected by GFP fluorescence signal.
B) Immunolabelling for K_{2P}9.1 using Proteintech polyclonal anti-K_{2P}9.1 antibody.
E) No primary antibody incubation control.
C, F) Overlapped fluorescence signals including nuclear stain (DAPI).

ii) HEK293 cells transiently expressing N-terminally GFP tagged human K_{2P}9.1.
A, D) Transfected channel was detected by GFP fluorescence signal.
B) Immunolabelling for K_{2P}9.1 using Santa Cruz polyclonal anti-K_{2P}9.1 antibody (2 µg/ml).
E) No primary antibody incubation control.
C, F) Overlapped fluorescence signals including nuclear stain (DAPI).

All scale bars are 30 µm.

4.3.2.2 Detection of $K_{2P}9.1$ channel protein expression by western blotting

Initially, the ability of three commercially available $K_{2P}9.1$ antibodies (APC-044 Alomone, sc-11320 Santa Cruz, and K0514 Sigma) to detect $K_{2P}9.1$ protein by western blotting was examined. As with $K_{2P}3.1$ protein detection by western blotting, $K_{2P}9.1$ antibody specificity was determined by comparing GFP and $K_{2P}9.1$ antibody binding. To determine the optimal $K_{2P}9.1$ antibody, human GFP-$K_{2P}9.1$ transfected COS-7 cell lysate was purified using a GFP pull down (Method 2.5.4.3); collecting two samples the unbound lysate and the enriched bound fraction eluted from the GFP beads. Untransfected COS-7 whole cell lysate was used as a negative control. GFP-$K_{2P}9.1$ has a predicted molecular weight of 72 kDa.

Incubation of the bound cell lysate with the GFP antibody (Abcam; Figure 4.10 i) produced two bands one which ran at approximately 66 kDa, which is most likely to be GFP-$K_{2P}9.1$, and a higher band above the 116 kDa ladder. The higher band was also present in the unbound cell lysate; this is likely to be improperly solubilised and aggregated proteins. Incubation with Santa Cruz anti-$K_{2P}9.1$ antibody (1 µg/ml; Figure 4.10 ii) also produced two bands against the enriched bound lysate, at similar sizes to those seen with the GFP antibody (Figure 4.10 i). Neither Alomone anti-$K_{2P}9.1$ (1.88 µg/ml; Figure 4.10 iii) or Sigma anti-$K_{2P}9.1$ (12 µg/ml; Figure 4.10 iv) produced bands that were comparable to the GFP staining detected (Figure 4.10 i), although both antibodies detected a higher molecular weight band above 116 kDa. Additionally, Alomone anti-$K_{2P}9.1$ (Figure 4.10 iii) showed some non-specific binding in the untransfected COS-7 lysate lane. From these blots, it can be concluded that Santa Cruz anti-$K_{2P}9.1$ binds to transfected GFP-$K_{2P}9.1$ protein (which has been enriched by GFP pull down) compared to the other human $K_{2P}9.1$ antibodies analysed.

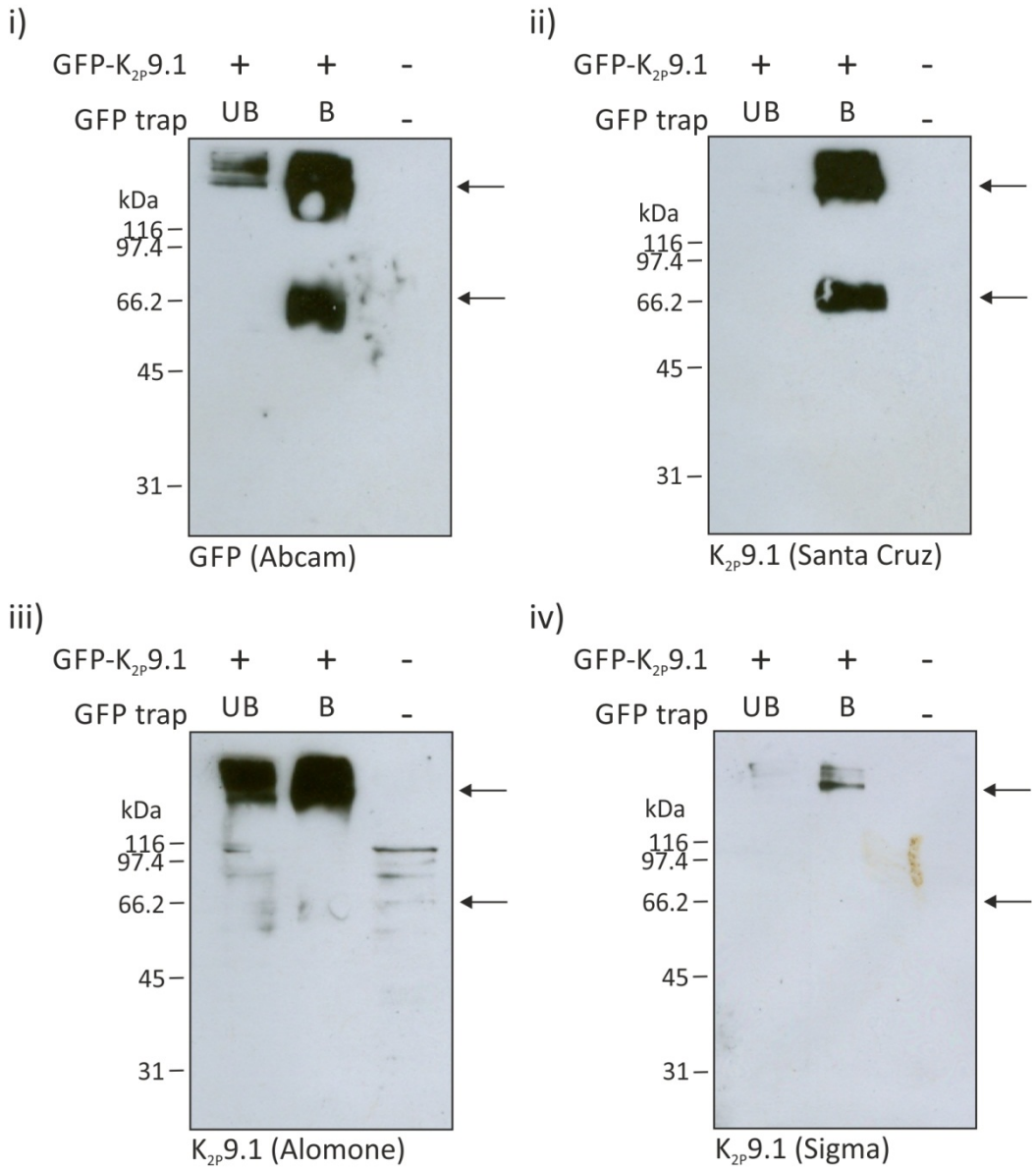

Figure 4.10: Analysis of K_{2P}9.1 antibody specificity by western blot detection

COS-7 cells transiently expressing GFP-K_{2P}9.1 (+) were lysed 24 h post transfection. Untransfected COS-7 cells (-) were run as a negative expression control.

GFP-K_{2P}9.1 was purified using a GFP-trap® matrix resulting in two fractions, unbound (UB) which did not bind to the beads and bound (B) which were eluted from the GFP-trap® matrix.

Protein was detected using antibodies against (i) GFP (Abcam), (ii) K_{2P}9.1 (Santa Cruz), (iii) K_{2P}9.1 (Alomone), and (iv) K_{2P}9.1 (Sigma).

The expected size for GFP-K_{2P}9.1 is 72 kDa.

A pull down method cannot be used to examine endogenous proteins. Therefore, in comparable experiments to those performed to optimise $K_{2P}3.1$ detection, the ability of Santa Cruz anti-$K_{2P}9.1$ to detect GFP-$K_{2P}9.1$ when crude membrane fractionation is used to enrich for membrane proteins was examined (Method 2.5.4.2). As before, the binding patterns resulting from GFP antibody incubation were compared to the $K_{2P}9.1$ antibody (Figure 4.11 B). The same antibody binding patterns were observed when the samples were purified using membrane fractionation (Figure 4.11) or a GFP pull down (Figure 4.10 A, B). Immunoblotting for $K_{2P}9.1$ protein (Santa Cruz) resulted in a comparable band pattern to a GFP antibody; a lower band at 66 kDa and a higher band above the 116 kDa ladder. Both antibodies showed binding that was specific to the transfected protein lane and no binding was detected in the untransfected lane (Figure 4.11). The band detected at 66 kDa by Santa Cruz anti-$K_{2P}9.1$ was fainter when the cell lysates were membrane fractionated (Figure 4.11 B). This may have been due to poor protein recovery in this sample or the presence of the higher molecular weight band (which was likely to be an improperly solubilised or aggregated protein). Therefore, to combat poor $K_{2P}9.1$ protein solubilisation a range of cell lysis buffers (cell lysis (CL), IP, or RIPA buffer; Table 2.25) were tested; in comparable optimisation experiments to those performed for $K_{2P}3.1$ detection. For this, SW620 colorectal cancer cells (which expresses $K_{2P}9.1$ mRNA; Figure 4.2) were harvested from T175 culture flasks and lysed using one of the three cell lysis buffers, combined with manual homogenisation or sonication. As before, the lysate was enriched for the membrane protein fraction and incubated, at either 37 or 90 °C, in loading buffer prior to gel loading (Table 2.26).

Native $K_{2P}9.1$ protein has a predicted molecular weight of 45 kDa. When blotting for $K_{2P}9.1$ protein in SW620 cells (Figure 4.12 A), a band was detected in lanes 2-8 with a molecular weight of approximately 85 kDa making it unlikely to be $K_{2P}9.1$ protein. This band was strongest in the samples which were lysed in RIPA buffer and preheated to 37 °C, with the homogenisation procedure not impacting the protein recovery (lanes 5 and 6; Figure 4.12 A). These data supported using the same conditions for $K_{2P}9.1$ sample preparation that were selected for $K_{2P}3.1$: using RIPA buffer, sonication, and a 37 °C pre-loading incubation (lane 6; Figure 4.12 A). These conditions were used, alongside membrane fractionation, to assess if $K_{2P}9.1$ expression could be detected in other human cancer cell lines (Figure 4.12 B).

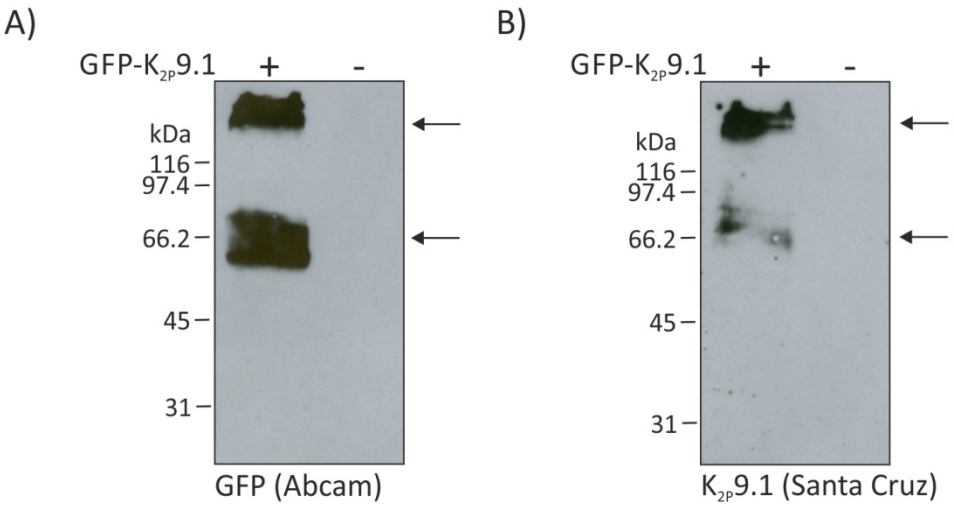

Figure 4.11: Detection of GFP-K_{2P}9.1 protein following membrane fractionation

HEK293 cells transiently expressing human GFP-K_{2P}9.1 (+) were lysed 24 h post transfection. Untransfected HEK293 cells (-) were run as a negative expression control.
Samples were enriched for membrane faction by ultracentrifugation.
Proteins were visualised using antibodies for (A) GFP (Abcam) and (B) K_{2P}9.1 (Santa Cruz).

The expected size for GFP-K_{2P}9.1 is 72 kDa.

A)

Cell lysis	CL	CL	IP	IP	RIPA	RIPA	RIPA	RIPA
Homogenisation	M	S	M	S	M	S	M	S
Preheated (° C)	37	37	37	37	37	37	90	90

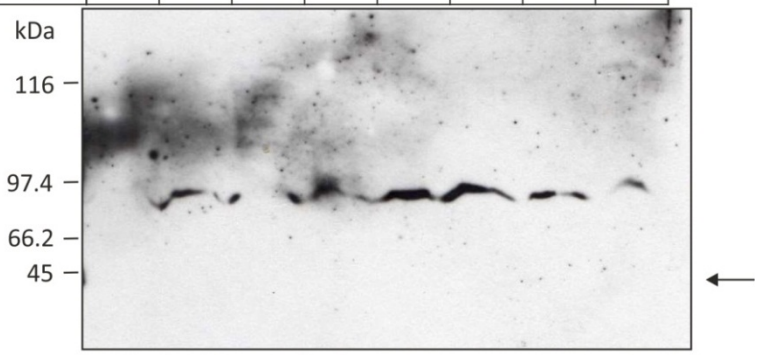

K_{2P}9.1 (Santa Cruz)

B)

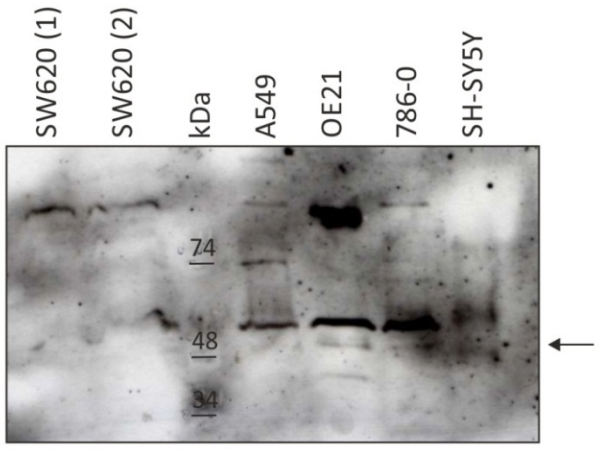

K_{2P}9.1 (Santa Cruz)

Figure 4.12: Endogenous K_{2P}9.1 protein detection in human cancer cell lines

A) Optimisation of western blot conditions to detect K_{2P}9.1 protein in SW620 colorectal cancer cell line.

Cells were lysed in either cell lysis buffer (CL), IP lysis buffer (IP) or RIPA buffer (RIPA), and homogenised manually (M) or by sonication (S). Cell lysates were enriched for the channel by membrane fractionation and preheated to 37 or 90 °C for 10 min before separation by SDS-PAGE electrophoresis on 12 % acrylamide gels (+ 8 M urea).

B) Failed detection of K_{2P}9.1 protein in human cancer cell lines.

Cells were lysed in RIPA buffer and membrane fraction was resuspended directly into loading buffer (LB) for all samples, except SW620 (2) which was resuspended in RIPA buffer before LB addition. Cell lines: A549 lung (positive for K_{2P}9.1 mRNA), SW620 colorectal (positive for K_{2P}9.1 mRNA), OE21 oesophageal (negative for K_{2P}9.1 mRNA), 786-0 renal (negative for K_{2P}9.1 mRNA), and SH-SY5Y neuroblastoma (positive for K_{2P}9.1 mRNA) cancer cell lines.

Santa Cruz anti-K_{2P}9.1 was used for immunolabelling. The expected size for K_{2P}9.1 protein is 45 kDa (indicated by arrow).

Five human cancer cell lines were assessed for native $K_{2P}9.1$ expression detection (Figure 4.12 B). Immunoblotting for $K_{2P}9.1$ (Santa Cruz) in these cell lines did not result in a band at the predicted molecular weight (45 kDa; Figure 4.12 B). As with $K_{2P}3.1$, increasing the solubility of membrane fraction pellet was examined to improve detection, however no improvement of $K_{2P}9.1$ protein detection was achieved (SW620 lanes 1 and 2; Figure 4.12 B). In three cell lines (A549, OE21, and 786-0), a band was detected at approximately 55 kDa (Figure 4.12 B); however only A549 cells express $K_{2P}9.1$ mRNA (Figure 4.2) and this band was stronger in the OE21 and 786-0 lanes (which do not express $K_{2P}9.1$ mRNA; Figure 4.2) making it unlikely that this band represented $K_{2P}9.1$ protein detection.

Data from these experiments showed that, like Sigma anti-$K_{2P}3.1$, Santa Cruz anti-$K_{2P}9.1$ is suitable for detection of overexpressed $K_{2P}9.1$ channel protein by immunofluorescence and western blotting. However, this antibody does not allow the detection of endogenous $K_{2P}9.1$ channel protein by western blotting, which may also be due to sub-optimal protein solubilisation conditions. Therefore, to assess endogenous $K_{2P}9.1$ protein expression in cancer cell lines, immunofluorescent staining in combination with confocal microscopy will be required (Result 4.4.1).

4.3.3 Detection of human $K_{2P}15.1$ protein expression

To detect the third member of the TASK channel family, two commercially available antibodies (Proteintech polyclonal anti-$K_{2P}15.1$ and Lifespan Biosciences polyclonal anti-$K_{2P}15.1$; Table 2.16) were tested by immunofluorescence against GFP tagged human $K_{2P}15.1$ expressing cells.

Proteintech anti-$K_{2P}15.1$ polyclonal antibody (0.13 µg/ml) did not recognise GFP tagged human $K_{2P}15.1$, when the GFP tag was located at either the C- or N-termini (Figure 4.13 i, ii). Incubation with the primary antibody against N-terminal GFP-$K_{2P}15.1$ transfected COS-7 cells resulted in some degree of signal overlap (Figure 4.13 i; C), however this staining was not an exact overlap to the tagged channel. In addition, antibody staining was present at low levels in untransfected cells (Figure 4.13 i; B). Incubation of the primary antibody against C-terminal $K_{2P}15.1$-GFP expressing COS-7 cells also failed to result in any detectable staining (Figure 4.13 ii; C).

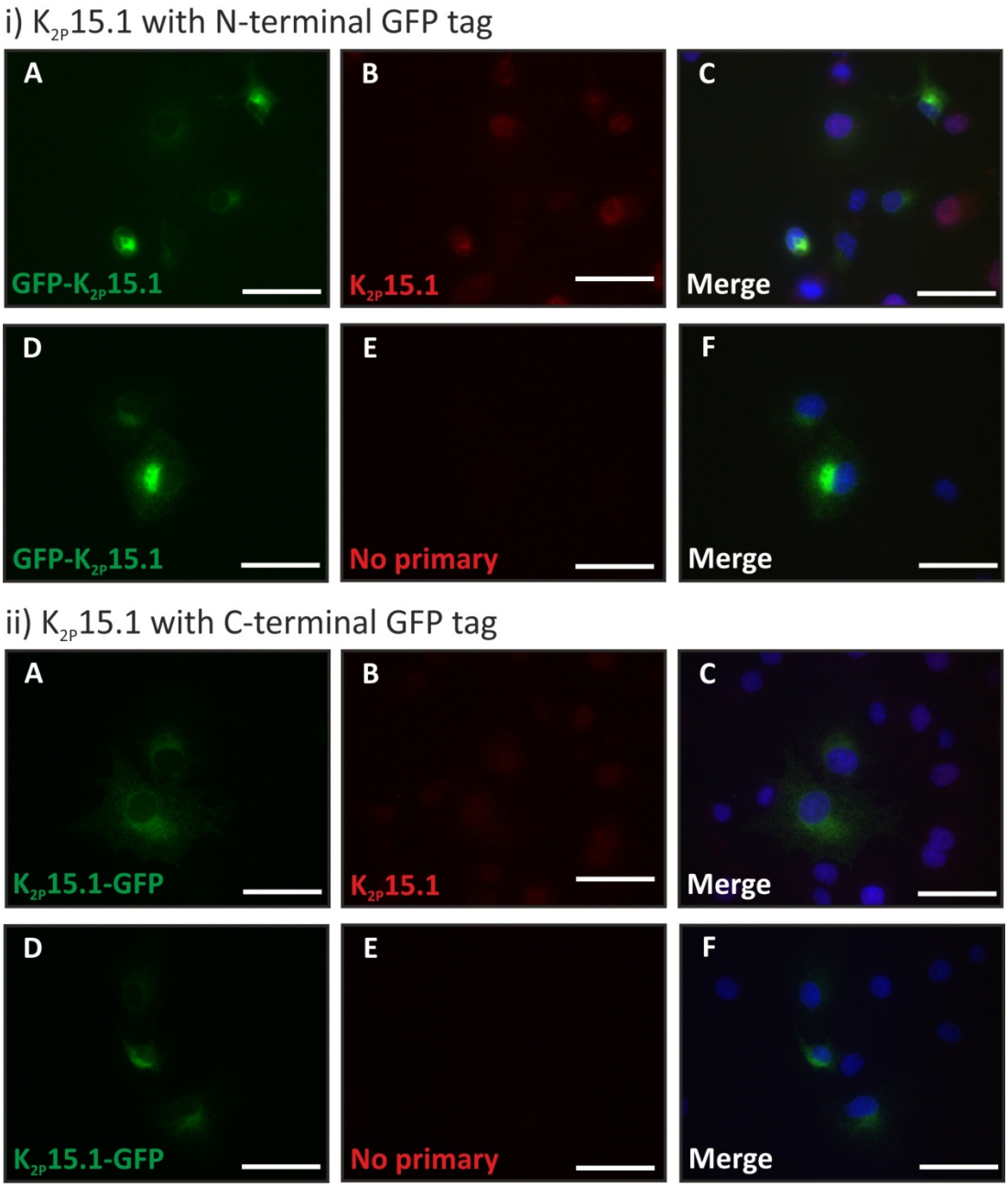

Figure 4.13: Failed detection of GFP tagged K_{2P}15.1 protein by Proteintech K_{2P}15.1 antibody

COS-7 cells transiently expressing (i) N-terminal tagged GFP-K_{2P}15.1 or (ii) C-terminal tagged K_{2P}15.1-GFP.

A, D) Transfected channel was detected by GFP fluorescence signal.

B) Immunolabelling for K_{2P}9.1 using Proteintech polyclonal anti-K_{2P}15.1 antibody.

E) No primary antibody incubation control.

C, F) Overlapped fluorescence signals including nuclear stain (DAPI).

All scale bars are 40 µm.

Lifespan anti-K_{2P}15.1 polyclonal antibody (20 µg/ml) also failed to recognise C- or N-terminally GFP tagged K_{2P}15.1 (Figure 4.14 i, ii). The presence of transfected channel was confirmed by GFP fluorescence (Figure 4.14 i, ii; A, D), however no binding of the primary antibody could be detected (Figure 4.14 i, ii; B). These antibodies were not examined further in this study, as both antibodies failed to identify GFP tagged K_{2P}15.1 expressing cells.

4.3.4 Antibodies available to detect TASK channel protein expression

The aim of the experiments presented in this section was to characterise the specificity of a number of commercially available TASK channel antibodies for TASK channel protein. Prior to this study, a limitation of studying TASK channel protein expression within the field has been a lack of reliable and validated antibodies. These experiments showed that both Sigma anti-K_{2P}3.1 and Santa Cruz anti-K_{2P}9.1 were suitable to detect overexpressed GFP tagged channels, using immunofluorescent staining and western blotting. However, the two K_{2P}15.1 antibodies tested here failed to produce a comparable staining pattern to GFP tagged human K_{2P}15.1 channels. Currently, no specific antibodies targeting K_{2P}15.1 protein have been produced either commercially or in our lab (Roncoroni, Thesis). This is an on-going limitation when studying K_{2P}15.1 channels and meant that K_{2P}15.1 protein expression could not be examined in this thesis.

When Sigma anti-K_{2P}3.1 and Santa Cruz anti-K_{2P}9.1 antibodies were used to identify their target GFP tagged channel by western blotting, additional high molecular weight bands were also detected. This was likely to be caused by poor protein solubility or aggregation. To improve this, a range of sample preparation conditions were tested with the most denaturing method for cell lysis (using RIPA lysis buffer) being selected for subsequent preparations. Despite this, both antibodies failed to detect endogenous TASK channel expression in human cancer cells lines. This may have been caused by a combination of poor channel solubility and the low levels of native channel expression.

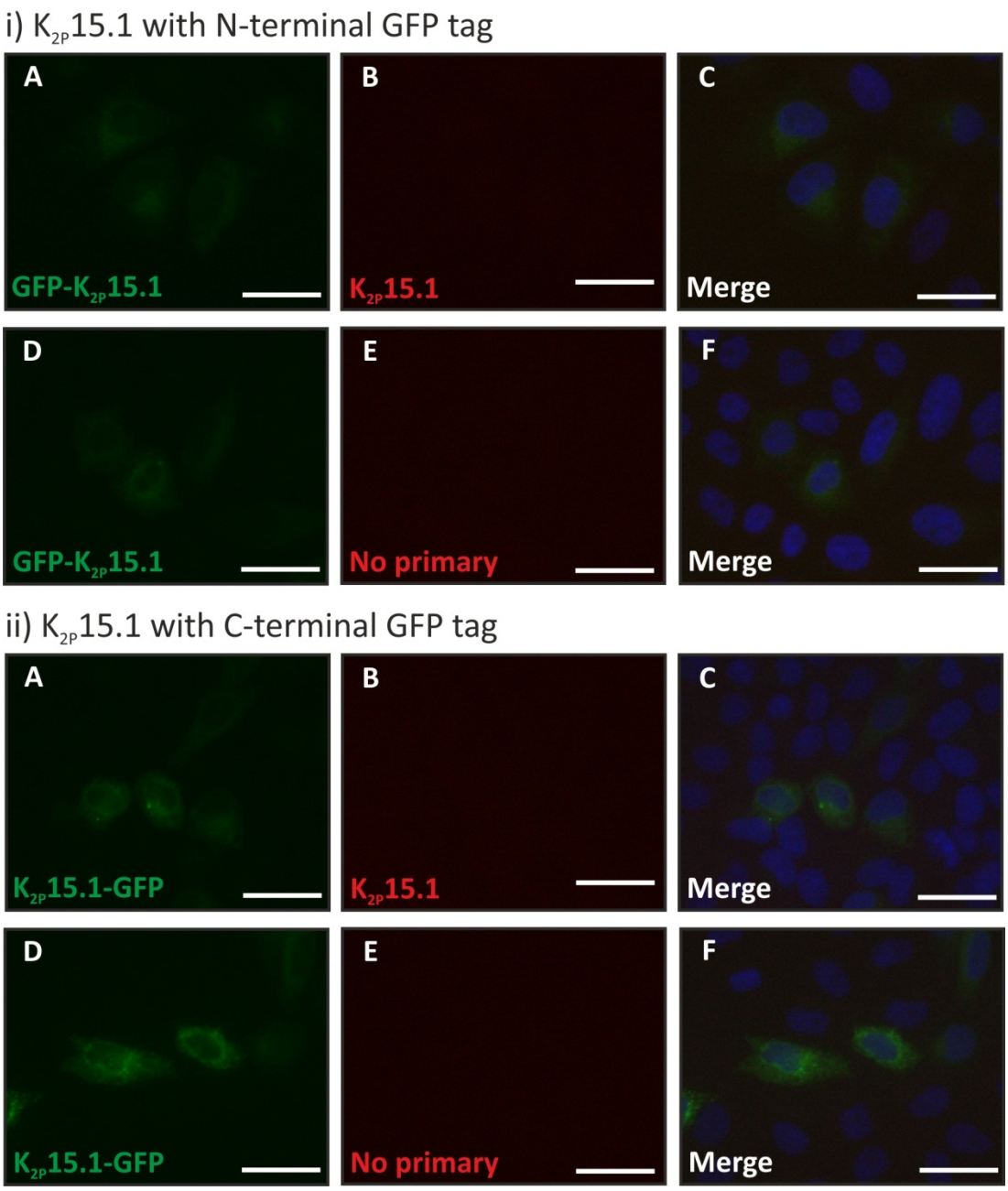

Figure 4.14: Failed detection of GFP tagged K_{2P}15.1 by Lifespan Bioscience K_{2P}15.1 antibody

HeLa cells transiently expressing (i) N-terminal tagged GFP-K_{2P}15.1 or (ii) C-terminal tagged K_{2P}15.1-GFP.

A, D) Transfected channel was detected by GFP fluorescence signal.

B) Immunolabelling for K_{2P}9.1 using Lifespan Bioscience polyclonal anti-K_{2P}15.1 antibody.

E) No primary antibody incubation control.

C, F) Overlapped fluorescence signals including nuclear stain (DAPI).

All scale bars are 30 µm.

In conclusion, these experiments showed that Sigma anti-K_{2P}3.1 and Santa Cruz anti-K_{2P}9.1 antibodies could successfully identify their target GFP tagged channel, however that these antibodies were not sensitive enough to detect endogenous protein by western blotting. Therefore, to study the expression of endogenous TASK channel protein in cancer cell lines immunofluorescent staining in combination with confocal microscopy was required. This combination of techniques was selected to give the highest sensitivity for staining detection (Result 4.4). Consequently, examining the TASK channel protein expression in cancer cells using the two antibodies characterised in this section with immunofluorescent staining and confocal microscopy was the next area of focus.

4.4 TASK channel protein expression in human cancer cell lines

The aim of this section was to assess the endogenous expression of TASK channel protein in the cancer cell lines examined in Result 4.2 that were positive for TASK channel mRNA (Table 4.1). Data presented in Result 4.3, identified the optimal antibody conditions for K_{2P}3.1 and K_{2P}9.1 protein detection by immunofluorescent staining, using Sigma anti-K_{2P}3.1 (12 µg/ml) and Santa Cruz anti-K_{2P}9.1 (20 µg/ml), respectively. For immunofluorescent labelling cancer cell lines were fixed (4 % PFA) and permeabilised (0.1 % Triton X-100; Method 2.5.3), before immunolabelling with antibody conditions described above.

TASK channel immunolabelling was detected using confocal microscopy (Method 2.6.2), comparing the staining to a no primary incubation control. For each cell line, the exposure times for the detection of channel staining were kept constant between the stained sample and no primary control, whereas to observe the DAPI nuclear stain the exposure times were varied to give the optimal detection. Confocal microscopy was used instead of epifluorescent microscopy, due to the increased imaging resolution and sensitivity. This allowed the detection of native protein expression levels which are significantly lower than the overexpressed protein levels examined in previous experiments (Results 4.3.1 and 4.3.2).

4.4.1 $K_{2P}3.1$ channel protein expression in cancer cell lines

$K_{2P}3.1$ protein expression was assessed in five cancer cell lines which were positive for $K_{2P}3.1$ mRNA (Figure 4.1 and Table 4.1): MCF-7 breast (Figure 4.15), HeLa cervical (Figure 4.16), A549 lung (Figure 4.17), 786-0 renal (Figure 4.18 i), and SH-SY5Y neuroblastoma (Figure 4.18 ii). In all cell lines, $K_{2P}3.1$ staining was compared to any background fluorescence in the no primary antibody incubation control (Panel C).

In MCF-7 cells, diffuse $K_{2P}3.1$ expression was observed across the cytoplasm with occasional brighter punctate fluorescence staining (Figure 4.15 A). The staining pattern detected in HeLa cells (Figure 4.16 A) was comparable to MCF-7 cells; however the punctate bright staining was more frequent. In A549 cells, faint $K_{2P}3.1$ expression was detected across the cytoplasm with occasional brighter spots within the cells (Figure 4.17 A). In 786-0 cells, as in the other cell lines examined, faint $K_{2P}3.1$ staining was detected across the cell cytoplasm with occasional brighter punctate regions of staining (Figure 4.18 i; A). However, in this cell line a brighter perinuclear network of $K_{2P}3.1$ expression was also detected (Figure 4.18 i; B). Finally, diffuse $K_{2P}3.1$ staining was observed across the cytoplasm of SH-SY5Y cells (Figure 4.18 ii; A).

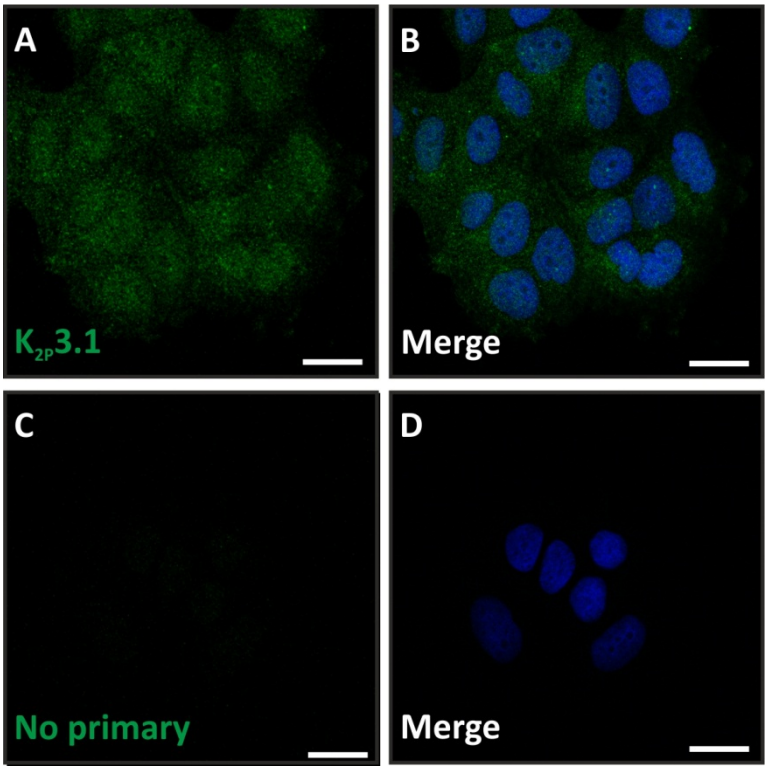

Figure 4.15: $K_{2P}3.1$ protein detected in MCF-7 breast cancer cell line
$K_{2P}3.1$ protein staining in MCF-7 cells, shown is a single confocal Z-slice.
A) Immunolabelling for $K_{2P}3.1$ using Sigma anti-$K_{2P}3.1$ antibody (shown in green).
C) No primary antibody incubation control.
B, D) Overlapped fluorescence with nuclear stain (DAPI, shown in blue).

All scale bars are 20 µm.

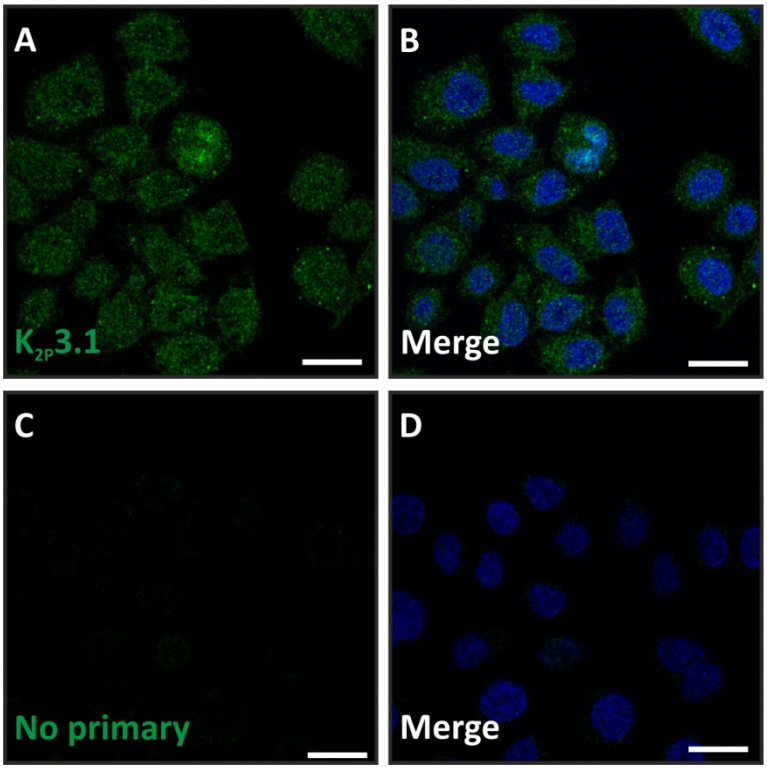

Figure 4.16: $K_{2P}3.1$ protein detected in HeLa cervical cancer cell line
$K_{2P}3.1$ protein staining in HeLa cells, shown is a confocal Z-slice.
A) Immunolabelling for $K_{2P}3.1$ using Sigma anti-$K_{2P}3.1$ antibody (shown in green).
C) No primary antibody incubation control.
B, D) Overlapped fluorescence with nuclear stain (DAPI, shown in blue).

All scale bars are 20 µm.

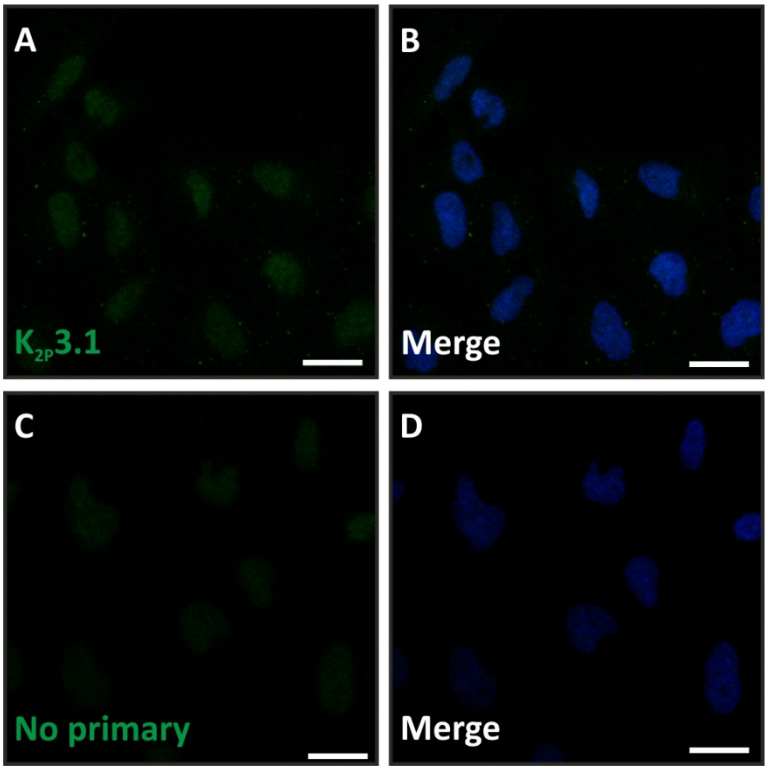

Figure 4.17: $K_{2P}3.1$ protein detected in A549 lung cancer cell line
$K_{2P}3.1$ protein staining in A549 cells, shown is a confocal Z-slice stack.
A) Immunolabelling for $K_{2P}3.1$ using Sigma anti-$K_{2P}3.1$ antibody (shown in green).
C) No primary antibody incubation control.
B, D) Overlapped fluorescence with nuclear stain (DAPI, shown in blue).

All scale bars are 20 μm.

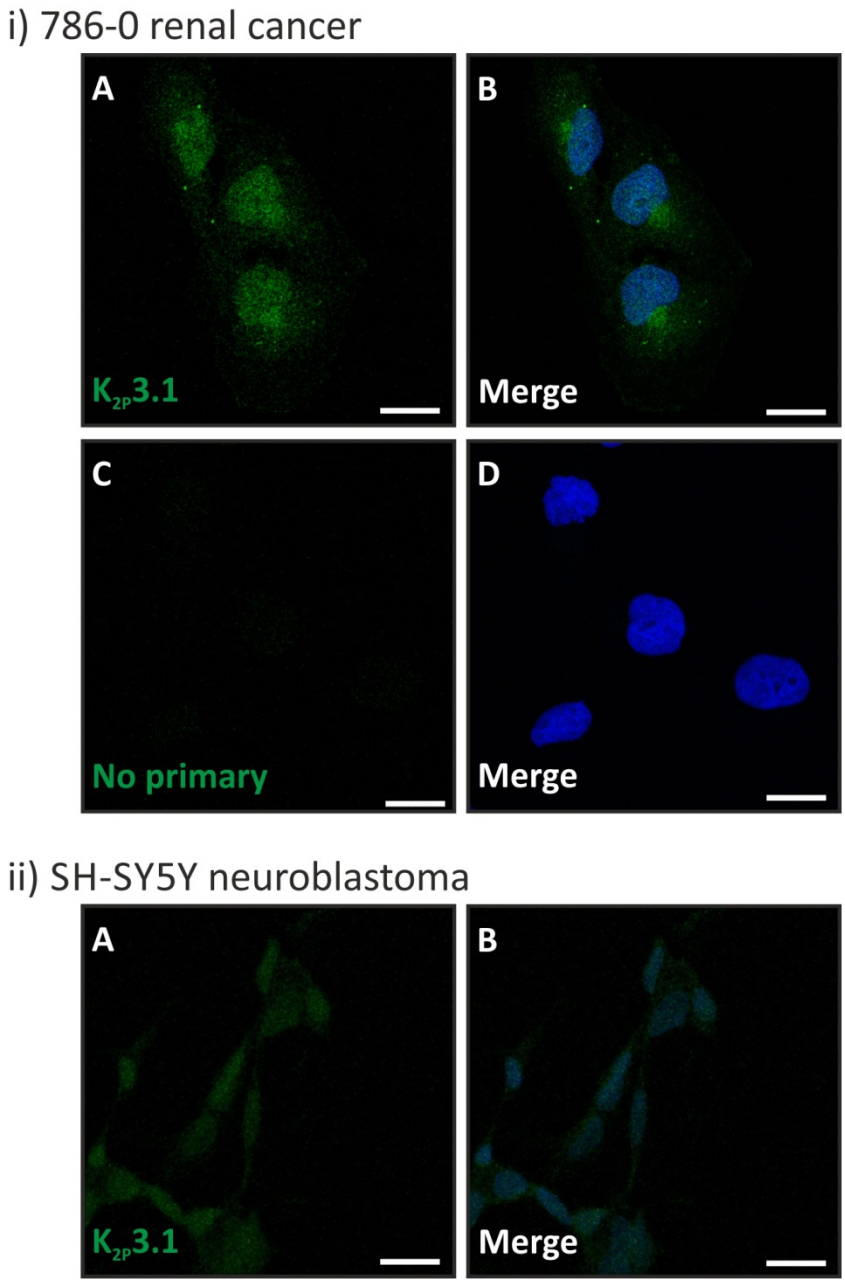

Figure 4.18: $K_{2P}3.1$ protein detected in renal cancer and neuroblastoma cells

i) $K_{2P}3.1$ protein staining in 786-0 cells, shown is a single confocal Z-slice.
A) Immunolabelling for $K_{2P}3.1$ using Sigma anti-$K_{2P}3.1$ antibody (shown in green).
C) No primary antibody incubation control.
B, D) Overlapped fluorescence with nuclear stain (DAPI, shown in blue).

ii) $K_{2P}3.1$ protein staining in SH-SY5Y cells, shown is a confocal Z-slide stack.
A) Immunolabelling for $K_{2P}3.1$ using Sigma anti-$K_{2P}3.1$ antibody (shown in green).
B) Overlapped fluorescence with nuclear stain (DAPI, shown in blue).

All scale bars are 20 μm.

4.4.2 K_{2P}9.1 channel protein expression in cancer cell lines

K_{2P}9.1 protein expression was assessed in six cancer cell lines which were positive for K_{2P}9.1 mRNA (Figure 4.2 and Table 4.1): MCF-7 breast (Figure 4.19), HCT116 colorectal (Figure 4.20), SW480 colorectal (Figure 4.21), SW620 colorectal (Figure 4.22), A549 lung (Figure 4.23 i), and SH-SY5Y neuroblastoma (Figure 4.23 ii). As before, the K_{2P}9.1 staining detected was above any background fluorescence detected in the no primary antibody incubation control (Panel C).

In MCF-7 cells, diffuse K_{2P}9.1 staining was detected across the cytoplasm (Figure 4.19 A) and this staining pattern was similar to the K_{2P}3.1 expression observed in these cells (Figure 4.15 A). As well as the diffuse cytoplasmic staining, a brighter perinuclear K_{2P}9.1 staining ring was detected within the cells (Figure 4.19 B). High levels of K_{2P}9.1 staining were detected in three colorectal carcinoma cell lines: HCT116 (Figure 4.20 A), SW480 (Figure 4.21 A), and SW620 (Figure 4.22 A). In HCT116 and SW620 cells, diffuse cytoplasmic K_{2P}9.1 expression was detected with a brighter perinuclear staining, and this staining pattern was comparable to MCF-7 cells (Figure 4.19). In SW480 cells, the same K_{2P}9.1 staining pattern was observed (diffuse cytoplasmic expression with a brighter perinuclear ring), in addition to brighter regions of K_{2P}9.1 staining within localised regions of the cell surface (Figure 4.21 A). In A549 cells, diffuse K_{2P}9.1 cytoplasmic staining was detected with brighter punctate regions of staining (Figure 4.23 i), this was comparable to the K_{2P}3.1 expression pattern observed. However, additional prominent K_{2P}9.1 staining was detected around the nucleus and on the plasma membrane in A549 cells (Figure 4.23 i). Finally, diffuse K_{2P}9.1 staining was observed within the SH-SY5Y neuroblastoma cell cytoplasm (Figure 4.23 i; A), and this was comparable to the K_{2P}3.1 staining detected in these cells. A brighter ring of K_{2P}9.1 staining was also observed around the nuclei of SH-SY5Y cells (Figure 4.23 ii; B); this nuclear staining was detected in all cancer cell lines examined for K_{2P}9.1 protein expression.

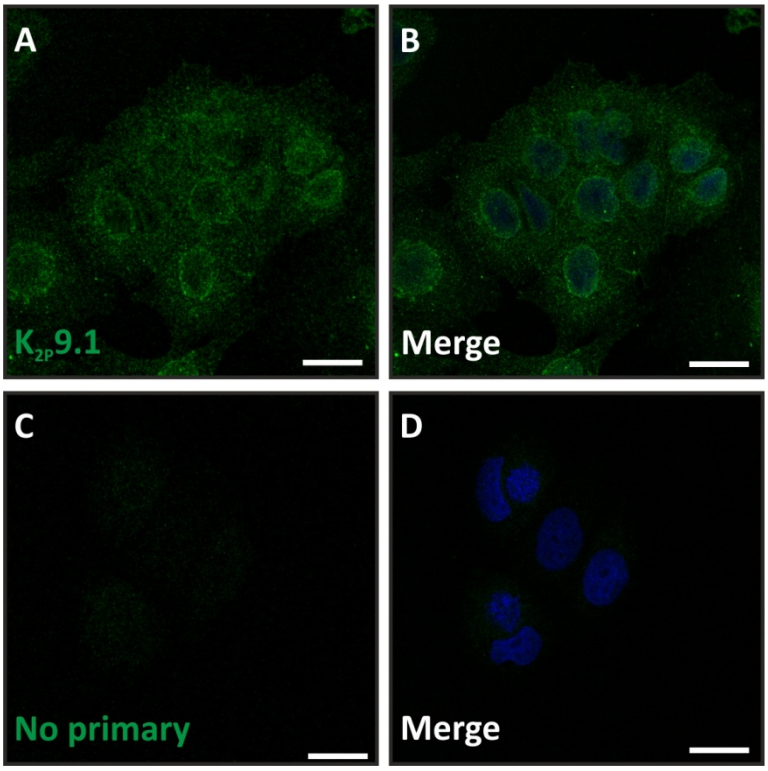

Figure 4.19: K_{2P}9.1 protein detected in MCF-7 breast cancer cell line
K_{2P}9.1 protein staining in MCF-7 cells, shown is a single confocal Z-slice.
A) Immunolabelling for K_{2P}9.1 using Santa Cruz anti-K_{2P}9.1 antibody (shown in green).
C) No primary antibody incubation control.
B, D) Overlapped fluorescence with nuclear stain (DAPI, shown in blue).

All scale bars are 20 µm.

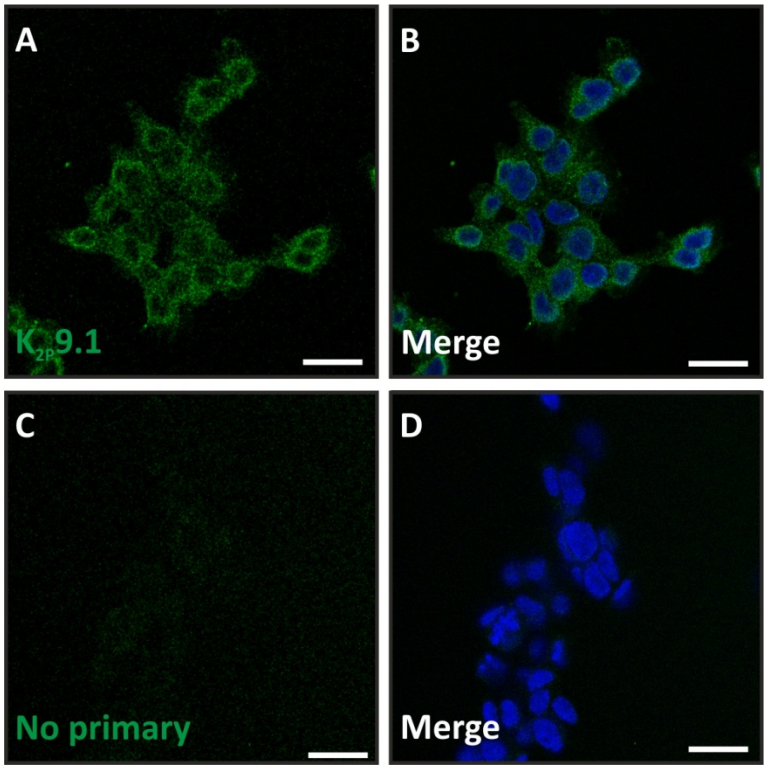

Figure 4.20: K_{2P}9.1 protein detected in HCT116 colorectal cancer cell line
K_{2P}9.1 protein staining in HCT116 cells, shown is a single confocal Z-slice.
A) Immunolabelling for K_{2P}9.1 using Santa Cruz anti-K_{2P}9.1 antibody (shown in green).
C) No primary antibody incubation control.
B, D) Overlapped fluorescence with nuclear stain (DAPI, shown in blue).

All scale bars are 20 μm.

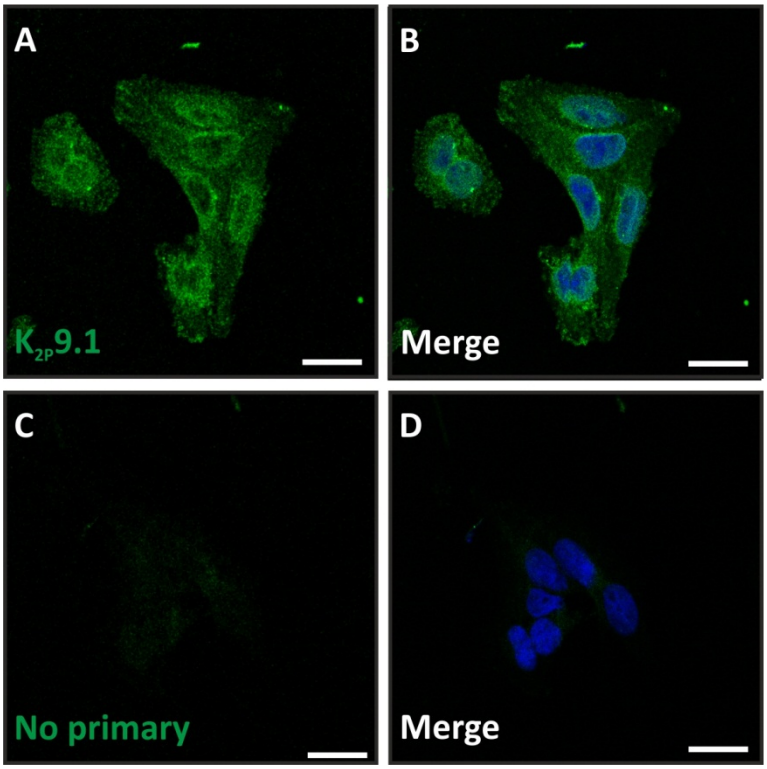

Figure 4.21: K_{2P}9.1 protein detected in SW480 colorectal cancer cell line
K_{2P}9.1 protein staining in SW480 cells, shown is a single confocal Z-slice.
A) Immunolabelling for K_{2P}9.1 using Santa Cruz anti-K_{2P}9.1 antibody (shown in green).
C) No primary antibody incubation control.
B, D) Overlapped fluorescence with nuclear stain (DAPI, shown in blue).

All scale bars are 20 μm.

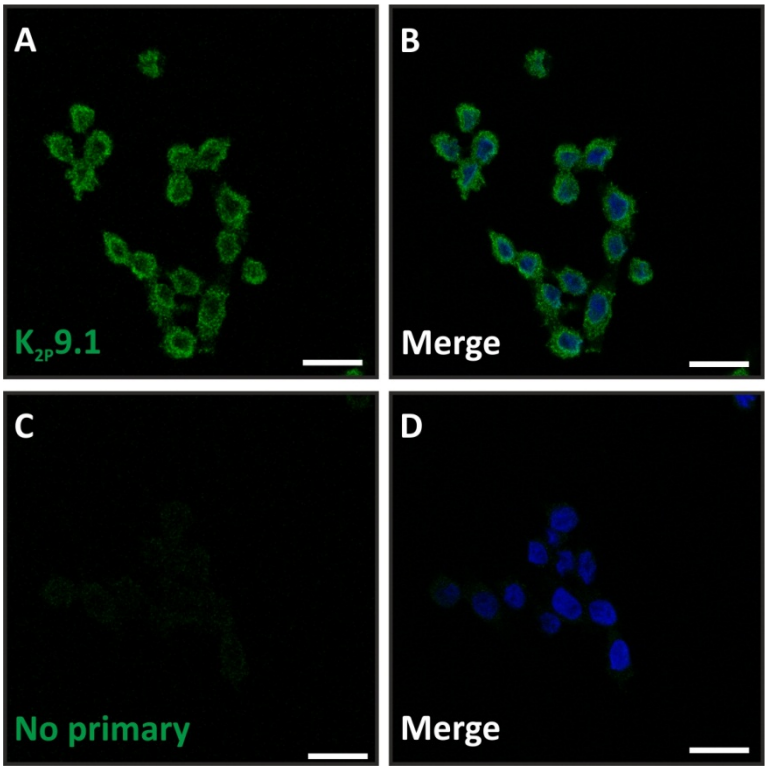

Figure 4.22: K_{2P}9.1 protein detected in SW620 colorectal cancer cell line
K_{2P}9.1 protein staining in SW620 cells, shown is a single confocal Z-slice.
A) Immunolabelling for K_{2P}9.1 using Santa Cruz anti-K_{2P}9.1 antibody (shown in green).
C) No primary antibody incubation control.
B, D) Overlapped fluorescence with nuclear stain (DAPI, shown in blue).

All scale bars are 20 μm.

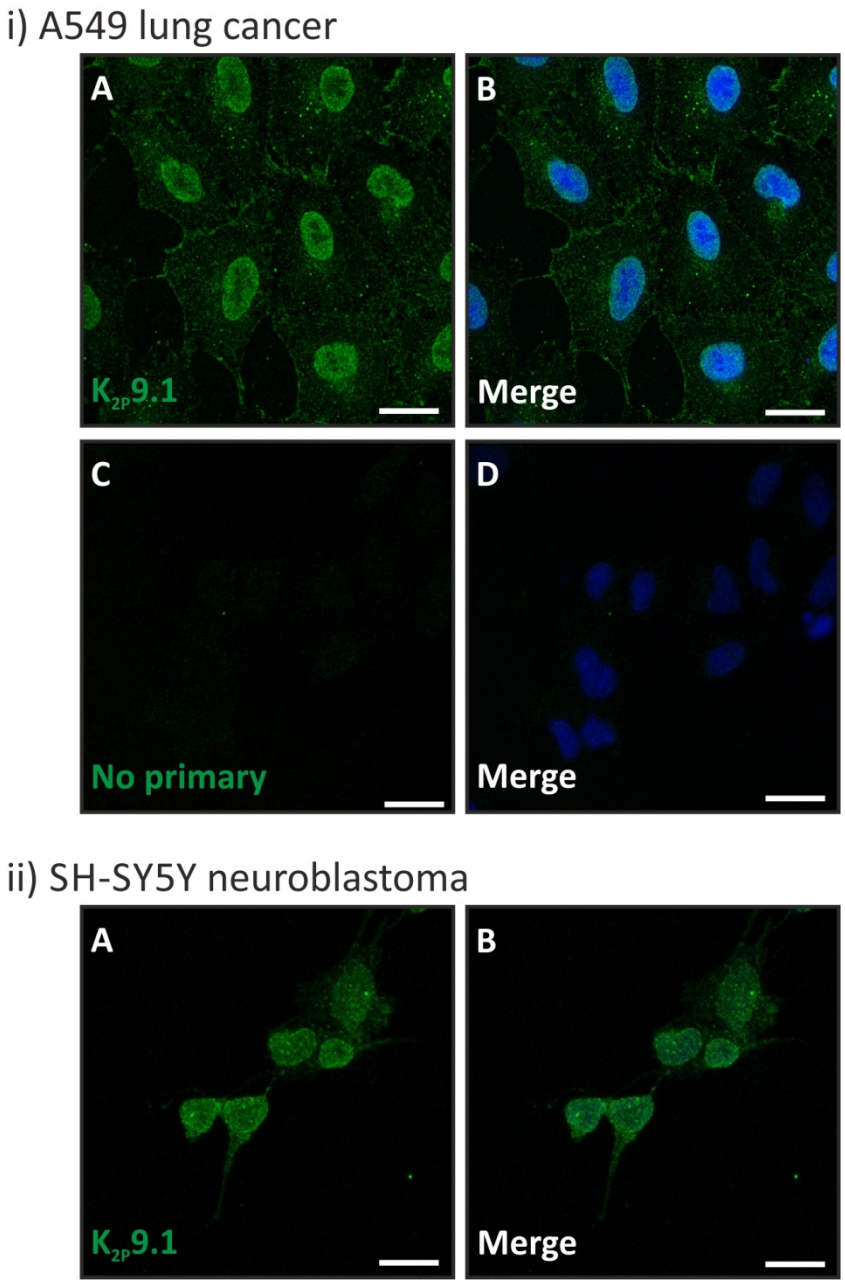

Figure 4.23: K_{2P}9.1 protein detected in lung cancer and neuroblastoma cells

i) K_{2P}9.1 protein staining in A549 cells, shown is a single confocal Z-slice.
A) Immunolabelling for K_{2P}9.1 using Santa Cruz anti-K_{2P}9.1 antibody (shown in green).
C) No primary antibody incubation control.
B, D) Overlapped fluorescence with nuclear stain (DAPI, shown in blue).

ii) K_{2P}9.1 protein staining in SH-SY5Y cells, shown is a confocal Z-slice stack.
A) Immunolabelling for K_{2P}9.1 using Santa Cruz anti-K_{2P}9.1 antibody (shown in green).
B) Overlapped fluorescence with nuclear stain (DAPI, shown in blue).

All scale bars are 20 µm.

4.4.3 The expression of $K_{2P}3.1$ and $K_{2P}9.1$ protein in cancer cell lines

This series of experiments aimed to assess the native TASK channel protein expression in human cancer cell lines (summarised in Table 4.2). Of the cancer cells lines positive for $K_{2P}3.1$ mRNA (Table 4.2), all had detectable levels of $K_{2P}3.1$ protein expression. High levels of $K_{2P}3.1$ protein staining were observed in HeLa and MCF-7 cells, which had diffuse $K_{2P}3.1$ expression across the cell cytoplasm with regions of brighter punctate staining (Figure 4.15 and Figure 4.16). $K_{2P}9.1$ protein expression was also observed in all cancer cell lines positive for $K_{2P}9.1$ mRNA (Table 4.2), with high levels of $K_{2P}9.1$ protein staining observed in colorectal cancer cell lines (HCT116 (Figure 4.20), SW480 (Figure 4.21), and SW620 (Figure 4.22)). The mRNA and protein expression data presented has shown that three cancer cell lines are positive for all three TASK channels (SH-SY5Y, MCF-7, and A549 cells; Table 4.2).

There were several limitations to the methodology used here. Firstly, immunofluorescent staining is not quantitative and the exposure times selected for imaging were based on the level of background fluorescence, therefore these varied between the cell lines examined. This meant that the levels of expression observed cannot be quantitatively compared. Secondly, the binding epitopes of these antibodies are located on the intracellular C-termini of the channels (Table 2.16), which meant that the cells needed to be permeabilised for protein detection. Therefore, it was not possible to specifically determine the plasma membrane expression of these channels; which would have allowed differences in the cell surface channels (which are presumed to be functional) within these cell lines to be identified. To determine if the presence of TASK channel protein resulted in functional channels whole-cell patch clamp experiments were the next area of investigation.

Table 4.2: TASK channel mRNA and protein expression in human cancer cell lines

Summary of the mRNA and protein expression of TASK channel family ($K_{2P}3.1$, $K_{2P}9.1$, and $K_{2P}15.1$) in eleven human cancer cell lines.
Positive and negative expression is shown by + and - respectively.
* indicates confirmation of mRNA product by DNA sequencing.

Cancer	Cell line	TASK channel expression				
		$K_{2P}3.1$		$K_{2P}9.1$		$K_{2P}15.1$
		mRNA	Protein	mRNA	Protein	mRNA
Brain	SH-SY5Y	+	+	+*	+	+
Breast	MCF-7	+	+	+	+	+
Cervical	HeLa	+	+	-	-	+
Colorectal	HCT116	-	-	+	+	+
	SW480	-	-	+	+	+*
	SW620	-	-	+	+	+
Lung	A549	+*	+	+*	+	+*
Oesophageal	OE19	-	-	-	-	+*
	OE21	-	-	-	-	-
Prostate	PC3	-	-	-	-	+
Renal	786-0	+*	+	-	-	-

4.5 Electrophysiological characterisation of A549 cells

The experiments performed in this section aimed to determine if TASK channel mRNA and protein expression correlated with functional TASK-like K^+ currents in the cancer cell lines characterised so far in this chapter. A549 lung cancer cells were selected for these experiments as the cells had been found to express mRNA for all three TASK channels ($K_{2P}3.1$, $K_{2P}9.1$, and $K_{2P}15.1$) and protein for both $K_{2P}3.1$ and $K_{2P}9.1$ channels (Table 4.2).

The electrophysiological properties of A549 lung cancer cells were examined by whole-cell patch clamp experiments (Method 2.8.2). To identify any TASK-like currents, the characteristics of the outward whole-cell currents were examined following exposure to published KCh modulators. First, 30 mM TEA was applied to cells to isolate the TEA-insensitive currents, which include K_{2P} channels. At this concentration, TEA will inhibit multiple non-leak KCh including members of K_V and K_{Ca} families (Table 1.1). The TEA-insensitive currents were then characterised by exposure to TASK channel modulation, either 30 µM methanandamide (a non-hydrolysable analogue of anandamide; Figure 4.24 C, D) or extracellular acidification to pH 6.0 (Figure 4.24 E, F). 30 µM methanandamide was selected to ensure complete inhibition of $K_{2P}3.1$ and $K_{2P}9.1$ channel activity, since 3 µM methanandamide results in over 50 % inhibition of both $K_{2P}3.1$ and $K_{2P}9.1$ channel currents (Veale et al., 2007a). The pK values for TASK channel inhibition by extracellular acidification are pH 7.3 for $K_{2P}3.1$ and pH 6.5 for $K_{2P}9.1$ (Chapman et al., 2000; Duprat et al., 1997; Veale et al., 2007a), therefore pH 6.0 was used to ensure inhibition of both channels.

When a voltage step protocol (-100 to +90 mV in 10 mV increments, for 70 ms duration) was applied using buffer conditions optimised to record outward K^+ currents (Table 2.31), predominately outward whole-cell currents were elicited from A549 cells (example current family; Figure 4.24 B). The outward currents showed almost instantaneous kinetics, following the application of all voltage steps, and reached maximal activation within 5 ms (Figure 4.28 B). Throughout the voltage pulse, little time dependence and no overall inactivation of the currents were observed (Figure 4.24 B). At higher voltages (over +60 mV) some current fluctuations were observed throughout the voltage pulse (up to a 25 pA change in current, for 5 ms), which suggested instability of the patch at these voltages (Figure 4.24 B). The *I-V* relationship of A549 cells under these control

conditions (pH 7.4) had a reversal potential of -34.6 ± 2.2 mV (Figure 4.24 A) and an estimated RMP of -24.4 ± 2.7 (n = 14).

Application of TEA (30 mM) altered the *I-V* relationship of A549 cells causing a reduction in the gradient and amplitude of relationship (Figure 4.24 C). TEA resulted in a significant 47 % reduction in current amplitude (+40 mV) compared to uninhibited cells ($p < 0.01$; Figure 4.24 D). In addition, TEA causes a significant positive shift in the reversal potential (from -34.6 ± 2.2 mV to -21.0 ± 2.6 mV; $p < 0.005$). The positive shift in the reversal potential indicated that was a reduction in outward K^+ flux, due to the inhibition of TEA sensitive KCh. To date, two TEA-sensitive KCh ($K_V1.3$ and $K_{Ca}1.1$) have been identified in A549 cells (Jang et al., 2011; Jovanović et al., 2003; Ridge et al., 1997), and the inhibition observed may have resulted from a block of these channels.

A non-significant reduction in the amplitude of the TEA-insensitive currents was observed following the application of 30 µM methanandamide (44 % reduction, $p = 0.31$; Figure 4.24 D) together with a non-significant positive shift in the reversal potential ($p = 0.79$). Extracellular acidification (pH 6.0) also caused a similar effect resulting in a non-significant reduction of the TEA-insensitive currents (31 % reduction, $p = 0.26$; Figure 4.28 F) and a non-significant positive shift of the reversal potential ($p = 0.64$). The lack of inhibition caused by TASK channel modulators suggested that there is no substantial TASK-like current in these cells.

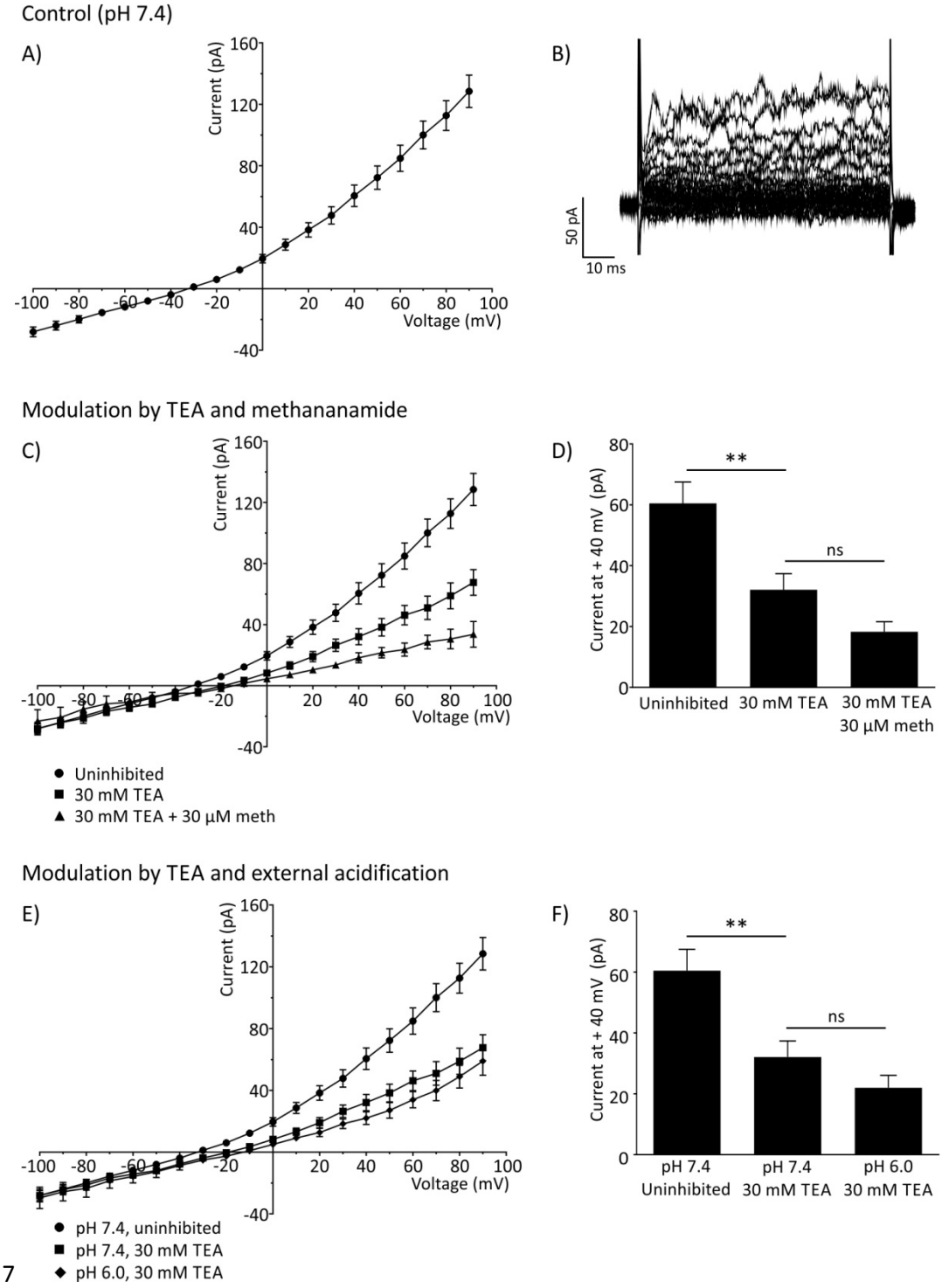
Control (pH 7.4)
A)
Current (pA)
Voltage (mV)
B)
50 pA
10 ms
Modulation by TEA and methananamide
C)
Current (pA)
Voltage (mV)
Uninhibited
30 mM TEA
30 mM TEA + 30 µM meth
D)
Current at + 40 mV (pA)
**
ns
Uninhibited
30 mM TEA
30 mM TEA
30 µM meth
Modulation by TEA and external acidification
E)
Current (pA)
Voltage (mV)
pH 7.4, uninhibited
pH 7.4, 30 mM TEA
pH 6.0, 30 mM TEA
F)
Current at + 40 mV (pA)
**
ns
pH 7.4
Uninhibited
pH 7.4
30 mM TEA
pH 6.0
30 mM TEA

Figure 4.24: Electrophysiological characterisation of A549 lung cancer cell line

Electrophysiological characterisation of the whole-cell outward currents recorded from A549 lung cancer cells. Currents were evoked by voltage steps from -100 to +90 mV in 10mV increments, for 70 ms duration.
To identify the leak K^+ current, broad spectrum KCh inhibition (targeting members of the K_V and K_{Ca} channel families) was used, by applying 30 mM TEA. To determine if TEA insensitive currents have the characteristics of the TASK channel family, 30 µM methanandamide (meth) or extracellular acidification (pH 6.0) was applied, in addition to 30 mM TEA.

A) *I-V* relationship for A549 under control conditions, pH 7.4. The data shown are the average of n = 53 cells, ± SEM.
B) Representative recording from a single A549 cell at pH 7.4.

C) *I-V* relationship for A549 cells under different KCh modulation conditions: uninhibited (circles, n = 53), 30 mM TEA (squares, n = 25), and 30mM TEA with 30 µM methanandamide (triangles, n = 4). Data shown are the average of n ≥ 4 cells, ± SEM
D) Average current (+ SEM) elicited at +40 mV voltage step, for all conditions (n ≥ 4 cells).

E) *I-V* relationship for A549 cells under different KCh modulation conditions: uninhibited at pH 7.4 (circles, n = 53), 30 mM TEA at pH 7.4 (squares, n = 25), and 30 mM TEA at pH 6.0 (diamonds, n = 12). Data shown are the average of n ≥ 12 cells, ± SEM
F) Average current (+ SEM) elicited at +40 mV voltage step, for all conditions (n ≥ 12 cells).

Statistical significance was calculated using a one-way ANOVA, with Sidak's multiple comparisons post-hoc test (ns: non-significant, ** $p < 0.01$). The comparisons performed are indicated by horizontal lines.

These data showed that up to 50 % of the endogenous whole-cell K^+ currents in A549 cells are from TEA-insensitive channels. This is a property which is exhibited by, but is not exclusive to, the K_{2P} channel family and suggested that there is substantial K_{2P} channel activity in A549 cells (Duprat et al., 1997; Enyedi and Czirják, 2010; Meadows and Randall, 2001). Following the identification of the TEA-insensitive currents, it was expected that TASK channel inhibition by either methanandamide or extracellular acidification would cause an additional reduction in the outward K^+ currents and a positive shift in the reversal potential. A non-significant inhibition was observed for both conditions (methanandamide and extracellular acidification). These findings suggested that despite K_{2P}3.1 and K_{2P}9.1 protein expression in A549 cells, that there is not a significant TASK-like current and that other K_{2P} channels may provide the dominant background K^+ currents. The mRNA expression data presented in this chapter showed that multiple non-TASK channels from other K_{2P} subfamilies are present within A549 cells (Table 4.1).

The idea that functional TASK channels may be present within A549 cells was supported by immunofluorescence data which showed that K_{2P}3.1 and K_{2P}9.1 protein colocalised with components of the secretory and endocytic pathways (Mant et al., 2013a). Expression of TASK channel protein within secretory and endocytic pathways indicated that channels are reaching the cell surface (Mant et al., 2013a). However, only a non-significant proportion of the whole-cell outward K^+ currents in A549 cells fulfil the criteria for a TASK-like current. This suggested either that only a small proportion of the TASK channel protein expressed in A549 cells reaches the cell surface, or that the protein is rapidly endocytosed. Therefore, that there is no significant TASK channel activity on the plasma membrane of A549 cells (discussed further in Section 4.7.3). A key limitation of this investigation was that, due to time restrictions, the presence of TASK channel activity was only examined in one cancer cell line (see Section 4.7.4 for a discussion of the implications of this limitation).

4.6 Analysis of TASK channel protein expression in human cancer tissue

To determine if there is a clinical relevance to the cell line expression data presented so far in this thesis, the expression of TASK channel protein in human cancer tissue samples was assessed. In order to conduct these experiments the antibodies

validated for the immunofluorescent detection of GFP tagged channels (Sigma anti-K_{2P}3.1 (12 µg/ml) and Santa Cruz anti-K_{2P}9.1 (20 µg/ml)) were optimised for protein detection in formalin fixed samples.

4.6.1 Optimisation of TASK channel protein detection by immunohistochemistry

The aim of these experiments was to determine the antigen retrieval conditions required for TASK channel protein detection in formalin fixed samples. For this, transfected HEK293 cell line samples expressing either K_{2P}3.1 or K_{2P}9.1 channels were fixed and mounted in comparable conditions to human cancer tissue samples (Method 2.5.2.1). Transfected cells were used so that channel protein detection could be confirmed in an expression system with high levels of TASK channel protein. Prior to primary antibody incubation samples underwent antigen retrieval, this involved boiling the samples in 0.1 M sodium citrate buffer (pH 6.0) for between 0 to 15 min followed by cooling for 20 min (Method 2.5.2.7). This method has been used to successfully detect K_{2P}9.1 protein expression in gastrointestinal tissue (Kovacs et al., 2005). Tissue sections were then labelled using both fluorescent and enzymatic (horse radish peroxidase, HRP) staining (Method 2.5.2.7).

K_{2P}3.1 expression was detected in embedded transfected cells by Sigma anti-K_{2P}3.1 antibody by both enzymatic (Figure 4.15) and fluorescent (Figure 4.16) staining. For both detection methods, K_{2P}3.1 staining was observed after antigen retrieval pre-treatment compared to the no primary controls (Figure 4.25 and Figure 4.26). Little K_{2P}3.1 staining was present without antigen retrieval (Figure 4.25 A and Figure 4.26 A). 5 min antigen retrieval significantly increased the staining for K_{2P}3.1 (Figure 4.25 C and Figure 4.26 C) and K_{2P}3.1 continued to be detected after 10 and 15 min treatments (Figure 4.25 E, G, and Figure 4.26 E, G).

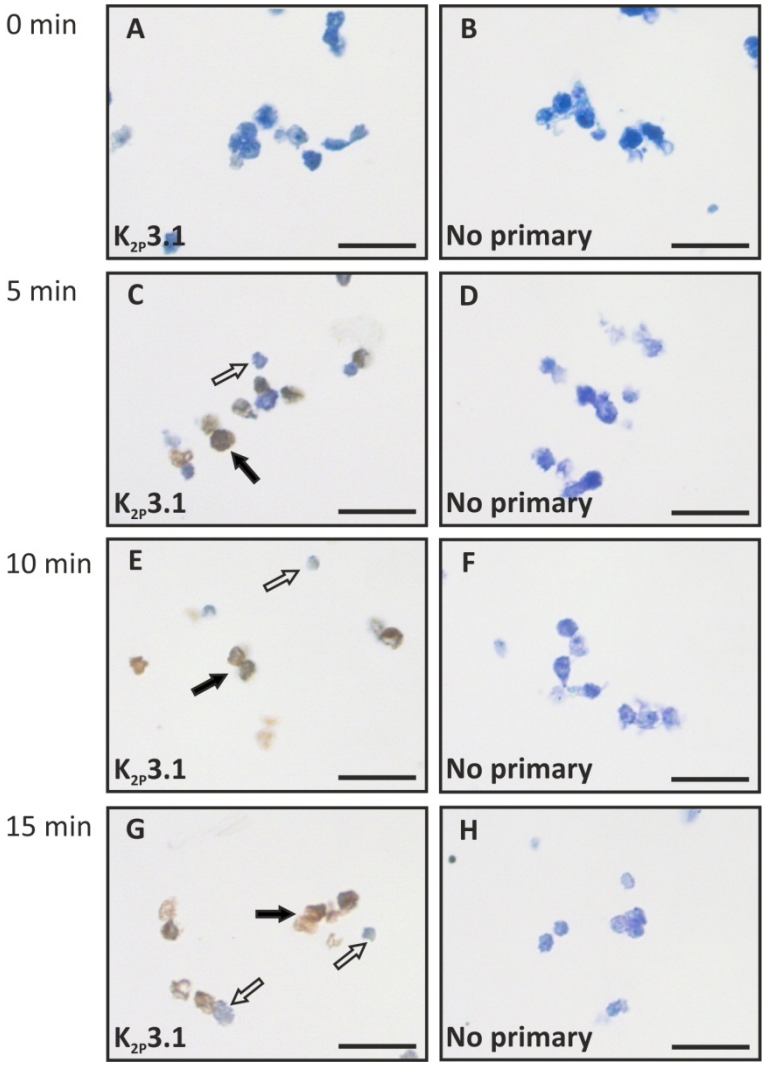

Figure 4.25: Enzymatic detection of K_{2P}3.1 in formalin fixed embedded cells

HEK293 cells transiently expressing human K_{2P}3.1 were fixed 24 h post transfection and embedded in paraffin blocks. Different antigen retrieval, boiling in 0.1 M sodium citrate pH 6.0, pre-treatment times ranging from 0 to 15 min were tested.
Immunolabelling with Sigma anti-K_{2P}3.1 antibody is shown in brown (DAB) and sections counterstained with toluidine blue.

A, C, E, G) Staining patterns for K_{2P}3.1 with increasing antigen retrieval times as indicated.
B, D, F, H) No primary antibody incubation control staining for each pre-treatment.

Filled in arrows indicate cells with K_{2P}3.1 staining. Open arrows indicate cells which do not appear to have K_{2P}3.1 staining.
All scale bars are 30 µm.

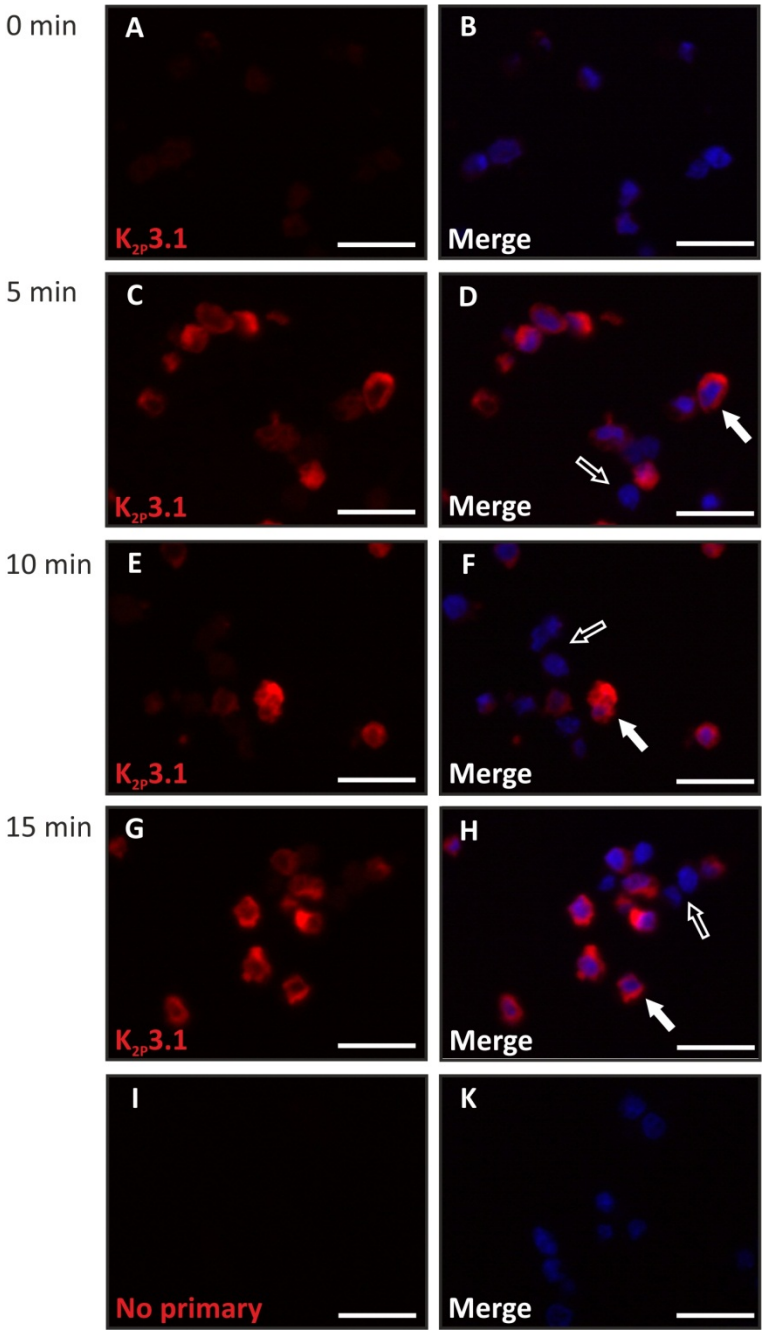

Figure 4.26: Fluorescent detection of $K_{2P}3.1$ in formalin fixed embedded cells

HEK293 cells transiently expressing human $K_{2P}3.1$ were fixed 24 h post transfection and embedded in paraffin blocks. Different antigen retrieval, boiling in 0.1 M sodium citrate pH 6.0, pre-treatment times ranging from 0 to 15 min were tested.

A, C, E, G) Immunolabelling for $K_{2P}3.1$ using Sigma anti-$K_{2P}3.1$ (shown in red) with increasing antigen retrieval times as indicated.

B, D, F, H) Merge of antibody staining and nuclear stain (DAPI, shown in blue).

I, K) No primary antibody incubation control staining.

Filled in arrows indicate cells with $K_{2P}3.1$ staining, Open arrows indicate cells which do not appear to have $K_{2P}3.1$ staining.

All scale bars are 30 µm.

K_{2P}9.1 protein expression was examined in embedded transfected cells using Santa Cruz anti-K_{2P}9.1 antibody by enzymatic (Figure 4.27) and fluorescent (Figure 4.28) detection. For both detection methods, K_{2P}9.1 staining was observed after antigen retrieval and no staining was present in the no primary antibody incubation control (Figure 4.27 and Figure 4.28). Without antigen retrieval little K_{2P}9.1 staining was observed (Figure 4.27 A and Figure 4.28 A). 5 min antigen retrieval significantly increased the K_{2P}9.1 staining (Figure 4.27 C and Figure 4.28 C) and this was still detected following 10 and 15 min pre-treatments (Figure 4.27 E, G, and Figure 4.28 E, G).

The specificity of the immunohistochemical detection of the K_{2P}3.1 and K_{2P}9.1 protein presented here could not be confirmed. This was due to the lack of an untransfected cell control. Nevertheless, clear staining differences were observed within the fields of view examined for K_{2P}3.1 transfected HEK293 cells stained with Sigma anti-K_{2P}3.1 (Figure 4.25 and Figure 4.26). Thus, some cells showed positive K_{2P}3.1 staining and these were presumed to be transfected (filled in arrows; Figure 4.25 and Figure 4.26), compared to cells with no K_{2P}3.1 staining that were likely to be untransfected HEK293 cells (open arrows) which do not express endogenous K_{2P}3.1 mRNA (Figure 4.1). These comparisons could not be made for K_{2P}9.1 expressing HEK293 cells, due to the presence of endogenous K_{2P}9.1 channel mRNA (Figure 4.2), although differences in the level of staining were observed (Figure 4.27 and Figure 4.28). This may have been due to the difference between endogenous and exogenous K_{2P}9.1 protein levels. Both of the antibodies used for immunohistochemical staining successfully detected GFP tagged K_{2P}3.1 or K_{2P}9.1 protein by immunofluorescent staining in this chapter (Figure 4.5 and Figure 4.9 B). However, this technique requires different staining conditions (using 4 % PFA fixed cells and o/n primary antibody incubation) and secondary antibodies, so will not directly compare to immunohistochemical staining (using formalin fixed cells and o/n primary antibody incubation).

In conclusion, both K_{2P}3.1 and K_{2P}9.1 protein appeared to be detected in formalin fixed cells (enzymatic and fluorescent staining) and this staining was enhanced by the addition of an antigen retrieval step. Thus, boiling tissue samples in sodium citrate buffer (pH 6.0) for up to 10 min was selected as the optimal pre-treatment conditions and was utilised to examine the expression of K_{2P}3.1 and K_{2P}9.1 channel protein in 19 human cancer tissue samples using immunohistochemistry (Results 4.6.2 and 4.6.3).

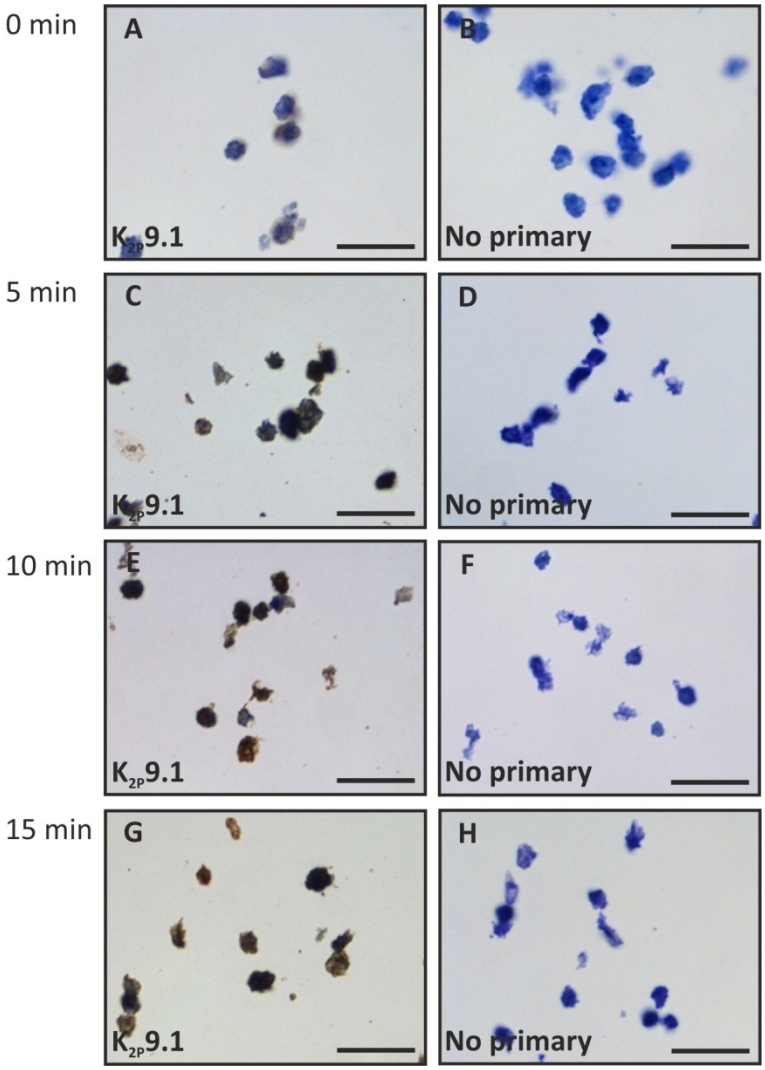

Figure 4.27: Enzymatic detection of $K_{2P}9.1$ in formalin fixed embedded cells

HEK293 cells transiently expressing human $K_{2P}9.1$ were fixed 24 h post transfection and embedded in paraffin blocks. Different antigen retrieval, boiling in 0.1 M sodium citrate pH 6.0, pre-treatment times ranging from 0 to 15 min were tested.
Immunolabelling with Santa Cruz anti-$K_{2P}9.1$ antibody is shown in brown (DAB) and sections counterstained with toluidine blue.

A, C, E, G) Staining patterns for $K_{2P}9.1$ with increasing antigen retrieval times as indicated.
B, D, F, H) No primary antibody incubation control staining for each pre-treatment.

All scale bars are 30 µm.

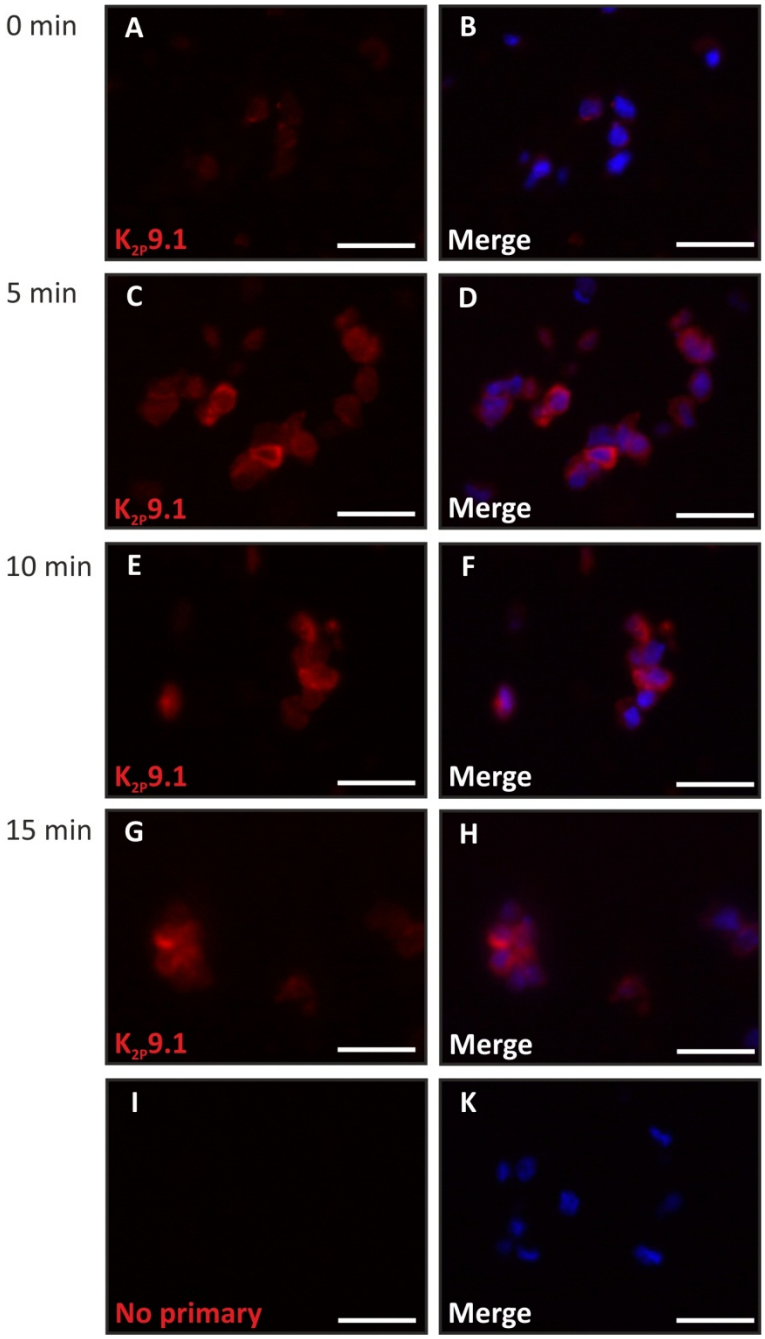

Figure 4.28: Fluorescent detection of $K_{2P}9.1$ in formalin fixed embedded cells

HEK293 cells transiently expressing human $K_{2P}9.1$ were fixed 24 h post transfection and embedded in paraffin blocks. Different antigen retrieval, boiling in 0.1 M sodium citrate pH 6.0, pre-treatment times ranging from 0 to 15 min were tested.

A, C, E, G) Immunolabelling for $K_{2P}9.1$ using Santa Cruz anti-$K_{2P}9.1$ (shown in red) with increasing antigen retrieval times as indicated.

B, D, F, H) Merge of antibody staining and nuclear stain (DAPI, shown in blue).

I, K) No primary antibody incubation control staining.

All scale bars are 30 µm.

4.6.2 K_{2P}3.1 protein expression in human cancer tissue

Using the optimal antigen retrieval conditions established in Result 4.6.1, the experiments in this and the following section (Result 4.6.3) aimed to establish the expression of K_{2P}3.1 and K_{2P}9.1 channel protein in four cancer types. The tissue samples selected for this study represent lung, pancreatic, oesophageal, and renal cancers (Table 2.17 and Method 2.5.2). The selection of these cancers was based on bioinformatic data (Table 3.4), which identified lung, pancreatic, and renal cancers as potential avenues for researching altered K_{2P}3.1 expression in cancer. In addition to the tissue available from collaboration with Dr A. Bateman whose research is focused on oesophageal cancer. Matched normal tissue controls were not available for the cancers used in this study due to the precious nature of patient tissue. Instead, it was decided that the expression studies presented in this section would provide initial data on whether the channel protein was expressed within these cancers. Therefore, this work provided an insight into the expression of TASK channel protein within these four cancers and suggested that this study should be expanded using larger sample numbers and tissue matched normal controls.

For immunohistochemical detection of K_{2P}3.1 channel protein, tissue sections were immunolabelled (following antigen retrieval; Method 2.5.2.7) using the commercially available Sigma anti-K_{2P}3.1 antibody which was characterised in this chapter (12 µg/ml; Result 4.3). As a positive expression control, tissue samples were also stained for a panel of cytokeratins (cytokeratins 5, 6, 8, 17, and 19; DakoCytomation (2.32 µg/ml)). Cytokeratins are part of the intermediate filament family that make up the cell cytoskeleton and a marker of epithelial tissue. Therefore, positive expression was expected in the tissue samples examined here (Barak et al., 2004). This was true for all of the cancer tissue samples used in this thesis where cytokeratin staining was detected. The staining observed for K_{2P}3.1 (Result 4.6.2), K_{2P}9.1 (Result 4.6.3), and cytokeratins (Results 4.6.2 and 4.6.3) is summarised in Table 4.3 (page 258).

4.6.2.1 Detection of K_{2P}3.1 protein in oesophageal adenocarcinomas

Of the ten oesophageal adenocarcinoma tissue samples (A-J) examined, three samples (classified as tumour stage 2 or 3) showed positive K_{2P}3.1 protein expression

compared to a no primary antibody incubation: B (Figure 4.29), I (Figure 4.30), and J (Figure 4.31). $K_{2P}3.1$ staining was observed within the cytoplasm of tumour cells in malignant glandular structures in tissue samples B and I (Figure 4.29 C, D and Figure 4.30 C, D), whereas $K_{2P}3.1$ staining was observed within malignant squamous cell tissue in sample J (Figure 4.31 C, D). Cytokeratin protein staining was also observed in all three adenocarcinomas; within the abnormal glandular structures in samples B and I (Figure 4.29 E and Figure 4.30 E), and the malignant squamous cell tissue in sample J (Figure 4.31 E).

The remaining seven oesophageal adenocarcinomas samples (A, C-H) showed no detectable staining for $K_{2P}3.1$ protein (Table 4.3, shown for sample A: Figure 4.32). For all samples, cytokeratin protein staining was present within the adenocarcinoma tissue, except in sample A where cytokeratin staining was detected within the malignant glands (Figure 4.32 E).

4.6.2.2 Detection of $K_{2P}3.1$ protein in lung squamous cell carcinomas

Three lung carcinoma tissue samples (K, L, and M) were examined and one showed positive $K_{2P}3.1$ protein expression compared to a no primary antibody incubation control (sample M; Figure 4.33). Diffuse $K_{2P}3.1$ protein staining was detected in the cytoplasm of the large pleomorphic tumour cells comprising atypical cell nests within the undifferentiated large cell carcinoma tissue (Figure 4.33 C, D). Cytokeratin protein staining was also observed within these atypical cell nests (Figure 4.33 E). The remaining two samples examined (K and L) showed no detectable $K_{2P}3.1$ protein staining (Table 4.3, shown for sample L: Figure 4.34 C, D), however cytokeratin staining was detected in both of these samples (Figure 4.34 E).

4.6.2.3 Detection of $K_{2P}3.1$ protein in pancreatic adenocarcinomas

Three pancreatic adenocarcinoma tissue samples (N, O, and P) were examined for $K_{2P}3.1$ protein expression and one showed positive $K_{2P}3.1$ staining compared to a no primary antibody incubation control (tissue sample N; Figure 4.35). $K_{2P}3.1$ protein was detected in the cytoplasm of select tumour cells which formed irregular glandular structures within the invasive ductal adenocarcinoma tissue (Figure 4.35 C, D). Positive

cytokeratin expression was also observed within these glandular structures (Figure 4.35 E). The remaining two pancreatic adenocarcinoma samples (P and O) were negative for $K_{2P}3.1$ expression (Table 4.3, shown for sample O: Figure 4.36 C, D). Cytokeratin protein staining was detected in both samples and was present within the malignant glandular structures in tissue sample O (Figure 4.36 E).

4.6.2.4 Detection of $K_{2P}3.1$ protein in renal carcinomas

All three of the renal carcinoma tissue samples examined showed positive $K_{2P}3.1$ protein expression compared to a no primary antibody incubation control: Q (Figure 4.37), R (Figure 4.38), and S (Figure 4.39). In renal oncocytoma tissue (sample Q), $K_{2P}3.1$ staining was present within the cytoplasm of cells within the oncocytic cell nests (Figure 4.37 C, D). $K_{2P}3.1$ staining was present within the cytoplasm of eosinophilic tumour cells (Figure 4.38 C, D) of a high grade renal cell carcinoma (tissue sample R). $K_{2P}3.1$ expression was also observed in a low grade clear cell renal carcinoma (tissue sample S) within the cytoplasm of the clear tumour cells (Figure 4.39 C, D). The level of $K_{2P}3.1$ protein staining detected in this sample was lower than the other renal carcinomas examined. Cytokeratin protein expression was detected in the eosinophilic tumour cells for sample Q (Figure 4.37 E) and within the clear tumour cells for sample S (Figure 4.39 E). However, for sample R, cytokeratin protein staining was observed within different structures to $K_{2P}3.1$ protein which have a more glandular structure appearance (Figure 4.38 E).

4.6.2.5 Expression of $K_{2P}3.1$ protein in human cancers

Prior to this investigation, $K_{2P}3.1$ protein had not been described in cancer tissue within the literature. The data presented in this section identified $K_{2P}3.1$ protein within the cancerous cells of human oesophageal, lung, pancreatic, and renal cancer tissues. These data supported the expression of $K_{2P}3.1$ channels in cancer and the findings from Chapter 3, which showed significant alterations to $K_{2P}3.1$ mRNA in six cancers (Table 3.4). The protein expression data presented here was limited by a lack of matched normal tissue controls and small sample numbers. However, the potential implications of these findings and the limitations of this work are discussed further detail in Result 4.6.4.

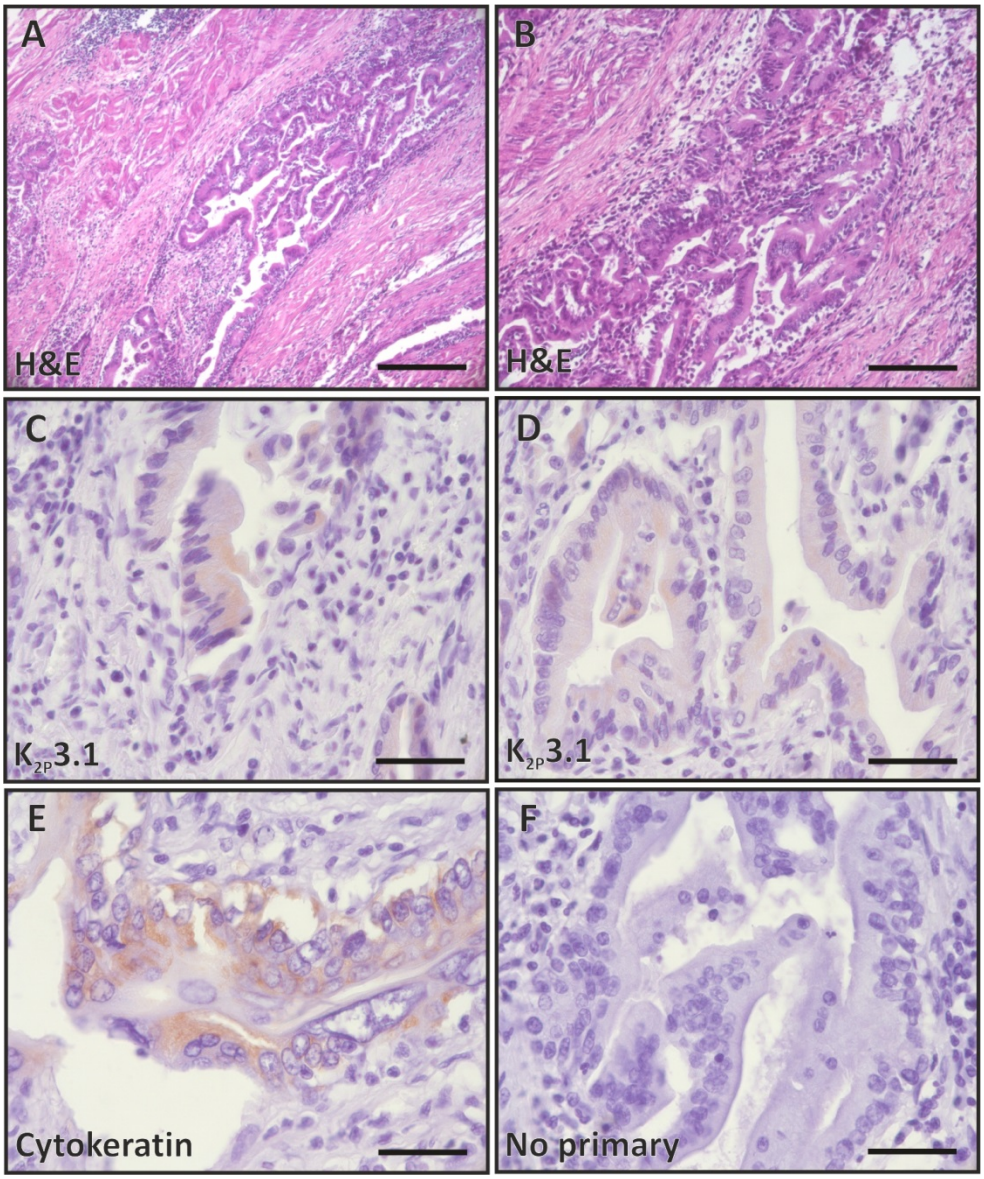

Figure 4.29: $K_{2P}3.1$ protein expression in oesophageal adenocarcinoma (tissue sample B)

Tissue sample B originated from the oesophago-gastro junction and is classed as tumour stage 3 with N1 lymph node involvement (pT3N1).
Sections were incubated with 0.01 M sodium citrate pH 6.0 for 5 min prior to antibody incubation. Antibody labelling is shown in brown (DAB) and sections counterstained with haematoxylin.

A, B) H&E staining.
C, D) Immunolabelling for $K_{2P}3.1$ protein, using Sigma $K_{2P}3.1$ antibody.
E) Immunolabelling for cytokeratin protein, using DakoCytomation cytokeratin antibody.
F) No primary antibody incubation control.

Scale bars are (A) 250 µm, (B) 125 µm, and (C-F) 40 µm.

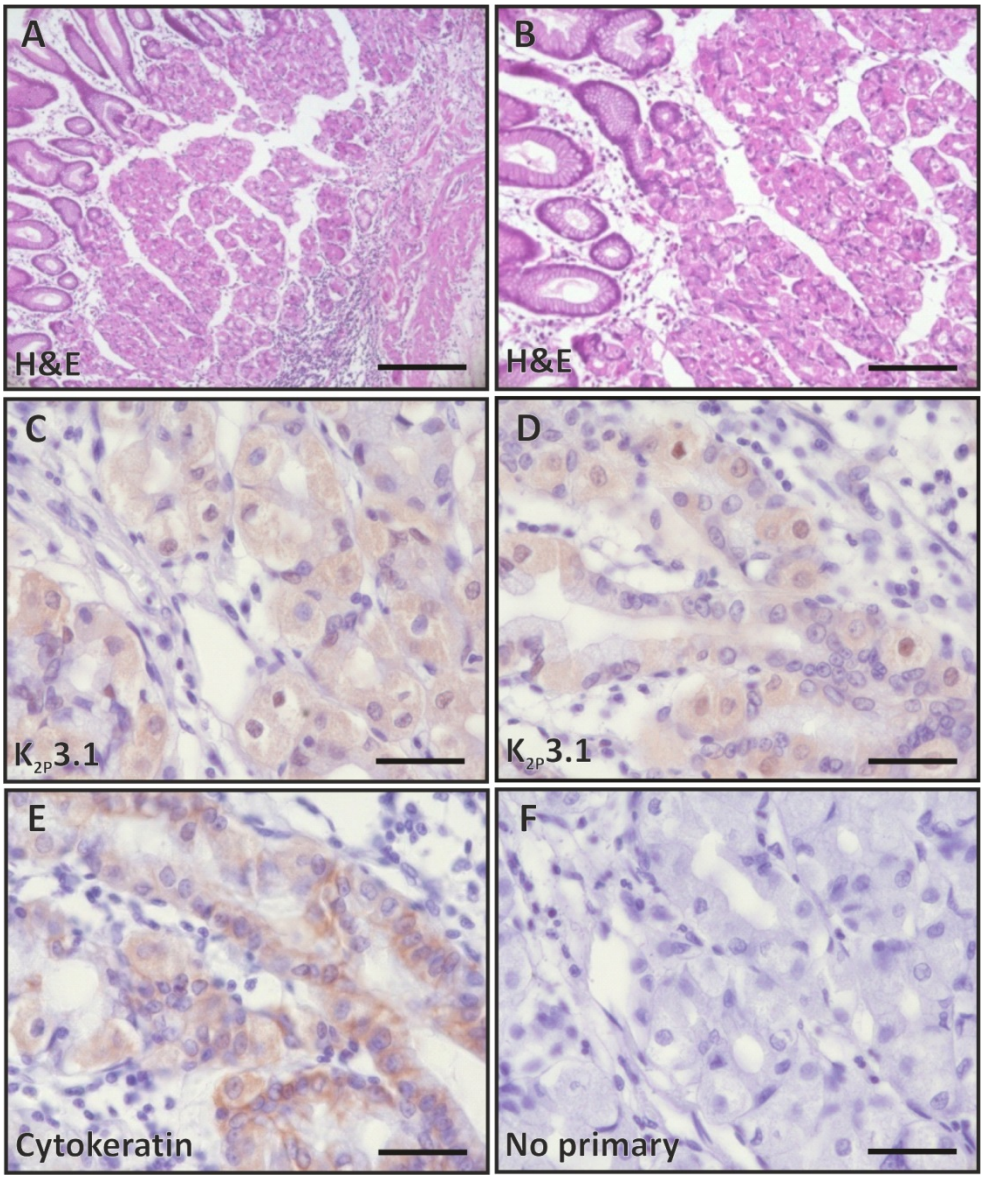

Figure 4.30: $K_{2P}3.1$ protein expression in oesophageal adenocarcinoma (tissue sample I)

Tissue sample I originated from the lower third of the oesophagus and is classed as tumour stage 2 with no lymph node involvement (pT2N0).

Sections were incubated with 0.01 M sodium citrate pH 6.0 for 5 min prior to antibody incubation. Antibody labelling is shown in brown (DAB) and sections counterstained with haematoxylin.

A, B) H&E staining.

C, D) Immunolabelling for $K_{2P}3.1$ protein, using Sigma $K_{2P}3.1$ antibody.

E) Immunolabelling for cytokeratin protein, using DakoCytomation cytokeratin antibody.

F) No primary antibody incubation control.

Scale bars are (A) 250 µm, (B) 125 µm, and (C-F) 40 µm.

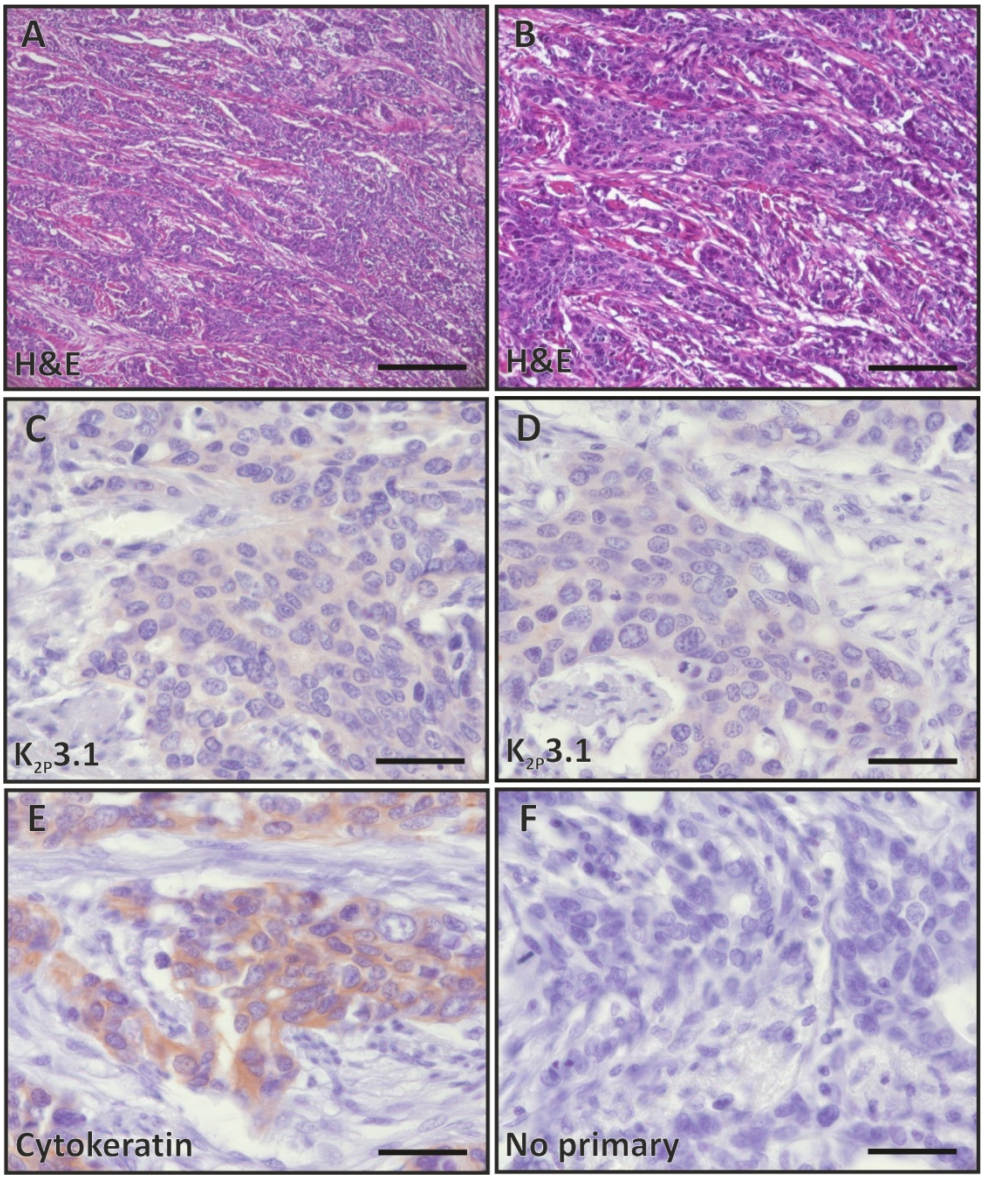

Figure 4.31: $K_{2P}3.1$ protein expression in oesophageal adenocarcinoma (tissue sample J)

Tissue sample J is a tumour stage 3 oesophageal adenocarcinoma with no lymph node involvement (pT3N0).

Sections were incubated with 0.01 M sodium citrate pH 6.0 for 5 min prior to antibody incubation. Antibody labelling is shown in brown (DAB) and sections counterstained with haematoxylin.

A, B) H&E staining.

C, D) Immunolabelling for $K_{2P}3.1$ protein, using Sigma $K_{2P}3.1$ antibody.

E) Immunolabelling for cytokeratin protein, using DakoCytomation cytokeratin antibody.

F) No primary antibody incubation control.

Scale bars are (A) 250 µm, (B) 125 µm, and (C-F) 40 µm.

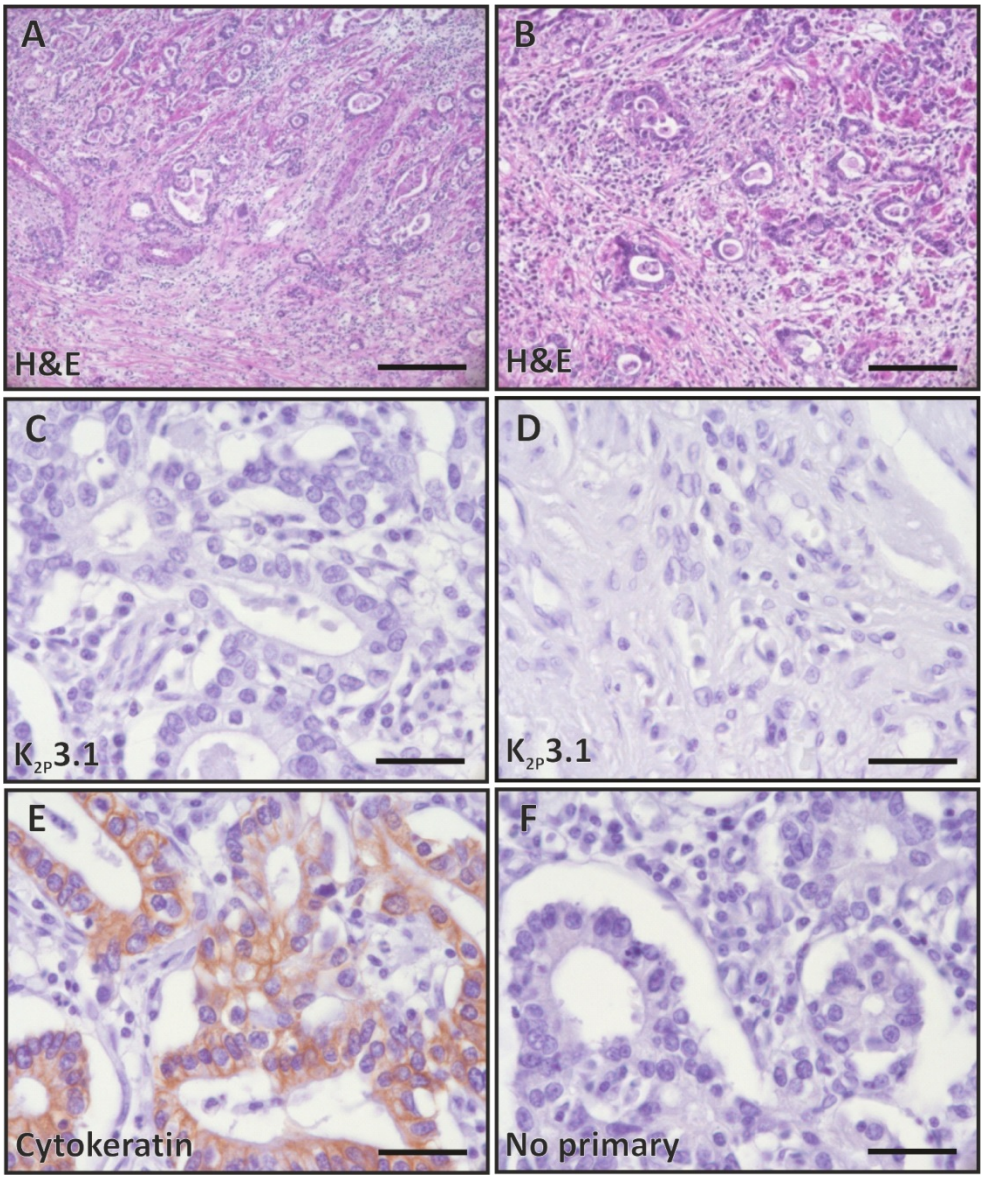

Figure 4.32: Negative $K_{2P}3.1$ protein staining in oesophageal adenocarcinoma (tissue sample A)

Tissue sample A is a tumour stage 3 oesophageal adenocarcinoma with no lymph node involvement (pT3N0).

Sections were incubated with 0.01 M sodium citrate pH 6.0 for 5 min prior to antibody incubation. Antibody labelling is shown in brown (DAB) and sections counterstained with haematoxylin.

A, B) H&E staining.

C, D) Immunolabelling for $K_{2P}3.1$ protein, using Sigma $K_{2P}3.1$ antibody.

E) Immunolabelling for cytokeratin protein, using DakoCytomation cytokeratin antibody.

F) No primary antibody incubation control.

Scale bars are (A) 250 µm, (B) 125 µm, and (C-F) 40 µm.

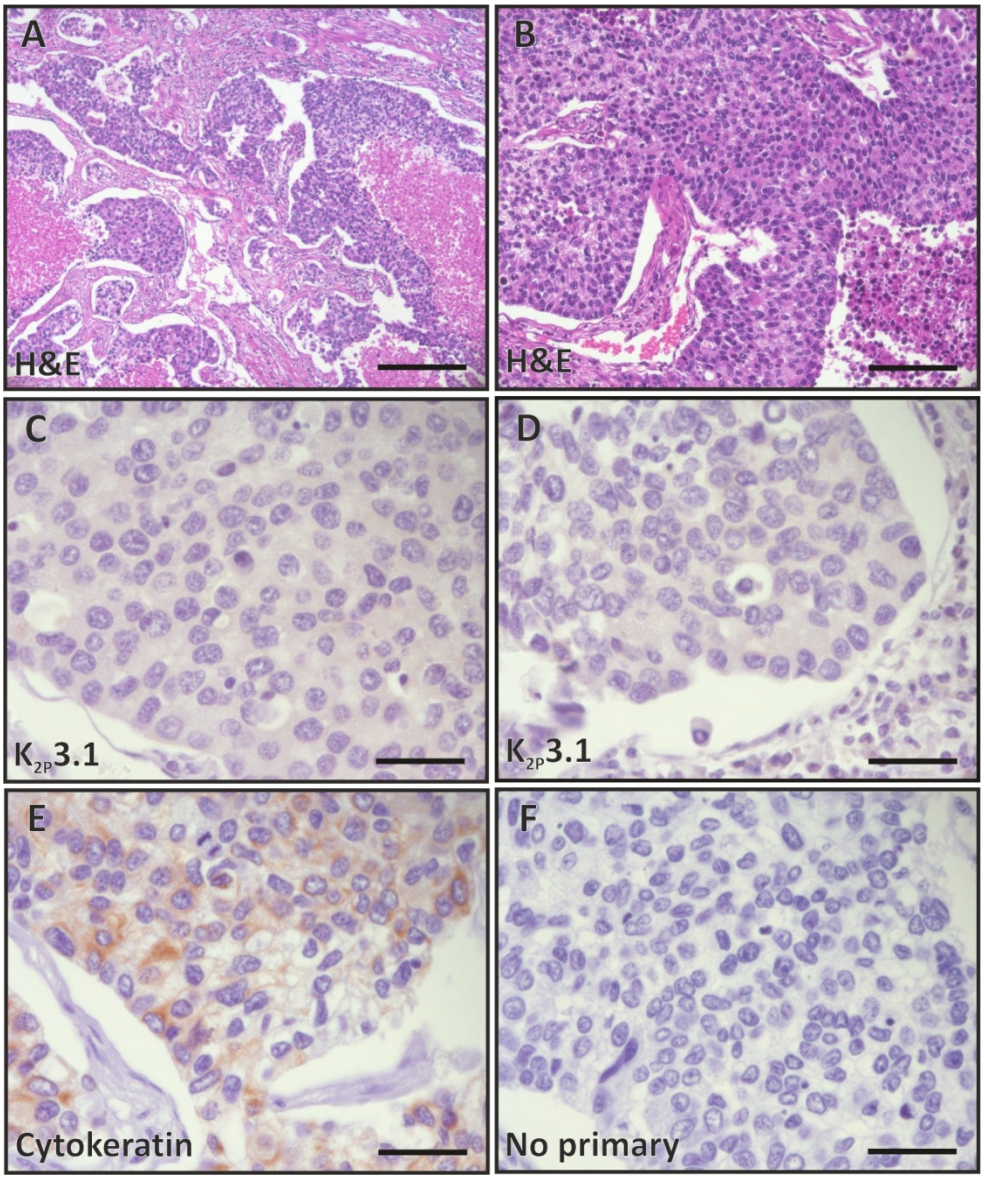

Figure 4.33: $K_{2P}3.1$ protein expression in undifferentiated large cell lung carcinoma (tissue sample M)

Tissue sample M is an undifferentiated large cell lung carcinoma, which is composed of infiltrating nests of large atypical cells, and classed as tumour stage 3 with no lymph node involvement (pT3N0).

Sections were incubated with 0.01 M sodium citrate pH 6.0 for 5 min prior to antibody incubation. Antibody labelling is shown in brown (DAB) and sections counterstained with haematoxylin.

A, B) H&E staining.
C, D) Immunolabelling for $K_{2P}3.1$ protein, using Sigma $K_{2P}3.1$ antibody.
E) Immunolabelling for cytokeratin protein, using DakoCytomation cytokeratin antibody.
F) No primary antibody incubation control.

Scale bars are (A) 250 µm, (B) 125 µm, and (C-F) 40 µm.

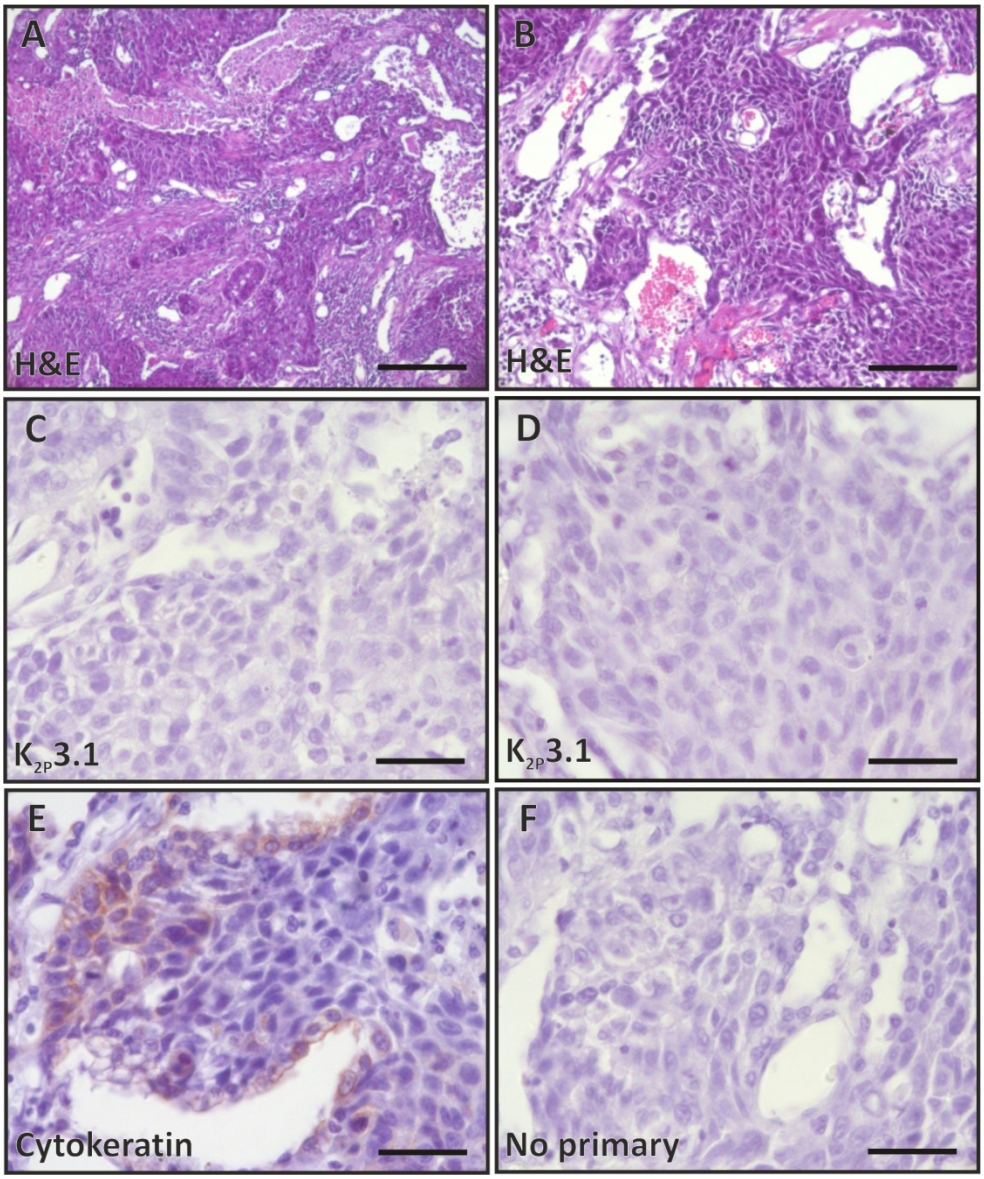

Figure 4.34: Negative $K_{2P}3.1$ protein staining in poorly differentiated lung squamous cell carcinoma (tissue sample L)

Tissue sample L is a moderate to poorly differentiated squamous cell lung carcinoma, classified as tumour stage 1 with regional lymph node metastases (pT1N1).
Sections were incubated with 0.01 M sodium citrate pH 6.0 for 5 min prior to antibody incubation. Antibody labelling is shown in brown (DAB) and sections counterstained with haematoxylin.

A, B) H&E staining.
C, D) Immunolabelling for $K_{2P}3.1$ protein, using Sigma $K_{2P}3.1$ antibody.
E) Immunolabelling for cytokeratin protein, using DakoCytomation cytokeratin antibody.
F) No primary antibody incubation control.

Scale bars are (A) 250 µm, (B) 125 µm, and (C-F) 40 µm.

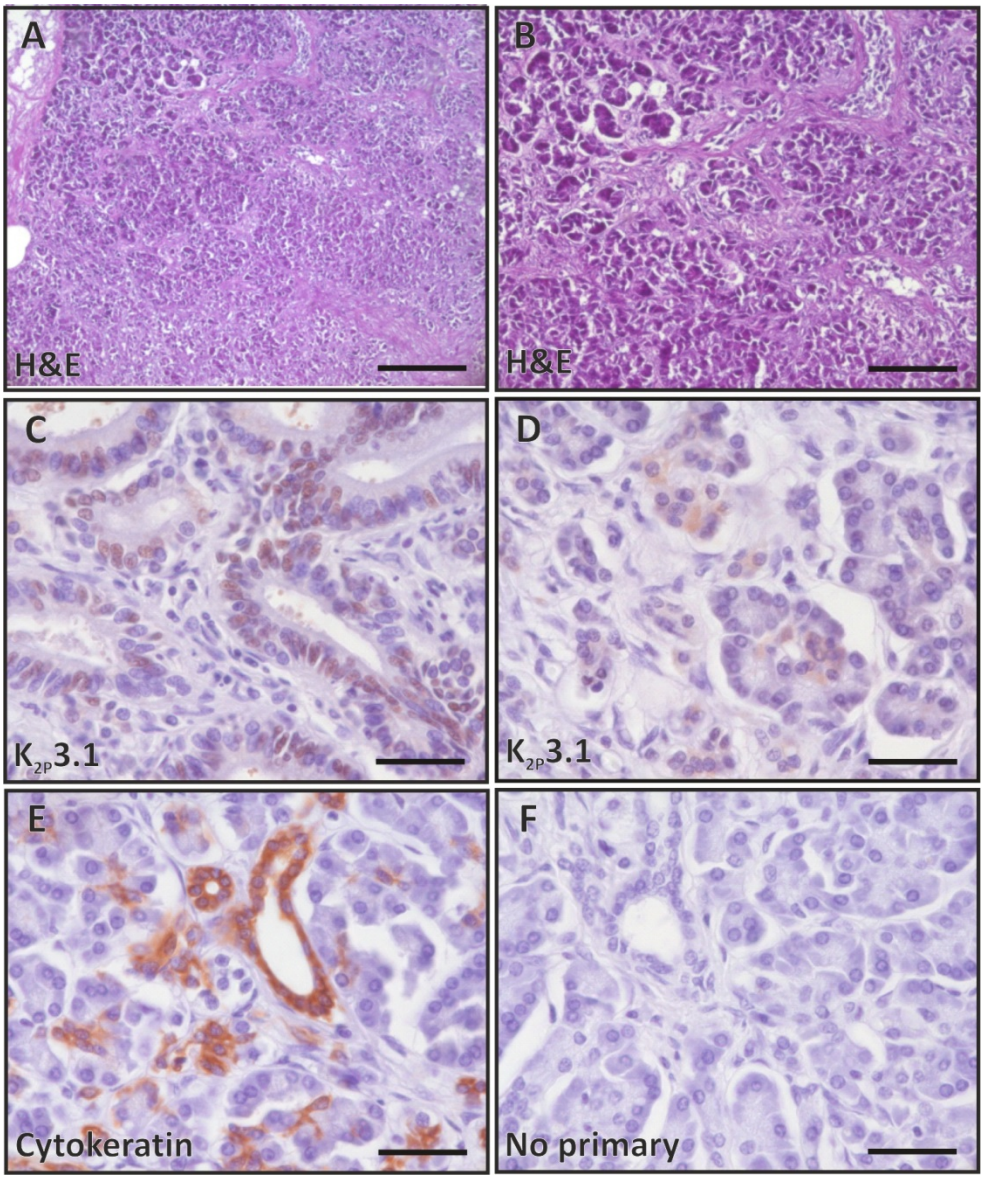

Figure 4.35: $K_{2P}3.1$ protein expression in ductal pancreatic adenocarcinoma (tissue sample N)

Tissue sample N is an invasive ductal adenocarcinoma with neural invasion, classified as tumour stage 1 (pT1) with unknown lymph node status.

Sections were incubated with 0.01 M sodium citrate pH 6.0 for 5 min prior to antibody incubation. Antibody labelling is shown in brown (DAB) and sections counterstained with haematoxylin.

A, B) H&E staining.

C, D) Immunolabelling for $K_{2P}3.1$ protein, using Sigma $K_{2P}3.1$ antibody.

E) Immunolabelling for cytokeratin protein, using DakoCytomation cytokeratin antibody.

F) No primary antibody incubation control.

Scale bars are (A) 250 µm, (B) 125 µm, and (C-F) 40 µm.

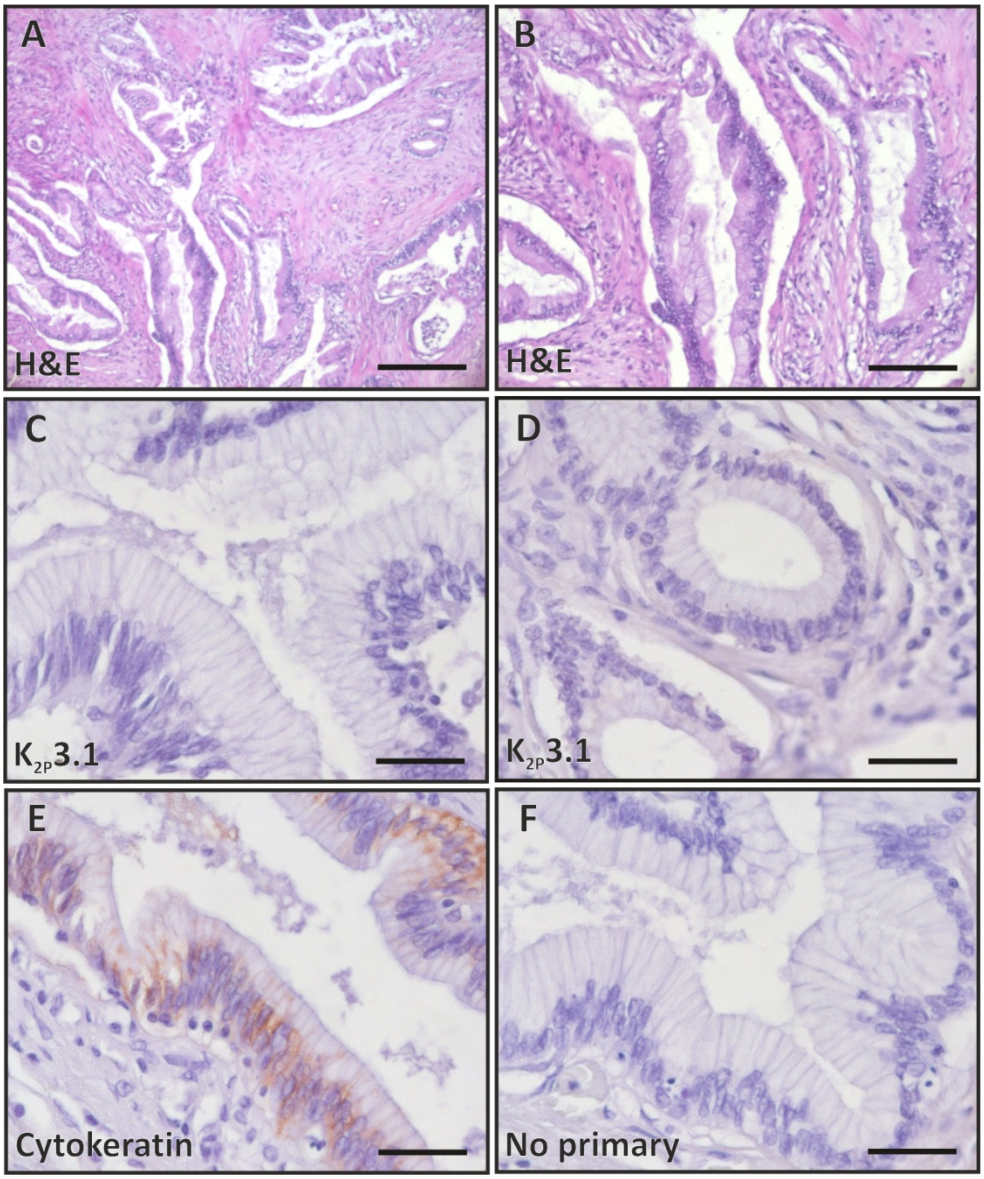

Figure 4.36: Negative $K_{2P}3.1$ protein staining in moderately differentiated pancreatic adenocarcinoma (tissue sample O)

Tissue sample O is moderately differentiated invasive pancreatic adenocarcinoma, classified as tumour stage 4 with local lymph node invasion and no metastases (pT4N1Mx). Sections were incubated with 0.01 M sodium citrate pH 6.0 for 5 min prior to antibody incubation. Antibody labelling is shown in brown (DAB) and sections counterstained with haematoxylin.

A, B) H&E staining.
C, D) Immunolabelling for $K_{2P}3.1$ protein, using Sigma $K_{2P}3.1$ antibody.
E) Immunolabelling for cytokeratin protein, using DakoCytomation cytokeratin antibody.
F) No primary antibody incubation control.

Scale bars are (A) 250 µm, (B) 125 µm, and (C-F) 40 µm.

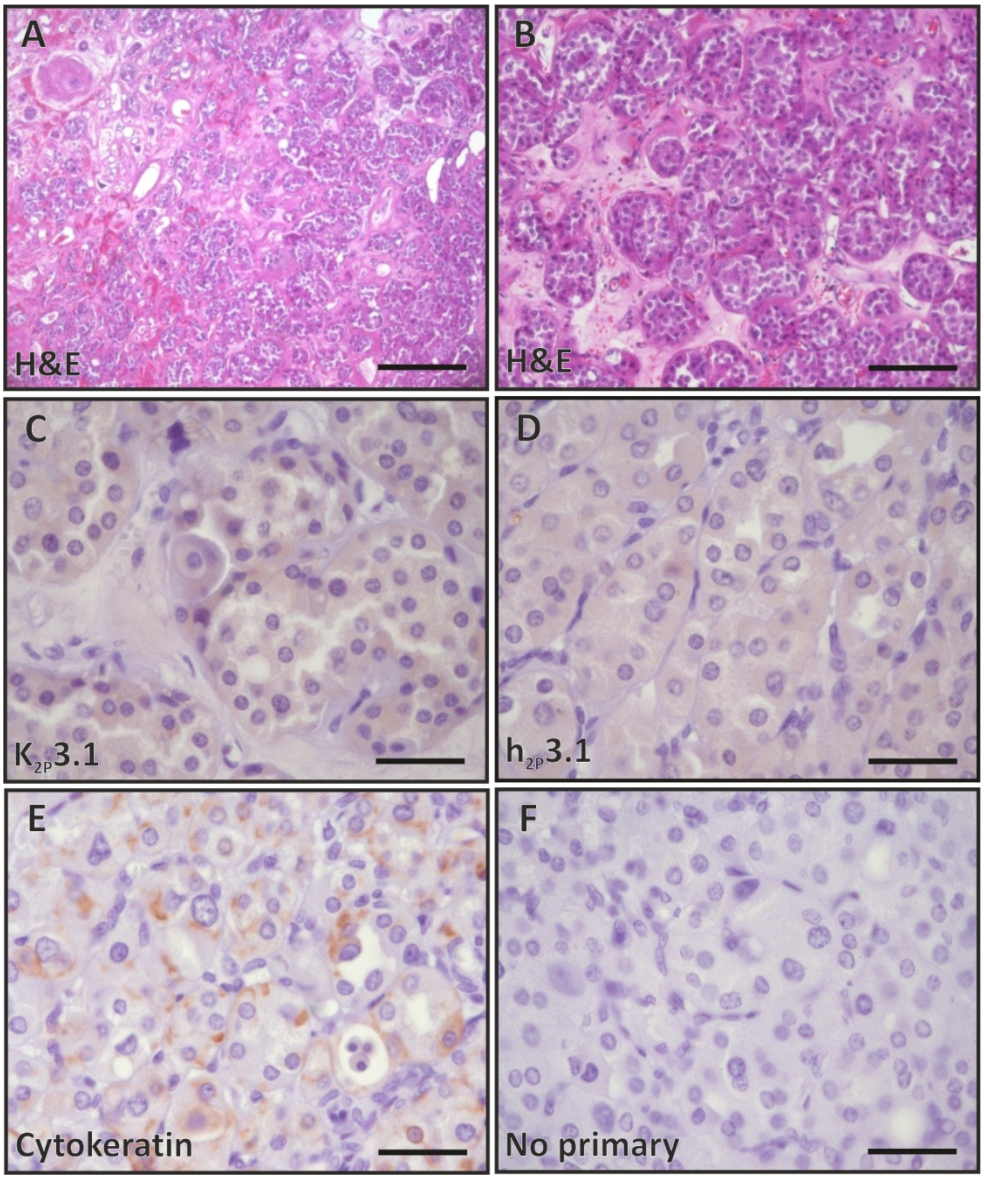

Figure 4.37: $K_{2P}3.1$ protein expression in renal oncocytoma (tissue sample Q)

Tissue sample Q is renal oncocytoma, where the tumour is composed of nests of oncocytic cells with characteristic round nuclei and eosinophilic granular cytoplasm. Pathologically renal oncocytomas are benign tumours, so do not have TNM grading.
Sections were incubated with 0.01 M sodium citrate pH 6.0 for 5 min prior to antibody incubation. Antibody labelling is shown in brown (DAB) and sections counterstained with haematoxylin.

A, B) H&E staining.
C, D) Immunolabelling for $K_{2P}3.1$ protein, using Sigma $K_{2P}3.1$ antibody.
E) Immunolabelling for cytokeratin protein, using DakoCytomation cytokeratin antibody.
F) No primary antibody incubation control.

Scale bars are (A) 250 µm, (B) 125 µm, and (C-F) 40 µm.

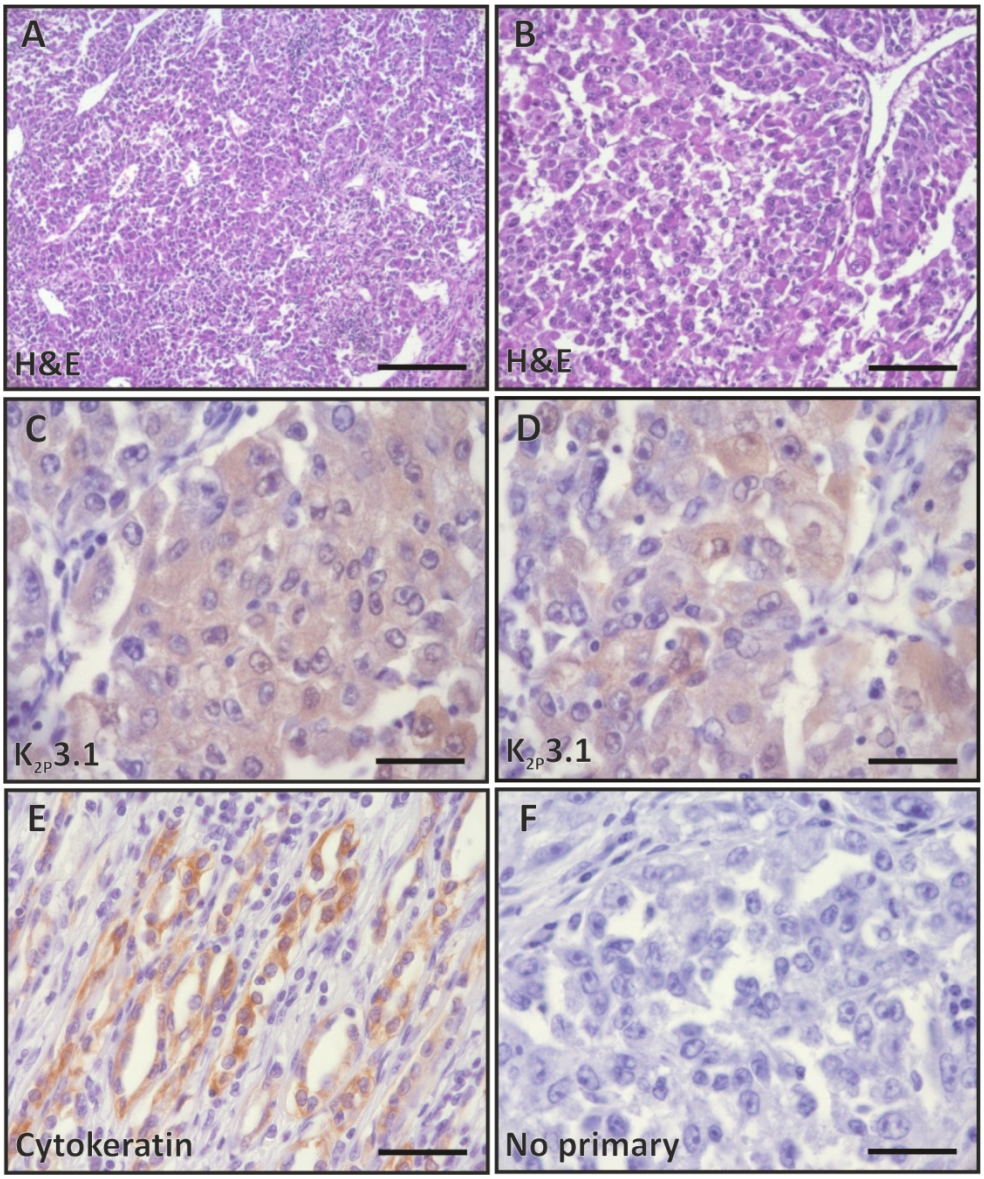

Figure 4.38: $K_{2P}3.1$ protein expression in high grade renal carcinoma (tissue sample R)

Tissue sample R is a high grade renal carcinoma, composed of some clear but mainly eosinophilic granular cells, and is classified as tumour stage 3 (pT3).

Sections were incubated with 0.01 M sodium citrate pH 6.0 for 5 min prior to antibody incubation. Antibody labelling is shown in brown (DAB) and sections counterstained with haematoxylin.

A, B) H&E staining.

C, D) Immunolabelling for $K_{2P}3.1$ protein, using Sigma $K_{2P}3.1$ antibody.

E) Immunolabelling for cytokeratin protein, using DakoCytomation cytokeratin antibody.

F) No primary antibody incubation control.

Scale bars are (A) 250 µm, (B) 125 µm, and (C-F) 40 µm.

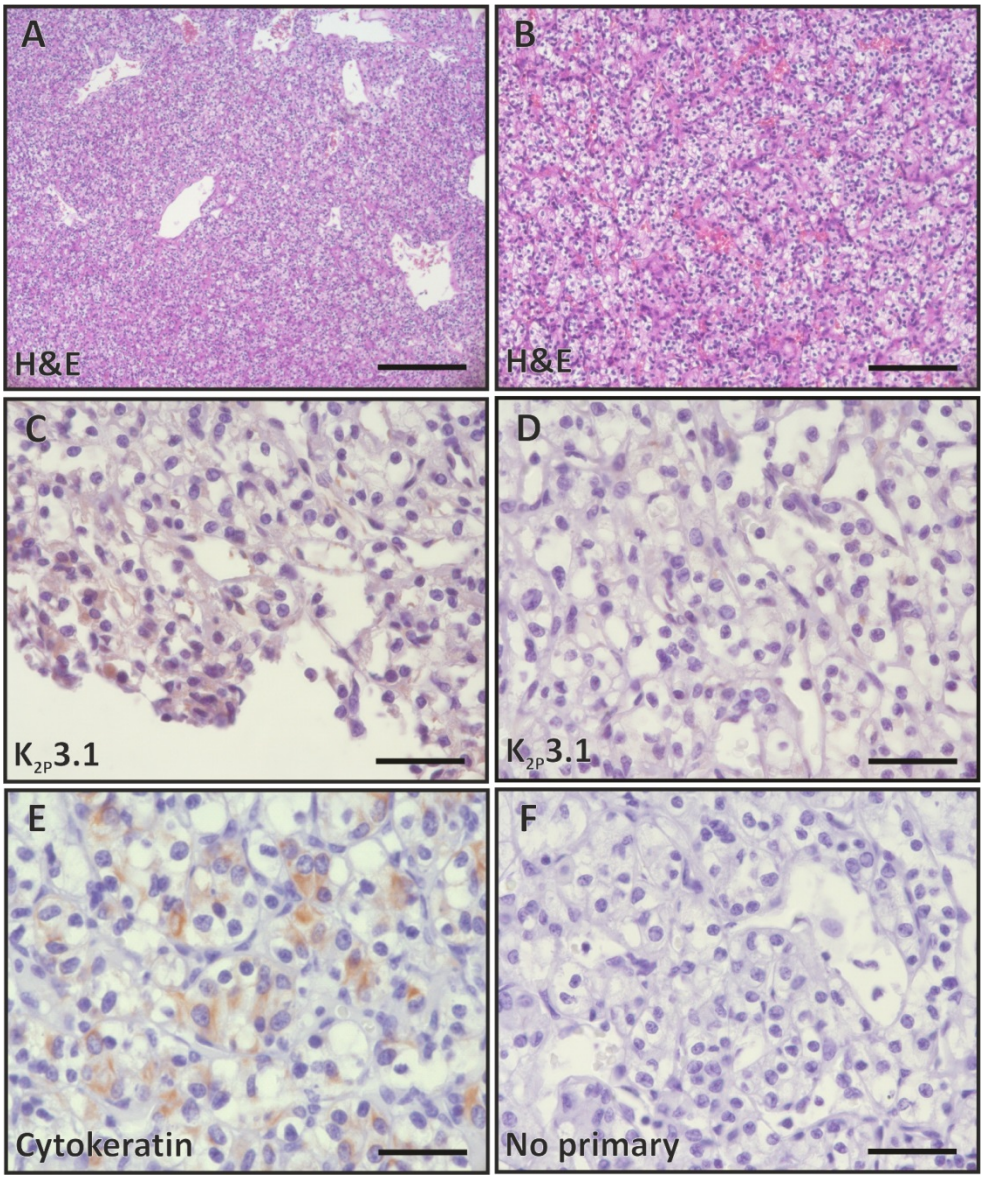

Figure 4.39: $K_{2P}3.1$ protein expression in low grade renal carcinoma (tissue sample S)

Tissue sample S is a low grade clear cell renal carcinoma and has not been classified with the TNM grading.

Sections were incubated with 0.01 M sodium citrate pH 6.0 for 5 min prior to antibody incubation. Antibody labelling is shown in brown (DAB) and sections counterstained with haematoxylin.

A, B) H&E staining.

C, D) Immunolabelling for $K_{2P}3.1$ protein using Sigma $K_{2P}3.1$ antibody.

E) Immunolabelling for cytokeratin protein, using DakoCytomation cytokeratin antibody.

F) No primary antibody incubation control.

Scale bars are (A) 250 µm, (B) 125 µm, and (C-F) 40 µm.

4.6.3 K_{2P}9.1 protein expression in human cancer tissue

K_{2P}9.1 protein expression was examined in the same 19 human cancer tissues which were assessed for K_{2P}3.1 protein. The tissue samples studied represent oesophageal, lung, pancreatic, and renal cancers (see Section 4.6.2 for the rationale for this selection). It should be noted that this expression study was limited by a lack of matched normal tissue controls. Therefore, the data presented here can only provide an initial assessment of K_{2P}9.1 protein expression in these cancers. The optimal antigen retrieval conditions utilised to detect K_{2P}9.1 protein were established in Result 4.6.1 (boiling in sodium citrate buffer (pH 6.0) for 10 min). Following antigen retrieval the sections were immunolabelled using Santa Cruz anti-K_{2P}9.1 (20 µg/ml; Method 2.5.2), and this antibody was found to specifically detect K_{2P}9.1 protein in Result 4.3.2. Cytokeratins were also used as a positive expression control for K_{2P}9.1 staining experiments (staining performed using 2.32 µg/ml DakoCytomation anti-cytokeratins antibody).

4.6.3.1 Detection of K_{2P}9.1 protein in oesophageal adenocarcinomas

The same ten oesophageal adenocarcinoma tissue samples (A-J) were examined for K_{2P}9.1 expression. Three samples showed positive K_{2P}9.1 expression (A (Figure 4.40), B (Figure 4.41) and C (Figure 4.42)) and in each case staining was compared to a no primary antibody incubation control. Expression of both K_{2P}3.1 and K_{2P}9.1 protein was only detected in one sample, B (K_{2P}3.1: Figure 4.29 and K_{2P}9.1: Figure 4.41). In sample B, K_{2P}9.1 staining was detected within the cytoplasm of the tumour cells in malignant glands (Figure 4.41 C, D), which was same pattern that was observed for K_{2P}3.1 (Figure 4.29 C, D). K_{2P}9.1 protein was also detected within the malignant glandular structures in samples A (Figure 4.40 C, D) and C (Figure 4.42 C, D). In all three tissues, cytokeratin protein staining was observed within the abnormal glandular structures (A: Figure 4.40 E, B: Figure 4.41 E, and C: Figure 4.42 E). The remaining seven oesophageal adenocarcinoma samples (D-H) showed no detectable K_{2P}9.1 protein staining (Table 4.3, shown for sample I; Figure 4.43).

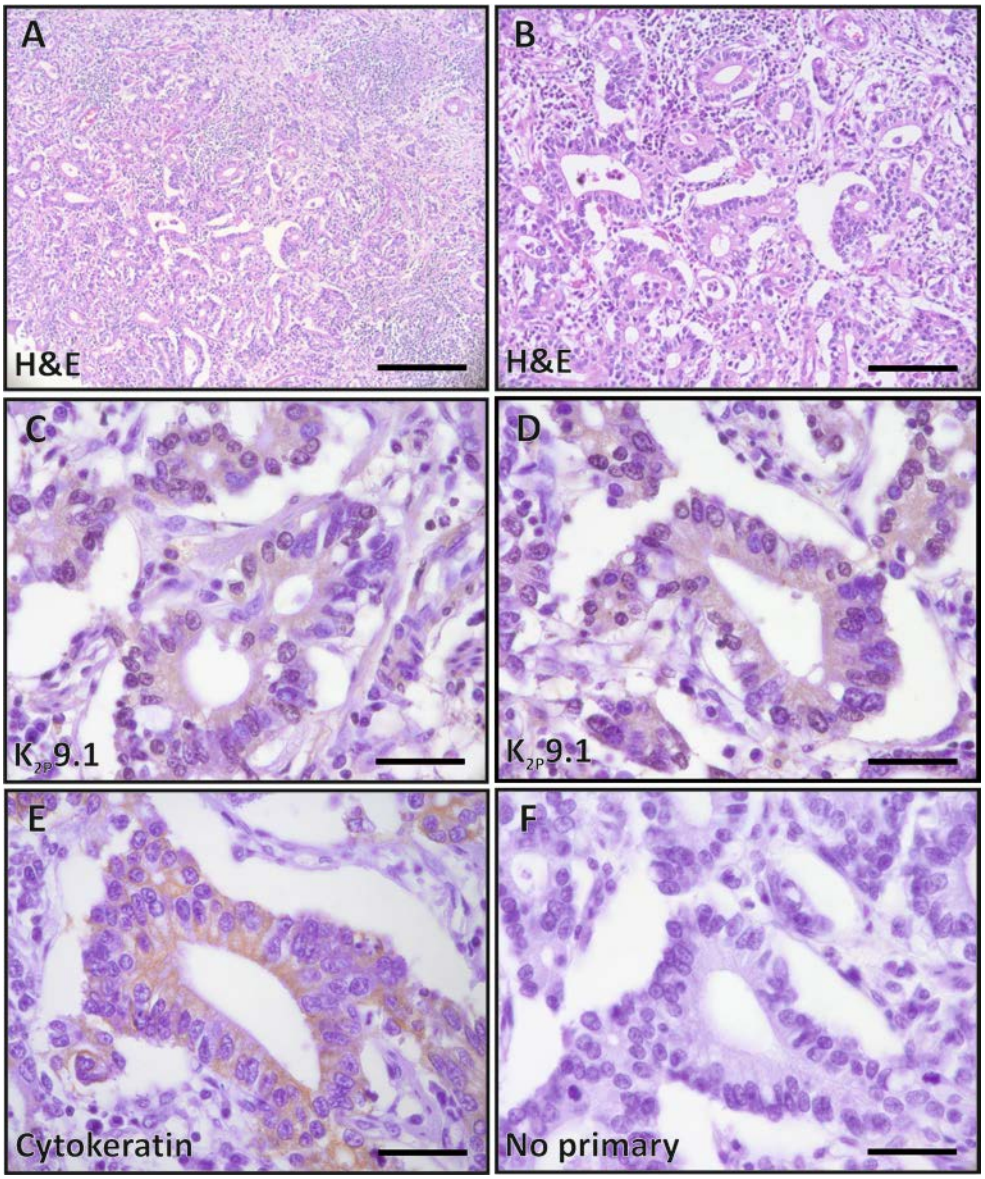

Figure 4.40: K_{2P}9.1 protein expression in oesophageal adenocarcinoma (tissue sample A)

Tissue sample A is a tumour stage 3 oesophageal adenocarcinoma with no lymph node involvement (pT3N0).

Sections were incubated with 0.01 M sodium citrate pH 6.0 for 5 min prior to antibody incubation. Antibody labelling is shown in brown (DAB) and sections counterstained with haematoxylin.

A, B) H&E staining.

C, D) Immunolabelling for K_{2P}9.1 protein, using Santa Cruz K_{2P}9.1 antibody.

E) Immunolabelling for cytokeratin protein, using DakoCytomation cytokeratin antibody.

F) No primary antibody incubation control.

Scale bars are (A) 250 µm, (B) 125 µm, and (C-F) 40 µm.

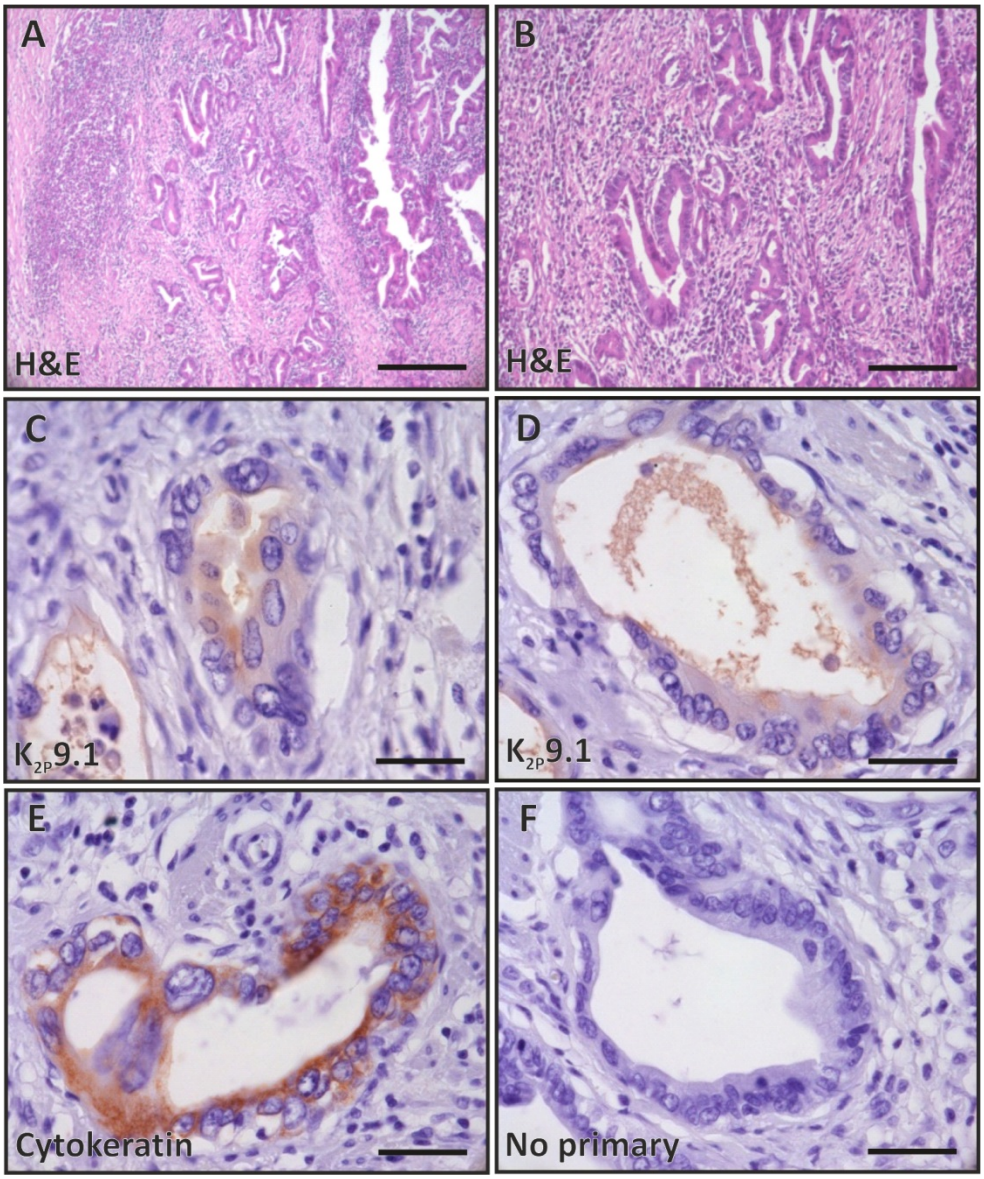

Figure 4.41: K_{2P}9.1 protein expression in oesophageal adenocarcinoma (tissue sample B)

Tissue sample B originated from the oesophago-gastro junction and is classed as tumour stage 3 with N1 lymph node involvement (pT3N1).

Sections were incubated with 0.01 M sodium citrate pH 6.0 for 5 min prior to antibody incubation. Antibody labelling is shown in brown (DAB) and sections counterstained with haematoxylin.

A, B) H&E staining.

C, D) Immunolabelling for K_{2P}9.1 protein, using Santa Cruz K_{2P}9.1 antibody.

E) Immunolabelling for cytokeratin protein, using DakoCytomation cytokeratin antibody.

F) No primary antibody incubation control.

Scale bars are (A) 250 µm, (B) 125 µm, and (C-F) 40 µm.

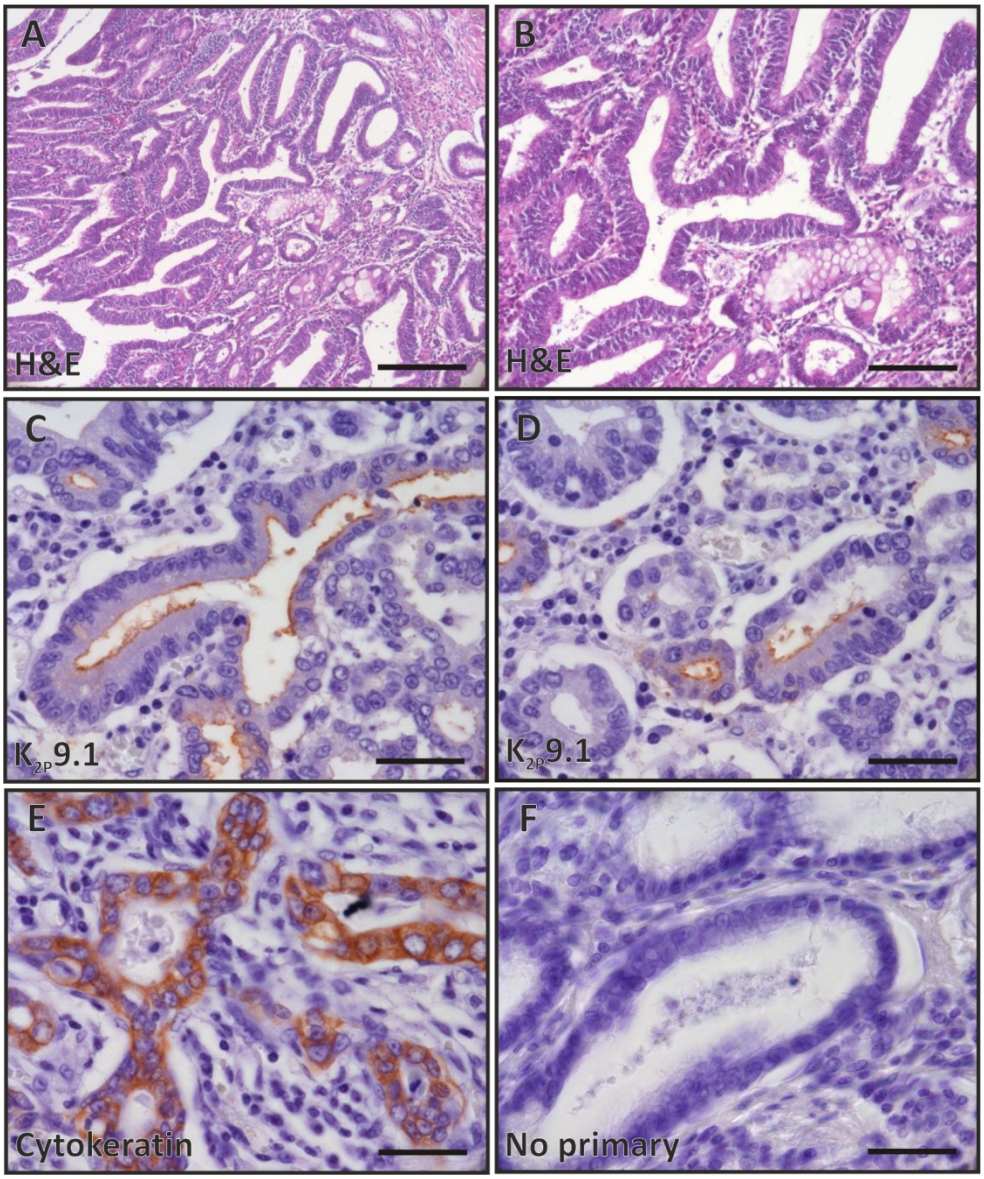

Figure 4.42: K_{2P}9.1 protein expression in oesophageal adenocarcinoma (tissue sample C)

Tissue sample C is oesophageal adenocarcinoma, classified as tumour stage 3 with N1 lymph node involvement (pT3N1).

Sections were incubated with 0.1 M sodium citrate pH 6.0 for 5 min prior to antibody incubation. Antibody labelling is shown in brown (DAB) and sections counterstained with haematoxylin.

A, B) H&E staining.

C, D) Immunolabelling for K_{2P}9.1 protein, using Santa Cruz K_{2P}9.1 antibody.

E) Immunolabelling for cytokeratin protein, using DakoCytomation cytokeratin antibody.

F) No primary antibody incubation control.

Scale bars are (A) 250 µm, (B) 125 µm, and (C-F) 40 µm.

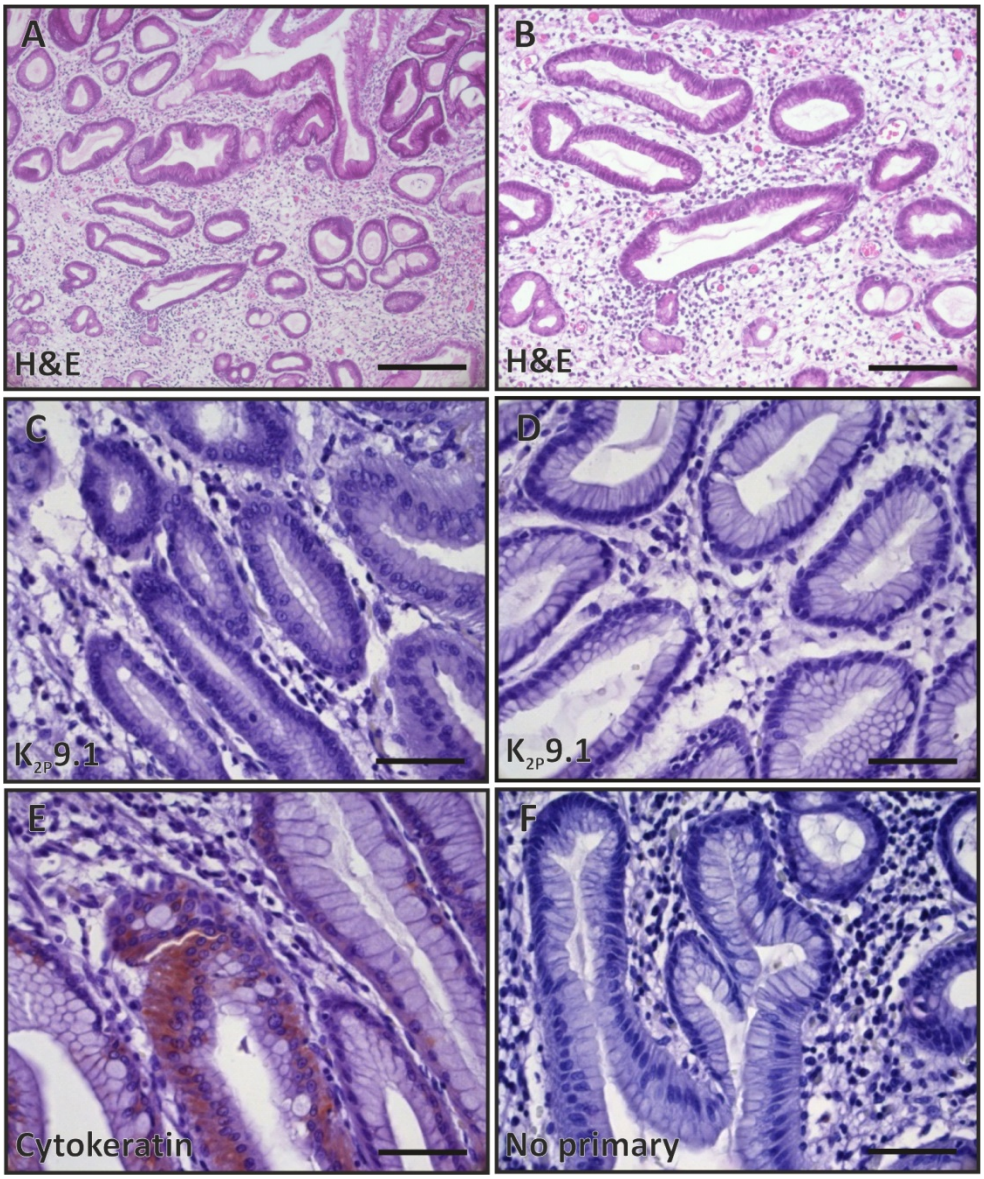

Figure 4.43: Negative $K_{2P}9.1$ protein staining in oesophageal adenocarcinoma (tissue sample I)

Tissue sample I originated in the lower third of the oesophagus and is classed as tumour stage 2 with no lymph node involvement (pT2N0).

Sections were incubated with 0.1 M sodium citrate pH 6.0 for 5 min prior to antibody incubation. Antibody labelling is shown in brown (DAB) and sections counterstained with haematoxylin.

A, B) H&E staining.

C, D) Immunolabelling for $K_{2P}9.1$ protein, using Santa Cruz $K_{2P}9.1$ antibody.

E) Immunolabelling for cytokeratin protein, using DakoCytomation cytokeratin antibody.

F) No primary antibody incubation control.

Scale bars are (A) 250 µm, (B) 125 µm, and (C-F) 40 µm.

4.6.3.2 Detection of $K_{2P}9.1$ protein in lung squamous cell carcinomas

Of the three lung squamous cell carcinoma tissues examined (K, L, and M), two showed $K_{2P}9.1$ staining: K (Figure 4.44) and M (Figure 4.45). $K_{2P}9.1$ protein was observed in the cytoplasm of the large pleomorphic cells forming the malignant tissue within a poorly differentiated invasive squamous cell lung carcinoma (Figure 4.44 C, D). $K_{2P}9.1$ expression was also observed in an undifferentiated large cell carcinoma (Figure 4.45), where diffuse $K_{2P}9.1$ staining was observed in the cytoplasm of the large pleomorphic tumour cells (Figure 4.45 C), and this was similar to the $K_{2P}3.1$ expression detected (Figure 4.33 C, D). In addition, $K_{2P}9.1$ staining was observed in some of the cells surrounding these atypical cell nests (Figure 4.45 D). The final tissue sample, a poorly differentiated squamous cell lung carcinoma (sample L: Figure 4.46), showed no detectable $K_{2P}9.1$ staining (Figure 4.46 C, D). Cytokeratin protein staining was also observed within the abnormal tumour cells in these samples (Figure 4.44 E, Figure 4.45 E, and Figure 4.46 E).

4.6.3.3 Detection of $K_{2P}9.1$ protein in pancreatic adenocarcinomas

Three pancreatic adenocarcinoma tissue samples were examined (N, O, and P) and two showed positive $K_{2P}9.1$ protein staining: N (Figure 4.47) and P (Figure 4.48). $K_{2P}9.1$ staining was observed in the cytoplasm of some tumour cells within the irregular gland-like structures present in the invasive ductal adenocarcinoma tissue (Figure 4.47 C, D), and this was similar to the $K_{2P}3.1$ expression detected (Figure 4.35). The level of $K_{2P}9.1$ staining in this tissue appeared to be stronger and in a larger number of cells (Figure 4.47 C, D), compared to $K_{2P}3.1$ (Figure 4.35). $K_{2P}9.1$ expression was also detected in moderately differentiated pancreatic adenocarcinoma (Figure 4.48 C, D), where diffuse $K_{2P}9.1$ staining was detected in the cytoplasm of tumour cells forming irregular gland-like structures (Figure 4.49 C, D). The third tissue examined, sample O, showed no detectable $K_{2P}9.1$ staining (Figure 4.49 C, D). In all samples, cytokeratin protein expression was observed within the tumour cells forming the irregular gland-like structures (Figure 4.47 E, Figure 4.48 E, and Figure 4.49 E).

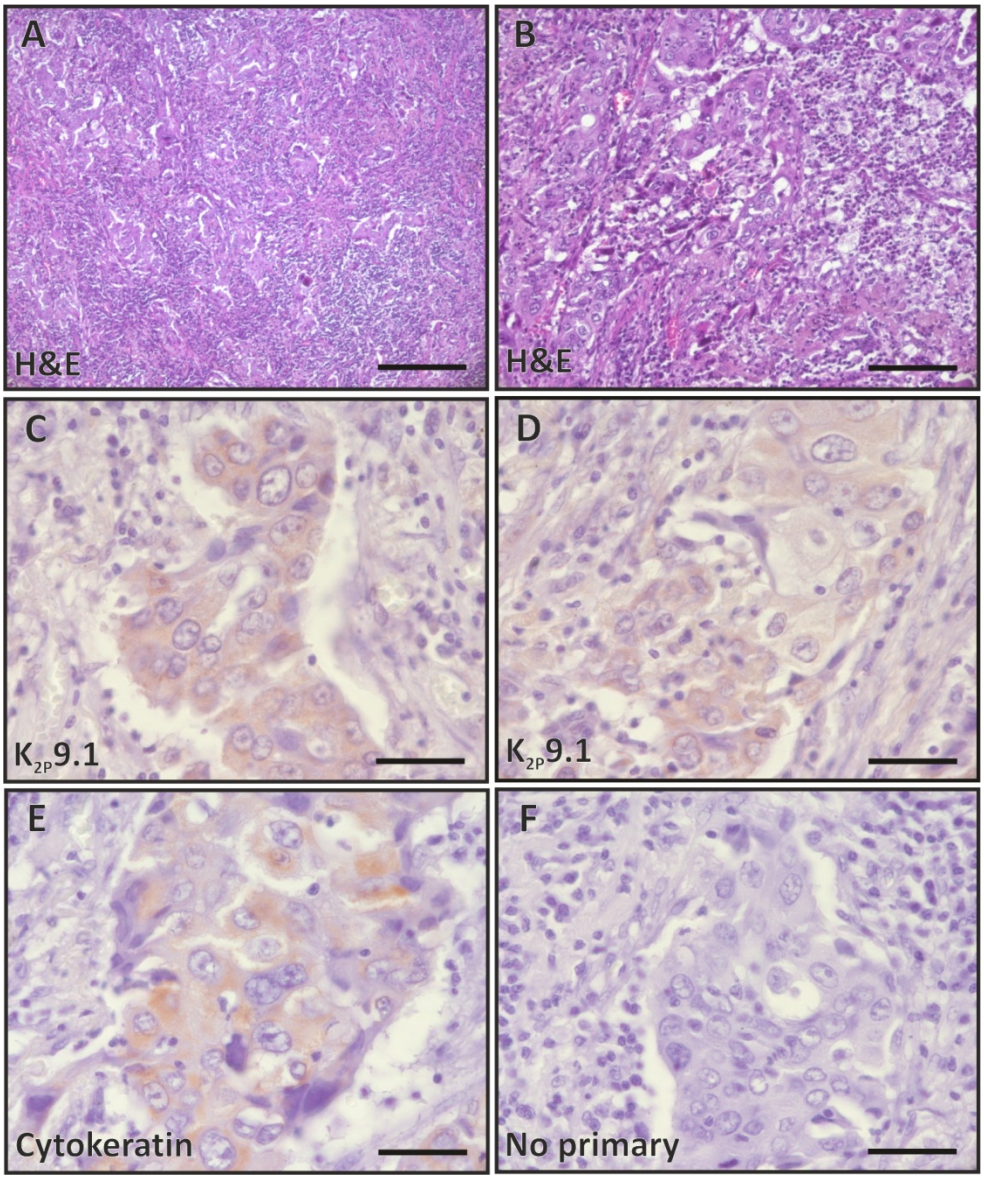

Figure 4.44: K_{2P}9.1 protein expression in poorly differentiated invasive lung squamous cell carcinoma (tissue sample K)

Tissue sample K is an invasive poorly differentiated squamous cell lung carcinoma, which is classified as tumour cell stage 2 with no lymph node involvement (pT2N0).
Sections were incubated with 0.01 M sodium citrate pH 6.0 for 5 min prior to antibody incubation. Antibody labelling is shown in brown (DAB) and sections counterstained with haematoxylin.

A, B) H&E staining.
C, D) Immunolabelling for K_{2P}9.1 protein, using Santa Cruz K_{2P}9.1 antibody.
E) Immunolabelling for cytokeratins protein, using DakoCytomation cytokeratin antibody.
F) No primary antibody incubation control.

Scale bars are (A) 250 µm, (B) 125 µm, and (C-F) 40 µm.

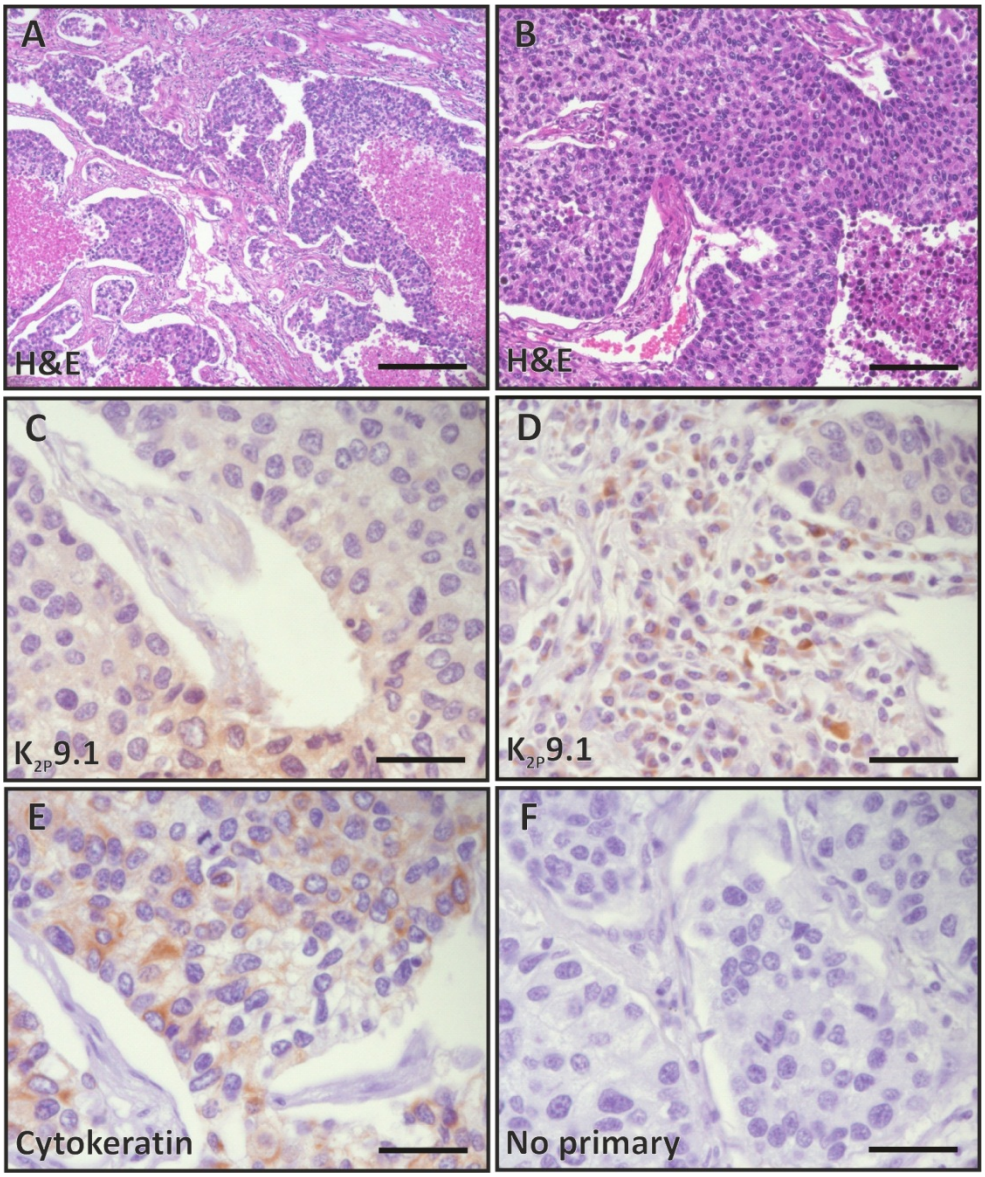

Figure 4.45: $K_{2P}9.1$ protein expression in undifferentiated large cell lung carcinoma (tissue sample M)

Tissue sample M is an undifferentiated large cell lung carcinoma, which is composed of infiltrating nests of large atypical cells, and classed as tumour stage 3 with no lymph node involvement (pT3N0).

Sections were incubated with 0.01 M sodium citrate pH 6.0 for 5 min prior to antibody incubation. Antibody labelling is shown in brown (DAB) and sections counterstained with haematoxylin.

A, B) H&E staining.
C, D) Immunolabelling for $K_{2P}9.1$ protein, using Santa Cruz $K_{2P}9.1$ antibody.
E) Immunolabelling for cytokeratin protein, using DakoCytomation cytokeratin antibody.
F) No primary antibody incubation control.

Scale bars are (A) 250 µm, (B) 125 µm, and (C-F) 40 µm.

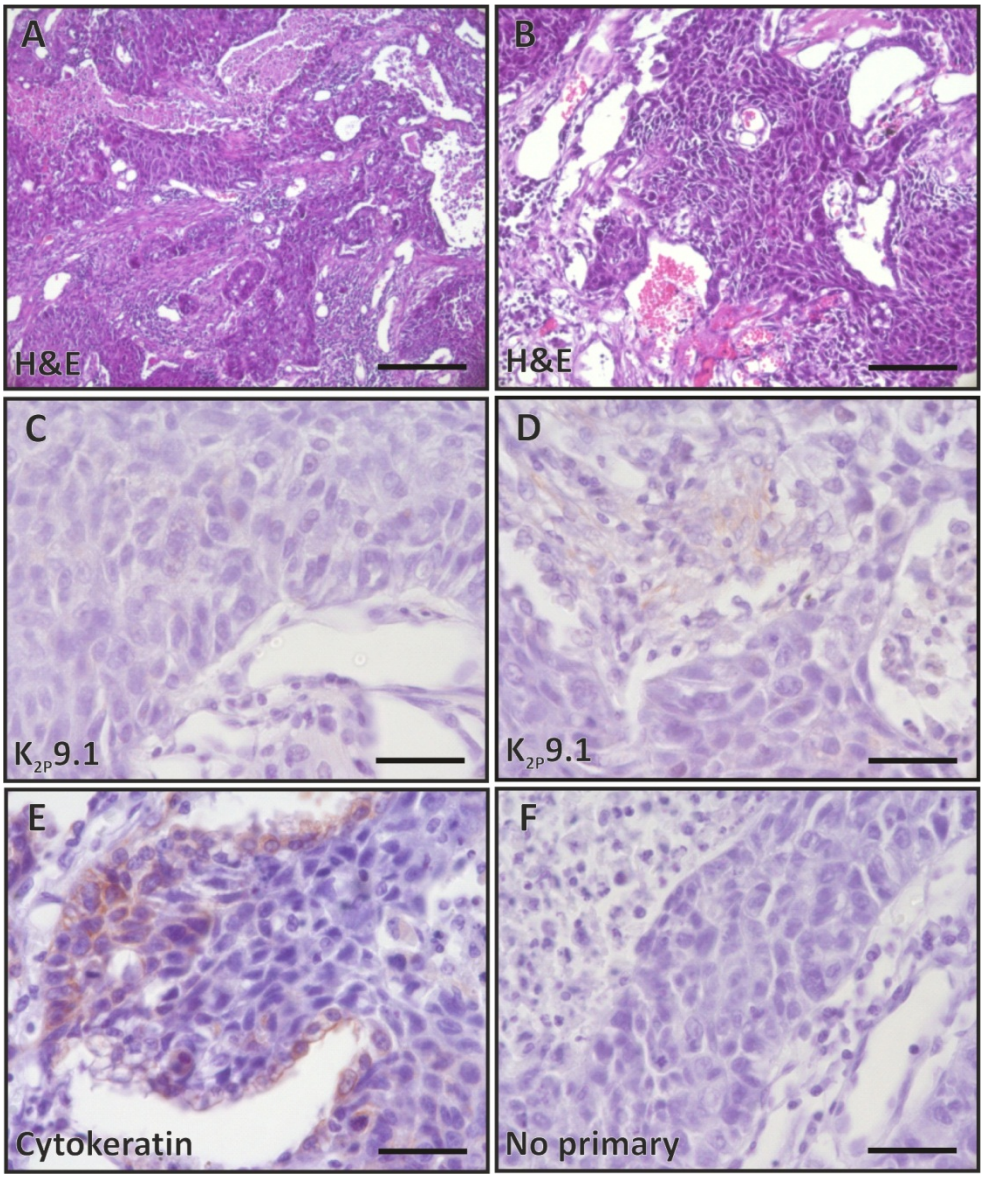

Figure 4.46: Negative $K_{2P}9.1$ protein staining in poorly differentiated lung squamous cell carcinoma (tissue sample L)

Tissue sample L is a moderate to poorly differentiated squamous cell lung carcinoma, classified as tumour stage 1 with regional lymph node metastases (pT1N1).
Sections were incubated with 0.01 M sodium citrate pH 6.0 for 5 min prior to antibody incubation. Antibody labelling is shown in brown (DAB) and sections counterstained with haematoxylin.

A, B) H&E staining.
C, D) Immunolabelling for $K_{2P}9.1$ protein, using Santa Cruz $K_{2P}9.1$ antibody.
E) Immunolabelling for cytokeratin protein, using DakoCytomation cytokeratin antibody.
F) No primary antibody incubation control.

Antibody labelling is shown in brown (DAB) and sections counterstained with haematoxylin.

Scale bars are (A) 250 µm, (B) 125 µm, and (C-F) 40 µm.

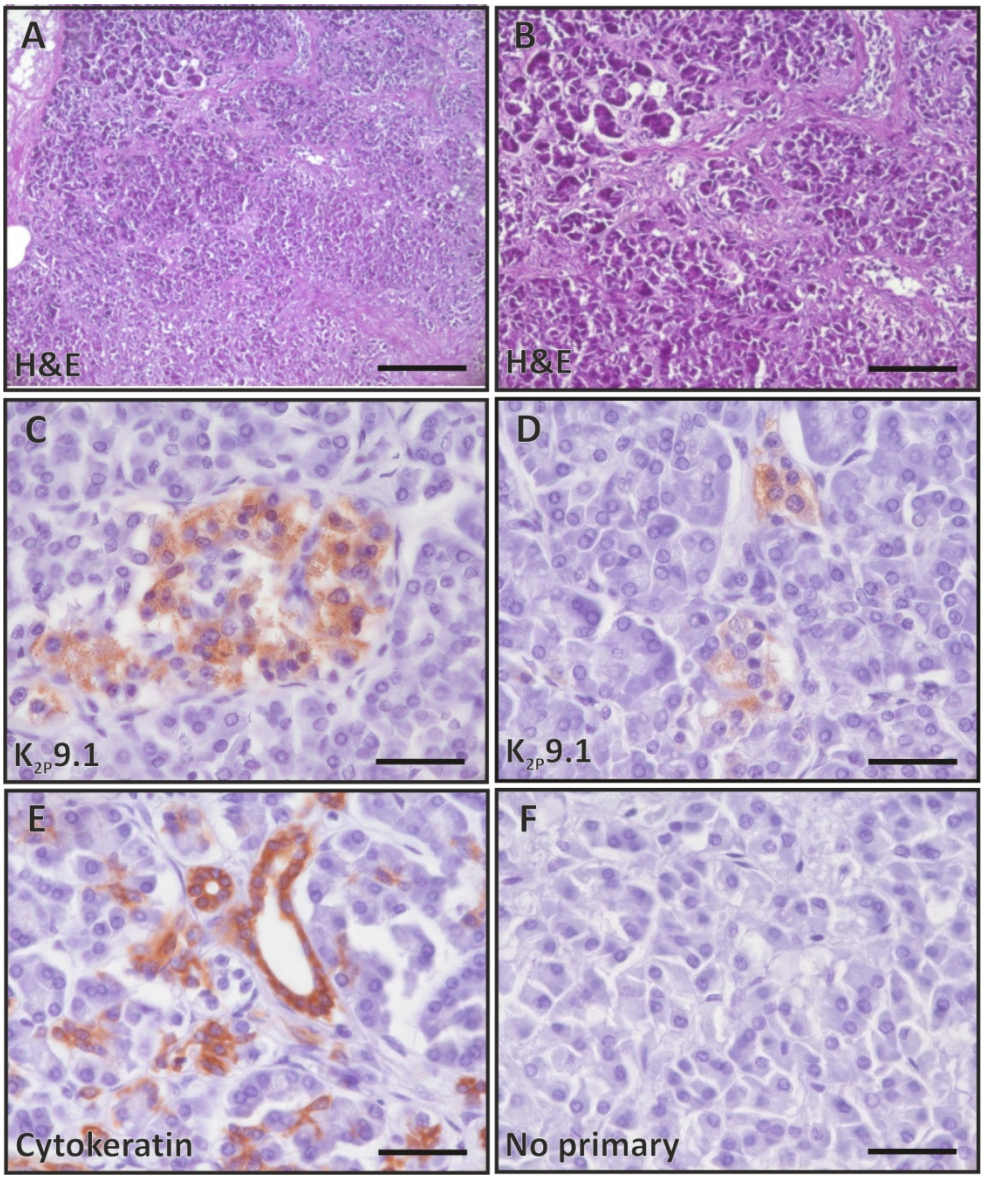

Figure 4.47: $K_{2P}9.1$ protein expression in invasive ductal pancreatic adenocarcinoma (tissue sample N)

Tissue sample N is an invasive ductal adenocarcinoma with neural invasion, classified as tumour stage 1 (pT1), lymph node status unknown.

Sections were incubated with 0.01 M sodium citrate pH 6.0 for 5 min prior to antibody incubation. Antibody labelling is shown in brown (DAB) and sections counterstained with haematoxylin.

A, B) H&E staining.

C, D) Immunolabelling for $K_{2P}9.1$ protein, using Santa Cruz $K_{2P}9.1$ antibody.

E) Immunolabelling for cytokeratin protein, using DakoCytomation cytokeratin antibody.

F) No primary antibody incubation control.

Antibody labelling is shown in brown (DAB) and sections counterstained with haematoxylin.

Scale bars are (A) 250 µm, (B) 125 µm, and (C-F) 40 µm.

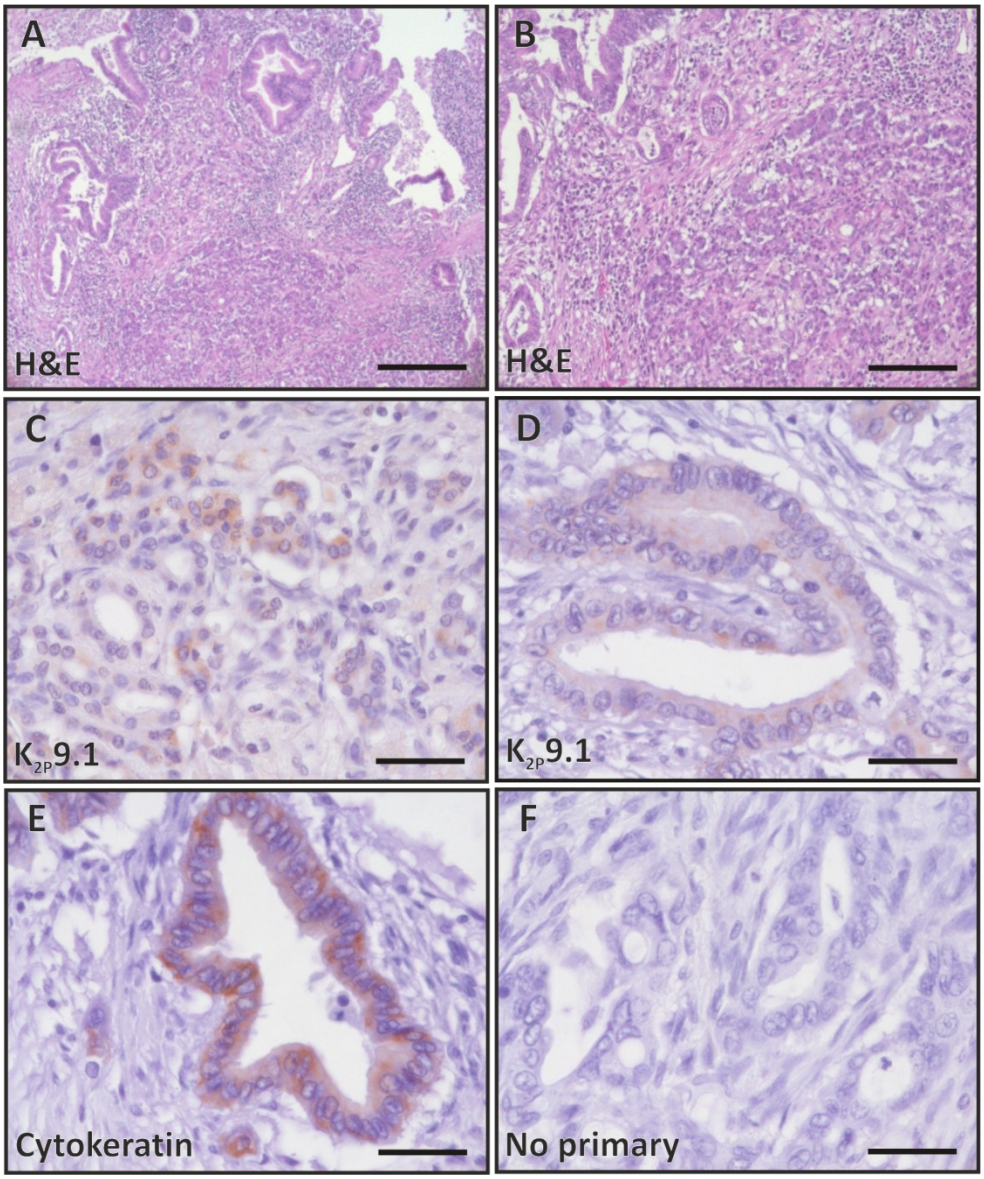

Figure 4.48: $K_{2P}9.1$ protein expression in moderately differentiated pancreatic adenocarcinoma (tissue sample P)

Tissue sample P is a moderately differentiated pancreatic adenocarcinoma, classified as tumour stage 2 with no lymph node involvement or metastases (pT2N0Mx)
Sections were incubated with 0.01 M sodium citrate pH 6.0 for 5 min prior to antibody incubation.

A, B) H&E staining.
C, D) Immunolabelling for $K_{2P}9.1$ protein, using Santa Cruz $K_{2P}9.1$ antibody.
E) Immunolabelling for cytokeratin protein, using DakoCytomation cytokeratin antibody.
F) No primary antibody incubation control.
Antibody labelling is shown in brown (DAB) and sections counterstained with haematoxylin.

Scale bars are (A) 250 µm, (B) 125 µm, and (C-F) 40 µm.

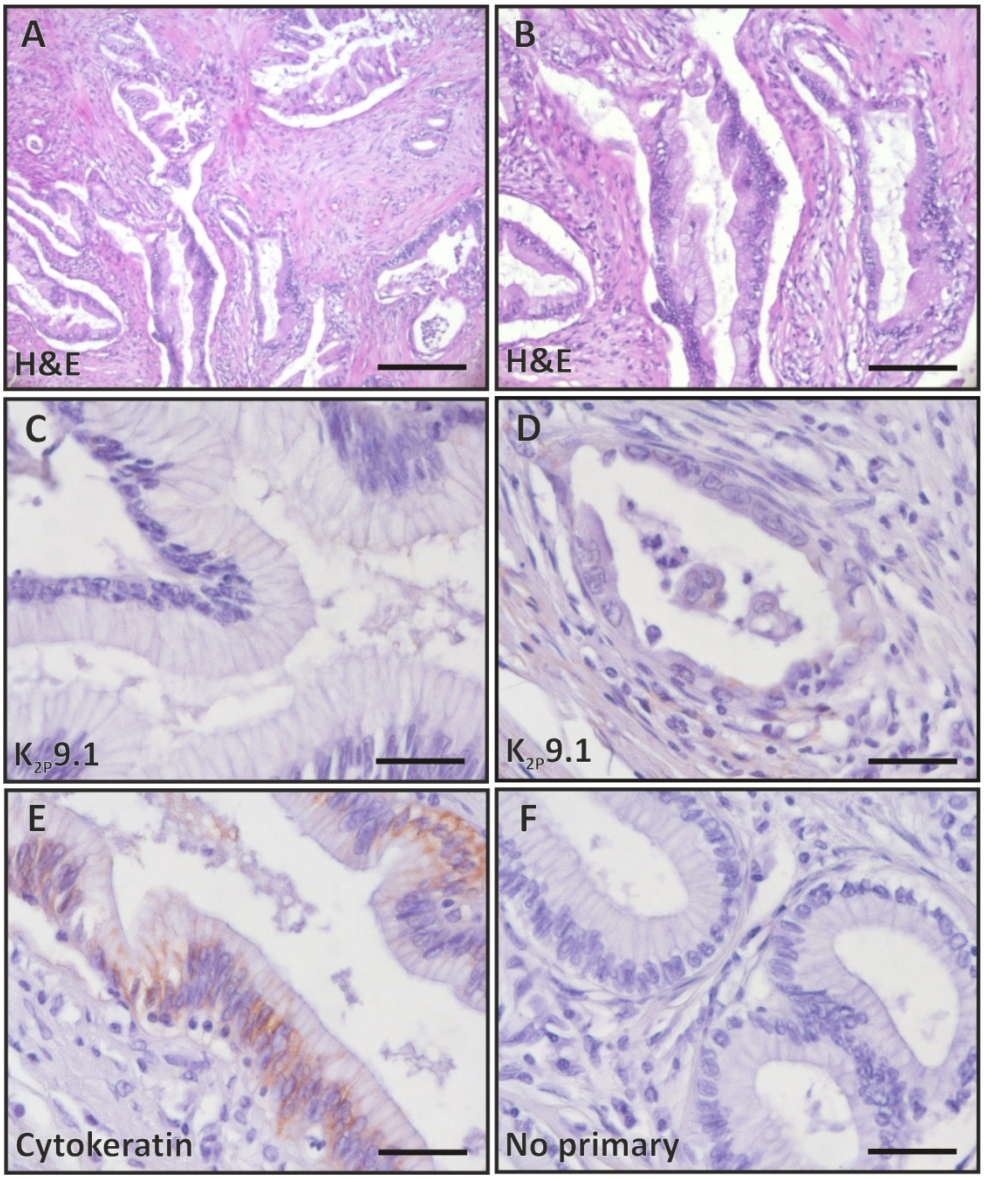

Figure 4.49: Negative $K_{2P}9.1$ protein staining in moderately differentiated pancreatic adenocarcinoma (tissue sample O)

Tissue sample O is moderately differentiated invasive pancreatic adenocarcinoma, classified as tumour stage 4 with local lymph node invasion and no metastases (pT4N1Mx). Sections were incubated with 0.01 M sodium citrate pH 6.0 for 5 min prior to antibody incubation.

A, B) H&E staining.
C, D) Immunolabelling for $K_{2P}9.1$ protein, using Santa Cruz $K_{2P}9.1$ antibody.
E) Immunolabelling for cytokeratin protein, using DakoCytomation cytokeratin antibody.
F) No primary antibody incubation control.
Antibody labelling is shown in brown (DAB) and sections counterstained with haematoxylin.

Scale bars are (A) 250 µm, (B) 125 µm, and (C-F) 40 µm.

4.6.3.4 Detection of $K_{2P}9.1$ protein in renal carcinomas

$K_{2P}9.1$ protein expression was detected in all three renal carcinoma tissue samples: Q (Figure 4.50), R (Figure 4.51), and S (Figure 4.52). In renal oncocytoma tissue (sample Q), $K_{2P}9.1$ staining was present in the cytoplasm of cells within the oncocytic cell nests (Figure 4.50 C, D) and this staining pattern was comparable to the $K_{2P}3.1$ expression detected (Figure 4.37). $K_{2P}9.1$ staining was observed in the cytoplasm of eosinophilic tumour cells within a high grade renal cell carcinoma (sample R; Figure 4.51 C, D) and this was also comparable to the $K_{2P}3.1$ staining observed (Figure 4.38). The level of $K_{2P}9.1$ staining was lowest in this sample compared to the other renal carcinoma tissues examined. $K_{2P}9.1$ expression was detected in the cytoplasm of tumour cells within a low grade clear cell renal carcinoma (sample S; Figure 4.52 C, D); this was similar to the $K_{2P}3.1$ staining observed (Figure 4.39), although the level of $K_{2P}9.1$ expression appeared to be greater. As before, cytokeratin protein expression was detected in all three tissue samples (Figure 4.50 E, Figure 4.51 E, and Figure 4.52 E) and in sample R cytokeratin staining was observed in more glandular structures compared to $K_{2P}9.1$ and $K_{2P}3.1$ protein.

4.6.3.5 Expression of $K_{2P}9.1$ protein in human cancers

The data presented in this section identified $K_{2P}9.1$ protein within the cancerous cells of human oesophageal, lung, pancreatic, and renal cancer tissue. In some cases $K_{2P}9.1$ protein was detected within the same tissue samples as $K_{2P}3.1$ protein (Table 4.3). However, without performing colocalisation experiments it cannot be confirmed if $K_{2P}3.1$ and $K_{2P}9.1$ channel protein are expressed within the same cells. $K_{2P}9.1$ protein had not been described within these cancer types prior to this study, although protein expression had been identified in breast, colorectal, ovarian, and melanoma cancer tissues (Innamaa et al., 2013b, Kim et al., 2004, Mu et al., 2003, Pocsai et al., 2006). The protein expression data presented here differed from the bioinformatic data presented in Chapter 3, which did not identify any alterations to $K_{2P}9.1$ mRNA in the same cancer types (Table 3.4). This may indicate that $K_{2P}9.1$ alterations only occur at the protein level in the cancers types examined. However, it should be noted that these observations cannot be confirmed without further studies that include matched normal tissue controls and larger sample numbers. The potential implications of these findings and the limitations of this work are discussed in further detail in Result 4.6.4.

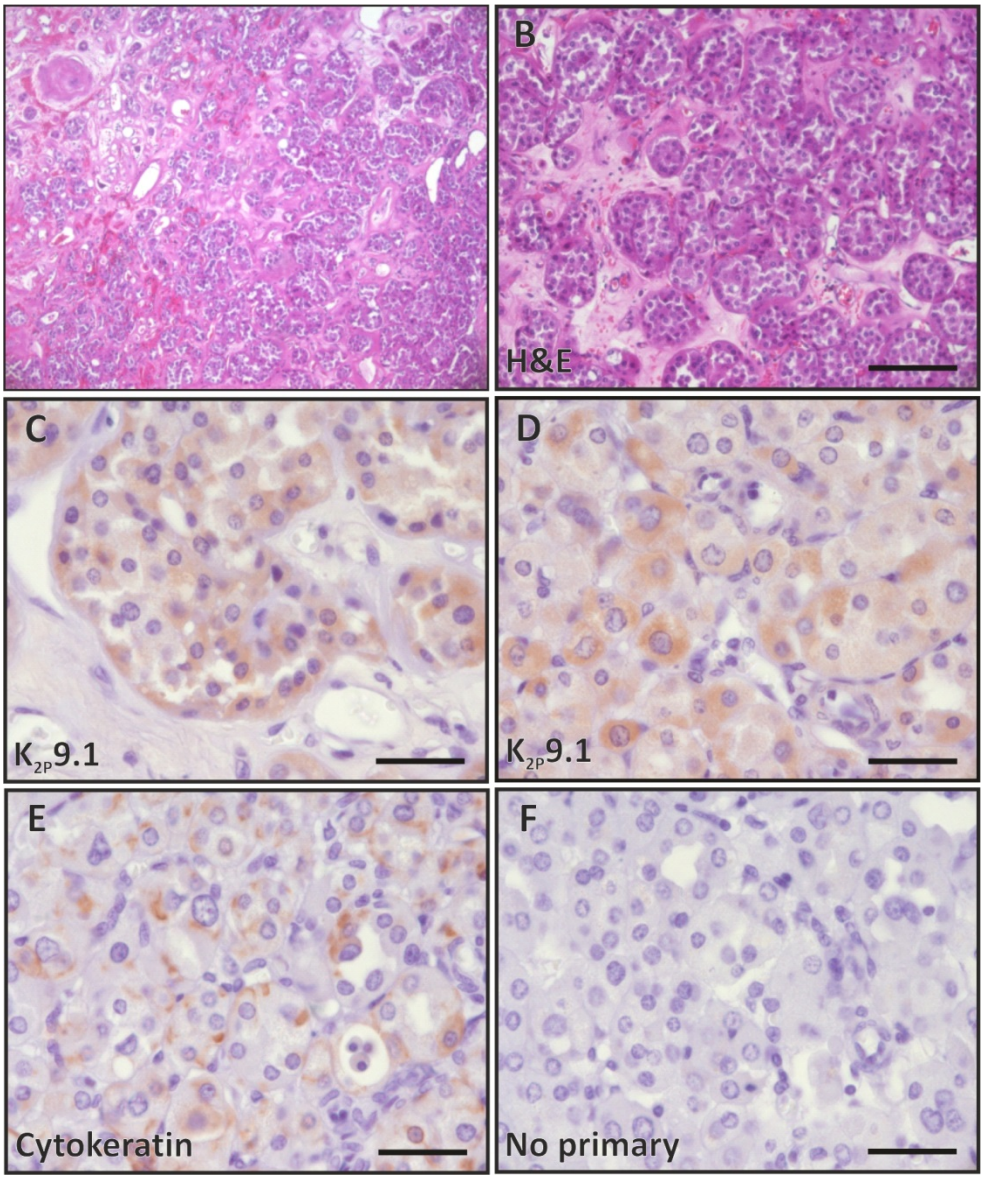

Figure 4.50: K_{2P}9.1 protein expression in renal oncocytoma (tissue sample Q)

Tissue sample Q is renal oncocytoma, where the tumour is composed of nests of oncocytic cells with characteristic round nuclei and eosinophilic granular cytoplasm. Pathologically renal oncocytomas are benign tumours, so do not have TNM grading.
Sections were incubated with 0.01 M sodium citrate pH 6.0 for 5 min prior to antibody incubation. Antibody labelling is shown in brown (DAB) and sections counterstained with haematoxylin.

A, B) H&E staining.
C, D) Immunolabelling for K_{2P}9.1 protein, using Santa Cruz K_{2P}9.1 antibody.
E) Immunolabelling for cytokeratin protein, using DakoCytomation cytokeratin antibody.
F) No primary antibody incubation control.
Antibody labelling is shown in brown (DAB) and sections counterstained with haematoxylin.

Scale bars are (A) 250 µm, (B) 125 µm, and (C-F) 40 µm.

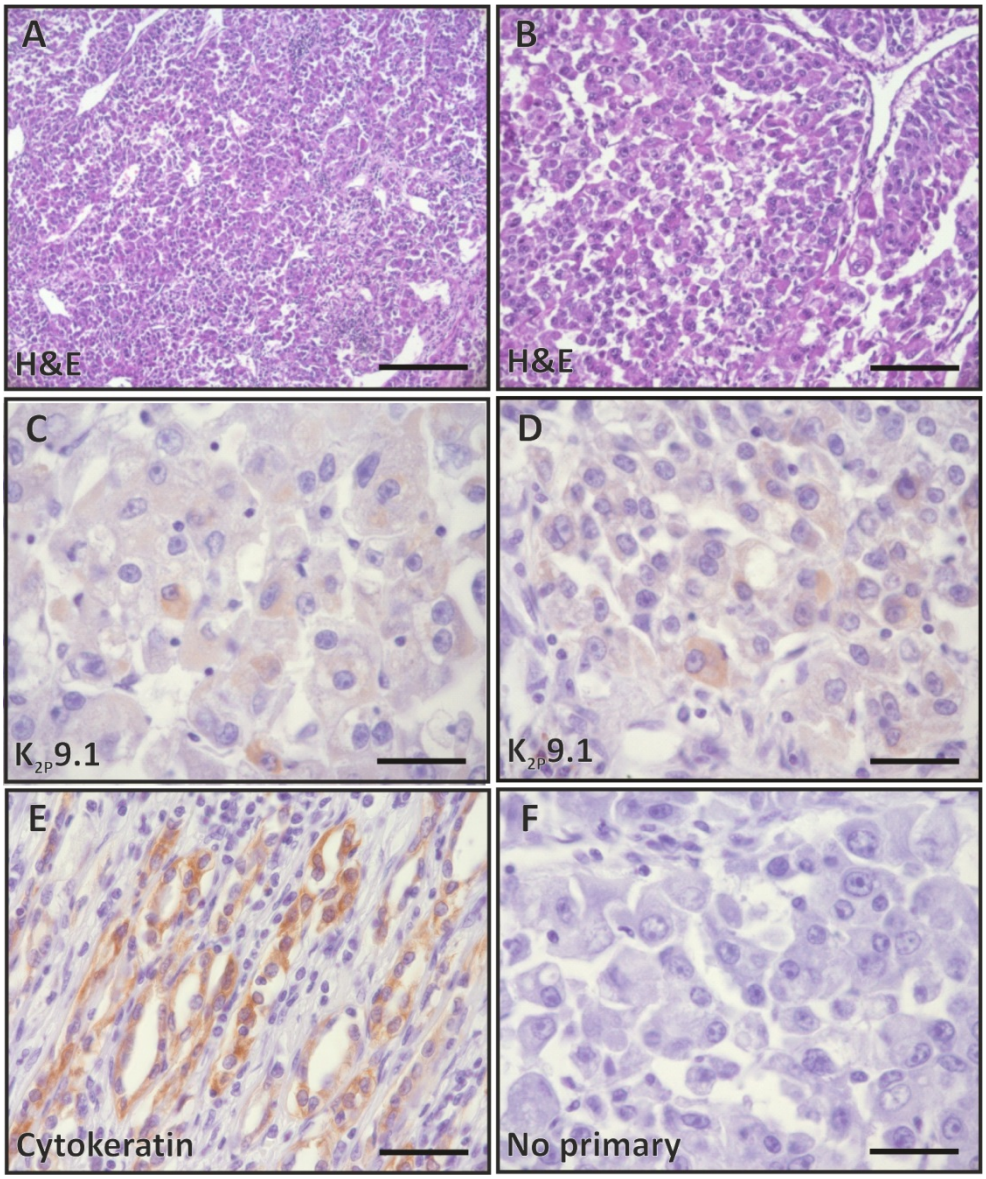

Figure 4.51: K_{2P}9.1 protein expression in high grade renal carcinoma (tissue sample R)

Tissue sample R is a high grade renal carcinoma, composed of some clear but mainly eosinophilic granular cells and is classified as tumour stage 3 (pT3).
Sections were incubated with 0.01 M sodium citrate pH 6.0 for 5 min prior to antibody incubation. Antibody labelling is shown in brown (DAB) and sections counterstained with haematoxylin.

A, B) H&E staining.
C, D) Immunolabelling for K_{2P}9.1 protein, using Santa Cruz K_{2P}9.1 antibody.
E) Immunolabelling for cytokeratin protein, using DakoCytomation cytokeratin antibody.
F) No primary antibody incubation control.

Scale bars are (A) 250 µm, (B) 125 µm, and (C-F) 40 µm.

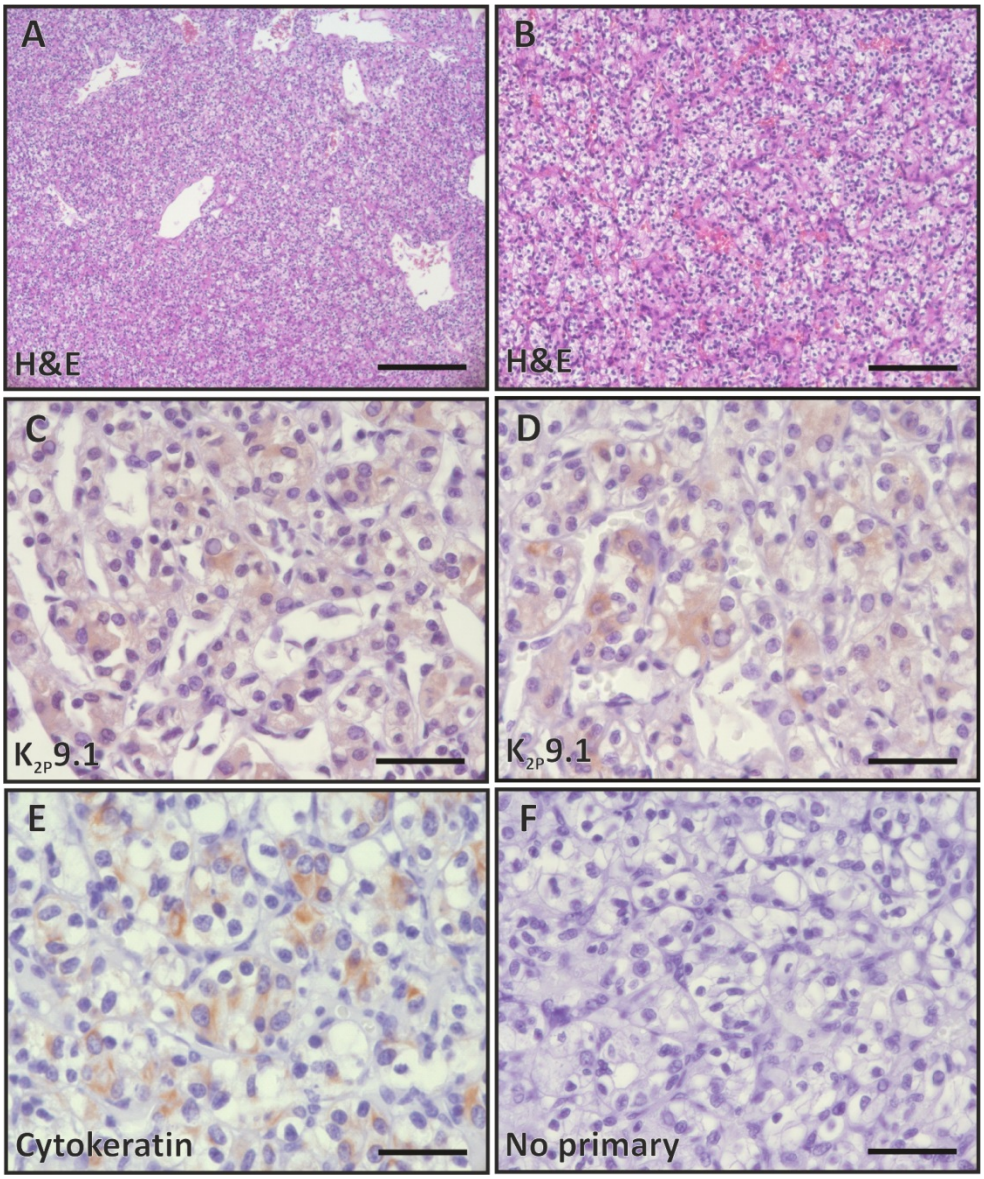

Figure 4.52: K_{2P}9.1 protein expression in low grade renal carcinoma (tissue sample S)

Tissue sample S is a low grade clear cell renal carcinoma and has not been classified with the TNM grading.

Sections were incubated with 0.01 M sodium citrate pH 6.0 for 5 min prior to antibody incubation. Antibody labelling is shown in brown (DAB) and sections counterstained with haematoxylin.

A, B) H&E staining.
C, D) Immunolabelling for K_{2P}9.1 protein, using Santa Cruz K_{2P}9.1 antibody.
E) Immunolabelling for cytokeratin protein, using DakoCytomation cytokeratin antibody.
F) No primary antibody incubation control.

Scale bars are (A) 250 µm, (B) 125 µm, and (C-F) 40 µm.

4.6.4 Summary of $K_{2P}3.1$ and $K_{2P}9.1$ protein expression in human cancer tissue

The aim of the staining experiments presented in this section was to identify if $K_{2P}3.1$ and $K_{2P}9.1$ protein could be detected within human oesophageal, lung, pancreatic, and renal cancer tissues. The data presented here provided the first evidence for $K_{2P}3.1$ and $K_{2P}9.1$ protein expression within the tumour cells in these cancer types (summarised in Table 4.3). The small sample numbers studied and the lack of matched normal tissue controls meant that these findings are currently of little value. However, examination of the published TASK channel expression data in cancer and the bioinformatic data presented in Chapter 3 gave a preliminary indication to whether the staining observed here could have a clinical relevance. This relevance will be outlined in the following paragraphs.

In lung cancer tissue, the absence of $K_{2P}3.1$ protein in two samples and the low level of expression detected in one sample (Table 4.3) are in agreement with the downregulation of $K_{2P}3.1$ mRNA, as predicated by bioinformatic analyses (Table 3.4). This is further supported by the detection of $K_{2P}3.1$ mRNA in healthy human and rat lung tissue (Duprat et al., 1997), although this study did not include protein expression analysis. $K_{2P}9.1$ protein was also detected in two lung squamous cell cancer tissues. No alterations to $K_{2P}9.1$ mRNA in lung cancers were found in Chapter 3, however Mu et al. (2003) observed increased $K_{2P}9.1$ mRNA in 35 % of the lung cancer samples they examined. Therefore, the protein expression data presented here may indicate that $K_{2P}9.1$ protein overexpression occurs in lung cancer. In support of this, $K_{2P}9.1$ mRNA has not been detected in normal human lung tissue (Chapman et al., 2000).

$K_{2P}3.1$ protein was detected in one of the three pancreatic adenocarcinoma tissue samples examined (Table 4.3). This supports the downregulation of $K_{2P}3.1$ mRNA in pancreatic adenocarcinomas which was observed in Chapter 3 (Table 3.4), in addition high levels of $K_{2P}3.1$ mRNA have been detected in normal human pancreatic tissue (Duprat et al., 1997; Medhurst et al., 2001). However, in these studies the corresponding protein expression was not performed. In two pancreatic adenocarcinoma tissue samples, $K_{2P}9.1$ protein was detected (Table 4.3). There have been no published studies describing altered $K_{2P}9.1$ expression in pancreatic cancer and bioinformatic analysis did not predict any changes to $K_{2P}9.1$ mRNA (Table 3.4). However, $K_{2P}9.1$ channel mRNA and protein has been

detected in normal human pancreatic tissue (Chapman et al., 2000; Kovacs et al., 2005; Medhurst et al., 2001).

K_{2P}3.1 and K_{2P}9.1 protein was detected in all three renal carcinoma tissue samples (Table 4.3). Bioinformatic data indicated that K_{2P}3.1 mRNA is increased in renal clear cell carcinomas (Table 3.4). Low levels of K_{2P}3.1 mRNA have been detected in normal human kidney tissue (Duprat et al., 1997); however K_{2P}3.1 protein expression has not been examined. Therefore, the expressed data presented in this thesis and published data from normal tissue indicated that K_{2P}3.1 (mRNA and protein) may be overexpressed in renal cancers compared to normal kidney tissue. It is unclear whether K_{2P}9.1 expression is altered in renal cancers; since bioinformatic data revealed no changes to K_{2P}9.1 at an mRNA level and K_{2P}9.1 mRNA was not detectable in normal human kidney tissue (Chapman et al., 2000).

No conclusions can be made about the expression K_{2P}3.1 and K_{2P}9.1 protein in oesophageal adenocarcinomas (Table 4.3), since TASK channel expression (mRNA and protein) has not been examined in the normal oesophagus. In addition, bioinformatic data did not describe any alterations to K_{2P}3.1 or K_{2P}9.1 mRNA in oesophageal cancers (Chapter 3).

Overall, the published expression data highlighted in the previous paragraphs indicated that there are some differences between the normal expression reported for TASK channels and the staining observed in this thesis (both mRNA in Chapter 3 and protein in this Chapter). However, without conducting further studies with a larger number of samples and matched normal tissue controls this cannot be confirmed. Therefore, no firm conclusions about the clinical relevance of the TASK channel expression detected in these tissues can be drawn at this time. Prior to this study, the lack of reliable and validated antibodies to detect TASK channel protein has limited expression studies in human tissue. The series of experiments performed in this chapter, characterised commercially available TASK channel antibodies and optimised the detection method for both K_{2P}3.1 and K_{2P}9.1 protein in fixed pathology samples. This will allow for future expression studies to be performed on both normal and cancerous human tissue samples.

Table 4.3: Expression of TASK channel protein in human cancer tissue
Summary of TASK channel ($K_{2P}3.1$ and $K_{2P}9.1$) and cytokeratin (CK) protein expression detected in the 19 carcinoma samples examined (Tissue A-S).
Tumour stage grading indicates the size and extent of the primary tumour biopsied (T1-4). The presence of positive (+) or negative (-) staining is indicated.

Tissue	Cancer	Stage	Expression		
			$K_{2P}3.1$	$K_{2P}9.1$	CK
A	Oesophageal adenocarcinoma	T3	-	+	+
B	Oesophageal adenocarcinoma	T3	+	+	+
C	Oesophageal adenocarcinoma	T3	-	+	+
D	Oesophageal adenocarcinoma	T1	-	-	+
E	Oesophageal adenocarcinoma	T3	-	-	+
F	Oesophageal adenocarcinoma	T3	-	-	+
G	Oesophageal adenocarcinoma	T3	-	-	+
H	Oesophageal adenocarcinoma	T3	-	-	+
I	Oesophageal adenocarcinoma	T2	+	-	+
J	Oesophageal adenocarcinoma	T3	+	-	+
K	Lung squamous cell carcinoma	T2	-	+	+
L	Lung squamous cell carcinoma	T1	-	-	+
M	Lung squamous cell carcinoma	T3	+	+	+
N	Pancreatic ductal adenocarcinoma	T1	+	+	+
O	Pancreatic adenocarcinoma	T4	-	-	+
P	Pancreatic adenocarcinoma	T2	-	+	+
Q	Renal oncocytoma	Benign	+	+	+
R	Renal carcinoma	T3	+	+	+
S	Renal carcinoma	Low grade	+	+	+

4.7 Discussion

The aim of this chapter was to define the TASK channel expression profile in clinically relevant human cancer cell lines in order to determine which cell lines to use as models for functional studies in subsequent chapters. To address this aim, cancer cell lines were evaluated for mRNA, protein, and functional TASK channel expression, using RT-PCR, immunofluorescent staining, and whole-cell patch clamp experiments, respectively.

The techniques used in this chapter were selected for a number of reasons (see Section 4.1). RT-PCR allowed TASK channel mRNA expression to be examined in eleven cancer cell lines. RT-PCR is a well-established tool and has been used in multiple investigations to determine if TASK channel mRNA is expressed in a range of cell types (Duprat et al., 1997, Hartness et al., 2001, Lee et al., 2012, Rajan et al., 2000). Immunofluorescent staining has been commonly utilised in published studies to identify TASK channel proteins in endogenous expression systems (Meuth et al., 2008; Plant et al., 2012; Rusznak et al., 2008). In this chapter, two antibodies were found to be suitable for the immunofluorescent detection of $K_{2P}3.1$ and $K_{2P}9.1$ channel protein. This approach enabled the detection of endogenous channel protein in cancer cell lines. To detect if TASK channel protein expression would result in functional channels, whole-cell patch clamp experiments were performed. In these experiments established pharmacological agents were used to look for an endogenous outward K^+ current with TASK channel properties (TEA-insensitive, acid/methanandamide-sensitive). Insensitivity to a broad spectrum KCh blocker (either TEA or 4-AP), followed by addition of a TASK channel inhibitor (acid or methanandamide) is a pharmacological strategy that has been previously been used by others to isolate currents with TASK-like characteristics (Gurney et al., 2003; Hsu et al., 2004; Johnson et al., 2003; Lin et al., 2004).

This study had three main experimental conclusions: (i) within a single cancer cell line multiple TASK/K_{2P} channels are expressed, (ii) in cell lines where $K_{2P}3.1$ and $K_{2P}9.1$ mRNA was detected the protein was also present, and (iii) that TASK channel protein expression does not necessarily result in the detection of a functional TASK-like current. Based on the data described in this Chapter, three cancer cell lines (A549, HCT116, and 786-0) were selected for use in subsequent experiments to assess the role of TASK

channels in cancer cell functions. Each of these conclusions will be discussed in further detail below.

4.7.1 Expression of TASK channel mRNA in human cancer cell lines

RT-PCR analysis aimed to characterise the mRNA expression of the TASK channel family in the cancer cell lines examined. These experiments identified that TASK channels were expressed in a wide range of cancer cell lines (Table 4.1). Of the eleven cancer cell lines examined, only OE21 oesophageal cells were negative for all members of the TASK channel family at an mRNA level (Table 4.1). In the cancer cell lines examined here, high levels of $K_{2P}3.1$ mRNA were observed in A549 lung and 786-0 renal cancer cell lines (Figure 4.1). This reflected the mRNA expression data reported in Chapter 3, where significant alterations were observed in lung and renal cancers (Table 3.4).

No changes in $K_{2P}9.1$ mRNA expression were detected in the cancers studied in Chapter 3, however high levels of PCR product were identified in breast (MCF-7), and colorectal (HCT116, SW480, and SW620; Figure 4.2) cancer cell lines. Expression of $K_{2P}9.1$ channels in MCF-7 cells was published during the course of this study, and found to be linked to cell migration (Lee et al., 2012). In colorectal cancers, levels of $K_{2P}9.1$ protein have been found to be higher in carcinomas compared to benign adenomas (Kim et al., 2004). This suggested that any expression changes may only occur at a protein level, but provided a clinical relevance to the detection of $K_{2P}9.1$ mRNA in colorectal cell lines.

Both $K_{2P}3.1$ and $K_{2P}9.1$ mRNA were detected in SH-SY5Y neuroblastoma cells. This was not surprising as these channels have been identified to be significantly expressed across the CNS (Introduction 1.4.1) and have been identified in both glioma and medulloblastoma brain cancer cell lines (Ernest et al., 2010; Meuth et al., 2008b).

The third member of the TASK channel family, $K_{2P}15.1$ was found to be expressed in nine of the eleven cancer cell lines examined (Figure 4.3). This result was unexpected because $K_{2P}15.1$ channels have not been shown to pass currents despite wide expression of $K_{2P}15.1$ mRNA in normal (Appendix 1) and cancer tissues (Table 3.4). Currently, there are no

known implications of K_{2P}15.1 channel expression within the cell or knowledge of how K_{2P}15.1 can influence other TASK, or other K_{2P} channel types within cancer.

In addition to the data on the expression of individual TASK channels, RT-PCR experiments identified that multiple TASK and other K_{2P} channels are expressed within a single cancer cell line (Table 4.1). These findings supported the bioinformatic data presented in Chapter 3, which found that multiple K_{2P} channels are expressed within a given cancer. As discussed previously (Result 3.3), there is no evidence to indicate how the simultaneous activity of multiple K_{2P} channels will impact the physiology or pathological potential of a cell. However, the expression of multiple K_{2P} channel subunits may result in channel heterodimers and the ability to respond to a range of internal and external stimuli, such as changes in pH and O_2.

It is important to note that the experiments described in this chapter could not quantify the level of K_{2P} channel expression in each individual cell lines. A quantitative RT-PCR (RT-qPCR) approach was tested in this thesis but was unsuccessful (see Section 4.2.11 for more details). As a result of this, the mRNA expression data presented in the chapter can only establish whether the mRNA product is present. Thus, this work identified two main questions: (i) do the levels of K_{2P} channel expression vary between cancer cell lines? and (ii) does the presence of K_{2P} channel mRNA result in protein expression? The first question could not be answered at this time (due to RT-qPCR experimental limitations), however the second question was answered in this chapter by determining if the presence of TASK channel mRNA results in protein expression.

4.7.2 Expression of TASK channel protein in human cancer cell lines

In this chapter, the identification of two commercially available antibodies (Sigma anti-K_{2P}3.1 and Santa Cruz anti-K_{2P}9.1) which could successfully detect K_{2P}3.1 and K_{2P}9.1 protein allowed the endogenous expression of TASK channel protein to be determined in cancer cell lines. The immunofluorescent data presented in this chapter showed that in cancer cell lines where K_{2P}3.1 and/or K_{2P}9.1 mRNA were detected, protein expression for the channel(s) could be observed (Table 4.2).

Quantification of the endogenous protein levels observed in this chapter was not possible, as western blot analysis proved unsuccessful (Figures 4.7 and 4.12). This may have been due to a combination of poor protein solubility and insufficient detection sensitivity. Therefore, the overall limitation of experiments performed here to characterise TASK channel expression was that no conclusions could be reliably drawn on the mRNA and protein expression levels observed between different channels and cell lines. As a result of this, the data presented in this chapter only provided information on whether the channel protein is present.

A further limitation of this work was that the subcellular localisation of $K_{2P}3.1$ and $K_{2P}9.1$ channel protein within these cancer cell lines was not examined. For this research project, establishing the precise localisation was not a priority. Therefore, future studies will be required to determine the precise subcellular localisation of $K_{2P}3.1$ and $K_{2P}9.1$ channels and if these channels are expressed on the plasma membrane. Some information on the localisation of $K_{2P}3.1$ and $K_{2P}9.1$ protein in these cells lines can be inferred based on the staining patterns observed and the published data. The majority of the channel staining detected in these cancer cell lines appeared to be cytoplasmic with little protein on the cell surface. This staining pattern may seem counterintuitive for a plasma membrane protein. However, cytoplasmic staining is commonly observed when examining K_{2P} channel protein expression, due to the presence of the channels within the secretory and endocytic pathways (Mant et al., 2013a; Mant et al., 2013b). In addition, this staining pattern has been reported in published studies examining other cancer cell lines (Pocsai et al., 2006) and was observed in this chapter when detecting GFP tagged channel proteins (Results 4.3.1.1 and 4.3.2.1). Additionally, the $K_{2P}3.1$ and $K_{2P}9.1$ staining pattern appeared to have an element of nuclear staining. This was most likely a non-specific staining artefact caused by the primary antibodies, and was only clearly observed when examining the endogenous expression due to the high sensitivity needed to detect the low levels of channel expression. Nuclear staining has been observed by others and was also considered to be a non-specific artefact (Berg et al., 2004; Callahan et al., 2004; Kovacs et al., 2005) or related to the mitochondrial expression of $K_{2P}9.1$ channels (Pocsai et al., 2006; Rusznak et al., 2008). However, other classes of KCh have been found to localise within the nuclear membrane of cancer cells, for example $K_{ir}2.3$ and $K_{ir}4.1$ channels are localised in the nuclear membrane of glioma cells compared to the plasma membrane in normal astrocytes (Olsen and Sontheimer, 2004). Therefore, the possibility of TASK channels localising on the nuclear

membranes in these cancer cell lines cannot be eliminated, since no experiments to determine the subcellular localisation were performed. In melanoma cell lines, $K_{2P}9.1$ channel protein has been found to have an altered localisation and to colocalise with the mitochondria (Pocsai et al., 2006; Rusznak et al., 2008). Mitochondrial localisation may explain the perinuclear staining pattern observed for $K_{2P}9.1$ channel protein in all the cancer cell lines examined (Figures 4.19-23). Functional expression of $K_{2P}9.1$ channels within the mitochondria has not been confirmed; however the mitochondrial function of melanoma cells was reduced when $K_{2P}9.1$ expression was knocked down (Kosztka et al., 2011). The protein staining patterns observed in this chapter along with the published evidence identifying altered KCh localisation in cancer cells, suggested that understanding the precise subcellular localisation of K_{2P} channel protein in cancer cells is an area of interest for future studies.

In A549 cells, which were found to express both $K_{2P}3.1$ and $K_{2P}9.1$ protein, we have shown that the $K_{2P}3.1$ and $K_{2P}9.1$ staining detected colocalises with markers of the secretory pathway (protein disulfide isomerase (ER) and 58 kDa Golgi protein (Golgi apparatus); Mant et al., 2013a). This staining pattern was expected for a membrane protein. Furthermore, the brighter punctate staining observed for $K_{2P}3.1$ and $K_{2P}9.1$ channels in A549 cells (Figure 4.23) colocalised with components of the endocytosis and protein recycling pathways (early endosome antigen 1 (EEA1) and Rab7/Rab11 vesicles; Mant et al., 2013a). This finding supported the hypothesis that some of the TASK channel protein detected in A549 cells had been endocytosed from the plasma membrane (Mant et al., 2013a). If this was true for the other cancer cell lines studied here, the bright punctate staining observed by immunofluorescent staining may indicate channel expression in endocytic vesicles.

In addition to channel homodimers, when both $K_{2P}3.1$ and $K_{2P}9.1$ channels are expressed within the same cells there is a potential for channel heterodimers to be formed (Czirjak and Enyedi, 2002a). Functional TASK channel heterodimers have been identified in the rat carotid body glomus cells and motor neurons (Berg et al., 2004; Kim et al., 2009). In A549, MCF-7, and SH-SY5Y cancer cell lines staining for both $K_{2P}3.1$ and $K_{2P}9.1$ channels was detected (Table 4.2). The formation of channel heterodimers within cancer cell lines was not investigated in this study. However, the subtle differences in the channel staining patterns detected by immunofluorescence may suggest that the channels have distinct

subcellular localisations. Generally, the K_{2P}3.1 staining observed was diffuse across the cytoplasm, whereas K_{2P}9.1 channel protein showed intense perinuclear fluorescence in addition to cytoplasmic staining. These differences suggested that K_{2P}3.1 and K_{2P}9.1 are not found in the same subcellular compartments and therefore that TASK channel heterodimers may not be the primary dimer formed by the channels.

The final limitation of the protein staining presented in this thesis was that no antibody which could successfully detect K_{2P}15.1 protein could be identified. Therefore, it was not possible to determine if K_{2P}15.1 mRNA results in protein production. This is a significant limitation when studying K_{2P}15.1 and has prevented any studies examining the channel protein in an endogenous setting. This practical limitation and the lack of function associated with this channel meant that the role of K_{2P}15.1 channels in cancer cells could not be further studied in this thesis.

In summary, the immunofluorescent data presented in this thesis showed that K_{2P}3.1 and K_{2P}9.1 protein was present in cancer cell lines (Table 4.2). However, at this time the precise subcellular localisation of the channels is unknown. For A549 cells, published data indicated that these channels may be functionally expressed based on their localisation in secretory and endocytic vesicles (Mant et al., 2013a). To confirm that protein expression resulted in functional channels at the cell membrane, electrophysiological data on these cells were required. Therefore, the next aim of this work was to study the electrical properties of cancer cells using whole-cell patch-clamp recordings.

4.7.3 Lack of functional TASK-like currents in A549 lung cancer cells

A549 lung cancer cells were analysed for functional TASK channel expression by whole-cell patch clamp experiments. A549 cells were selected based on the expression data in this chapter which found that both K_{2P}3.1 and K_{2P}9.1 channel protein was present (Table 4.2). Significant inhibition of the whole-cell currents by TEA and clear isolation of the TEA-insensitive outward K^+ currents suggested that there is a significant K_{2P} channel current in A549 cells. Further modulation with TASK channel inhibition failed to result in a significant reduction in the outward K^+ current. This finding was unexpected because within A549 cells there was substantial K_{2P}3.1 and K_{2P}9.1 protein expression. In addition, we

showed that both $K_{2P}3.1$ and $K_{2P}9.1$ colocalise with secretory and endocytic vesicles, suggesting that the channels are reaching the cell surface and achieving functional protein expression (Mant et al., 2013a). There are four reasons why TASK channels may reach the cell surface in A549 cells but do not result in a significant TASK-like conductance:

(i) There are only a small number of channels expressed on the plasma membrane at any given time. When expressed on the cell surface, K_{2P} channels are always open (except if modulated by external and internal stimuli) and will result in background K^+ currents (Enyedi and Czirják, 2010; Goldstein et al., 2005). Therefore, it is important to regulate the number of K_{2P} channels undergoing forward transport to the plasma membrane (Mant et al., 2011; O'Kelly and Goldstein, 2008). As this can prevent excessive K^+ efflux which could result in cell death (Dezaki et al., 2012; Lang et al., 2005; Lauritzen et al., 2003; Wang, 2004).

(ii) TASK channels reaching the cell surface may be rapidly removed by endocytosis. This is another important mechanism to regulate the number of K_{2P} channels on the surface at any one time and has been found to regulate $K_{2P}1.1$, $K_{2P}3.1$, and $K_{2P}9.1$ protein expression (Mant et al., 2013a; Matsuoka et al., 2013; Feliciangeli et al., 2010).

(iii) Expression of $K_{2P}1.1$ mRNA was also found in A549 cells and this may result in TASK channel silencing by SUMOylation. In rCGN, heterodimers formed between TASK and $K_{2P}1.1$ channels have been shown to be silenced on the cell surface by SUMOylation (Plant et al., 2012).

(iv) No experiments were conducted to establish if $K_{2P}3.1$ and $K_{2P}9.1$ channels are solely targeted to the cell surface and the proteins may be targeted to intracellular locations, such as the mitochondria. Altered targeting of $K_{2P}9.1$ protein to the mitochondria has been observed in WM35 melanoma cells (Kosztka et al., 2011; Rusznak et al., 2008). Whole-cell patch clamp experiments would not reveal any mitochondrial TASK-like channel currents and mitoplast preparations would have been required to investigate this hypothesis.

These four hypotheses were not investigated further in this thesis but represent important areas for future study. Thus, currently, from these data it can be concluded that A549 cells do not possess TASK-like currents. This may mean that other K_{2P} channels

provide the main background K^+ currents within A549 cells, for example $K_{2P}1.1$ and $K_{2P}5.1$ (Table 4.1).

It is important to appreciate the limitations of the experimental approaches used to characterise the A549 whole-cell currents in this study. The pharmacological blockers used here to target $K_{2P}3.1$ and $K_{2P}9.1$ channels are not specific and can have other targets within the cell. The ideal experiments to modulate TASK channels would have involved using targeted channel knockdowns. In this study, A549 cells were successfully transfected with a pore mutant channel that will knockdown endogenous currents (GFP tagged $K_{2P}9.1_{G97E}$; see Figure 5.8, page 287) and the cells remained viable (see Figure 5.21 for apoptosis data). However, patch clamp recordings were problematic. Despite GΩ seal recordings, transfected A549 cells show linear *I-V* relationships (pH 7.4; data not shown) indicating voltage independent ion flux or non-specific leak current.

The second limitation of the electrophysiological experiments performed in this chapter was time. Ideally, the TASK channel protein expression identified in this chapter needed to be confirmed at a functional level in all of the cancer cell lines. However, time restrictions meant that only one cancer cell line (A549 cells) was characterised during this study. Therefore, until these experiments are conducted or the cell surface expression is quantified, an assumption was made that if the channel protein is present within a cancer cell line then functional expression was possible.

4.7.4 Selection of clinically relevant model cancer cell lines with TASK channel protein expression

In order to address the overall aim of this research (Introduction 1.9) and the aim of this chapter (Section 4.1.1), clinically relevant model cancer cell lines with TASK channel expression needed to be selected. For this three cell lines were chosen: A549 lung, HCT116 colorectal, and 786-0 renal cancer cells.

A549 lung cancer cells were chosen as a clinically relevant model for both $K_{2P}3.1$ and $K_{2P}9.1$ channel expression in cancer. This selection was made for two reasons and in spite of the fact that functional TASK-like currents could not be isolated from this cell line:

(i) A549 cells express all members of the TASK channel family ($K_{2P}3.1$, $K_{2P}9.1$, and $K_{2P}15.1$) at an mRNA level, in addition protein staining was observed for $K_{2P}3.1$ and $K_{2P}9.1$ (Table 4.3). There are a number of explanations for why a TASK-like K^+ current was not observed in A549 cells (see Section 4.7.3). For example, if the majority of TASK channel protein expressed in A549 cells was intracellular this may provide functional benefits by preventing apoptosis which can result from excessive K^+ efflux (Figure 1.11; Bortner and Cidlowski, 2007; Lang et al., 2005; Wang, 2004; Yu, 2003). Therefore, modulations to TASK channel activity may still reveal interesting consequences for cellular functions in A549 cells.

(ii) Expression of TASK channels in lung cancer has a clinical relevance. $K_{2P}9.1$ and $K_{2P}3.1$ mRNA expression has been described in lung cancer tissue (Table 3.4; Mu *et al.,* 2003). Additionally, $K_{2P}9.1$ and $K_{2P}3.1$ channel protein was identified within lung squamous cell cancer tissue in this chapter (Table 4.3).

These reasons were the justification for continuing to use A549 cells in this study.

Two other clinically relevant model cell lines were selected to represent cancers that only express one functional TASK channel ($K_{2P}3.1$ or $K_{2P}9.1$). In renal clear cell carcinomas, overexpression of $K_{2P}3.1$ mRNA was identified by bioinformatic analysis (Table 3.4); in addition $K_{2P}3.1$ protein was detected in the three renal cancer tissue samples examined in this chapter (Table 4.3). In this chapter, 786-0 cells were found to only express $K_{2P}3.1$ mRNA and protein (Table 4.2). Therefore, 786-0 renal cancer cells were selected as a model cell line for $K_{2P}3.1$ channel expression in cancer. HCT116 colorectal cancer cells were selected as a model cell line for $K_{2P}9.1$ channel expression in cancer, these cells expressed $K_{2P}9.1$ channel mRNA and protein (in addition to $K_{2P}15.1$ mRNA; Table 4.2). $K_{2P}9.1$ expression in colorectal cancers has a clinical relevance, since $K_{2P}9.1$ protein overexpression has been detected in 46 % of colorectal carcinomas compared to colorectal adenomas (Kim et al., 2004). It should be highlighted that the presence of TASK channel activity was not tested in these cell lines due to time restrictions. Therefore, the selection of 786-0 and HCT116 cells was purely based on the presence of TASK channel protein (Table 4.3). Characterising the whole-cell K^+ currents of 786-0 and HCT116 cells will be a key future experiment. However, continuing to use 786-0 and HCT116 cells in this study may have

revealed any cancer cell functions which are related to the expression of TASK channel protein.

In summary, despite the limitations in the expression data presented in this chapter and the ambiguity surrounding whether $K_{2P}3.1$ and $K_{2P}9.1$ channels are functional in the cancer cell lines studied. The identification of three clinically relevant model cell lines, with characterised TASK channel mRNA and protein expression, will allow any consequences for cellular functions which can be related to the expression of TASK channels in cancer to be investigated further. Consequently, this was the focus of the following chapters.

4.8 Publications arising

Data from figures 1.1, 1.2, 1.5, 1.9 B, 1.21, and 1.27 A are published in: Mant, A., Williams, S. & O'Kelly, I. 2013. Acid sensitive background potassium channels $K_{2P}3.1$ and $K_{2P}9.1$ undergo rapid dynamin-dependent endocytosis. *Channels,* 7**,** 0-14.

Chapter 5

Results

Do TASK channels play a role in cancer cell functions?

5.1 Introduction

The primary aim of the work presented in this chapter was to establish the impact of TASK channel protein expression in cancer cell lines on three cellular functions (proliferation, apoptosis, and migration). The second aim of the study was to determine if any functional roles can be linked to the differences in TASK channel protein expression identified within three model cell lines: A549, HCT116, and 786-0 (Chapter 4). Three model cell lines were chosen for further studies based on their differential expression of TASK channel protein (Table 4.3) so that channel specific roles could be investigated. Two cancer cell lines were selected as models which only express one functional TASK channel: 786-0 and HCT116 cells, which express $K_{2P}3.1$ and $K_{2P}9.1$ protein, respectively. Of note, these cell line selections were based on protein expression data and a clinical relevance, TASK channel activity was not investigated in these cell lines, therefore it is not known if the channels are expressed on the plasma membrane or if they are functional. Despite these limitations, it was worthwhile investigating if TASK channel modulation has consequences for cellular functions and to determine if there were potential roles for TASK channel activity in the model cell lines chosen. A549 cells were selected as a clinically relevant cell line which expressed both $K_{2P}3.1$ and $K_{2P}9.1$ protein. A549 cells were extensively characterised in Chapter 4 and no TASK-like currents could be isolated from the cells following whole-cell patch clamp experiments. Despite this finding, A549 cells may still provide information on the functional implications of $K_{2P}3.1$ and $K_{2P}9.1$ expression in cancer, therefore they were still utilised in this chapter for a number of reasons (see discussion in Section 4.7.3). For example, the TASK channels in A549 cells might be localised to intracellular membranes, such as the mitochondrial membranes. Therefore, the expression of $K_{2P}3.1$ and $K_{2P}9.1$ protein in A549 cells may still have functional implications. Subcellular localisation experiments were not performed in this thesis, therefore this and related hypotheses are speculative and based on the published knowledge of $K_{2P}9.1$ channels in cancer (Kosztka et al., 2011; Rusznak et al., 2008).

Published studies have indicated that $K_{2P}9.1$ channel activity can have multiple functional roles within cancer cells, and that the functional impact may depend on the cancer cell type (Introduction 1.8). Advantageous cellular functions which result from $K_{2P}9.1$ expression and activity include promotion of cell proliferation in $K_{2P}9.1$ expressing C8 fibroblasts, Ben lung cancer cells, and WM35 melanoma cells (Kosztka et al., 2011; Pei et al.,

2003). Additionally, in ovarian cancer cell lines and $K_{2P}9.1$ expressing C8 fibroblasts, $K_{2P}9.1$ activity has been found to resist apoptotic stimuli (Innamaa et al., 2013b; Pei et al., 2003).

$K_{2P}9.1$ activity has not always been found to promote beneficial cellular functions. For example, using isoflurane to increase K_{2P} channel activity in $K_{2P}3.1$ and $K_{2P}9.1$ expressing glioma cell lines was found to promote cell death (Meuth et al., 2008b). Addtionally, in MDA-MB-231 breast cancer cells, $K_{2P}9.1$ channel activity reduced cell migration (Lee et al., 2012). From these data, it is unclear whether $K_{2P}9.1$ channel activity is advantageous or detrimental in cancer cells, or what causes $K_{2P}9.1$ activity to have cell-specific functional impacts. It is likely that this effect is determined by the other classes of ion channel expressed within the cancer cells (see Table 1.3 for an overview of ion channels which have been linked to cancer hallmark functions). However, a limitation of the published studies examining the role of K_{2P} channels in cancer is that only one TASK channel subtype (usually $K_{2P}9.1$) and cancer type was assessed. This limitation has prevented any conclusions being drawn on whether the expression of multiple TASK channels can influence the role of $K_{2P}9.1$ channels in cancer cells. The data presented in this chapter aimed to investigate this hypothesis by utilising the three model cancer cell lines selected in Chapter 4, which represent different cancer types and have distinct TASK channel expression patterns (described above), including the expression of multiple TASK channel subtypes (A549 cells).

Experimental tools that can modulate endogenous TASK channel expression or activity were required to address the overall aim of this chapter. For this, the specificity of RNA interference (RNAi: using siRNA and siRNA plasmids) targeted against $K_{2P}3.1$ and $K_{2P}9.1$ channels was assessed using immunofluorescent staining and RT-PCR, which were techniques established in Chapter 4 for the detection of TASK channel expression. A targeted approach using siRNA was tested, as this would reduce channel expression within cancer cell lines with minimal off-target effects. Experiments using RNAi revealed that the commercial tools available at this time were not suitable to reduce TASK channel expression. Therefore, a second approach was examined using channel constructs with a mutated pore domain. Mutation of the pore domain within K_{2P} channels disrupts the functionality of the channel and has been found in published studies to reduce WT channel activity when expressed in either heterologous or endogenous systems (Pei et al., 2003; Voloshyna et al., 2008). The constructs generated in this study (GFP-$K_{2P}3.1_{G97E}$ and GFP-$K_{2P}9.1_{G97E}$) were characterised by whole-cell patch clamp experiments. Whole-cell patch

clamp experiments revealed that WT GFP-K_{2P}3.1 channels are non-functional as the channels failed to achieve cell surface expression. Therefore, expression of GFP-K_{2P}3.1 channels was not used further in this study. GFP-$K_{2P}9.1_{G97E}$ channels were shown to be non-functional compared to WT GFP-K_{2P}9.1, therefore based on published work it is predicted that this channel would reduce endogenous K_{2P}9.1 channel activity (Pei et al., 2003). Producing polyclonal transfected cell populations, using antibiotic selection pressures, was examined as a technique to modulate endogenous K_{2P}9.1 channel expression in A549 and HCT116 cells using GFP-$K_{2P}9.1_{G97E}$. This technique was used as a method to rapidly select for cells expressing GFP-$K_{2P}9.1_{G97E}$ and to produce a heterogeneous transfected cell population which could then be used for functional assays. A loss of the channel expression was observed during the culture period required for selection of the transfected cell population. This finding meant that transfection of GFP-$K_{2P}9.1_{G97E}$ was not suitable for assays that did not allow for direct selection of GFP positive cells, such as proliferation and migration assays.

Because neither the use of RNAi nor mutated channel expression were suitable strategies to assess the contribution of endogenous TASK channels to cancer cell function, a pharmacological approach was employed. Three available pharmacological agents were selected: methanandamide, genistein, and ruthenium red. These published inhibitors of TASK channels are not without limitations: the agents are not specific and can have multiple targets within the cell (see Introduction 1.4.2.6 for a description of these targets). Therefore, the cell function data produced in this chapter needs to be interpreted with the limitations of using TASK channel inhibitors in mind (these are discussed further in Section 5.4.1).

Once a strategy for TASK channel modulation was established, assays to determine the effect of channel inhibition on cancer cell functions could be performed. Three key cancer hallmark functions, proliferation, apoptosis, and migration, were assessed in this chapter. These hallmark functions were selected for study because K_{2P} channel activity had previously been linked to these functions in published studies (Introduction 1.7).

MTS assays were used to assess cell proliferation. This approach allows for multiple cell lines and inhibitor concentrations to be assessed in a comparable manner. This assay has been used in multiple studies to determine the role of K_{2P} channels in cell growth

(Innamaa et al., 2013b; Pei et al., 2003; Voloshyna et al., 2008). However, MTS assays are not without limitations and this assay does not provide a direct read out of cell growth and the resulting absorbance values are a measure of cell numbers. Therefore, it cannot be distinguished whether an observed reduction of cell numbers is caused by reduced cell growth or increased cell death. To address this limitation of MTS assays and to determine if TASK channel inhibition impacts on cell death, flow cytometry with annexin V staining was used to perform apoptosis assays. The advantage of annexin V staining was that non-permeabilised cells were required, therefore living cells could be stained and allowed for a rapid time period (< 1 h) between cell harvesting and data collection (Zhang et al., 1997). This assay has been commonly utilised to determine the role of K_{2P} channels in cell death (Innamaa et al., 2013b; Meuth et al., 2008). The final cell function assessed in this chapter was cell migration, for this wound healing assays were performed. Wound healing assays are a basic measure of cell migration and provide data on the motility of the cells in response to channel modulation. A better measure of cell migration would have been to use Transwell assays or organotypic cultures, which require cell movement through a membrane or cell layer. However, wound healing assays were selected as they are easy to perform, require little specialised equipment, and provide an initial measure of cell migration (Liang et al., 2007). Additionally, wound healing assays have been previously used to determine the role of K_{2P}9.1 channels in breast cancer cell migration (Lee et al., 2012). Therefore, in summary the overall and specific aims of this chapter are as follows:

5.1.1 Aims

To establish (i) the functional impact of TASK channel inhibition on the model cancer cell lines (A549, HCTT16, and 786-0) selected in Chapter 4, and (ii) to determine any functional roles which can be linked to differences in TASK channel protein expression within the model cell lines. To achieve this, this work had three specific aims:

1. To establish if commercially available RNAi tools were suitable to reduce endogenous TASK channel expression in cancer cell lines.
2. To assess if a mutation in the pore domain of TASK channels resulted in non-functional channels which could be used to knockdown endogenous channel activity in cancer cell lines.

3. To determine the effect of TASK channel inhibition on three cancer cell functions in the model cancer cell lines (A549, HCT116, and 786-0) selected in Chapter 4. For this, cell proliferation, apoptosis, and migration assays were performed.

5.2 Tools available to modulate endogenous TASK channel expression

In order to assess functional roles of TASK channel expression in cancer cell lines, tools to modulate native channel expression and/or function needed to be characterised. For this, a series of experiments were conducted to assess the suitability of RNAi to knockdown TASK channel expression (Result 5.2.1) and channels with mutated pore domains to knockdown channel activity (Result 5.2.2).

5.2.1 Use of RNA interference to knockdown TASK channel expression

The ability of commercially available small interfering RNA (siRNA, Qiagen; Method 2.3.4) to reduce native $K_{2P}3.1$ and $K_{2P}9.1$ channel expression in A549 and HCT116 cancer cells, respectively, were characterised. A549 and HCT116 cancer cell lines were tested since they were selected as model cancer cell lines in Chapter 4 and would be used in subsequent functional studies. Due to time restrictions only two of the three model cell lines selected in this thesis were tested for siRNA optimisation experiments. For siRNA optimisation experiments, cells were transfected with 50 nM siRNA (Method 2.4.4.2) and the TASK channel protein expression was assessed after 72 h, by immunofluorescent staining in combination with confocal microscopy (Methods 2.5.3 and 2.6.2). A time point of 72 h was selected to give sufficient time for knockdown of TASK channel protein expression. To quantify the level of TASK channel protein staining in untransfected (UT) and siRNA transfected cells, the mean fluorescence intensity of each image was analysed using the LAS AF Lite software (Leica; Method 2.6.2).

In A549 cells transfected with *KCNK3* siRNA, no reduction in $K_{2P}3.1$ protein staining was detected (Figure 5.1 ii; A) compared to the native $K_{2P}3.1$ protein expression (Figure 5.1

i; A). Quantification of the mean fluorescence intensity for $K_{2P}3.1$ protein staining showed that siRNA transfected cells had almost twice the level of $K_{2P}3.1$ fluorescence compared to UT cells (Figure 5.1 iii). An altered morphology of the siRNA transfected A549 cells was observed and was likely to be caused by the reduced cell density within the field of view (Figure 5.1 ii). Transfection of HCT116 cells with *KCNK9* siRNA resulted in comparable levels of $K_{2P}9.1$ protein staining in both transfected (Figure 5.2 ii) and UT cells (Figure 5.2 i).

A limitation of using siRNA was that the transfection efficiency could not be directly quantified, therefore commercially available plasmids encoding TASK channel siRNA and GFP (abm®, Method 2.3.4) were utilised. This allowed direct quantification of the siRNA transfection in cancer cell lines. A549 and HCT116 cells were successfully transfected with siRNA plasmids (confirmed by the presence of GFP fluorescence; data not shown), and polyclonal transfected cell lines were created using puromycin selection (Method 2.4.4.3). The polyclonal siRNA transfected cells were harvested and the mRNA expression was analysed by RT-PCR, utilising the same conditions as in Chapter 4 (Table 2.12 and Method 2.3.12).

In A549 cells, $K_{2P}3.1$ mRNA expression was assessed in UT, *KCNK3* siRNA plasmids transfected (pool of four separate plasmids used), and a scrambled siRNA plasmid transfected cells (Figure 5.3). $K_{2P}3.1$ mRNA product (430 bp) was detected by RT-PCR under all three conditions and in the positive pooled cDNA control (Figure 5.3 A). Quantification of $K_{2P}3.1$ mRNA showed that there was no difference between the level of expression in endogenous cells and *KCNK3* siRNA transfected cells, and that there was a slight increase in $K_{2P}3.1$ mRNA when cells were transfected with the control scrambled siRNA (Figure 5.3 C). Comparable experiments were performed to assess $K_{2P}9.1$ knockdown in HCT116 cells (Figure 5.4), $K_{2P}9.1$ mRNA product (413 bp) was detected by RT-PCR under all three conditions and in the positive pooled cDNA control (Figure 5.4 A). Quantification of $K_{2P}9.1$ mRNA revealed that in *KCNK9* siRNA plasmids transfected cells there was a 50 % increase in $K_{2P}9.1$ mRNA compared to the endogenous expression (Figure 5.4 C). No differences were observed between native and the scrambled siRNA plasmid transfected HCT116 cells (Figure 5.4 C).

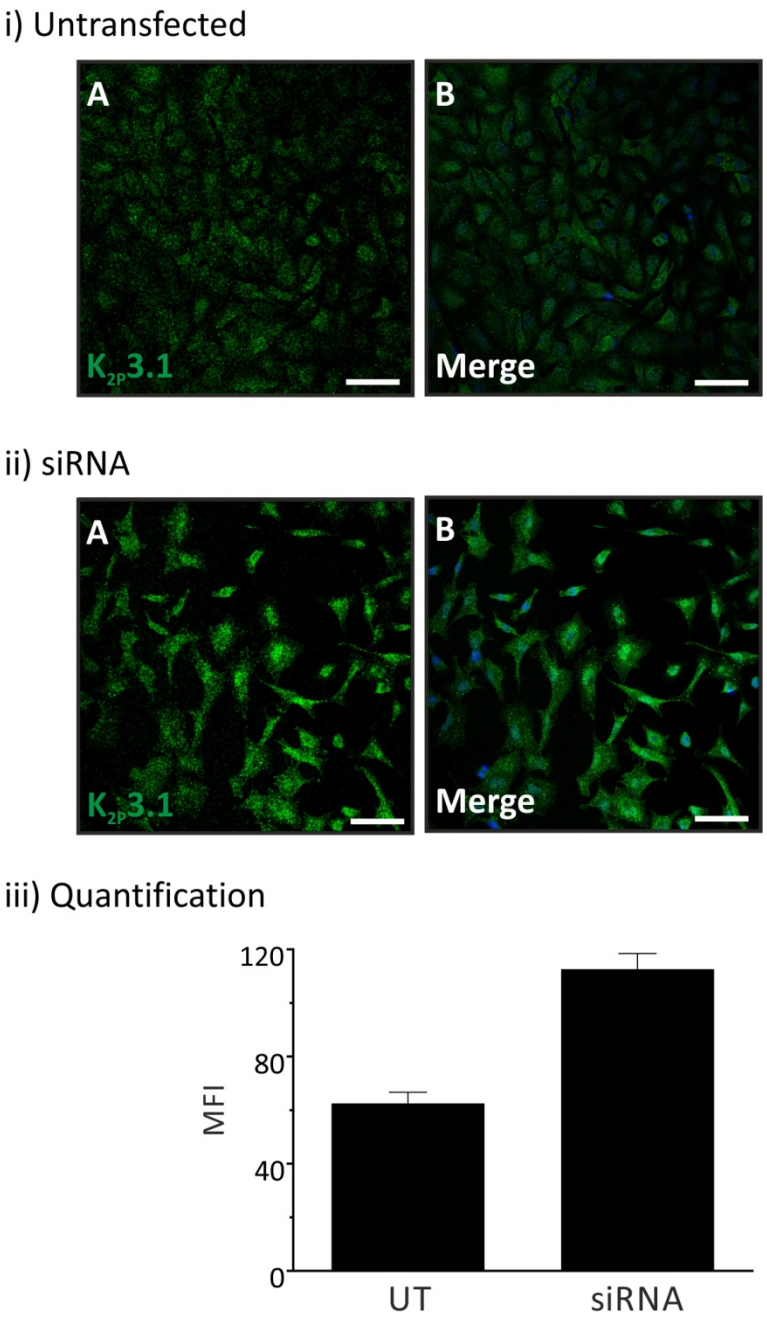

Figure 5.1: $K_{2P}3.1$ protein is detected following siRNA transfection in A549 lung cancer cell line

Singe confocal Z-slices showing $K_{2P}3.1$ staining in A549 cells, 72 h post transfection in (i) untransfected (UT) and (ii) *KCNK3* siRNA transfected cells (siRNA).
A) Immunolabelling for $K_{2P}3.1$ protein (Sigma anti-$K_{2P}3.1$).
B) Overlapped fluorescence with DAPI nuclear stain.
All scale bars are 20 µm.

iii) Quantification of $K_{2P}3.1$ expression.
Mean fluorescence intensity (MFI + SEM) from randomly selected region of interest (ROI) transects across 20 cells in two fields of view for UT and siRNA transfected A549 cells.

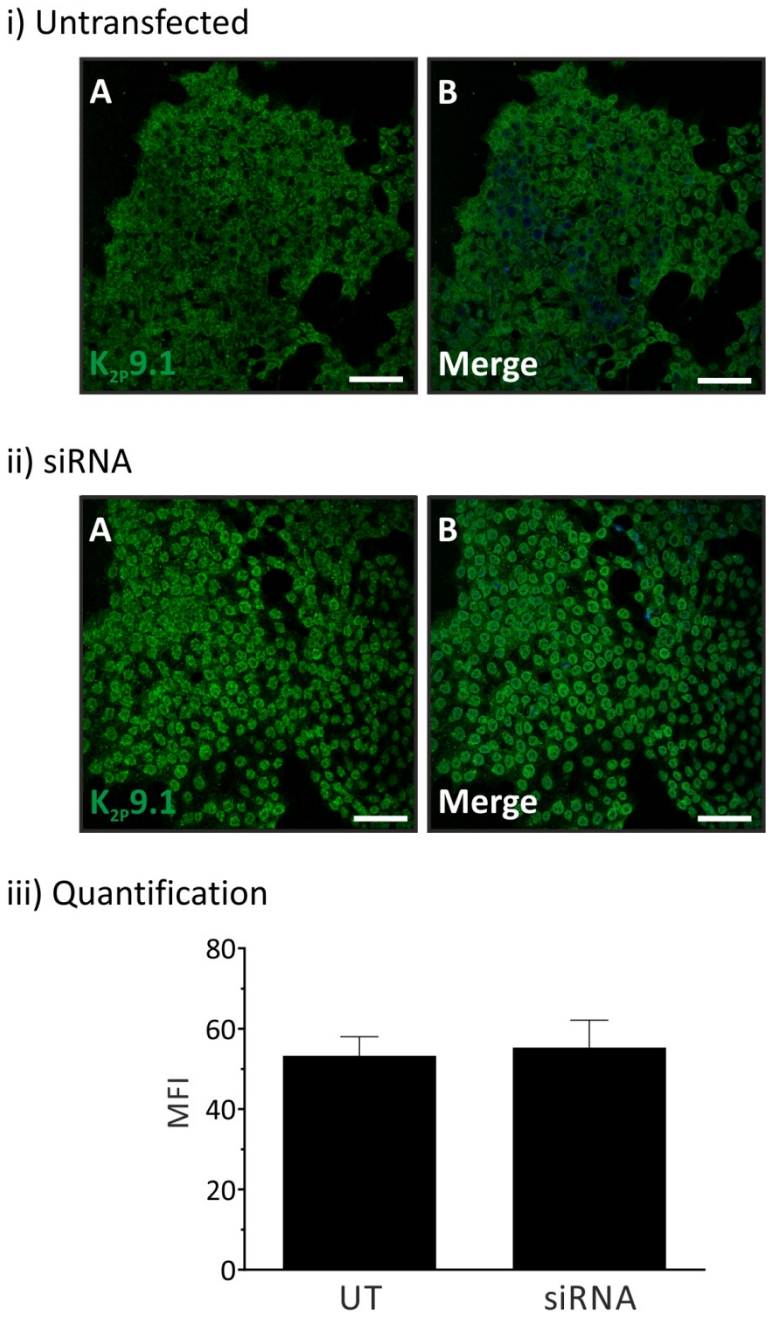

Figure 5.2: K_{2P}9.1 protein detected following siRNA transfection in HCT116 colorectal cancer cell line

Singe confocal Z-slices showing K_{2P}9.1 staining in HCT116 cells, 72 h post transfection in (i) untransfected (UT) and (ii) *KCNK9* siRNA transfected cells (siRNA).
A) Immunolabelling for K_{2P}9.1 protein (Santa Cruz anti-K_{2P}9.1).
B) Overlapped fluorescence with DAPI nuclear stain.
All scale bars are 20 µm.

iii) Quantification of K_{2P}9.1 expression.
Mean fluorescence intensity (MFI + SEM) of three different fields of view was calculated for UT and siRNA transfected HCT116 cells.

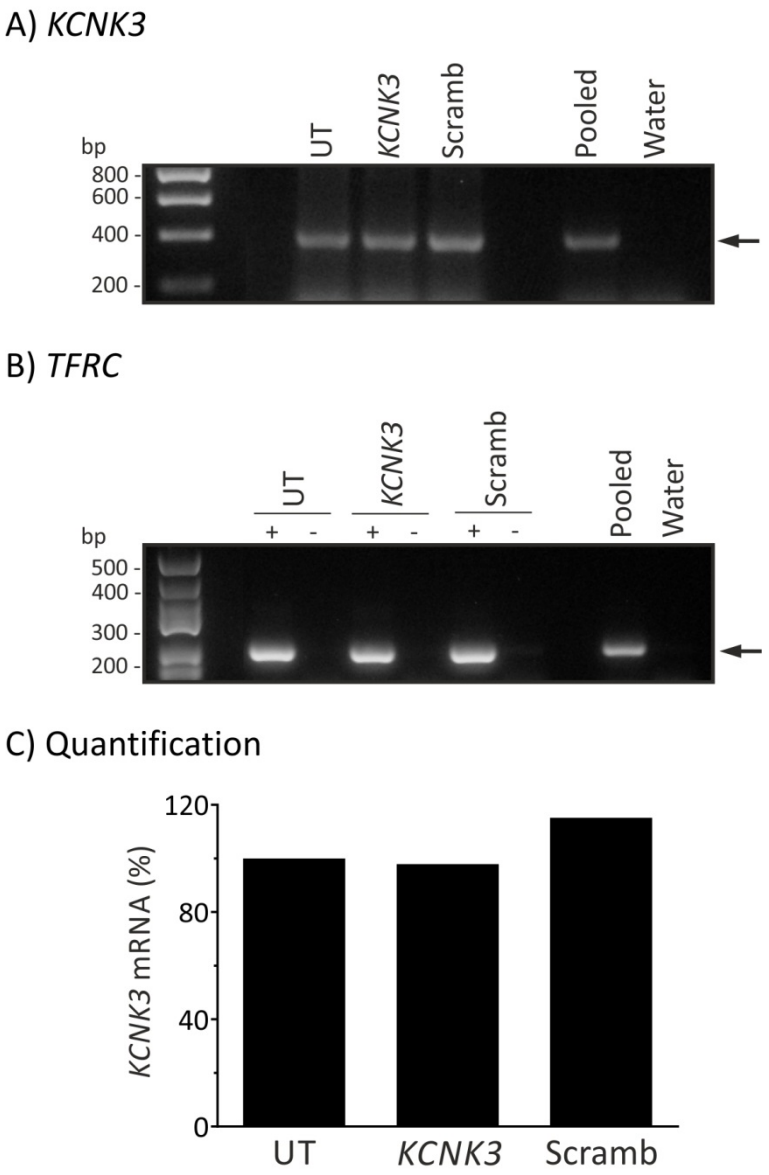

Figure 5.3: $K_{2P}3.1$ mRNA detected following polyclonal siRNA plasmid expression in A549 lung cancer cell line

$K_{2P}3.1$ mRNA expression detected in untransfected (UT) and cells transfected with either *KCNK3* siRNA or scrambled siRNA (scramb) plasmids.
Pooled cDNA and water were run as positive and a no cDNA template control respectively.

A) $K_{2P}3.1$ mRNA expression: PCR products were amplified using KCNK3F and KCNK3R primers and have a predicted size of 430 bp, indicated by an arrow.

B) Transferrin receptor (TFRC) mRNA expression: PCR products were amplified using TFRC-F and TFRC-R primers and have a predicted size of 252 bp, indicated by an arrow.

C) Quantified $K_{2P}3.1$ mRNA expression
$K_{2P}3.1$ mRNA expression is shown as percentage of UT cells.

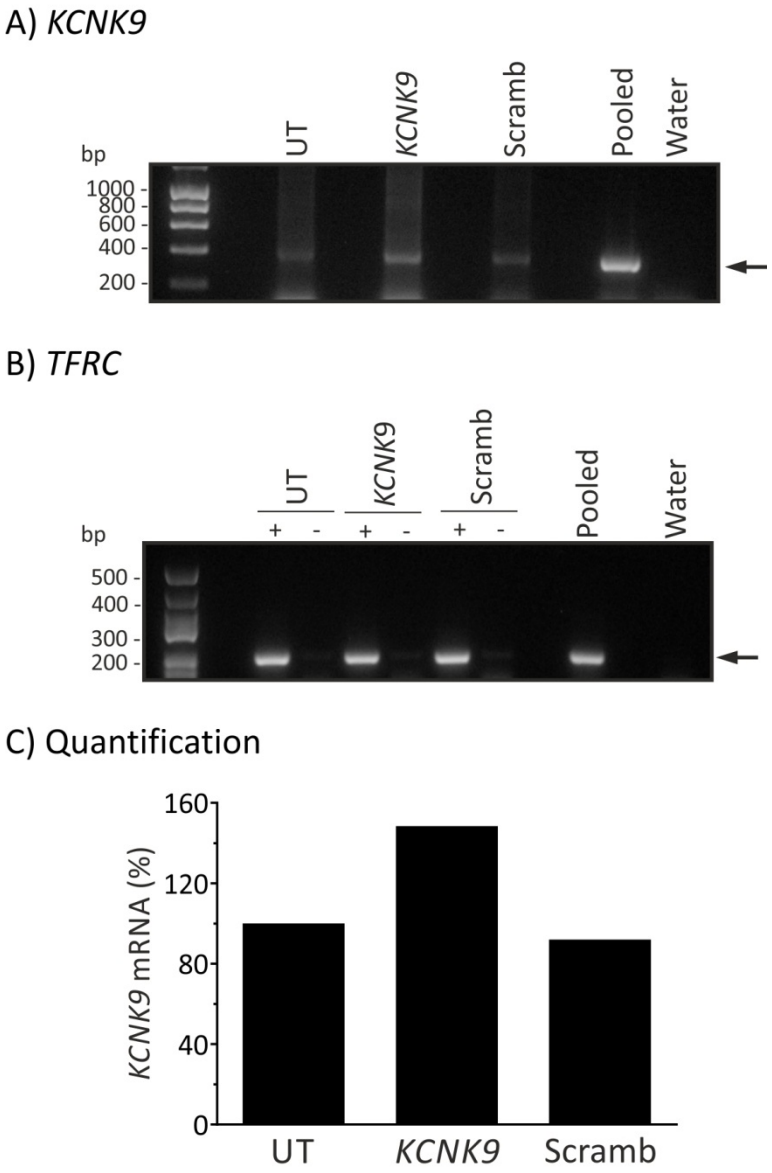

Figure 5.4: $K_{2P}9.1$ mRNA detected following polyclonal siRNA plasmid expression in HCT116 colorectal cancer cell line

$K_{2P}9.1$ mRNA expression detected in untransfected (UT) and cells transfected with either *KCNK9* siRNA or scrambled siRNA (scramb) plasmids.
Pooled cDNA and water were run as positive and a no cDNA template control respectively.

A) $K_{2P}9.1$ mRNA expression: PCR products were amplified using KCNK9F and KCNK9R primers and have a predicted size of 413 bp, indicated by an arrow.

B) Transferrin receptor (TFRC) mRNA expression: PCR products were amplified using TFRC-F and TFRC-R primers and have a predicted size of 252 bp, indicated by an arrow.

C) Quantified $K_{2P}9.1$ mRNA expression
$K_{2P}9.1$ mRNA expression is shown as percentage of UT cells.

To date, there have only been two published studies which have successfully used siRNA knockdowns to reduce TASK channel expression in cancer cell lines, and neither study used the constructs examined here. To successfully reduce $K_{2P}9.1$ mRNA and protein expression in MCF-7 cells, Lee et al. (2012) required 100 nM of *KCNK9* siRNA (Dharmacon). In WM35 melanoma cells, a siRNA plasmid system successfully decreased $K_{2P}9.1$ mRNA and protein 48 h post transfection (Kosztka et al., 2011). From the current study, it can be concluded that TASK channel expression cannot be knocked down at an mRNA or protein level using the siRNA constructs tested.

5.2.2 Generation of pore mutant TASK channel constructs

The failure of commercially available RNAi tools to reduce TASK channel expression (Result 5.2.1) meant that an alternative strategy to modulate TASK channels was required. For this, $K_{2P}3.1$ and $K_{2P}9.1$ channels with mutated pore domains were generated. This strategy was selected because mutation of the selectivity filter within a KCh was predicted to disrupt channel function by preventing K^+ ion transport. This approach has been found to be successful in cell lines with native $K_{2P}9.1$ channel expression, where expression of $K_{2P}9.1$ channels with a mutated pore domain has been shown to have a dominant negative effect and to create a functional knockdown (Pei et al., 2003). To create TASK channels with a mutated pore domain, site-directed mutagenesis was used to mutate glycine 97 (G97; the second glycine residue in the first pore domain (GYG)) into a glutamate (G97E; Figure 5.5 and Method 2.3.5). This successfully generated mutant GFP tagged human $K_{2P}3.1$ and $K_{2P}9.1$ channels (GFP-$K_{2P}3.1_{G97E}$ and GFP-$K_{2P}9.1_{G97E}$), confirmed by DNA sequencing (Appendix 4). Pei et al. (2003) utlised a similar mutation of $K_{2P}9.1$ to the one created here, which disrupted the first glycine in the first pore domain (G95E). Pei et al. found that when $K_{2P}9.1_{G95E}$ cRNA was co-injected into *Xenopus* oocytes alongside the WT channel the recorded currents were 60 % lower than the WT alone, this showed that this mutant had a dominant negative effect on the WT channel function (Pei et al., 2003). Furthermore, when both pore domains were disrupted in $K_{2P}2.1$ channels (G161E and G268E) and the mutant channel was expressed in PC3 prostate carcinoma cells it abolished native $K_{2P}2.1$ channel currents (Voloshyna et al., 2008). To establish if the mutation of G97 disrupted the function of $K_{2P}3.1$ and $K_{2P}9.1$ channels, the whole-cell currents produced by HEK293 cells expressing the mutant channel were compared to the WT channel (Method 2.8.2). For whole-cell patch clamp experiments, a voltage step protocol (-100 to + 90 mV, 10 mV increments, for

50 ms duration) was applied to transfected HEK293 cells using buffer conditions optimised to record outward K^+ currents (Table 2.31).

Prior to this study, whether or not functional GFP tagged $K_{2P}3.1$ (GFP-$K_{2P}3.1$) channels reached the cell surface had not been characterised by electrophysiology or immunofluorescence (Table 2.3). Therefore, before experiments to characterise GFP-$K_{2P}3.1_{G97E}$ channel function were conducted, the functionality of WT GFP-$K_{2P}3.1$ was compared to untagged human $K_{2P}3.1$, which was known to be functional based on published work (Table 2.3; Mant et al., 2011; O'Kelly et al., 2002). Expression of untagged human $K_{2P}3.1$ in HEK293 cells produced instantaneous currents which are non-inactivating throughout the voltage pulse, as expected for a voltage-insensitive background potassium channel (Figure 5.6 A). Thus, the *I-V* relationship of untagged $K_{2P}3.1$ was typical for a K_{2P} channel and showed outward rectification in the physiological K^+ gradients used for recordings (150 mM $[K^+]_{in}$ and 5 mM $[K^+]_{ex}$, see Table 2.31; Figure 5.6 B). Additionally, the currents produced by untagged $K_{2P}3.1$ expression at pH 7.8 were different to UT cells, with a significantly larger current amplitude at +60 mV ($p < 0.0001$; Figure 5.6 C) and hyperpolarised reversal potential (-60.3 ± 2.4 compared to -39.1 ± 3.2 mV ($p < 0.05$); Figure 5.6 B). This shift showed that there was higher K^+ flux in transfected cells and was consistent with the published literature on this channel (Mant et al., 2011; O'Kelly et al., 2002). As predicted for a TASK channel, the untagged $K_{2P}3.1$ currents were inhibited by exposure to external acidification which caused a significant positive shift in the reversal potential (from -60.3 ± 2.4 mV to -30.0 ± 6.0 mV ($p < 0.05$); Figure 5.6 B).

Expression of WT GFP-$K_{2P}3.1$ in HEK293 cells failed to produce currents that were significantly different from UT cells (Figure 5.6). Consistent with this observation, the reversal potential of cells expressing GFP-$K_{2P}3.1$ was comparable to UT cells (-34.8 ± 8.5 mV for GFP-$K_{2P}3.1$ compared to -39.1 ± 3.2 mV for UT; $p = 0.95$) and significantly different from untagged $K_{2P}3.1$ expressing cells ($p < 0.05$; Figure 5.6 B). This suggested that there was no increase in K^+ ion flux in GFP-$K_{2P}3.1$ expressing cells and was supported by the lower current amplitude in these cells which was similar to UT cells ($p = 0.10$; Figure 5.6 C). In addition, the GFP-$K_{2P}3.1$ currents showed no inhibition following extracellular acidification which further suggested that GFP-$K_{2P}3.1$ was a non-functional TASK channel (Figure 5.6 C).

A) Location of G97

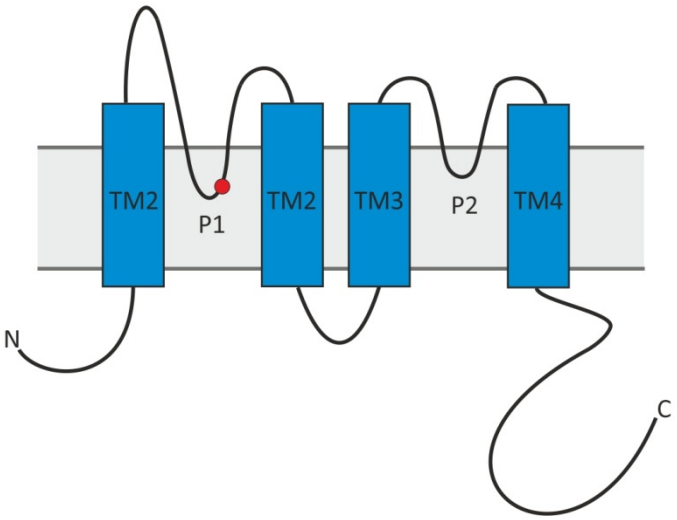

B) Pore mutant channels

WT $K_{2P}3.1$	60	PHKAGVQWRFAGSFYFAITVITTIGYGHAAPSTDGGKVFC	110
$K_{2P}3.1_{G97E}$	60	PHKAGVQWRFAGSFYFAITVITTIGY**E**HAAPSTDGGKVFC	110
WT $K_{2P}9.1$	60	PHRAGVQWKFAGSFYFAITVITTIGYGHAAPGTDAGKAFC	110
$K_{2P}9.1_{G97E}$	60	PHRAGVQWKFAGSFYFAITVITTIGY**E**HAAPGTDAGKAFC	110

Figure 5.5: Pore mutant channels

A) Cartoon representing a channel subunit, highlighting the location of glycine 97 (G97) in red.

B) Partial amino acid sequence alignments of wild type (WT) and pore mutant (G97E) human $K_{2P}3.1$ and $K_{2P}9.1$. The channel pore selectivity sequence is underlined and mutated glutamate (E) is shown in bold. The external domain is highlighted in light grey and the pore-forming loop in darker grey.

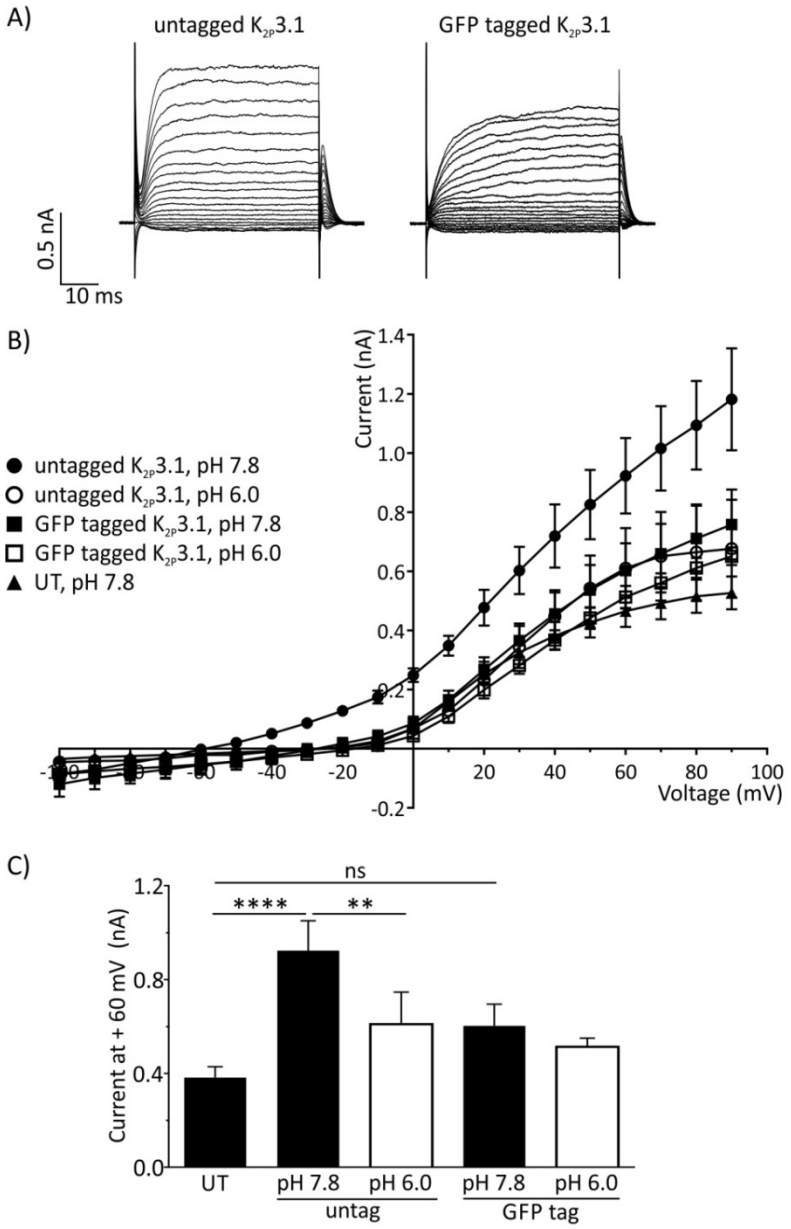

Figure 5.6: Electrophysiological properties of untagged and GFP tagged $K_{2P}3.1$

Whole-cell recordings from HEK293 cells transiently expressing either untagged $K_{2P}3.1$ co-transfected with GFP (untag; 2 µg untagged $K_{2P}3.1$ and 0.5 µg GFP DNA) or GFP tagged wild type $K_{2P}3.1$ (GFP tag; 2 µg GFP-$K_{2P}3.1$ DNA). Cells were analysed 24 h post-transfection and ≈70 % of cells were transfected (identified by GFP fluorescence). Currents were evoked by voltage steps from -100 to +90 mV in 10 mV increments, for 50 ms duration.

A) Representative recordings from cells expressing untagged $K_{2P}3.1$ or GFP tagged $K_{2P}3.1$, at pH 7.8.

B) *I-V* relationship for both channels at pH 7.8 and pH 6.0, in addition to untransfected (UT) cells at pH 7.8. The data shown are the average of n ≥ 5 cells, ± SEM.

C) Average current (+ SEM) elicited at +60 mV voltage step for all conditions (n ≥ 5 cells).

Statistical significance was calculated using a one-way ANOVA, with Dunnett's multiple comparisons post-hoc test (**** $p < 0.0001$). The comparisons performed are indicated by horizontal lines.

To assess if the lack of functionality of GFP-K_{2P}3.1 was due to improper trafficking, we sought to determine the subcellular localisation of the channel (experiments performed by Dr A. Mant; Figure 5.7). As TASK channels are membrane proteins, expression is expected within the secretory pathway (ER and Golgi apparatus) as well as on the plasma membrane. The subcellular localisation of GFP-K_{2P}3.1 was determined by examining colocalisation (fluorescence intensity overlap) between the GFP tagged channel (panel A) and staining for a compartment marker protein (panel B): ER (calnexin staining; Figure 5.7 i), Golgi apparatus (58K Golgi protein; Figure 5.7 ii), and plasma membrane (lectins; Figure 5.7 iii).

GFP-K_{2P}3.1 colocalised with the ER resident protein calnexin (Figure 5.7 i), as fluorescence overlap was observed between calnexin staining and GFP fluorescence in GFP-K_{2P}3.1 expressing COS-7 cells. The localisation of GFP-K_{2P}3.1 was also compared to the Golgi apparatus resident 58K Golgi protein (Figure 5.7 ii), with moderate colocalisation detected between 58K Golgi staining and GFP fluorescence (Figure 5.7 ii; C). This demonstrated that a proportion of GFP-K_{2P}3.1 undergoes forward trafficking from the ER to the Golgi apparatus. Although, without quantifying further transects and fields of view the proportion of GFP-K_{2P}3.1 in the Golgi apparatus cannot be determined. When colocalisation was examined between GFP-K_{2P}3.1 and cell surface staining for lectins (Figure 5.7 iii), no signal overlap was observed (Figure 5.7 iii; C). This demonstrated that GFP-K_{2P}3.1 was not expressed in the plasma membrane of COS-7 cells.

These experiments revealed that GFP-K_{2P}3.1 was not localised to the plasma membrane, although some of the protein undergoes forward transport from the ER to the Golgi apparatus. Therefore, it is likely that the lack of GFP-K_{2P}3.1 channel activity was due to disrupted forward trafficking. This may be caused by the GFP protein or the linker region between the two proteins disrupting trafficking motifs or preventing recruitment of accessory proteins needed for K_{2P}3.1 transport, such as 14-3-3β (O'Kelly et al., 2002). Since WT GFP-K_{2P}3.1 channels cannot achieve functional surface expression, it was unlikely that expression of GFP-$K_{2P}3.1_{G97E}$ would modulate endogenous K_{2P}3.1 channel function. Consequently, this construct was not examined further in this thesis. From this point, whenever expression of WT K_{2P}3.1 channels was used, the untagged K_{2P}3.1 construct was transfected alongside GFP in separate plasmids.

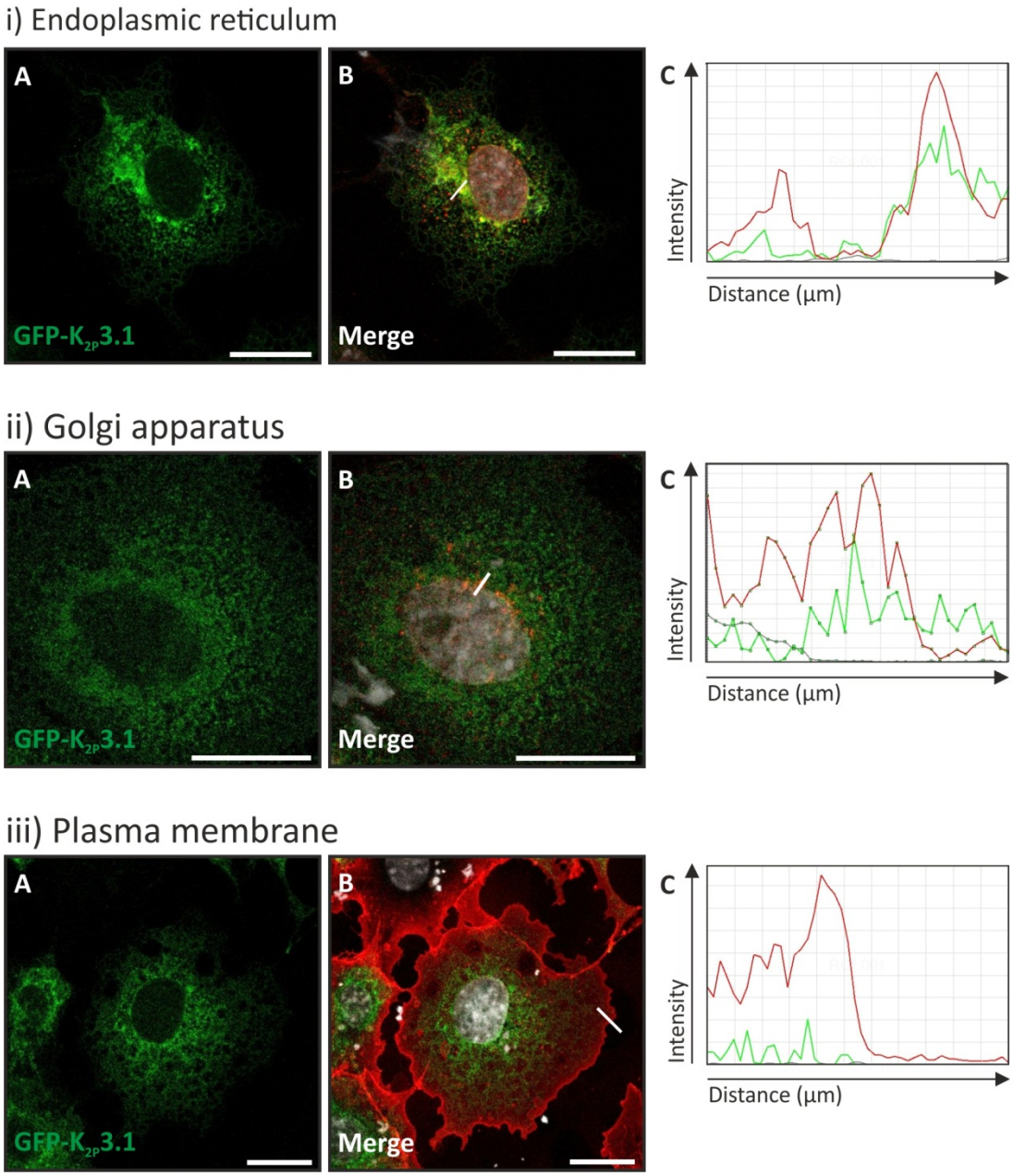

Figure 5.7: Subcellular localisation of human GFP tagged $K_{2P}3.1$
Confocal Z-slice images showing the subcellular localisation of GFP-$K_{2P}3.1$ expressed in COS-7 cells.
i) Endoplasmic reticulum staining, labelling for ER resident protein calnexin (shown in red).
ii) Golgi apparatus staining, labelling for 58K Golgi resident protein (shown in red).
iii) Plasma membrane staining, labelling for lectins (shown in red).

A) Transfected GFP-$K_{2P}3.1$ detected by GFP fluorescence signal.
B) Merge of GFP-$K_{2P}3.1$ (green), compartment marker (red) and DAPI nuclear stain (grey).
C) Quantification of fluorescence intensity across a transfect line (white line on panel B) of GFP fluorescence (green line) and compartment marker (red line). Colocalisation results in overlap of the intensity peaks for the two signals.

All scale bars are 20 µm.

Unlike GFP-K_{2P}3.1, the subcellular localisation of WT GFP-K_{2P}9.1 had been shown to be correct prior to this study (Table 2.3), and when whole-cell patch clamp experiments were performed this construct functioned as predicted for a TASK channel (Figure 5.8). WT GFP-K_{2P}9.1 expressing HEK293 cells produced instantaneous currents that are non-inactivating throughout the voltage pulse (Figure 5.8 A). The *I-V* relationship of GFP-K_{2P}9.1 was typical of a K_{2P} channel and showed outward rectification in the physiological K^+ gradients used for recordings (150 mM $[K^+]_{in}$ and 5 mM $[K^+]_{ex}$, Table 2.31; Figure 5.8 B). Compared to UT cells, WT GFP-K_{2P}9.1 expressing cells had a significantly hyperpolarised reversal potential (-65.8 ± 3.0 mV compared to -39.1 ± 3.2 mV; $p < 0.001$) and increased current amplitude ($p < 0.0001$; Figure 5.8 C). As predicted for a TASK channel, WT GFP-K_{2P}9.1 currents were inhibited by external acidification (pH 6.0; Chapman et al., 2000) which caused a significant reduction in the current amplitude ($p < 0.05$; Figure 5.8C) and a positive shift in the reversal potential (from -65.8 ± 3.0 mV to -40.0 ± 7.4 mV ($p < 0.01$); Figure 5.8 B).

Expression of pore mutant GFP-$K_{2P}9.1_{G97E}$ in HEK293 cells produced an *I-V* relationship that was comparable to UT cells (Figure 5.8 B). Compared to UT cells, expression of GFP-$K_{2P}9.1_{G97E}$ resulted in a non-significant depolarisation of the reversal potential (-26.8 ± 4.2 mV for GFP-$K_{2P}9.1_{G97E}$ compared to -39.1 ± 3.2 mV for UT ($p = 0.20$); Figure 5.8 B). The current amplitude for GFP-$K_{2P}9.1_{G97E}$ expressing HEK293 cells was significantly lower than WT GFP-K_{2P}9.1 ($p < 0.0001$) and comparable to UT cells ($p = 0.81$; Figure 5.8 C). These data suggested that GFP-$K_{2P}9.1_{G97E}$ is a non-functional channel; based on these data and published work (Pei et al., 2003; Voloshyna et al., 2008) this channel was likely to knockdown native channels when expressed in cancer cell lines.

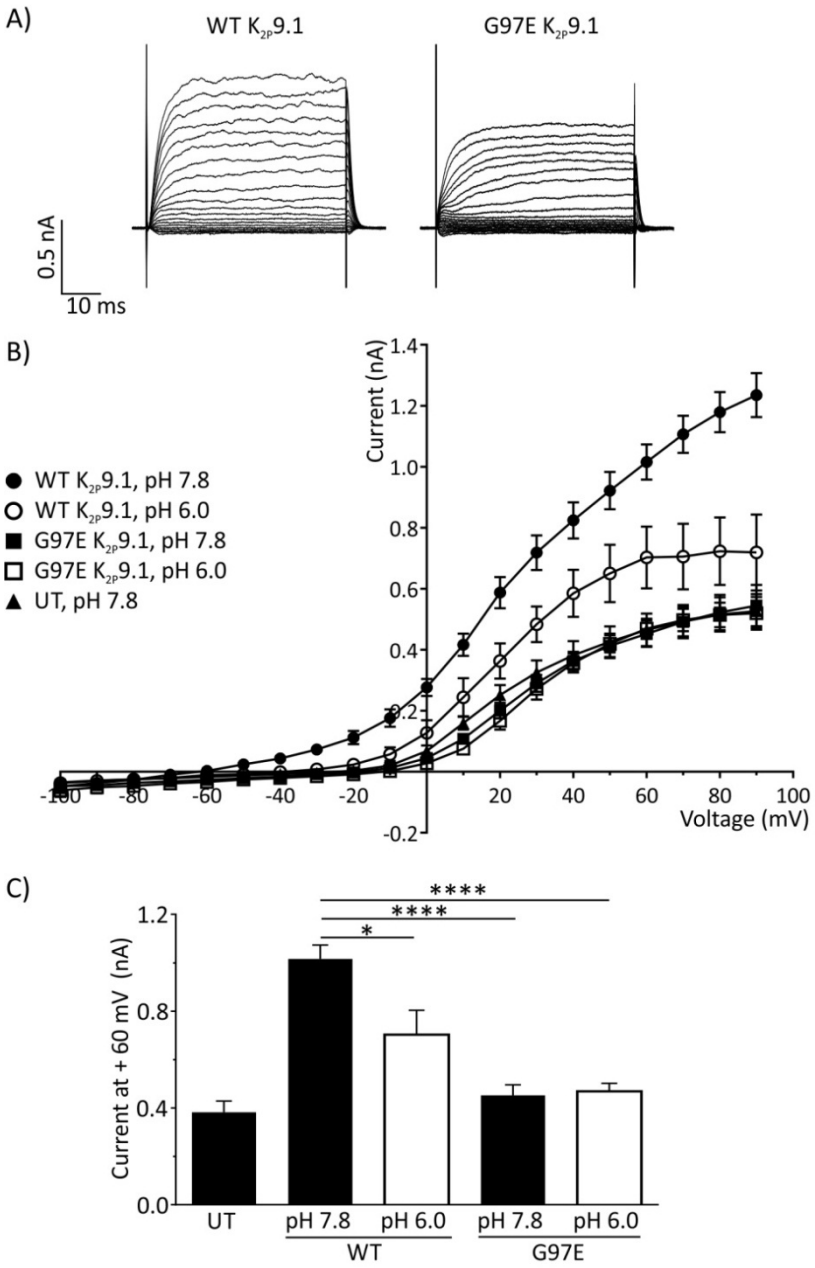

Figure 5.8: Electrophysiological properties of $K_{2P}9.1_{G97E}$ pore mutant

Whole-cell recordings from HEK293 cells transiently expressing either; GFP tagged wild type $K_{2P}9.1$ (WT; 1 µg GFP-$K_{2P}9.1$ DNA) or GFP tagged pore mutant $K_{2P}9.1_{G97E}$ (G97E; 1 µg GFP-$K_{2P}9.1_{G97E}$ DNA). Cells were analysed 24 h post-transfection and, ≈50 % of cells were transfected (identified by GFP fluorescence). Currents were evoked by voltage steps from -100 to +90 mV in 10mV increments, for 50 ms duration.

A) Representative recordings from cells expressing WT $K_{2P}9.1$ or G97E $K_{2P}9.1$, at pH 7.8.

B) *I-V* relationship for both channels at pH 7.8 and pH 6.0, in addition to untransfected (UT) cells at pH 7.8. The data shown are the average of n ≥ 4 cells, ± SEM.

C) Average current (+ SEM) elicited at +60 mV voltage step for all conditions (n ≥ 4 cells). Statistical significance was calculated using a one-way ANOVA, with Dunnett's multiple comparisons post-hoc test (* $p < 0.05$, **** $p < 0.0001$). The comparisons performed are indicated by horizontal lines.

5.2.2.1 Polyclonal transfected cell line generation

The aim of the work conducted in this section was to generate a polyclonal transfected population of cancer cells expressing GFP-$K_{2P}9.1_{G97E}$ channels. This strategy was explored because transfection of cancer cell lines was found to have a relatively low efficiency of between 5-20 % (data not shown). This level of GFP-$K_{2P}9.1_{G97E}$ channel expression would not have been sufficient to perform functional assays using transfected HCT116 and A549 cancer cells, where you would ideally be looking for the entire cell population to be affected by the modulation used. $K_{2P}9.1$ was subcloned into a pEGFP-C1 plasmid to create GFP tagged $K_{2P}9.1$ (Table 2.2); this plasmid contained a neomycin resistance gene which can be used to select for transfected mammalian cells (Method 2.4.4.3). For generation of polyclonal transfected cell lines, the effect of neomycin on cell survival was compared between a transfected and untransfected cell population. When all the cells in the untransfected cell population had died, the transfected cells were considered to be a polyclonal transfected population and this usually took between 1-3 weeks (Method 2.4.4.3). Despite successful transfection of GFP-$K_{2P}9.1_{G97E}$ into A549 and HCT116 cancer cell lines (shown for HCT116 cells; Appendix 5), generation of polyclonal transfected cell lines was not successful. Transfection was assessed by GFP fluorescence, which was initially detected by immunofluorescent microscopy, but after prolonged cell culture became undetectable. This was deduced to be caused by a loss of the channel expression during extended cell culture (> 7 days), even in the presence of antibiotic selection pressures (up to 1 mg/ml G418; Appendix 5). Therefore, generation of polyclonal transfected cell population with GFP-$K_{2P}9.1_{G97E}$ was not possible in A549 and HCT116 cell lines and this strategy was abandoned. However, transient channel transfections allowed certain functional studies to be performed, when either a high transfection efficiency was achieved (such as in HEK293 cells) or GFP positive cells could be selected (for example using flow cytometry).

5.2.3 Pharmacological modulation of TASK channels

The impact of TASK channels on cancer cell functions was studied using pharmacological modulators because transfection of GFP-$K_{2P}9.1_{G97E}$ channels into cancer cell lines was not suitable for proliferation and migration assays which were performed in

this chapter, and no tools targeted against $K_{2P}3.1$ channel expression were generated in this chapter. Thus, Three published TASK inhibitors were selected for use in this study: genistein, methanandamide, and ruthenium red (Czirják and Enyedi, 2003; Gierten et al., 2008; Veale et al., 2007a). These inhibitors were chosen due to their different selectivities for TASK channels; methanandamide and genistein will inhibit both $K_{2P}3.1$ and $K_{2P}9.1$ channels (Gierten et al., 2008; Maingret et al., 2001; Veale et al., 2007a), whereas ruthenium red is selective for $K_{2P}9.1$ and will not inhibit $K_{2P}3.1$ (Czirják and Enyedi, 2003). The different selectivities of these published inhibitors may allow any differential effects of $K_{2P}3.1$ and $K_{2P}9.1$ to be distinguished. Although, the TASK channel inhibitors used in this study are published modulators of the channels, they are not specific for the TASK channel family and have a wide range of cellular targets including other cell surface channels and receptors (see Introduction 1.4.2.6 for details of other cellular targets). The relevance of the other cellular targets for each inhibitor will depend on the individual cell lines and were not characterised in this study. However, this meant that any impacts of TASK channel inhibition on cell line functions may not be solely due to TASK channel modulation. This limitation was taken into consideration when interpreting the data presented in this chapter (see Section 5.4).

The concentrations for each of the three TASK channel inhibitors used in this chapter were selected based on published electrophysiological and functional data. Genistein was used in the concentration range of 0.5-100 µM; this range was selected since published electrophysiological data show that the IC_{50} for $K_{2P}3.1$ inhibition is 10 µM and that a 60 % inhibition of $K_{2P}9.1$ currents will occur with 100 µM genistein (Gierten et al., 2008). Methanandamide is the non-hydrolysable analogue of anandamide, which inhibits both $K_{2P}3.1$ and $K_{2P}9.1$ channels, with 60 % inhibition being observed at concentrations of 3 µM (Maingret et al., 2001; Veale et al., 2007a). Thus, a concentration range of 0.5-50 µM was selected to ensure TASK channel inhibition and up to 50 µM methanandamide has been used in published studies (Innamaa et al., 2013b; Meuth et al., 2008b). Ruthenium red is an inhibitor of homodimeric $K_{2P}9.1$ channels, with an IC_{50} of 0.7 µM (Czirjak and Enyedi, 2002a). Up to 100 µM ruthenium red has been used when studying $K_{2P}9.1$ channels in published studies (Czirják and Enyedi, 2003; Lee et al., 2012), therefore a concentration range of 0.5-100 µM was selected.

5.3 Role of TASK channels in cancer cell functions

To determine the functional roles of TASK channels in cancer cells, assays to examine three key cancer hallmark functions (proliferation, apoptosis, and migration) were conducted. These assays were performed in the presence of the semi-selective TASK channel inhibitors (genistein, methanandamide, and ruthenium red). Additionally, the effect of GFP-$K_{2P}9.1_{G97E}$ expression on apoptosis was examined, since this assay allowed for the selection of GFP positive (transfected) cells.

By regulation of the membrane potential, K_{2P} channels are thought to influence the activity of multiple types of ion channels, and this may include K_V channels (Blackiston et al., 2009; Campanucci et al., 2005; Enyedi and Czirják, 2010; Lesage and Lazdunski, 2000; Patel and Lazdunski, 2004; Rajan et al., 2000; Schwab et al., 2012). Therefore, in this study the functional role of other classes of KCh (non-TASK channels) were examined in the same cancer cell lines, using 4-AP; 4-AP is broad spectrum inhibitor and can modulate a wide range of KCh, but will not inhibit K_{2P} channels. Targets of 4-AP include members of the K_V1, K_V2, K_V3, K_V4, and K_V11 subfamilies, in addition to $K_{ir}3.4$ and $K_{ir}7.1$ channels (Table 1.1; Adelman et al., 2013; Gutman et al., 2013b). Concentrations from 0.1-20 mM 4-AP were used in this study to ensure broad spectrum channel inhibition, this range was selected based on the IC_{50} values of the target KCh (Table 1.1).

5.3.1 Proliferation

MTS assays were utilised to study the effect of KCh inhibition on cell growth, where the resulting absorbance is proportional to the number of cells (Method 2.7.2). Data are presented as dose-response curves which show the average change in cell numbers compared to untreated cells (% inhibition ± SEM). In cases where the cell numbers were reduced by 50 %, the IC_{50} value was calculated and the significance was determined between untreated cells and the highest drug concentration used. Proliferation was measured following a 24 h exposure to a range of inhibitor concentrations: 4-AP (0.5-20 mM), genistein (0.5-100 µM), methanandamide (0.5-50 µM), and ruthenium red (0.5-100 µM). A time point of 24 h was selected so that sufficient time was given for chronic KCh modulation and cell cycle progression to occur, without the nutrients in the cell media

becoming a limiting factor. Cell proliferation was assessed in the three model cell lines, A549, HCT116, and 786-0, selected in Chapter 4. In order to provide additional information which addressed the second aim of this chapter (to determine any functional roles which can be linked to differences in TASK channel protein expression within cancer cell lines), six additional cancer cell lines (MCF-7, SW480, SW620, OE19, OE21, and SH-SY5Y) characterised in Chapter 4 for TASK channel expression (Table 4.2) were also assessed by MTS assays.

In A549 lung cancer cells (selected as a model for $K_{2P}3.1$ and $K_{2P}9.1$ protein expression in cancer; Chapter 4) no significant changes in cell numbers were observed following incubation with either 4-AP or TASK channel inhibitors (Figure 5.9). Additionally, in 786-0 renal cancer cells (selected as a model for $K_{2P}3.1$ protein expression in cancer; Chapter 4) exposure to TASK channel inhibitors had no significant effect on cell numbers (Figure 5.10 B-D). However, 4-AP caused a significant reduction in 786-0 cell numbers (IC_{50} = 7.2 mM, $p < 0.05$; Figure 5.10 A), suggesting that non-leak KChs have a role in regulating 786-0 cell numbers by affecting either cell growth or death (see Section 5.4.3 for further discussion of this finding).

Three colorectal cancer cell lines were assessed by MTS assays: HCT116 cells (Figure 5.11), SW480 cells (Figure 5.12) and SW620 cells (Figure 5.13). All three cell lines were positive for $K_{2P}9.1$ protein expression and HCT116 cells were selected as a model for $K_{2P}9.1$ protein expression in cancer (Chapter 4). Methanandamide had similar effects on all three colorectal cell lines causing a dose-dependent reduction in cell numbers and this was significant at 50 µM methanandamide (HCT116: $p < 0.05$, IC_{50} = 32.0 µM (Figure 5.11 C), SW480: IC_{50} = 47.5 µM, $p < 0.01$ (Figure 5.12 C), and SW620: IC_{50} = 32.4 µM, $p < 0.01$ (Figure 5.13 C)). Ruthenium red also resulted in a significant reduction in cell numbers in both SW480 cells (IC_{50} = 66.6 µM ($p < 0.05$); Figure 5.12 D) and SW620 cells (IC_{50} = 79.0 µM ($p < 0.05$); Figure 5.13 D), but had no effect on cell numbers in HCT116 cells. The finding that colorectal cancer cell numbers were reduced following exposure to methanandamide and ruthenium red suggested that $K_{2P}9.1$ channels have a role in regulating cell numbers by influencing cell growth or cell death. Therefore, cell death assays were required to determine if this effect is proliferative or apoptotic (see Section 5.3.2)

In all three colorectal cancer cell lines, 4-AP treatment resulted in a significant reduction in cell numbers compared to untreated cells (20 mM, $p < 0.05$; Figures 5.11-13 A) and suggested that non-leak KCh are involved in regulating cell numbers. However, it is likely that some of the effects of 4-AP at concentrations greater than 5 mM were due to increased cell death, since in SW620 cells 20 mM 4-AP resulted in over 100 % reduction in cell numbers. This was a limitation of MTS assays, as the difference between reduced cell growth and increased cell death could not be determined. For this reason, apoptosis assays were performed to determine the levels of cell death in response to the inhibitors used (Result 5.3.2).

TASK channel modulation had no significant effects on cell numbers in the other six cell lines tested: MCF-7 (Figure 5.14), OE19 (Figure 5.15), OE21 (Figure 5.16), and SH-SY5Y (Figure 5.17). This was despite TASK channel protein expression in some of these cell lines (Table 4.3), although in this thesis it was not confirmed if protein expression results in TASK channel activity. In these six cell lines, 4-AP treatment caused a dose-dependent reduction in cell numbers, although in some cases this was not significant: MCF-7 (IC_{50} = 7.9 mM, $p = 0.11$), OE19 (IC_{50} = 20.8 mM, $p = 0.11$), OE21 (IC_{50} = 8.1, $p < 0.001$), and SH-SY5Y (IC_{50} = 7.9 mM, $p = 0.08$). These data suggested that non-leak KCh have a role in the control of cell numbers either by regulating cell proliferation or cell death. Due to time limitations, the six additional cell lines investigated by MTS assays were not included for the other assays performed in this chapter. However, the potential implication of the finding, that non-leak KCh may be involved in the regulation of cellular functions, is discussed in Section 5.4.3.

In the cell lines examined, TASK channel modulation had little impact on cell numbers, and the only significant decrease in cell numbers observed was in $K_{2P}9.1$ expressing colorectal cancer cell lines (HCT116, SW480, and SW620). A limitation of using MTS assays was that it could not be determined if the observed reduction in cell numbers was due to decreased cell growth or increased cell death. Therefore, apoptosis assays were performed with the same four channel inhibitors (methanandamide, genistein, ruthenium red, and 4-AP) to investigate if TASK channels and non-leak KCh have a role in cancer cell apoptosis. In addition, apoptosis assays will clarify if the effects observed in this section were due to decreased cell growth.

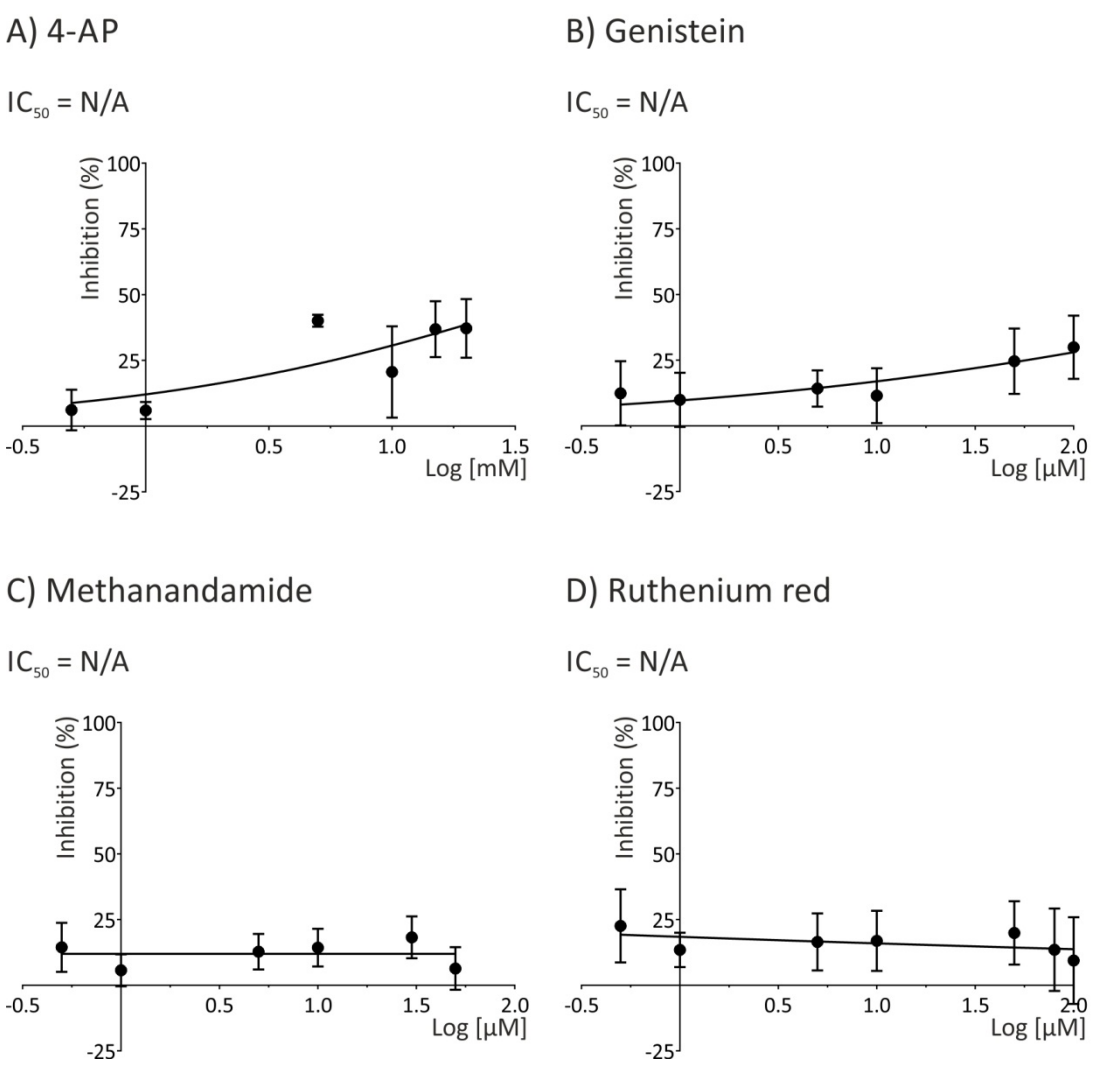

Figure 5.9: Effect of potassium channel modulation on A549 lung cancer cell proliferation

Proliferation of A549 cells measured following a 24 h exposure to KCh inhibitors.
A) 4-AP (4-aminopyridine; 0.5-20 mM).
B) Genistein (0.5-100 µM).
C) Methanandamide (0.5-50 µM).
D) Ruthenium red (0.5-100 µM).

Data are presented as dose-response curves (± SEM) and the IC_{50} values calculated.
All data sets are n = 3 experimental repeats.

If the inhibition observed reached 50 %, the statistical significance was calculated using a paired two-tailed Student's t-test by comparing highest inhibitor concentration against untreated cells.

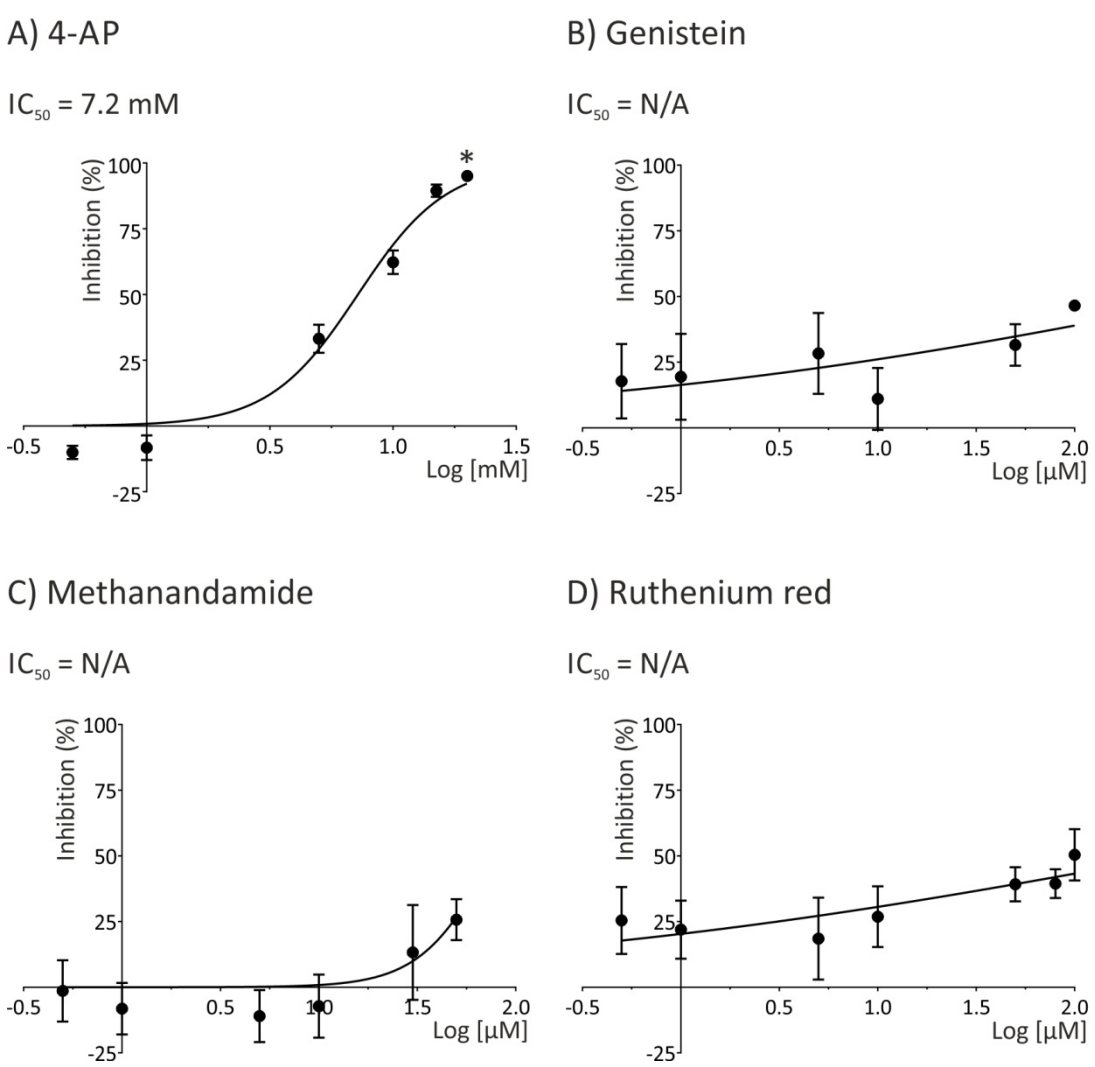

Figure 5.10: Effect of potassium channel modulation on 786-0 renal cancer cell proliferation

Proliferation of 786-0 cells measured following a 24 h exposure to KCh inhibitors.
A) 4-AP (4-aminopyridine; 0.5-20 mM).
B) Genistein (0.5-100 µM).
C) Methanandamide (0.5-50 µM).
D) Ruthenium red (0.5-100 µM).

Data are presented as dose-response curves (± SEM) and the IC_{50} values calculated.
All data sets are n = 3 experimental repeats.

If the inhibition observed reached 50 %, the statistical significance was calculated using a paired two-tailed Student's t-test by comparing highest inhibitor concentration against untreated cells (* $p < 0.05$).

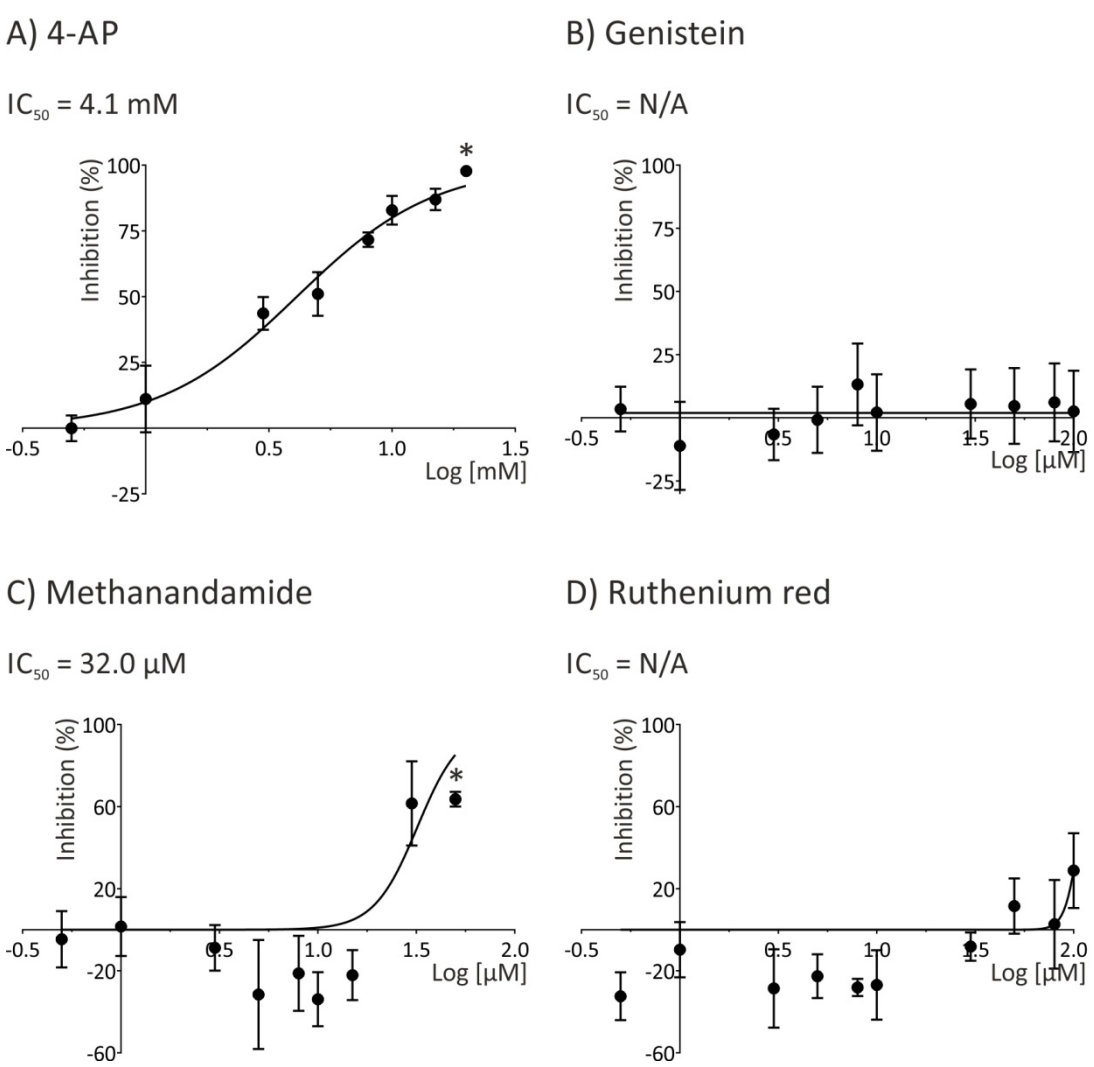

Figure 5.11: Effect of potassium channel modulation on HCT116 colorectal cell cancer proliferation

Proliferation of HCT116 cells measured following a 24 h exposure to KCh inhibitors.
A) 4-AP (4-aminopyridine; 0.5-20 mM).
B) Genistein (0.5-100 µM).
C) Methanandamide (0.5-50 µM).
D) Ruthenium red (0.5-100 µM).

Data are presented as dose-response curves (± SEM) and the IC_{50} values calculated.
All data sets are n = 3 experimental repeats.

If the inhibition observed reached 50 %, the statistical significance was calculated using a paired two-tailed Student's t-test by comparing highest inhibitor concentration against untreated cells (* $p < 0.05$).

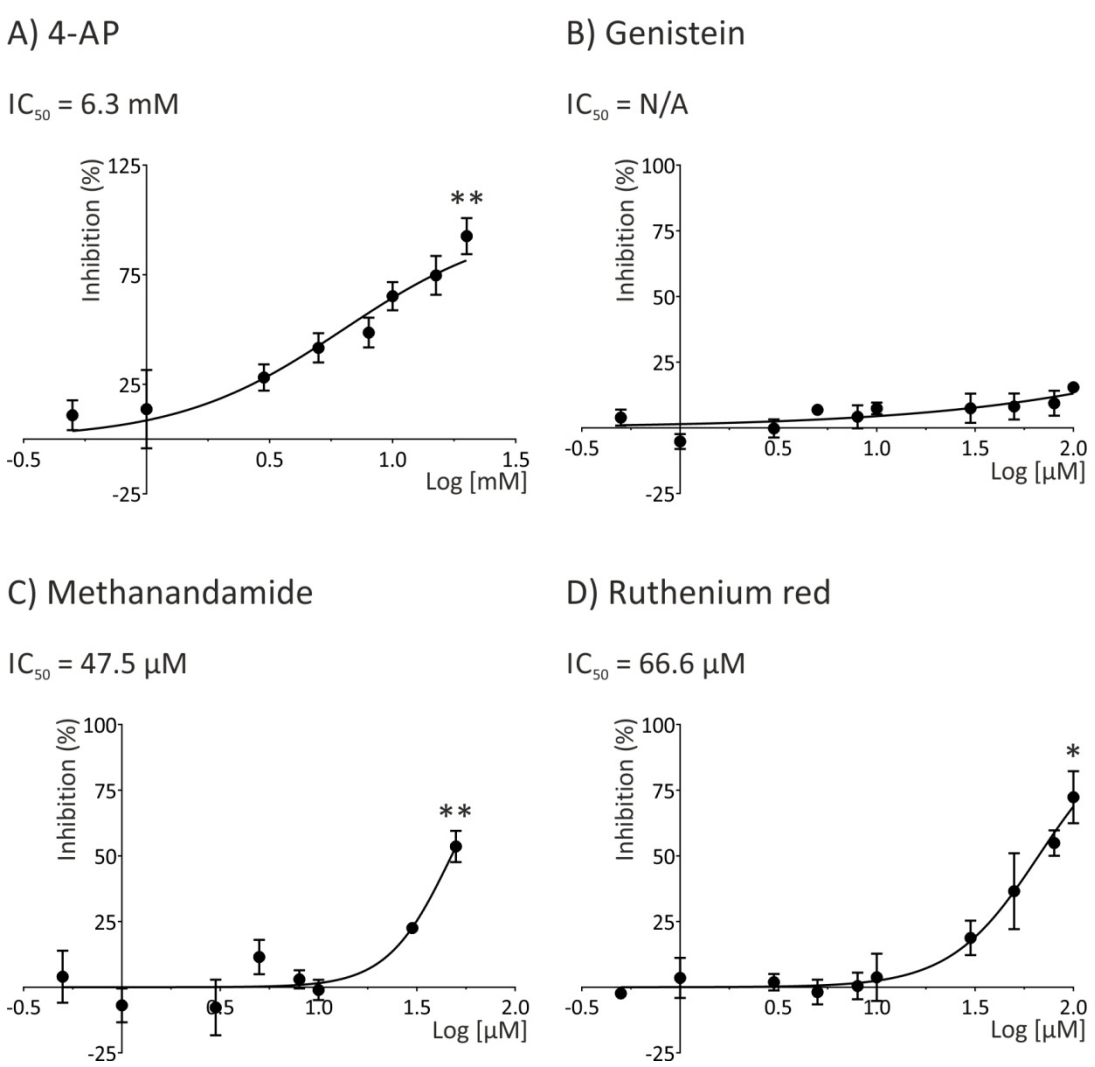

Figure 5.12: Effect of potassium channel modulation on SW480 colorectal cancer cell proliferation

Proliferation of SW480 cells measured following a 24 h exposure to KCh inhibitors.
A) 4-AP (4-aminopyridine; 0.5-20 mM).
B) Genistein (0.5-100 µM).
C) Methanandamide (0.5-50 µM).
D) Ruthenium red (0.5-100 µM).

Data are presented as dose-response curves (± SEM) and the IC_{50} values calculated.
All data sets are n = 3 experimental repeats.

If the inhibition observed reached 50 %, the statistical significance was calculated using a paired two-tailed Student's t-test by comparing highest inhibitor concentration against untreated cells (* $p < 0.05$, ** $p < 0.01$).

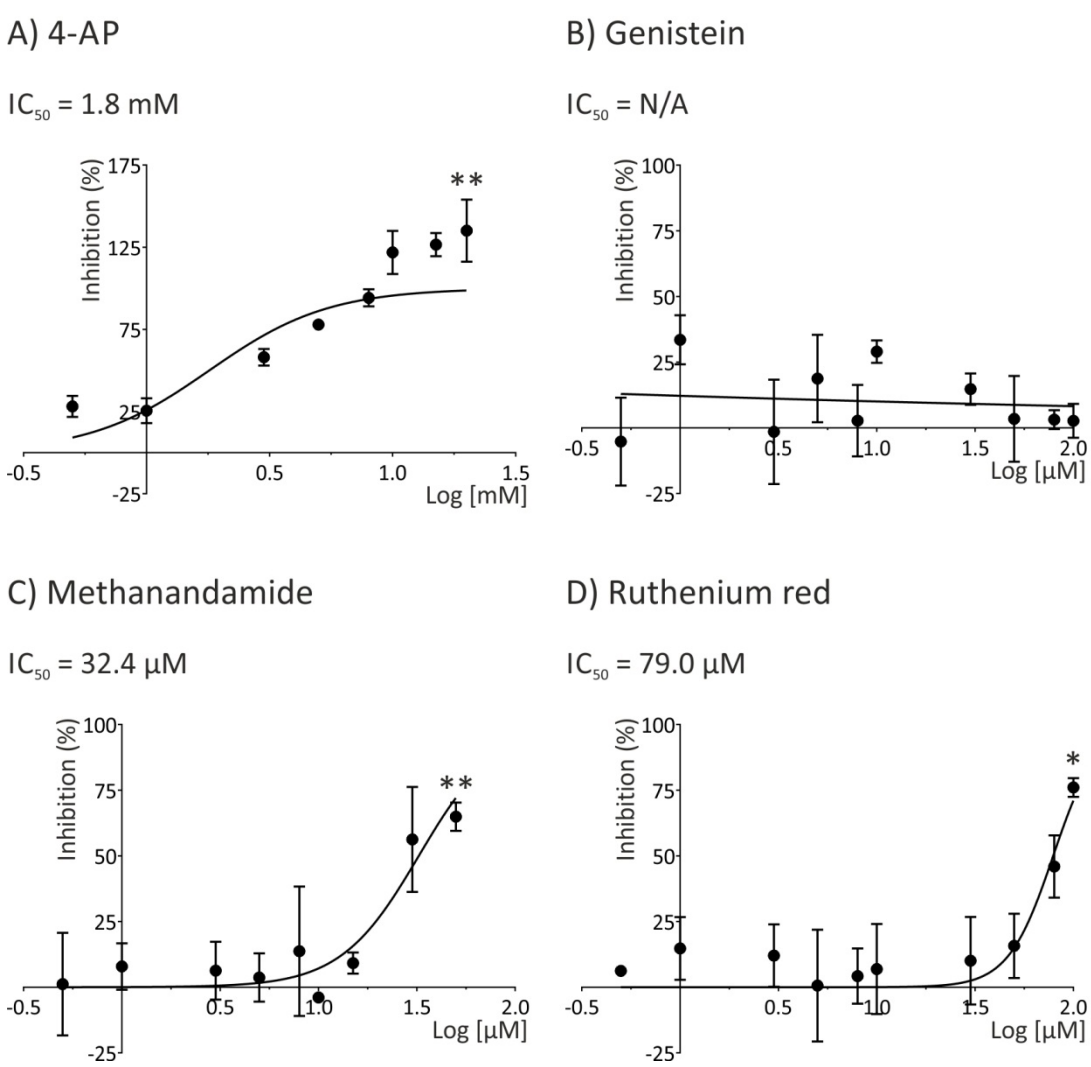

Figure 5.13: Effect of potassium channel modulation on SW620 colorectal cancer cell proliferation

Proliferation of SW480 cells measured following a 24 h exposure to KCh inhibitors.
A) 4-AP (4-aminopyridine; 0.5-20 mM).
B) Genistein (0.5-100 µM).
C) Methanandamide (0.5-50 µM).
D) Ruthenium red (0.5-100 µM).

Data are presented as dose-response curves (± SEM) and the IC_{50} values calculated.
All data sets are n = 3 experimental repeats.

If the inhibition observed reached 50 %, the statistical significance was calculated using a paired two-tailed Student's t-test by comparing highest inhibitor concentration against untreated cells (* $p < 0.05$, ** $p < 0.01$).

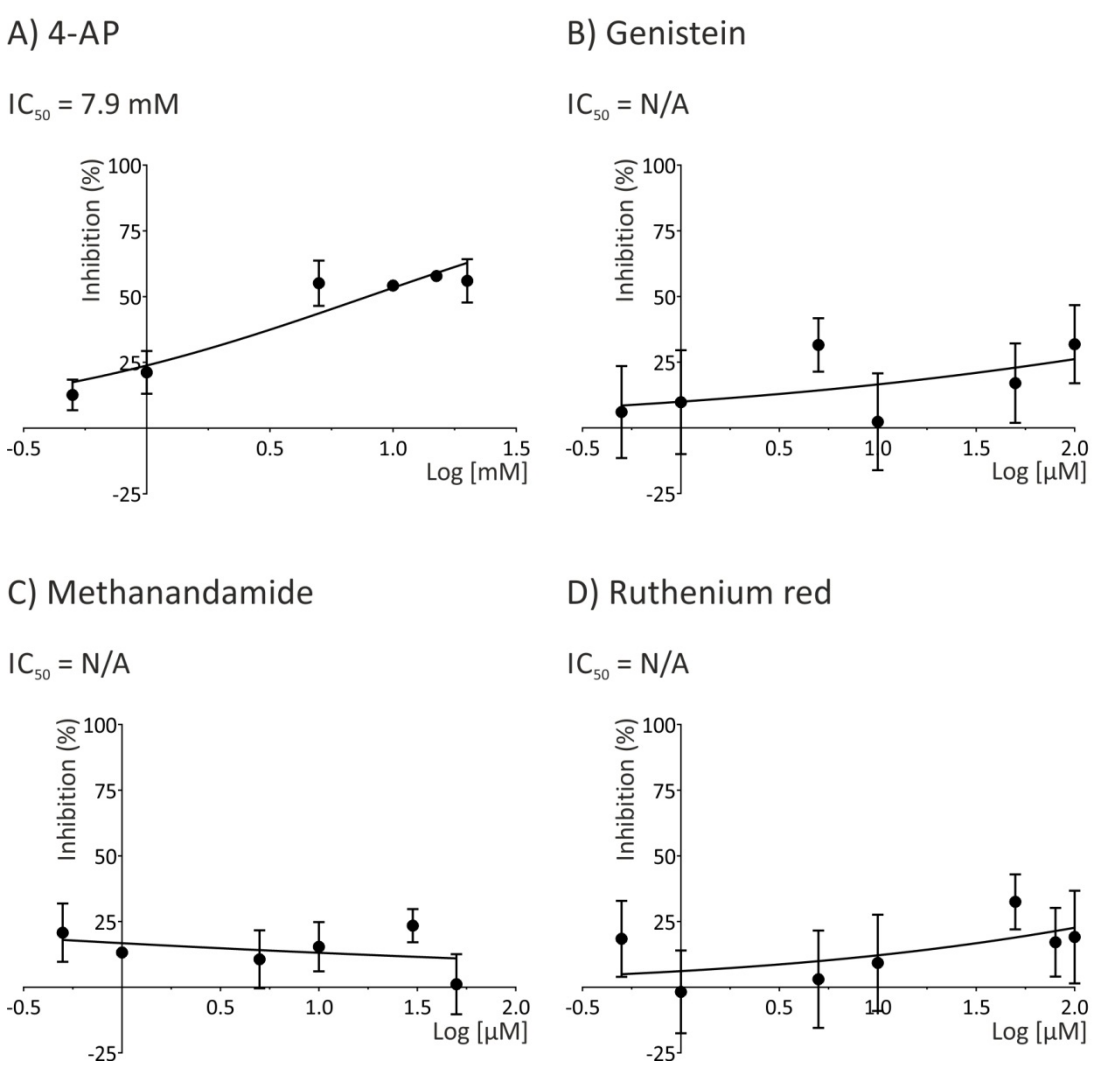

Figure 5.14: Effect of potassium channel modulation on MCF7 breast cancer cell proliferation

Proliferation of MCF7 cells measured following a 24 h exposure to KCh inhibitors.
A) 4-AP (4-aminopyridine; 0.5-20 mM).
B) Genistein (0.5-100 µM).
C) Methanandamide (0.5-50 µM).
D) Ruthenium red (0.5-100 µM).

Data are presented as dose-response curves (± SEM) and the IC_{50} values calculated.
All data sets are n = 3 experimental repeats.

If the inhibition observed reached 50 %, the statistical significance was calculated using a paired two-tailed Student's t-test by comparing highest inhibitor concentration against untreated cells.

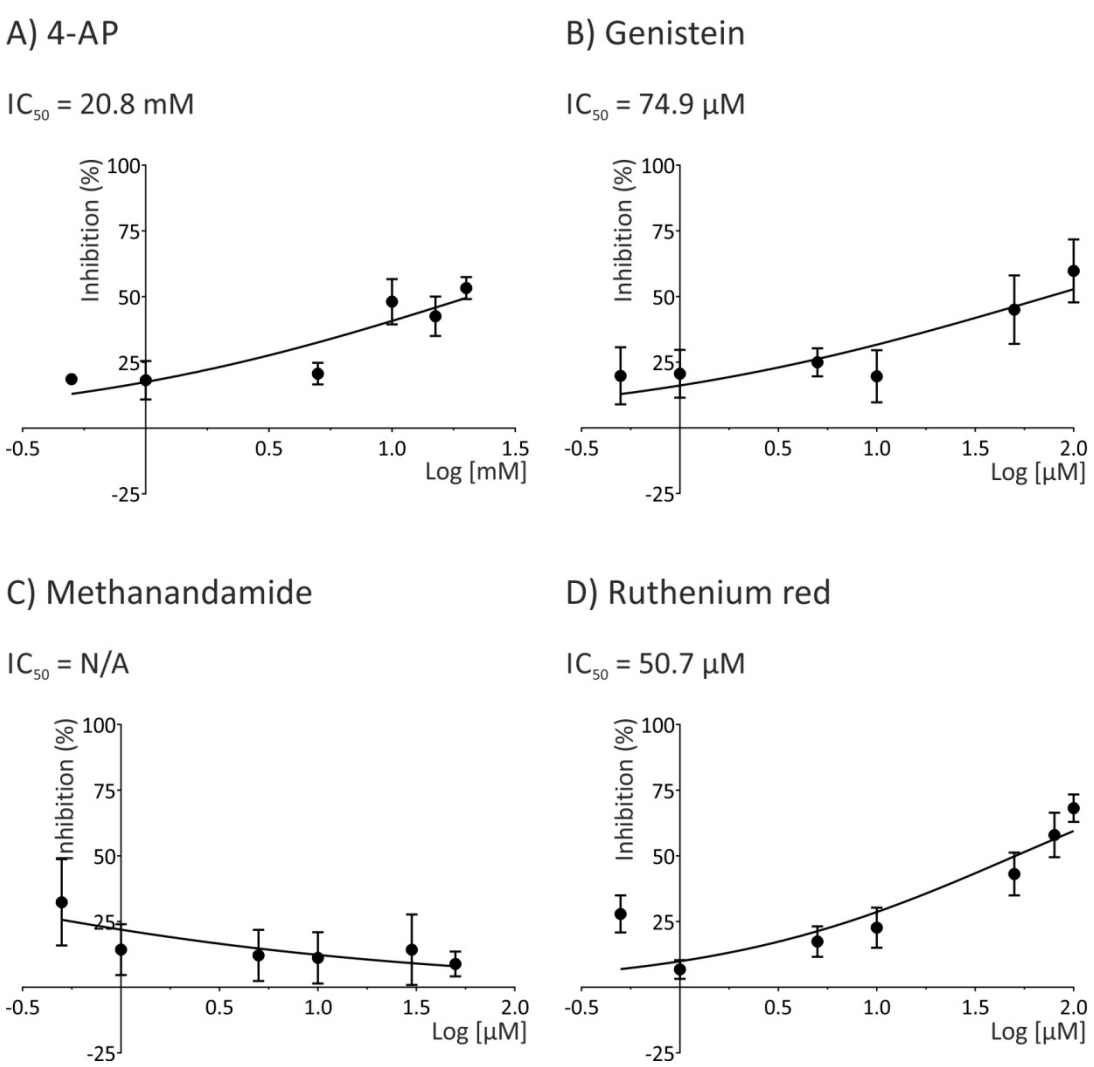

Figure 5.15: Effect of potassium channel modulation on OE19 oesophageal cancer cell proliferation

Proliferation of OE19 cells measured following a 24 h exposure to KCh inhibitors.
A) 4-AP (4-aminopyridine; 0.5-20 mM).
B) Genistein (0.5-100 µM).
C) Methanandamide (0.5-50 µM).
D) Ruthenium red (0.5-100 µM).

Data are presented as dose-response curves (± SEM) and the IC_{50} values calculated.
All data sets are n = 3 experimental repeats.

If the inhibition observed reached 50 %, the statistical significance was calculated using a paired two-tailed Student's t-test by comparing highest inhibitor concentration against untreated cells.

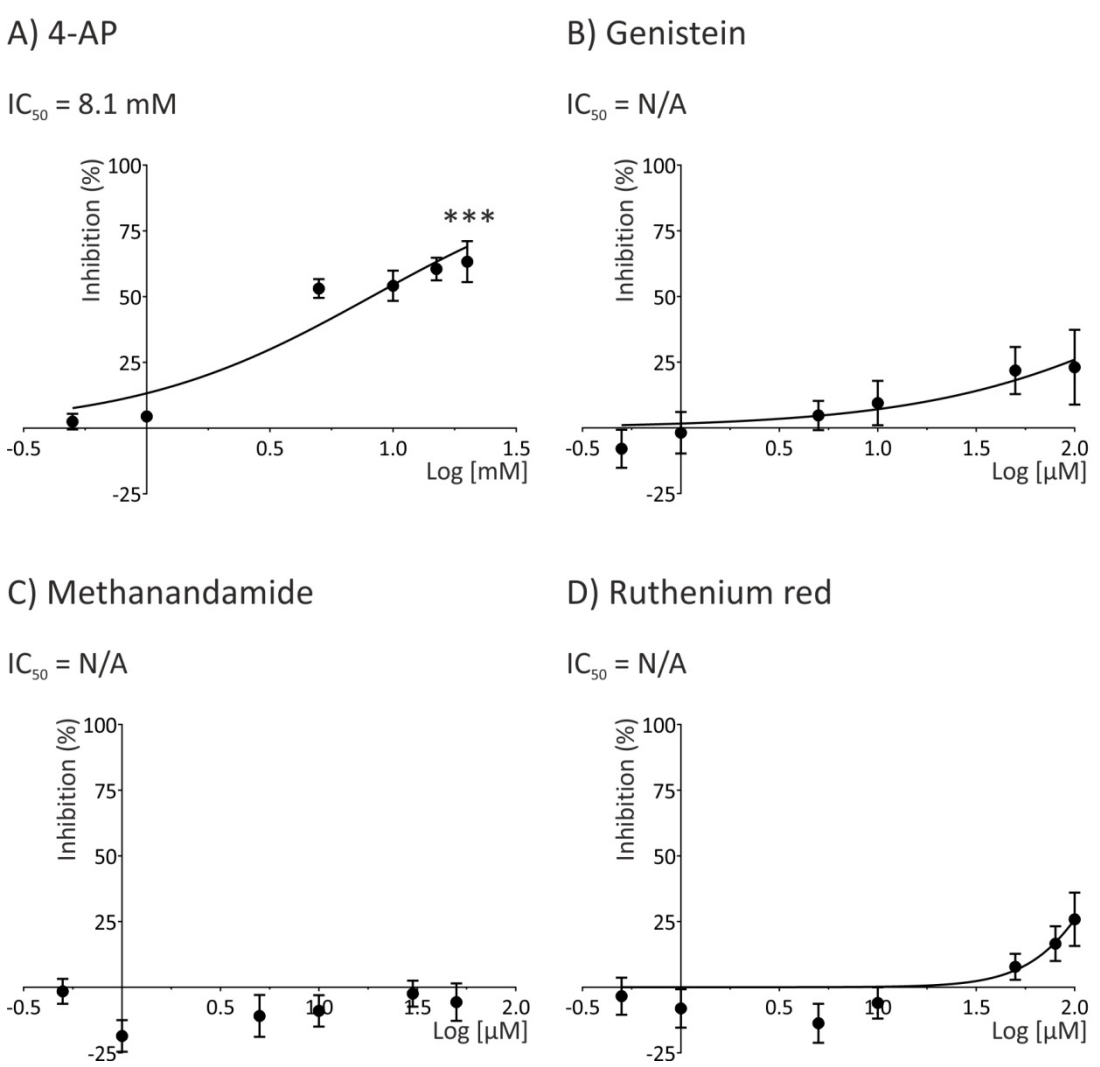

Figure 5.16: Effect of potassium channel modulation on OE21 oesophageal cancer cell proliferation

Proliferation of OE21 cells measured following a 24 h exposure to KCh inhibitors.
A) 4-AP (4-aminopyridine; 0.5-20 mM).
B) Genistein (0.5-100 µM).
C) Methanandamide (0.5-50 µM).
D) Ruthenium red (0.5-100 µM).

Data are presented as dose-response curves (± SEM) and the IC_{50} values calculated.
All data sets are n = 3 experimental repeats.

If the inhibition observed reached 50 %, the statistical significance was calculated using a paired two-tailed Student's t-test by comparing highest inhibitor concentration against untreated cells (*** $p < 0.001$).

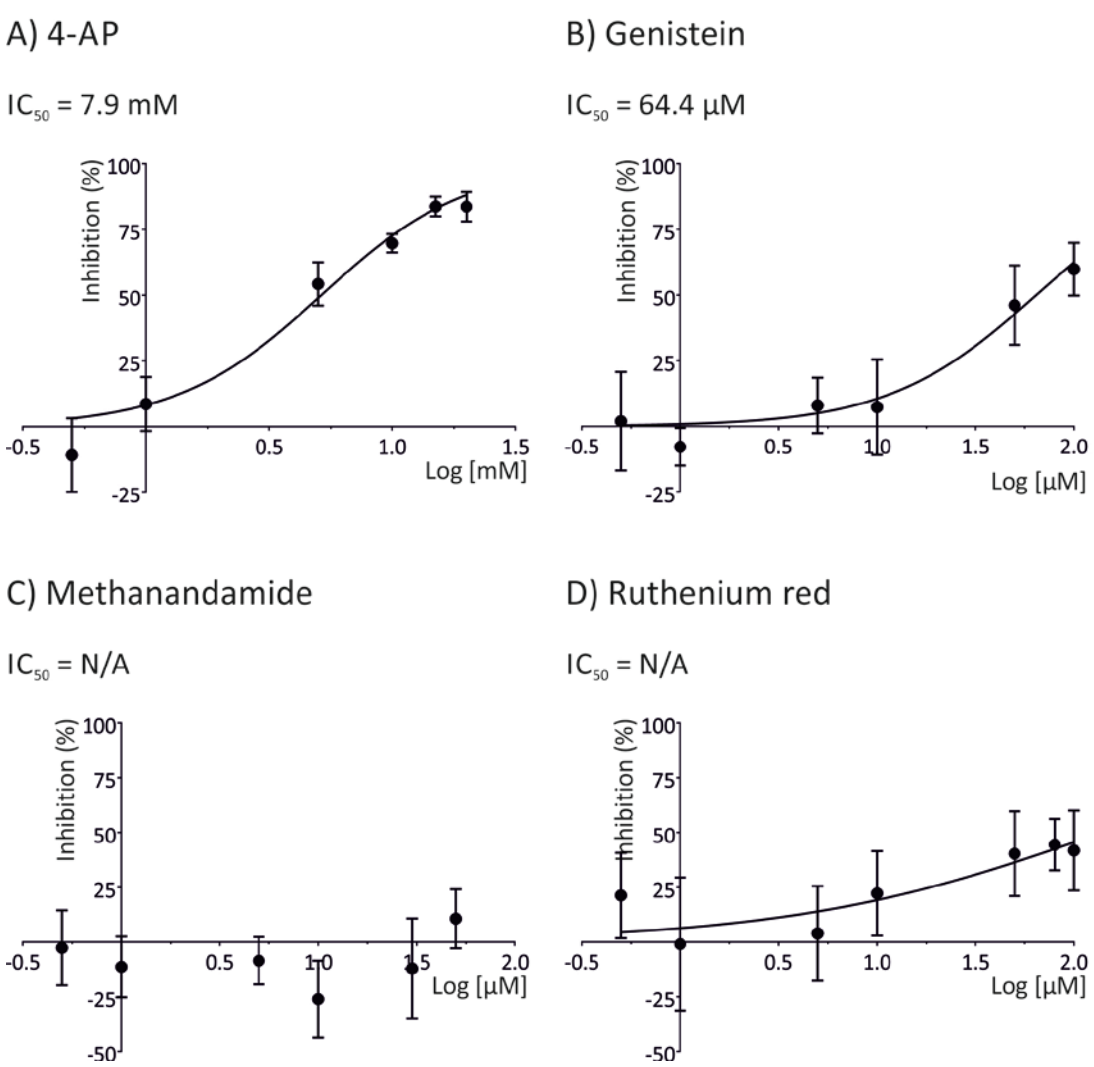

Figure 5.17: Effect of potassium channel modulation on SH-SY5Y neuroblastoma cell proliferation

Proliferation of SH-SY5Y cells measured following a 24 h exposure to KCh inhibitors.
A) 4-AP (4-aminopyridine; 0.5-20 mM).
B) Genistein (0.5-100 µM).
C) Methanandamide (0.5-50 µM).
D) Ruthenium red (0.5-100 µM).

Data are presented as dose-response curves (± SEM) and the IC_{50} values calculated.
All data sets are n = 3 experimental repeats.

If the inhibition observed reached 50 %, the statistical significance was calculated using a paired two-tailed Student's t-test by comparing highest inhibitor concentration against untreated cells.

5.3.2 Apoptosis

To assess the apoptotic response of cancer cell lines to either channel modulation or a functional $K_{2P}9.1$ knockdown, flow cytometry with annexin V staining was used (Method 2.7.3). Annexin V will bind to extracellular phosphatidylserines; in viable cells phosphatidylserines are located on the cytoplasmic side of the plasma membrane and during apoptosis they are moved onto the extracellular surface, which will allow annexin V binding. In this assay, apoptotic cells were defined as the population positive for annexin V staining shown was Quadrant 4 (Q4: early apoptosis, annexin V stained) and Quadrant 2 (Q2: late apoptosis, annexin V and SYTOX stained) on the dot plots presented in this thesis). The effect of channel modulation on cell death was examined in the three model cell lines selected in Chapter 4: A549, HCT116, and 786-0 cells. Apoptosis assays were performed at a time point of 48 h, to allow sufficient time for cell death to occur and to make comparisons with the effects observed in proliferation assays. The same inhibitors used for MTS assays were utilised for apoptosis assays. For genistein, methanandamide, and ruthenium red, the highest concentrations used in MTS assays were selected for apoptosis experiments, 100 µM, 50 µM, and 100 µM, respectively. These concentrations were selected so that the data from apoptosis assays could be compared to the changes in cell numbers observed in the previous section (Result 5.3.1). Clear toxic effects were observed in MTS assays at high concentrations of 4-AP (up to 20 mM), therefore it was decided that 5 mM 4-AP would give a better measure of apoptosis. The pro-apoptotic agent etoposide was used as a positive control, which induced cell death by causing DNA damage leading to cell cycle arrest and apoptosis (Hande, 1998). For this, cells were exposed to 10 µM etoposide 16 h prior to the beginning of the experimental time course.

Treatment of HCT116 colorectal cancer cells with etoposide resulted in a significant increase in the percentage of apoptotic cells ($p < 0.05$; Figure 5.18 B). TASK channel modulation had no effect on HCT116 cell death, while 4-AP caused a greater increase in apoptosis than etoposide, which was significant compared to untreated cells ($p < 0.01$; Figure 5.18 B). This finding suggests that the reduction in cell numbers observed following 4-AP treatment (Figure 5.11) was caused by an increase in HCT116 apoptosis and not reduced proliferation.

Etoposide treatment also resulted in a significant increase in A549 lung cancer cell death ($p < 0.05$; Figure 5.19 B). Additionally, 4-AP treatment caused a significant increase in A549 apoptosis, which was comparable to etoposide and significantly different to untreated cells ($p < 0.05$; Figure 5.19 B). In a similar manner to HCT116 cells, TASK channel inhibition resulted in no difference in the number of apoptotic A549 cells (Figure 5.19). The effect of 4-AP on A549 cells suggested that non-leak KCh have a role in preventing cell death. The data presented in Figures 5.9 and 5.19 suggested that TASK channels have no role in regulating A549 cell growth or death. These findings are discussed in Section 5.4.2.

In 786-0 renal cancer cells, the apoptotic response was measured at two time points: 24 and 48 h (Figure 5.20). This was due to a low number (under 10,000) of cell events being detected after a 48 h exposure to 4-AP and methanandamide. These data suggested that 786-0 cells were more sensitive to KCh modulation than A549 and HCT116 cells. Therefore, to get a reliable measure of apoptosis, a shorter time point of 24 h was also examined. At both time points, etoposide and 4-AP caused an increase in 786-0 apoptosis, although this did not reach significance (Figure 5.20 B, C). Methanandamide also resulted in an increase in 786-0 cell death, which was comparable to 4-AP and etoposide treatments, but did not reach significance (Figure 5.20 B). This trend was also observed after a 48 h exposure to methanandamide (Figure 5.20 C), but may be under represented in the data because of the low cell numbers recorded in this sample (average of 3,500 cell events). Thus, these data indicated that the small reduction in 786-0 cell numbers observed following methanandamide treatment (Figure 5.10) were likely to be due to increased apoptosis. No differences in 786-0 cell death were observed following exposure to genistein or ruthenium red (Figure 5.20 B, C).

The final TASK channel modulation examined by apoptosis assays was the expression of GFP-$K_{2P}9.1_{G97E}$ channels in $K_{2P}9.1$ expressing model cell lines (A549 and HCT116). Apoptosis was assessed 24 h post-transfection (Method 2.4.4.1) using flow cytometry with transfected cells being selected by GFP fluorescence and compared to UT cells (Method 2.7.3). These data showed that expression of GFP-$K_{2P}9.1_{G97E}$ or GFP alone, in both A549 and HCT116 cells, did not result in any change in apoptosis compared to UT cells (Figure 5.21 A, B). This finding supported the data which showed that pharmacological modulation of $K_{2P}9.1$ channels had no effect on HCT116 (Figure 5.18) or A549 cell death (Figure 5.19).

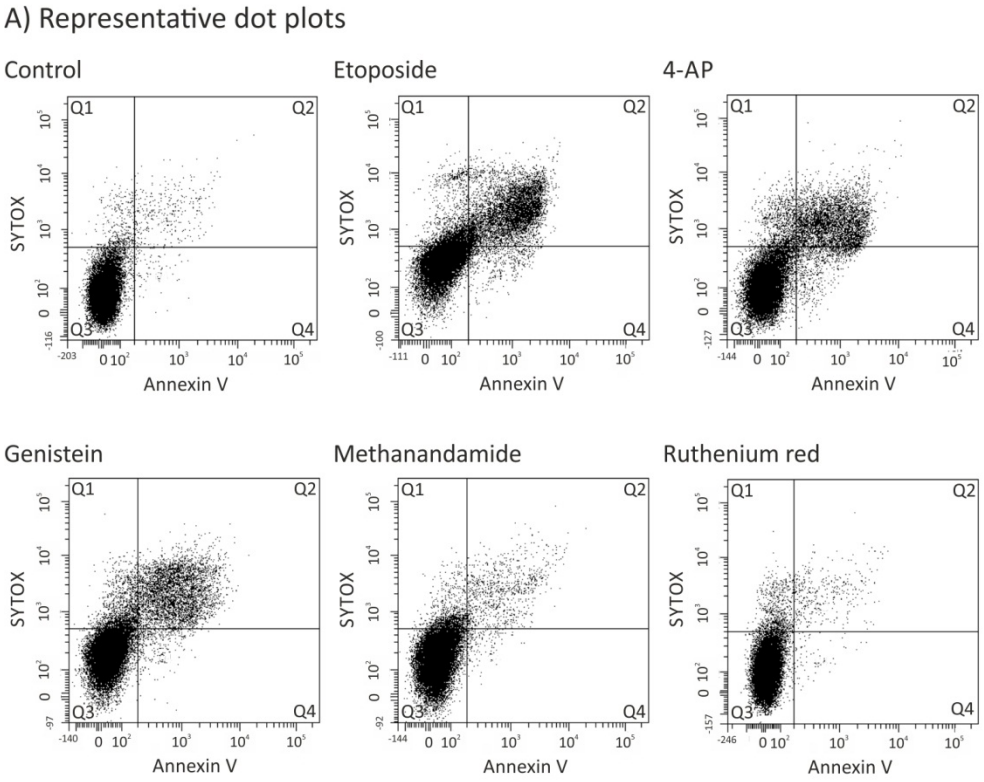

Figure 5.18: Effect of potassium channel modulation on HCT116 colorectal cancer cell apoptosis

Apoptotic response of HCT116 cells following a 48 h exposure to inhibitors, measured by flow cytometry. Inhibitors: etoposide (apoptosis inducer, 10 µM), 4-AP (5 mM), genistein (100 µM), methanandamide (meth, 50 µM), and ruthenium red (RR, 100 µM).

A) Representative dot plots for each condition.

B) Quantification of cell death in response to each treatment, shown is the average percentage of annexin V positive cells (%) + SEM. All data sets are n ≥ 3 experimental repeats.

Statistical significance was calculated using a one-way ANOVA, with Dunnett's multiple comparisons post-hoc test, comparing inhibited cells against control (untreated) cells (* $p < 0.05$, ** $p < 0.01$). Significant comparisons, where present, are indicated by horizontal lines.

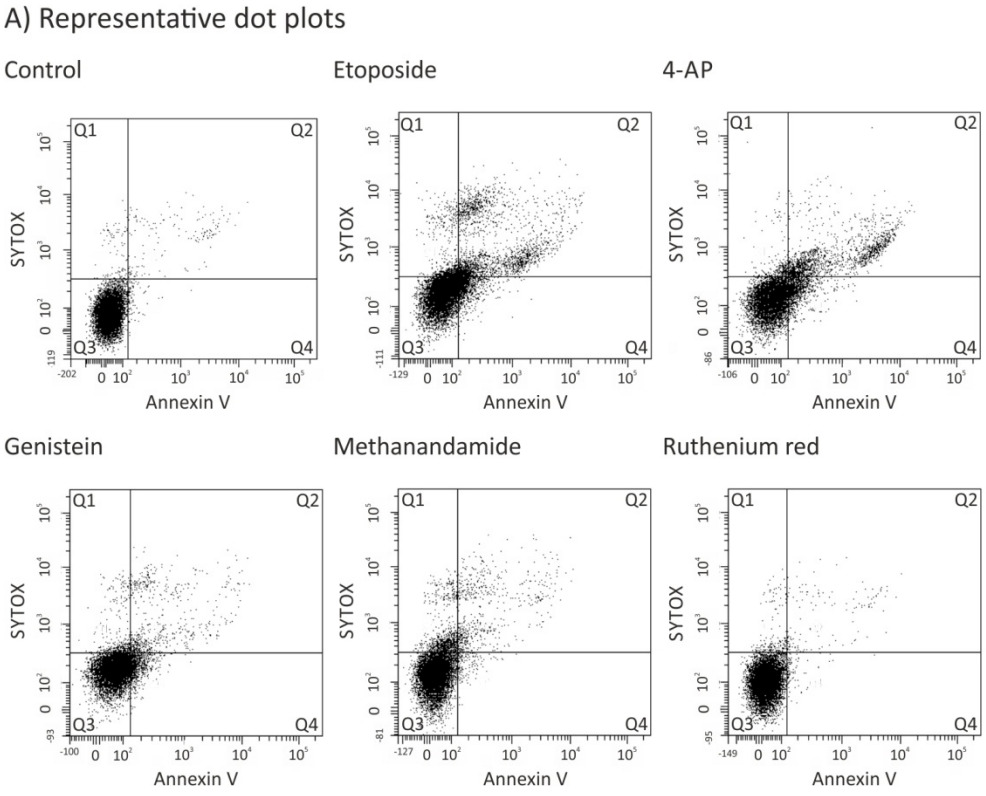

Figure 5.19: Effect of potassium channel modulation A549 lung cancer cell apoptosis

Apoptotic response of A549 cells following a 48 h exposure to inhibitors, measured by flow cytometry. Inhibitors: etoposide (apoptosis inducer, 10 µM), 4-AP (5 mM), genistein (100 µM), methanandamide (meth, 50 µM), and ruthenium red (RR, 100 µM).

A) Representative dot plots for each condition.

B) Quantification of cell death in response to each treatment, shown is the average percentage of annexin V positive cells (%) + SEM. All data sets are n ≥ 3 experimental repeats.

Statistical significance was calculated using a one-way ANOVA, with Dunnett's multiple comparisons post-hoc test, comparing inhibited cells against control (untreated) cells (* $p < 0.05$). Significant comparisons, where present, are indicated by horizontal lines.

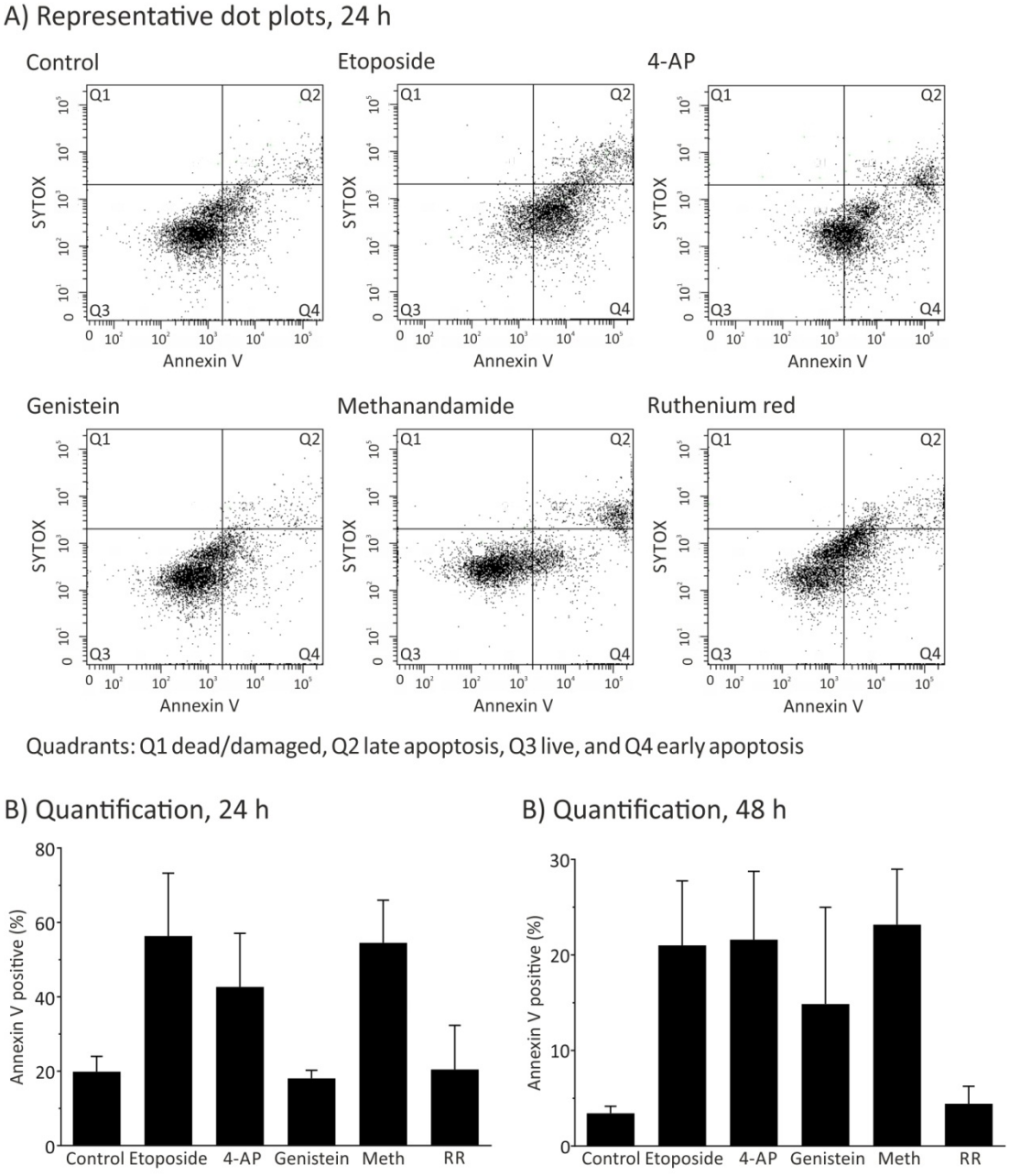

Figure 5.20: Effect of potassium channel modulation 786-0 renal cancer cell apoptosis

Apoptotic response of 786-0 cells following a (A) 24 h or (B) 48 h exposure to inhibitors, measured by flow cytometry. Inhibitors: etoposide (apoptosis inducer, 10 µM), 4-AP (5 mM), genistein (100 µM), methanandamide (meth, 50 µM), and ruthenium red (RR, 100 µM).

A) Representative dot plots for each condition at 24 h.

B & C) Quantification of cell death in response to each treatment at B) 24 h or C) 48 h, shown is the average percentage of annexin V positive cells (%) + SEM. All data sets are n ≥ 3 experimental repeats.

Statistical significance was calculated using a one-way ANOVA, with Dunnett's multiple comparisons post-hoc test, comparing inhibited cells against control (untreated) cells. Significant comparisons, where present, are indicated by horizontal lines.

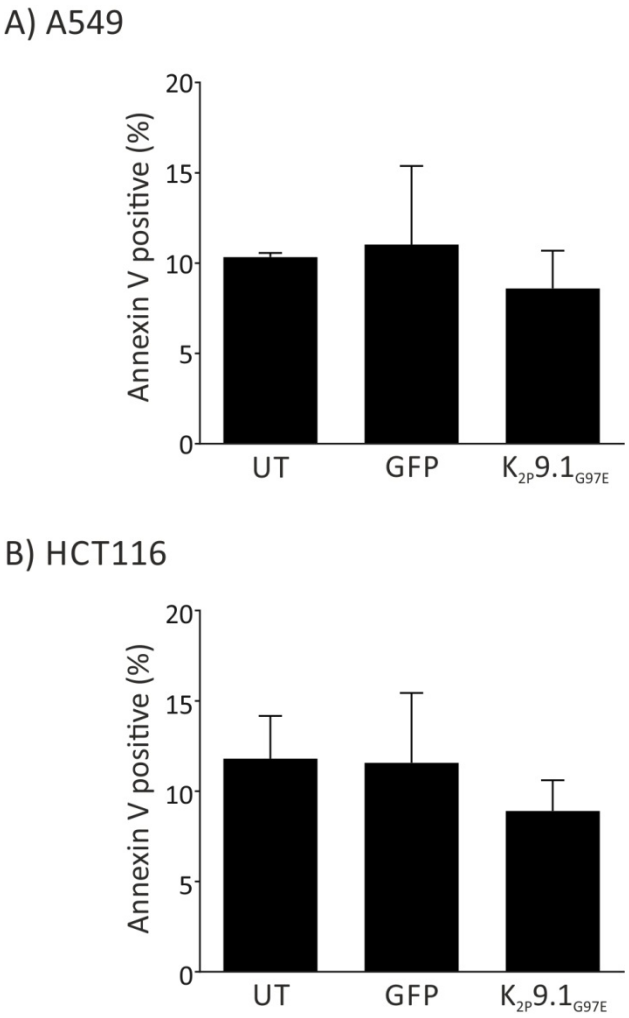

Figure 5.21: Effect of functional $K_{2P}9.1$ knockdown on cancer cell apoptosis

Apoptotic response of cancer cell lines (A) A549 lung cancer cells and (B) HCT116 cancer cells, measured 24 h post-transfection (2 µg DNA transfected).
UT: untransfected.
GFP: green fluorescent protein.
$K_{2P}9.1_{G97E}$: pore mutant GFP tagged $K_{2P}9.1_{G97E}$.

Data presented are the average percentage of annexin V positive cells (+ SEM), three transfection replicates were performed for each conditions (n = 3).

Statistical significance was calculated using a one-way ANOVA, with Dunnett's multiple comparisons post-hoc test, comparing transfected cells against untransfected cells. Significant comparisons, where present, are indicated by horizontal lines.

Apoptosis assays showed that 4-AP treatment resulted in an increase of cell death that was comparable to etoposide, a known inducer of apoptosis, in A549 and HCT116 cells. This finding indicated that the reduced cell numbers observed in MTS assays following 4-AP exposure were likely to be caused by increased cell death. The precise channels involved in this cannot be determined without further investigation, since 4-AP is a broad spectrum inhibitor; however some of the non-leak KCh which may be involved in prevention of cell death in A549 and HCT116 cells are discussed in Section 5.4.3. TASK channel inhibition had no significant effects on apoptosis in A549, HCT116, and 786-0 cells. This indicated that the reduction in cell numbers observed in HCT116 cells (Figure 5.11) was likely to be caused by reduced proliferation. In 786-0 cells, methanandamide treatment resulted in a trend for increased cell death (although this was not-significant), which may indicate that K^+ efflux through $K_{2P}3.1$ channels could have a role in the prevention of apoptosis. The data presented so far in this chapter showed that in A549 lung cancer cells, no functional impacts (reduced cell numbers or increased apoptosis) were observed following TASK channel inhibition. $K_{2P}9.1$ channels have been published to be involved in cell migration (Lee et al., 2012). Therefore, to investigate the role of TASK channels in this cancer hallmark functional, cell migration was investigated in A549 cells.

5.3.3 Migration

Wound healing assays were used as a measure of A549 cell migration in response to channel modulation (Method 2.7.4). A549 cell motility was assessed in the presence of the same KCh modulators as used previously, namely 4-AP (5 mM), methanandamide (50 µM), and ruthenium red (100 µM; Figure 5.22). Wound closure (%) was determined by comparing the area covered by cells at two time points, 0 h and 9 h, using the TScratch analysis software (Gebäck et al., 2009). An end point of 9 h was selected based on optimisation experiments, where untreated A549 cells closed the wound between 9-12 h (data not shown).

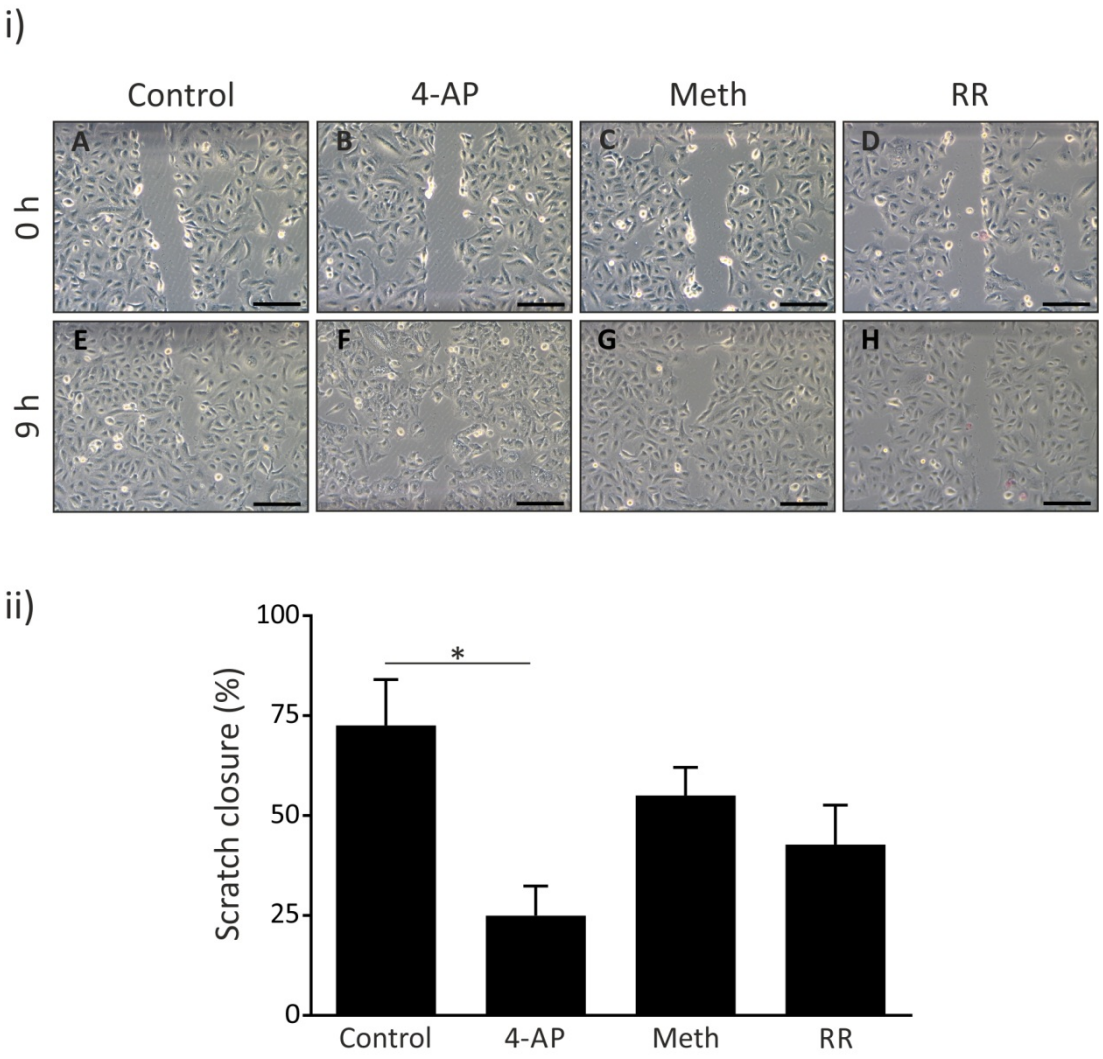

Figure 5.22: Effect of potassium channel modulation on A549 lung cancer cell migration

Migration of A549 cells in the presence of KCh inhibitors, using scratch assay to assess the wound closure from 0 h to 9 h.

i) Example images at 0 and 9 h time points.

A, E) Control, untreated cells.

B, F) 4-AP (5 mM).

C, G) Methanandamide (meth; 50 µM).

D, H) Ruthenium red (RR; 100 µM).

All scales bars are 250 µm.

ii) Quantification.

Average scratch closure (+ SEM) at 9 h compared to 0 h.

All data sets are n = 3 experimental replicates, each replicate values are calculated from n ≥ 3 fields of view.

Statistical significance was calculated using a one-way ANOVA, with Dunnett's multiple comparisons post-hoc test (* $p < 0.05$). Significant comparisons are indicated by horizontal lines.

Some degree of A549 cell migration was observed in each condition (example images; Figure 5.22 i). In untreated cells there was a 72.5 ± 11.5 % closure after 9 h (Figure 5.22 ii), and exposure to 4-AP caused a significant reduction in this closure ($p < 0.05$; Figure 5.22 ii). Exposure to the TASK channel inhibitors, methanandamide or ruthenium red, had no effect on A549 cell motility. In summary, the data presented on A549 cellular functions in this chapter indicated that 4-AP significantly increases apoptosis and this increase is likely to cause the observed reduction in cell motility. The potential 4-AP-sensitive channels responsible for regulating A549 cell death are discussed in Section 5.4.3. Although, immunofluorescence assays reported that both $K_{2P}3.1$ and $K_{2P}9.1$ channel protein is observed at the surface of A549 cells, no whole-cell outward K^+ currents with TASK-like characteristics could be isolated (Chapter 4). In support of these electrophysiological data, the data on cellular functions presented in this chapter showed that TASK channel inhibition, using pharmacological agents, had no effect on the rate of A549 cell death, proliferation or migration. The relevance of these findings and the limitations of the techniques used in the chapter are discussed in detail below.

5.4 Discussion

The primary aim of the work presented in this chapter was to establish the impact of TASK channel protein expression in cancer cell lines on three cellular functions (proliferation, apoptosis, and migration). The second aim was to determine if any functional roles can be linked to the differences in TASK channel protein expression identified in the model cell lines selected in Chapter 4 (A549, HCT116, and 786-0). To address these aims, the effect of TASK channel modulation on cancer cell line proliferation, apoptosis, and migration was investigated, using MTS assays, flow cytometry with annexin V staining, and wound healing assays, respectively. MTS assays were used because they allowed proliferation to be assessed under a range of conditions. Hence this assay allowed the effects of four inhibitors (4-AP, methanandamide, genistein, and ruthenium red) to be investigated in the three model cell lines (A549, HCT116, 786-0) and the six other cell lines characterised in the Chapter 4 (MCF-7, SW480, SW620, OE19, OE21, and SH-SY5Y). Flow cytometry with annexin V staining was used to determine the apoptotic response of cancer cell lines to KCh inhibition, this technique was selected as it provided a rapid method to test cell death in non-permeabilised cells. The final cellular function assessed in this chapter

was cell migration. Wound healing assays were selected to assess cell migration as they were a simple technique that provided data on the motility of the cells in response to channel modulation.

The experimental approaches used in this chapter lead to three main conclusions:

(i) K_{2P}9.1 channels play a role in the proliferation of colorectal cancer cell lines which express K_{2P}9.1 protein

(ii) In the majority of cancer cell lines which express TASK channel protein, channel inhibition has no significant impact on the cellular functions examined in this chapter

(iii) Non-leak KCh (which are sensitive to 4-AP inhibition) regulate cell numbers in eight of the nine cell lines examined in this chapter and that this role is likely to involve the regulation of apoptosis.

Each of these findings is described in detail below, and the functional responses observed in this chapter are summarised in Table 5.1.

5.4.1 K_{2P}9.1 channels have a role in colorectal cancer cell proliferation

In this chapter, the proliferation of K_{2P}9.1 expressing colorectal cancer cell lines was significantly reduced in response to the TASK channel inhibitors, methanandamide and ruthenium red (Figures 5.11-13). A proliferative role of K_{2P}9.1 channels in cancer was not unexpected based on the literature, where K_{2P}9.1 channels have been found to be involved in cell growth of breast, lung, and melanoma cancer cell lines (Kosztka et al., 2011; Mu et al., 2003; Pei et al., 2003). It is proposed that K_{2P} channel activity is beneficial to cancer cells by modulating the membrane potential, which may cause alterations to the activity of other ion channels (See Introduction 1.8; Enyedi and Czirják, 2010; Lesage and Lazdunski, 2000; Mu et al., 2003; Pei et al., 2003). The approach selected in this chapter to modulate TASK channels using the published TASK channel inhibitors had limitations based on the selectivity of the agents used. Therefore, to determine if the response observed is caused by K_{2P}9.1 channel inhibition, future experiments will be required. However, considering the published knowledge on the other cellular targets of the inhibitors used in colorectal cancer cell lines, it may indicate if the effects observed are likely to be due to K_{2P}9.1 channel modulation.

Table 5.1: Effects of TASK channel modulation on human cancer cell line functions

The impacts of TASK channel inhibition on cancer cell functions (proliferation, apoptosis, and migration) that were examined in this chapter are summarised. Channel modulation was performed using TASK channel inhibitors (genistein, methanandamide, and ruthenium red), or pore mutant $K_{2P}9.1_{G97E}$ channel expression (to cause a functional $K_{2P}9.1$ knockdown). ↑ indicates an increase and ↓ a decrease in a particular cell function. The significance of response is also indicated.

Where cells are left blank in the table, the modulation was not examined in that cancer cell line.

Cancer cell line	**TASK channel expression**	**Effect on cellular functions**			**Knockdown $K_{2P}9.1_{G97E}$**
		Genistein	**Meth-anandamide**	**Ruthenium red**	
SH-SY5Y brain	$K_{2P}3.1$ $K_{2P}9.1$ $K_{2P}15.1$	↓ growth (trend)	No effect	No effect	
MCF-7 breast	$K_{2P}3.1$ $K_{2P}9.1$ $K_{2P}15.1$	No effect	No effect	No effect	
HCT116 colorectal	$K_{2P}9.1$ $K_{2P}15.1$	No effect	↓ growth ($p < 0.05$)	No effect	No effect
SW480 colorectal	$K_{2P}9.1$ $K_{2P}15.1$	No effect	↓ growth ($p < 0.01$)	↓ growth ($p < 0.05$)	
SW620 colorectal	$K_{2P}9.1$ $K_{2P}15.1$	No effect	↓ growth ($p < 0.01$)	↓ growth ($p < 0.05$)	
A549 lung	$K_{2P}3.1$ $K_{2P}9.1$ $K_{2P}15.1$	No effect	No effect	No effect	No effect
786-0 Renal	$K_{2P}3.1$	No effect	↑ apoptosis (trend)	No effect	No effect

Methanandamide was used in this thesis as a $K_{2P}3.1$ and $K_{2P}9.1$ inhibitor (Veale et al., 2007a), however it will also inhibit cannabinoid receptor (CB1 and CB2) signalling and this can impact on cancer cell functions (Pisanti et al., 2013). Inhibition of CB1 receptor signalling by anandamide (25 μM) in HCT116 cells induced apoptosis when Bax, an apoptosis regulator protein, is not expressed (Patsos et al., 2010). The data presented in this chapter showed that the apoptosis of HCT116 cells was unaffected by methanandamide (Figure 5.18). This finding suggested that the reduction in cell numbers observed following methanandamide treatment was caused by reduced cell proliferation and this may be a result of $K_{2P}9.1$ channel inhibition. It should be acknowledged that, at this time, a role for cannabinoid signalling in HCT116 cell proliferation cannot be eliminated since this has not been investigated in this study or in published work. Methanandamide also reduced the proliferation of SW480 (Figure 5.12) and SW620 (Figure 5.13) colorectal cancer cell lines. This effect has been observed in published studies following reduced CB1 receptor activation in SW620 cells (Patsos et al., 2005; Proto et al., 2012). However, the data presented in this chapter showed that SW480 and SW620 cell numbers were also reduced by ruthenium red (Figures 5.12 and 5.13), which is a published $K_{2P}9.1$ channel inhibitor (Czirják and Enyedi, 2003). It is likely that ruthenium red modulated other targets within SW480 and SW620 cells which may have functional consequences, such as Ca^{2+} binding proteins and Ca_V channels (see Introduction 1.4.2.6 for a comprehensive list of targets). However, the only known target for both methanandamide and ruthenium red are $K_{2P}9.1$ channels, therefore it is likely that $K_{2P}9.1$ channel activity is involved in the proliferation of both SW480 and SW620 colorectal cancer cells. In summary, the data presented in this chapter and published studies indicated that the reduction of HCT116, SW480, and SW620 cell numbers observed here was caused by $K_{2P}9.1$ channel inhibition and that $K_{2P}9.1$ activity is involved in proliferation in colorectal cancer cells.

To confirm the role of $K_{2P}9.1$ channels in colorectal cancer cell line proliferation, future studies will need to be conducted. For this, there are two main lines of investigation:

(i) To determine if $K_{2P}9.1$ channels are functional within colorectal cancers cell lines.

(ii) To confirm that the proliferative effect observed is a result of $K_{2P}9.1$ channel inhibition.

A limitation of the cell line characterisation experiments conducted in this thesis were that in colorectal cell lines TASK channel expression was only confirmed at a protein level. To overcome this limitation, electrophysiological experiments will be required to

confirm that $K_{2P}9.1$ channel activity is present in colorectal cancer cell lines. Targeted modulation will need to be used to determine if the proliferative response observed in this chapter was due to $K_{2P}9.1$ channel inhibition. A limitation of the channel modulation strategy selected in this chapter was the selectivity of the published pharmacological modulators of TASK channels. This approach was selected in this chapter based upon the failure of more targeted tools (siRNA and pore mutant channels) to modulate channel expression or to cause long term modulation. One strategy to address this limitation may be to use cDNA plasmids with a different mammalian selection antibiotic for stable cell line generation. Data presented in this chapter showed that neomycin selection was not suitable for polyclonal stable cell line generation experiments due to loss of the channel construct after a 7 day culture period (Result 5.2.2.1). An alternative approach may be to use plasmids with a puromycin resistance gene, as this antibiotic is more toxic and can take just two days to kill UT cells. In addition, this selection treatment allowed successful selection of polyclonal siRNA plasmid transfected cells in this study (Result 5.2.1).

In addition to the limitations described above, there are two other limiting factors to the functional data presented in this chapter which need to be considered when pursuing future experiments to examine proliferation in $K_{2P}9.1$ expressing colorectal cancer cells:

(i) Some of the assays used in this chapter were limited in what information they provide on cellular functions. For example, MTS assays were utilised as a measure of cell growth, however this assay measures changes in cell numbers which can also be caused by an increase in cell death. Therefore, more assays may be required to determine if cell cycle arrest is occurring.

(ii) In this chapter only one time point was investigated for each of the assays performed. Although this was suitable to allow an initial examination of the role of TASK channels in cancer cell functions, a longer time course may be required to further investigate any functional roles.

5.4.2 TASK channel inhibition had no impact on cellular functions in the majority of cancer cell lines examined

A conclusion that can be drawn from the experimental data presented in this chapter is that, in the majority of cancer cell lines which express TASK channel mRNA and

protein (Chapter 4) no functional effects were detected following pharmacological channel inhibition (Table 5.1). This conclusion is in contrast to published studies which have found that $K_{2P}9.1$ channel mRNA and proteins expression has a tumour promoting role in cancer cell lines (Innamaa et al., 2013b; Pei et al., 2003; Kosztka et al., 2011). However, in these published studies, no experiments were conducted to assess if the expression of $K_{2P}9.1$ channel mRNA and protein resulted in channel activity.

The data presented in this chapter found that TASK channel modulation did not impact on the cellular biology of three of the six cancer cell lines examined which had $K_{2P}9.1$ protein expression (Table 5.1). This finding might reflect functional compensation from other TASK channels expressed within the cells. For example, colorectal cancer cell lines showed a significant decrease in cell proliferation in response to TASK channel modulation and only express $K_{2P}9.1$ channels. However, in other cancer cell lines where TASK channel modulators did not impact cell proliferation, only $K_{2P}3.1$ is expressed, or $K_{2P}3.1$ is expressed alongside $K_{2P}9.1$. These observations suggested that $K_{2P}3.1$ channel expression may alter the oncogenic role of $K_{2P}9.1$. This hypothesis is based upon the protein expression data presented in Chapter 4 and this thesis did not investigate if the presence of TASK channel protein results in TASK channel activity in all of the cancer cell lines used in this study. Though, in A549 lung cancer cells $K_{2P}3.1$ and $K_{2P}9.1$ channel protein expression did not result in significant whole-cell currents with TASK-like characteristics. $K_{2P}3.1$ and $K_{2P}9.1$ channels can form functional heterodimers (Berg et al., 2004; Czirjak and Enyedi, 2002a; Kang et al., 2004a; Kim et al., 2009), and this may be a potential mechanism for $K_{2P}3.1$ channels to alter the oncogenic role of $K_{2P}9.1$. However, the immunofluorescent data presented in Chapter 4 (Figures 4.19-27) indicated that the subcellular localisation of $K_{2P}3.1$ and $K_{2P}9.1$ channel protein within a single cancer cell line may not be identical and this would suggest that heterodimers may not be formed. Further investigation will be required to determine if TASK channel heterodimers are formed in these cancer cell lines. A limitation of the TASK channel inhibitors used in this thesis was that, in cell lines where both channels were expressed, roles of $K_{2P}3.1$ could not be separated from $K_{2P}9.1$ channels as no tools to specifically target $K_{2P}3.1$ could be identified in this study and the recently published inhibitor (A1899) which is more selective for $K_{2P}3.1$ channels was not available (Streit et al., 2011).

Data presented in previous chapters showed significant alterations to $K_{2P}3.1$ mRNA in a range of cancers (Table 3.4) and that $K_{2P}3.1$ protein expression was detected in several cancer cell lines (Table 4.2). However, no functional roles for $K_{2P}3.1$ channel activity in cancer cells were identified in this series of experiments. In 786-0 renal cancer cells, methanandamide treatment resulted in a trend for increased cell death; however genistein did not have the same impact (Figure 5.20). Therefore, in 786-0 cells the effect of methanandamide may be caused by other cellular targets. To further investigate a role for $K_{2P}3.1$ channels in cancer, $K_{2P}3.1$ channel activity in the cancer cells examined in thesis will need to be confirmed before determining if $K_{2P}3.1$ channels have a functional role using targeted modulation.

5.4.3 Role of non-leak potassium channels in cancer cell functions

In cancer cells, K_{2P} channels are hypothesised to influence the activity of multiple types of ion channels through the regulation of the membrane potential (Blackiston et al., 2009; Campanucci et al., 2005; Enyedi and Czirják, 2010; Lesage and Lazdunski, 2000; Patel and Lazdunski, 2004; Rajan et al., 2000; Schwab et al., 2012). One class of ion channel which may be influenced by K_{2P} channel activity are K_V channels, therefore the functional role of non-leak KCh were examined in the same cancer cell lines using 4-AP in this chapter. The data presented in this chapter showed that exposure to 4-AP caused a significant reduction in cell numbers in eight of the nine cancer cell lines examined (Figures 5.9-17). Apoptosis assays revealed that this response was likely to be caused by increased cell death (Figures 5.18-20). Overall, these data highlighted the importance of non-leak KCh activity in cancer cell functions and suggested that 4-AP-sensitive K^+ efflux is involved in the prevention of cell death within these cell lines.

The wide range of KCh that can be inhibited by 4-AP (Table 1.1) does not help identify the individual channels involved in cellular functions. Extensive studies on KCh expression within the cancer cell lines used in this thesis have not been reported in the literature; however the published data which is available highlight channels which may be involved in the functional responses observed in this chapter.

The data presented in this chapter showed that 4-AP treatment caused a significant increase in A549 cell death, and that this apoptotic increase was responsible for the

observed reduction in A549 cell numbers (Figure 5.9) and motility (Figure 5.22). Expression of one 4-AP sensitive channel, $K_V1.3$, has been identified in A549 cells in the literature (Jang et al., 2011). However, Jang et al. (2011) found that $K_V1.3$ activity promoted A549 cell proliferation. Therefore, it is unlikely that inhibition of $K_V1.3$ channels by 4-AP caused the increase in A549 cell death observed here (Figure 5.19). A channel which may be involved in A549 apoptosis is $K_V11.1$. Inhibition of $K_V11.1$ channel activity increased apoptosis in transfected HEK293, colorectal cancer, and gastrointestinal cancer cell lines (Gong et al., 2010; Shao et al., 2005; Thomas et al., 2008). In addition, this channel is expressed in a wide range of cancers (Table 1.4) including a small cell lung cancer cell line (Glassmeier et al., 2012). $K_V11.1$ channel activity may also be responsible for the increase in HCT116 cell death which was observed in this chapter, because inhibition or knockdown of $K_V11.1$ has been shown to increase HCT116 apoptosis in published studies (in addition to reducing cell proliferation and motility; Bischoff et al., 2000; Gong et al., 2010). In 786-0 renal cells, the increase in cell death observed following 4-AP exposure did not reach significance and there is no published knowledge on the expression of non-leak KCh. Therefore, it is currently unclear whether 4-AP-sensitive KCh are involved in the apoptotic response of 786-0 cells (Figure 5.20).

A substantial limitation of using 4-AP to modulate non-leak KCh was that a wide range of channels can be inhibited (Table 1.1), therefore it is possible that 4-AP can impact on multiple cancer cell functions by modulating specific channels. In addition, a proliferative role for 4-AP-sensitive channels cannot be eliminated in cell lines where apoptosis assays were not performed, such as MCF-7 and SH-SY5Y cells. These limitations meant that functional data produced from experiments using 4-AP does not provide information which will progress the understanding of the roles played by non-leak KCh in cancer cells. However, the data presented in this chapter supported published studies showing that regulation of K^+ efflux is critical for cancer cell survival (See Introduction 1.6.4; Lang et al., 2005; Wang, 2004; Wonderlin and Strobl, 1996).

5.4.4 Conclusions from the functional data presented in this chapter

In conclusion, the data presented in this chapter suggested that TASK channels may have a cell-specific role in cancer and that expression of TASK channel protein does not have an impact on cellular functions in all cancer cell lines (Table 5.1). These data indicated

that there is no functional role for TASK channels when protein for both $K_{2P}3.1$ and $K_{2P}9.1$ are present (brain, breast, and lung), compared to colorectal cell lines which just express $K_{2P}9.1$ protein (Table 5.1). In colorectal cancer cell lines expressing $K_{2P}9.1$ channel protein, different functional roles were identified for $K_{2P}9.1$ channels (which are likely to be involved in cell growth) and 4-AP-sensitive KCh (which appear to prevent apoptosis). Potential explanations for this finding is that $K_{2P}9.1$ channels can either, directly regulate proliferation, or that the channels are modulating 4-AP-insensitive channels. K^+ efflux through $K_{2P}9.1$ channel activity may influence the driving force for Ca^{2+} entry through TRP channels, and a channel potentially involved in this is TRPV6. TRPV6 protein overexpression has been detected in colorectal cancers, and in prostate cancer cell lines K^+ efflux will stimulate Ca^{2+} entry through TRPV6 channels causing proliferation (Lehen'kyi et al., 2007; Lehen'kyi et al., 2012). At this time, these conclusions are speculative and further experiments are required to determine if $K_{2P}9.1$ channel activity is present in colorectal cancer cells and to confirm that the channels are involved in proliferation (see Section 5.4.1).

In conclusion the data presented in this chapter has shown that TASK channel protein expression does not result in functional benefits in all cancer cell lines. This finding differed from published data which has found that expression of $K_{2P}9.1$ channels can result in cell type specific functional advantages (see Introduction 1.8; Innamaa et al., 2013b; Lee et al., 2012; Meuth et al., 2008b; Mu et al., 2003; Pei et al., 2003). An alternative published hypothesis is that TASK channel expression in cancer cells will only provide a functional advantage when cells are cultured under environmental stress conditions, such as low O_2 tensions and serum starvation (Liu et al., 2005; Mu et al., 2003; Pei et al., 2003). Investigating if TASK channel expression provided a functional advantage to cells cultured in conditions commonly experienced within the cancer microenvironment was the focus of the following chapter.

Chapter 6

Results

Does environmental regulation impact on cancer cell functions in TASK channel expressing cell lines?

6.1 Introduction

The aim of the studies presented in this chapter was to investigate the effect of two chronic environmental changes commonly experienced in cancer, hypoxia and low glucose, on $K_{2P}3.1$ and $K_{2P}9.1$ channel activity. In addition, the experiments aimed to determine if chronic hypoxia or low glucose altered cellular functions in cell lines expressing TASK channel protein. These aims were predicated on the data presented in Chapter 5, which showed that inhibition of TASK channels has no impact on cellular functions in the majority of cancer cell lines which express TASK channel protein under control culture conditions (20 % O_2, 2-4.5 g/l glucose). Colorectal cancer cell lines which expressed $K_{2P}9.1$ protein were the exception to this finding, where it appeared that channel inhibition significantly reduced proliferation (see Section 5.4.1 for a discussion of this finding).

A549 lung cancer cells were selected in this study as a model for $K_{2P}3.1$ and $K_{2P}9.1$ protein expression in cancer based on the data presented in Chapter 4. In A549 cells it was shown that despite $K_{2P}3.1$ and $K_{2P}9.1$ channel protein expression (Table 4.2), no whole-cell currents with TASK-like characteristics could be identified using electrophysiology. A549 cells were still included for the analysis of cellular functions in Chapter 5, as no experiments were conducted in this thesis to determine if this finding was due the channels failing to achieve functional expression on the cell surface or whether it was due to altered subcellular localisation (see Section 4.7.3). Data presented in Chapter 5 showed that when A549 cells were exposed to TASK channel inhibitors there was no impact on cell proliferation, apoptosis, or migration (Table 5.1). This finding may have been due to a lack of TASK channel activity within A549 cells, or it could indicate that TASK channels do not have a significant role in A549 cells under normal culture conditions.

Abnormal environmental conditions are commonly experienced by cancer cells (hypoxia, acidosis, or nutrient starvation) and this can induce a selection pressure for cells that can survive in these conditions (Introduction 1.5.2). Mu et al. (2003) and Liu et al. (2005) proposed the hypothesis that in some cancer cells TASK channel expression may only be beneficial under cellular stress conditions. In support of this hypothesis, Lui et al. (2005) have shown that when C8 fibroblasts expressing $K_{2P}3.1$ or $K_{2P}9.1$ channels are exposed to serum starvation (0.5-1 % serum) or hypoxia (0-10 % O_2), enhanced proliferation and decreased apoptosis is observed compared to untransfected cells or

control conditions (10 % serum and 20 % O_2). The idea that TASK channel activity has a beneficial role in cancer cells under environmental stress conditions is further supported by the roles of TASK channels in non-cancerous cells (carotid body glomus cells, lung NEB cells, and chemo-sensing neurons) where acute changes in environmental parameters (such as pH and O_2) inhibit TASK channel activity and can lead to cellular depolarisation (Chapman et al., 2000; Duprat et al., 1997; González et al., 2009; Johnson et al., 2004; Kim et al., 2009; Lewis et al., 2001; López-Barneo et al., 2008; O'Kelly et al., 1999; Ortiz et al., 2013; Plant et al., 2002). TASK channel involvement in chemo-sensing has been well-documented, however there are still a number of gaps in the field. At this time no research has been conducted to determine the effect of chronic hypoxia on TASK channel expression and activity. However, TASK channel activity has been shown to be inhibited by acute hypoxia (5-10 % O_2) in both heterologous ($K_{2P}3.1$ expressing HEK293 cells) and endogenous expressing cells (carotid body glomus cells, rCGN, and lung NEB cells; Buckler, 2007; Buckler et al., 2000; Hartness et al., 2001; Kim et al., 2009; Lewis et al., 2001; O'Kelly et al., 1998; O'Kelly et al., 1999; Plant et al., 2002). In addition, pre-treatment of carotid body glomus cells with chronic intermittent hypoxia (5 % O_2 for 20 s, every 5 min, for 8 h/day, for 7 days) has been found to result in a larger and faster inhibition of the TASK-like currents by acute hypoxia (Ortiz et al., 2013). There is also evidence to suggest that TASK channels are regulated by changes in glucose concentrations (Burdakov et al., 2006). In mouse hypothalamic orexin neurons, the whole-cell outward K^+ currents are modulated by physiological variations in glucose (between 1 to 2.5 mM), with high glucose concentrations (4.5 mM) increasing the amplitude of the TASK-like currents recorded (Burdakov et al., 2006). The mechanism by which glucose regulated TASK channel activity was unknown prior to this study. Therefore, investigating the effect of chronic hypoxia and low glucose on TASK channel activity will be the focus of this chapter.

To determine the impact of chronic hypoxia on $K_{2P}3.1$ and $K_{2P}9.1$ channel activity, whole-cell patch clamp experiments were conducted in transiently transfected HEK293 cells exposed to 5 % O_2 for 24 h prior to recordings. This approach was selected as the quantitative approaches to assess TASK channel expression, at a mRNA or protein level, proved unsuccessful in this study (Chapter 4). Therefore, any effects of chronic hypoxia on channel expression could not be determined, however examining channel activity may give an idea if any chronic hypoxia has an effect on the number of channels on the cell surface.

In this chapter *N*-linked glycosylation was investigated as the mechanism responsible for the regulation of TASK channels by glucose. For this, it was first established if the channels of interest are glycoproteins using western blot analysis. Western blot was used to determine if the de-glycosylation of a potential *N*-glycan attachment site in $K_{2P}3.1$ and $K_{2P}9.1$ channels (asparagine 53; N53) by mutation or tunicamycin treatment caused a motility shift in the protein size. Western blotting was selected for these experiments as differences in protein size are detectable by observing band shifts, therefore it would be expected that channels which cannot be glycosylated will have increased mobility on the blot (i.e. run at a smaller size). Once it was established that both $K_{2P}3.1$ and $K_{2P}9.1$ channels were modified by *N*-linked glycosylation at N53, the impact of this modification on channel activity was determined using whole-cell patch clamp experiments in transfected HEK293 cells. Whole-cell patch clamp experiments were performed as they gave a measure of how *N*-linked glycosylation would regulate channel activity.

Once the effects of chronic hypoxia and low glucose (determined indirectly by assessing channel glycosylation) on TASK channel activity were investigated. Whole-cell patch clamp experiments were performed to examine the impact of culturing A549 cells under chronic hypoxia or low glucose on the electrophysiological characteristics of the cells, for example by revealing a TASK-like whole-cell current. To determine how these environmental conditions impacted the TASK channel mediated component of the whole-cell current specifically, cells were studied in the presence and absence of TEA and acidified external recording solution. These channel modulation conditions were selected so that experimental results were comparable to the data presented in Chapter 4, which found that no significant TASK-like whole-cell currents can be isolated in A549 cells under control culture conditions.

The final experiments presented in this chapter aimed to assess the impact of chronic hypoxia and low glucose on cellular functions in TASK channel expressing cell lines. The same functional assays as those presented in Chapter 4 were used for these experiments: MTS assays, flow cytometry with annexin V staining, and wound healing assays, to determine proliferation, apoptosis, and migration, respectively. Cellular functions were assessed in both a heterologous (transfected HEK293 cells) and endogenous (A549 cells) expression system. HEK293 cells were utilised for these experiments as it had been shown in Chapter 5 that transfection of channel cDNA constructs (WT GFP-$K_{2P}9.1$ and

untagged WT K_{2P}3.1 channels) resulted in TASK channel activity. This approach was selected as a limitation of using cancer cell lines with endogenous TASK channel protein expression in this thesis was that, either TASK channel activity was not investigated due to time restrictions, or no TASK-like currents could be identified despite the presence of channel protein (A549 cells). A549 cells were also utilised for functional assays to investigate cellular functions in this chapter, as data presented so far in this thesis has not identified significant TASK-like currents or functional roles for TASK channels in these cells under normal conditions. Therefore, as hypothesised by Lui et al. (2005), the expression of TASK channel protein in A549 cells may only provide a functional advantage under altered environmental conditions. Thus, in summary the overall and specific aims of this chapter are as follows:

6.1.1 Aims

To investigate the effect of chronic environmental alterations, hypoxia and low glucose, on K_{2P}3.1 and K_{2P}9.1 channel activity. As well as determining if altered environmental conditions will impact on cellular functions in cells expressing TASK channels, either HEK293 cells (transfected with cDNA constructs shown to be functional in Chapter 5), or A549 cells (which express native TASK channels at an mRNA and protein level). To address these questions, this work has four specific aims:

1. To determine the impact of chronic hypoxia on K_{2P}3.1 and K_{2P}9.1 channel activity, by utilising whole-cell patch clamp experiments in transiently transfected HEK293 cells.
2. To investigate if *N*-linked glycosylation is responsible for the regulation of TASK channels by glucose, by establishing if the channels are glycoproteins and studying the effect of this on channel activity.
3. To examine the impact of chronic hypoxia and low glucose on the electrophysiological characteristics of A549 lung cancer cells.
4. To assess the impact of chronic hypoxia and low glucose on cellular functions in TASK channel expressing HEK293 cells (transfected with cDNA constructs shown to be functional in Chapter 5) and A549 cells (which express native TASK channels at an mRNA and protein level)

6.2 Regulation of TASK channels by chronic hypoxia

TASK channel activity is inhibited by acute hypoxia (Introduction 1.4.2.3); however no investigations have been performed to examine the effect of chronic hypoxia on $K_{2P}3.1$ and $K_{2P}9.1$ activity. When cells are chronically exposed to hypoxia they undergo adaptive changes, this can involve the regulation of gene expression, via HIF transcription factors interacting with hypoxia response elements (HRE; Bertout et al., 2008; Weir and Olschewski, 2006). Transcriptional regulation of $K_{2P}3.1$ and $K_{2P}9.1$ mRNA by chronic hypoxia has not been reported. However, *in silico* analysis conducted within the lab, on the 5000 bp upstream of the start codons in both genes, indicated that at least four HRE (consensus sequence ACGTG or GCGTG) are present for each channel (analysis performed using www.cbrc.jp/research/db/TFSEARCH.html; Dr L. Roncoroni, personal communication). Chronic hypoxia has been found to regulate other K_{2P} channels at a transcriptional level (Brazier et al., 2005; Nielsen et al., 2013). Alternatively, chronic hypoxia may regulate TASK channel expression at a post-translational level and this has been described for $K_V1.3$ and $K_V11.1$ channels (Chimote et al., 2012; Nanduri et al., 2009; Nanduri et al., 2008). Since quantitative approaches to assess TASK channel expression, at a mRNA or protein level, proved unsuccessful in this study (Chapter 4), whole-cell patch clamp experiments were used to examine the impact of chronic hypoxia on TASK channel activity (Method 2.8.2). HEK293 cells expressing either untagged human WT $K_{2P}3.1$ or GFP tagged human WT $K_{2P}9.1$ channels were cultured in 5 % O_2 (hypoxia) or 20 % O_2 (normoxia) for 24 h after DNA transfection (Methods 2.4.4.1 and 2.8.1). Whole-cell patch clamp experiments performed in Chapter 5 found that transfection with these cDNA constructs results in the production of functional TASK channels (see Figure 5.6 (page 283) for untagged $K_{2P}3.1$ and Figure 5.8 (page 287) for GFP-$K_{2P}9.1$). 5 % O_2 was selected for chronic hypoxia experiments based on published studies examining the acute modulation of TASK channels (Hartness et al., 2001; Lewis et al., 2001; Ortiz et al., 2013), preliminary work conducted within the lab (Dr L. Roncoroni; unpublished data), and the hypoxia incubator available (where the lowest O_2 tension possible was 5 %). After a 24 h exposure to either 5 or 20 % O_2, TASK channel activity was assessed by whole-cell patch clamp experiments, using comparable recording conditions to those utilised in Chapter 5 (Method 2.8.2).

Culturing untransfected (UT) HEK293 cells in 5 % O_2 resulted in an non-significant increase in the outward currents of the *I-V* relationship compared to those cultured in 20 %

O_2 (at +60 mV p = 0.15; Figure 6.1 B). Since the difference in current amplitude was not significant this was not expected to influence the reliability of the data obtained from whole-cell current recordings with transfected TASK channels. As shown in Chapter 5, HEK293 cells expressing $K_{2P}3.1$ cultured in control conditions (20 % O_2) elicited an *I-V* relationship that was typical of a K_{2P} channel (Figure 6.1 A). The currents produced by $K_{2P}3.1$ expressing cells were significantly different to UT cells, with a more hyperpolarised reversal potential ($p < 0.01$; Figure 6.1 A) and larger current amplitude ($p < 0.01$; Figure 6.1 B). When cultured in 5 % O_2, the *I-V* relationship of $K_{2P}3.1$ expressing cells was comparable to cells cultured in 20 % O_2, with equivalent reversal potentials (p = 1.00; Figure 6.1 A) and current amplitude (p = 0.49; Figure 6.1 B). These data indicated that there is no difference in the outward K^+ currents of $K_{2P}3.1$ expressing cells cultured in 5 or 20 % O_2. The reversal potential of $K_{2P}3.1$ expressing cells cultured in 5 % O_2 was significantly more negative than UT cells, indicating increased outward K^+ currents (-62.0 ± 6.6 mV compared to -36.1 ± 5.1 mV ($p < 0.01$); Figure 6.1 A). The current amplitude was not significantly higher in $K_{2P}3.1$ expressing cells compared to UT cells when both cell groups were cultured in chronic hypoxia (p = 0.32; Figure 6.1 B), and this may have been due to the perceived increase in UT cells current amplitude.

The same comparisons were performed for $K_{2P}9.1$ expressing HEK293 cells cultured in 5 and 20 % O_2. As shown in Chapter 5, $K_{2P}9.1$ expression in cells cultured in control conditions (20 % O_2) resulted in characteristic K_{2P} channel currents (Figure 6.2 A). Compared to UT cells, $K_{2P}9.1$ expressing cells cultured in 20 % O_2 had a significantly more hyperpolarised reversal potential ($p < 0.001$: Figure 6.2 A) and higher current amplitude ($p < 0.05$; Figure 6.2 B). Expression of $K_{2P}9.1$ in cells cultured in 5 % O_2 resulted in significantly different currents compared to UT cells, with more hyperpolarised reversal potential (-64.4 ± 2.4 mV compared to -36.1 ± 5.1 mV ($p < 0.001$); Figure 6.2 A) and larger current amplitude ($p < 0.001$; Figure 6.2 B). Culturing $K_{2P}9.1$ expressing cells in 5 or 20 % O_2 resulted in comparable *I-V* relationships, with equivalent reversal potentials (p = 1.00; Figure 6.2 A). The equivalent reversal potentials indicated that there is no difference in the outward K^+ currents. The data presented in Figure 6.2 B appeared to show an increase in the current amplitude in 5 % cultured $K_{2P}9.1$ expressing cells, compared to 20 % O_2 cells. This difference was not significant (p = 0.18) and resulted from the range of currents recorded (from 0.66-3.35 nA in 5 % O_2 cells compared to 0.74-1.13 nA in 20 % O_2 cells) which reflect the inherent variability in current expression which is observed in transfected cells.

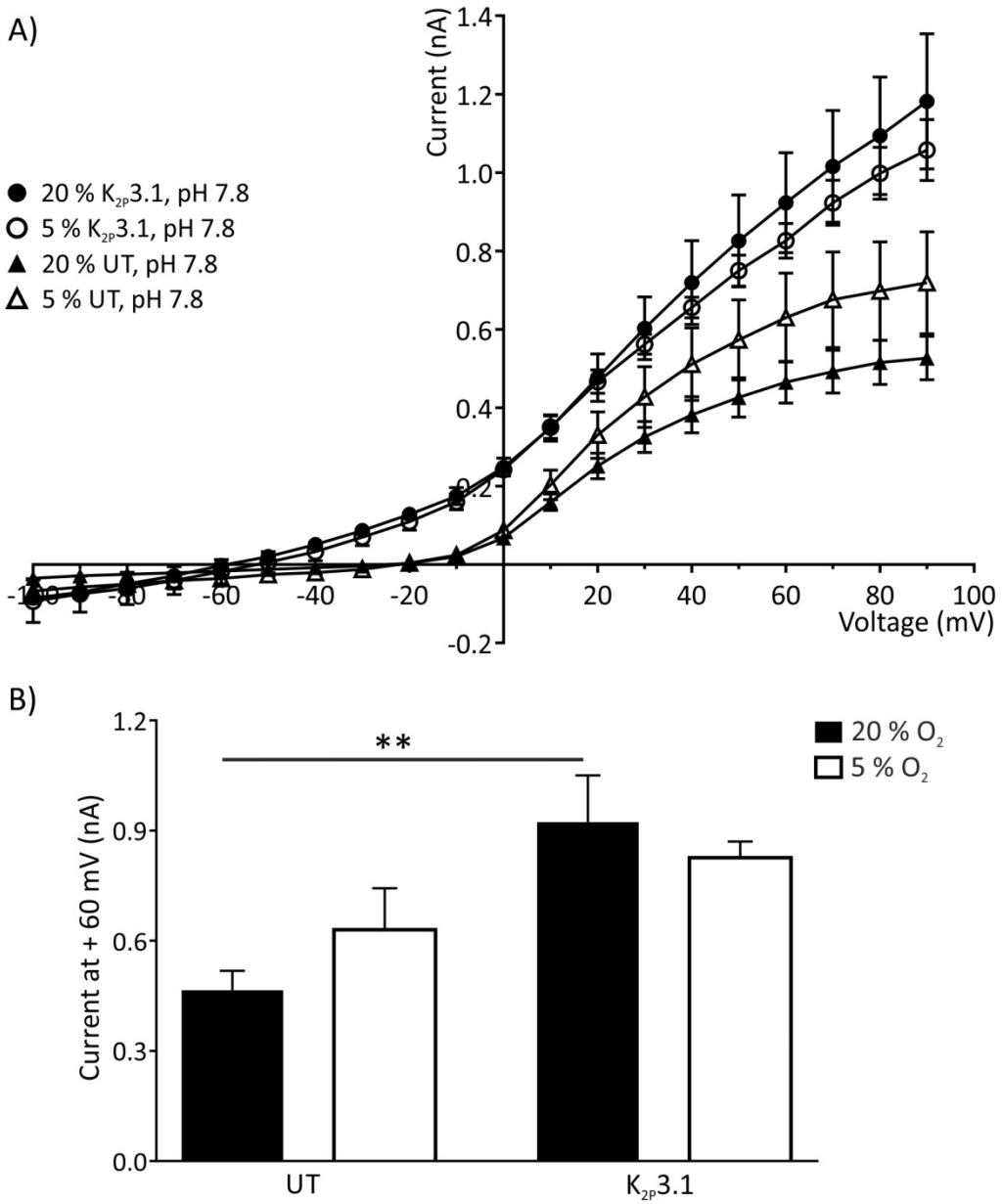

Figure 6.1: Electrophysiological properties of $K_{2P}3.1$ after exposure to chronic hypoxia

Whole-cell recordings from HEK293 cells transiently expressing untagged $K_{2P}3.1$ co-transfected with GFP (2 µg untagged $K_{2P}3.1$ DNA co-transfected with 0.5 µg GFP DNA), cultured in 5 % O_2 or 20 % O_2, for 24 h, prior to recordings. Cells were analysed 24 h post-transfection and ≈70 % of cells were transfected (identified by GFP fluorescence). Currents were evoked by voltage steps from -100 to +90 mV in 10 mV increments, for 50 ms duration. All recordings were made at pH 7.8.

A) *I-V* relationship for $K_{2P}3.1$ expressing cells and untransfected (UT) cells cultured in 5 % or 20 % O_2. The data shown are the average of n ≥ 5 cells, ± SEM.

B) Average current (+ SEM) elicited at +60 mV for all conditions (n ≥ 5 cells).

Statistical significance was calculated using a one-way ANOVA, with Dunnett's multiple comparisons post-hoc test (** $p < 0.01$). Significant comparisons, where present, are indicated by horizontal lines.

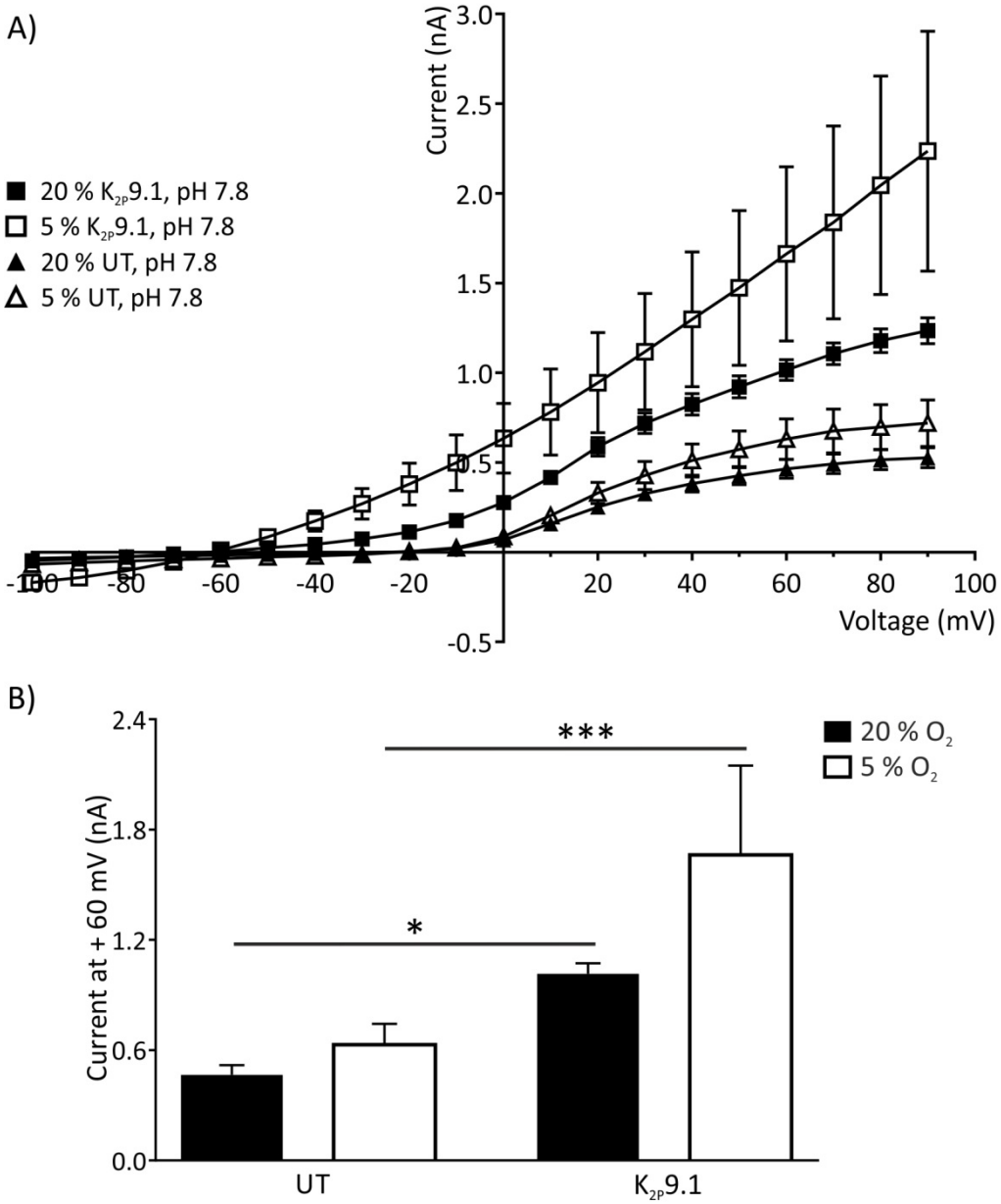

Figure 6.2: Electrophysiological properties of $K_{2P}9.1$ after exposure to chronic hypoxia

Whole-cell recordings from HEK293 cells transiently expressing GFP tagged $K_{2P}9.1$ (1 µg DNA transfected), cultured in 5 % O_2 or 20 % O_2, for 24 h, prior to recordings. Cells were analysed 24 h post-transfection and ≈50 % of cells were transfected (identified by GFP fluorescence). Currents were evoked by voltage steps from -100 to +90 mV in 10 mV increments, for 50 ms duration. All recordings were made at pH 7.8.

A) *I-V* relationship for $K_{2P}9.1$ expressing cells and untransfected (UT) cells cultured in 5 % or 20 % O_2. The data shown are the average of n ≥ 5 cells, ± SEM.

B) Average current (+ SEM) elicited at +60 mV voltage step for all conditions (n ≥ 5 cells).

Statistical significance was calculated using a one-way ANOVA, with Sidak's multiple comparisons post-hoc test (* $p < 0.05$, *** $p < 0.001$). Significant comparisons, where present, are indicated by horizontal lines.

In conclusion, the data presented in this section suggested that chronic hypoxia (5 % O_2, 24 h) had no effect on $K_{2P}3.1$ or $K_{2P}9.1$ channel activity, when the channels are expressed in HEK293 cells. There were two limitations to this experimental set up which need to be highlighted and taken into consideration when interpreting the findings presented here. (i) Overexpression of TASK channels in HEK293 cells may have meant that the channel mRNA and protein was above the regulatory capacity of the native hypoxia response systems in HEK293 cells. Therefore, the entire channel population may not be modulated by chronic hypoxia appropriately. (ii) The experimental replicate number was low and only five cells were recorded for some conditions. This may have meant that any subtle expression changes, at an mRNA or protein level, are not detected in the whole-cell current recordings reported here. Chronic hypoxia triggers adaptive changes, which can involve expression regulation at a transcriptional and post-translational level (Bertout et al., 2008; Brazier et al., 2005; Chimote et al., 2012; Nanduri et al., 2009; Weir and Olschewski, 2006). However, quantitative approaches to assess TASK channel expression, at a mRNA or protein level, proved unsuccessful in this study (Chapter 4), therefore the impact of chronic hypoxia on TASK channel expression could not be studied and the effect on channel activity was examined. As a result of these technical limitations, additional experiments will be required to determine the expression of TASK channels at an mRNA and protein level in both normoxic and hypoxic conditions. In addition, to increasing the replicate number to expand upon the data presented in this chapter which suggested that at a functional level heterologously expressed $K_{2P}3.1$ and $K_{2P}9.1$ channels are not regulated by chronic hypoxia. The limitations of this work and the direction for future studies to analyse the regulation of TASK channels by chronic hypoxia are discussed further in Section 6.6.1.

6.3 Regulation of TASK channels by glucose

It is predicted that changes in glucose concentrations will regulate TASK channel activity (Burdakov et al., 2006). A potential mechanism for this regulation is via *N*-linked glycosylation, since changes in external glucose concentrations have been reported to influence protein glycosylation (Hayter et al., 1992). Additionally, *N*-linked glycosylation has been shown to be a critical regulator of ion channel gating, trafficking, and surface stability (Egenberger et al., 2010; Hagen and Sanders, 2006; Zhu et al., 2012). Therefore, we aimed

to determine if $K_{2P}3.1$ and $K_{2P}9.1$ channels are glycoproteins, and whether this post-translational modification has an impact on the functionality of the channels.

6.3.1 TASK channels are *N*-linked glycoproteins

N-linked glycosylation will occur at conserved asparagine (N) residues in the consensus sequence NX(S/T). The protein sequences of $K_{2P}3.1$ and $K_{2P}9.1$ (human, mouse, and rat) were analysed for the presence of *N*-linked glycosylation sites on the external surface of the channel, since these regions are internal in the Golgi apparatus where protein glycosylation will occur (analysis performed using the NetNGlyc 1.0 server, by Dr A. Mant; Blom et al., 2004). These analyses revealed that both $K_{2P}3.1$ and $K_{2P}9.1$ channels possess a single *N*-linked glycosylation site, asparagine 53 (N53), that is conserved across the species examined and located within the first extracellular loop of the channels (Figure 6.3). To determine if N53 is a target for *N*-linked glycan attachment this site was first ablated, via site-directed mutagenesis of N53 to a glutamine (Q), to create the glycosylation mutant channels rat $K_{2P}3.1_{N53Q}$ and rat $K_{2P}9.1_{N53Q}$ (created by Drs A. Mant and D. Johnson).

To examine whether the WT and N53Q channels are glycosylated, the relative protein motilities of both WT and N53Q GFP and HA tagged rat channels expressed in COS-7 cells (GFP-r$K_{2P}3.1$-HA and GFP-r$K_{2P}9.1$-HA) were analysed by western blotting (Method 2.5.4). Prior to this study, WT GFP-r$K_{2P}3.1$-HA and GFP-r$K_{2P}9.1$-HA channels had been shown to have the correct subcellular localisation (Table 2.3; Mant et al., 2011). These cDNA constructs were used for western blot experiments as antibodies directed against the protein could be used. This prevented any issues from the low sensitivity of the TASK channel antibodies analysed in Chapter 4 for western blot detection. The functionality of GFP-r$K_{2P}3.1$-HA and GFP-r$K_{2P}9.1$-HA cDNA constructs was not determined in this thesis and this was not considered to be a problem for western blot experiments. However, for the whole-cell patch experiments conducted in Section 6.3.2 untagged channels were used since protein tags can interfere with channel function and this was shown to be the case for human GFP-$K_{2P}3.1$ channels in Chapter 5. Transfected cells were treated with either 1.0 g/ml tunicamycin (+), to block synthesis of all *N*-linked glycoproteins, or with its vehicle

Me_2SO alone (-) for 16 h prior to protein harvesting. Both GFP-rK_{2P}3.1-HA and GFP-rK_{2P}9.1-HA channels have a predicated molecular weight of 72 kDa.

When examining the protein mobility of rK_{2P}3.1 (Figure 6.4 A), the WT channel produced two distinct bands (between 50-60 kDa in the untreated condition). Tunicamycin treatment reduced the intensity of the upper band, while increasing the lower band intensity and this indicated that inhibition of protein glycosylation increased the mobility of WT K_{2P}3.1 channels (Figure 6.4 A). The protein mobility of r$K_{2P}3.1_{N53Q}$ was equivalent to the tunicamycin treated WT channel (a faint upper band and more intense lower band) and r$K_{2P}3.1_{N53Q}$ mobility was not enhanced by tunicamycin treatment (Figure 6.5 A). These data indicated that r$K_{2P}3.1_{N53Q}$ channels have increased mobility compared to untreated WT channels, which could not be further increased by tunicamycin treatment and showed that $K_{2P}3.1_{N53Q}$ channels were not glycosylated (Figure 6.4 A).

The protein mobility of WT and N53Q rK_{2P}9.1 channels were examined in equivalent experiments. WT rK_{2P}9.1 was detected as a single band at approximately 72 kDa (Figure 6.4 B) and following tunicamycin treatment two bands were present (a lower band at 60 kDa and the higher band at 72 KDa; Figure 6.4 B). This indicated that the WT channel was glycosylated, since tunicamycin increased the mobility in a proportion of the WT rK_{2P}9.1 protein. The protein mobility of r$K_{2P}9.1_{N53Q}$ was similar to the tunicamycin treated WT channel, and the mobility of r$K_{2P}9.1_{N53Q}$ could not be further increased by tunicamycin treatment (Figure 6.4 B). In conclusion, these data showed that both rK_{2P}3.1 and rK_{2P}9.1 channels are glycoproteins, with *N*-linked glycosylation occurring at N53 (Figure 6.4).

6.3.2 Impact of *N*-linked glycosylation on TASK channel activity

To assess the implications of TASK channel glycosylation on channel activity, the electrophysiological properties of HEK293 cells transfected with either untagged WT or N53Q rat channels, alongside GFP on separate plasmids, were assessed by whole-cell patch clamp experiments (Method 2.8.2). The untagged rat K_{2P}3.1 and K_{2P}9.1 channel constructs had been confirmed to be functional prior to this study (Table 2.3; Mant et al., 2011). The same recording conditions to those utilised in Chapter 5 and Result 6.2 were applied (Method 2.8.2).

Figure 6.3: Conserved *N*-linked glycosylation motif in TASK channels

Alignment of amino acids 50-100 for $K_{2P}3.1$ and $K_{2P}9.1$ channels (mouse (m), rat (r), and human (h)).

The conserved *N*-linked glycosylation consensus site asparagine 53 (N53) and channel selectivity filter (GYG) are highlighted.

The external domain is highlighted in light grey and the pore-forming loop in darker grey.

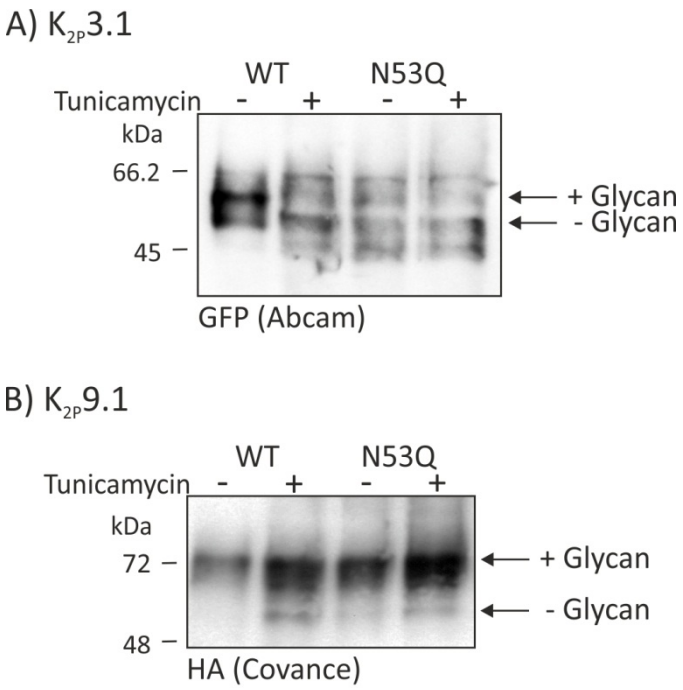

Figure 6.4: TASK channels are *N*-linked glycoproteins

Protein mobility of wild type (WT) and glycosylation mutant (N53Q) rat TASK channels expressed in COS-7 cells. Transfected COS-7 cells were either untreated (-) or tunicamycin treated (+) for 16 h prior cell lysis. Samples were harvested 24 h post transfection.

A) GFP and HA tagged rK_{2P}3.1; WT and N53Q. K_{2P}3.1 protein was visualised using a rabbit polyclonal anti-GFP antibody (Abcam).

B) GFP and HA tagged rK_{2P}9.1; WT and N53Q. K_{2P}9.1 protein was visualised using a mouse monoclonal anti-HA tag antibody (Covance).

WT rK_{2P}3.1 protein was detected at 60 kDa and WT rK_{2P}9.1 at 72 kDa. Indicated by + glycan arrow.

HEK293 cells expressing WT rK$_{2P}$3.1 produced an *I-V* relationship with the expected characteristics for a K$_{2P}$ channel (Figure 6.5 A) and these were comparable to the WT untagged human K$_{2P}$3.1 channel (Figure 5.6). As predicted for WT rK$_{2P}$3.1 channel, extracellular acidification (pH 6.5) caused a significant positive shift in the reversal potential (from -60.9 ± 3.2 mV to -29.9 ± 5.6 mV ($p < 0.01$); Figure 6.5 A) and reduction of the current amplitude ($p = 0.007$; Figure 6.5 B). The amplitude of the acid inhibited WT rK$_{2P}$3.1 currents (pH 6.5) were comparable to UT cells at pH 7.8 ($p = 0.98$; Figure 6.5 B). The *I-V* relationship of rK$_{2P}$3.1$_{N53Q}$ expressing cells was significantly different from WT rK$_{2P}$3.1 channels, and equivalent to acid inhibited WT currents or UT cells (Figure 6.5 A). At pH 7.8, rK$_{2P}$3.1$_{N53Q}$ channels have a significantly more positive reversal potential (-31.2 ± 6.0 mV compared to -60.9 ± 3.2 mV; $p < 0.01$) and lower current amplitude ($p < 0.01$; Figure 6.5 B) compared to WT rK$_{2P}$3.1 channels. These differences indicated that rK$_{2P}$3.1$_{N53Q}$ expressing cells have reduced outward K^+ currents compared to WT rK$_{2P}$3.1 expressing cells. Unlike WT rK$_{2P}$3.1 expressing cells, rK$_{2P}$3.1$_{N53Q}$ currents were not inhibited by extracellular acidification ($p = 1.00$; Figure 6.5 B), indicating that no acid-sensitive currents are expressed in these cells. These data showed that K$_{2P}$3.1$_{N53Q}$ expressing cells have reduced outward K^+ currents compared to WT K$_{2P}$3.1 expressing cells and elicit currents that are comparable to UT cells. This suggested that *N*-linked glycosylation was required to produce functional K$_{2P}$3.1 currents.

The electrophysiological properties of WT and N53Q rK$_{2P}$9.1 channels were studied in equivalent experiments (Figure 6.6). WT rK$_{2P}$9.1 expressing cells also elicited an *I-V* relationship that was typical for a K$_{2P}$ channel (Figure 6.6 A) and had similar characteristics to the WT human K$_{2P}$9.1 channel (Figure 5.8). Extracellular acidification (pH 6.5) resulted in a modest reduction in WT rK$_{2P}$9.1 currents, although this was not significant ($p = 0.49$; Figure 6.6 B). No significant differences were observed between the *I-V* relationships elicited by cells expressing rK$_{2P}$9.1$_{N53Q}$ or WT rK$_{2P}$9.1 channels (Figure 6.6), with equivalent reversal potentials (-60.0 ± 5.8 mV for rK$_{2P}$9.1$_{N53Q}$ versus -67.2 ± 1.3 mV for WT rK$_{2P}$9.1; $p = 0.57$) and current amplitudes detected ($p = 0.83$). These data indicated that there was no difference in the outward K^+ currents between WT rK$_{2P}$9.1 and rK$_{2P}$9.1$_{N53Q}$ expressing cells. Extracellular acidification also caused no reduction in current amplitude of rK$_{2P}$9.1$_{N53Q}$ expressing cells ($p = 0.99$; Figure 6.6 B). These data showed that unlike rK$_{2P}$3.1, glycosylation of rK$_{2P}$9.1 channels was not critical for the production of functional K$_{2P}$9.1 currents. The apparent lack of acid sensitivity of both WT and N53Q rK$_{2P}$9.1 channels in

these experiments was likely to be due to pH used for extracellular acidification (pH 6.5). K_{2P}9.1 channels are less sensitive to changes in extracellular pH (pK 6.7; Kim et al., 2000) than K_{2P}3.1 channels (pK 7.3; Duprat et al., 1997). However, pH 6.5 was selected so that the recording conditions were identical to those used to study K_{2P}3.1 channels.

In conclusion, these data indicated that both K_{2P}3.1 and K_{2P}9.1 channels are glycoproteins, with *N*-linked glycosylation occurring at asparagine 53 (N53). *N*-linked glycosylation appeared to be critical for the production of functional rK_{2P}3.1 currents and we have shown that when channel glycosylation is prevented the localisation of rK_{2P}3.1 protein was altered (Mant et al., 2013b). In tunicamycin treated WT rK_{2P}3.1 expressing COS-7 cells, or cells expressing $rK_{2P}3.1_{N53Q}$, little expression of the channel was detected on the plasma membrane by flow cytometry and immunofluorescent staining (Mant et al., 2013b). However, a loss of rK_{2P}9.1 channel glycosylation only caused a modest reduction in the cell surface expression; in tunicamycin treated cells a 40 % decrease in cell surface rK_{2P}9.1 protein was detected by flow cytometry (Mant et al., 2013b). These data showed that *N*-linked glycosylation has different impacts on TASK channel expression and function, for K_{2P}3.1 channels glycosylation was critical for the surface expression and therefore the functionality of the channel. However, *N*-linked glycosylation was not critical for K_{2P}9.1 surface expression or function. Additionally, to determine if K_{2P}3.1 protein glycosylation was regulated by changes in external glucose concentrations, we showed that culturing COS-7 cells expressing WT rK_{2P}3.1 in reduced glucose concentrations (1.0 g/l glucose, for 16 h) decreased the channel surface expression by 25 % compared to normal glucose concentrations (4.5 g/l glucose; Mant et al., 2013b). These data indicated that chronic cell culture under reduced glucose concentrations altered K_{2P}3.1 glycosylation and this may impact on K_{2P}3.1 channel activity.

In the mammalian brain, glucose levels typically vary between 1-2.5 mM (Burdakov et al., 2006); however the cell culture media used in this study ranged from 11-25 mM glucose (2.0-4.5 g/l glucose; Method 2.4.2). Based on the modest reduction of K_{2P}3.1 surface expression observed following treatment with 1.0 g/l glucose (5.6 mM), a lower concentration of 0.5 g/l glucose (2.8 mM) was selected for subsequent experiments investigating low glucose. Although 0.5 g/l glucose (2.8 mM) is nearly a 10-fold decrease compared to DMEM media (4.5 g/l or 25 mM glucose), this value was at the upper limit of the typical physiological glucose concentrations observed within the brain.

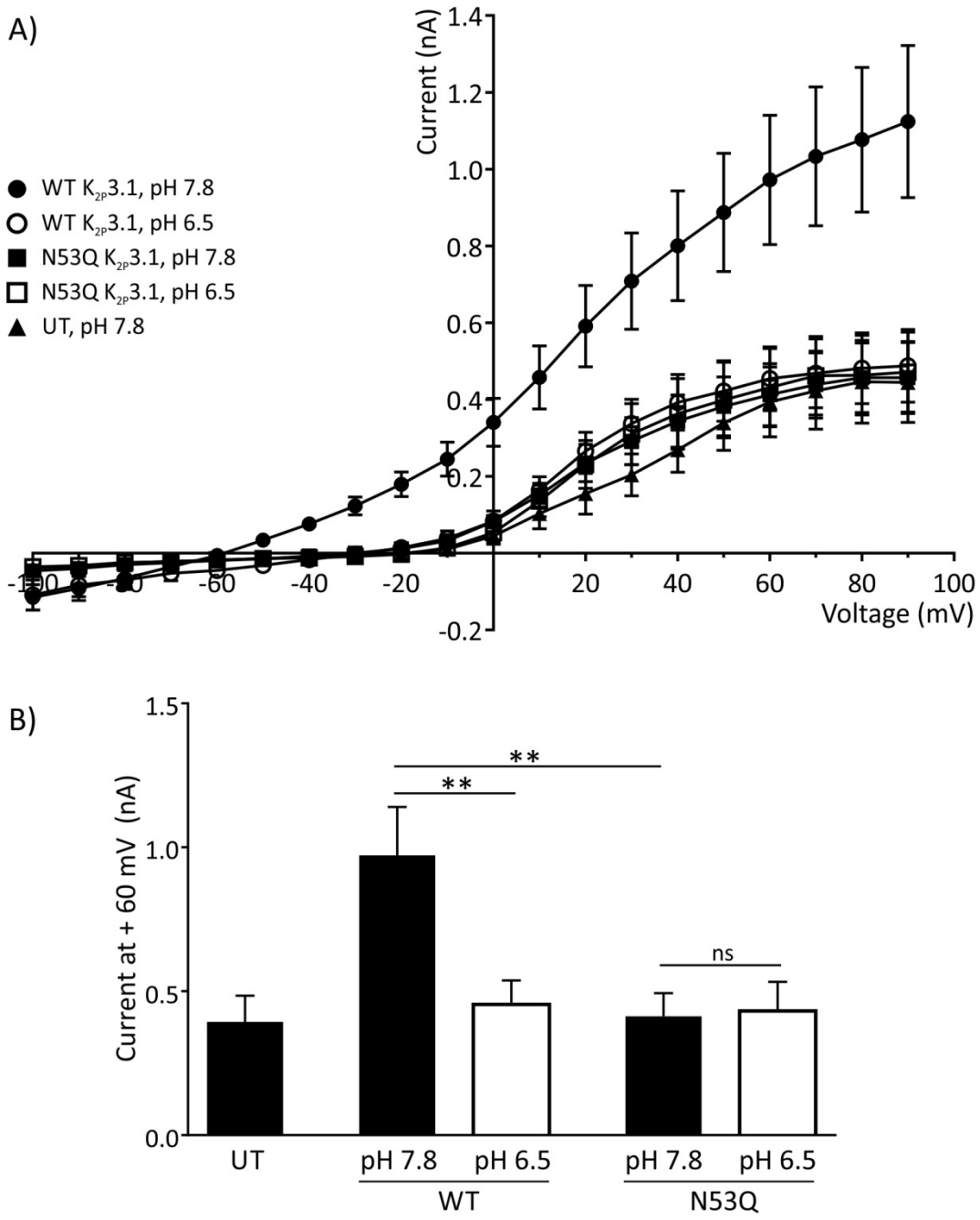

Figure 6.5: Electrophysiological modulation of rat $K_{2P}3.1$ by glycosylation
Showing the electrophysiological properties of HEK293 cells expressing WT $rK_{2P}3.1$ or $rK_{2P}3.1_{N53Q}$ channels (1.5 µg channel DNA co-transfected with 0.5 µg GFP DNA). The currents for untransfected (UT) cells are shown. Cells were analysed 24 h post-transfection and ≈70 % of cells were transfected (identified by GFP fluorescence). Currents were evoked by voltage steps from -100 to +90 mV in 10 mV increments, for 50 ms duration.
A) *I-V* relationship for both channels at pH 7.8 and pH 6.5, in addition to untransfected (UT) cells at pH 7.8. The data shown are the average of n ≥ 7 cells, ± SEM.
B) Average current (+ SEM) elicited at +60 mV voltage step for all conditions (n ≥ 7 cells). Statistical significance was calculated using a one-way ANOVA, with Dunnett's multiple comparisons post-hoc test (** $p < 0.01$, ns: non-significant). The statistical comparisons performed are indicated by horizontal lines.

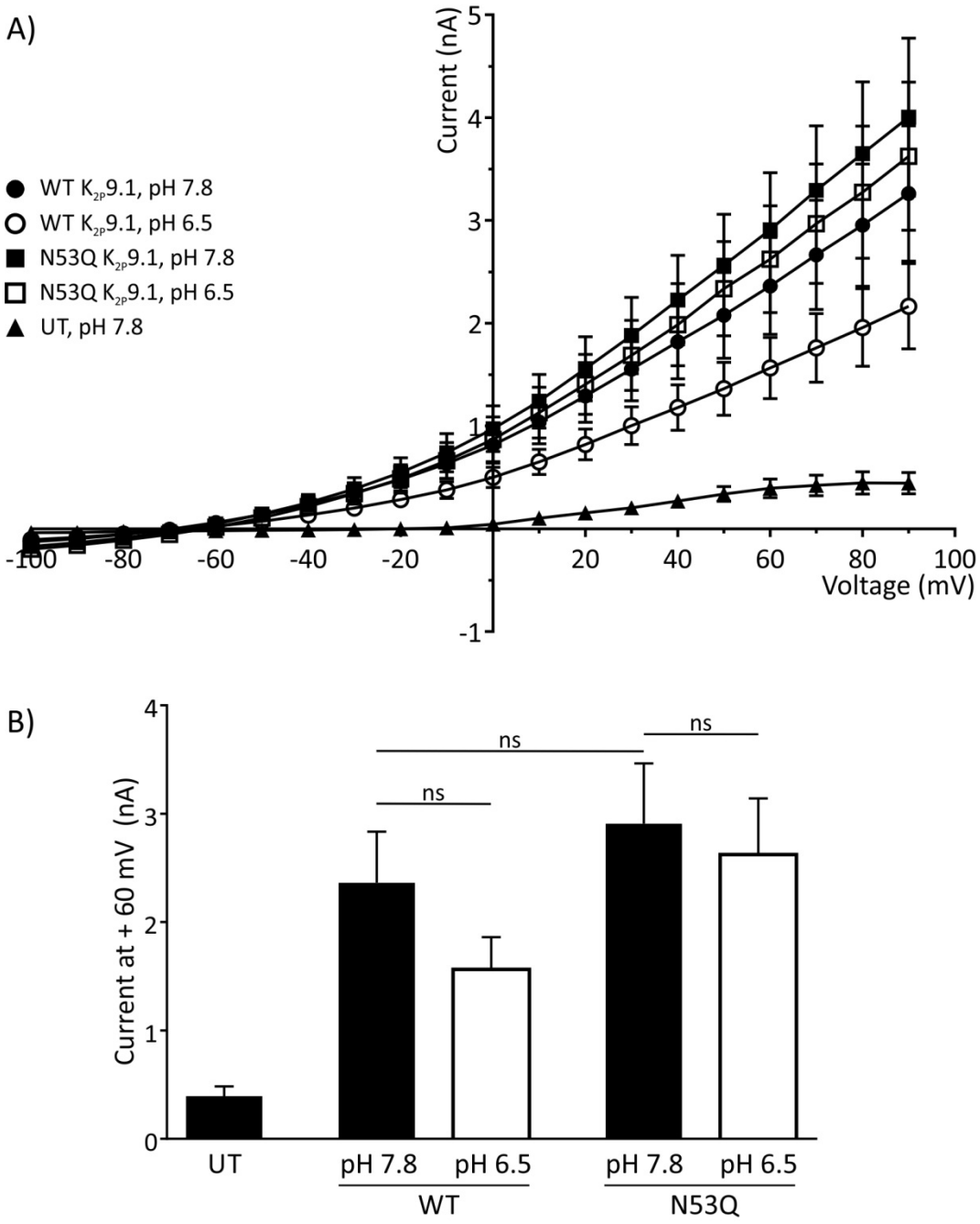

Figure 6.6: Electrophysiological modulation of rat K_{2P}9.1 by glycosylation
Showing the electrophysiological properties of HEK293 cells expressing either WT rK_{2P}9.1 or r$K_{2P}9.1_{N53Q}$ channels (0.5 µg channel DNA co-transfected with 0.5 µg GFP). The currents for untransfected (UT) HEK293 cells are also shown. Cells were analysed 24 h post-transfection and ≈40 % of cells were transfected (identified by GFP fluorescence). Currents were evoked by voltage steps from -100 to +90 mV in 10 mV increments, for 50 ms duration.
A) *I-V* relationship for both channels at pH 7.8 and pH 6.5, in addition to untransfected (UT) cells at pH 7.8. The data shown are the average of n ≥ 7 cells, ± SEM.
B) Average current (+ SEM) elicited at +60 mV voltage step for all conditions (n ≥ 7 cells). Statistical significance was calculated using a one-way ANOVA, with Dunnett's multiple comparisons post-hoc test (ns: non-significant). The statistical comparisons performed are indicated by horizontal lines.

6.4 Environmental regulation of endogenous TASK channel function

Data presented in Chapter 4 showed that, despite $K_{2P}3.1$ and $K_{2P}9.1$ protein expression, A549 cells do not exhibit significant currents with TASK-like properties (discussed in Section 4.7.3). The experiments presented in this section aimed to determine if altered environmental conditions (chronic hypoxia or low glucose) change the whole-cell outward K^+ current characteristics in A549 lung cancer cells. To examine the effect of chronic hypoxia (5 % O_2) or low glucose (0.5 g/l) the whole-cell currents of A549 cells cultured in these conditions, for 24 h prior to recordings were compared to control culture conditions (20 % O_2, 3.2 g/l glucose). No control recordings were achieved on the same experimental day as cells cultured in hypoxia or low glucose. Therefore, the control data presented here are from the two experimental days prior to environmental assessment of A549 whole-cell currents. These recordings were made using the same batch of cells, culture media, and electrophysiological buffers. For whole-cell recordings, the same ionic gradients, voltage protocol, and channel modulation conditions to those used in Chapter 4 were applied (Method 2.8.2). To assess if any TASK-like whole-cell K^+ currents were present in A549 cells cultured under altered environmental conditions, the same pharmacological protocol as used in Chapter 4 was applied by first identifying the TEA-insensitive currents (application of 30 mM TEA) followed by extracellular acidification (pH 6.0).

The *I-V* relationships recorded at pH 7.4 for cells in 5 % O_2 or 0.5 g/l glucose were similar to control culture conditions (20 % O_2, 3.2 g/l glucose), with no differences in the shape or amplitude of the *I-V* relationships observed (Figure 6.7). For A549 cells cultured in 5 and 20 % O_2, both the reversal potential ($p = 1.00$; Figure 6.7 A) and current amplitude were comparable ($p = 0.39$; Figure 6.7 B). Additionally, compared to control cells, in 0.5 g/l glucose cultured cells an equivalent reversal potential ($p = 0.95$; Figure 6.7 C) and current amplitude was observed ($p = 0.86$; Figure 6.7 D).

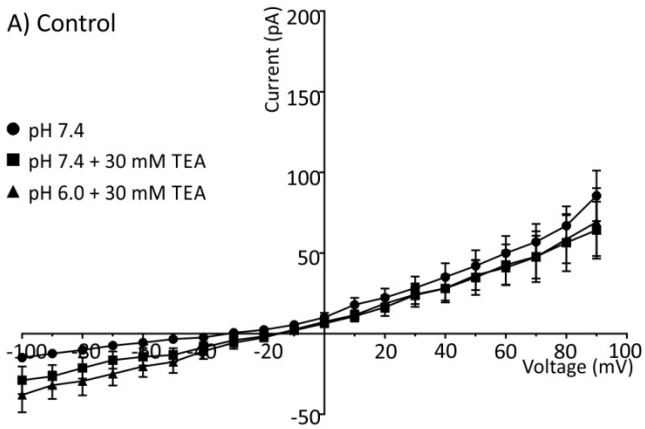
A) Control
pH 7.4
pH 7.4 + 30 mM TEA
pH 6.0 + 30 mM TEA
Current (pA)
Voltage (mV)

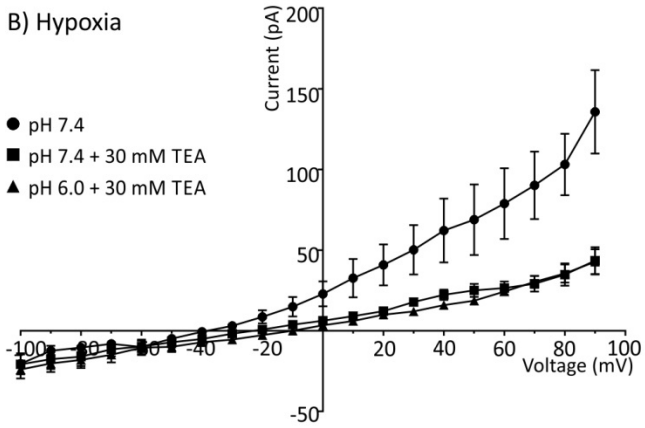
B) Hypoxia
pH 7.4
pH 7.4 + 30 mM TEA
pH 6.0 + 30 mM TEA
Current (pA)
Voltage (mV)

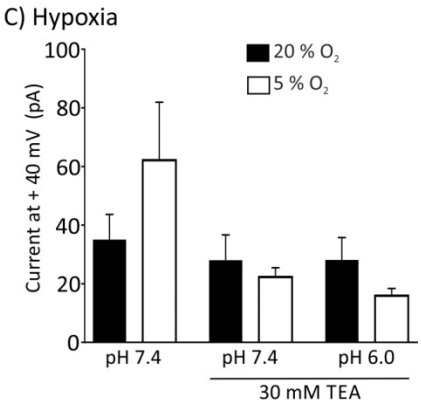
C) Hypoxia
20 % O2
5 % O2
Current at + 40 mV (pA)
pH 7.4
pH 7.4
pH 6.0
30 mM TEA

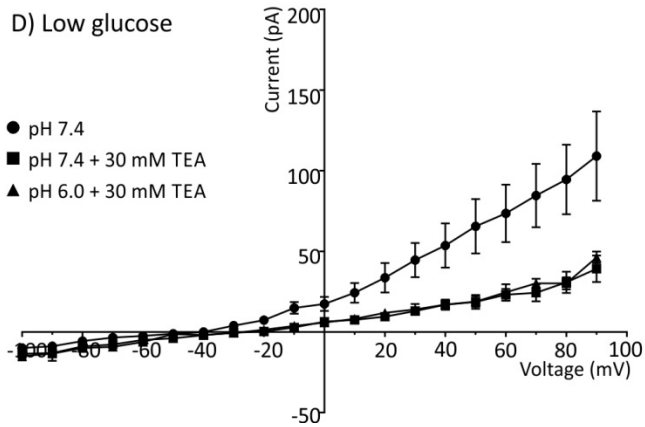
D) Low glucose
pH 7.4
pH 7.4 + 30 mM TEA
pH 6.0 + 30 mM TEA
Current (pA)
Voltage (mV)

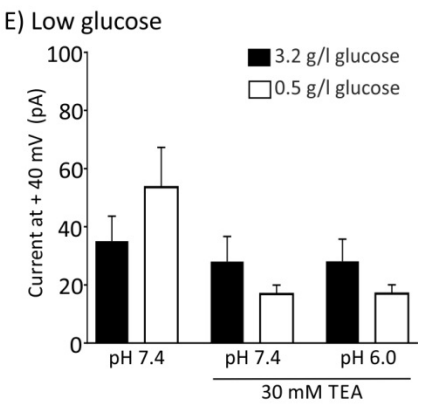
E) Low glucose
3.2 g/l glucose
0.5 g/l glucose
Current at + 40 mV (pA)
pH 7.4
pH 7.4
pH 6.0
30 mM TEA

Figure 6.7: Environmental modulation of A549 lung cancer whole-cell currents

Electrophysiological characterisation of the whole-cell outward currents recorded from A549 cells cultured in control conditions (20 % O_2, 3.2 g/l glucose), hypoxia (5 % O_2) or low glucose (0.5 g/l). To identify any TASK-like currents, the leak K^+ current was first identified using 30 mM TEA followed by extracellular acidification (pH 6.0). Currents were evoked by voltage steps from -100 to +90 mV in 10 mV increments, for 70 ms duration.

A) *I-V* relationships of cells cultured in control conditions under different modulation conditions. The data shown are the average of n > 4 cells, ± SEM.
B) *I-V* relationships of cells cultured in hypoxia under different modulation conditions. The data shown are the average of n > 4 cells, ± SEM.
C) Average current (+ SEM) elicited at +40 mV voltage step, for all conditions (n ≥ 4 cells).
D) *I-V* relationship of cells cultured in low glucose under different modulation conditions. The data shown are the average of n > 4 cells, ± SEM.
E) Average current (+ SEM) elicited at +40 mV voltage step, for all conditions (n ≥ 4 cells).

Statistical significance was calculated using a one-way ANOVA, with Sidak's multiple comparisons post-hoc test.

In Chapter 4, 30 mM TEA significantly inhibited the whole-cell outward K^+ currents of A549 cells cultured in control conditions. These data showed that the addition of TEA to cells cultured in control conditions resulted in a non-significant positive shift of the reversal potential ($p = 0.27$; Figure 6.7 A) and a reduction in the current amplitude ($p = 0.82$; Figure 6.7 B). TEA inhibition did not reach significance in this set of experiments and this may have been due to the low sample number ($n < 7$ cells). The same trend was observed following the addition of TEA to A549 cells cultured in altered environmental conditions and no differences were observed between the *I-V* relationships recorded (Figure 6.7). In Chapter 4, a no significant current with TASK-like properties (TEA-insensitive and acid-sensitive) could be isolated from A549 cells. The data presented in this chapter also showed that in control conditions extracellular acidification (pH 6.0) caused no modulation of the TEA-insensitive currents, with equivalent reversal potentials ($p = 1.00$; Figure 6.7 A) and current amplitudes detected ($p = 1.00$; Figure 6.7 B). The same effect was observed in A549 cells cultured in 5 % O_2, Figure 6.7 A, B) and 0.5 g/l glucose ($p = 1.00$; Figure 6.7 C, D).

In summary, the data presented in this chapter show that culturing A549 cells in either chronic hypoxia (5 % O_2) or low glucose (0.5 g/l glucose) had no significant effect on the whole-cell outward currents compared to control culture conditions (20 % O_2, 3.2 g/l glucose). Comparably to the data presented in Chapter 4, there was no indication of whole-cell currents with TASK-like characteristics in A549 cells cultured under both control and altered conditions. As discussed in Chapter 4, without robust tools to specifically isolate TASK channel function this study is limited (discussed in Section 4.7.3). Therefore, at this time there is no evidence to support that the presence of $K_{2P}3.1$ and $K_{2P}9.1$ channel protein in A549 cells resulted in TASK channel activity at the cell surface.

6.5 Environmental regulation of cancer cell functions

Chronic cell stress conditions, low serum (0.2-1 %) and hypoxia (0-10 % O_2), have been found to promote cell growth and survival in $K_{2P}3.1$ or $K_{2P}9.1$ expressing C8 fibroblasts (Liu et al., 2005; Mu et al., 2003). These published studies suggested that TASK channels provide an advantage to cells cultured under environmental stress conditions. The aim of the data presented in this section was to determine if the altered environmental conditions (chronic hypoxia (5 % O_2) or low glucose (0.5 g/l glucose)) assessed in this chapter have an

impact on cellular functions in cell lines with heterologous (HEK293 cells) or native (A549 cells) TASK channel protein expression. For this, comparable functional assays to those performed in Chapter 5 were utilised. As before, it should be highlighted that no evidence has been generated in this thesis which proved TASK channel activity at the cell surface of A549 cells, despite the expression of both $K_{2P}3.1$ and $K_{2P}9.1$ channel protein (discussed in Section 4.7.3). One hypothesis for this finding could be that TASK channel protein is located on the intracellular membranes of A549 cells, for example in the mitochondria. In the interest of further characterising A549 cells and to investigate whether TASK channel inhibition has significant impacts on A549 cellular functions in environmental stress conditions, this cell line continued to be utilised for this study.

6.5.1 Impact of environmental conditions on TASK channel expressing HEK293 cell functions

Utilisation of cancer cell lines with endogenous TASK channel protein expression in this thesis has been limited by the fact that extensive studies to characterise the TASK channel activity were not performed. Therefore, the work presented in this section aimed to use HEK293 cells as an expression system where cDNA constructs known to produce functional TASK channel activity at the cell surface could be utilised. This would then allow cellular functions to be assessed in a cell population with TASK channel activity. This experimental technique has been utilised in several published studies to determine if $K_{2P}9.1$ expression resulted in any alterations to cellular functions (Liu et al., 2005; Mu et al., 2003; Pei et al., 2003). It should be noted that HEK293 cells do not originate from a cancer source and therefore the experiments presented here may not accurately represent the role played by TASK channel activity in a cancer situation. However, these experiments may give an indication of research areas which require further investigation.

In the experiments presented in this section HEK293 cells transiently expressing either WT $K_{2P}3.1$ (untagged WT $K_{2P}3.1$ co-transfected with GFP), WT $K_{2P}9.1$ (GFP tagged WT $K_{2P}9.1$), non-functional $K_{2P}9.1_{G97E}$ (pore mutant GFP-$K_{2P}9.1_{G97E}$), or GFP (GFP alone) were used to assess the effect of environmental conditions on cell proliferation and apoptosis. Expression of GFP controlled for any functional changes that may be caused by the pEGFP-C1 plasmid, which encodes both GFP and the $K_{2P}9.1$ channel constructs. The cDNA

constructs used were characterised and shown to be functional in this thesis (untagged $K_{2P}3.1$ (Figure 5.6, page 283), WT GFP-$K_{2P}9.1$ (Figure 5.8, page 287), and GFP-$K_{2P}9.1_{G97E}$ (Figure 5.8, page 287)), or prior to this study (GFP; Table 2.3). HEK293 cells were transfected with 5 µg of channel or GFP plasmid cDNA and incubated overnight (Method 2.4.4.1). Cells were then re-plated for each assay and seeded for 24 h, before culturing in either control (20 % O_2, 4.5 g/l glucose), hypoxic (5 % O_2), or low glucose (0.5 g/l glucose) conditions, for an additional 24 h prior to the assessment of cell proliferation (Method 2.7.2) or apoptosis (Method 2.7.3).

6.5.1.1 Proliferation

MTS assays were utilised to study the effects of channel expression on cell growth, with the resulting absorbance being proportional to the number of cells (Method 2.7.2). Following this assay, the absorbance values (at 490 nm) detected had a large amount of variability for each experimental replicate, in both untransfected (UT) and transfected cells (for example from 0.13 to 1.57 (n = 6) for GFP expressing cells). Therefore, to allow comparison between the experimental replicates, the absorbance values observed were normalised to GFP expressing HEK293 cells.

Expression of functional TASK channels or non-functional $K_{2P}9.1_{G97E}$ in cells cultured in control conditions (20 % O_2, 4.5 g/l glucose) did not significantly alter cell numbers compared to UT cells (Figure 6.8). The same trend was observed when cells were cultured in 5 % O_2 (Figure 6.9 A) and 0.5 g/l glucose (Figure 6.8 B). Comparing between each transfection condition, hypoxia caused a significant decrease in the numbers of UT and WT $K_{2P}3.1$ expressing cells ($p < 0.0001$; Figure 6.8 A). Reduced cell numbers were also observed in WT $K_{2P}3.1$ expressing cells in low glucose compared to control conditions, although this was not significant ($p = 0.09$; Figure 6.8 B). In conclusion, MTS assays showed that the expression of functional $K_{2P}3.1$ and $K_{2P}9.1$ channels in HEK293 cells cultured in control or altered environmental conditions does not result in any significant change to cell numbers compared to UT cells. Therefore, TASK channel activity in HEK293 cells does not result in any proliferative advantage.

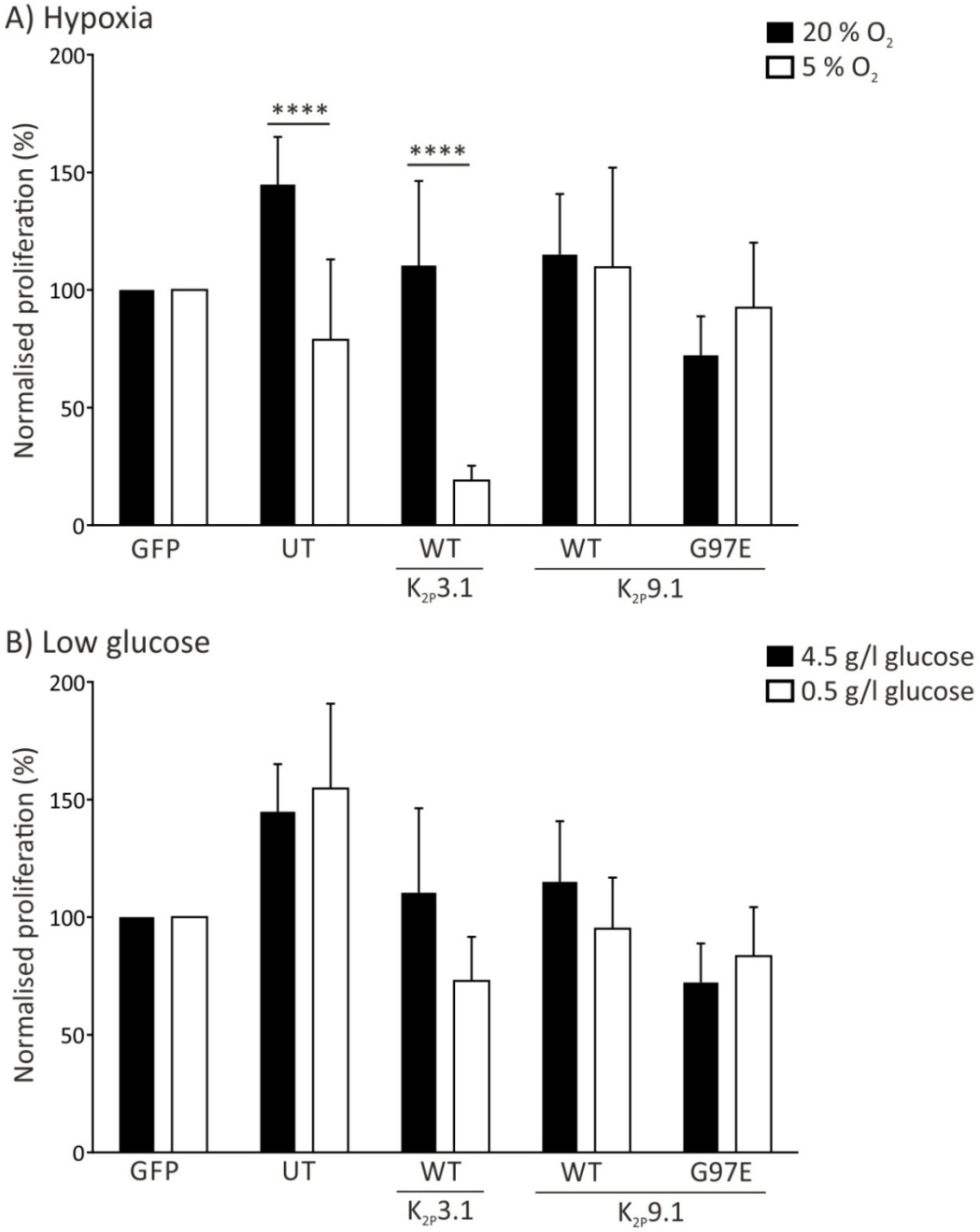

Figure 6.8: Assessment of proliferation under altered environmental conditions in a heterologous expression system

Proliferation of transfected HEK293 cells was measured 48-72 h post-transfection following 24 h cell culture in (A) hypoxia (5 % O_2) or (B) low glucose (0.5 g/l) compared to control conditions (20 % O_2, 4.5g/l glucose).

GFP: green fluorescent protein. UT: untransfected. WT K_{2P}3.1: wild type untagged K_{2P}3.1 co-transfected with GFP. WT K_{2P}9.1: wild type GFP tagged K_{2P}9.1. G97E K_{2P}9.1: pore mutant GFP tagged $K_{2P}9.1_{G97E}$.

Data are presented as normalised proliferation compared to GFP expressing cells (average % + SEM), n ≥ 3 experimental repeats.

Statistical significance was calculated by a two-way ANOVA with Dunnett's multiple comparisons post-hoc test (**** $p < 0.0001$). Significant comparisons, where present, are indicated by horizontal lines.

6.5.1.2 Apoptosis

Apoptosis was examined utilising the same conditions as Chapter 5, by detecting the percentage of annexin V stained cells with flow cytometry (Method 2.7.3). In cells cultured in control conditions (20 % O_2, 4.5 g/l glucose) expression of WT channels or non-functional $K_{2P}9.1_{G97E}$ resulted in a slight, but non-significant, increase of cell death compared to UT cells (Figure 6.9). Culturing transfected cells in 5 % O_2 resulted in the same trend; TASK channel expression caused a non-significant increase in cell death that did not depend on the channel being functional (Figure 6.9 A). For each transfection condition, no differences were detected in apoptosis between 5 and 20 % O_2 cultured cells (Figure 6.9 A). Culturing cells in 0.5 g/l glucose caused a reduction of UT cell death compared to 4.5 g/l glucose, although this was not significant ($p = 0.34$; Figure 6.9 B). $K_{2P}9.1_{G97E}$ expression in 0.5 g/l glucose cultured cells caused a significant increase in apoptosis compared to UT cells, and this could have resulted from a knockdown of native $K_{2P}9.1$ channels in HEK293 cells (positive for $K_{2P}9.1$ mRNA; Chapter 4). However, no difference was detected between the cell death caused by $K_{2P}9.1_{G97E}$ expression in 0.5 and 4.5 g/l glucose cultured cells ($p = 0.88$; Figure 6.9 B). This suggested that the increase in cell death of $K_{2P}9.1_{G97E}$ expressing cells in low glucose was related to the decrease of UT cell apoptosis. In conclusion, these data indicated that expression of functional $K_{2P}3.1$ and $K_{2P}9.1$ channels in HEK293 cells has no significant impact on cell death under all conditions examined. In summary, the data presented in this section showed that utilisation of transfected HEK293 cells for functional assays did not reveal any proliferative or apoptotic effects which were related to TASK channel activity.

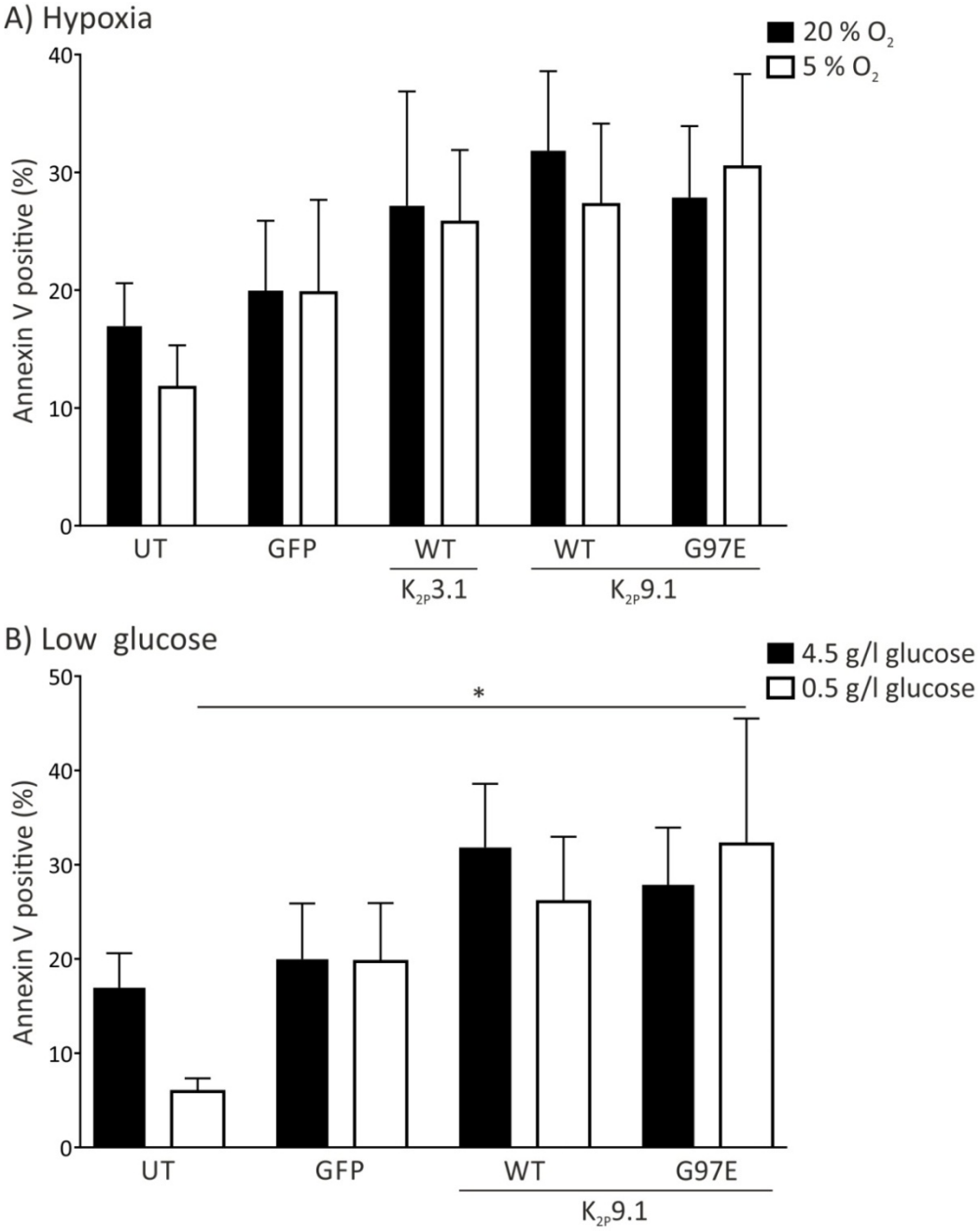

Figure 6.9: Assessment of apoptosis under altered environmental conditions in a heterologous expression system

Apoptotic response of transfected HEK cells measured 48-72 h post-transfection following a 24 h exposure to (A) hypoxia (5 % O_2) or (B) low glucose (0.5 g/l glucose) compared to control culture conditions (20 % O_2, 4.5g/l glucose).

UT: untransfected. GFP: green fluorescent protein. WT K_{2P}3.1: wild type untagged K_{2P}3.1 co-transfected with GFP. WT K_{2P}9.1: wild type GFP tagged K_{2P}9.1. G97E K_{2P}9.1: pore mutant GFP tagged $K_{2P}9.1_{G97E}$.

Data are presented as average number of annexin V positive cells (%) + SEM, n ≥ 3 experimental repeats.

Statistical significance was calculated by a two-way ANOVA with Dunnett's multiple comparisons post-hoc test (* $p < 0.05$). Significant comparisons, where present, are indicated by horizontal lines.

6.5.2 Impact of environmental conditions on A549 cancer cell functions

Utilisation of HEK293 cells allowed functional assays to be performed on a cell system where TASK channel activity could be induced by cDNA construct expression, however this system was also limited by the fact it did not represent a cancerous model. Data presented in Chapter 5 show that TASK channel modulation has no effect on A549 cell functions in control culture conditions (20 % O_2, 3.2 g/l glucose). This finding may not be surprising as no significant TASK channel activity could be detected on the cell surface of A549 by whole-cell patch clamping under both normal (Chapter 4) and altered environmental conditions (Result 6.4). However, a lack of cell surface activity does not eliminate the potential for TASK channel expression and function on intracellular membranes. Therefore, in the interest of completeness, equivalent functional assays to those used in Chapter 5 were performed to assess if TASK channels play a role in A549 cell functions when cultured in hypoxia or low glucose. The assays used were MTS assays, flow cytometry with annexin V staining, and wound healing assays, to determine proliferation, apoptosis, and migration, respectively. These assays were performed in the presence of TASK channel inhibitors (genistein (100 µM), methanandamide (50 µM), and ruthenium red (100 µM)), as well as 5mM 4-AP for broad spectrum KCh inhibition (which modulates non-leak KCh channels). In addition, the effect of a functional $K_{2P}9.1$ knockdown (using GFP-$K_{2P}9.1_{G97E}$ expression) in A549 cells on cell apoptosis was examined. Expression of GFP-$K_{2P}9.1_{G97E}$ in A549 cells could be used for apoptosis assay as flow cytometry allowed for the selection of GFP positive A549 cells (i.e. transfected cells) and therefore the low transfection efficiency (5-20 %) in A549 cells was not a limiting factor.

6.5.2.1 Proliferation

MTS assays were utilised to assess the regulation of A549 cell growth in different environmental conditions, (Method 2.7.2). The response observed following KCh modulation in A549 cells cultured in control conditions (20 % O_2, 3.2 g/l glucose) was equivalent to the proliferation data presented in Chapter 5 (Figure 5.9), where TASK channel inhibition and 4-AP (24 h exposure) caused no alteration to cell numbers compared to untreated cells (Figure 6.10). The same effect of KCh modulation on cell numbers was observed when A549 cells were cultured in 5 % O_2 (Figure 6.10 A). When comparing A549

cell numbers between 5 and 20 % O_2, hypoxia caused a non-significant increase of cell numbers regardless of the KCh modulation ($p > 0.21$; Figure 6.10 A). Culturing A549 cells in 0.5 g/l glucose also caused no alterations to cell numbers, with no differences observed between KCh inhibited and untreated cells ($p = 1.00$ for all; Figure 6.10 B). Additionally, increased A549 cell numbers were observed in low glucose culture conditions regardless of the inhibitor treatment, and this increase was significant for methanandamide treated cells ($p < 0.05$; Figure 6.10 B). In conclusion, these data showed that A549 cell numbers are unaffected by alterations in the cell culture conditions and that TASK channel inhibition has no effect on the regulation of cell numbers in A549 cells under all conditions examined.

6.5.2.2 Apoptosis

To assess the apoptotic response of A549 cells to either channel modulation or a functional $K_{2P}9.1$ knockdown, flow cytometry with annexin V staining was used (Method 2.7.3). As shown in Chapter 5, when A549 cells are cultured in normoxia (20 % O_2) 4-AP significantly increased the cell apoptosis compared to untreated cells ($p < 0.05$), whereas TASK channel modulation failed to alter cell death (Figure 6.11). In matched experiments, A549 cells were exposed to channel inhibitors and hypoxia (5 % O_2) for 48 h prior to the assessment of cell death (Figure 6.11 A). KCh modulation had the same effect in A549 cells cultured in 5 % O_2; 4-AP caused an increase in cell death compared to untreated cells, although this did not reach significance ($p = 0.16$), and TASK channel inhibition had no effect on apoptosis (Figure 6.11 A). No significant differences were observed between the apoptosis of A549 cells cultured in 5 and 20 % O_2 for each modulation condition (Figure 6.11 A).

The impact of low glucose on A549 cell death was assessed in separate experiments. For this, the effect of TASK channel modulation using methanandamide (50 µM, 24 h exposure) was measured in A549 cells cultured in either low (0.5 g/l) or control (3.2 g/l) glucose for 24 h. These data showed that methanandamide has no effect on A549 cell death in either condition ($p < 0.97$; Figure 6.11 B).

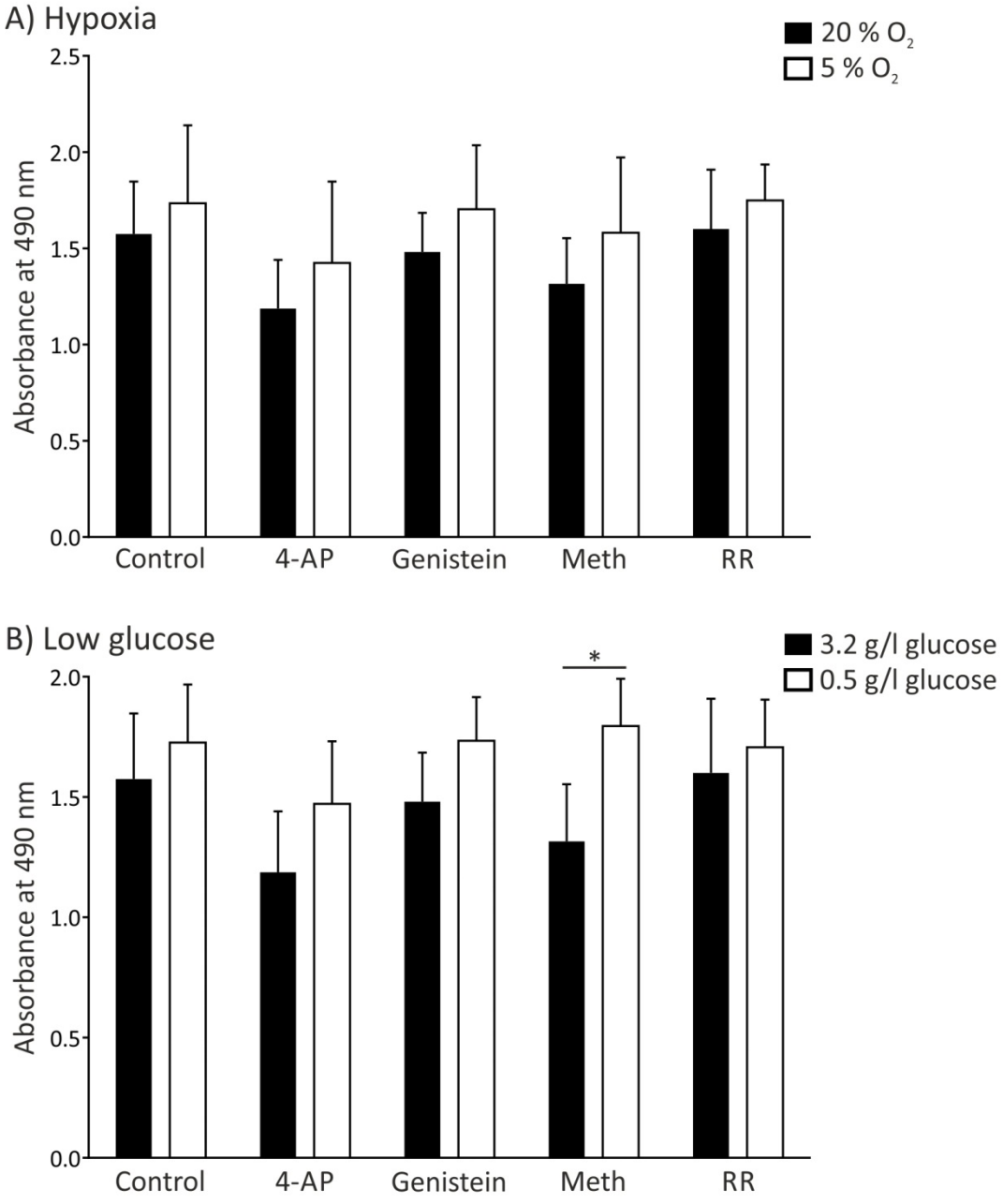

Figure 6.10: Assessment of A549 lung cancer cell proliferation under altered environmental conditions

Proliferation of A549 cells measured following a 24 h exposure to channel inhibitors in (A) hypoxia (5 % O_2) or (B) low glucose (0.5 g/l) compared to control culture conditions (20 % O_2, 3.2 g/l glucose).
Control (untreated), 5 mM 4-AP, 100 µM genistein, 50 µM methanandamide (meth), and 100 µM ruthenium red (RR).

Data are presented average absorbance at 490 nm + SEM, n = 3 experimental repeats.
Statistical significance was calculated by a two-way ANOVA with Turkey's post-hoc multiple comparisons test (* $p < 0.05$). Significant comparisons, where present, are indicated by horizontal lines.

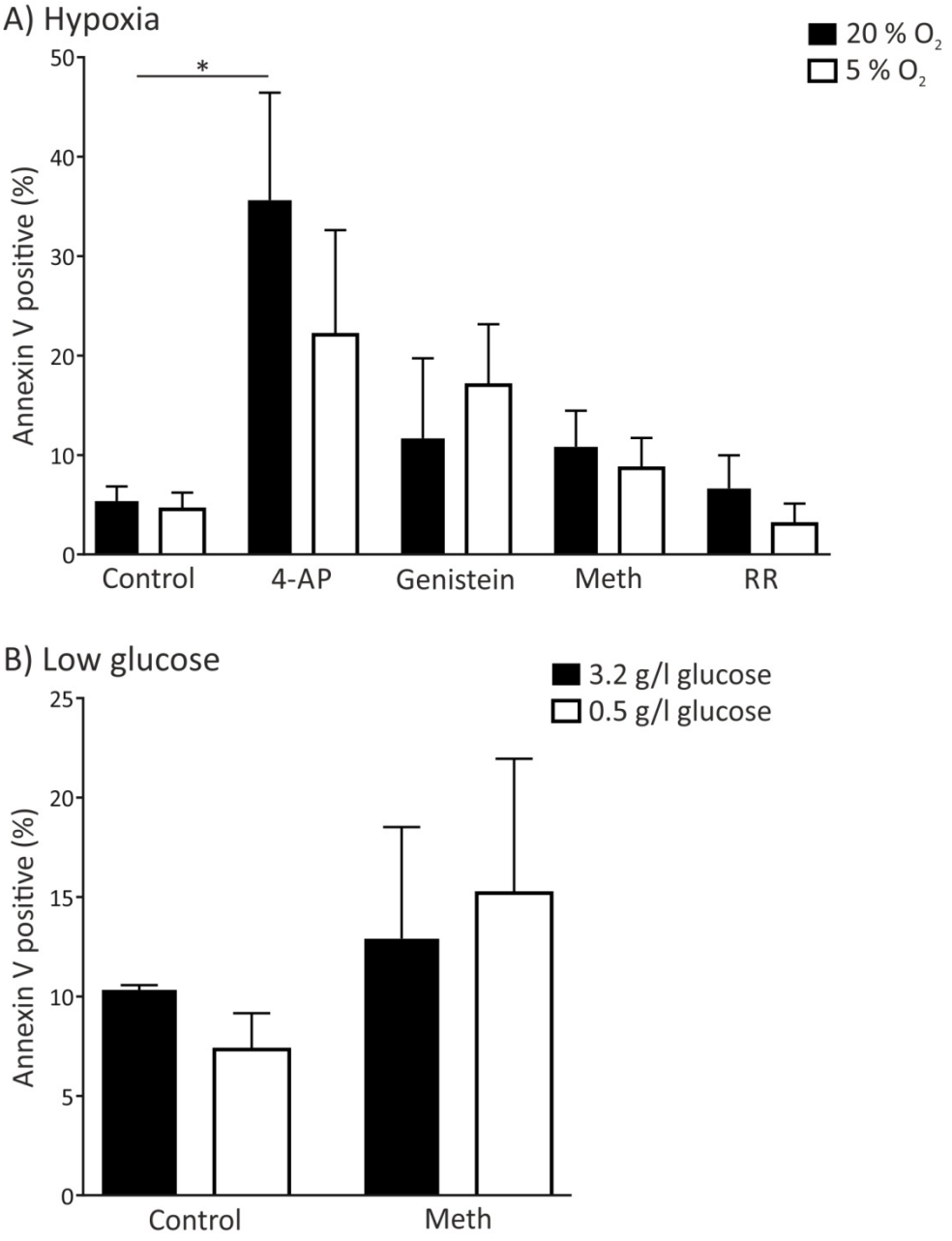

Figure 6.11: Assessment of A549 lung cancer cell apoptosis under altered environmental conditions

Apoptotic response of A549 cells measured following exposure to inhibitors when cultured in (A) hypoxia for 48 h (5 % O_2) or (B) low glucose for 24 h (0.5 g/l glucose) compared to control culture conditions (20 % O_2, 3.2 g/l glucose).
Control (untreated), 10 µM etoposide (apoptosis inducer), 5 mM 4-AP, 100 µM genistein, 50 µM methanandamide (meth), and 100 µM ruthenium red (RR).

Data are presented as average percentage of annexin V positive cells (%) + SEM, n ≥ 3 experimental repeats.
Statistical significance was calculated by a two-way ANOVA with Sidak's post-hoc multiple comparisons test (* $p < 0.05$). Significant comparisons, where present, are indicated by horizontal lines.

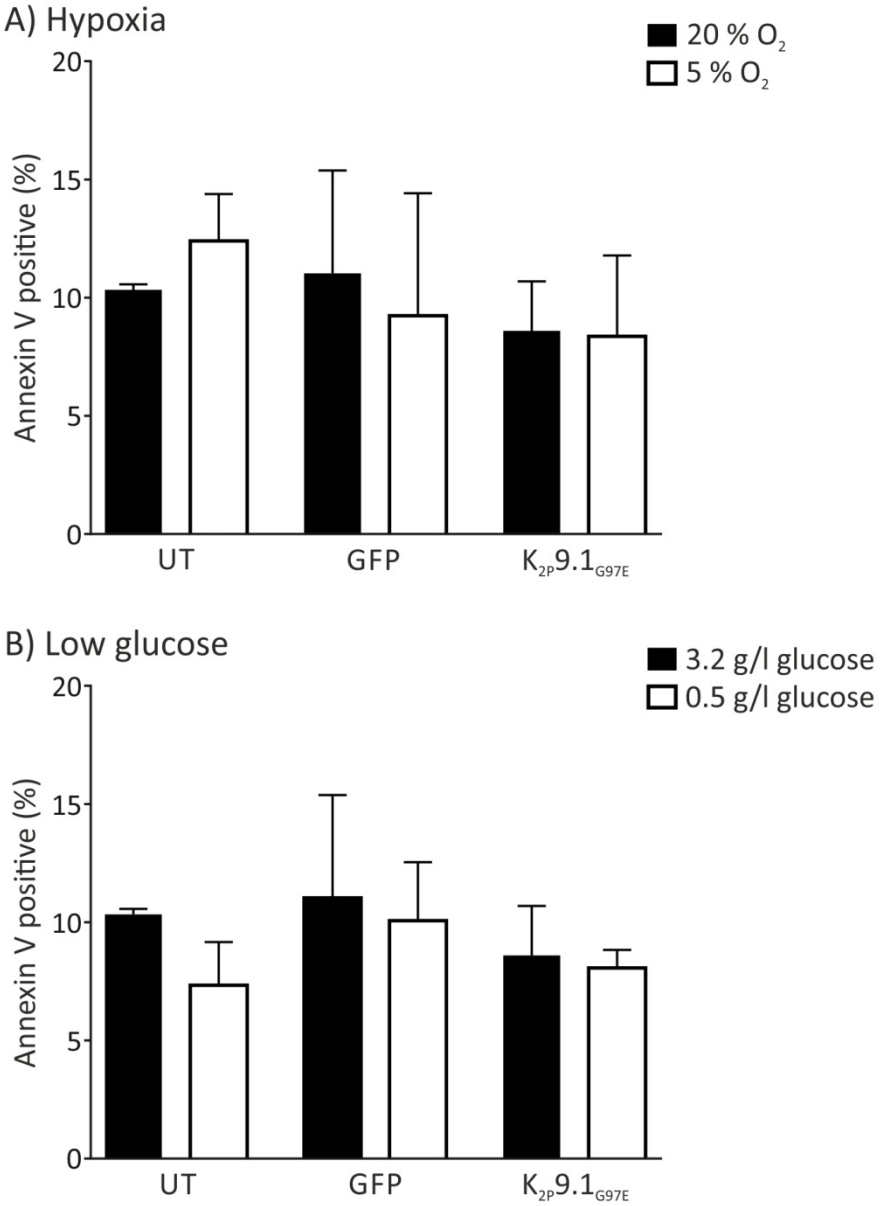

Figure 6.12: Assessment of functional $K_{2P}9.1$ channel knockdown on A549 lung cancer cell apoptosis under altered environmental conditions

Apoptotic response of A549 cells, measured 24 h post-transfection (2 µg DNA transfected), following a 24 h cell culture in (A) hypoxia (5 % O_2) or (B) low glucose (0.5 g/l glucose) compared to control culture conditions (20 % O_2, 3.2 g/l glucose).
UT: untransfected. GFP: green fluorescent protein. $K_{2P}9.1_{G97E}$: pore mutant GFP tagged $K_{2P}9.1$.

Data are presented as average percentage of annexin V positive cells (%) + SEM, n ≥ 3 experimental repeats.
Statistical significance was calculated by a two-way ANOVA with Sidak's post-hoc multiple comparisons test. Significant comparisons, where present, are indicated by horizontal lines.

The effect of a functional $K_{2P}9.1$ knockdown on A549 cell apoptosis when cells were cultured in chronic hypoxia and low glucose was also studied, by expression of non-functional $K_{2P}9.1_{G97E}$ channels (characterised in Chapter 5; Figure 5.8, page 287). Following DNA transfection (2 µg DNA transfected, Method 2.4.4.1), cells were cultured in control conditions (20 % O_2, 3.2 g/l glucose), hypoxia (5 % O_2), or low glucose (0.5 g/l glucose) for 24 h prior to the assessment of the cell death. In all three cell culture conditions, expression of $K_{2P}9.1_{G97E}$ or GFP failed to cause any alterations to A549 cell death ($p < 0.95$; Figure 6.12). In conclusion, data from apoptosis assays showed that pharmacological TASK channel modulation or expression of non-functional GFP-$K_{2P}9.1_{G97E}$ channels in A549 cells caused no alteration to cell death under control, hypoxia or low glucose culture conditions. 4-AP was used in this thesis to examine the role of non-leak KCh in cell death. The data presented here showed that 4-AP increases A549 cell death in both control and hypoxic conditions and that there was no difference in 4-AP induced apoptosis between the two culture conditions.

6.5.2.3 Migration

To assess A549 cell migration, wound healing assays were performed in comparable experiments to Chapter 5, by measuring the wound closure over a 9 h period in response to KCh modulation (Method 2.7.4). Cells were cultured in either hypoxia (5 % O_2) or low glucose (0.5 g/l) for 24 h prior to the start of the assay and these conditions were then maintained throughout the assay, in combination with the addition of KCh modulation (5 mM 4-AP, 50 µM methanandamide, and 100 µM ruthenium red).

As shown in Chapter 5, in control culture conditions (20 % O_2, 3.2 g/l glucose) 4-AP significantly reduced A549 cell migration ($p < 0.05$; Figure 6.13), however TASK channel modulation had no effect. The same trend was observed in matched experiments where A549 cells were cultured in 5 % O_2, with the effect of KCh modulation on cell migration being equivalent for 5 and 20 % O_2 cultured cells ($p = 1.00$; Figure 6.13 A). In separate experiments, methanandamide exposure did not alter A549 cell migration compared to untreated cells, when cultured in both low (0.5 g/l; $p = 0.70$) and control glucose (3.2 g/l, $p > 0.94$; Figure 6.13 B) conditions. In conclusion, these experiments showed that the environmental conditions tested in this chapter (hypoxia and low glucose) had no effect on

A549 cell motility. In addition, these data showed that TASK channel inhibition had no effect on A549 cell motility in control, hypoxic or low glucose culture conditions. In summary, the data presented in this chapter showed that TASK channel inhibition and environmental conditions have no impact on A549 cellular functions (proliferation, apoptosis, and migration).

6.6 Discussion

The primary aim of the data presented in this chapter was to investigate the effect of two chronic environmental changes commonly experienced in cancer, hypoxia and low glucose, on $K_{2P}3.1$ and $K_{2P}9.1$ channel activity. In addition, the effects of chronic hypoxia and low glucose on cellular functions were studied in cell lines expressing TASK channel protein.

To address these aims the effects of chronic hypoxia on $K_{2P}3.1$ and $K_{2P}9.1$ channel activity and the ability of *N*-linked glycosylation (which was investigated as the mechanism for channel regulation by glucose) to modulate channel activity was investigated using whole-cell patch clamp experiments with transfected HEK293 cells. This approach was selected as it provided a direct measure of TASK channel activity on the cell surface. The impact of chronic hypoxia and low glucose on cellular functions in TASK channel expressing cell lines was also assessed in this chapter. For this, MTS assays, flow cytometry with annexin V staining, and wound healing assays were used to determine proliferation, apoptosis, and migration, respectively. The same three assays as used in Chapter 4 were utilised for these experiments so that the results were comparable. Cellular functions were assessed in both a heterologous (transfected HEK293 cells) and endogenous (A549 cells) expression system. HEK293 cells were utilised as an expression system which could easily be transfected so that the presence of TASK channel activity could be guaranteed. This approach was utilised as identifying cancer cell lines which endogenously express significant levels of TASK channel activity has been a limitation in this thesis.

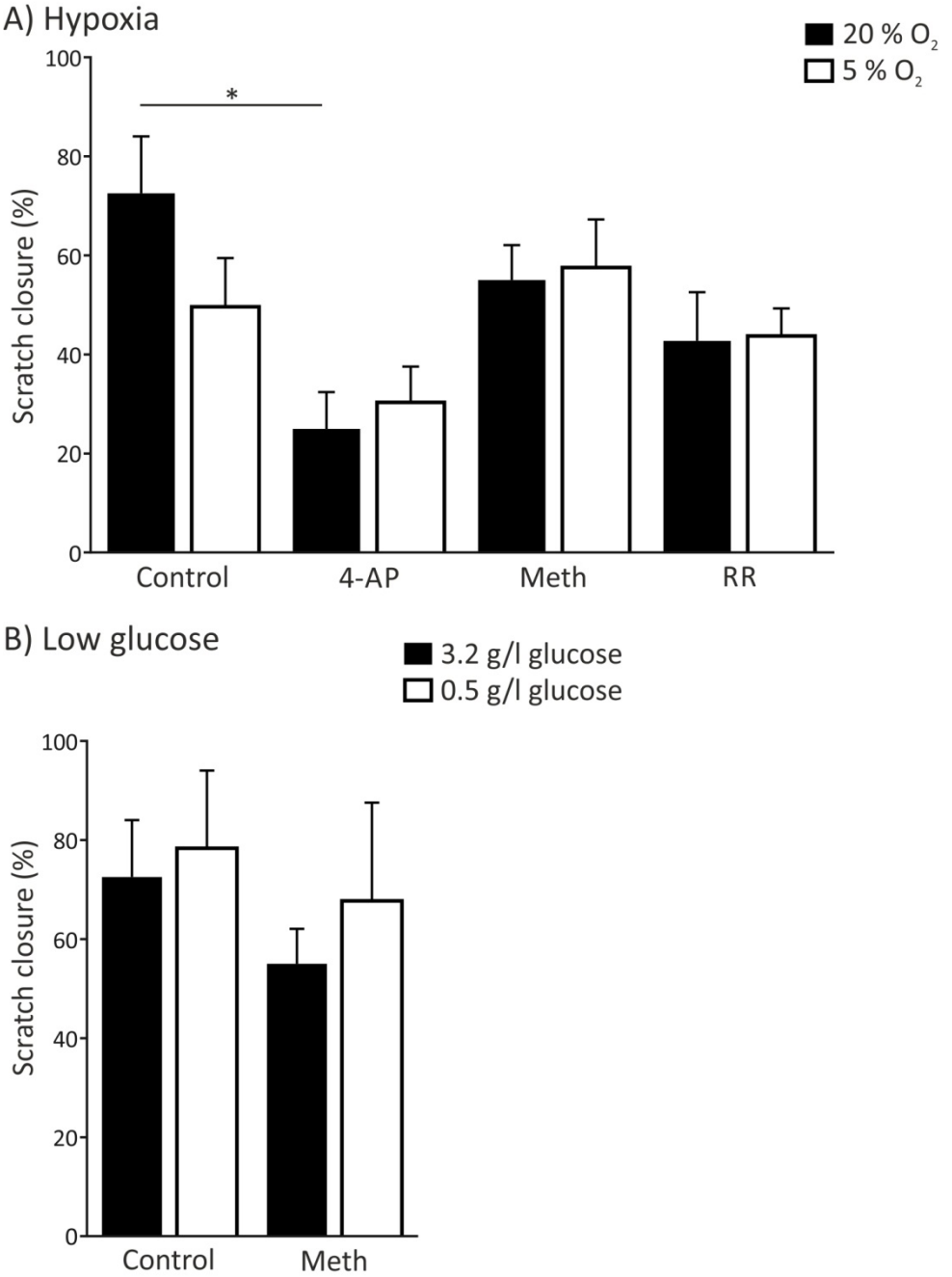

Figure 6.13: Assessment of A549 lung cancer cell migration under altered environmental conditions

Migration of A549 cells in the presence of inhibitors following 24 h cell culture in (A) hypoxia (5 % O_2) or (B) low glucose (0.5 g/l glucose) compared to control conditions (20 % O_2, 3.2 g/l glucose).
Control (untreated), 5 mM 4-AP, 50 µM methanandamide (meth), and 100 µM ruthenium red (RR).

Data are shown as average scratch closure (% + SEM) at 9 h compared to 0 h, n ≥ 3 experimental repeats. Each replicate was calculated from n ≥ 3 fields of view.
Statistical significance was calculated by a two-way ANOVA with Sidak's post-hoc test (* $p < 0.05$). Significant comparisons, where present, are indicated by horizontal lines.

The experimental approaches used in this chapter led to four main conclusions, including that:

(i) Chronic hypoxia does not regulate TASK channel activity.

(ii) Both $K_{2P}3.1$ and $K_{2P}9.1$ channel proteins were glycosylated at N53, but that this post-translation modification was only critical for the cell surface expression and function of $K_{2P}3.1$ channels.

(iii) Culturing TASK channel expressing HEK293 cells in chronic hypoxia or low glucose had no impact on cellular functions.

(iv) In A549 cells, expression of $K_{2P}3.1$ and $K_{2P}9.1$ protein does not result in cell surface TASK channel activity or functional benefits in both normal and altered cell culture conditions.

Each of these findings is discussed in detail below.

6.6.1 $K_{2P}3.1$ and $K_{2P}9.1$ channel activity was not regulated by chronic hypoxia

The data presented in this chapter showed that chronic hypoxia (5 % O_2, 24 h) had no effect on $K_{2P}3.1$ or $K_{2P}9.1$ channel activity when the channels are expressed in HEK293 cells (Figures 6.1 and 6.2). This finding was surprising as *in silico* analyses conducted within the lab indicated that at least four HRE are present within the *KCNK3* (encoding $K_{2P}3.1$) and *KCNK9* genes (encoding $K_{2P}9.1$; Dr L. Roncoroni, personal communication), which would suggest that chronic hypoxia can regulate both channels. Within the K_{2P} channel family, chronic hypoxia has been found to downregulate $K_{2P}5.1$ channel mRNA expression in H416 cancer cells and this results in a depolarised RMP compared to control cells (Brazier et al., 2005). A limitation of the work presented in this chapter was that because quantitative approaches to assess TASK channel expression at a mRNA or protein level proved unsuccessful in this thesis (Chapter 4), assessment of the effect of chronic hypoxia on channel mRNA and protein expression could not be performed. Therefore, whole-cell patch clamp experiments were used to examine the impact of chronic hypoxia on TASK channel activity, however this assessment was limited by a small replicate number. To confirm the findings presented here, additional whole-cell patch clamp experiments will be required along with quantitative expression experiments (at an mRNA and protein level) to determine if chronic hypoxia has any effects on TASK channel expression. Additionally, by transfecting cDNA constructs into HEK293 cells the expressed mRNA and protein may be

above the regulatory capacity of the native hypoxia response systems. Therefore, to confirm the findings presented in this chapter, the same experiments will need to be repeated in an endogenous system with robust TASK channel activity, such as rCGN or carotid body glomus cells (Buckler, 2007; Buckler et al., 2000; Kim et al., 2009; Plant et al., 2002).

A further limitation of the experiments presented in this chapter was the environmental conditions utilised (0.5 g/l glucose and 5 % O_2), which were relatively mild compared to physiological conditions. These conditions were selected based on published work studying acute hypoxia (Hartness et al., 2001; Lewis et al., 2001; Ortiz et al., 2013), previous studies conducted within the lab using low glucose conditions (Mant et al., 2013b), and equipment limitations (for example the hypoxia incubator used has a minimum value of 5 % O_2). However, published studies examining the impact of environmental stresses on TASK channel expressing cells have used more extreme conditions (0.2-1 % serum and 0-10 % O_2; Liu et al., 2005; Mu et al., 2003). Therefore, to further characterise the environmental regulation of TASK channels more extreme conditions which may be closer to those experienced within tumours need to be analysed, such as less than 2 % O_2 (Bertout et al., 2008; Mucaj et al., 2012).

In summary, the experiments presented in this chapter provided a preliminary assessment of TASK channel activity following exposure to chronic hypoxia and indicated that channel activity was not regulated by this condition. However, due to the limitations of the experimental set up these findings will require further investigation before firm conclusions can be made.

6.6.2 $K_{2P}3.1$ and $K_{2P}9.1$ channels are glycoproteins, and this was critical for $K_{2P}3.1$ channel surface expression and function

Burdakov et al. (2006) showed that high glucose concentrations (4.5 mM) increased the amplitude of TASK-like currents recorded in mouse hypothalamic orexin neurons. The data presented in this chapter revealed that *N*-linked glycosylation is likely to be the mechanism for $K_{2P}3.1$ and $K_{2P}9.1$ channel regulation by changes in glucose concentrations. These data showed both $K_{2P}3.1$ and $K_{2P}9.1$ channels are *N*-linked glycoproteins (Figure 6.4), and that this post-translational modification was critical for the surface expression and

functionality of $K_{2P}3.1$ channels (Figure 6.5). We showed that glycosylation is critical for stable surface expression of $K_{2P}3.1$ channels and when glycosylation is prevented, by mutation (N53Q) or tunicamycin treatment, $K_{2P}3.1$ channel protein reaches the cell surface but is rapidly removed (Mant et al., 2013b). Although, $K_{2P}9.1$ channels are also glycosylated at N53, this post-translational modification was less critical for the surface expression and activity of the channel, and $K_{2P}9.1$ currents were still recorded from cells expressing the $K_{2P}9.1_{N53Q}$ mutant (Figure 6.6; Mant et al., 2013b). This finding indicated that high glucose expression might encourage the glycosylation and stable expression of TASK channels on the cell surface and that low glucose may reduce the surface expression. Published evidence showed *N*-linked glycosylation is dependent on extracellular glucose concentrations (Hayter et al., 1992), and we proved that exposure to low glucose culture conditions reduced the expression of $K_{2P}3.1$ and $K_{2P}9.1$ protein on the cell surface in COS-7 cells (Mant et al., 2013b). The findings from these data indicated that exposure to low glucose, for example in cancer, can impact on TASK channel expression and $K_{2P}3.1$ channel activity.

6.6.3 Environmental stress conditions have no impact on cellular functions in TASK channel expressing HEK293 cells

The data presented in this chapter aimed to determine if environmental conditions can regulate cellular functions in TASK channel expressing cell lines, since rapid cancer cell growth and changes in cell metabolism can trigger environmental stress conditions (Introduction 1.5.2). The functional data presented here showed that expression of $K_{2P}3.1$ or $K_{2P}9.1$ channels provide no cell growth or survival advantage to HEK293 cells in control or environmental stress (chronic hypoxia and low glucose) culture conditions (Result 6.5.1). This finding differed from published work; Liu et al. (2005) showed that C8 fibroblasts expressing $K_{2P}3.1$ or $K_{2P}9.1$ channels have a growth advantage (compared to untransfected cells) when cultured for 72 h in low serum concentration (0.2-1 % serum), chronic hypoxia (0 % O_2), or a combination of both conditions (0.2 % serum and 0 % O_2). The difference in the data presented in this chapter and data from Lui et al (2005) could reflect differences in the experimental conditions and the cell lines used. The environmental stresses used in this chapter were mild and may not be extreme enough to induce changes in cellular functions. For example, 5 % O_2 was used for hypoxia experiments, however most tissues will normally experience O_2 tensions of between 2-9 % O_2 (Bertout et al., 2008; Mucaj et al., 2012).

Secondly, in this chapter, a shorter time period was examined compared to Liu et al. (2005) who utilised a longer time course of 72 h. Thus, a functional advantage resulting from prolonged exposure (over 24 h) to altered environmental conditions cannot be excluded. Finally, HEK293 cells were used in this chapter compared to mouse C8 fibroblasts by Liu et al. (2005), therefore the expression of endogenous ion channels and cellular receptors within HEK293 cells and C8 fibroblasts may alter the role of TASK channel activity under environmental stress conditions. To further investigate if TASK channels play a role in cell survival under environmental stress conditions, a study will need to be conducted with both HEK293 cells and C8 fibroblasts utilising the same environmental conditions and experimental time course.

6.6.4 Do TASK channels have a functional role in A549 lung cancer cells?

A549 lung cancer cells have been studied extensively in thesis. The data presented here showed that expression of $K_{2P}3.1$ and $K_{2P}9.1$ protein with A549 cells (Result 4.4) does not result in cell surface TASK channel activity (Results 4.5 and 6.4) or functional benefits in both normal and altered cell culture conditions (Results 5.3 and 6.5.2). Because TASK channel activity on the cell surface of A549 cells was not observed, the finding that TASK channels do play a functional role in cellular proliferation, migration or apoptosis is not surprising. However, it remains possible that TASK channel protein could influence cell function in other ways. For example, published data has indicated that in WM35 melanoma cells $K_{2P}9.1$ channel protein is predominately located on the mitochondrial membranes compared to the plasma membrane (Rusznak et al., 2008). Consistent with this idea, in melanoma cells a knockdown of $K_{2P}9.1$ channels significantly reduces mitochondrial function and cell proliferation (Kosztka et al., 2011). The hypothesis that TASK channels could have an altered subcellular localisation in A549 cells was one of the reasons for continuing to examine this cell line in this thesis. However, no experiments were conducted to investigate the subcellular locations of TASK channel protein in A549 cells and this is therefore an area for further investigation (Result 4.7.2).

The functional assays conducted in this thesis examined the effect of TASK channel inhibition on A549 cell proliferation, apoptosis, and migration. These experiments did not identify any cellular functions which could be related to the expression of $K_{2P}3.1$ and $K_{2P}9.1$

channel protein. These findings suggested that if TASK channel protein was targeted to intracellular locations within A549 cells, it provides no functional advantages.

Another hypothesis for the lack of a functional role for TASK channel protein expression in A549 cells under normal cell culture conditions was that the channels may only provide a functional benefit under cell stress conditions. This hypothesis was investigated in this chapter and the data presented here found that no TASK-like currents are detected in A549 cells following a 24 h exposure to cell stress conditions (hypoxia and low glucose). In addition, no proliferative, apoptotic, and migratory differences were observed between normal and environmental stress conditions. The experiments performed in this thesis to examine cellular functions have been limited by the tools available to modulate $K_{2P}3.1$ and $K_{2P}9.1$ channels. No targeted tools which were suitable to reduce TASK channel expression or function could be identified in Chapter 5 and this led to a pharmacological approach being selected (Result 5.2.3). The pharmacological approach utilised in this thesis had significant drawbacks, particularly a lack of inhibitor selectivity (discussed in Results 5.2.3 and 5.4). Therefore, to confirm that TASK channels have no role in regulating A549 cellular functions, more specific reagents than are currently available will be required.

In summary, the data presented in this thesis showed that the expression of native $K_{2P}3.1$ and $K_{2P}9.1$ channel protein in A549 cells provides no functional advantages under both normal and environmental stress culture conditions. A potential hypothesis which could be drawn from these findings is that other K_{2P} channels may provide the dominant background outward K^+ currents in A549 cells and that these K_{2P} channels may have functional roles. The idea that additional K_{2P} channels are active on the cell surface of A549 cells is supported by data presented in this thesis. Data presented in Chapter 4 found that multiple K_{2P} channels are presented in A549 cells at an mRNA level (Table 4.1) and that 50 % of the whole-cell currents are TEA-insensitive, a property fulfilled by the K_{2P} channel family (Result 4.5 and discussed in Section 4.7.3). The functional implications resulting from the expression of multiple K_{2P} channels within a single cell type have not been characterised within the literature. However, this could mean that the activity of other K_{2P} channels can compensate for the inhibition of another, which may explain why TASK channel modulation does not significantly impact A549 cell functions.

6.7 Publications arising

Figures 6.5, 6.7, and 6.8 are published in: Mant, A., Williams, S., Roncoroni, L., Lowry, E., Johnson, D. & O'Kelly, I. 2013. *N*-glycosylation-dependent control of functional expression of background potassium channels $K_{2P}3.1$ and $K_{2P}9.1$. *J Biol Chem,* 288**,** 3251-3264.

Chapter 7

General Discussion

7.1 Role of TASK channels in cancer

The aim of this thesis was to investigate the role of TASK channels in the function of cancer cells. The rationale for this research was based on published studies which suggested that K_{2P} channels may be a target for future cancer therapies.

TASK channel expression has been identified in several cancers, leading to the hypothesis that TASK channel overexpression provides a functional advantage to cancer cells (Mu et al., 2003; Pei et al., 2003). This hypothesis is supported by multiple studies which show that $K_{2P}9.1$ activity promotes cell growth and apoptosis resistance (Innamaa et al., 2013b; Kosztka et al., 2011; Mu et al., 2003; Pei et al., 2003). Additionally, it has been suggested that TASK channel expression provides a functional advantage by enabling cell survival in altered environmental conditions (Liu et al., 2005; Mu et al., 2003). The exact pathways by which TASK channel activity might provide a functional advantage to cancer cells have not been determined. One possible mechanism is via the modulation of the RMP, because K_{2P} channels are active across the physiological voltage-range, one of their primary roles in cell biology is to regulate the membrane potential (Enyedi and Czirják, 2010; Lesage and Lazdunski, 2000; Patel and Lazdunski, 2004). Thus, modifications of K_{2P} channel function in cancer cells might in-turn influence the operation of other ion channels and cellular pathways, by direct alteration of the membrane potential or, secondarily, by altering calcium signalling for example (Goldstein et al., 2001; Enyedi and Czirjak, 2010; Plant, 2012a). Based on this idea, K_{2P} channels are predicted to play a role in multiple cancer types. However, despite the evidence that has accumulated to support this hypothesis over the last decade, a systematic evaluation of K_{2P} channel expression across multiple cancer types was lacking. Therefore, this project sought to determine the expression of K_{2P} channels in cancer tissues and cell lines, to investigate the role of TASK channels in cancer cell functions, and to assess if altered environmental conditions modulate the role of TASK channels in cancer cells. This study adopted a multidisciplinary approach to evaluate the mRNA, protein, and functional expression of multiple K_{2P} channels in a range of cancer cell types, focusing on the TASK channels $K_{2P}3.1$, $K_{2P}9.1$, and $K_{2P}15.1$. The implications and results of this research are discussed below.

7.1.1 K_{2P} channel expression in cancer

Both cancer tissue and cell line expression data showed that multiple K_{2P} channels were expressed, at an mRNA level, within a single cancer type (Results 3.2 and 4.2). In Chapter 3, the mRNA transcripts for multiple K_{2P} channels were found to be both over- and underexpressed across a wide range of cancer types, with the alterations in expression varying between cancer subtypes (Result 3.2). Whilst K_{2P} channel overexpression has been reported (Kim et al., 2004; Mu et al., 2003; Voloshyna et al., 2008), this was the first evidence of underexpression and indicated that K_{2P} channel underexpression may be more prevalent in cancer. Broadly speaking, the potential implication of these data is that variations in K_{2P} channel expression may provide different functional advantages to cancer cells by causing membrane potential alterations which could affect other ion channels expressed within the cancer cells (discussed in Section 7.2). However, the specific effect of differential K_{2P} channel expression patterns will depend on the cell type in question. To date, most studies that have investigated the impact of altered K_{2P} channel function have focused on acute changes in the excitability of neurons (Plant, 2012a). For example, reducing the activity of TASK channels in neurons by extracellular acidification increases excitability by decreasing the magnitude of the background K^+ conductance, this depolarises the membrane potential closer to the firing threshold for action potentials and increases the cellular input resistance (Plant et al., 2012b). In the same study, the opposite effects on excitability were observed when cells were treated with halothane, a volatile anaesthetic that augments the activity of TASK channels.

7.1.2 What is the functional role of TASK channels in cancer cells?

TASK channel protein expression differences were detected in the cancer cell lines examined in this thesis and this may have proliferative implications. The functional data presented in Chapter 5 showed that TASK channel inhibition significantly reduced proliferation in K_{2P}9.1 channel protein expressing colorectal cancer cells, but had no effects on cancer cells expressing K_{2P}3.1 protein, or on K_{2P}3.1 and K_{2P}9.1 protein (Result 5.3). These data suggested that K_{2P}9.1 protein overexpression in colorectal cancer tissue (Kim et al., 2004) may provide proliferative benefits. The lack of a functional role in cells expressing K_{2P}3.1 protein alone or alongside K_{2P}9.1 indicated that there may be a cell-specific nature to

the impact of TASK channel protein expression on cancer cells. A cell-specific nature to the role of TASK channels in cancer cells is supported by published studies which have found multiple functional roles for $K_{2P}9.1$ channels in different cancer cells (Innamaa et al., 2013b; Lee et al., 2012; Meuth et al., 2008b; Mu et al., 2003; Patel and Lazdunski, 2004; Pei et al., 2003).

By regulation of the membrane potential, K_{2P} channels are thought to influence the activity of multiple types of ion channels, and this may include K_V channels (Blackiston et al., 2009; Campanucci et al., 2005; Enyedi and Czirják, 2010; Patel and Lazdunski, 2004; Schwab et al., 2012). Therefore, the roles of non-K_{2P} KChs in cancer cell functions were also investigated in this thesis using the K_V channel pore blocker, 4-AP. Data presented in Chapter 5 showed that 4-AP treatment caused a reduction of cell numbers in eight cancer cell lines (Result 5.3.1). Apoptosis assays revealed that in A549 lung and HCT116 colorectal cancer cells the observed reduction in cell numbers was correlated to increased cell death (Result 5.3.2). A wide range of KCh can be inhibited by 4-AP (Table 1.1), therefore the experiments conducted in this thesis did not identify the specific channels involved in regulating cellular functions. However based on published data, $K_V11.1$ was hypothesised as a 4-AP-sensitive channel which may be involved in regulating A549 and HCT116 cell death (discussed in Section 5.4.3). For A549 cells, K^+ efflux through 4-AP-sensitive KCh appeared to be essential for cell survival and suggested that non-K_{2P} KChs are critical in this cell line. This finding was supported by electrophysiological data which found that in A549 cells a significant proportion (47 %) of the whole-cell outward K^+ currents were inhibited by broad spectrum KCh inhibition (using TEA), but that no TASK-like currents could be isolated (Result 4.5). In contrast, different roles were identified for $K_{2P}9.1$ channels (which were likely to be involved in cell growth) and 4-AP-sensitive KCh (which appeared to prevent apoptosis) in HCT116 colorectal cancer cells. This difference suggested that in HCT116 cells, $K_{2P}9.1$ channel activity may not influence 4-AP-sensitive KCh, therefore K^+ efflux through K_{2P} channels may impact on the activity of other ion channels in this cell line (candidate channels are discussed in Section 7.2). Whilst 4-AP treatment could not identify the specific channel(s) involved in cancer cell functions, these data highlighted the importance of K^+ efflux and non-K_{2P} KCh activity in cancer cell functions (for an overview of the published roles of KCh in cancer see Table 1.4). To investigate the role(s) of non-K_{2P} KCh in the cancer

cell lines examined in this thesis, a comprehensive analysis of the ion channels and transporters expressed in each cell type will be required (discussed in Section 7.5).

Because the microenvironment in which cancer cells reside is often deprived of nutrients such as O_2 and glucose (Chiche et al., 2010; Gillies et al., 2008; Luo et al., 2009), the role of TASK channels was also studied in cells cultured under hypoxic and low glucose conditions. Chronic hypoxia had no impact on the magnitude of TASK channel currents despite prior studies showing that the activity of channels is reduced by exposure to acute hypoxia (Buckler, 2007; Hartness et al., 2001; Kim et al., 2009; Lewis et al., 2001). This finding indicated that chronic hypoxia might not be a modulating factor for TASK channels in HEK293 cells (Result 6.2). *N*-linked glycosylation was investigated as the mechanism for channel regulation by varying glucose concentrations (Hayter et al., 1992). Both $K_{2P}3.1$ and $K_{2P}9.1$ were found to be *N*-linked glycoproteins, and this post-translational modification proved to be critical for the activity of cell surface $K_{2P}3.1$, however the activity of $K_{2P}9.1$ channels did not change (Result 6.3).

Chronic exposure to low glucose or hypoxia had no impact on the proliferation, apoptosis, and migration of A549 cells (Result 6.5) which express TASK channel mRNA and protein (Results 4.2 and 4.3). This contrasts with published work which indicated that $K_{2P}3.1$ or $K_{2P}9.1$ channel expression promotes cell survival in C8 fibroblasts cultured in deprived conditions (hypoxia and low serum; Liu et al., 2005; Mu et al., 2003). These findings might reflect different expression levels of active TASK channels at the surface of A549 cells and C8 fibroblasts. Indeed, whole-cell patch clamp recordings did not provide evidence for TASK channel activity in A549 cells (Results 4.5 and 6.4). Additionally, it was not confirmed that TASK channel activity could be detected at the cell surface following the transfection of channel cDNA constructs into C8 fibroblasts (Liu et al., 2005). These data questioned whether or not active TASK channels were present at the surface of the other cancer cell lines investigated in the study. Time limitations precluded the electrophysiological evaluation of the other cell lines and this remains an important avenue for future studies. However, TASK channel inhibitors did alter the proliferation of HCT116, SW480, and SW620 colorectal cancer cells under control culture conditions (Result 5.4.1), suggesting there is a role for active TASK channels in colorectal cancer cells. The differences between these data (Chapters and 5 and 6) and published work (Liu et al., 2005; Mu et al.,

2003) further suggested that there is a cell-specific role for TASK channel activity in cancer cells.

A cell-specific role of TASK channel expression in cancer may depend on the complement of K_{2P} channels and other ion channels expressed within the cell. The functional implications resulting from the expression of multiple K_{2P} channel subfamilies in cancer have not been identified, since published work has investigated the functional roles of a single K_{2P} channel in cancer and this study focused on the TASK channel subfamily. A potential functional consequence which may result from the expression of multiple K_{2P} channels in cancer is compensation of channel activity. This hypothesis is discussed below.

7.1.3 Is functional compensation occurring within the K_{2P} channel family in cancer?

The combination of expression data (showing multiple K_{2P} channels are expressed in different cancers; Results 3.2 and 4.2) and functional data (indicating that there is functional benefit to $K_{2P}9.1$ channel protein expression when $K_{2P}3.1$ protein is not expressed; Result 5.3) presented in this thesis suggested that the functional compensation for K_{2P} channel activity might occur in cancer cells (Figure 7.1). This hypothesis could mean that the activity of other K_{2P} channels present within cancer cells may prevent background K^+ currents being lost from the cancer cell when TASK channels are inhibited, and this may preclude any consequences for cellular functions (Figure 7.1 B). K_{2P} channel activity compensation may also occur under altered environmental conditions (Figure 7.1 C, D) when K_{2P} channels are differentially regulated by physiological stimuli (e.g. hypoxia, glucose, and pH; Appendix 1). Differential regulation of K_{2P} channel activity was demonstrated in this thesis, where it was shown that *N*-linked glycosylation was only critical for $K_{2P}3.1$ functionality despite the similarities between $K_{2P}3.1$ and $K_{2P}9.1$ channel activity and regulation (Appendix 1, Result 6.3; Mant et al., 2013b).

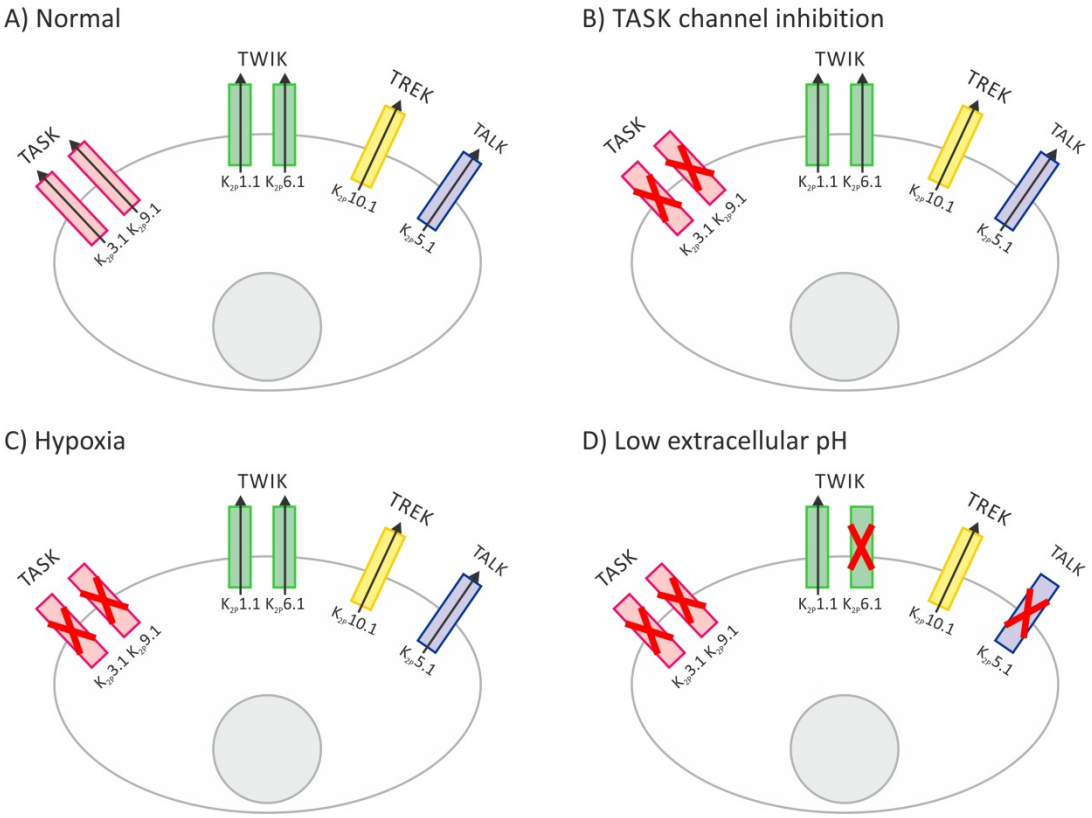

Figure 7.1: Functional compensation of K_{2P} channel activity in cancer cells
Multiple K_{2P} channels are expressed within a single cancer cell; this may result in functional compensation under different modulatory conditions. The model shown is for breast cancer cells, which express K_{2P} channels from the TASK (K_{2P}3.1 and K_{2P}9.1), TWIK (K_{2P}1.1 and K_{2P}6.1), TREK (K_{2P}10.1), and TALK (K_{2P}5.1) subfamilies.
A) Under normal conditions, K_{2P} channel expression will result in outward K^+ currents and an efflux of K^+ ions.
B) TASK channel inhibition will prevent K^+ efflux via TASK channels. However, K^+ efflux can still occur due to the activity of the remaining K_{2P} channels.
C) In hypoxic conditions, TASK channels will be inhibited, however K^+ efflux is maintained due to the activity of the remaining K_{2P} channels.
D) In low extracellular pH, K_{2P}3.1, K_{2P}5.1, K_{2P}6.1, and K_{2P}9.1 channels will be inhibited, however K^+ efflux can still occur due to K_{2P}1.1 and K_{2P}10.1 channel activity.

The expression of K_{2P} channels in breast cancer cells is based on data from this study (Result 3.2) and published work: Mu et al. (2003) and Alvarez-Baron et al. (2011).

The idea that functional compensation can occur within the K_{2P} channel family is supported by data from mouse KO studies which suggested that other channels can compensate for the genetic loss of one K_{2P} channel (Dobler et al., 2007; Linden et al., 2008; Ortega-Saenz et al., 2010; Turner and Buckler, 2013). $K_{2P}3.1/K_{2P}9.1$ heterodimers regulate the RMP in mouse carotid body glomus cells, with channel inhibition causing cell depolarisation and a rise in intracellular Ca^{2+} (Buckler et al., 2000; Kim et al., 2009; Ortega-Saenz et al., 2010; Turner and Buckler, 2013). Turner and Buckler (2013) proposed that in $K_{2P}3.1/K_{2P}9.1^{-/-}$ KO cells the activity of other ion channels will compensate for a loss of TASK channel currents, as no differences in intracellular Ca^{2+} levels and only a small depolarisation of the RMP were observed (compared to WT cells; Turner and Buckler, 2013). Ionic compensation in $K_{2P}3.1/K_{2P}9.1^{-/-}$ KO cells was supported by data from Ortega-Saenz et al. (2010) which showed that the voltage-dependent Ca^{2+} currents were 50 % lower in KO cells. Ionic compensation has also been observed in other mouse KO models; in $K_{2P}3.1^{-/-}$ KO brain tissue, the function of the $GABA_A$ receptor is upregulated and this is thought to prevent a loss of neurological functions (Linden et al., 2008). A functional $K_{2P}18.1$ KO in mouse dorsal root ganglion neurons resulted in a reduction in background outward K^+ currents, but failed to alter the RMP compared to WT cells (Dobler et al., 2007). Additionally, $K_{2P}18.1$ KO neurons have an increased hyperpolarisation phase following action potential generation, this was not explained by a loss of KCh activity suggesting that ionic compensation was occurring, potentially by the upregulation of other KCh (Dobler et al., 2007). These published studies suggested that other ion channels can compensate for the loss of K_{2P} channel activity. Functional compensation in cancer may explain why multiple types of K_{2P} channels (Results 3.2 and 4.2) and other ion channels (Tables 1.3 and 1.4) are expressed within a single cancer type, however this remains unknown and an area for future studies. Thus, to understand the functional implications of background outward K^+ currents in cancer cells, the contributions of all the K_{2P} channels expressed with the cancer type will need to be considered.

7.1.4 Is cancer cell signalling responsible for cell-specific roles of the K_{2P} channel family in cancer?

Understanding the regulation of K_{2P} channels (by external and internal factors) may be critical to clarify the cell-specific roles of these channels and to understand why K_{2P} channel overexpression is beneficial in some cancers, but detrimental in others. Cancer cell signalling pathways have been shown to play an essential role in ion channel regulation and can influence cellular functions (Brackenbury and Djamgoz, 2007; Campbell et al., 2013; Frede et al., 2013; Peña et al., 2000). Two published studies have demonstrated K_{2P} channel regulation by signalling pathways commonly present in cancer cells (Alvarez-Baron et al., 2011; El Hachmane et al., 2014). In breast cancer cell lines, stimulation of K_{2P}5.1 activity by oestrogen signalling provided a proliferative advantage (Alvarez-Baron et al., 2011). K_{2P}9.1 activity was increased by TNFα (via the ASK1/MAPK/JNK-p38 pathway); this stimulated apoptosis in K_{2P}9.1 expressing tsA-201 cells and suggested that K_{2P}9.1 channels were mediating some of the TNFα pro-apoptotic effects (El Hachmane et al., 2014). These studies indicated that, in specific cells, K_{2P} channel activity may not have a significant impact on cellular functions without stimulation from signalling pathways (Alvarez-Baron et al., 2011; El Hachmane et al., 2014). Therefore, K_{2P} channel regulation by cell signalling pathways may be essential in cancer cells and this may explain the limited functional role for TASK channels in the cancer cell lines examined here (Result 5.3).

7.2 Functional consequences of altered K_{2P} channel expression in cancer

The precise functional consequences of altered K_{2P} channel expression in cancer cells are likely to depend on the other ion channels and transporters expressed (Figure 7.2), in addition to cancer cell signalling pathways. Multiple types of ion channels and transporters have been identified in cancer and linked to cancer cell functions (Table 1.3).

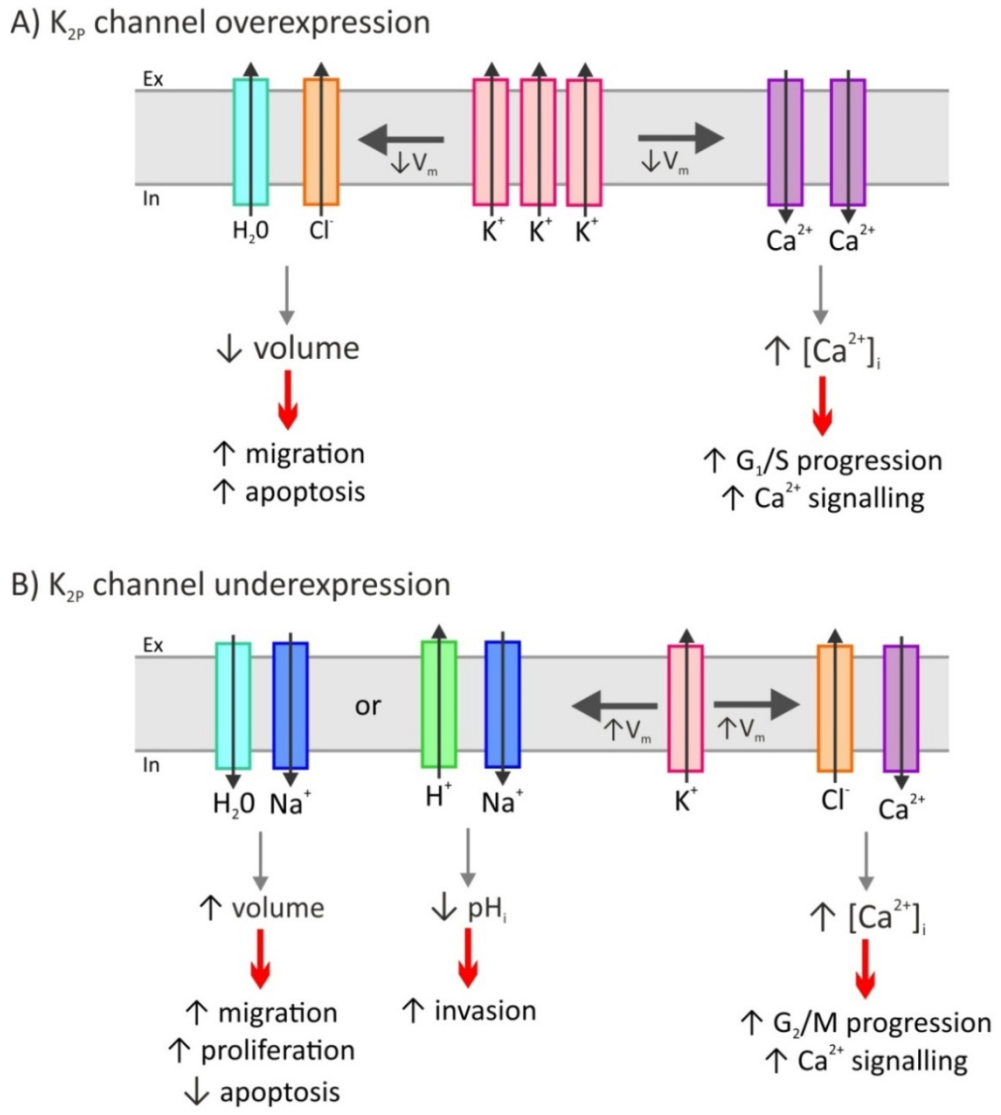

Figure 7.2: Potential functional consequences of altered K_{2P} channel activity in cancer cells

Model indicating the potential functional consequences of altered K_{2P} channel expression and activity on other transmembrane ion conduction pathways in cancer cells.

A) Overexpression of K_{2P} channels will result in increased K^+ efflux and membrane hyperpolarisation ($\downarrow V_m$). Depending on the other ion channels expressed within the cancer cell, K^+ efflux may cause either increased Ca^{2+} entry (e.g. via TRP channels) and downstream Ca^{2+}-dependent signalling events, or result in Cl^- and water efflux which causes cell shrinkage. Additionally, hyperpolarisation is expected to close and reduce the functional activity of voltage-gated Na^+, Ca^{2+} and K^+ channels.

B) Underexpression of K_{2P} channels will result in decreased K^+ efflux and membrane depolarisation ($\uparrow V_m$). Membrane depolarisation can also increase Ca^{2+} entry (e.g. activation of Ca_V channels) and downstream Ca^{2+}-dependent signalling events, or trigger the activation of K_V channels and Na_V channels. Na_V channels are involved in cell swelling pathways and the regulation of intracellular pH, which promotes cell invasion.

Figure adapted from Becchetti (2011), Blackiston et al. (2009), Cuddapah and Sontheimer (2011), Kunzelmann (2005), Pedersen et al. (2013), Schwab et al. (2012), and Yu (2003).

7.2.1 Potential impacts of K_{2P} channel overexpression on cancer cell functions

At a cellular level there are three published consequences of increased K^+ efflux: membrane hyperpolarisation, modulation of Ca^{2+} signalling, and cell volume regulation (Figure 7.2 A). Transient membrane hyperpolarisation, caused by K^+ efflux, is critical for cell cycle progression through the G_1/S checkpoint (Massague, 2004; Wang et al., 1998; Wonderlin and Strobl, 1996). Unless K_{2P} channel activity is regulated throughout the cell cycle, K_{2P} channel overexpression would be unlikely to cause a transient hyperpolarisation. However, this cannot be eliminated as cell cycle regulation of KCh activity has been observed in SH-SY5Y cells, where increased K_V11.1 mRNA levels correlate with membrane hyperpolarisation (Crociani et al., 2003). Membrane hyperpolarisation is expected to close and reduce the functional activity of voltage-gated Na^+, Ca^{2+}, and K^+ channels. Closure of voltage-gated ion channels is likely to have functional consequences for cancer cells, however, at this time, the published knowledge investigating the role of increased KCh activity in cancer have not established these implications.

K^+ efflux and membrane hyperpolarisation will increase the electrical driving force for Ca^{2+} entry (Figure 7.2 A). Even though the activity of Ca_V channels is expected to be reduced at hyperpolarised membrane potentials, influx of Ca^{2+} through voltage-independent Ca^{2+} channels, including certain TRP and specific GluR receptor channels, may be augmented (Fioro Pla et al., 2011; Fioro Pla et al., 2013; Hamadi et al., 2014; Oh et al., 2012; Lallet-Daher et al., 2009). Although this question has not been addressed specifically in the K_{2P} channel literature, the functional consequences of increased Ca^{2+} influx in response to K_{2P} channel-mediated hyperpolarisation may be similar to those described for other KCh subtypes (Figure 7.2 A). One functional consequence of K^+-dependent Ca^{2+} entry is cell proliferation, such as in MCF-7 breast cancer cells, where growth is stimulated by K_V11.1 and K_{Ca}3.1 activity (Ouadid-Ahidouch and Ahidouch, 2008). Similarly in LNCap prostate cancer cells where K_{Ca}3.1 activity triggers Ca^{2+} entry, via TRPV6 channels, and cell growth (Lallet-Daher et al., 2009). Additionally, K^+-dependent Ca^{2+} entry can trigger apoptosis (such as CaCo-2 colorectal cancer cells; Gerbino et al., 2009) or promote cell migration (such as MDA-MB-231 breast cancer cells, where K_V10.1 activity stimulated Ca^{2+} entry via Orai1 channels; Hammadi et al., 2012).

Alternatively, K^+ efflux could impact on the cell volume through cooperative activity with Cl^- channels, leading to loss of water and cell shrinkage (Figure 7.2 A). In Ehrlich ascites tumour cells, $K_{2P}5.1$ channels are activated by cell swelling, and this in combination with VRAC activity will result in a volume decrease (Kirkegaard et al., 2010; Niemeyer et al., 2001). Cell volume control pathways are critical in the regulation of proliferation, apoptosis, and migration (Lang et al., 2007; McFerrin et al., 2012; Pardo, 2004; Pedersen et al., 2013; Schwab et al., 2012; Tao et al., 2008); however the functional consequence of $K_{2P}5.1$ activation in Ehrlich ascites tumour cells has not been determined.

The range of ionic signalling pathways that can be induced by increased K^+ efflux indicates that K_{2P} channel overexpression may have several functional consequences. Therefore, K_{2P} channel activity may have cancer cell-specific effects due to the expression of other ion channels and transporters. Cancer cell-specific roles resulting from differences in TASK channel expression were shown in Chapter 5 (Result 5.3 and Section 5.4.2), in addition to published studies where $K_{2P}9.1$ activity has been linked to proliferation, apoptosis, and migration (Innamaa et al., 2013b; Kosztka et al., 2011; Lee et al., 2012; Meuth et al., 2008b; Mu et al., 2003; Pei et al., 2003).

7.2.2 Potential impacts of K_{2P} channel underexpression on cancer cell functions

K_{2P} channel underexpression in cancer may provide a different set of functional advantages compared to channel overexpression, depending on ion channels and transporters expressed within the cell (Figure 7.2 B). Therefore, a loss of K_{2P} channel activity is also likely to have cancer cell-specific effects. In the cancers examined in Chapter 3, K_{2P} channel mRNA underexpression was more prevalent compared to overexpression (Result 3.2). Reduced K^+ efflux will trigger membrane depolarisation; a depolarised membrane potential has been found to correlate with highly proliferative/invasive cancer cells, in addition to being a requirement for cell cycle progression at the G_2/M checkpoint (Arcangeli et al., 1995; Blackiston et al., 2009; Molenaar, 2011; Olsen and Sontheimer, 2004; Sundelacruz et al., 2009).

Membrane depolarisation can also stimulate Ca^{2+} influx, via increased Ca_V channel activity, and Ca^{2+}-dependent signalling events (Capiod, 2012; Chen et al., 2013; Fiske et al., 2006; Li and Xiong, 2011; Monteith et al., 2012; Prevarskaya et al., 2013). TASK channel inhibition results in membrane depolarisation and increased Ca^{2+} entry in rat carotid body glomus and human adrenocortical cells (H295R cell line; Buckler, 2007; Kim et al., 2009; Nogueira et al., 2010; Turner and Buckler, 2013). The precise Ca^{2+} channels activated by TASK channel inhibition have not been defined; however in carotid body glomus cells this response is proposed to involve L- and P/Q-type Ca_V channels (Buckler, 2007; Buckler and Vaughan-Jones, 1994; Buckler and Vaughan-Jones, 1998; Kim et al., 2009; Nogueira et al., 2010; Turner and Buckler, 2013).

K_{2P} channel underexpression may be associated with cancer progression and invasive cancer phenotypes, by stimulating membrane depolarisation and increasing the activity of voltage-gated ion channels. Invasive cancer phenotypes correlate with the expression of Na_V channels, such as $Na_V1.5$ (breast cancer) and $Na_V1.7$ (non-small cell lung and prostate cancers; Brackenbury, 2012; Brackenbury and Djamgoz, 2007; Campbell et al., 2013; Fraser et al., 2014). Na^+ influx and persistent Na_V channel activity promotes cell invasion, by regulating cell swelling which is required for cell protrusion, or reducing intracellular pH which leads to extracellular acidification and pH-dependent extracellular matrix degradation (Figure 7.2 B; Arcangeli, 2011; Brackenbury, 2012; Brackenbury and Djamgoz, 2007; Campbell et al., 2013; Pedersen et al., 2013; Schwab et al., 2012). Na_V channels are activated by membrane depolarisation and will usually be closed at resting (negative) membrane potentials (Blackiston et al., 2009; Brackenbury, 2012). Therefore, if K_{2P} channel activity is reduced in cancer cells and this resulted in a depolarised membrane potential, it may promote persistent Na_V channel activity and invasive cancer phenotypes.

The data presented in this thesis showed that K_{2P} channels were not exclusively over- or underexpressed, and the majority of cancer subtypes had both channel over- and underexpression (at an mRNA level; Result 3.2). The consequence of this is currently unknown but this may result in different functional advantages depending on the ionic signalling pathways present and K_{2P} channel regulation (for example, by cancer signalling pathways or the environment).

7.3 What is the role of multiple ionic signalling pathways in cancer?

Multiple types of ion channels or transporters can result in the same functional advantages (Figure 7.2). An example of functional redundancy within the ionic signalling networks present in cancer cells is the multiple mechanisms which can be employed to increase intracellular pH (Amith and Fliegel, 2013; Damaghi et al., 2013; Pouyssegur et al., 2006). These include: anion exchangers, ATPases (Na^+/K^+, H^+-, and V-), carbonic anhydrases, Na_V channels, H^+/lactate transporters, Na^+-HCO_3 co-transporters, NHE1 transporters, and MCT transporters (Amith and Fliegel, 2013; Pedersen and Stock, 2013; Pouyssegur et al., 2006). A consequence of this is that a loss of one class of channel or transporter may not significantly impact H^+ extrusion from the cancer cell. Functional redundancy has not been described for other cellular functions dependent on ion transport, such as regulation of intracellular Ca^{2+}. However, multiple channels can be utilised by cancer cells to facilitate Ca^{2+} entry including TRP, Orai, and Ca_V channels (Capiod, 2012; Fiorio Pla et al., 2011; Monteith et al., 2012). The different properties of these channels may mean that if Ca^{2+} influx is prevented through one channel subtype, Ca^{2+} entry may still occur through the other channel subtypes expressed (Lehen'kyi et al., 2007; Lehen'kyi et al., 2011; Schwab et al., 2012). For example, if Ca_V channels are inactive due to membrane hyperpolarisation, Ca^{2+} entry may still occur through TRP channels which are less sensitive to changes in voltage (Fioro Pla and Gkika, 2013).

The variety of ion channels and transporters which have been identified in cancer cells may explain why K_{2P} channel mRNA upregulation was detected in some cancers, but in others downregulation was observed (Result 3.2). In cancer cells where TRP and VRAC channels are expressed, K_{2P} channel overexpression may be beneficial by promoting K^+-dependent Ca^{2+} entry and regulating cell volume decreases (Figure 7.2 A). Alternatively, in cancer cells where Ca_V and Na_V channels are expressed, K_{2P} channel underexpression may be advantageous by promoting voltage-gated channel activity and invasive phenotypes (Figure 7.2 B). Additionally, if specific K_{2P} channels can modulate different ion channels and cellular functions, this may explain why certain members are overexpressed but others are underexpressed within the same cancer subtype. Furthermore, the alterations which occur in cellular signalling pathways in cancer (Figure 1.9) may contribute to the stimulation of

different functional advantages from the same combination of ion channels. Therefore, the precise role of ion channel signalling in cancer cells is likely to depend on the specific channels and transporters expressed, as well as the conditions experienced. The cell-specific nature of ionic signalling in cancer is likely to impact on the potential for these proteins to be used as therapeutic targets.

7.4 Are K_{2P} channels a suitable target for future cancer therapies?

The data presented in this thesis indicate that targeting a single K_{2P} subfamily or channel, such as TASK channels or K_{2P}9.1, may not be as clinically beneficial as previous studies have suggested (Innamaa et al., 2013b; Kosztka et al., 2011; Liu et al., 2005; Mu et al., 2003; Pei et al., 2003). Functional data (proliferation, apoptosis, and migration assays) provided evidence that TASK channel protein expression may result in cell-specific effects for cellular functions (Result 5.3). Multiple K_{2P} channels were found to be expressed within different cancer tissues (mRNA) and cell lines (mRNA and protein) in this study (Results 3.2 and 4.2), and this may result in functional compensation (Figure 7.1) which could limit the effect of any targeted modulation. Therefore, designing a cancer therapy to target a single K_{2P} channel is unlikely to be clinically useful, until the interactions of K_{2P} channels with each other and other types of ion channels expressed in cancer are further investigated.

7.5 Future lines of investigation

Without conducting further studies, the suitability of TASK channels as a target for cancer therapy appears to be limited. To address this, there are two main lines of investigation. The first is to determine the clinical relevance of the K_{2P} channel expression data presented in this thesis. For this, a number of additional studies need to be undertaken:

1. To establish the expression of K_{2P} channel protein in cancer tissue compared to normal matched controls using immunohistochemistry. This will provide information on whether the over- or underexpression of K_{2P} channels correlate

with a cancer stage. Furthermore, by performing co-staining experiments, the presence of multiple K_{2P} channels at a protein level within cancer cells can be confirmed.

2. The protein and functional expression was not assessed for all K_{2P} channels in the cancer cell lines examined in this thesis. Therefore, experiments need to be conducted to assess if functional K_{2P} channel activity can be detected in these cell lines using electrophysiology. In addition, different pharmacological modulators of K_{2P} channels can be used and this may determine the contribution of the individual K_{2P} channels to the whole-cell currents. At present, there is a dearth of selective pharmacological agents that inhibit or augment the activity of specific K_{2P} channels. Therefore, the inhibitors used in this thesis were the only TASK channel blockers which are currently available for research use.
3. To assess the subcellular localisation of the K_{2P} channel protein staining detected in cancer cell lines. This will establish if/which K_{2P} channels show altered subcellular localisation in cancer, as this may have functional impacts. We have developed a protocol to assess the intracellular localisation and trafficking of endogenous TASK channel protein in cancer cells, refer to Mant et al., 2013a and Mant et al., 2013b for detailed protocols. In brief, for colocalisation experiments, the endogenous channel protein can be labelled using the antibodies optimised in this thesis (Chapter 4) and then the intracellular compartment of interest is labelled using a primary antibody raised in a different species (see Table 2.24 for examples of compartment markers used in this study). This will enable two secondary antibodies with different fluorophores to be used for the detection of primary antibody immunolabelling. Following confocal microscopy the colocalisation (or proximity) of the two fluorophores can be determined by using LAS lite software (as in Chapter 5.2.2) or Imaris imaging software (Bitplane).

The second line of investigation is to assess what impact K_{2P} channel activity has on cancer cell functions. Despite the limitations of the experimental techniques used in this thesis, the functional data presented here suggested that the differences in TASK channel protein expression may have a cell-specific effect on cancer cell proliferation (see Chapter 5). This may be caused by functional compensation within the K_{2P} channel family and the existence of multiple pathways to achieve a specific cellular function. 4-AP treatment was

found to reduce cell numbers in eight of the nine cancer cell lines examined in this thesis (Chapter 5). To determine which KCh are regulated by 4-AP treatment and have functional consequences, comprehensive characterisation of the ion channel and transporter expression in each cancer cell line will be required. In order to investigate these hypotheses and to confirm the functional data presented in this thesis, the following studies can be conducted:

1. To establish targeted experimental tools that can be used to modulate K_{2P} channel expression and activity. A lack of targeted $K_{2P}3.1$ and $K_{2P}9.1$ modulation was a limitation in this thesis and to further investigate TASK channel expression and activity in endogenously expressing cells, specific and reliable modulation is required. Areas of focus for this investigation will include examining the reliability of published RNAi tools (Kosztka et al., 2011; Lee et al., 2012) and establishing if the recently published channel inhibitors, A1899 for $K_{2P}3.1$ channels and Compound 23 for $K_{2P}9.1$ channels (which were not available for this study), can be used to selectively modulate the channels.
2. To confirm a proliferative role of $K_{2P}9.1$ channel protein expression in colorectal cancer cells. For this, subcellular localisation and whole-cell patch clamp experiments need to be conducted to determine the expression and activity of $K_{2P}9.1$ channels in colorectal cancer cells. Following these experiments, targeted modulation to reduce $K_{2P}9.1$ channel expression/activity will be required to determine if the proliferative effect observed in this chapter was due to $K_{2P}9.1$ channel modulation or off-target effects.
3. To identify potential ionic signalling networks present within cancer cells by characterising the ion channels and transporters expressed. For this, qRT-PCR will allow screening for ion channel and transporter mRNA expression within cancer cell lines. The specific ion channels/transporters which are expressed will depend on the cancer cell type in question, and a wide variety of ion channels and transporters have been identified in cancer (Table 1.3). Due to the breadth of candidate channels, a reasonable starting location would be to use an ion channel and transporter array, such as Qiagen Human Neuroscience Ion Channels and Transporters RT² Profiler™ PCR Array which determines the expression prolife of a panel of 84 ion channel and transporter genes. Following the establishment of an

expression prolife, individual channels/transporters which show significant expression can then be explored further.

4. Once candidate channels/pathways are established, the next area to investigate would be what cellular functions are caused by the activity of different complements of channels. For this, initial experiments may involve using cellular dyes and imaging experiments to examine any changes in the membrane potential (such as ANEP or RH dyes; Life Technologies), intracellular Ca^{2+} levels (such as Fluo-4 or Rhod-3; Life Technologies), or pH (such as pHrodo™; Life Technologies) following targeted modulation of the candidate channels identified following qRT-PCR analysis.
5. To determine if functional compensation occurs within the K_{2P} channel family a number of experiments will need to be performed. Utilisation of K_{2P} channel knockdowns, in combination with qRT-PCR, will elucidate if changes in the mRNA expression of K_{2P} channels or other ion channels occur in response to the loss of a specific channel. Whole-cell patch clamp experiments would need to be conducted alongside these experiments to assess if changes in ionic currents occur, since any changes may only occur at a functional level.
6. The influence of the cancer environment and cell signalling pathways on K_{2P} channels (expression and activity) may also result in cell-specific functional impacts on cancer cells. To examine K_{2P} channel regulation in cancer, the same lines of investigation listed in points 3-5 can be conducted under different modulation conditions.

7.6 Conclusion

In conclusion, this work has shown that K_{2P} channels are expressed in a wider range of cancers than had been previously identified, with both K_{2P} channel over- and underexpression occurring in cancer. In addition, multiple K_{2P} channels are expressed within a given cancer type. At a functional level, data presented in this thesis suggested that the expression of TASK channel protein appeared to have cell-specific functional consequences in the cancer cell lines examined, with TASK channel inhibition only causing a significant proliferative impact on cell lines that only expressed K_{2P}9.1 protein. The characterisation of roles for TASK channel activity in cancer cells in this study was limited by

the modulation tools available and incomplete cell line characterisation. However, the findings that the mRNA for multiple K_{2P} channels are expressed in cancer tissues and cell lines combined with the finding that TASK channel inhibition does not always impact on cell proliferation suggested that functional redundancy may occur in cancer. Functional redundancy may mean that other K_{2P} channels and ion channels can compensate for the loss of TASK channel activity (caused by pharmacological inhibition). Therefore, to further investigate the role of K_{2P} channels in cancer, the functional impacts of K_{2P} channel expression on cancer cells will need to be characterised in terms of upstream and downstream ionic signalling events. Initial experiments which should be conducted to further the research in this field, should aim to further characterise the expression of K_{2P} channels in cancer cell lines, both in terms of where the channels are expressed within the cells and which channels are active on the cell surface.

Appendices

Appendix 1: Summary of the properties of the K_{2P} channel family

The expression profiles, biophysical properties, and regulators of the fifteen K_{2P} channels. Channels are grouped by the six channel subfamilies: TWIK, TREK, TASK, TALK, THIK, and TRESK.

The abbreviated regulators and pharmacological agents that modulate the channels are: AA arachidonic acid, LA local anaesthetics, PUFA polyunsaturated fatty acids, SSRI selective serotonin reuptake inhibitors, and VA volatile anaesthetics.

Other abbreviations: PBL peripheral blood lymphocytes.

↑ indicates channel activation and ↓ inhibition.

(1) Lesage et al. (1996), (2) Lesage and Lazdunski (2000), (3) Enyedi and Czirják (2010), (4) Plant et al. (2012), (5) Chatelain et al. (2012), (6) Chavez et al. (1999), (7) Patel et al. (2000), (8) Medhurst et al. (2001), (9) Mhatre et al. (2004), (10) Salinas et al. (1999), (11) Fink et al. (1998), (12) Honore (2007), (13) Duprat et al. (2000), (14) Fink et al. (1996), (15) Noël et al. (2011), (16) Maingret et al. (1999a), (17) Kréneisz et al. (2009), (18) Lesage et al. (2000), (19) Duprat et al. (1997), (20) Gierten et al. (2008), (21) Streit et al. (2011), (22) Patel et al. (1999), (23) Meadows and Randall (2001), (24) Maingret et al. (2001), (25) O'Kelly et al. (1999), (26) O'Kelly et al. (2002), (27) O'Kelly and Goldstein (2008), (28) Talley and Bayliss (2002), (29) Mant et al. (2012), (30) Mant et al. (2013a), (31) Papreck et al. (2012), (32) Bai et al. (2005), (33) Czirjak and Enyedi (2002a), (34) Clarke et al. (2004), (35) Coburn et al. (2012), (36) Czirják and Enyedi (2003), (37) Brenner and O'Shaughnessy (2008), (38) Kovacs et al. (2005), (39) Kim and Gnatenco (2001), (40) Karschin et al. (2001), (41) Ashmole et al. (2001), (42) Reyes et al. (1998), (43) Duprat et al. (2005), (44) Girard et al. (2001), (45) Han et al. (2003), (46) Decher et al. (2001), (47) Rajan et al. (2001), (48) Campanucci et al. (2005), (49) Sano et al. (2003), (50) Liu et al. (2004), (51) Czirják et al. (2008).

Family	Channel	Expression	Current (sym. K^+)	Pharmacological modulators	Physiological regulation	Unique Properties	Ref
TWIK	K_{2P}1.1 (TWIK1)	Brain, colon, heart, kidney, liver, lung, ovary, pancreas, placenta, prostate, small intestine, spleen, testis.	Weak inward rectification	↓ Ba^{2+} ↓Quinine, ↓Quinidine	↓ Decrease intracellular pH ↑PKC activators (indirect)	SUMOylation of K247 silences K_{2P}1.1. Dileucine L293/L294 endocytosis motif on C-terminus. Pass Na^+ ions at acidic pH.	1-5
	K_{2P}6.1 (TWIK2)	Brain, bone marrow, cochlea, colon, heart, liver, lung, oesophagus, pancreas, PBL, placenta, prostate, salivary gland, small intestine, spleen, stomach, testis, thymus.	Weak inward rectification	↓ Ba^{2+} ↓Quinine ↓Quinidine	↓ Decrease extracellular pH ↑PKC activators ↓ Heat	Partial time dependent inactivation at depolarised potentials.	2-3 6-9
	K_{2P}7.1	Brain, lung, spinal cord.	Non-functional	Unknown	Unknown	GLE in P2 domain.	10-12
TREK	K_{2P}2.1 (TREK1)	Brain, kidney, ovary, pancreas, prostate, skeletal muscle, small intestine, testis.	Open rectification	↓Quinidine ↑ VA ↓ SSRI ↑ Riluzole	↑ Membrane stretch ↑ AA, PUFA ↓ PKA/PKC phosphorylation ↑ Decrease intracellular pH ↓ Decrease extracellular pH ↑ Heat ↓ O_2	Functionally active splice variants. Alternative start site, Sensitivity to extracellular divalent cations. AKAP150 binding partner modifies the functional properties of the channel.	2 12-18

	K_{2P}4.1 (TRAAK)	Brain, kidney, placenta, prostate, retina, small intestine, spinal cord, testis.	Open rectification	↑ Riluzole	↑ Membrane stretch ↑ AA, PUFA ↑ Heat ↑ Increase intracellular pH	Functionally active splice variants. Non-functional truncated variant detected.	2-3 11 13 15 16
	K_{2P}10.1 (TREK2)	Brain, colon, heart, kidney, liver, prostate, pancreas, PBL, small intestine, testis, thymus.	Open rectification	↑ VA ↓ SSRI ↑ Riluzole	↑ Membrane stretch ↑ AA, PUFA ↓ PKA/PKC phosphorylation ↑ Heat ↑ Decrease intracellular pH ↑ Decrease extracellular pH	Functionally active splice variants. Alternative start site. AKAP150 binding partner modifies the functional properties of the channel.	3 15 19
TASK	K_{2P}3.1 (TASK1)	Brain, carotid body, colon, heart, kidney, lung, pancreas, placenta, prostate, small intestine, uterus.	Open rectification	↓ Anandamide ↓ Genistein ↓ A1899 ↓ LA ↑ VA	↓ Decrease extracellular pH ↓ Gq GPCR ↓ Acute hypoxia ↓ Intracellular H_2O_2	C-terminal binding of 14-3-3β is required for surface expression. N-terminal binding of β-COP causes ER retention. Undergo clathrin-dependent endocytosis.	19-32
	K_{2P}9.1 (TASK3)	Adrenal, brain, carotid body, gastrointestinal tract, pancreas, pituitary gland.	Open rectification	↓ Anandamide ↓ Genistein ↓ Ruthenium red ↓ Zn^{2+} ↓Compound 23 ↓LA ↑ VA	↓ Extracellular decrease pH ↓ Acute hypoxia ↓ Gq GPCR ↓ Intracellular H_2O_2	C-terminal binding of 14-3-3β is required for surface expression. N-terminal binding of β-COP causes ER retention. Undergo clathrin-dependent pathways	19 22-28 30 33-38

						endocytosis.	
	K_{2P}15.1 (TASK5)	Adrenal gland, brain, central auditory system heart, kidney, liver, lung, pancreas, placenta, ovary, skeletal muscle, testis.	Non-functional	Unknown	Unknown	Polymorphism in P1 domain with GYG or EFG.	39-41
TALK	K_{2P}5.1 (TASK2)	Kidney, pancreas, placenta, liver, lung, ovary, small intestine.	Open rectification	↓ Quinine ↓ Quinidine ↓LA ↑ VA	↑ Increases extracellular pH		2 3 42
	K_{2P}16.1 (TALK1)	Pancreas.	Slight outward rectification	↓ Ba^{2+} ↓ Quinine ↓ Quinidine ↓ Chloroform ↓ VA	↑ Increases extracellular pH ↑ ROS	Four splice variants, only two are functional.	3 8 45
	K_{2P}17.1 (TALK2)	Brain, colon, heart, liver, lung, ovary, pancreas, PBL, placenta, small intestine, spleen, thymus, testis.	Slight outward rectification	↓ Quinine, ↓ Quinidine, ↓ Ba^{2+}, ↓ Chloroform ↓ Halothane ↑ Isoflurane	↑ Increases extracellular pH ↑ NO, ROS		3 43 44 46
THIK	K_{2P}13.1	Brain, heart, kidney,	Outward	↓Halothane	↓ Acute hypoxia		3

	(THIK1)	muscle, liver, lung, spleen, stomach, testis.	rectification	↑ AA			47-48
	K_{2P}12.1 (THIK2)	Brain, heart, kidney, liver, lung, skeletal muscle, pancreas, placenta, spleen, stomach.	Non-functional	Unknown	Unknown		3 44 47
TRESK	K_{2P}18.1 (TRESK)	Brain, spinal cord.	Outward rectification	↓ Ba^{2+} ↓ Quinine ↓ Quinidine ↓ LA ↑ VA ↓ Propafenone ↓ Glyburide ↓ Triethanolamine	↓ Decreases intracellular pH ↓ AA, PUFA	Activation by Ca^{2+}-dependent phosphorylation is regulated by binding of 14-3-3 to intracellular TM2-TM3 loop.	49-51

Appendix 2: Oncomine dataset reference list

Datasets are referenced from 1-80 in each data table presented in Chapter 3. For each reference the Oncomine nomenclature for a study and the original publication reference is given.

Ref	Oncomine dataset	Publication
1	Blaveri Bladder 2	Blaveri E, Simko JP, Korkola JE, Brewer JL, Baehner F, et al. (2005) Bladder cancer outcome and subtype classification by gene expression. Clin Cancer Res 11: 4044-4055.
2	Sanchez-Carbayo Bladder 2	Sanchez-Carbayo M, Socci ND, Lozano J, Saint F, Cordon-Cardo C (2006) Defining molecular profiles of poor outcome in patients with invasive bladder cancer using oligonucleotide microarrays. J Clin Oncol 24: 778-789.
3	Bredel Brain 2	Bredel M, Bredel C, Juric D, Harsh GR, Vogel H, et al. (2005) Functional network analysis reveals extended gliomagenesis pathway maps and three novel MYC-interacting genes in human gliomas. Cancer Res 65: 8679-8689.
4	French Brain	French PJ, Swagemakers SM, Nagel JH, Kouwenhoven MC, Brouwer E, et al. (2005) Gene expression profiles associated with treatment response in oligodendrogliomas. Cancer Res 65: 11335-11344.
5	Lee Brain	38. Lee J, Kotliarova S, Kotliarov Y, Li A, Su Q, et al. (2006) Tumor stem cells derived from glioblastomas cultured in bFGF and EGF more closely mirror the phenotype and genotype of primary tumors than do serum-cultured cell lines. Cancer Cell 9: 391-403.
6	Murat Brain	Murat A, Migliavacca E, Gorlia T, Lambiv WL, Shay T, et al. (2008) Stem cell-related "self-renewal" signature and high epidermal growth factor receptor expression associated with resistance to concomitant chemoradiotherapy in glioblastoma. J Clin Oncol 26: 3015-3024.
7	Pomeroy Brain	Pomeroy SL, Tamayo P, Gaasenbeek M, Sturla LM, Angelo M, et al. (2002) Prediction of central nervous system embryonal tumour outcome based on gene expression. Nature 415: 436-442.
8	Rickman Brain	Rickman DS, Bobek MP, Misek DE, Kuick R, Blaivas M, et al. (2001) Distinctive Molecular Profiles of High-Grade and Low-Grade Gliomas Based on Oligonucleotide Microarray Analysis. Cancer Res 61: 6885-6891.
9	Sun Brain	Sun L, Hui AM, Su Q, Vortmeyer A, Kotliarov Y, et al. (2006) Neuronal and glioma-derived stem cell factor induces angiogenesis within the brain. Cancer Cell 9: 287-300.
10	TCGA Brain	The Cancer Genome Atlas - Glioblastoma Gene Expression Data http://tcga-data.nci.nih.gov/tcga/
11	Finak Breast	Finak G, Bertos N, Pepin F, Sadekova S, Souleimanova M, et. Al. (2008). Stromal gene expression predicts clinical outcome in breast cancer. Nat Med 14, 518-527.
12	Ma Breast 4	Ma X-J, Dahiya S, Richardson E, Erlander M, Sgroi DC (2009) Gene expression profiling of the tumor microenvironment during breast cancer progression. Breast Cancer Res 11.
13	Perou Breast	Perou CM, Sorlie T, Eisen MB, van de Rijn M, Jeffrey SS, et al. (2000) Molecular portraits of human breast tumours. Nature 406: 747-752.
14	Radvanyi Breast	Radvanyi L, Singh-Sandhu D, Gallichan S, Lovitt C, Pedyczak A, et al. (2005) The gene associated with trichorhinophalangeal syndrome in humans is overexpressed in breast cancer. Proc Natl Acad Sci U S A 102: 11005-11010.
15	Sorlie Breast	Sørlie T, Perou CM, Tibshirani R, Aas T, Geisler S, et al. (2001) Gene expression patterns of breast carcinomas distinguish tumor subclasses with clinical implications. Proceedings of the National Academy of Sciences 98: 10869-10874.

16	Sorlie Breast 2	Sørlie T, Tibshirani R, Parker J, Hastie T, Marron JS, et al. (2003) Repeated observation of breast tumor subtypes in independent gene expression data sets. Proceedings of the National Academy of Sciences 100: 8418-8423.
17	TCGA Breast	The Cancer Genome Atlas - Invasive Breast Carcinoma Gene Expression Data http://tcga-data.nci.nih.gov/tcga/
18	Turashvili Breast	Turashvili G, Bouchal J, Baumforth K, Wei W, Dziechciarkova M, et al. (2007) Novel markers for differentiation of lobular and ductal invasive breast carcinomas by laser microdissection and microarray analysis. BMC Cancer 7: 55.
19	Zhao Breast	Zhao H, Langerød A, Ji Y, Nowels KW, Nesland JM, et al. (2004) Different Gene Expression Patterns in Invasive Lobular and Ductal Carcinomas of the Breast. Molecular Biology of the Cell 15: 2523-2536.
20	Pyeon Multi-cancer	Pyeon D, Newton MA, Lambert PF, den Boon JA, Sengupta S, et al. (2007) Fundamental differences in cell cycle deregulation in human papillomavirus-positive and human papillomavirus-negative head/neck and cervical cancers. Cancer Res 67: 4605-4619.
21	Scotto Cervix 2	56. Scotto L, Narayan G, Nandula SV, Arias-Pulido H, Subramaniyam S, et al. (2008) Identification of copy number gain and overexpressed genes on chromosome arm 20q by an integrative genomic approach in cervical cancer: potential role in progression. Genes Chromosomes Cancer 47: 755-765.
22	Zhai Cervix	79. Zhai Y, Kuick R, Nan B, Ota I, Weiss SJ, et al. (2007) Gene expression analysis of preinvasive and invasive cervical squamous cell carcinomas identifies HOXC10 as a key mediator of invasion. Cancer Res 67: 10163-10172.
23	Hong Colorectal	Hong Y, Downey T, Eu KW, Koh PK, Cheah PY (2010) A 'metastasis-prone' signature for early-stage mismatch-repair proficient sporadic colorectal cancer patients and its implications for possible therapeutics. Clin Exp Metastasis 27: 83-90.
24	Sabates-Bellver Colon	Sabates-Bellver J, Van der Flier LG, de Palo M, Cattaneo E, Maake C, et al. (2007) Transcriptome profile of human colorectal adenomas. Mol Cancer Res 5: 1263-1275.
25	Skrzypczak Colorectal 2	Skrzypczak M, Goryca K, Rubel T, Paziewska A, Mikula M, et al. (2010) Modeling Oncogenic Signaling in Colon Tumors by Multidirectional Analyses of Microarray Data Directed for Maximization of Analytical Reliability. PLoS One 5: e13091.
26	TCGA colorectal	The Cancer Genome Atlas - Colon and Rectum Adenocarcinoma Gene Expression Data http://tcga-data.nci.nih.gov/tcga/
27	Cho Gastric	Cho JY, Lim JY, Cheong JH, Park YY, Yoon SL, et al. (2011) Gene expression signature-based prognostic risk score in gastric cancer. Clin Cancer Res 17: 1850-1857.
28	Derrico Gastric	D'Errico M, de Rinaldis E, Blasi MF, Viti V, Falchetti M, et al. (2009) Genome-wide expression profile of sporadic gastric cancers with microsatellite instability. Eur J Cancer 45: 461-469.
29	Wang Gastric	Wang Q, Wen YG, Li DP, Xia J, Zhou CZ, et al. (2012) Upregulated INHBA expression is associated with poor survival in gastric cancer. Med Oncol 29: 77-83.
30	Cromer Head-Neck	Cromer A, Carles A, Millon R, Ganguli G, Chalmel F, et al. (2004) Identification of genes associated with tumorigenesis and metastatic potential of hypopharyngeal cancer by microarray analysis. Oncogene 23: 2484-2498.
31	Estilo Head-Neck	Estilo CL, P Oc, Talbot S, Socci ND, Carlson DL, et al. (2009) Oral tongue cancer gene expression profiling: Identification of novel potential prognosticators by oligonucleotide microarray analysis. BMC Cancer 9: 11.
32	Ginos Head-Neck	Ginos MA (2004) Identification of a Gene Expression Signature Associated with Recurrent Disease in Squamous Cell Carcinoma of the Head and Neck. Cancer Res 64: 55-63.
33	Pyeon Multi-cancer	Pyeon D, Newton MA, Lambert PF, den Boon JA, Sengupta S, Marsit CJ, Woodworth CD, Connor JP, Haugen TH, Smith EM, Kelsey KT, Turek LP & Ahlquist P. (2007).

		Fundamental differences in cell cycle deregulation in human papillomavirus-positive and human papillomavirus-negative head/neck and cervical cancers. Cancer research 67, 4605-4619.
34	Talbot Lung	Talbot SG, Estilo C, Maghami E, Sarkaria IS, Pham DK, et al. (2005) Gene expression profiling allows distinction between primary and metastatic squamous cell carcinomas in the lung. Cancer Res 65: 3063-3071.
35	Ye Head-Neck	Ye H, Yu T, Temam S, Ziober B, Wang J, et al. (2008) Transcriptomic dissection of tongue squamous cell carcinoma. BMC Genomics 9: 69.
36	Beroukhim Renal	Beroukhim R, Brunet JP, Di Napoli A, Mertz KD, Seeley A, et al. (2009) Patterns of gene expression and copy-number alterations in von-hippel lindau disease-associated and sporadic clear cell carcinoma of the kidney. Cancer Res 69: 4674-4681.
37	Cutcliffe Renal	Cutcliffe C, Kersey D, Huang CC, Zeng Y, Walterhouse D, et al. (2005) Clear cell sarcoma of the kidney: up-regulation of neural markers with activation of the sonic hedgehog and Akt pathways. Clin Cancer Res 11: 7986-7994.
38	Gumz Renal	Gumz ML, Zou H, Kreinest PA, Childs AC, Belmonte LS, et al. (2007) Secreted frizzled-related protein 1 loss contributes to tumor phenotype of clear cell renal cell carcinoma. Clin Cancer Res 13: 4740-4749.
39	Jones Renal	Jones J, Otu H, Spentzos D, Kolia S, Inan M, et al. (2005) Gene signatures of progression and metastasis in renal cell cancer. Clin Cancer Res 11: 5730-5739.
40	Lenburg Renal	Lenburg ME, Liou LS, Gerry NP, Frampton GM, Cohen HT, et al. (2003) Previously unidentified changes in renal cell carcinoma gene expression identified by parametric analysis of microarray data. BMC Cancer 3.
41	Yusenko Renal	Yusenko MV, Kuiper RP, Boethe T, Ljungberg B, van Kessel AG, et al. (2009) High-resolution DNA copy number and gene expression analyses distinguish chromophobe renal cell carcinomas and renal oncocytomas. BMC Cancer 9: 152.
42	Choi Leukemia	Choi YL, Tsukasaki K, O'Neill MC, Yamada Y, Onimaru Y, et al. (2007) A genomic analysis of adult T-cell leukemia. Oncogene 26: 1245-1255.
43	Haferlach Leukemia	Haferlach T, Kohlmann A, Wieczorek L, Basso G, Kronnie GT, et al. (2010) Clinical utility of microarray-based gene expression profiling in the diagnosis and subclassification of leukemia: report from the International Microarray Innovations in Leukemia Study Group. J Clin Oncol 28: 2529-2537.
44	Stegmair Leukemia	Stegmaier K, Ross KN, Colavito SA, O'Malley S, Stockwell BR, et al. (2004) Gene expression-based high-throughput screening(GE-HTS) and application to leukemia differentiation. Nat Genet 36: 257-263.
45	Wurmbach Liver	Wurmbach E, Chen YB, Khitrov G, Zhang W, Roayaie S, et al. (2007) Genome-wide molecular profiles of HCV-induced dysplasia and hepatocellular carcinoma. Hepatology 45: 938-947.
46	Beer Lung	Beer DG, Kardia SL, Huang CC, Giordano TJ, Levin AM, et al. (2002) Gene-expression profiles predict survival of patients with lung adenocarcinoma. Nat Med 8: 816-824.
47	Bhattaherjee Lung	Bhattacharjee A, Richards WG, Staunton J, Li C, Monti S, et al. (2001) Classification of human lung carcinomas by mRNA expression profiling reveals distinct adenocarcinoma subclasses. Proc Natl Acad Sci U S A 98: 13790-13795.
48	Garber Lung	Garber ME, Troyanskaya OG, Schluens K, Petersen S, Thaesler Z, et al. (2001) Diversity of gene expression in adenocarcinoma of the lung. Proc Natl Acad Sci U S A 98: 13784-13789.
49	Hou Lung	Hou J, Aerts J, den Hamer B, van Ijcken W, den Bakker M, et al. (2010) Gene Expression-Based Classification of Non-Small Cell Lung Carcinomas and Survival Prediction. PLoS One 5: e10312.
50	Landi Lung	Landi MT, Dracheva T, Rotunno M, Figueroa JD, Liu H, et al. (2008) Gene expression signature of cigarette smoking and its role in lung adenocarcinoma development and

		survival. PLoS One 3: e1651.
51	Stearman Lung	Stearman RS, Dwyer-Nield L, Zerbe L, Blaine SA, Chan Z, et al. (2005) Analysis of Orthologous Gene Expression between Human Pulmonary Adenocarcinoma and a Carcinogen-Induced Murine Model. The American Journal of Pathology 167: 1763-1775.
52	Su Lung	Su LJ, Chang CW, Wu YC, Chen KC, Lin CJ, et al. (2007) Selection of DDX5 as a novel internal control for Q-RT-PCR from microarray data using a block bootstrap re-sampling scheme. BMC Genomics 8: 140.
53	Wachi Lung	Wachi S, Yoneda K, Wu R (2005) Interactome-transcriptome analysis reveals the high centrality of genes differentially expressed in lung cancer tissues. Bioinformatics 21: 4205-4208.
54	Brune Lymphoma	Brune V, Tiacci E, Pfeil I, Doring C, Eckerle S, et al. (2008) Origin and pathogenesis of nodular lymphocyte-predominant Hodgkin lymphoma as revealed by global gene expression analysis. J Exp Med 205: 2251-2268.
55	Storz Lymphoma	Storz MN, van de Rijn M, Kim YH, Mraz-Gernhard S, Hoppe RT, et al. (2003) Gene expression profiles of cutaneous B cell lymphoma. J Investig Dermatol 120: 865-870.
56	Haqq Melanoma	Haqq C, Nosrati M, Sudilovsky D, Crothers J, Khodabakhsh D, et al. (2005) The gene expression signatures of melanoma progression. Proc Natl Acad Sci U S A 102: 6092-6097.
57	Riker Melanoma	Riker A, Enkemann S, Fodstad O, Liu S, Ren S, et al. (2008) The gene expression profiles of primary and metastatic melanoma yields a transition point of tumor progression and metastasis. BMC Medical Genomics 1: 13.
58	Talantov Melanoma	Talantov D, Mazumder A, Yu JX, Briggs T, Jiang Y, et al. (2005) Novel genes associated with malignant melanoma but not benign melanocytic lesions. Clin Cancer Res 11: 7234-7242.
59	Zhan Myeloma 3	Zhan F, Barlogie B, Arzoumanian V, Huang Y, Williams DR, et al. (2007) Gene-expression signature of benign monoclonal gammopathy evident in multiple myeloma is linked to good prognosis. Blood 109: 1692-1700.
60	Hao Oesophagus	Hao Y, Triadafilopoulos G, Sahbaie P, Young HS, Omary MB, et al. (2006) Gene expression profiling reveals stromal genes expressed in common between Barrett's esophagus and adenocarcinoma. Gastroenterology 131: 925-933.
61	Kim Oesophagus	Kim SM, Park Y-Y, Park ES, Cho JY, Izzo JG, et al. (2010) Prognostic Biomarkers for Esophageal Adenocarcinoma Identified by Analysis of Tumor Transcriptome. PLoS One 5: e15074.
2	Kimchi Oesophagus	Kimchi ET, Posner MC, Park JO, Darga TE, Kocherginsky M, et al. (2005) Progression of Barrett's metaplasia to adenocarcinoma is associated with the suppression of the transcriptional programs of epidermal differentiation. Cancer Res 65: 3146-3154.
63	Wang Oesophagus	Wang S, Zhan M, Yin J, Abraham JM, Mori Y, et al. (2006) Transcriptional profiling suggests that Barrett's metaplasia is an early intermediate stage in esophageal adenocarcinogenesis. Oncogene 25: 3346-3356.
64	Crabtree Uterus (Other)	Crabtree JS, Jelinsky SA, Harris HA, Choe SE, Cotreau MM, et al. (2009) Comparison of human and rat uterine leiomyomata: identification of a dysregulated mammalian target of rapamycin pathway. Cancer Res 69: 6171-6178.
65	Giordana Adrenal (Other)	Giordano TJ, Thomas DG, Kuick R, Lizyness M, Misek DE, et al. (2003) Distinct Transcriptional Profiles of Adrenocortical Tumors Uncovered by DNA Microarray Analysis. The American Journal of Pathology 162: 521-531.
66	Gordon Mesotheliom a (Other)	Gordon GJ, Rockwell GN, Jensen RV, Rheinwald JG, Glickman JN, et al. (2005) Identification of Novel Candidate Oncogenes and Tumor Suppressors in Malignant Pleural Mesothelioma Using Large-Scale Transcriptional Profiling. The American Journal of Pathology 166: 1827-1840.

67	Korkola Seminoma (Other)	Korkola JE, Houldsworth J, Chadalavada RS, Olshen AB, Dobrzynski D, et al. (2006) Down-regulation of stem cell genes, including those in a 200-kb gene cluster at $1_{2P}13.31$, is associated with in vivo differentiation of human male germ cell tumors. Cancer Res 66: 820-827.
68	Nindl Skin (Other)	Nindl I, Dang C, Forschner T, Kuban RJ, Meyer T, et al. (2006) Identification of differentially expressed genes in cutaneous squamous cell carcinoma by microarray expression profiling. Mol Cancer 5: 30.
69	Quade Uterus (Other)	Quade BJ, Wang TY, Sornberger K, Dal Cin P, Mutter GL, et al. (2004) Molecular pathogenesis of uterine smooth muscle tumors from transcriptional profiling. Genes Chromosomes Cancer 40: 97-108.
70	Skotheim Testis (Other)	Skotheim RI, Lind GE, Monni O, Nesland JM, Abeler VM, et al. (2005) Differentiation of human embryonal carcinomas in vitro and in vivo reveals expression profiles relevant to normal development. Cancer Res 65: 5588-5598.
71	Badea Pancreas	Badea L, Herlea V, Dima SO, Dumitrascu T, Popescu I (2008) Combined gene expression analysis of whole-tissue and microdissected pancreatic ductal adenocarcinoma identifies genes specifically overexpressed in tumor epithelia. Hepatogastroenterology 55: 2016-2027.
72	Iacobuzio-Danahue Pancreas 2	Iacobuzio-Donahue CA, Maitra A, Olsen M, Lowe AW, Van Heek NT, et al. (2003) Exploration of Global Gene Expression Patterns in Pancreatic Adenocarcinoma Using cDNA Microarrays. The American Journal of Pathology 162: 1151-1162.
73	Logsdon Pancreas	Logsdon CD, Simeone DM, Binkley C, Arumugam T, Greenson JK, et al. (2003) Molecular Profiling of Pancreatic Adenocarcinoma and Chronic Pancreatitis Identifies Multiple Genes Differentially Regulated in Pancreatic Cancer. Cancer Res 63: 2649-2657.
74	Pei Pancreas	Pei H, Li L, Fridley BL, Jenkins GD, Kalari KR, et al. (2009) FKBP51 affects cancer cell response to chemotherapy by negatively regulating Akt. Cancer Cell 16: 259-266.
75	Segara Pancreas	Segara D, Biankin AV, Kench JG, Langusch CC, Dawson AC, et al. (2005) Expression of HOXB2, a retinoic acid signaling target in pancreatic cancer and pancreatic intraepithelial neoplasia. Clin Cancer Res 11: 3587-3596.
76	Arredouani Prostate	Arredouani MS, Lu B, Bhasin M, Eljanne M, Yue W, et al. (2009) Identification of the transcription factor single-minded homologue 2 as a potential biomarker and immunotherapy target in prostate cancer. Clin Cancer Res 15: 5794-5802.
77	Grasso Prostate	Grasso CS, Wu YM, Robinson DR, Cao X, Dhanasekaran SM, et al. (2012) The mutational landscape of lethal castration-resistant prostate cancer. Nature 487: 239-243.
78	Tomlins Prostate	Tomlins SA, Mehra R, Rhodes DR, Cao X, Wang L, et al. (2007) Integrative molecular concept modeling of prostate cancer progression. Nat Genet 39: 41-51.
79	Vermbally Prostate	Varambally S, Yu J, Laxman B, Rhodes DR, Mehra R, et al. (2005) Integrative genomic and proteomic analysis of prostate cancer reveals signatures of metastatic progression. Cancer Cell 8: 393-406.
80	Detwiller Sarcoma	Detwiller KY, Fernando NT, Segal NH, Ryeom SW, D'Amore PA, et al. (2005) Analysis of hypoxia-related gene expression in sarcomas and effect of hypoxia on RNA interference of vascular endothelial cell growth factor A. Cancer Res 65: 5881-5889.

Appendix 3: Expression of K_{2P} channel mRNA in cancers which were excluded from comparative meta-analysis

The above threshold data for K_{2P} channel mRNA expression in cancer subtypes where insufficient study numbers were available to enable inclusion in meta-analysis (n ≤ 2) are shown. Data are grouped by gene name and divided into each cancer type and subtypes.

The p-value, fold change, and gene rank percentile (%) for data which scored above threshold values (p-value < 0.05, fold change > 2 and gene rank percentile < 10 %) are shown.

Overexpression (↑) and underexpression (↓) are indicated in red and blue respectively.

Gene	Cancer	Subtype	Above threshold analyses				Median value		
			p-value	Fold change	%	Ref	p-value	Gene rank	n
KCNK1	Brain	Medulloblastoma	↓ 2.60E-08	-14.207	2	7	2.74E-05	69.5	2
			↓ 5.48E-05	-10.211	2	7			
KCNK2	Head and Neck	Squamous cell	↓ 2.24E-05	-3.693	2	30	4.58E-01	4694.5	2
KCNK5	Leukaemia	Chronic Lymphocytic	↓ 4.97E-39	-2.039	5	43	3.92E-01	5370.5	2
	Lung	Squamous cell	↓ 9.14E-14	-2.192	6	49	1.20E-02	1618	2
KCNK6	Melanoma	Melanoma	↓ 2.01E-04	-2.209	3	57	3.20E-01	5582	2
KCNK7	Oesophageal	Adenocarcinoma	↓ 2.40E-17	-2.681	4	61	1.87E-04	418	2
			↓ 3.74E-04	-9.38	2	62			
		Barrett's	↓ 1.12E-10	-2.608	5	61	1.00E-03	597.5	2
			↓ 3.00E-03	-2.586	3	60			
KCNK10	Colorectal	Adenoma	↓ 3.61E-11	-2.758	1	25	6.86E-.04	1116	2
KCNK12	Brain	Astrocytoma	↓ 8.77E-08	-4.126	5	9	2.00E-03	1332.5	2
			↓ 3.00E-03	-3.054	10	9			

A) G97E GFP-K_{2P}3.1

GAGCTGTACAAGTCCGGACTCAGATCTCGAGCTCAAGCTTGGTACCACTTGTTCTTTTTGCAGAA
GCTCAGAATAAACGCTCAACTTTGGGCCCCTCGAGGTCGACGAATTCGCCCTTCG**ATG**AAGCGG
CAGAACGTGCGCACGCTGGCGCTCATCGTGTGCACCTTCACCTACCTGCTGGTGGGCGCCGCGG
TCTTCGACGCGCTGGAGTCGGAGCCCGAGCTGATCGAGCGGCAGCGGCTGGAGCTGCGGCAGC
AGGAGCTGCGGGCGCGCTACAACCTCAGCCAGGGCGGCTACGAGGAGCTGGAGCGCGTCGTG
CTGCGCCTCAAGCCGCACAAGGCCGGCGTGCAGTGGCGCTTCGCCGGCTCCTTCTACTTCGCCA
TCACCGTCATCACCACCATCGGCTAC**GAG**CACGCGGCACCCAGCACGGATGGCGGCAAGGTGTT
CTGCATGTTCTACGCGCTGCTGGGCATCCCGCTCACGCTCGTCATGTTCCAGAGCCTGGGCGAGC
GCATCAACACCTTGGTGAGGTACCTGCTGCACCGCGCCAAGAAGGGGCTGGGCATGCGGCGCG
CCGACGTGTCCATGGCCAACATGGTGCTCATCGGCTTCTTCTCGTGCATCAGCACGCTGTGCATC
GGCGCCGCCGCCTTCTCCCACTACGAGCACTGGACCTTCTTCCAGGCCTACTACTACTGCTTCATC
ACCCTCACCACCATCGGCTTCGGCGACTACGTGGCGCTGCAGAAGGACCAGGCCCTGCAGACGC
AGCCGCAGTACGTGGCCTTCAGCTTCGTCTACATCCTTACGGGCCTCACGGTCATCGGCGCCTTC
CTCAACCTCGTGGTGCTGCGCTTCATGACCATGAACGCCGAGGACGAGAAGCGCGACGCCGAG
CACCGCGCGCTGCTCACGCGCAACGGGCAGGCGGGCGGCGGCGGAGGGGGTGGCAGCGCGC
ACACTACGGACACCGCCTCATCCACGGCGGCAGCGGGCGGCGGCGGCTTCCGCAACGTCTACG
CGGAGGTGCTGCACTTCCAGTCCATGTGCTCGTGCCTGTGGTACAAGAGCCGCGAGAAGCTGCA
GTACTCCATCCCCATGATCATCCCGCGGGACCTCTCCACGTCCGACACGTGCGTGGAGCAGAGCC
ACTCGTCGCCGGGAGGGGGCGGCCGCTACAGCGACACGCCCTCGCGACGCTGCCTGTGCAGCG
GGGCGCCACGCTCCGCCATCAGCTCGGTGTCCACGGGTCTGCACAGCCTGTCCACCTTCCGCGG
CCTCATGAAGCGCAGGAGCTCCGTG**TGA**CTGCCCCGAGGGACCTGGAGCACCTGGGGGCGCGA
AGGGCGAATTCCGC

B) G97E GFP-K_{2P}9.1

GCTGGACGAGCTGTACAGTCCGGACTCAGATCTCGAGCTCAAGCTTCGAATTCA**ATG**AAGAGGC
AGAACGTGCGGACTCTGTCCCTCATCGTCTGCACCTTCACCTACCTGCTGGTGGGCGCCGCCGTG
TTCGACGCCCTCGAGTCGGACCACGAGATGCGCGAGGAGGAGAAACTCAAAGCCGAGGAGATC
CGGATCAAGGGGAAGTACAACATCAGCAGCGAGGACTACCGGCAGCTGGAGCTGGTGATCCTG
CAGTCGGAACCGCACCGCGCCGGCGTCCAGTGGAAATTCGCCGGCTCCTTCTACTTTGCGATCA
CGGTCATCACCACCATAGGTTAT**GAG**CACGCTGCACCTGGCACCGATGCGGGCAAGGCCTTCTG
CATGTTCTACGCCGTGCTGGGCATCCCGCTGACACTGGTCATGTTCCAGAGCCTGGGCGAGCGCA
TGAACACCTTCGTGCGCTACCTGCTGAAGCGCATTAAGAAGTGCTGTGGCATGCGCAACACTGA
CGTGTCTATGGAGAACATGGTGACTGTGGGCTTCTTCTCCTGCATGGGGACGCTGTGCATCGGG
GCGGCCGCCTTCTCCCAGTGTGAGGAGTGGAGCTTCTTCCACGCCTACTACTACTGCTTCATCAC
GTTGACTACCATTGGGTTCGGGGACTACGTGGCCCTGCAGACCAAGGGCGCCCTGCAGAAGAA
GCCGCTCTACGTGGCCTTTAGCTTTATGTATATCCTGGTGGGGCTGACGGTCATCGGGGCCTTCCT
CAACCTGGTCGTCCTCAGGTTCTTGACCATGAACAGTGAGGATGAGCGGCGGGATGCTGAAGA
GAGGGCATCCCTCGCCGGAAACCGCAACAGCATGGTCATTCACATCCCTGAGGAGCCGCGGCCC
AGCCGGCCCAGGTACAAGGCGGACGTCCCGGACCTGCAGTCTGTGTGCTCCTGCACCTGCTACC
GCTCGCAGGACTATGGCGGCCGCTCGGTGGCACCGCAGAACTCCTTCAGCGCCAAGCTTGCCCC
CCACTACTTCCACTCCATCTCTTACAAGATCGAGGAGATCTCACCAAGCACATTAAAAAACAGCCT
CTTCCCATCGCCTATTAGCTCCATCTCTCCTGGGTTACACAGCTTTACCGACCACCAGAGGCTGAT
GAAACGCCGGAAGTCCGTT**TGA**GGATCCACCGGATCTAGATAACTGATCATAATCAGCCATACCA
CATTTGTAGAGGTTTTACTTGCTTTAAAAAACCTCCCACACCTCCCCCTGAACCTGAAACATAAAA
TGAATGCAATTGT

Appendix 4: Pore mutant channel DNA sequencing

DNA sequencing results for (A) G97E GFP-K_{2P}3.1 and (B) G97E GFP-K_{2P}9.1. Sequencing results from site-directed mutagenesis experiments which created channels with a mutated pore domain by mutating glycine 97 into glutamate. The mutated DNA codon (GAG) is highlighted in grey.
The start (ATG) and stop (TGA) codons are also highlighted.

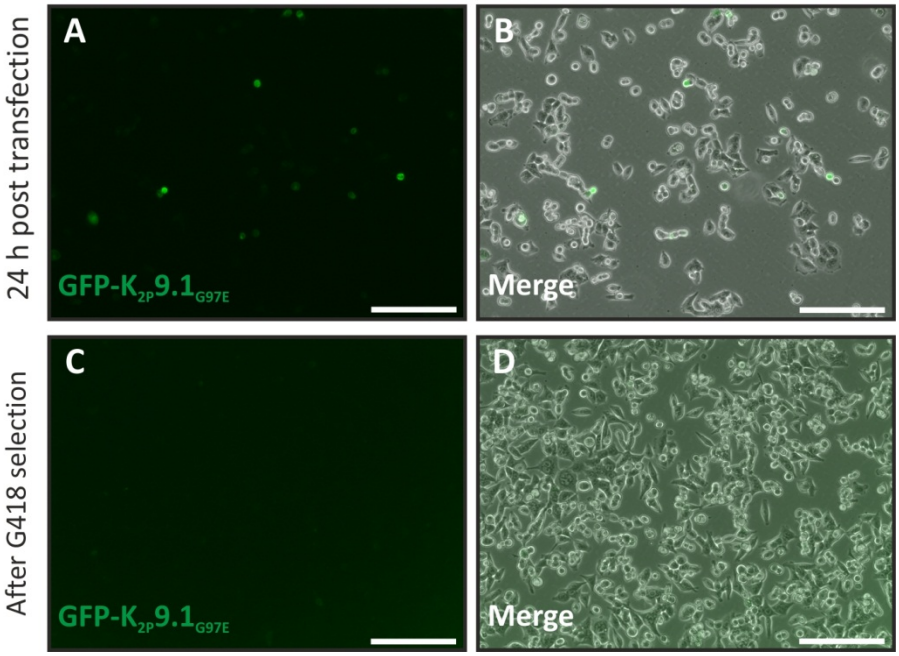

Appendix 5: HCT116 colorectal carcinoma transfection

HCT116 cells expressing GFP-$K_{2P}9.1_{G97E}$. Channel expression was analysed 24 h post transfection and after G418 antibiotic (1 mg/ml) selection.

A&C) Transfected channel was detected by GFP fluorescence signal.
B&D) GFP fluorescence signal overlapped with phase contrast.

All scale bars are 200 µm.

References

Abbott, G. W., Sesti, F., Splawski, I., Buck, M. E., Lehmann, M. H., Timothy, K. W., Keating, M. T. & Goldstein, S. A. N. 1999. MiRP1 forms IKr potassium channels with HERG and is associated with cardiac arrhythmia. *Cell,* 97**,** 175-187.

Abdul, M. & Hoosein, N. 2006. Reduced $K_V1.3$ potassium channel expression in human prostate cancer. *J Membr Biol,* 214**,** 99-102.

Adams, J. M. & Cory, S. 2007. The Bcl-2 apoptotic switch in cancer development and therapy. *Oncogene,* 26**,** 1324-1337.

Adelman, J. P., Clapham, D. E., Hibino, H., Inanobe, A., Jan, L. Y., Karschin, A., Kubo, Y., Kurachi, Y., Lazdunski, M., Miki, T., Nichols, C. G., Pearson, W. L., Seino, S. & C.A., V. 2013. *Inwardly rectifying potassium channels* [Online]. IUPHAR database (IUPHAR-DB). Available: http://www.iuphar-db.org/DATABASE/FamilyMenuForward?familyId=74 [Accessed 20/09/2013].

Adelman, J. P., Maylie, J. & Sah, P. 2012. Small-conductance Ca^{2+}-activated K^+ channels: form and function. *Annu Rev Physiol,* 74**,** 245-269.

Afrasiabi, E., Hietamäki, M., Viitanen, T., Sukumaran, P., Bergelin, N. & Törnquist, K. 2010. Expression and significance of HERG (*KCNH2*) potassium channels in the regulation of MDA-MB-435S melanoma cell proliferation and migration. *Cell Signal,* 22**,** 57-64.

Agarwal, J., Griesinger, F., Stuhmer, W. & Pardo, L. 2010. The potassium channel Ether à go-go is a novel prognostic factor with functional relevance in acute myeloid leukemia. *Mol Cancer,* 9.

Aidley, D. J. & Stanfield, P. R. 1996. *Ion channels: molecules in action,* Cambridge, Cambridge University Press.

Akiyama, T., Ishida, J., Nakagawa, S., Ogawara, H., Watanabe, S., Itoh, N., Shibuya, M. & Fukami, Y. 1987. Genistein, a specific inhibitor of tyrosine-specific protein kinases. *J Biol Chem,* 262**,** 5592-5595.

Akiyama, T. & Ogawara, H. 1991. [30] Use and specificity of genistein as inhibitor of protein-tyrosine kinases. *In:* Tony Hunter, B. M. S. (ed.) *Methods Enzymol.* Academic Press.

Akl, H. & Bultynck, G. 2013. Altered Ca^{2+} signaling in cancer cells: proto-oncogenes and tumor suppressors targeting IP_3 receptors. *BBA - Rev Cancer,* 1835**,** 180-193.

Alberts, B. 2008. *Molecular biology of the cell,* New York, Garland Science.

Alloui, A., Zimmermann, K., Mamet, J., Duprat, F., Noel, J., Chemin, J., Guy, N., Blondeau, N., Voilley, N., Rubat-Coudert, C., Borsotto, M., Romey, G., Heurteaux, C., Reeh, P., Eschalier, A. & Lazdunski, M. 2006. TREK-1, a K^+ channel involved in polymodal pain perception. *EMBO J,* 25**,** 2368-2376.

Alvarez-Baron, C. P., Jonsson, P., Thomas, C., Dryer, S. E. & Williams, C. 2011. The two-pore domain potassium channel *KCNK5*: induction by estrogen receptor α and role in proliferation of breast cancer cells. *Mol Endocrinol,* 25**,** 1326-1336.

Amith, S. R. & Fliegel, L. 2013. Regulation of the Na^+/H^+ exchanger (NHE1) in breast cancer metastasis. *Cancer Res,* 73**,** 1259-1264.

Amorós, I., Barana, A., Caballero, R., Gómez, R., Osuna, L., Lillo, M. P., Tamargo, J. & Delpón, E. 2010. Endocannabinoids and cannabinoid analogues block human cardiac $K_V4.3$ channels in a receptor-independent manner. *J Mol Cell Cardiol,* 48**,** 201-210.

Andersen, A. P., Moreira, J. M. A. & Pedersen, S. F. 2014. Interactions of ion transporters and channels with cancer cell metabolism and the tumour microenvironment. *Philos Trans R Soc Lond B Biol Sci,* 369.

Anderson, A. R. A., Weaver, A. M., Cummings, P. T. & Quaranta, V. 2006. Tumor morphology and phenotypic evolution driven by selective pressure from the microenvironment. *Cell,* 127**,** 905-915.

Arcangeli, A. 2011. Ion channels and transporters in cancer. 3. Ion channels in the tumor cell-microenvironment cross talk. *Am J Physiol Cell Physiol,* 301**,** C762-771.

Arcangeli, A. & Becchetti, A. 2010. New trends in cancer therapy: targeting ion channels and transporters. *Pharmaceuticals,* 3**,** 1202-1224.

Arcangeli, A., Bianchi, L., Becchetti, A., Faravelli, L., Coronnello, M., Mini, E., Olivotto, M. & Wanke, E. 1995. A novel inward-rectifying K^+ current with a cell-cycle dependence governs the resting potential of mammalian neuroblastoma cells. *J Physiol,* 489**,** 455-471.

Artandi, S. E. & DePinho, R. A. 2010. Telomeres and telomerase in cancer. *Carcinogenesis,* 31**,** 9-18.

Artym, V. V. & Petty, H. R. 2002. Molecular proximity of $K_V1.3$ voltage-gated potassium channels and β_1-integrins on the plasma membrane of melanoma cells: effects of cell adherence and channel blockers. *J Gen Physiol,* 120**,** 29-37.

Arvind, S., Arivazhagan, A., Santosh, V. & Chandramouli, B. A. 2012. Differential expression of a novel voltage gated potassium channel – $K_V1.5$ in astrocytomas and its impact on prognosis in glioblastoma. *Br J Neurosurg,* 26**,** 16-20.

Ashcroft, F. M. 2010. New uses for old drugs: neonatal diabetes and sulphonylureas. *Cell Metab,* 11**,** 179-181.

Asher, V., Khan, R., Warren, A., Shaw, R., Schalkwyk, G., Bali, A. & Sowter, H. 2010. The Eag potassium channel as a new prognostic marker in ovarian cancer. *Diagn Pathol,* 5**,** 78.

Asher, V., Warren, A., Shaw, R., Sowter, H., Bali, A. & Khan, R. 2011. The role of Eag and HERG channels in cell proliferation and apoptotic cell death in SK-OV-3 ovarian cancer cell line. *Cancer Cell Int,* 11.

Ashmole, I., Goodwin, P. & Stanfield, P. 2001. TASK-5, a novel member of the tandem pore K^+ channel family. *Pflugers Arch,* 442**,** 828-833.

Baeriswyl, V. & Christofori, G. 2009. The angiogenic switch in carcinogenesis. *Semin Cancer Biol,* 19**,** 329-337.

Bai, X., Bugg, G. J., Greenwood, S. L., Glazier, J. D., Sibley, C. P., Baker, P. N., Taggart, M. J. & Fyfe, G. K. 2005. Expression of TASK and TREK, two-pore domain K^+ channels, in human myometrium. *Reproduction,* 129**,** 525-530.

Banderali, U., Belke, D., Singh, A., Jayanthan, A., Giles, W. R. & Narendran, A. 2011. Curcumin blocks $K_V11.1$ (Erg) potassium current and slows proliferation in the infant acute monocytic leukemia cell line THP-1. *Cell Physiol Biochem,* 28**,** 1169-1180.

Barak, V., Goike, H., Panaretakis, K. W. & Einarsson, R. 2004. Clinical utility of cytokeratins as tumor markers. *Clin Biochem,* 37**,** 529-540.

Barriere, H., Belfodil, R., Rubera, I., Tauc, M., Lesage, F., Poujeol, C., Guy, N., Barhanin, J. & Poujeol, P. 2003. Role of TASK-2 potassium channels regarding volume regulation in primary cultures of mouse proximal tubules. *J Gen Physiol,* 122**,** 177-190.

Bayliss, D. A. & Barrett, P. Q. 2008. Emerging roles for two-pore domain potassium channels and their potential therapeutic impact. *Trends Pharmacol Sci,* 29**,** 566-575.

Bayliss, D. A., Sirois, J. E. & Talley, E. M. 2003. The TASK family: two-pore domain background K^+ channels. *Mol Interv,* 3**,** 205-219.

Becchetti, A. 2011. Ion channels and transporters in cancer. 1. Ion channels and cell proliferation in cancer. *Am J Physiol Cell Physiol,* 301**,** C255-C265.

Becchetti, A., Munaron, L. & Arcangeli, A. 2013. The role of ion channels and transporters in cell proliferation and cancer. *Front Physiol,* 4.

Behrends, J. C. 2012. Evolution of the ion channel concept: the historical perspective. *Chem Rev,* 112**,** 6218-6226.

Benesova, J., Rusnakova, V., Honsa, P., Pivonkova, H., Dzamba, D., Kubista, M. & Anderova, M. 2012. Distinct expression/function of potassium and chloride channels contributes to the diverse volume regulation in cortical astrocytes of GFAP/EGFP mice. *PLoS One,* 7**,** e29725.

Benga, O. & Huber, V. J. 2012. Brain water channel proteins in health and disease. *Mol Aspects Med,* 33**,** 562-578.

Berdasco, M. & Esteller, M. 2010. Aberrant epigenetic landscape in cancer: how cellular identity goes awry. *Dev Cell,* 19**,** 698-711.

Berg, A. P., Talley, E. M., Manger, J. P. & Bayliss, D. A. 2004. Motoneurons express heteromeric TWIK-related acid-sensitive K^+ (TASK) channels containing TASK-1 (*KCNK3*) and TASK-3 (*KCNK9*) subunits. *J Neurosci,* 24**,** 6693-6702.

Berkefeld, H., Fakler, B. & Schulte, U. 2010. Ca^{2+}-activated K^+ xhannels: from protein complexes to function. *Physiol Rev,* 90**,** 1437-1459.

Berridge, M. J. 1993. Inositol trisphosphate and calcium signalling. *Nature,* 361**,** 315-325.

Bertout, J. A., Patel, S. A. & Simon, M. C. 2008. The impact of O_2 availability on human cancer. *Nat Rev Cancer,* 8**,** 967-975.

Bhowmick, N. A., Neilson, E. G. & Moses, H. L. 2004. Stromal fibroblasts in cancer initiation and progression. *Nature,* 432**,** 332-337.

Bi, D., Toyama, K., Lemaître, V., Takai, J., Fan, F., Jenkins, D. P., Wulff, H., Gutterman, D. D., Park, F. & Miura, H. 2013. The intermediate conductance calcium-activated potassium channel $K_{Ca}3.1$ regulates vascular smooth muscle cell proliferation via controlling calcium-dependent signaling. *J Biol Chem,* 288**,** 15843-15853.

Bianco, R., Melisi, D., Ciardiello, F. & Tortora, G. 2006. Key cancer cell signal transduction pathways as therapeutic targets. *Eur J Cancer,* 42**,** 290-294.

Biedler, J. L., Roffler-Tarlov, S., Schachner, M. & Freedman, L. S. 1978. multiple neurotransmitter synthesis by human neuroblastoma cell Lines and clones. *Cancer Res,* 38**,** 3751-3757.

Bielanska, J., Hernández-Losa, J., Pérez-Verdaguer, M., Moline, T., Somoza, R., Y, R., Cajal, S., Condom, E., Ferreres JC & A., F. 2009. Voltage-dependent potassium channels $K_V1.3$ and $K_V1.5$ in human cancer. *Curr Cancer Drug Targets,* 9**,** 904-914.

Bischoff, U., Schmidt, C., Netzer, R. & Pongs, O. 2000. Effects of fluoroquinolones on HERG currents. *Eur J Pharmacol,* 406**,** 341-343.

Bittner, S., Bobak, N., Herrmann, A. M., Göbel, K., Meuth, P., Höhn, K. G., Stenner, M.-P., Budde, T., Wiendl, H. & Meuth, S. G. 2010. Upregulation of $K_{2P}5.1$ potassium channels in multiple sclerosis. *Ann Neurol,* 68**,** 58-69.

Bittner, S., Ruck, T., Schuhmann, M. K., Herrmann, A. M., ou Maati, H. M., Bobak, N., Gobel, K., Langhauser, F., Stegner, D., Ehling, P., Borsotto, M., Pape, H.-C., Nieswandt, B., Kleinschnitz, C., Heurteaux, C., Galla, H.-J., Budde, T., Wiendl, H. & Meuth, S. G. 2013. Endothelial TWIK-related potassium channel-1 (TREK-1) regulates immune-cell trafficking into the CNS. *Nat Med,* 19**,** 1161-1165.

Black, Joel A. & Waxman, Stephen G. 2013. Noncanonical roles of voltage-gated sodium channels. *Neuron,* 80**,** 280-291.

Blackiston, D. J., McLaughlin, K. A. & Levin, M. 2009. Bioelectric controls of cell proliferation: ion channels, membrane voltage and the cell cycle. *Cell Cycle,* 8**,** 3527-3536.

Blankman, J. L. & Cravatt, B. F. 2013. Chemical probes of endocannabinoid metabolism. *Pharmacol Rev,* 65**,** 849-871.

Blaustein, M. P. & Lederer, W. J. 1999. Sodium/calcium exchange: its physiological implications. *Physiol Rev,* 79**,** 763-854.

Blom, N., Sicheritz-Pontén, T., Gupta, R., Gammeltoft, S. & Brunak, S. 2004. Prediction of post-translational glycosylation and phosphorylation of proteins from the amino acid sequence. *Proteomics,* 4**,** 1633-1649.

Bobak, N., Bittner, S., Andronic, J., Hartmann, S., Muhlpfordt, F., Schneider-Hohendorf, T., Wolf, K., Schmelter, C., Gobel, K., Meuth, P., Zimmermann, H., Doring, F., Wischmeyer, E., Budde, T., Wiendl, H., Meuth, S. G. & Sukhorukov, V. L. 2011. Volume regulation of murine T lymphocytes relies on voltage-dependent and two-pore domain potassium channels. *Biochim Biophys Acta,* 1808**,** 2036-2044.

Bonnet, S., Archer, S. L., Allalunis-Turner, J., Haromy, A., Beaulieu, C., Thompson, R., Lee, C. T., Lopaschuk, G. D., Puttagunta, L., Bonnet, S., Harry, G., Hashimoto, K., Porter, C. J., Andrade, M. A., Thebaud, B. & Michelakis, E. D. 2007. A mitochondria-K^+ channel axis is suppressed in cancer and its normalization promotes apoptosis and inhibits cancer growth. *Cancer Cell,* 11**,** 37-51.

Borowiec, A.-S., Hague, F., Gouilleux-Gruart, V., Lassoued, K. & Ouadid-Ahidouch, H. 2011. Regulation of IGF-1-dependent cyclin D1 and E expression by hEag1 channels in MCF-7 cells: The critical role of hEag1 channels in G_1 phase progression. *BBA - Mol Cell Res,* 1813**,** 723-730.

Borowiec, A.-S., Hague, F., Harir, N., Guénin, S., Guerineau, F., Gouilleux, F., Roudbaraki, M., Lassoued, K. & Ouadid-Ahidouch, H. 2007. IGF-1 activates hEAG K^+ channels through an Akt-dependent signaling pathway in breast cancer cells: role in cell proliferation. *J Cell Physiol,* 212**,** 690-701.

Bortner, C. D. & Cidlowski, J. A. 2007. Cell shrinkage and monovalent cation fluxes: role in apoptosis. *Arch Biochem Biophys,* 462**,** 176-188.

Bortner, C. D., Hughes, F. M. & Cidlowski, J. A. 1997. A primary role for K^+ and Na^+ efflux in the activation of apoptosis. *J Biol Chem,* 272**,** 32436-32442.

Brackenbury, W. J. 2012. Voltage-gated sodium channels and metastatic disease. *Channels,* 6**,** 352-361.

Brackenbury, W. J. & Djamgoz, M. B. A. 2007. Nerve growth factor enhances voltage-gated Na^+ channel activity and Transwell migration in Mat-LyLu rat prostate cancer cell line. *J Cell Physiol,* 210**,** 602-608.

Brattain, M. G., Fine, W. D., Khaled, F. M., Thompson, J. & Brattain, D. E. 1981. Heterogeneity of malignant cells from a human colonic carcinoma. *Cancer Res,* 41**,** 1751-1756.

Brazier, S. P., Mason, H. S., Bateson, A. N. & Kemp, P. J. 2005. Cloning of the human TASK-2 (*KCNK5*) promoter and its regulation by chronic hypoxia. *Biochem Biophys Res Commun,* 336**,** 1251-1258.

Brenner, T. & O'Shaughnessy, K. M. 2008. Both TASK-3 and TREK-1 two-pore loop K^+ channels are expressed in H295R cells and modulate their membrane potential and aldosterone secretion. *Am J Physiol Endoc M,* 295**,** E1480-E1486.

Brevet, M., Fucks, D., Chatelain, D., Regimbeau, J.-M., Delcenserie, R., Sevestre, H. & Ouadid-Ahidouch, H. 2009a. Deregulation of 2 potassium channels in pancreas adenocarcinomas: implication of $K_V1.3$ gene promoter methylation. *Pancreas,* 38**,** 649-654.

Brevet, M., Haren, N., Sevestre, H., Merviel, P. & Ouadid-Ahidouch, H. 2009b. DNA methylation of $K_V1.3$ potassium channel gene promoter is associated with woorly differentiated breast adenocarcinoma. *Cell Physiol Biochem,* 24**,** 25-32.

Brohawn, S. G., del Mármol, J. & MacKinnon, R. 2012. Crystal structure of the human K_{2P} TRAAK, a lipid- and mechano-sensitive K^+ ion channel. *Science,* 335**,** 436-441.

Brown, C. J., Lain, S., Verma, C. S., Fersht, A. R. & Lane, D. P. 2009. Awakening guardian angels: drugging the p53 pathway. *Nat Rev Cancer,* 9**,** 862-873.

Buckler, K. J. 2007. TASK-like potassium channels and oxygen sensing in the carotid body. *Respir Physiol Neurobiol,* 157**,** 55-64.

Buckler, K. J. & Vaughan-Jones, R. D. 1994. Effects of hypoxia on membrane potential and intracellular calcium in rat neonatal carotid body type I cells. *J Physiol,* 476**,** 423-428.

Buckler, K. J. & Vaughan-Jones, R. D. 1998. Effects of mitochondrial uncouplers on intracellular calcium, pH and membrane potential in rat carotid body type I cells. *J Physiol,* 513**,** 819-833.

Buckler, K. J., Williams, B. A. & Honore, E. 2000. An oxygen-, acid- and anaesthetic-sensitive TASK-like background potassium channel in rat arterial chemoreceptor cells. *J Physiol,* 525**,** 135-142.

Burdakov, D., Jensen, L. T., Alexopoulos, H., Williams, R. H., Fearon, I. M., O'Kelly, I., Gerasimenko, O., Fugger, L. & Verkhratsky, A. 2006. Tandem-pore K^+ channels mediate inhibition of orexin neurons by glucose. *Neuron,* 50**,** 711-722.

Burdall, S. E., Hanby, A. M., Lansdown, M. R. J. & Speirs, V. 2003. Breast cancer cell lines: friend or foe? *Breast Cancer Res*, 5**,**89-95

Buttigieg, J., Pan, J., Yeger, H. & Cutz, E. 2012. NOX2 (gp91phox) is a predominant O_2 sensor in a human airway chemoreceptor cell line: biochemical, molecular, and electrophysiological evidence. *Am J Physiol Lung Cell Mol Physiol,* 303**,** L598-L607.

Cahalan, M. D., Wulff, H. & Chandy, K. G. 2001. Molecular properties and physiological roles of ion channels in the immune system. *J Clin Immunol,* 21**,** 235-252.

Callahan, R., Labunskiy, D. A., Logvinova, A., Abdallah, M., Liu, C., Cotten, J. F. & Yost, C. S. 2004. Immunolocalization of TASK-3 (*KCNK9*) to a subset of cortical neurons in the rat CNS. *Biochem Biophys Res Commun,* 319**,** 525-530.

Cambien, B., Rezzonico, R., Vitale, S., Rouzaire-Dubois, B., Dubois, J., Barthel, R., Karimdjee, B., Mograbi, B., Schmid-Alliana, A. & Schmid-Antomarchi, H. 2008. Silencing of hSlo potassium channels in human osteosarcoma cells promotes tumorigenesis. *Int J Cancer,* 123**,** 365-371.

Campanucci, V. A., Brown, S. T., Hudasek, K., O'Kelly, I. M., Nurse, C. A. & Fearon, I. M. 2005. O_2 sensing by recombinant TWIK-related halothane-inhibitable K^+ channel-1 background K^+ channels heterologously expressed in human embryonic kidney cells. *Neuroscience,* 135**,** 1087-1094.

Campbell, T. M., Main, M. J. & Fitzgerald, E. M. 2013. Functional expression of the voltage-gated Na^+-channel $Na_V1.7$ is necessary for EGF-mediated invasion in human non-small cell lung cancer cells. *J Cell Sci,* 126**,** 4939-4949.

Capiod, T. 2012. The need for calcium channels in cell proliferation. *Recent Pat Anticancer Drug Discov,* 8**,** 4-17.

Carafoli, E. 2002. Calcium signaling: a tale for all seasons. *Proc Natl Acad Sci U S A,* 99**,** 1115-1122.

Catacuzzeno, L., Aiello, F., Fioretti, B., Sforna, L., Castigli, E., Ruggieri, P., Tata, A. M., Calogero, A. & Franciolini, F. 2011. Serum-activated K^+ and Cl^- currents underlay U87-MG glioblastoma cell migration. *J Cell Physiol,* 226**,** 1926-1933.

Catterall, A. W. 1995. Structure and function of voltage-gated ion channels. *Annu Rev Biochem,* 64**,** 493-531.

Cavalieri, D., Dolara, P., Mini, E., Luceri, C., Castagnini, C., Toti, S., Macaig, K., De Filippo, C., Nobili, S., Morganti, M., Napoli, C., Tonini, G., Baccini, M., Biggeri, A., Tonelli, F., Valanzano, R., Orlando, C., Gelmini, S., Cianchi, F., Messerini, L. & Luzzatto, L. 2007. Analysis of gene expression profiles reveals novel correlations with the clincal course of colorectal cancer. *Oncol Res,* 16**,** 535-548.

Chalhoub, N. & Baker, S. J. 2009. PTEN and the PI3-Kinase pathway in cancer. *Annu Rev Pathol Mech,* 4**,** 127-150.

Chantôme, A., Girault, A., Potier, M., Collin, C., Vaudin, P., Pagès, J.-C., Vandier, C. & Joulin, V. 2009. K_{Ca}2.3 channel-dependent hyperpolarization increases melanoma cell motility. *Exp Cell Res,* 315**,** 3620-3630.

Chantôme, A., Potier-Cartereau, M., Clarysse, L., Fromont, G., Marionneau-Lambot, S., Guéguinou, M., Pagès, J.-C., Collin, C., Oullier, T., Girault, A., Arbion, F., Haelters, J.-P., Jaffrès, P.-A., Pinault, M., Besson, P., Joulin, V., Bougnoux, P. & Vandier, C. 2013. Pivotal role of the lipid raft SK3–Orai1 complex in human cancer cell migration and bone metastases. *Cancer Res,* 73**,** 4852-4861.

Chapman, C. G., Meadows, H. J., Godden, R. J., Campbell, D. A., Duckworth, M., Kelsell, R. E., Murdock, P. R., Randall, A. D., Rennie, G. I. & Gloger, I. S. 2000. Cloning, localisation and functional expression of a novel human, cerebellum specific, two pore domain potassium channel. *Brain Res Mol Brain Res,* 82**,** 74-83.

Charuk, J. H. M., Pirraglia, C. A. & Reithmeier, R. A. F. 1990. Interaction of ruthenium red with Ca^{2+}-binding proteins. *Anal Biochem,* 188**,** 123-131.

Chatelain, F. C., Bichet, D., Douguet, D., Feliciangeli, S., Bendahhou, S., Reichold, M., Warth, R., Barhanin, J. & Lesage, F. 2012. TWIK-1, a unique background channel with variable ion selectivity. *Proc Natl Acad Sci U S A,* 109**,** 5499-5504.

Chavez, R. A., Gray, A. T., Zhao, B. B., Kindler, C. H., Mazurek, M. J., Mehta, Y., Forsayeth, J. R. & Yost, C. S. 1999. TWIK-2, a new weak inward rectifying member of the tandem pore domain potassium channel family. *J Biol Chem,* 274**,** 7887-7892.

Chen, Y.-F., Chen, Y.-T., Chiu, W.-T. & Shen, M.-R. 2013. Remodeling of calcium signaling in tumor progression. *J Biomed Sci,* 20**,** 23.

Chiche, J., Brahimi-Horn, M. C. & Pouysségur, J. 2010. Tumour hypoxia induces a metabolic shift causing acidosis: a common feature in cancer. *J Cell Mol Med,* 14**,** 771-794.

Chimote, A. A., Kuras, Z. & Conforti, L. 2012. Disruption of K_V1.3 channel forward vesicular trafficking by hypoxia in human T lymphocytes. *J Biol Chem,* 287**,** 2055-2067.

Choi, K.-H., Song, C., Shin, D. & Park, S. 2011a. hERG channel blockade by externally applied quaternary ammonium derivatives. *BBA - Biomembranes,* 1808**,** 1560-1566.

Choi, M., Scholl, U. I., Yue, P., Björklund, P., Zhao, B., Nelson-Williams, C., Ji, W., Cho, Y., Patel, A., Men, C. J., Lolis, E., Wisgerhof, M. V., Geller, D. S., Mane, S., Hellman, P., Westin, G., Åkerström, G., Wang, W., Carling, T. & Lifton, R. P. 2011b. K^+ channel mutations in adrenal aldosterone-producing adenomas and hereditary hypertension. *Science,* 331**,** 768-772.

Cibulsky, S. M. & Sather, W. A. 1999. Block by ruthenium red of cloned neuronal voltage-gated calcium channels. *J Pharmacol Exp Ther,* 289**,** 1447-1453.

Cidad, P., Jiménez-Pérez, L., García-Arribas, D., Miguel-Velado, E., Tajada, S., Ruiz-McDavitt, C., López-López, J. R. & Pérez-García, M. T. 2012. K_V1.3 channels can modulate cell proliferation during phenotypic switch by an ion-flux independent mechanism. *Arterioscler Thromb Vasc Biol*, 2**,** 1299-1307

Clapham, D. E. 2007. Calcium signaling. *Cell,* 131**,** 1047-1058.

Clarke, C. E., Veale, E. L., Green, P. J., Meadows, H. J. & Mathie, A. 2004. Selective block of the human 2-P domain potassium channel, TASK-3, and the native leak potassium current, IK_{SO}, by zinc. *J Physiol,* 560**,** 51-62.

Clarke, C. E., Veale, E. L., Wyse, K., Vandenberg, J. I. & Mathie, A. 2008. The M1P1 loop of TASK-3 K_{2P} channels apposes the selectivity filter and influences channel function. *J Biol Chem,* 283**,** 16985-16992.

Coburn, C. A., Luo, Y., Cui, M., Wang, J., Soll, R., Dong, J., Hu, B., Lyon, M. A., Santarelli, V. P., Kraus, R. L., Gregan, Y., Wang, Y., Fox, S. V., Binns, J., Doran, S. M., Reiss, D. R., Tannenbaum, P. L., Gotter, A. L., Meinke, P. T. & Renger, J. J. 2012. Discovery of a

pharmacologically active antagonist of the two-pore domain potassium channel K_{2P}9.1 (TASK-3). *ChemMedChem,* 7**,** 123-133.

Coiret, G., Borowiec, A.-S., Mariot, P., Ouadid-Ahidouch, H. & Matifat, F. 2007. The anti-estrogen tamoxifen activates BK Channels and stimulates proliferation of MCF-7 breast cancer cells. *Mol Pharmacol,* 71**,** 843-851.

Coiret, G., Matifat, F., Hague, F. & Ouadid-Ahidouch, H. 2005. 17-β-Estradiol activates maxi-K channels through a non-genomic pathway in human breast cancer cells. *FEBS Lett,* 579**,** 2995-3000.

Collins, K., Jacks, T. & Pavletich, N. P. 1997. The cell cycle and cancer. *Proc Natl Acad Sci U S A,* 94**,** 2776-2778.

Conway, K. E. & Cotten, J. F. 2012. Covalent modification of a volatile anaesthetic regulatory site activates TASK-3 (*KCNK9*) tandem-pore potassium channels. *Mol Pharmacol,* 81**,** 393-400.

Crociani, O., Guasti, L., Balzi, M., Becchetti, A., Wanke, E., Olivotto, M., Wymore, R. S. & Arcangeli, A. 2003. Cell cycle-dependent expression of HERG1 and HERG1B isoforms in tumor cells. *J Biol Chem,* 278**,** 2947-2955.

Crociani, O., Zanieri, F., Pillozzi, S., Lastraioli, E., Stefanini, M., Fiore, A., Fortunato, A., D'Amico, M., Masselli, M., De Lorenzo, E., Gasparoli, L., Chiu, M., Bussolati, O., Becchetti, A. & Arcangeli, A. 2013. hERG1 channels modulate integrin signalling to trigger angiogenesis and tumour progression in colorectal cancer. *Sci Rep,* 3**,** 1-13.

Cuddapah, V. A. & Sontheimer, H. 2010. Molecular interaction and functional regulation of ClC-3 by Ca^{2+}/calmodulin-dependent protein kinase II (CaMKII) in human malignant glioma. *J Biol Chem,* 285**,** 11188-11196.

Cuddapah, V. A. & Sontheimer, H. 2011. Ion channels and tranporters in cancer. 2. Ion channels and the control of cancer cell migration. *Am J Physiol Cell Physiol,* 301**,** 541-549.

Curran, M. E., Splawski, I., Timothy, K. W., Vincen, G. M., Green, E. D. & Keating, M. T. 1995. A molecular basis for cardiac arrhythmia: hERG mutations cause long QT syndrome. *Cell,* 80**,** 795-803.

Cutz, E. & Jackson, A. 1999. Neuroepithelial bodies as airway oxygen sensors. *Respir Physiol,* 115**,** 201-214.

Czirjak, G. & Enyedi, P. 2002a. Formation of functional heterodimers between the TASK-1 and TASK-3 two-pore domain potassium channel subunits. *J Biol Chem,* 277**,** 5426-5432.

Czirjak, G. & Enyedi, P. 2002b. TASK-3 dominates the background potassium conductance in rat adrenal glomerulosa cells. *Mol Endocrinol,* 16**,** 621-629.

Czirják, G. & Enyedi, P. 2003. Ruthenium red inhibits TASK-3 potassium channel by interconnecting glutamate 70 of the two subunits. *Mol Pharmacol,* 63**,** 646-652.

Czirjak, G., Fischer, T., Spät, A., Lesage, F. & Enyedi, P. 2000. TASK (TWIK-related acid-sensitive K^+ channel) is expressed in glomerulosa cells of rat adrenal cortex and inhibited by angiotensin II. *Mol Endocrinol,* 14**,** 863-874.

Czirják, G., Vuity, D. & Enyedi, P. 2008. Phosphorylation-dependent binding of 14-3-3 proteins controls TRESK regulation. *J Biol Chem,* 283**,** 15672-15680.

D'Amico M, Gasparoli L & A., A. 2013. Potassium channels: novel emerging biomarkers and targets for therapy in cancer. *Recent Pat Anticancer Drug Discov,* 8**,** 53-65.

da Cunha Santos, G., Shepherd, F. A. & Tsao, M. S. 2011. EGFR mutations and lung cancer. *Annu Rev Pathol Mech,* 6**,** 49-69.

Damaghi, M., Wojtkowiak, J. W. & Gillies, R. J. 2013. pH Sensing and regulation in cancer. *Front Physiol,* 4.

Das, A., Pushparaj, C., Bahí, N., Sorolla, A., Herreros, J., Pamplona, R., Vilella, R., Matias-Guiu, X., Martí, R. M. & Cantí, C. 2012. Functional expression of voltage-gated calcium channels in human melanoma. *Pigment Cell Melanoma Res,* 25**,** 200-212.

Davis, F., Parsonage, M., Cabot, P., Parat, M.-O., Thompson, E., Roberts-Thomson, S. & Monteith, G. 2013. Assessment of gene expression of intracellular calcium channels, pumps and exchangers with epidermal growth factor-induced epithelial-mesenchymal transition in a breast cancer cell line. *Cancer Cell Int,* 13**,** 76.

De Marchi, U., Sassi, N., Fioretti, B., Catacuzzeno, L., Cereghetti, G. M., Szabo, I. & Zoratti, M. 2009. Intermediate conductance Ca^{2+}-activated potassium channel ($K_{Ca}3.1$) in the inner mitochondrial membrane of human colon cancer cells. *Cell Calcium,* 45**,** 509-516.

DeBerardinis, R. J., Lum, J. J., Hatzivassiliou, G. & Thompson, C. B. 2008. The biology of cancer: metabolic reprogramming fuels cell growth and proliferation. *Cell Metab,* 7**,** 11-20.

Decher, N., Maier, M., Dittrich, W., Gassenhuber, J., Brüggemann, A., Busch, A. E. & Steinmeyer, K. 2001. Characterization of TASK-4, a novel member of the pH-sensitive, two-pore domain potassium channel family. *FEBS Lett,* 492**,** 84-89.

DeCoursey, T. E. 2013. Voltage-gated proton channels: molecular biology, physiology, and pathophysiology of the H_V family. *Physiol Rev,* 93**,** 599-652.

DeCoursey, T. E., Chandy, K. G., Gupta, S. & Cahalan, M. D. 1984. Voltage-gated K^+ channels in human T lymphocytes: a role in mitogenesis? *Nature,* 307**,** 465-468.

Dezaki, K., Maeno, E., Sato, K., Akita, T. & Okada, Y. 2012. Early-phase occurrence of K^+ and Cl^- efflux in addition to Ca^{2+} mobilization is a prerequisite to apoptosis in HeLa cells. *Apoptosis,* 17**,** 821-831.

Dick, F. A. & Rubin, S. M. 2013. Molecular mechanisms underlying Rb protein function. *Nat Rev Mol Cell Biol,* 14**,** 297-306.

Ding, X.-W., Luo, H.-S., Luo, B., Xu, D.-Q. & Gao, S. 2008a. Overexpression of hERG1 in resected esophageal squamous cell carcinomas: a marker for poor prognosis. *J Surg Oncol,* 97**,** 57-62.

Ding, X.-W., Wang, X.-G., Luo, H.-S., Tan, S.-Y., Gao, S., Luo, B. & Jiang, H. 2008b. Expression and prognostic roles of Eag1 in resected esophageal squamous cell carcinomas. *Dig Dis Sci,* 53**,** 2039-2044.

Ding, X.-W., Yan, J.-J., An, P., Lü, P. & Luo, H.-S. 2007. Aberrant expression of Ether à go-go potassium channel in colorectal cancer patients and cell lines. *World J Gastroenterol,* 13**,** 1257-1261.

Ding, X., He, Z., Zhou, K., Cheng, J., Yao, H., Lu, D., Cai, R., Jin, Y., Dong, B., Xu, Y. & Wang, Y. 2010. Essential role of TRPC6 channels in G_2/M phase transition and development of human glioma. *J Natl Cancer Inst,* 102**,** 1052-1068.

Dobler, T., Springauf, A., Tovornik, S., Weber, M., Schmitt, A., Sedlmeier, R., Wischmeyer, E. & Döring, F. 2007. TRESK two-pore-domain K^+ channels constitute a significant component of background potassium currents in murine dorsal root ganglion neurones. *J Physiol,* 585**,** 867-879.

Dong, H., Shim, K. N., Li, J. M., Estrema, C., Ornelas, T.A., Nguyen, F., Liu, S., Ramamoorthy, S. L., Ho, S., Carethers, J. M. & Chow, J. Y. Molecular mechanisms underlying Ca^{2+}-mediated motility of human pancreatic duct cells. *Am J Physiol Cell Physiol*, 299**,** 1493-1503.

Doupnik, C. A., Davidson, N. & Lester, H. A. 1995. The inward rectifier potassium channel family. *Curr Opin Neurobiol,* 5**,** 268-277.

Downie, B. R., Sánchez, A., Knötgen, H., Contreras-Jurado, C., Gymnopoulos, M., Weber, C., Stühmer, W. & Pardo, L. A. 2008. Eag1 expression interferes with hypoxia homeostasis and induces angiogenesis in tumors. *J Biol Chem,* 283**,** 36234-36240.

Doyle, D. A. 1998. The structure of the potassium channel: molecular basis of K^+ conduction and selectivity. *Science,* 280**,** 69-77.

Dray, A., Forbes, C. A. & Burgess, G. M. 1990. Ruthenium red blocks the capsaicin-induced increase in intracellular calcium and activation of membrane currents in sensory neurones as well as the activation of peripheral nociceptors *in vitro*. *Neurosci Lett,* 110**,** 52-59.

Du, G., Chen, X., Todorovic, M. S., Shu, S., Kapur, J. & Bayliss, D. A. 2011. TASK channel deletion reduces sensitivity to local anesthetic-induced seizures. *Anesthesiology,* 115**,** 1003-1011.

Duprat, F., Girard, C., Jarretou, G. & Lazdunski, M. 2005. Pancreatic two P domain K^+ channels TALK-1 and TALK-2 are activated by nitric oxide and reactive oxygen species. *J Physiol,* 562**,** 235-244.

Duprat, F., Lauritzen, I., Patel, A. & Honore, E. 2007. The TASK background K_{2P} channels: chemo- and nutrient sensors. *Trends Neurosci,* 30**,** 573-580.

Duprat, F., Lesage, F., Fink, M., Reyes, R., Heurteaux, C. & Lazdunski, M. 1997. TASK, a human background K^+ channel to sense external pH variations near physiological pH. *EMBO J,* 16**,** 5464-5471.

Duprat, F., Lesage, F., Patel, A. J., Fink, M., Romey, G. & Lazdunski, M. 2000. The neuroprotective agent riluzole activates the two P domain K^+ channels TREK-1 and TRAAK. *Mol Pharmacol,* 57**,** 906-912.

Egenberger, B., Polleichtner, G., Wischmeyer, E. & Döring, F. 2010. *N*-linked glycosylation determines cell surface expression of two-pore-domain K^+ channel TRESK. *Biochem Biophys Res Commun,* 391**,** 1262-1267.

El Hachmane, M.-F., Rees, K. A., Veale, E. L., Sumbayev, V. V. & Mathie, A. 2014. Enhancement of TWIK-related acid-sensitive potassium channel 3 (TASK3) two-pore domain potassium channel activity by tumor necrosis factor α. *J Biol Chem,* 289**,** 1388-1401.

Engbring, J. A. & Kleinman, H. K. 2003. The basement membrane matrix in malignancy. *J Pathol,* 200**,** 465-470.

Enyedi, P. & Czirják, G. 2010. Molecular background of leak K^+ currents: two-pore domain potassium channels. *Physiol Rev,* 90**,** 559-605.

Erdogan, A., Schaefer, C. A., Schaefer, M., Luedders, D. W., Stockhausen, F., Abdallah, Y., Schaefer, C., Most, A. K., Tillmanns, H., Piper, H. M. & Kuhlmann, C. R. W. 2005. Margatoxin inhibits VEGF-induced hyperpolarization, proliferation and nitric oxide production of human endothelial cells. *J Vasc Res,* 42**,** 368-376.

Ernest, N. J., Logsdon, N. J., McFerrin, M. B., Sontheimer, H. & Spiller, S. E. 2010. Biophysical properties of human medulloblastoma cells. *J Membr Biol,* 237**,** 59-69.

Fanger, C. M., Ghanshani, S., Logsdon, N. J., Rauer, H., Kalman, K., Zhou, J., Beckingham, K., Chandy, K. G., Cahalan, M. D. & Aiyar, J. 1999. Calmodulin mediates calcium-dependent activation of the intermediate conductance K_{Ca} channel, $IK_{Ca}1$. *J Biol Chem,* 274**,** 5746-5754.

Faouzi, M., Chopin, V., Ahidouch, A. & Ouadid-Ahidouch, H. 2010. Intermediate Ca^{2+}-sensitive K^+ channels are necessary for prolactin-induced proliferation in breast cancer cells. *J Membr Biol,* 234**,** 47-56.

Feliciangeli, S., Tardy, M. P., Sandoz, G., Chatelain, F. C., Warth, R., Barhanin, J., Bendahhou, S. & Lesage, F. 2010. Potassium channel silencing by constitutive endocytosis and intracellular sequestration. *J Biol Chem,* 285**,** 4798-4805.

Felipe, A., Vicente, R., Villalonga, N., Roura-Ferrer, M., Martinez-Marmol, R., Sole, L., Ferreres, J. C. & Condom, E. 2006. Potassium channels: new targets in cancer therapy. *Cancer Detect Prev,* 30**,** 375-385.

Feng, M., Grice, D. M., Faddy, H. M., Nguyen, N., Leitch, S., Wang, Y., Muend, S., Kenny, P. A., Sukumar, S., Roberts-Thomson, S. J., Monteith, G. R. & Rao, R. 2010. Store-independent activation of Orai1 by SPCA2 in mammary tumors. *Cell,* 143**,** 84-98.

Ferlay, J., Shin, H. R., Bray, F., Forman, D., Mathers, C. & Parkin, D. M. 2008. *GLOBOCAN 2008 v1.2, Cancer incidence and mortality worldwide: IARC CancerBase No. 10* [Online]. Lyon, France: International Agency for Research on Cancer; 2010. . Available: Available from: http://globocan.iarc.fr [Accessed 11/01/2012].

Fink, M., Duprat, F., Lesage, F., Reyes, R., Romey, G., Heurteaux, C. & Lazdunski, M. 1996. Cloning, functional expression and brain localization of a novel unconventional outward rectifier K^+ channel. *EMBO J,* 15**,** 6854-6862.

Fink, M., Lesage, F., Duprat, F., Heurteaux, C., Reyes, R., Fosset, M. & Lazdunski, M. 1998. A neuronal two P domain K^+ channel stimulated by arachidonic acid and polyunsaturated fatty acids. *EMBO J,* 17**,** 3297-3308.

Fiorio Pla, A., Avanzato, D., Munaron, L. & Ambudkar, I. S. 2011. Ion channels and transporters in cancer. 6. Vascularizing the tumor: TRP channels as molecular targets. *Am J Physiol Cell Physiol,* 302**,** C9-C15.

Fioro Pla, A. & Gkika, D. 2013. Emerging role of TRP channels in cell migration: from tumor vascularization to metastasis. *Front Physiol,* 4.

Firth, A. L., Remillard, C. V., Platoshyn, O., Fantozzi, I., Ko, E. A. & Yuan, J. X. 2011. Functional ion channels in human pulmonary artery smooth muscle cells: Voltage-dependent cation channels. *Pulm Circ,* 1**,** 48-71.

Fiske, J., Fomin, V., Brown, M., Duncan, R. & Sikes, R. 2006. Voltage-sensitive ion channels and cancer. *Cancer Metastasis Rev,* 25**,** 493-500.

Fortunato, P., Pillozzi, S., Tamburini, A., Pollazzi, L., Franchi, A., La Torre, A. & Arcangeli , A. 2010. Irresponsiveness of two retinoblastoma cases to conservative therapy correlates with upregulation of hERG1 channels and of the VEGF-A pathway. *BMC Cancer,* 10.

Franks, N. P. & Honoré, E. 2004. The TREK K_{2P} channels and their role in general anesthesia and neuroprotection. *Trends Pharmacol Sci,* 25**,** 601-608.

Fraser, S. P. Ozerlat-Gunduz, I., Brackenbury, W. J., Fitzgerald, E. M., Campbell, T. M., Coombes, R. C. & and Djamgoz, M. B. A. 2014. Regulation of voltage-gated sodium channel expression in cancer: hormones, growth factors and auto-regulation. *Philos Trans R Soc Lond B Biol Sci*, 369.

Fraser, S. P. & Pardo, L. A. 2008. Ion channels: functional expression and therapeutic potential in cancer. *EMBO Rep,* 9**,** 512-515.

Frede, J., Fraser, S. P., Oskay-Özcelik, G., Hong, Y., Ioana Braicu, E., Sehouli, J., Gabra, H. & Djamgoz, M. B. A. 2013. Ovarian cancer: ion channel and aquaporin expression as novel targets of clinical potential. *Eur J Cancer,* 49**,** 2331-2344.

Freshney, N. W., Goonesekera, S. D. & Feig, L. A. 1997. Activation of the exchange factor Ras-GRF by calcium requires an intact Dbl homology domain. *FEBS Lett*, 407**,** 111-115.

Gamper, N. G., Fillon, S. F., Huber, S. H., Feng, Y. F., Kobayashi, T. K., Cohen, P. C. & Lang, F. L. 2002. IGF-1 upregulates K^+ channels via PI3-kinase, PDK1 and SGK1. *Pflugers Arch,* 443**,** 625-634.

Garzon-Muvdi, T., Schiapparelli, P., ap Rhys, C., Guerrero-Cazares, H., Smith, C., Kim, D.-H., Kone, L., Farber, H., Lee, D. Y., An, S. S., Levchenko, A. & Quiñones-Hinojosa, A.

2012. Regulation of brain tumor dispersal by NKCC1 through a novel role in focal adhesion regulation. *PLoS Biol,* 10**,** e1001320.

Gatenby, R. A., Smallbone, K., Maini, P. K., Rose, F., Averill, J., Nagle, R. B., Worrall, L. & Gillies, R. J. 2007. Cellular adaptations to hypoxia and acidosis during somatic evolution of breast cancer. *Br J Cancer,* 97**,** 646-653.

Gebäck, T., Schulz, M. M. P., Koumoutsakos, P. & Detmar, M. 2009. TScratch: a novel and simple software tool for automated analysis of monolayer wound healing assays. *Biotechniques,* 46**,** 265-274.

Gerbino, A., Ranieri, M., Lupo, S., Caroppo, R., Debellis, L., Maiellaro, I., Caratozzolo, M. F., Lopez, F. & Colella, M. 2009. Ca^{2+}-dependent K^+ efflux regulates deoxycholate-induced apoptosis of BHK-21 and Caco-2 cells. *Gastroenterology,* 137**,** 955-964, 964 e951-952.

Ghiani, C. A., Yuan, X., Eisen, A. M., Knutson, P. L., DePinho, R. A., McBain, C. J. & Gallo, V. 1999. Voltage-activated K^+ channels and membrane depolarization regulate accumulation of the cyclin-dependent kinase inhibitors p27Kip1 and p21CIP1 in glial progenitor cells. *J Neurosci,* 19**,** 5380-5392.

Giard, D. J., Aaronson, S. A., Todaro, G. J., Arnstein, P., Kersey, J. H., Dosik, H. & Parks, W. P. 1973. *In vitro* cultivation of human tumors: establishment of cell lines derived from a series of solid tumors. *J Natl Cancer Inst,* 51**,** 1417-1423.

Gierten, J., Ficker, E., Bloehs, R., Schlomer, K., Kathofer, S., Scholz, E., Zitron, E., Kiesecker, C., Bauer, A., Becker, R., Katus, H. A., Karle, C. A. & Thomas, D. 2008. Regulation of two-pore domain (K_{2P}) potassium leak channels by the tyrosine kinase inhibitor genistein. *Br J Pharmacol,* 154**,** 1680-1690.

Gillet, L., Roger, S., Besson, P., Lecaille, F., Gore, J., Bougnoux, P., Lalmanach, G. & Le Gunnec, J.-Y. 2009. Voltage-gated sodium channel activity promotes cysteine cathepsin-dependent invasiveness and colony growth of human cancer cells. *J Biol Chem*, 284**,** 8680-8691.

Gillies, R. J., Robey, I. & Gatenby, R. A. 2008. Causes and consequences of increased glucose metabolism of cancers. *J Nucl Med,* 49**,** 24S-42S.

Girard, C., Duprat, F., Terrenoire, C., Tinel, N., Fosset, M., Romey, G., Lazdunski, M. & Lesage, F. 2001. Genomic and functional characteristics of novel human pancreatic $_{2P}$ domain K^+ channels. *Biochem Biophys Res Commun,* 282**,** 249-256.

Glassmeier, G., Hempel, K., Wulfsen, I., Bauer, C. K., Schumacher, U. & Schwarz, J. R. 2012. Inhibition of hERG1 K^+ channel protein expression decreases cell proliferation of human small cell lung cancer cells. *Pflugers Arch,* 463**,** 365-376.

Gluzman, Y. 1981. SV40-transformed simian cells support the replication of early SV40 mutants. *Cell,* 23**,** 175-182.

Goldstein, S. A., Bayliss, D. A., Kim, D., Lesage, F., Plant, L. D. & Rajan, S. 2005. International Union of Pharmacology. LV. Nomenclature and molecular relationships of two-P potassium channels. *Pharmacol Rev,* 57**,** 527-540.

Goldstein, S. A. N., Bockenhauer, D., O'Kelly, I. & Zilberberg, N. 2001. Potassium leak channels and the KCNK family of two-pore domain subunits. *Nat Rev Neurosci,* 2**,** 175-184.

Goldstein, S. A. N., Price, L. A., Rosenthal, D. N. & Pausch, M. H. 1996. ORK1, a potassium-selective leak channel with two pore domains cloned from Drosophila melanogaster by expression in Saccharomyces cerevisiae. *Proc Natl Acad Sci U S A,* 93**,** 13256-13261.

Gong, J., Liu, X., Shang, B., Chen, S. & Zhen, Y. 2010. hERG K^+ channel related chemosensitivity to sparfloxacin in colon cancer cells. *Oncol Rep,* 23**,** 1747-1756.

González, J. A., Jensen, L. T., Doyle, S. E., Miranda-Anaya, M., Menaker, M., Fugger, L., Bayliss, D. A. & Burdakov, D. 2009. Deletion of TASK-1 and TASK-3 channels disrupts intrinsic excitability but does not abolish glucose or pH responses of orexin/hypocretin neurons. *Eur J Neurosci,* 30**,** 57-64.

Graeber, T. G., Osmanian, C., Jacks, T., Housman, D. E., Koch, C. J., Lowe, S. W. & Giaccia, A. J. 1996. Hypoxia-mediated selection of cells with diminished apoptotic potential in solid tumours. *Nature,* 379**,** 88-91.

Graeber, T. G., Osmanian, C., Jacks, T., Housman, D. E., Koch, C. J., Lowe, S. W. & Giaccia, A. J. 1996. Hypoxia-mediated selection of cells with diminished apoptotic potential in solid tumours. *Nature*, 379**,** 88-91.

Graham, F. L., Smiley, J., Russell, W. C. & Nairn, R. 1977. Characteristics of a human cell line transformed by DNA from human adenovirus type 5. *J Gen Virol,* 36**,** 59-72.

Grgic, I., Eichler, I., Heinau, P., Si, H., Brakemeier, S., Hoyer, J. & Köhler, R. 2005. Selective blockade of the intermediate-conductance Ca^{2+}-activated K^+ channel suppresses proliferation of microvascular and macrovascular endothelial cells and angiogenesis *in vivo*. *Arterioscler Thromb Vasc Biol,* 25**,** 704-709.

Grivennikov, S. I., Greten, F. R. & Karin, M. 2010. Immunity, inflammation, and cancer. *Cell,* 140**,** 883-899.

Gulbins, E., Sassi, N., Grassmè, H., Zoratti, M. & Szabò, I. 2010. Role of $K_V1.3$ mitochondrial potassium channel in apoptotic signalling in lymphocytes. *BBA - Bioenergetics,* 1797**,** 1251-1259.

Gurney, A. M, Osipenko, O. N., MacMillan, D., McFarlane, K. M., Tate, R. J. & Kempsill, F. E. 2003. Two-pore domain K^+ channel, TASK-1, in pulmonary artery smooth muscle cells. *Circ Res,* 93**,** 957-964.

Gutman, G. A., Aldrich, R., Chandy, K. G., Grissmer, S., Wei, A. D. & Wulff, H. 2013a. *Calcium-activated potassium channels* [Online]. IUPHAR database (IUPHAR-DB). Available: http://www.iuphar-db.org/DATABASE/FamilyMenuForward?familyId=69 [Accessed 20/09/2013].

Gutman, G. A., Chandy, K. G., Adelman, J. P., Aiyar, J., Bayliss, D. A., Clapham, D. E., Covarriubias, M., Desir, G. V., Furuichi, K., Ganetzky, B., Garcia, M. L., Grissmer, S., Jan, L. Y., Karschin, A., Kim, D., Kuperschmidt, S., Kurachi, Y., Lazdunski, M., Lesage, F., Lester, H. A., McKinnon, D., Nichols, C. G., O'Kelly, I., Robbins, J., Robertson, G. A., Rudy, B., Sanguinetti, M., Seino, S., Stuehmer, W., Tamkun, M. M., Vandenberg, C. A., Wei, A., Wulff, H. & Wymore, R. S. 2003. International Union of Pharmacology. XLI. Compendium of voltage-gated ion channels: potassium channels. *Pharmacol Rev,* 55**,** 583-586.

Gutman, G. A., Chandy, K. G., Grissmer, S., Lazdunski, M., Mckinnon, D., Pardo, L. A., Robertson, G. A., Rudy, B., Sanguinetti, M. C., Stühmer, W. & Wang, X. 2013b. *Voltage-gated potassium channels* [Online]. IUPHAR database (IUPHAR-DB). Available: http://www.iuphar-db.org/DATABASE/FamilyMenuForward?familyId=81 [Accessed 20/09/2013].

Hagen, B. M. & Sanders, K. M. 2006. Deglycosylation of the β1-subunit of the BK channel changes its biophysical properties. *Am J Physiol Cell Physiol,* 291**,** C750-C756.

Hahn, W. C., Counter, C. M., Lundberg, A. S., Beijersbergen, R. L., Brooks, M. W. & Weinberg, R. A. 1999. Creation of human tumour cells with defined genetic elements. *Nature,* 400**,** 464-468.

Hale, M., Hayden, J. & Grabsch, H. 2013. Tumour-microenvironment interactions: role of tumour stroma and proteins produced by cancer-associated fibroblasts in chemotherapy response. *Cell Oncol (Dordr),* 36**,** 95-112.

Hammadi, M., Chopin, V., Matifat, F., Dhennin-Duthille, I., Chasseraud, M., Sevestre, H. & Ouadid-Ahidouch, H. 2012. Human Ether à go-go K^+ channel 1 (hEag1) regulates MDA-MB-231 breast cancer cell migration through Orai1-dependent calcium entry. *J Cell Physiol,* 227**,** 3837-3846.

Hamadi, A., Giannone, G., Takeda, K. & Rondé, P. 2014. Glutamate involvement in calcium–dependent migration of astrocytoma cells. *Cancer Cell Int*, 14.

Han, J., Kang, D. & Kim, D. 2003. Functional properties of four splice variants of a human pancreatic tandem-pore K^+ channel, TALK-1. *Am J Physiol Cell Physiol,* 285**,** C529-C538.

Han, X., Wang, F., Yao, W., Xing, H., Weng, D., Song, X., Chen, G., Xi, L., Zhu, T., Zhou, J., Xu, G., Wang, S., Meng, L., Iadecola, C., Wang, G. & Ma, D. 2007. Heat shock proteins and p53 play a critical role in K^+ channel-mediated tumor cell proliferation and apoptosis. *Apoptosis,* 12**,** 1837-1846.

Han, X., Xi, L., Wang, H., Huang, X., Ma, X., Han, Z., Wu, P., Ma, X., Lu, Y., Wang, G., Zhou, J. & Ma, D. 2008. The potassium ion channel opener NS1619 inhibits proliferation and induces apoptosis in A2780 ovarian cancer cells. *Biochem Biophys Res Commun,* 375**,** 205-209.

Hanahan, D. & Weinberg, R. A. 2000. The hallmarks of cancer. *Cell,* 100**,** 57-70.

Hanahan, D. & Weinberg, R. A. 2011. Hallmarks of cancer: the next generation. *Cell,* 144**,** 646-674.

Hande, K. R. 1998. Etoposide: four decades of development of a topoisomerase II inhibitor. *Eur J Cancer,* 34**,** 1514-1521.

Harris, C. C. 1996. COMMENTARY: p53 Tumor suppressor gene: from the basic research laboratory to the clinic—an abridged historical perspective. *Carcinogenesis,* 17**,** 1187-1198.

Hartness, M. E., Lewis, A., Searle, G. J., O'Kelly, I., Peers, C. & Kemp, P. J. 2001. Combined antisense and pharmacological approaches implicate hTASK as an airway O_2 sensing K^+ channel. *J Biol Chem,* 276**,** 26499-26508.

Harvey, A. L. 2001. Twenty years of dendrotoxins. *Toxicon,* 39**,** 15-26.

Haupt, S., Berger, M., Goldberg, Z. & Haupt, Y. 2003. Apoptosis - the p53 network. *J Cell Sci,* 116**,** 4077-4085.

Hayabuchi, Y., Willars, G. B., Standen, N. B. & Davies, N. W. 2008. Insulin-like growth factor-I inhibits rat arterial K_{ATP} channels through PI3-kinase. *Biochem Biophys Res Commun,* 374**,** 742-746.

Hayflick, L. 2000. The illusion of cell immortality. *Br J Cancer,* 83**,** 841-846.

Hayter, P. M., Curling, E. M. A., Baines, A. J., Jenkins, N., Salmon, I., Strange, P. G., Tong, J. M. & Bull, A. T. 1992. Glucose-limited chemostat culture of chinese hamster ovary cells producing recombinant human interferon-γ. *Biotechnol Bioeng,* 39**,** 327-335.

Heurteaux, C., Guy, N., Laigle, C., Blondeau, N., Duprat, F., Mazzuca, M., Lang-Lazdunski, L., Widmann, C., Zanzouri, M., Romey, G. & Lazdunski, M. 2004. TREK-1, a K^+ channel involved in neuroprotection and general anesthesia. *EMBO J,* 23**,** 2684-2695.

Hibino, H., Inanobe, A., Furutani, K., Murakami, S., Findlay, I. & Kurachi, Y. 2010. Inwardly rectifying potassium channels: their structure, function, and physiological roles. *Physiol Rev,* 90**,** 291-366.

Hodgkin, A. L. & Huxley, A. F. 1945. Resting and action potentials in single nerve fibres. *J Physiol,* 104**,** 176-195.

Hodgkin, A. L. & Huxley, A. F. 1947. Potassium leakage from an active nerve fibre. *J Physiol,* 106**,** 341-367.

Hodgkin, A. L. & Katz, B. 1949. The effect of sodium ions on the electrical activity of the giant axon of the squid. *J Physiol,* 108**,** 37-77.

Hoeben, A., Landuyt, B., Highley, M. S., Wildiers, H., Van Oosterom, A. T. & De Bruijn, E. A. 2004. Vascular endothelial growth factor and angiogenesis. *Pharmacol Rev,* 56**,** 549-580.

Honore, E. 2007. The neuronal background K_{2P} channels: focus on TREK-1. *Nat Rev Neurosci,* 8**,** 251-261.

Hsu, K., Seharaseyon, J., Dong, P., Bour, S. & Marbán, E. 2004. Mutual functional destruction of HIV-1 Vpu and host TASK-1 channel. *Mol Cell,* 14**,** 259-267.

Hu, M. & Polyak, K. 2008. Microenvironmental regulation of cancer development. *Curr Opin Genet Dev,* 18**,** 27-34.

Huang, D. Y., Yu, B. W. & Fan, Q. W. 2008. Roles of TRESK, a novel two-pore domain K^+ channel, in pain pathway and general anesthesia. *Neurosci Bull,* 24**,** 166-172.

Huang, L., Li, B., Li, W., Guo, H. & Zou, F. 2009. ATP-sensitive potassium channels control glioma cells proliferation by regulating ERK activity. *Carcinogenesis,* 30**,** 737-744.

Huang, X., Dubuc, A. M., Hashizume, R., Berg, J., He, Y., Wang, J., Chiang, C., Cooper, M. K., Northcott, P. A., Taylor, M. D., Barnes, M. J., Tihan, T., Chen, J., Hackett, C. S., Weiss, W. A., James, C. D., Rowitch, D. H., Shuman, M. A., Jan, Y. N. & Jan, L. Y. 2012. Voltage-gated potassium channel EAG2 controls mitotic entry and tumor growth in medulloblastoma via regulating cell volume dynamics. *Genes Dev,* 26**,** 1780-1796.

Innamaa, A., Jackson, L., Asher, V., Schalkwyk, G., Warren, A., Keightley, A., Hay, D., Bali, A., Sowter, H. & Khan, R. 2013a. Expression and effects of modulation of the K_{2P} potassium channels TREK-1 (*KCNK2*) and TREK-2 (*KCNK10*) in the normal human ovary and epithelial ovarian cancer. *Clini Transl Oncol***,** 1-9.

Innamaa, A., Jackson, L., Asher, V., Van Shalkwyk, G., Warren, A., Hay, D., Bali, A., Sowter, H. & Khan, R. 2013b. Expression and prognostic significance of the oncogenic K_{2P} potassium channel *KCNK9* (TASK-3) in ovarian carcinoma. *Anticancer Res,* 33**,** 1401-1408.

Izumi, H., Torigoe, T., Ishiguchi, H., Uramoto, H., Yoshida, Y., Tanabe, M., Ise, T., Murakami, T., Yoshida, T., Nomoto, M. & Kohno, K. 2003. Cellular pH regulators: potentially promising molecular targets for cancer chemotherapy. *Cancer Treat Rev,* 29**,** 541-549.

Jang, S., Kang, K., Ryu, P. & Lee, S. 2009a. $K_V1.3$ voltage-gated K^+ channel subunit as a potential diagnostic marker and therapeutic target for breast cancer. *BMB Rep,* 42**,** 535-539.

Jang, S. H., Choi, C., Hong, S.-G., Yarishkin, O. V., Bae, Y. M., Kim, J. G., O'Grady, S. M., Yoon, K.-A., Kang, K.-S., Ryu, P. D. & Lee, S. Y. 2009b. Silencing of $K_V4.1$ potassium channels inhibits cell proliferation of tumorigenic human mammary epithelial cells. *Biochem Biophys Res Commun,* 384**,** 180-186.

Jang, S. H., Choi, S. Y., Ryu, P. D. & Lee, S. Y. 2011. Anti-proliferative effect of $K_V1.3$ blockers in A549 human lung adenocarcinoma *in vitro* and *in vivo*. *Eur J Pharmacol,* 651**,** 26-32.

Jehle, J., Schweizer, P. A., Katus, H. A. & Thomas, D. 2011. Novel roles for hERG K^+ channels in cell proliferation and apoptosis. *Cell Death Dis,* 2**,** e193.

Jemal, A., Bray, F., Center, M. M., Ferlay, J., Ward, E. & Forman, D. 2011. Global cancer statistics. *CA Cancer J Clin,* 61**,** 69-90.

Jensen, M. Ø., Jogini, V., Borhani, D. W., Leffler, A. E., Dror, R. O. & Shaw, D. E. 2012. Mechanism of voltage gating in potassium channels. *Science,* 336**,** 229-233.

Jiang, B., Sun, X., Cao, K. & Wang, R. 2002. Endogenous K_V channels in human embryonic kidney (HEK293) cells. *Mol Cell Biochem,* 238**,** 69-79.

Johnson, R. P., O'Kelly, I. M. & Fearon, I. M. 2004. System-specific O_2 sensitivity of the tandem pore domain K^+ channel TASK-1. *Am J Physiol Cell Physiol,* 286**,** C391-397.

Jones, R. G. & Thompson, C. B. 2009. Tumor suppressors and cell metabolism: a recipe for cancer growth. *Genes Dev,* 23**,** 537-548.

Jovanović, S., Crawford, R. M., Ranki, H. J. & Jovanović, A. 2003. Large conductance Ca^{2+}-activated K^+ channels sense acute changes in oxygen tension in alveolar epithelial cells. *Am J Respir Cell Mol Biol,* 28**,** 363-372.

Kalluri, R. & Weinberg, R. A. 2009. The basics of epithelial-mesenchymal transition. *J Clin Invest,* 119**,** 1420-1428.

Kang, D., Han, J., Talley, E. M., Bayliss, D. A. & Kim, D. 2004a. Functional expression of TASK-1/TASK-3 heteromers in cerebellar granule cells. *J Physiol,* 554**,** 64-77.

Kang, D., Mariash, E. & Kim, D. 2004b. Functional expression of TRESK-2, a new member of the tandem-pore K^+ channel family. *J Biol Chem,* 279**,** 28063-28070.

Karschin, C., Wischmeyer, E., Preisig-Müller, R., Rajan, S., Derst, C., Grzeschik, K.-H., Daut, J. & Karschin, A. 2001. Expression pattern in brain of TASK-1, TASK-3, and a tandem pore domain K^+ channel subunit, TASK-5, associated with the central auditory nervous system. *Mol Cell Neurosci,* 18**,** 632-648.

Kemp, P. J., Lewis, A., Hartness, M. E., Searle, G. J., Miller, P., O'Kelly, I. & Peers, C. 2002. Airway chemotransduction: from oxygen sensor to cellular effector. *Am J Respir Crit,* 166**,** S17-S24.

Ketchum, K. A., Joiner, W. J., Sellers, A. J., Kaczmarek, L. K. & Goldstein, S. A. N. 1995. A new family of outwardly rectifying potassium channel proteins with two pore domains in tandem. *Nature,* 376**,** 690-695.

Khaitan, D., Sankpal, U., Weksler, B., Meister, E., Romero, I., Couraud, P.-O. & Ningaraj, N. 2009. Role of *KCNMA1* gene in breast cancer invasion and metastasis to brain. *BMC Cancer,* 9.

Kim, C. J., Cho, Y. G., Jeong, S. W., Kim, Y. S., Kim, S. Y., Nam, S. W., Lee, S. H., Yoo, N. J., Lee, J. Y. & Park, W. S. 2004. Altered expression of *KCNK9* in colorectal cancers. *APMIS,* 112**,** 588-594.

Kim, D., Cavanaugh, E. J., Kim, I. & Carroll, J. L. 2009. Heteromeric TASK-1/TASK-3 is the major oxygen-sensitive background K^+ channel in rat carotid body glomus cells. *J Physiol,* 587**,** 2963-2975.

Kim, D. & Gnatenco, C. 2001. TASK-5, a new member of the tandem-pore K^+ channel family. *Biochem Biophys Res Commun,* 284**,** 923-930.

Kim, H.-J., Jang, S. H., Jeong, Y. A., Ryu, P. D., Kim, D.-Y. & Lee, S. Y. 2010. Involvement of $K_V4.1$ K^+ Channels in Gastric Cancer Cell Proliferation. *Biol Pharm Bull,* 33**,** 1754-1757.

Kim, Y., Bang, H. & Kim, D. 2000. TASK-3, a new member of the tandem pore K^+ channel family. *J Biol Chem,* 275**,** 9340-9347.

King, R. J. B. & Robins, M. W. 2006. *Cancer biology*, Pearson Education Limited.

Kirkegaard, S. S., Lambert, I. H., Gammeltoft, S. & Hoffmann, E. K. 2010. Activation of the TASK-2 channel after cell swelling is dependent on tyrosine phosphorylation. *Am J Physiol Cell Physiol,* 299**,** C844-C853.

Knowles, M. A. & Selby, P. J. 2005. *Introduction to the cellular and molecular biology of cancer*, Oxford University Press.

Köhler, R., Degenhardt, C., Kühn, M., Runkel, N., Paul, M. & Hoyer, J. 2000. Expression and function of endothelial Ca^{2+}-activated K^+ channels in human mesenteric artery: a single-cell reverse transcriptase–polymerase chain reaction and electrophysiological study *in situ*. *Circ Res,* 87**,** 496-503.

Koster, J. C., Permutt, M. A. & Nichols, C. G. 2005. Diabetes and insulin Secretion: the ATP-sensitive K^+ channel (K_{ATP}) connection. *Diabetes,* 54**,** 3065-3072.

Kosztka, L., Rusznak, Z., Nagy, D., Nagy, Z., Fodor, J., Szucs, G., Telek, A., Gonczi, M., Ruzsnavszky, O., Szentandrassy, N. & Csernoch, L. 2011. Inhibition of TASK-3 (*KCNK9*) channel biosynthesis changes cell morphology and decreases both DNA content and mitochondrial function of melanoma cells maintained in cell culture. *Melanoma Res,* 21**,** 308-322.

Kovacs, I., Pocsai, K., Czifra, G., Sarkadi, L., Szucs, G., Nemes, Z. & Rusznak, Z. 2005. TASK-3 immunoreactivity shows differential distribution in the human gastrointestinal tract. *Virchows Arch,* 446**,** 402-410.

Kréneisz, O., Benoit, J. P., Bayliss, D. A. & Mulkey, D. K. 2009. AMP-activated protein kinase inhibits TREK channels. *J Physiol,* 587**,** 5819-5830.

Kunzelmann, K. 2005. Ion channels and cancer. *J Membr Biol,* 205**,** 159-173.

L'Hoste, S., Barriere, H., Belfodil, R., Rubera, I., Duranton, C., Tauc, M., Poujeol, C., Barhanin, J. & Poujeol, P. 2007a. Extracellular pH alkalinization by Cl^-/HCO_3^- exchanger is crucial for TASK-2 activation by hypotonic shock in proximal cell lines from mouse kidney. *Am J Physiol Renal Physiol,* 292**,** F628-F638.

L'Hoste, S., Poet, M., Duranton, C., Belfodil, R., Barriere, H. é., Rubera, I., Tauc, M., Poujeol, C., Barhanin, J. & Poujeol, P. 2007b. Role of TASK-2 in the control of apoptotic volume decrease in proximal kidney cells. *J Biol Chem,* 282**,** 36692-36703.

Lafreniere, R. G., Cader, M. Z., Poulin, J.-F., Andres-Enguix, I., Simoneau, M., Gupta, N., Boisvert, K., Lafreniere, F., McLaughlan, S., Dube, M.-P., Marcinkiewicz, M. M., Ramagopalan, S., Ansorge, O., Brais, B., Sequeiros, J., Pereira-Monteiro, J. M., Griffiths, L. R., Tucker, S. J., Ebers, G. & Rouleau, G. A. 2010. A dominant-negative mutation in the TRESK potassium channel is linked to familial migraine with aura. *Nat Med,* 16**,** 1157-1160.

Lai, W., Chen, S., Wu, H., Guan, Y., Liu, L., Zeng, Y., Zhao, H., Jiang, J. & Chu, Z. 2011. PRL-3 promotes the proliferation of LoVo cells via the upregulation of *KCNN4* channels. *Oncol Rep,* 26**,** 909-917.

Lallet-Daher, H., Roudbaraki, M., Bavencoffe, A., Mariot, P., Gackiere, F., Bidaux, G., Urbain, R., Gosset, P., Delcourt, P., Fleurisse, L., Slomianny, C., Dewailly, E., Mauroy, B., Bonnal, J. L., Skryma, R. & Prevarskaya, N. 2009. Intermediate-conductance Ca^{2+}-activated K^+ channels ($IK_{Ca}1$) regulate human prostate cancer cell proliferation through a close control of calcium entry. *Oncogene,* 28**,** 1792-1806.

Land, H., Parada, L. F. & Weinberg, R. A. 1983. Tumorigenic conversion of primary embryo fibroblasts requires at least two cooperating oncogenes. *Nature,* 304**,** 596-602.

Lane, D. P. 1992. p53, guardian of the genome. *Nature,* 358**,** 15-16.

Lang, F., Busch, G. L., Ritter, M., Völkl, H., Waldegger, S., Gulbins, E. & Häussinger, D. 1998. Functional significance of cell volume regulatory mechanisms. *Physiol Rev,* 78**,** 247-306.

Lang, F., Föller, M., Lang, K., Lang, P., Ritter, M., Vereninov, A., Szabo, I., M. Huber, S. & Gulbins, E. 2007. Cell volume regulatory ion channels in cell proliferation and cell death. 428**,** 209-225.

Lang, F., Föller, M., Lang, K. S., Lang, P. A., Ritter, M., Gulbins, E., Vereninov, A. & Huber, S. M. 2005. Ion channels in cell proliferation and apoptotic cell death. *J Membr Biol,* 205**,** 147-157.

Lang, P. A., Kaiser, S., Myssina, S., Wieder, T., Lang, F. & Huber, S. M. 2003. Role of Ca^{2+}-activated K^+ channels in human erythrocyte apoptosis. *Am J Physiol Cell Physiol,* 285**,** C1553-C1560.

Laniado, M. E., Fraser, S. P. & Djamgoz, M. B. A. 2001. Voltage-gated K^+ channel activity in human prostate cancer cell lines of markedly different metastatic potential: Distinguishing characteristics of PC-3 and LNCaP cells. *Prostate,* 46**,** 262-274.

Larkin, N. D. & Jackson, S. P. 1999. Regulation of p53 in response to DNA damage. *Oncogene,* 18**,** 7644-7655.

Lastraioli, E. 2004. *herg1* Gene and hERG1 Protein Are Overexpressed in Colorectal Cancers and Regulate Cell Invasion of Tumor Cells. *Cancer Res,* 64**,** 606-611.

Lauritzen, I., Chemin, J., Honore, E., Jodar, M., Guy, N., Lazdunski, M. & Patel, A. J. 2005. Cross-talk between the mechano-gated K_{2P} channel TREK-1 and the actin cytoskeleton. *EMBO Rep,* 6**,** 642-648.

Lauritzen, I., Zanzouri, M., Honore, E., Duprat, F., Ehrengruber, M. U., Lazdunski, M. & Patel, A. J. 2003. K^+-dependent cerebellar granule neuron apoptosis. Role of TASK leak K^+ channels. *J Biol Chem,* 278**,** 32068-32076.

Lazarenko, R. M., Fortuna, M. G., Shi, Y., Mulkey, D. K., Takakura, A. C., Moreira, T. S., Guyenet, P. G. & Bayliss, D. A. 2010. Anesthetic activation of central respiratory chemoreceptor neurons involves inhibition of a THIK-1-like background K^+ current. *J Neurosci,* 30**,** 9324-9334.

Le, A., Lane, A. N., Hamaker, M., Bose, S., Gouw, A., Barbi, J., Tsukamoto, T., Rojas, C. J., Slusher, B.S., Zhang, H., Zimmerman, L. J., Liebler, D. C., Slebos, R. J. C., Lorkiewicz, P. K., Higashi, R. M., Fan, T. W. M. & Dang, C. V. 2012. Glucose-independent glutamine metabolism via TCA cycling for proliferation and survival in B Cells. *Cell Metab,* 15**,** 110-121.

Leanza, L., Biasutto, L., Manago, A., Gulbins, E., Zoratti, M. & Szabò, I. 2013. Intracellular ion channels and cancer. *Front Physiol,* 4.

Leanza, L., Henry, B., Sassi, N., Zoratti, M., Chandy, K. G., Gulbins, E. & Szabo, I. 2012. Inhibitors of mitochondrial $K_V1.3$ channels induce Bax/Bak-independent death of cancer cells. *EMBO Mol Med,* 4**,** 577-593.

Lee, G. W., Park, H. S., Kim, E. J., Cho, Y. W., Kim, G. T., Mun, Y. J., Choi, E. J., Lee, J. S., Han, J. & Kang, D. 2012. Reduction of breast cancer cell migration via upregulation of TASK-3 two-pore domain K^+ channel. *Acta Physiologica,* 204**,** 513-524.

Lee, I., Park, C. & Kang, W. K. 2010. Knockdown of inwardly rectifying potassium channel $K_{ir}2.2$ suppresses tumorigenesis by inducing reactive oxygen species–mediated cellular senescence. *Mol Cancer Ther,* 9**,** 2951-2959.

Lee, Y.-M., Kim, B.-J., Chun, Y.-S., So, I., Choi, H., Kim, M.-S. & Park, J.-W. 2006. NOX4 as an oxygen sensor to regulate TASK-1 activity. *Cell Signal,* 18**,** 499-507.

Lehen'kyi, V., Flourakis, M., Skryma, R. & Prevarskaya, N. 2007. TRPV6 channel controls prostate cancer cell proliferation via Ca^{2+}/NFAT-dependent pathways. *Oncogene,* 26**,** 7380-7385.

Lehen'kyi, V., Raphaël, M. & Prevarskaya, N. 2012. The role of the TRPV6 channel in cancer. *J Physiol,* 590**,** 1369-1376.

Lehen'kyi, V., Shapovalov, G., Skryma, R. & Prevarskaya, N. 2011. Ion channnels and transporters in cancer. 5. Ion channels in control of cancer and cell apoptosis. *Am J Physiol Cell Physiol,* 301**,** C1281-C1289.

Leibovitz, A., Stinson, J. C., McCombs, W. B., McCoy, C. E., Mazur, K. C. & Mabry, N. D. 1976. Classification of human colorectal adenocarcinoma cell lines. *Cancer Res,* 36**,** 4562-4569.

Lesage, F. 2003. Pharmacology of neuronal background potassium channels. *Neuropharmacology,* 44**,** 1-7.

Lesage, F., Guillemare, E., Fink, M., Duprat, F., Lazdunski, M., Romey, G. & Barhanin, J. 1996. TWIK-1, a ubiquitous human weakly inward rectifying K^+ channel with a novel structure. *EMBO J,* 15**,** 1004-1011.

Lesage, F. & Lazdunski, M. 2000. Molecular and functional properties of two-pore-domain potassium channels. *Am J Physiol Renal Physiol,* 279**,** F793-F801.

Lesage, F., Terrenoire, C., Romey, G. & Lazdunski, M. 2000. Human TREK-2, a $_{2P}$ domain mechano-sensitive K^+ Channel with multiple regulations by polyunsaturated fatty acids, lysophospholipids, and Gs, Gi, and Gq protein-coupled receptors. *J Biol Chem,* 275**,** 28398-28405.

Levite, M., Cahalon, L., Peretz, A., Hershkoviz, R., Sobko, A., Ariel, A., Desai, R., Attali, B. & Lider, O. 2000. Extracellular K^+ and opening of voltage-gated potassium channels activate T cell integrin function: physical and functional association between $K_V1.3$ channels and β_1 integrins. *J Exp Med,* 191**,** 1167-1176.

Lewis, A., Hartness, M. E., Chapman, C. G., Fearon, I. M., Meadows, H. J., Peers, C. & Kemp, P. J. 2001. Recombinant hTASK1 is an O_2-sensitive K^+ channel. *Biochem Biophys Res Commun,* 285**,** 1290-1294.

Li, M. & Xiong, Z. G. 2011. Ion channels as targets for cancer therapy. *Int J Physiol Pathophysiol Pharmacol,* 3**,** 156-166.

Li, Z. & Li, Z. 2012. Glucose regulated protein 78: a critical link between tumor microenvironment and cancer hallmarks. *BBA - Rev Cancer,* 1826**,** 13-22.

Liang, C. C., Park, A. Y. & Guan, J. L. 2007. *In vitro* scratch assay: a convenient and inexpensive method for analysis of cell migration *in vitro*. *Nat Protoc*, 2**,** 329-333.

Lin, W., Burks, C. A., Hansen, D. R., Kinnamon, S. C. & Gilbertson, T. A. 2004. Taste receptor cells express pH-sensitive leak K^+ channels. *J Neurophysiol*, 92**,** 2909-2919.

Linden, A.-M., Aller, M. I., Leppä, E., Rosenberg, P. H., Wisden, W. & Korpi, E. R. 2008. K^+ channel TASK-1 knockout mice show enhanced sensitivities to ataxic and hypnotic effects of $GABA_A$ receptor ligands. *J Pharmacol Exp Ther,* 327**,** 277-286.

Linsdell, P., Blay, J., Cowley, E., Vantol, B. & Roy, J. 2008. Pharmacological separation of hEAG and hERG K^+ channel function in the human mammary carcinoma cell line MCF-7. *Oncol Rep,* 19**,** 1511-1516.

Liu, C., Au, J. D., Zou, H. L., Cotten, J. F. & Yost, C. S. 2004. Potent activation of the human tandem pore domain K^+ channel TRESK with clinical concentrations of volatile anesthetics. *Anesth Analg,* 99**,** 1715-1722.

Liu, C., Cotten, J. F., Schuyler, J. A., Fahlman, C. S., Au, J. D., Bickler, P. E. & Yost, C. S. 2005. Protective effects of TASK-3 (*KCNK9*) and related $_{2P}$ K^+ channels during cellular stress. *Brain Res,* 1031**,** 164-173.

Long, S. B., Campbell, E. B. & MacKinnon, R. 2005. Crystal Structure of a mammalian voltage-dependent Shaker family K^+ channel. *Science,* 309**,** 897-903.

Lopatin, A. N., Makhina, E. N. & Nichols, C. G. 1994. Potassium channel block by cytoplasmic polyamines as the mechanism of intrinsic rectification. *Nature,* 372**,** 366-369.

Lopes, C. M. B., Gallagher, P. G., Buck, M. E., Butler, M. H. & Goldstein, S. A. N. 2000. Proton block and voltage Gating are potassium-dependent in the cardiac leak channel *KCNK3*. *J Biol Chem,* 275**,** 16969-16978.

López-Barneo, J., Ortega-Sáenz, P., Pardal, R., Pascual, A. & Piruat, J. I. 2008. Carotid body oxygen sensing. *Eur Respir J,* 32**,** 1386-1398.

Lowry, O. H., Rosebrough, N. J., Farr, A. L. & Randall, R. J. 1951. Protein measurement with the folin phenol reagent. *J Biol Chem,* 193**,** 265-275.

Luo, F., Liu, X., Yan, N., Li, S., Cao, G., Cheng, Q., Xia, Q. & Wang, H. 2006. Hypoxia-inducible transcription factor-1α promotes hypoxia-induced A549 apoptosis via a mechanism that involves the glycolysis pathway. *BMC Cancer,* 6**,** 26.

Luo, J., Solimini, N. L. & Elledge, S. J. 2009. Principles of cancer therapy: oncogene and non-oncogene addiction. *Cell,* 136**,** 823-837.

Luscher, C. & Slesinger, P. A. 2010. Emerging roles for G protein-gated inwardly rectifying potassium (GIRK) channels in health and disease. *Nat Rev Neurosci,* 11**,** 301-305.

Ma, L., Zhang, X. & Chen, H. 2011. TWIK-1 two-pore domain potassium channels change ion selectivity and conduct inward leak sodium currents in hypokalemia. *Sci Signal,* 4**,** ra37.

Ma, Y. G., Liu, W. C., Dong, S., Du, C., Wang, X. J., Li, J. S., Xie, X. P., Wu, L., Ma, D. C., Yu, Z. B. & Xie, M. J. 2012. Activation of BK_{Ca} channels in zoledronic acid-induced apoptosis of MDA-MB-231 breast cancer cells. *PLoS One,* 7**,** e37451.

Maingret, F., Fosset, M., Lesage, F., Lazdunski, M. & Honoré, E. 1999a. TRAAK is a mammalian neuronal mechano-gated K^+ channel. *J Biol Chem,* 274**,** 1381-1387.

Maingret, F., Patel, A. J., Lazdunski, M. & Honore, E. 2001. The endocannabinoid anandamide is a direct and selective blocker of the background K^+ channel TASK-1. *EMBO J,* 20**,** 47-54.

Maingret, F., Patel, A. J., Lesage, F., Lazdunski, M. & Honoré, E. 1999b. Mechano- or acid stimulation, two interactive modes of activation of the TREK-1 potassium channel. *J Biol Chem,* 274**,** 26691-26696.

Maingret, F., Patel, A. J., Lesage, F., Lazdunski, M. & Honoré, E. 2000. Lysophospholipids open the two-pore domain mechano-gated K^+ channels TREK-1 and TRAAK. *J Biol Chem,* 275**,** 10128-10133.

Maldonado, E. N. & Lemasters, J. J. 2012. Warburg revisited: regulation of mitochondrial metabolism by voltage-dependent anion channels in cancer cells. *J Pharmacol Exp Ther,* 342**,** 637-641.

Mant, A., Elliott, D., Eyers, P. A. & O'Kelly, I. M. 2011. Protein kinase A is central for forward transport of two-pore domain potassium channels $K_{2P}3.1$ and $K_{2P}9.1$. *J Biol Chem,* 286**,** 14110-14119.

Mant, A., Williams, S. & O'Kelly, I. 2013a. Acid sensitive background potassium channels $K_{2P}3.1$ and $K_{2P}9.1$ undergo rapid dynamin-dependent endocytosis. *Channels,* 7**,** 0-14.

Mant, A., Williams, S., Roncoroni, L., Lowry, E., Johnson, D. & O'Kelly, I. 2013b. *N*-glycosylation-dependent control of functional expression of background potassium channels $K_{2P}3.1$ and $K_{2P}9.1$. *J Biol Chem,* 288**,** 3251-3264.

Marinc, C., Preisig-Muller, R., Pruss, H., Derst, C. & Veh, R. W. 2011. Immunocytochemical localization of TASK-3 ($K_{2P}9.1$) channels in monoaminergic and cholinergic neurons. *Cell Mol Neurobiol,* 31**,** 323-335.

Marinc, C., Prüss, H., Derst, C. & Veh, R. 2012. Immunocytochemical localization of TASK-3 channels in rat motor neurons. *Cell Mol Neurobiol,* 32**,** 309-318.

Mark, M. D. & Herlitze, S. 2000. G-protein mediated gating of inward-rectifier K^+ channels. *Eur J Biochem,* 267**,** 5830-5836.

Marsh, B., Acosta, C., Djouhri, L. & Lawson, S. N. 2012. Leak K^+ channel mRNAs in dorsal root ganglia: relation to inflammation and spontaneous pain behaviour. *Mol Cell Neurosci,* 49**,** 375-386.

Mascia, F., Denning, M., Kopan, R. & Yuspa, S. H. 2012. The black box illuminated: signals and signaling. *J Invest Dermatol,* 132**,** 811-819.

Masi, A., Becchetti, A., Restano-Cassulini, R., Polvani, S., Hofmann, G., Buccoliero, A. M., Paglierani, M., Pollo, B., Taddei, G. L., Gallina, P., Di Lorenzo, N., Franceschetti, S., Wanke, E. & Arcangeli, A. 2005. hERG1 channels are overexpressed in glioblastoma multiforme and modulate VEGF secretion in glioblastoma cell lines. *Br J Cancer,* 93**,** 781-792.

Massague, J. 2004. G_1 cell-cycle control and cancer. *Nature,* 432**,** 298-306.

Matheu, M. P., Beeton, C., Garcia, A., Chi, V., Rangaraju, S., Safrina, O., Monaghan, K., Uemura, M. I., Li, D., Pal, S., de la Maza, L. M., Monuki, E., Flügel, A., Pennington, M. W., Parker, I., Chandy, K. G. & Cahalan, M. D. 2008. Imaging of effector memory T

cells during a delayed-type hypersensitivity reaction and suppression by $K_V1.3$ channel block. *Immunity,* 29**,** 602-614.

Mathie, A., Al-Moubarak, E. & Veale, E. L. 2010. Gating of two-pore domain potassium channels. *J Physiol,* 588**,** 3149-3156.

Matsuoka, H., Harada, K., Nakamura, J. & Inoue, M. 2013. Nerve growth factor-induced endocytosis of TWIK-related acid-sensitive K^+ 1 channels in adrenal medullary cells and PC12 cells. *Pflugers Arch,* 465**,** 1051-1064.

McAndrew, D., Grice, D. M., Peters, A. A., Davis, F. M., Stewart, T., Rice, M., Smart, C. E., Brown, M. A., Kenny, P. A., Roberts-Thomson, S. J. & Monteith, G. R. 2011. Orai1-mediated calcium influx in lactation and in breast cancer. *Mol Cancer Ther,* 10**,** 448-460.

McFerrin, M. B., Turner, K. L., Cuddapah, V. A. & Sontheimer, H. 2012. Differential role of IK and BK potassium channels as mediators of intrinsic and extrinsic apoptotic cell death. *Am J Physiol Cell Physiol,* 303**,** C1070-C1078.

McTaggart, J. S., Clark, R. H. & Ashcroft, F. M. 2010. The role of the K_{ATP} channel in glucose homeostasis in health and disease: more than meets the islet. *J Physiol,* 588**,** 3201-3209.

Meadows, H. J. & Randall, A. D. 2001. Functional characterisation of human TASK-3, an acid-sensitive two-pore domain potassium channel. *Neuropharmacology,* 40**,** 551-559.

Medhurst, A. D., Rennie, G., Chapman, C. G., Meadows, H., Duckworth, M. D., Kelsell, R. E., Gloger, I. I. & Pangalos, M. N. 2001. Distribution analysis of human two-pore domain potassium channels in tissues of the central nervous system and periphery. *Brain Res Mol Brain Res,* 86**,** 101-114.

Menéndez, S. T., Rodrigo, J. P., Allonca, E., García-Carracedo, D., Álvarez-Alija, G., Casado-Zapico, S., Fresno, M. F., Rodríguez, C., Suárez, C. & García-Pedrero, J. M. 2010. Expression and clinical significance of the $K_V3.4$ potassium channel subunit in the development and progression of head and neck squamous cell carcinomas. *J Pathol,* 221**,** 402-410.

Menendez, S. T., Villaronga, M. A., Rodrigo, J. P., Alvarez-Teijeiro, S., Garcia-Carracedo, D., Urdinguio, R. G., Fraga, M. F., Pardo, L. A., Viloria, C. G., Suarez, C. & Garcia-Pedrero, J. M. 2012. Frequent aberrant expression of the human Ether à go-go (hEAG1) potassium channel in head and neck cancer: pathobiological mechanisms and clinical implications. *J Mol Med (Berl),* 90**,** 1173-1184.

Meuth, S. G., Bittner, S., Meuth, P., Simon, O. J., Budde, T. & Wiendl, H. 2008a. TWIK-related acid-sensitive K^+ channel 1 (TASK-1) and TASK-3 critically influence T lymphocyte effector functions. *J Biol Chem,* 283**,** 14559-14570.

Meuth, S. G., Herrmann, A. M., Ip, C. W., Kanyshkova, T., Bittner, S., Weishaupt, A., Budde, T. & Wiendl, H. 2008b. The two-pore domain potassium channel TASK-3 functionally impacts glioma cell death. *J Neurooncol,* 87**,** 263-270.

Meyer, R. & Heinemann, S. H. 1998. Characterization of an Eag-like potassium channel in human neuroblastoma cells. *J Physiol,* 508**,** 49-56.

Mhatre, A. N., Li, J., Chen, A. F., Yost, C. S., Smith, R. J. H., Kindler, C. H. & Lalwani, A. K. 2004. Genomic structure, cochlear expression, and mutation screening of *KCNK6*, a candidate gene for DFNA4. *J Neurosci Res,* 75**,** 25-31.

Michaelis, U. R. & Fleming, I. 2006. From endothelium-derived hyperpolarizing factor (EDHF) to angiogenesis: epoxyeicosatrienoic acids (EETs) and cell signaling. *Pharmacol Ther,* 111**,** 584-595.

Mijatovic, T., Ingrassia, L., Facchini, V. & Kiss, R. 2008. Na^+/K^+-ATPase α subunits as new targets in anticancer therapy. *Expert Opin Ther Targets,* 12**,** 1403-1417.

Millar, J. A., Barratt, L., Southan, A. P., Page, K. M., Fyffe, R. E. W., Robertson, B. & Mathie, A. 2000. A functional role for the two-pore domain potassium channel TASK-1 in cerebellar granule neurons. *Proc Natl Acad Sci U S A,* 97**,** 3614-3618.

Miller, A. N. & Long, S. B. 2012. Crystal structure of the human two–pore domain potassium channel $K_{2P}1$. *Science,* 335**,** 432-436.

Millership, J. E., Devor, D. C., Hamilton, K. L., Balut, C. M., Bruce, J. I. E. & Fearon, I. M. 2011. Calcium-activated K^+ channels increase cell proliferation independent of K^+ conductance. *Am J Physiol Cell Physiol,* 300**,** C792-C802.

Molenaar, R. J. 2011. Ion channels in glioblastoma. *ISRN Neurol,* 2011**,** 7.

Monteith, G. R., Davis, F. M. & Roberts-Thomson, S. J. 2012. Calcium channels and pumps in cancer: changes and consequences. *J Biol Chem,* 287**,** 31666-31673.

Monteith, G. R., McAndrew, D., Faddy, H. M. & Roberts-Thomson, S. J. 2007. Calcium and cancer: targeting Ca^{2+} transport. *Nat Rev Cancer*, 7**,** 519-530.

Mu, D., Chen, L., Zhang, X., See, L.-H., Koch, C. M., Yen, C., Tong, J. J., Spiegel, L., Nguyen, K. C. Q., Servoss, A., Peng, Y., Pei, L., Marks, J. R., Lowe, S., Hoey, T., Jan, L. Y., McCombie, W. R., Wigler, M. H. & Powers, S. 2003. Genomic amplification and oncogenic properties of the *KCNK9* potassium channel gene. *Cancer Cell,* 3**,** 297-302.

Mucaj, V., Shay, J. S. & Simon, M. C. 2012. Effects of hypoxia and HIFs on cancer metabolism. *Int J Hematol,* 95**,** 464-470.

Nakagawa, Y., Numoto, K., Yoshida, A., Kunisada, T., Ohata, H., Takeda, K., Wai, D., Poremba, C. & Ozaki, T. 2006a. Chromosomal and genetic imbalances in synovial sarcoma detected by conventional and microarray comparative genomic hybridization. *J Cancer Res Clin Oncol,* 132**,** 444-450.

Nakagawa, Y., Yoshida, A., Numoto, K., Kunisada, T., Wai, D., Ohata, N., Takeda, K., Kawai, A. & Ozaki, T. 2006b. Chromosomal imbalances in malignant peripheral nerve sheath tumor detected by metaphase and microarray comparative genomic hybridization. . *Oncol Rep,* 15**,** 297-303.

Nanduri, J., Bergson, P., Wang, N., Ficker, E. & Prabhakar, N. R. 2009. Hypoxia inhibits maturation and trafficking of hERG K^+ channel protein: role of Hsp90 and ROS. *Biochem Biophys Res Commun,* 388**,** 212-216.

Nanduri, J., Wang, N., Bergson, P., Yuan, G., Ficker, E. & Prabhakar, N. R. 2008. Mitochondrial reactive oxygen species mediate hypoxic down-regulation of hERG channel protein. *Biochem Biophys Res Commun,* 373**,** 309-314.

Nayak, T. K., Harinath, S., Nama, S., Somasundaram, K. & Sikdar, S. K. 2009. Inhibition of human two-pore domain K^+ channel TREK-1 by local anesthetic lidocaine: negative cooperativity and half-of-sites saturation kinetics. *Mol Pharmacol,* 76**,** 903-917.

Nichols, C. G. & Lopatin, A. N. 1997. Inward rectifier potassium channels. *Annu Rev Physiol,* 59**,** 171-191.

Nielsen, G., Wandall-Frostholm, C., Sadda, V., Oliván-Viguera, A., Lloyd, E. E., Bryan, R. M., Simonsen, U. & Köhler, R. 2013. Alterations of N-3 polyunsaturated fatty acid-activated K_{2P} channels in hypoxia-induced pulmonary hypertension. *Basic Clin Pharmacol Toxicol,* 113**,** 250-258.

Niemeyer, M. I., Cid, L. P., Barros, L. F. & Sepúlveda, F. V. 2001. Modulation of the two-pore domain acid-sensitive K^+ channel TASK-2 (*KCNK5*) by changes in cell volume. *J Biol Chem,* 276**,** 43166-43174.

Niemeyer, M. I., González-Nilo, F. D., Zúñiga, L., González, W., Cid, L. P. & Sepúlveda, F. V. 2007. Neutralization of a single arginine residue gates open a two-pore domain, alkali-activated K^+ channel. *Proc Natl Acad Sci U S A,* 104**,** 666-671.

NIH, N. C. I. *Cancer Staging* [Online]. Available: http://www.cancer.gov/cancertopics/factsheet/detection/staging [Accessed 14/07/2013].

Noël, J., Sandoz, G. & Lesage, F. 2011. Molecular regulations governing TREK and TRAAK channel functions. *Channels,* 5**,** 402-409.

Nogueira, E. F., Gerry, D., Mantero, F., Mariniello, B. & Rainey, W. E. 2010. The role of TASK-1 in aldosterone production and its expression in normal adrenal and aldosterone-producing adenomas. *Clin Endocrinol (Oxf),* 73**,** 22-29.

Normanno, N., De Luca, A., Bianco, C., Strizzi, L., Mancino, M., Maiello, M. R., Carotenuto, A., De Feo, G., Caponigro, F. & Salomon, D. S. 2006. Epidermal growth factor receptor (EGFR) signaling in cancer. *Gene,* 366**,** 2-16.

Numata, T., Sato, K., Okada, Y. & Wehner, F. 2008. Hypertonicity-induced cation channels rescue cells from staurosporine-elicited apoptosis. *Apoptosis,* 13**,** 895-903.

Nunez, M., Medina, V., Cricco, G., Croci, M., Cocca, C., Rivera, E., Bergoc, R. & Martin, G. 2013. Glibenclamide inhibits cell growth by inducing G_0/G_1 arrest in the human breast cancer cell line MDA-MB-231. *BMC Pharmacol Toxicol,* 14.

Oh, M. C., Kim, J. M., Safaee, M., Kaur, G., Sun, M. Z., Kaur, R., Celli, A., Mauro, T.M., & Parsa, A. T. 2012. Overexpression of calcium-permeable glutamate receptors in glioblastoma derived brain tumor initiating cells. *PLoS One*, 7**,** e47846.

O'Kelly, I., Butler, M. H., Zilberberg, N. & Goldstein, S. A. N. 2002. Forward transport: 14-3-3 binding overcomes retention in endoplasmic reticulum by dibasic signals. *Cell,* 111**,** 577-588.

O'Kelly, I. & Goldstein, S. A. 2008. Forward transport of $K_{2P}3.1$: mediation by 14-3-3 and COPI, modulation by p11. *Traffic,* 9**,** 72-78.

O'Kelly, I., Peers, C. & Kemp, P. J. 2001. NADPH oxidase does not account fully for O_2-sensing in model airway chemoreceptor cells. *Biochem Biophys Res Commun,* 283**,** 1131-1134.

O'Kelly, I., Peers, C. & Kemp, P. J. 1998. O_2-sensitive K^+ channels in neuroepithelial body-derived small cell carcinoma cells of the human lung. *Am J Physiol Lung Cell Mol Physiol,* 275**,** L709-L716.

O'Kelly, I., Stephens, R. H., Peers, C. & Kemp, P. J. 1999. Potential identification of the O_2-sensitive K^+ current in a human neuroepithelial body-derived cell line. *Am J Physiol Lung Cell Mol Physiol,* 276**,** L96-L104.

Oeggerli, M., Tian, Y., Ruiz, C., Wijker, B., Sauter, G., Obermann, E., Güth, U., Zlobec, I., Sausbier, M., Kunzelmann, K. & Bubendorf, L. 2012. Role of *KCNMA1* in breast cancer. *PLoS One,* 7**,** e41664.

Olsen, M. L. & Sontheimer, H. 2004. Mislocalization of K_{ir} channels in malignant glia. *Glia,* 46**,** 63-73.

Oncomine. 2013. *Oncomine* [Online]. Compendia Bioscience, Ann Arbor, MI. Available: www.oncomine.org. [Accessed 30/01/2013].

Orio, P., Rojas, P., Ferreira, G. & Latorre, R. 2002. New disguises for an old channel: MaxiK channel β-subunits. *News Physiol Sci,* 17**,** 156-161.

Ortega-Saenz, P., Levitsky, K. L., Marcos-Almaraz, M. T., Bonilla-Henao, V., Pascual, A. & Lopez-Barneo, J. 2010. Carotid body chemosensory responses in mice deficient of TASK channels. *J Gen Physiol,* 135**,** 379-392.

Ortiz, F. C., Del Rio, R., Ebensperger, G., Reyes, V. R., Alcayaga, J., Varas, R. & Iturriaga, R. 2013. Inhibition of rat carotid body glomus cells TASK-like channels by acute hypoxia is enhanced by chronic intermittent hypoxia. *Respir Physiol Neurobiol,* 185**,** 600-607.

Ouadid-Ahidouch, H. & Ahidouch, A. 2008. K^+ channel expression in human breast cancer cells: involvement in cell cycle regulation and carcinogenesis. *J Membr Biol,* 221**,** 1-6.

Ouadid-Ahidouch, H., Chaussade, F., Roudbaraki, M., Slomianny, C., Dewailly, E., Delcourt, P. & Prevarskaya, N. 2000. $K_V1.1$ K^+ channels identification in human breast carcinoma cells: involvement in cell proliferation. *Biochem Biophys Res Commun,* 278**,** 272-277.

Ouadid-Ahidouch, H., Roudbaraki, M., Delcourt, P., Ahidouch, A., Joury, N. & Prevarskaya, N. 2004. Functional and molecular identification of intermediate-conductance Ca^{2+}-activated K^+ channels in breast cancer cells: association with cell cycle progression. *Am J Physiol Cell Physiol,* 287**,** C125-C134.

Ousingsawat, J., Spitzner, M., Puntheeranurak, S., Terracciano, L., Tornillo, L., Bubendorf, L., Kunzelmann, K. & Schreiber, R. 2007. Expression of voltage-gated potassium channels in human and mouse colonic carcinoma. *Clin Cancer Res,* 13**,** 824-831.

Ousingsawat, J., Spitzner, M., Schreiber, R. & Kunzelmann, K. 2008. Upregulation of colonic ion channels in $APC^{Min/+}$ mice. *Pflugers Arch,* 456**,** 847-855.

Ouyang, L., Shi, Z., Zhao, S., Wang, F. T., Zhou, T. T., Liu, B. & Bao, J. K. 2012. Programmed cell death pathways in cancer: a review of apoptosis, autophagy and programmed necrosis. *Cell Prolif,* 45**,** 487-498.

Pages, F., Galon, J., Dieu-Nosjean, M. C., Tartour, E., Sautes-Fridman, C. & Fridman, W. H. 2009. Immune infiltration in human tumors: a prognostic factor that should not be ignored. *Oncogene,* 29**,** 1093-1102.

Pandiella, A., Magni, M., Lovisolo, D. & Meldolesi, J. 1989. The effect of epidermal growth factor on membrane potential. Rapid hyperpolarization followed by persistent fluctuations. *J Biol Chem,* 264**,** 12914-12921.

Panyi, G., Varga, Z. & Gáspár, R. 2004. Ion channels and lymphocyte activation. *Immunol Lett,* 92**,** 55-66.

Papazian, D. M., Timpe, L. C., Jan, Y. N. & Jan, L. Y. 1991. Alteration of voltage-dependence of Shaker potassium channel by mutations in the S4 sequence. *Nature,* 349**,** 305-310.

Papreck, J., Martin, E., Lazzarini, P., Kang, D. & Kim, D. 2012. Modulation of $K_{2P}3.1$ (TASK-1), $K_{2P}9.1$ (TASK-3), and TASK-1/3 heteromer by reactive oxygen species. *Pflugers Arch,* 464**,** 471-480.

Pardo, L. A. 2004. Voltage-gated potassium channels in cell proliferation. *Physiology (Bethesda),* 19**,** 285-292.

Pardo, L. A. & Stuhmer, W. 2014. The roles of K^+ channels in cancer. *Nat Rev Cancer*, 14**,** 39-48.

Park, J. B., Lee, C. S., Jang, J.-H., Ghim, J., Kim, Y.-J., You, S., Hwang, D., Suh, P.-G. & Ryu, S. H. 2012. Phospholipase signalling networks in cancer. *Nat Rev Cancer,* 12**,** 782-792.

Park, S.-H., Ramachandran, S., Kwon, S.-H., Cha, S.-D., Seo, E. W., Bae, I., Cho, C. & Song, D.-K. 2008. Upregulation of ATP-sensitive potassium channels for estrogen-mediated cell proliferation in human uterine leiomyoma cells. *Gynecol Endocrinol,* 24**,** 250-256.

Patel, A., Honore, E., Maingret, F., Lesage, F., Fink, M., Duprat, F. & Lazdunski, M. 1998. A mammalian two pore domain mechano-gated S-like K^+ channel. *EMBO J,* 17**,** 4283-4290.

Patel, A. J., Honore, E., Lesage, F., Fink, M., Romey, G. & Lazdunski, M. 1999. Inhalational anesthetics activate two-pore-domain background K^+ channels. *Nat Neurosci,* 2**,** 422-426.

Patel, A. J. & Lazdunski, M. 2004. The $_{2P}$-domain K^+ channels: role in apoptosis and tumorigenesis. *Pflugers Arch,* 448**,** 261-273.

Patel, A. J., Maingret, F., Magnone, V., Fosset, M., Lazdunski, M. & Honoré, E. 2000. TWIK-2, an inactivating $_{2P}$ domain K^+ channel. *J Biol Chem,* 275**,** 28722-28730.

Patsos, H., Greenhough, A., Hicks, D., Al Kharusi, M., Collard, T., Lane, J., Paraskeva, C. & Williams, A. 2010. The endogenous cannabinoid, anandamide, induces COX-2-dependent cell death in apoptosis-resistant colon cancer cells. *Int J Oncol,* 37**,** 187-193.

Patsos, H. A., Hicks, D. J., Dobson, R. R. H., Greenhough, A., Woodman, N., Lane, J. D., Williams, A. C. & Paraskeva, C. 2005. The endogenous cannabinoid, anandamide, induces cell death in colorectal carcinoma cells: a possible role for cyclooxygenase 2. *Gut,* 54**,** 1741-1750.

Pedersen, S. F., Hoffmann, E. K. & Novak, I. 2013. Cell volume regulation in epithelial physiology and cancer. *Front Physiol,* 4.

Pedersen, S. F. & Stock, C. 2013. Ion channels and transporters in cancer: pathophysiology, regulation, and clinical Potential. *Cancer Res,* 73**,** 1658-1661.

Pei, L., Wiser, O., Slavin, A., Mu, D., Powers, S., Jan, L. Y. & Hoey, T. 2003. Oncogenic potential of TASK-3 (*KCNK9*) depends on K^+ channel function. *Proc Natl Acad Sci U S A,* 100**,** 7803-7807.

Peinado, H., Ballestar, E., Esteller, M. & Cano, A. 2004. Snail mediates E-cadherin repression by the recruitment of the Sin3A/histone deacetylase 1 (HDAC1)/HDAC2 complex. *Mol Cell Biol,* 24**,** 306-319.

Peña, T. L., Chen, S. H., Konieczny, S. F. & Rane, S. G. 2000. Ras/MEK/ERK upregulation of the fibroblast K_{Ca} channel FIK is a common mechanism for basic fibroblast growth factor and transforming growth factor-β suppression of myogenesis. *J Biol Chem,* 275**,** 13677-13682.

Peterson, G. 1995. Evaluation of the biochemical targets of genistein in tumor cells. *J Nutr,* 125**,** 784S-789S.

Pisanti, S., Picardi, P., D'Alessandro, A., Laezza, C. & Bifulco, M. 2013. The endocannabinoid signaling system in cancer. *Trends Pharmacol Sci,* 34**,** 273-282.

Placzek, W. J., Wei, J., Kitada, S., Zhai, D., Reed, J. C. & Pellecchia, M. 2010. A survey of the anti-apoptotic Bcl-2 subfamily expression in cancer types provides a platform to predict the efficacy of Bcl-2 antagonists in cancer therapy. *Cell Death Dis,* 1**,** e40.

Plant, L. D., Bayliss, D. A., Kim, D., Lesage, F. & S.A.N., G. 2014. *Two-P potassium channels* [Online]. IUPHAR database (IUPHAR-DB). Available: http://www.iuphar-db.org/DATABASE/FamilyMenuForward?familyId=79 [Accessed 05/07/2014].

Plant, L. D., Kemp, P. J., Peers, C., Henderson, Z. & Pearson, H. A. 2002. Hypoxic depolarization of cerebellar granule neurons by specific inhibition of TASK-1. *Stroke,* 33**,** 2324-2328.

Plant, L. D., Rajan, S. & Goldstein, S. A. 2005. K_{2P} channels and their protein partners. *Curr Opin Neurobiol,* 15**,** 326-333.

Plant, L. D. 2012a. A role for K_{2P} channels in the operation of somatosensory nociceptors. *Front. Mol. Neurosci*, 5.

Plant, L. D., Zuniga, L., Araki, D., Marks, J. D. & Goldstein, S. A. N. 2012b. SUMOylation silences heterodimeric TASK potassium channels containing K_{2P}1 subunits in cerebellar granule neurons. *Sci Signal,* 5**,** ra84.

Plummer, H., Dhar, M., Cekanova, M. & Schuller, H. 2005. Expression of G-protein inwardly rectifying potassium channels (GIRKs) in lung cancer cell lines. *BMC Cancer,* 5.

Pocsai, K., Kosztka, L., Bakondi, G., Gonczi, M., Fodor, J., Dienes, B., Szentesi, P., Kovacs, I., Feniger-Barish, R., Kopf, E., Zharhary, D., Szucs, G., Csernoch, L. & Rusznak, Z. 2006. Melanoma cells exhibit strong intracellular TASK-3-specific immunopositivity in both tissue sections and cell culture. *Cell Mol Life Sci,* 63**,** 2364-2376.

Poling, J. S., Rogawski, M. A., Salem Jr, N. & Vicini, S. 1996. Anandamide, an endogenous cannabinoid, inhibits Shaker-related voltage-gated K^+ channels. *Neuropharmacology,* 35**,** 983-991.

Polyak, K., Haviv, I. & Campbell, I. G. 2009. Co-evolution of tumor cells and their microenvironment. *Trends Genet,* 25**,** 30-38.

Portt, L., Norman, G., Clapp, C., Greenwood, M. & Greenwood, M. T. 2011. Anti-apoptosis and cell survival: a review. *BBA - Mol Cell Res,* 1813**,** 238-259.

Potier, M., Joulin, V., Roger, S., Besson, P., Jourdan, M.-L., LeGuennec, J.-Y., Bougnoux, P. & Vandier, C. 2006. Identification of SK3 channel as a new mediator of breast cancer cell migration. *Mol Cancer Ther,* 5**,** 2946-2953.

Potier, M., Tran, T. A., Chantome, A., Girault, A., Joulin, V., Bougnoux, P., Vandier, C. & Pierre, F. 2010. Altered SK3/K_{Ca}2.3-mediated migration in adenomatous polyposis coli (APC) mutated mouse colon epithelial cells. *Biochem Biophys Res Commun,* 397**,** 42-47.

Pouyssegur, J., Dayan, F. & Mazure, N. M. 2006. Hypoxia signalling in cancer and approaches to enforce tumour regression. *Nature,* 441**,** 437-443.

Preußat, K., Beetz, C., Schrey, M., Kraft, R., Wölfl, S., Kalff, R. & Patt, S. 2003. Expression of voltage-gated potassium channels K_V1.3 and K_V1.5 in human gliomas. *Neurosci Lett,* 346**,** 33-36.

Prevarskaya, N., Skryma, R., Bidaux, G., Flourakis, M. & Shuba, Y. 2007. Ion channels in death and differentiation of prostate cancer cells. *Cell Death Differ,* 14**,** 1295-1304.

Prevarskaya, N., Skryma, R. & Shuba, Y. 2013. Targeting Ca^{2+} transport in cancer: close reality or long perspective? *Expert Opin Ther Targets,* 17**,** 225-241.

Proto, M. C., Gazzerro, P., Di Croce, L., Santoro, A., Malfitano, A. M., Pisanti, S., Laezza, C. & Bifulco, M. 2012. Interaction of endocannabinoid system and steroid hormones in the control of colon cancer cell growth. *J Cell Physiol,* 227**,** 250-258.

Rada, C. C., Pierce, S. L., Nuno, D. W., Zimmerman, K., Lamping, K. G., Bowdler, N. C., Weiss, R. M. & England, S. K. 2012. Overexpression of the SK3 channel alters vascular remodeling during pregnancy, leading to fetal demise. *Am J Physiol Endoc M,* 303**,** E825-E831.

Raimondi, C. & Falasca, M. 2012. Phosphoinositides signalling in cancer: Focus on PI3K and PLC. *Adv Biol Regul,* 52**,** 166-182.

Rajan, S., Plant, L. D., Rabin, M. L., Butler, M. H. & Goldstein, S. A. N. 2005. Sumoylation silences the plasma membrane leak K^+ Channel K_{2P}1. *Cell,* 121**,** 37-47.

Rajan, S., Preisig-Muller, R., Wischmeyer, E., Nehring, R., Hanley, P. J., Renigunta, V., Musset, B., Schlichthorl, G., Derst, C., Karschin, A. & Daut, J. 2002. Interaction with 14-3-3 proteins promotes functional expression of the potassium channels TASK-1 and TASK-3. *J Physiol,* 545**,** 13-26.

Rajan, S., Wischmeyer, E., Karschin, C., Preisig-Müller, R., Grzeschik, K.-H., Daut, J., Karschin, A. & Derst, C. 2001. THIK-1 and THIK-2, a novel subfamily of tandem pore domain K^+ channels. *J Biol Chem,* 276**,** 7302-7311.

Rajan, S., Wischmeyer, E., Xin Liu, G., Preisig-Muller, R., Daut, J., Karschin, A. & Derst, C. 2000. TASK-3, a novel tandem pore domain acid-sensitive K^+ channel. An extracellular histiding as pH sensor. *J Biol Chem,* 275**,** 16650-16657.

Rao, J. N., Platoshyn, O., Li, L., Guo, X., Golovina, V. A., Yuan, J. X.-J. & Wang, J.-Y. 2002. Activation of K^+ channels and increased migration of differentiated intestinal epithelial cells after wounding. *Am J Physiol Cell Physiol,* 282**,** C885-C898.

Renganathan, M., Sidach, S. & Blight, A. R. 2009. Effects of 4-Aminopyridine on cloned hERG channels expressed in mammalian Cells. *Arch Drug Inf,* 2**,** 51-57.

Reyes, R., Duprat, F., Lesage, F., Fink, M., Salinas, M., Farman, N. & Lazdunski, M. 1998. Cloning and expression of a novel pH-sensitive two pore domain K^+ channel from human kidney. *J Biol Chem,* 273**,** 30863-30869.

Rhodes, D. R., Kalyana-Sundaram, S., Mahavisno, V., Varambally, R., Yu, J., Briggs, B. B., Barrette, T. R., Anstet, M. J., Kincead-Beal, C., Kulkarni, P., Varambally, S., Ghosh, D. & Chinnaiyan, A. M. 2007. Oncomine 3.0: genes, pathways, and networks in a collection of 18,000 cancer gene expression profiles. *Neoplasia,* 9**,** 166-180.

Rhodes, D. R., Yu, J., Shanker, K., Deshpande, N., Varambally, R., Ghosh, D., Barrette, T., Pandey, A. & Chinnaiyan, A. M. 2004. Oncomine: a cancer microarray database and integrated data-mining platform. *Neoplasia,* 6**,** 1-6.

Ridge, F. P. G., Duszyk, M. & French, A. S. 1997. A large conductance, Ca^{2+}-activated K^+ channel in a human lung epithelial cell line (A549). *BBA - Biomembranes,* 1327**,** 249-258.

Ridley, J. M., Milnes, J. T., Zhang, Y. H., Witchel, H. J. & Hancox, J. C. 2003. Inhibition of hERG K^+ current and prolongation of the guinea-pig ventricular action potential by 4-aminopyridine. *J Physiol,* 549**,** 667-672.

Riener, M.-O., Nikolopoulos, E., Herr, A., Wild, P. J., Hausmann, M., Wiech, T., Orlowska-Volk, M., Lassmann, S., Walch, A. & Werner, M. 2008. Microarray comparative genomic hybridization analysis of tubular breast carcinoma shows recurrent loss of the CDH13 locus on 16q. *Hum Pathol,* 39**,** 1621-1629.

Rockett, J. C., Larkin, K., Darnton, S. J., Morris, A. G. & Matthews, H. R. 1997. Five newly established oesophageal carcinoma cell lines: phenotypic and immunological characterization. *Br J Cancer,* 75**,** 258-263.

Roger, S., Rollin, J., Barascu, A., Besson, P., Raynal, P.I., Iochmann, S., Lei, M., Bougnoux, P., Gruel, Y. & Le Guennec, J. Y. 2007. Voltage-gated sodium channels potentiate the invasive capacities of human non-small-cell lung cancer cell lines. *Int J Biochem Cell Biol*, 39**,** 774-786.

Rodrigues, A. R. A., Arantes, E. C., Monje, F., Stuhmer, W. & Varanda, W. A. 2003. Tityustoxin-K(α) blockade of the voltage-gated potassium channel $K_V1.3$. *Br J Pharmacol,* 139**,** 1180-1186.

Rodriguez-Rasgado, J. A., Acuna-Macias, I. & Camacho, J. 2012. Eag1 channels as potential cancer biomarkers. *Sensors (Basel),* 12**,** 5986-5995.

Roncoroni, L. 2012. *Functional role of the background potassium channel $K_{2P}15.1$.* PhD Research, University of Southampton.

Rosenberg, S. A. 1969. A Computer Evaluation of Equations for Predicting the Potential across Biological Membranes. *Biophysical Journal,* 9**,** 500-509.

Rouzaire-Dubois, B. & Dubois, J. M. 1998. K^+ channel block-induced mammalian neuroblastoma cell swelling: a possible mechanism to influence proliferation. *J Physiol,* 510**,** 93-102.

Roy, J. W., Cowley, E. A., Blay, J. & Linsdell, P. 2010. The intermediate conductance Ca^{2+}-activated K^+ channel inhibitor TRAM-34 stimulates proliferation of breast cancer cells via activation of oestrogen receptors. *Br J Pharmacol,* 159**,** 650-658.

Ruscic, K. J., Miceli, F., Villalba-Galea, C. A., Dai, H., Mishina, Y., Bezanilla, F. & Goldstein, S. A. N. 2013. IKs channels open slowly because KCNE1 accessory subunits slow the movement of S4 voltage sensors in KCNQ1 pore-forming subunits. *Proc Natl Acad Sci U S A,* 110**,** E559-E566.

Rusznak, Z., Bakondi, G., Kosztka, L., Pocsai, K., Dienes, B., Fodor, J., Telek, A., Gonczi, M., Szucs, G. & Csernoch, L. 2008. Mitochondrial expression of the two-pore domain TASK-3 channels in malignantly transformed and non-malignant human cells. *Virchows Arch,* 452**,** 415-426.

Rusznák, Z., Pocsai, K., Kovács, I., Pór, Á., Pál, B., Bíró, T. & Szücs, G. 2004. Differential distribution of TASK-1, TASK-2 and TASK-3 immunoreactivities in the rat and human cerebellum. *Cell Mol Life Sci,* 61**,** 1532-1542.

Salinas, M., Reyes, R., Lesage, F., Fosset, M., Heurteaux, C., Romey, G. & Lazdunski, M. 1999. Cloning of a new mouse two-P domain channel subunit and a human homologue with a unique pore structure. *J Biol Chem,* 274**,** 11751-11760.

Sano, Y., Inamura, K., Miyake, A., Mochizuki, S., Kitada, C., Yokoi, H., Nozawa, K., Okada, H., Matsushime, H. & Furuichi, K. 2003. A novel two-pore domain K^+ channel, TRESK, is localized in the spinal cord. *J Biol Chem,* 278**,** 27406-27412.

Scherer, W. F., Syverton, J. T. & Gey, G. O. 1953. Studies on the propagation *in vitro* of poliomyelitis viruses: IV. Viral multiplication in a stable strain of human malignant epithelial cells (Strain HeLa) derived from an epidermoid carcinoma of the cervix. *J Exp Med,* 97**,** 695-710.

Schmidt, J., Friebel, K., Schonherr, R., Coppolino, M. G. & Bosserhoff, A.-K. 2010. Migration-associated secretion of melanoma inhibitory activity at the cell rear is supported by K_{Ca}3.1 potassium channels. *Cell Res,* 20**,** 1224-1238.

Schönherr, R. 2005. Clinical relevance of ion channels for diagnosis and therapy of cancer. *J Membr Biol,* 205**,** 175-184.

Schreiber, M. & Salkoff, L. 1997. A novel calcium-sensing domain in the BK channel. *Biophysical Journal,* 73**,** 1355-1363.

Schumacher, M. A., Rivard, A. F., Bachinger, H. P. & Adelman, J. P. 2001. Structure of the gating domain of a Ca^{2+}-activated K^+ channel complexed with Ca^{2+}/calmodulin. *Nature,* 410**,** 1120-1124.

Schwab, A., Fabian, A., Hanley, P. J. & Stock, C. 2012. Role of ion channels and transporters in cell migration. *Physiol Rev,* 92**,** 1865-1913.

Shao, X.-D., Wu, K.-C., Guo, X.-Z., Xie, M.-J., Zhang, J. & Fan, D.-M. 2008. Expression and significance of hERG protein in gastric cancer. *Cancer Biol Ther,* 7**,** 45-50.

Shao, X.-D., Wu, K., Hao, Z.-M., Hong, L., Zhang, J. & Fan, D. 2005. The potent inhibitory effects of cisapride, a specific blocker for human Ether-à-go-go-related gene (hERG) channel, on gastric cancer cells. *Cancer Biol Ther,* 4**,** 295-301.

Shaw, R. J. & Cantley, L. C. 2006. Ras, PI3K and mTOR signalling controls tumour cell growth. *Nature,* 441**,** 424-430.

Shay, J. W. & Wright, W. E. 2011. Role of telomeres and telomerase in cancer. *Semin Cancer Biol,* 21**,** 349-353.

Shieh, C.-C., Coghlan, M., Sullivan, J. P. & Gopalakrishnan, M. 2000. Potassium channels: molecular defects, diseases, and therapeutic opportunities. *Pharmacol Rev,* 52**,** 557-594.

Shiotani, B. & Zou, L. 2009. ATR signaling at a glance. *J Cell Sci,* 122**,** 301-304.

Shu, J., Jelinek, J., Chang, H., Shen, L., Qin, T., Chung, W., Oki, Y. & Issa, J. P. 2006. Silencing of bidirectional promoters by DNA methylation in tumorigenesis. *Cancer Res,* 66**,** 5077-5084.

Sontheimer, H. 2008. An unexpected role for ion channels in brain tumor metastasis. *Experimental Biology and Medicine,* 233**,** 779-791.

Soule, H. D., Vazquez, J., Long, A., Albert, S. & Brennan, M. 1973. A human cell line from a pleural effusion derived from a breast carcinoma. *J Natl Cancer Inst,* 51**,** 1409-1416.

Spitzner, M., Martins, J. R., Soria, R. B., Ousingsawat, J., Scheidt, K., Schreiber, R. & Kunzelmann, K. 2008. Eag1 and Bestrophin1 are upregulated in fast-growing colonic cancer cells. *J Biol Chem,* 283**,** 7421-7428.

Stansfeld, P. J., Grottesi, A., Sands, Z. A., Sansom, M. S. P., Gedeck, P., Gosling, M., Cox, B., Stanfield, P. R., Mitcheson, J. S. & Sutcliffe, M. J. 2008. Insight into the mechanism

of inactivation and pH sensitivity in potassium channels from molecular dynamics simulations. *Biochemistry,* 47**,** 7414-7422.

Steinle, M., Palme, D., Misovic, M., Rudner, J., Dittmann, K., Lukowski, R., Ruth, P. & Huber, S. M. 2011. Ionizing radiation induces migration of glioblastoma cells by activating BK K^+ channels. *Radiother Oncol,* 101**,** 122-126.

Stimers, J. R. & Byerly, L. 1982. Slowing of sodium current inactivation by ruthenium red in snail neurons. *J Gen Physiol,* 80**,** 485-497.

Streit, A. K., Netter, M. F., Kempf, F., Walecki, M., Rinné, S., Bollepalli, M. K., Preisig-Müller, R., Renigunta, V., Daut, J., Baukrowitz, T., Sansom, M. S. P., Stansfeld, P. J. & Decher, N. 2011. A specific two-pore domain potassium channel blocker defines the structure of the TASK-1 open pore. *J Biol Chem,* 286**,** 13977-13984.

Stringer, B. K., Cooper, A. G. & Shepard, S. B. 2001. Overexpression of the G-protein inwardly rectifying potassium channel 1 (GIRK1) in primary breast carcinomas correlates with axillary lymph node metastasis. *Cancer Res,* 61**,** 582-588.

Sundelacruz, S., Levin, M. & Kaplan, D. 2009. Role of membrane potential in the regulation of cell proliferation and differentiation. *Stem Cell Rev,* 5**,** 231-246.

Suzuki, Y., Inoue, T., Murai, M., Suzuki-Karasaki, M., Ochiai, T. & Ra, C. 2012. Depolarization potentiates TRAIL-induced apoptosis in human melanoma cells: role for ATP-sensitive K^+ channels and endoplasmic reticulum stress. *Int J Oncol,* 41**,** 465-475.

Tajima, N., Schonherr, K., Niedling, S., Kaatz, M., Kanno, H., Schonherr, R. & Heinemann, S. 2006. Ca^{2+}-activated K^+ channels in human melanoma cells are up-regulated by hypoxia involving hypoxia-inducible factor-1α and the von Hippel-Lindau protein. *J Physiol,* 571**,** 349 - 359.

Talley, E. M. & Bayliss, D. A. 2002. Modulation of TASK-1 (*KCNK3*) and TASK-3 (*KCNK9*) potassium channels: volatile anesthetics and neurotransmitters share a molecular site of action. *J Biol Chem,* 277**,** 17733-17742.

Talley, E. M., Lei, Q., Sirois, J. E. & Bayliss, D. A. 2000. TASK-1, a two-pore domain K^+ channel, is modulated by multiple neurotransmitters in motoneurons. *Neuron,* 25**,** 399-410.

Talley, E. M., Solórzano, G., Lei, Q., Kim, D. & Bayliss, D. A. 2001. CNS distribution of members of the two-pore domain (*KCNK*) potassium channel family. *J Neurosci,* 21**,** 7491-7505.

Talmadge, J. E. & Fidler, I. J. 2010. AACR centennial series: the biology of cancer metastasis: historical perspective. *Cancer Res,* 70**,** 5649-5669.

Tan, G., Sun, S.-q. & Yuan, D.-l. 2008. Expression of $K_{ir}4.1$ in human astrocytic tumors: correlation with pathologic grade. *Biochem Biophys Res Commun,* 367**,** 743-747.

Tao, R., Lau, C.-P., Tse, H.-F. & Li, G.-R. 2008. Regulation of cell proliferation by intermediate-conductance Ca^{2+}-activated potassium and volume-sensitive chloride channels in mouse mesenchymal stem cells. *Am J Physiol Cell Physiol,* 295**,** C1409-C1416.

Tapia, R. & Velasco, I. 1997. Ruthenium red as a tool to study calcium channels, neuronal death and the function of neural pathways. *Neurochem Int,* 30**,** 137-147.

Taylor, K. H., Pena-Hernandez, K. E., Davis, J. W., Arthur, G. L., Duff, D. J., Shi, H., Rahmatpanah, F. B., Sjahputera, O. & Caldwell, C. W. 2007. Large-scale CpG methylation analysis identifies novel candidate genes and reveals methylation hotspots in acute lymphoblastic leukemia. *Cancer Res,* 67**,** 2617-2625.

Teng, M. W. L., Swann, J. B., Koebel, C. M., Schreiber, R. D. & Smyth, M. J. 2008. Immune-mediated dormancy: an equilibrium with cancer. *J Leukoc Biol,* 84**,** 988-993.

Terlau, H. & Stühmer, W. 1998. Structure and function of voltage-gated ion channels. *Naturwissenschaften,* 85**,** 437-444.

Thomas, D., Bloehs, R., Koschny, R., Ficker, E., Sykora, J., Kiehn, J., Schlömer, K., Gierten, J., Kathöfer, S., Zitron, E., Scholz, E. P., Kiesecker, C., Katus, H. A. & Karle, C. A. 2008. Doxazosin induces apoptosis of cells expressing hERG K^+ channels. *Eur J Pharmacol,* 579**,** 98-103.

Tie, L., Lu, N., Pan, X. Y., Pan, Y., An, Y., Gao, J. W., Lin, Y. H., Yu, H. M. & Li, X. J. 2012. Hypoxia-induced upregulation of aquaporin-1 protein in prostate cancer cells in a p38-dependent manner. *Cell Physiol Biochem,* 29**,** 269-280.

Toyoshima, C., Kanai, R. & Cornelius, F. 2011. First crystal structures of Na^+,K^+-ATPase: new light on the oldest ion pump. *Structure,* 19**,** 1732-1738.

Trédan, O., Galmarini, C. M., Patel, K. & Tannock, I. F. 2007. Drug resistance and the solid tumor microenvironment. *J Natl Cancer Inst,* 99**,** 1441-1454.

Turner, P. J. & Buckler, K. J. 2013. Oxygen and mitochondrial inhibitors modulate both monomeric and heteromeric TASK-1 and TASK-3 channels in mouse carotid body type-1 cells. *J Physiol*.

Tyan, S.-W., Kuo, W.-H., Huang, C.-K., Pan, C.-C., Shew, J.-Y., Chang, K.-J., Lee, E. Y. H. P. & Lee, W.-H. 2011. Breast cancer cells induce cancer-associated fibroblasts to secrete hepatocyte growth factor to enhance breast tumorigenesis. *PLoS One,* 6**,** e15313.

Uysal-Onganer, P. & Djamgoz, M. 2007. Epidermal growth factor potentiates *in vitro* metastatic behaviour of human prostate cancer PC-3M cells: involvement of voltage-gated sodium channel. *Mol Cancer,* 6**,** 76.

Vander Heiden, M. G., Cantley, L. C. & Thompson, C. B. 2009. Understanding the Warburg effect: the metabolic requirements of cell proliferation. *Science,* 324**,** 1029-1033.

VanHouten, J., Sullivan, C., Bazinet, C., Ryoo, T., Camp, R., Rimm, D. L., Chung, G. & Wysolmerski, J. 2010. PMCA2 regulates apoptosis during mammary gland involution and predicts outcome in breast cancer. *Proc Natl Acad Sci U S A,* 107**,** 11405-11410.

vanTol, B. L., Missan, S., Crack, J., Moser, S., Baldridge, W. H., Linsdell, P. & Cowley, E. A. 2007. Contribution of KCNQ1 to the regulatory volume decrease in the human mammary epithelial cell line MCF-7. *Am J Physiol Cell Physiol,* 293**,** C1010-C1019.

Vaporidi, K., Tsatsanis, C., Georgopoulos, D. & Tsichlis, P. N. 2005. Effects of hypoxia and hypercapnia on surfactant protein expression proliferation and apoptosis in A549 alveolar epithelial cells. *Life Sci,* 78**,** 284-293.

Vara, J. Á. F., Casado, E., de Castro, J., Cejas, P., Belda-Iniesta, C. & González-Barón, M. 2004. PI3K/Akt signalling pathway and cancer. *Cancer Treat Rev,* 30**,** 193-204.

Veale, E. L., Buswell, R., Clarke, C. E. & Mathie, A. 2007a. Identification of a region in the TASK-3 two-pore domain potassium channel that is critical for its blockade by methanandamide. *Br J Pharmacol,* 152**,** 778-786.

Veale, E. L., Kennard, L. E., Sutton, G. L., MacKenzie, G., Sandu, C. & Mathie, A. 2007b. $G\alpha_q$-mediated regulation of TASK-3 two-pore domain potassium channels: the role of protein kinase C. *Mol Pharmacol,* 71**,** 1666-1675.

Veeravalli, K. K., Ponnala, S., Chetty, C., Tsung, A. J., Gujrati, M. & Rao, J. S. 2012. Integrin α9β1-mediated cell migration in glioblastoma via SSAT and K_{ir}4.2 potassium channel pathway. *Cell Signal,* 24**,** 272-281.

Vergara, C., Latorre, R., Marrion, N. & Adelman, J. 1998. Calcium-activated potassium channels. *Curr Opin Neurobiol,* 8**,** 321 - 329.

Voloshyna, I., Besana, A., Castillo, M., Matos, T., Weinstein, I. B., Mansukhani, M., Robinson, R. B., Cordon-Cardo, C. & Feinmark, S. J. 2008. TREK-1 is a novel molecular target in prostate cancer. *Cancer Res,* 68**,** 1197-1203.

Wadhwa, S., Wadhwa, P., Dinda, A. & Gupta, N. 2009. Differential expression of potassium ion channels in human renal cell carcinoma. *Int Urol Nephrol,* 41**,** 251-257.

Wang, J.-Y., Wang, J., Golovina, V. A., Li, L., Platoshyn, O. & Yuan, J. X.-J. 2000. Role of K^+ channel expression in polyamine-dependent intestinal epithelial cell migration. *Am J Physiol Cell Physiol,* 278**,** C303-C314.

Wang, J., Weigand, L., Wang, W., Sylvester, J. T. & Shimoda, L. A. 2005. Chronic hypoxia inhibits K_V channel gene expression in rat distal pulmonary artery. *Am J Physiol Lung Cell Mol Physiol,* 288**,** L1049-L1058.

Wang, L. H., Wang, N., Lu, X. Y., Liu, B. C., Yanda, M. K., Song, J. Z., Dai, H. M., Sun, Y. L., Bao, H. F., Eaton, D. C. & Ma, H. P. 2012. Rituximab inhibits K_V1.3 channels in human B lymphoma cells via activation of FcγRIIB receptors. *Biochim Biophys Acta,* 1823**,** 505-513.

Wang, S., Melkoumian, Z., Woodfork, K. A., Cather, C., Davidson, A. G., Wonderlin, W. F. & Strobl, J. S. 1998. Evidence for an early G_1 ionic event necessary for cell cycle progression and survival in the MCF-7 human breast carcinoma cell line. *J Cell Physiol,* 176**,** 456-464.

Wang, Z. 2004. Roles of K^+ channels in regulating tumour cell proliferation and apoptosis. *Pflugers Arch,* 448**,** 274-286.

Ward, C., Langdon, S. P., Mullen, P., Harris, A. L., Harrison, D. J., Supuran, C. T. & Kunkler, I. H. 2013. New strategies for targeting the hypoxic tumour microenvironment in breast cancer. *Cancer Treat Rev,* 39**,** 171-179.

Washburn, C. P., Bayliss, D. A. & Guyenet, P. G. 2003. Cardiorespiratory neurons of the rat ventrolateral medulla contain TASK-1 and TASK-3 channel mRNA. *Respir Physiol Neurobiol,* 138**,** 19-35.

Washburn, C. P., Sirois, J. E., Talley, E. M., Guyenet, P. G. & Bayliss, D. A. 2002. Serotonergic raphe neurons express TASK channel transcripts and a TASK-Like pH- and halothane-sensitive K^+ conductance. *J Neurosci,* 22**,** 1256-1265.

Wei, A. D., Gutman, G. A., Aldrich, R., Chandy, K. G., Grissmer, S. & Wulff, H. 2005. International Union of Pharmacology. LII. Nomenclature and molecular relationships of calcium-activated potassium channels. *Pharmacol Rev,* 57**,** 463-472.

Weinberg, R. A. 1995. The retinoblastoma protein and cell cycle control. *Cell,* 81**,** 323-330.

Weinberg, R. A. 2006. *The biology of cancer*, Garland Science.

Weir, E. K. & Olschewski, A. 2006. Role of ion channels in acute and chronic responses of the pulmonary vasculature to hypoxia. *Cardiovasc Res,* 71**,** 630-641.

Wickenden, A. D. 2002. K^+ channels as therapeutic drug targets. *Pharmacol Ther,* 94**,** 157-182.

Williams, A. C., Collard, T. J. & Paraskeva, C. 1999. An acidic environment leads to p53 dependent induction of apoptosis in human adenoma and carcinoma cell lines: implications for clonal selection during colorectal carcinogenesis. *Oncogene,* 18**,** 3199-3204.

Williams, C., Edvardsson, K., Lewandowski, S. A., Strom, A. & Gustafsson, J.-A. 2007a. A genome-wide study of the repressive effects of estrogen receptor beta on estrogen receptor alpha signaling in breast cancer cells. *Oncogene,* 27**,** 1019-1032.

Williams, R. D., Elliott, A. Y., Stein, N. & Fraley, E. E. 1978. *In vitro* cultivation of human renal cell cancer. *In Vitro,* 14**,** 779-786.

Williams, R. H., Jensen, L. T., Verkhratsky, A., Fugger, L. & Burdakov, D. 2007b. Control of hypothalamic orexin neurons by acid and CO_2. *Proc Natl Acad Sci U S A,* 104**,** 10685-10690.

Witsch, E., Sela, M. & Yarden, Y. 2010. Roles for growth factors in cancer progression. *Physiology (Bethesda),* 25**,** 85-101.

Wonderlin, W. F. & Strobl, J. S. 1996. Potassium channels, proliferation and G_1 progression. *J Membr Biol,* 154**,** 91-107.

Wu, J., Wu, X., Lian, K., Lin, B., Guo, L. & Ding, Z. 2012. Overexpression of potassium channel Ether à go-go in human osteosarcoma. *Neoplasma,* 59**,** 207-215.

Wu, S.-N., Jan, C.-R. & Li, H.-F. 1999. Ruthenium red-mediated inhibition of large-conductance Ca^{2+}-activated K^+ channels in rat pituitary GH3 cells. *J Pharmacol Exp Ther,* 290**,** 998-1005.

Wyatt, C. N., Mustard, K. J., Pearson, S. A., Dallas, M. L., Atkinson, L., Kumar, P., Peers, C., Hardie, D. G. & Evans, A. M. 2007. AMP-activated protein kinase mediates carotid body excitation by hypoxia. *J Biol Chem,* 282**,** 8092-8098.

Xia, X.-M., Fakler, B., Rivard, A., Wayman, G., Johnson-Pais, T., Keen, J. E., Ishii, T., Hirschberg, B., Bond, C. T., Lutsenko, S., Maylie, J. & Adelman, J. P. 1998. Mechanism of calcium gating in small-conductance calcium-activated potassium channels. *Nature,* 395**,** 503-507.

Xia, X.-M., Zeng, X. & Lingle, C. J. 2002. Multiple regulatory sites in large-conductance calcium-activated potassium channels. *Nature,* 418**,** 880-884.

Yan, G.-R., Xiao, C.-L., He, G.-W., Yin, X.-F., Chen, N.-P., Cao, Y. & He, Q.-Y. 2010. Global phosphoproteomic effects of natural tyrosine kinase inhibitor, genistein, on signaling pathways. *Proteomics*, 10**,** 976-986.

Yang, H., Li, X., Ma, J., Lv, X., Zhao, S., Lang, W. & Zhang, Y. 2013. Blockade of the intermediate-conductance Ca^{2+}-activated K^+ channel inhibits the angiogenesis induced by epidermal growth factor in the treatment of corneal alkali burn. *Exp Eye Res,* 110**,** 76-87.

Yang, J., Jan, Y. N. & Jan, L. Y. 1995. Determination of the subunit stoichiometry of an inwardly rectifying potassium channel. *Neuron,* 15**,** 1441-1447.

Yang, J. & Weinberg, R. A. 2008. Epithelial-Mesenchymal Transition: At the crossroads of development and tumor metastasis. *Dev Cell,* 14**,** 818-829.

Yang, M. & Brackenbury, W.J. 2013. Membrane potential and cancer progression. *Front Physiol*, 4.

Yang, S., Zhang, J. J. & Huang, X.-Y. 2009. Orai1 and STIM1 are critical for breast tumor cell migration and metastasis. *Cancer Cell,* 15**,** 124-134.

Yang, X., Hao, Y., Ding, Z., Pater, A. & Tang, S.-C. 1999. Differential expression of anti-apoptotic gene BAG-1 in human breast normal and cancer cell lines and tissues. *Clin Cancer Res,* 5**,** 1816-1822.

Yellen, G. 2002. The voltage-gated potassium channels and their relatives. *Nature,* 419**,** 35-42.

Yu, S. P. 2003. Regulation and critical role of potassium homeostasis in apoptosis. *Prog Neurobiol,* 70**,** 363-386.

Yu, S. P., Yeh, C.-H., Sensi, S. L., Gwag, B. J., Canzoniero, L. M. T., Farhangrazi, Z. S., Ying, H. S., Tian, M., Dugan, L. L. & Choi, D. W. 1997. Mediation of neuronal apoptosis by enhancement of outward potassium current. *Science,* 278**,** 114-117.

Yuill, K. H., Stansfeld, P. J., Ashmole, I., Sutcliffe, M. J. & Stanfield, P. R. 2007. The selectivity, voltage-dependence and acid sensitivity of the tandem pore potassium channel TASK-1: contributions of the pore domains. *Pflugers Arch,* 455**,** 333-348.

Zhang, G., Gurtu, V., Kain, S. R., & Yan, G. 1997. Early detection of apoptosis using a fluorescent conjugate of annexin V. *Biotechniques,* 23**,** 525-531.

Zhang, R., Tian, P., Chi, Q., Wang, J., Wang, Y., Sun, L., Liu, Y., Tian, S. & Zhang, Q. 2012. Human Ether-à-go-go-related gene expression is essential for cisplatin to induce apoptosis in human gastric cancer. *Oncol Rep,* 27**,** 433-440.

Zhao, J., Wei, X.-L., Jia, Y.-S. & Zheng, J.-Q. 2008. Silencing of hERG gene by shRNA inhibits SH-SY5Y cell growth *in vitro* and *in vivo*. *Eur J Pharmacol,* 579**,** 50-57.

Zheng, Y., Chen, L., Li, J., Yu, B., Su, L., Chen, X., Yu, Y., Yan, M., Liu, B. & Zhu, Z. 2011. Hypermethylated DNA as potential biomarkers for gastric cancer diagnosis. *Clin Biochem,* 44**,** 1405-1411.

Zhu, J., Yan, J. & Thornhill, W. B. 2012. *N*-glycosylation promotes the cell surface expression of K_V1.3 potassium channels. *FEBS J,* 279**,** 2632-2644.